Electrochemical Lignin Breakdown: From Bulk to Atomically Dispersed Catalysts

Dissertation

Zur Erlangung des Doktorgrades
der Naturwissenschaft (Dr. rer. nat.) in der Fachgruppe Chemie und Biologie
der Mathematisch Naturwissenschaftlichen Fakultät
der Bergischen Universität Wuppertal

vorgelegt von

Lucie Marie Lindenbeck

aus Wuppertal

- 2025 -

Dekan:	Prof. Dr. Fabian Mohr
Erster Gutachter:	Prof. Dr. Adam Slabon
Zweiter Gutachter:	Prof. Dr. Christian Lehmann
Tag der mündlichen Prüfung:	27.05.2025

February 2023 – March 2025

“Basically, I have been compelled by curiosity.”

— *Mary Leakey*

Comments on the structure of the dissertation

Comments on the structure of the dissertation

This dissertation follows a cumulative structure, integrating five first-author publications and two submitted manuscripts. Chapters 1 and 2 provide the scientific background and outline the motivation for the projects, while Chapter 3 presents a review article offering a comprehensive overview of electrochemical lignin depolymerization catalyst used in these processes. Chapters 4, 5, and 6 present published research articles, while Chapters 7 and 9 are currently under peer review - Chapter 9 has been also published as a preprint. Each research article begins with a preface to provide context for non-specialist readers and highlight key challenges and findings.

Chapter 8 provides a perspective article that explores the transition from bulk to advanced, complex electrocatalysts. The final Chapter 10 concludes with an overview, unpublished results and a discussion of future research directions.

The dissertation incorporates the remarks and suggestions of all authors involved in the manuscript preparation, as well as comments from reviewers and journal editors obtained during the peer-review process. To enhance clarity and readability, all references, figures, and tables have been renumbered sequentially throughout the dissertation, with the source of each original publication noted at the beginning of the respective chapter. Although the formatting has been modified to maintain consistency, the scientific content itself has remained unaltered. Variations in nomenclature, abbreviations, and structure reflect the differences in publication styles characteristic of various academic journals.

Publications

1) Lucie M. Lindenbeck, Björn B. Beele, Mohammad Morsali, Serhiy Budnyk, Marcella Frauscher, Jianhong Chen, Mika H. Sipponen, Adam Slabon, and Bruno V. M. Rodrigues, MoS_2 Nanoflower-Decorated Lignin Nanoparticles for Superior Lubricant Properties. *Nanoscale* **2023**, *15* (20), 9014–9021.

2) Lucie M. Lindenbeck, Yanbing Liu, Björn B. Beele, Adam Slabon, and Bruno V. M. Rodrigues, Sustainable Routes for the Depolymerization of Lignocellulosic Biomass. In *Encyclopedia of Inorganic and Bioinorganic Chemistry*; Scott, R. A., Ed.; Wiley, **2023**; pp 1–19.

3) Lucie M. Lindenbeck, Vanessa C. Barra, Sira Dahlhaus, Silas Brand, Luca M. Wende, Björn B. Beele, Nils H. Schebb, Bruno V. M. Rodrigues, and Adam Slabon, Organic Chemicals from Wood: Selective Depolymerization and Dearomatization of Lignin via Aqueous Electrocatalysis. *ChemSusChem* **2024**, *17* (9), e202301617.

4) Lucie M. Lindenbeck, Sira Dahlhaus, Luca M. Wende, Björn B. Beele, Marcella Frauscher, Nils H. Schebb, Christian W. Lehmann, Julia Bornhorst, Adam Slabon, and Bruno V. M. Rodrigues, Breaking down Lignin in Gamma-Valerolactone: Advances into a Bioelectrorefinery. *Green Chem. Lett. Rev.* **2024**, *17* (1), 2390867.

5) Lucie M. Lindenbeck, Vanessa C. Barra, Björn B. Beele, Bruno V. M. Rodrigues, and Adam Slabon, Revisiting the Electrocatalyst Role on Lignin Depolymerization. *Adv. Energy Sustainability Res.* **2024**, *5* (10), 2400130.

6) Lucie M. Lindenbeck, Björn B. Beele, Dirk F. Lützenkirchen-Hecht, Bruno V. M. Rodrigues, and Adam Slabon, Electrochemical Biomass Depolymerization: Will Complex Catalysts Trigger High Product Selectivity? *Chem. Mater.* **2024**, *36* (19), 9173–9188.

7) Jian Zhu, Thijs Mulder, Anna Rokicińska, Lucie M. Lindenbeck, Järi Van Den Hoek, Remco W. A. Havenith, Ana V. Cunha, Piotr Kuśtrowski, Adam Slabon, Shoubhik Das, and Pegie Cool, Synergistic Interaction between the Ni-Center and Glycine-Derived N-Doped Porous Carbon Material Boosts Electrochemical CO_2 Reduction. *ACS Catal.* **2024**, *14*, 10987–10997.

8) Lucie M. Lindenbeck, Silas Brand, Franka Stallmann, Vanessa C. Barra, Marcella Frauscher, Björn B. Beele, Adam Slabon, and Bruno V. M. Rodrigues, Silver-Catalyzed Aqueous Electrochemical Valorization of Soda Lignin into Aliphatics and Phenolics. *Polymers* **2024**, *16* (23), 3325.

9) Lucie M. Lindenbeck, Silas Brand, Finn Schatz, Franka Stallmann, Nele Petersen, Björn B. Beele, Jessica Pichler, Marcella Frauscher, Serhiy Budnyk, Adam Slabon, and Bruno V. M. Rodrigues, One-Pot Electrocatalytic Lignin Depolymerization with *In-Situ* Extraction: A Feasible Approach for the Production of Biomass-based Oils, *Green Chem.* **2025**, *27*, 9927-9936.

10) Lucie M. Lindenbeck, Anuja P. Nawadkar, Dirk Lützenkirchen-Hecht, Andreas Drichel, Marcella Frauscher, Björn B. Beele, Piotr Kuśtrowski, Prathamesh Patil, Christian M. Pichler, Yu Chen, Yi Yu, Christian W. Lehmann, Jiayin Yuan, Bruno V. M. Rodrigues, and Adam Slabon, Electrocatalytic Lignin Depolymerization enabled by a Biomass-derived Iron Dual-Atom Catalyst: from Synthesis to an *In-Operando* X-Ray Absorption Spectroscopy Study, *accepted in Green Chem. Lett. Rev*.

11) Lucie M. Lindenbeck, Laura Kubens, Sven Buschmann, Björn B. Beele, Andrij Pich, Serhiy Budnyk, Julia Bornhorst, Bruno V. M. Rodrigues, and Adam Slabon, Nature-Inspired Coatings: Chitosan Integrated Lignin-based Aliphatic Additives for Prolonging Fruit Shelf Life, *submitted*.

12) Lucie M. Lindenbeck, Björn B. Beele, Dirk Lützenkirchen-Hecht, Piotr Kuśtrowski, Bruno V. M. Rodrigues, and Adam Slabon, Lignin Meets Inorganics: Engineering Hybrid Interfaces for Sustainable Applications, *submitted*.

Table of contents

Abbreviations used

1G	First generation biomass feedstocks
2G	Second generation biomass feedstocks
4-HVA	4-Hydroxyvaleric acid
ACN	Acetonitrile
ads	Adsorption
AGC	Automatic gain control
AGU	Anhydroglucose unit
AP-XPS	Ambient pressure-X-ray photoelectron spectroscopy
AR-XPS	Angle-resolved-X-ray photoelectron spectroscopy
ATR-FTIR	Attenuated total reflection-infrared spectroscopy
BC	Biochar
BSE	Backscattered electrons
BTU	British thermal unit
CNT	Carbon nanotubes
CO_2RR	Electrochemical reduction of carbon dioxide
COF	Coefficient of friction
COSY	Correlation spectroscopy
CP	Carbon paper
CQD	Carbon quantum dots
Cu-AHP	Copper-catalyzed alkaline hydrogen peroxide
CV	Cyclic voltammetry
DAC	Dual-atom catalyst
DDO	Direct deoxygenation
DES	Deep eutectic solvent
DFT	Density functional theory
DI-ESI-HRMS	Direct injection electrospray ionization high-resolution mass spectrometry
DL	Depolymerized lignin
DME	Dimethoxyethane
DMP	Dess–Martin periodinane
DMSO	Dimethylsulfoxide
DSC	Differential scanning calorimetry
DTG	Derivative thermogravimetry
e.g.	exempli gratia (for example)
EC	Electrocatalysis
ECH	Electrocatalytic hydrogenation
ECO	Electrocatalytic oxidation
ECSA	Electrochemically active surface area
EDX	Energy dispersive X-ray spectroscopy
EELS	Electron energy loss spectroscopy
ELNES	Electron loss near edge structure
EPR	Electron paramagnetic resonance spectroscopy
et al.	et alia (and others)
ETEM	Environmental transmission electron microscopy
EXAFS	Extended X-ray absorption fine structure
EXELFS	Extended electron energy loss fine structure

FAL	Biomass-derived furfural
FE	Faradaic efficiency
FT	Fourier transformation
FTIR	Fourier transform infrared spectroscopy
GC	Gas chromatography
GC-FID	Gas chromatography-flame ionization detection
GC-MS	Gas chromatography–mass spectrometry
GPC	Gel permeation chromatography
GVL	Gamma-Valerolactone
HAADF	High-angle annular dark-field
HAADF-STEM	High-angle annular dark-field scanning transmission electron microscopy
HD	Hydrodeoxygenation
HDO	Hydrodeoxygenation
HEA	High-entropy alloy
HEB	High-entropy boride
HEN	High-entropy nitride
HER	Hydrogen evolution reaction
HESAC	High-entropy single-atom catalyst
HMBC	Heteronuclear multiple bond correlation
HOMO	Highest occupied molecular orbital
HPGe	High purity germanium radiation detector
HPLC	High performance liquid chromatography
HR-LC MS	High-resolution liquid chromatography mass spectrometry
HR-STEM	High-resolution scanning transmission electron microscope
HR-TEM	High-resolution transmission electron microscopy
HRMS	High-resolution mass spectrometry
HSQC	Heteronuclear single quantum coherence
ICP-OES	Inductively coupled plasma optical emission spectrometry
LA	Levulinic acid
LC-ESI-HRMS	Liquid chromatography electrospray ionization high-resolution mass spectrometry
LC-ESI-MS	Liquid chromatography electrospray ionization mass spectrometry
LC-MS	Liquid chromatography mass spectrometry
LC-UV	Liquid chromatography ultraviolet detection
LDH	Layered double hydroxide
LEIS	Low energy ion scattering
LFFC	Liquid flow fuel cell
LO	Lignin oil
M	Metal
m/z	Mass to charge ratio
MIBK	Methyl isobutyl ketone
MO	Metal oxide
MOF	Metal-organic framework
MP	Metal phosphides
MS	Mass spectrometry
MWCNT	Multi-walled arbon nanotubes
MWNT	Multi-walled nanotubes
NHPI	N-hydroxyphthalimide

NMR	Nuclear magnetic resonance
NP	Nanoparticle
NS	Nanosheets
OER	Oxygen evolution reaction
OP	Organic phase
ORR	Oxygen reduction reaction
PCDD	Polychlorinated dibenzo-dioxins
PCDF	Polychlorinated dibenzofurans
PE	Polyethylen
PET	Polyethylenterephthalat
PINO	Phthalifmide-N-oxyl
PIPS	Passivated implanted planar silicon detector
PMA	Methoxy propyl acetate
POM	Polyoxometalates
PP	Polypropylene
PPE	2-Phenoxy-1-phenylethanol
pXRD	Powder X-ray diffraction
RCF	Reductive catalytic fractionation
RDE	Rotating disk electrode
RFS	Renewable fuel standard
RHE	Reversible hydrogen electrode
ROS	Reactive oxygen species
rpm	Rounds per minute
RVC	Reticulated vitreous carbon
SAC	Single-atom catalyst
satd.	Saturated
SAXS	Small-angle X-ray scattering
SCE	Saturated calomel electrode
SDD	Silicon drift detector
SDG	Sustainable development goals
SE	Secondary electrons
SEM	Scanning electron microscopy
SEM-EDX	Scanning electron microscopy with energy-dispersive X-ray spectroscopy
SHE	Standard hydrogen electrode
SRV	Schwingungs-Reib-Verschleiß-Test (Reciprocating tribometer test)
STEM	Scanning transmission electron microscopy
STM	Scanning tunneling microscopy
SWCNT	Single-walled carbon nanotubes
TEA	Techno-economic analysis
TEM	Transmission electron microscopy
TEMPO	2,2,6,6-Tetramethylpiperidine-N-oxyl
TG	Thermogravimetry
TGA	Thermogravimetric analysis
TM	Transition metal
TMB	Transition metal boride
TMC	Transition metal carbide
TMN	Transition metal nitrides
TMP	Transition metal phosphides

TOF-MS	Time-of-flight mass spectrometry
UPLC-MS	Ultra-performance liquid chromatography–mass spectrometry
UV/Vis	Ultraviolet and visible spectroscopy
WP	Water phase
XANES	X-ray absorption near edge structure
XAS	X-ray absorption spectroscopy
XPS	X-ray photoelectron spectroscopy
XRD	X-ray diffraction
ZDDP	Zinc dialkyl dithiophosphate

Summary

The pressing challenges of our time—particularly man-made climate change and the depletion of fossil raw materials—call for a fundamental rethinking of the chemical industry. Given that most carbon-based chemicals currently originate from fossil sources, a transition to more sustainable, renewable, and nearly CO_2-neutral alternatives is imperative. Lignin, the second most abundant biopolymer on Earth after cellulose, presents significant potential as a renewable raw material. As a by-product of paper production, lignin can be used without additional infrastructure, so its carbon footprint is not increased by harvesting or transportation. Nevertheless, lignin is still mainly incinerated, because its complex and varying structure—additionally influenced by different extraction methods—makes it considerably more difficult to use for high-quality applications. A promising approach to better utilize lignin is depolymerization, which converts it into valuable organic chemicals. Among the various depolymerization methods, electrochemical depolymerization has emerged as a sustainable approach due to its compatibility with *Green Chemistry* principles and its ability to be conducted under mild conditions. The utilization of renewable energy further enhances the sustainability of the process, contributing to achieving carbon neutrality.

This dissertation investigates the influence of electrocatalysts on lignin depolymerization. A review of the extant literature reveals that the prevailing focus of research efforts is oriented towards the utilization of metal catalysts, such as copper, nickel, lead, and platinum. Nevertheless, carbon electrodes emerge as a promising alternative, offering enhanced sustainability and cost-effectiveness. Notably, the potential of silver as a catalyst remains under-explored. Moreover, reductive depolymerization conditions are comparatively under-researched in comparison to oxidative approaches.

In light of these observations, the present dissertation investigates the application of carbon and silver for the reductive depolymerization of technical lignins, such as Soda lignin and Kraft lignin. It is demonstrated that electrochemical depolymerization is achievable with both unmodified bulk carbon and silver electrodes. Despite the recognized challenges associated with lignin depolymerization, including its low selectivity and the complexity in characterizing the products, the use of both nuclear magnetic resonance and infrared spectroscopy, as well as high- resolution mass spectrometry, has enabled the identification of several predominant products. Furthermore, it has been demonstrated that the catalyst selection plays a pivotal role in determining the product distribution, even under conditions that are otherwise identical.

Utilizing carbon as a catalyst results in the complete dearomatization of lignin, yielding four major aliphatic products: levulinic acid, 4-hydroxyvaleric acid, acetic acid, and formic acid. Conversely, the employment of silver enables the production of a more extensive product spectrum, encompassing both aliphatic and aromatic monomers. The lower yield in the depolymerization of Kraft lignin compared to Soda lignin could be overcome by implementing a novel two-phase system. This system, consisting of an aqueous sodium carbonate/lignin solution and an organic methyl isobutyl ketone layer on top, expands the product spectrum, significantly increases the efficiency of lignin utilization, and thus lays the foundation for integration into future biorefineries.

To facilitate the transition from conventional oil refineries to biorefineries, it is of utmost importance to streamline processes and avoid unnecessary intermediate steps and the associated time- and energy-intensive processing. The solvent gamma-valerolactone (GVL), which can be derived from biomass, holds promise for direct lignin extraction from biomass. Currently, lignin extraction and solvent recovery require several complex steps. However, the findings of this study demonstrate that lignin can be directly depolymerized in GVL, thereby eliminating the necessity for multistep processing. This underscores the potential of GVL not only as an extractant but also as a reaction medium for depolymerization, which marks a significant advancement toward efficient and sustainable biorefinery processes.

While carbon and silver bulk catalysts have been demonstrated to be effective, the development of catalysts has been stagnant in comparison to advances in CO_2 reduction. Recent studies have demonstrated that the employment of complex catalysts, such as transition metal borides, nitrides, carbides, phosphides, MXenes, nanoparticles, and single-atom catalysts, can remarkably enhance Faradaic efficiency and product selectivity. It is hypothesized that these findings can be extrapolated to the domain of biomass depolymerization, and that the strategic exploitation of dynamic structural features and exceptional catalytic properties can facilitate the controlled cleavage of bonds in bio-based raw materials.

In this study, an iron dual-atom catalyst was utilized on coffee-based biochar, marking a pioneering application of methodologies employed in CO_2 reduction to biomass depolymerization. The findings demonstrate a substantial enhancement in electrocatalytic efficiency when compared to conventional bulk catalysts. The catalyst was synthesized *via* pyrolysis and underwent comprehensive characterization substantiating its atomic dispersion and chemical composition. Furthermore, the *in-operando* stability of the

catalyst was demonstrated by X-ray absorption spectroscopy measurements at varying potentials.

This dissertation thus demonstrates the potential of both bulk and atomically dispersed catalysts for lignin valorization, provides a basis for monitoring catalyst behavior at the atomic level during electrochemical depolymerization, and paves the way for future biorefineries. In particular, atomically dispersed catalysts open up new perspectives for sustainable and precisely controlled biomass conversion due to their high efficiency and selectivity.

Chapter 1

Motivation and Scope of the Thesis

Chapter 1 - Motivation and scope of the thesis

1.1 Motivation of the thesis

Significant environmental problems, such as climate change and pollution, are caused by the global dependence on finite fossil fuels for energy, chemicals, and materials. In 2024, the global warming threshold of 1.5 °C was exceeded for the first time, [1] which has led to an increased urgency for the transition to a bio-based economy. Lignocellulosic biomass is a promising candidate as a feedstock because it is perpetually renewable and can contribute to carbon neutrality. [2,3] Among the various components of lignocellulose, lignin stands out as the least utilized fraction and is predominantly incinerated. [4] It is the largest natural source of renewable aromatic compounds, thereby underscoring its significant potential to produce high-value chemicals, biofuels, and advanced materials. To harness this potential, innovative approaches are imperative to overcome the inherent structural complexity and heterogeneity of lignin. The development of efficient and sustainable depolymerization methods is imperative to break down lignin into valuable monomers and oligomers. [5] Electrochemical depolymerization of lignin has emerged as a *greener* alternative to conventional thermal or chemical processes. [3] Electrochemical methods offer precise control over reaction conditions, require lower energy inputs, and seamlessly integrate with renewable electricity sources, thereby aligning with the principles of *Green Chemistry*. [6–9] However, a crucial aspect for improving the efficiency of this approach is the transition from conventional "bulk" catalysts, which frequently exhibit deficiencies with respect to surface area, active site exposure, and the precision necessary for selective reactions, to nano- and atomically dispersed ones. [10] Conversely, nano- and atomically structured catalysts boast a higher density of active sites, thereby enhancing catalytic efficiency. Their surface chemistry can be fine-tailored to specific interactions with lignin and its intermediates and they require less loading, reducing overall costs. However, their synthesis and characterization are often more complex than those of bulk catalysts. Advanced analytical techniques are required to confirm active site structures as well as to confirm the stability of the catalysts in the context of lignin depolymerization. Additionally, achieving consistent reproducibility in large-scale production can be more difficult than with bulk catalysts. These challenges must be overcome in order to transition to atomically structured catalysts.

1.2 Scope of the thesis

- Development of electrochemical methods for lignin depolymerization using diverse electrocatalysts to produce high-value products.
- Comprehensive structural characterization of depolymerization products using analytical techniques such as Nuclear Magnetic Resonance (NMR), Fourier Transform Infrared Spectroscopy (FTIR), and Mass Spectrometry (MS) to identify key molecular components and their transformations.
- Design and synthesis of novel atomically dispersed electrocatalysts to enhance the efficiency and selectivity of the lignin depolymerization processes.
- Structural analysis of electrocatalysts utilizing techniques such as X-ray Diffraction (XRD), X-ray Photoelectron Spectroscopy (XPS), Low-Energy Ion Scattering (LEIS), and X-ray Absorption Spectroscopy (XAS), including *in-operando* XAS, to uncover atomic-scale details and evaluate their stability under reaction conditions.

Chapter 2

Background Information

Chapter 2 - Background information

2.1 The need for change

Climate change has emerged as the most pressing threat to the future of humanity, [11–13] driven by fundamental processes that regulate the Earth's temperature. Sunlight strikes the Earth's surface, with a portion being reflected and the remainder absorbed and subsequently radiated as heat. [14] The presence of greenhouse gases, such as carbon dioxide (CO_2), methane, and water vapor, impedes the dissipation of this heat into space, leading to an increase in the Earth's temperature. [15] In the absence of the greenhouse effect, it is estimated that the average surface temperature on Earth would be approximately −19 °C, [15] as opposed to the current average of 15.1 °C, [1] a condition that would preclude the existence of life as we know it. The concentration of CO_2 in the atmosphere has increased from approximately 280 ppm to over 400 ppm [16] as a result of human activities, leading to a global temperature increase of over 1.6 °C compared to pre-industrial levels. 2024 was the warmest year on record, surpassing 2023, and marked the first full calendar year with an average global temperature exceeding 1.5 °C above pre-industrial levels. [1] Observations show that each decade since the 1980s has been warmer than the previous one, with the last ten years being the warmest on record. [1,13,16] This warming phenomenon affects more than just air temperatures; it primarily impacts the oceans, which serve as a thermal reservoir for approximately 90% of the additional heat absorbed by the Earth's climate system. [16] The increased evaporation caused by warmer ocean temperatures leads to higher humidity and more intense rainfall. This, in turn, results in more frequent extreme weather events. Since 1980, there has been a quadruple increase in extreme climatological events, including high temperatures, droughts, and wildfires, while meteorological events such as extreme storms have doubled. [13] The year 2024 alone saw multiple global records broken, not only for greenhouse gas concentrations but also for air and sea surface temperatures, leading to devastating floods, wildfires, and heatwaves. [1] Furthermore, climate change has a profound impact on ecosystems, as plants and animals respond to altered environmental conditions by shifting their habitats. [16] The current rate of warming is more than 0.2 °C per decade, [1] which makes it highly probable that the 1.5 °C target established by the Paris Agreement will be consistently exceeded within the 2030s. Despite international agreements, global temperatures continue to rise due to the persistent use of fossil fuels and ongoing deforestation. [13] In the absence of a comprehensive energy transition, temperatures are projected to rise by 3 °C or more by the end of the century. [17]

2.2 Problems with fossil fuel utilization

This prognosis emphasizes the necessity of addressing the underlying causes of increased greenhouse gas emissions to mitigate the pace of climate change. The combustion of fossil fuels for energy production releases substantial quantities of CO_2, which persists in the atmosphere for extended periods, thereby amplifying the greenhouse effect by retaining heat radiation from the Earth's surface. [18] The most significant emissions are associated with the generation of electricity in coal-fired power plants, deforestation, and agricultural practices. [19]

Methane, a far more potent greenhouse gas than CO_2, has been shown to have a global warming potential that is 86 times higher over a 20-year period. This indicates that even minor leaks in the extraction and transportation of natural gas can have a substantial impact on global warming. [20] Nitrogen oxides (NO_x) are also produced during the combustion process of fossil fuels, contributing to the enhancement of the greenhouse effect. [21] The extraction of fossil fuels is often associated with significant ecological consequences, including widespread deforestation and soil degradation. [22,23] The clearance of forests, which function as natural carbon reservoirs, results in the release of stored CO_2 and the reduction of nature's capacity to absorb CO_2. Furthermore, the limited availability of fossil resources introduces an additional challenge, as the extraction of these materials results in rising environmental and economic costs. [22] Consequently, the continued reliance on fossil fuels becomes unsustainable over time.

Fossil raw materials consist of carbon that has been sequestered in the earth for millions of years. The rapid extraction and processing of these materials, which releases the stored carbon into the atmosphere, disrupts the natural balance of the carbon cycle. This, in consequence, results in an accelerated rise in the global average temperature. This warming triggers further amplification effects, which also lead to increased greenhouse gas emissions. Notable examples of this include the release of methane and CO_2 from thawing permafrost [24] and the reduction in reflectivity (albedo) [25] due to the melting of ice.

The overreliance on finite fossil resources not only exacerbates climate change but also underscores the urgent need for alternative, sustainable solutions that balance energy demands with environmental preservation. To address the present issues, it is essential to adopt a framework that aligns economic, social, and environmental priorities. This framework is encapsulated in the concept of sustainability, which emphasizes the need to meet present demands without compromising the ability of future generations to meet their own needs.

2.3 Principles of sustainability

The term "sustainability" is not clearly defined, and its interpretation and implementation vary significantly among individuals and organizations. Nonetheless, despite the divergent perspectives, there exists a consensus that sustainability is predicated on a multidimensional approach. [26] According to the Environmental Protection Agency (EPA), sustainability can be defined as "to create and maintain conditions, under which humans and nature can exist in productive harmony, that permit fulfilling the social, economic, and other requirements of present and future generations". [27] This definition is predicated on an extensive review of relevant literature, consultations with experts from governmental agencies, industry, academia, and NGOs, as well as intensive discussions within a dedicated committee. The committee held multiple meetings and public hearings in 2010 and 2011 to gather diverse perspectives on sustainable development and environmental stewardship. [27]

The three pillars of sustainability—the social, the economic, and the environmental dimension—must be closely interconnected and considered together to create viable long-term solutions. The social dimension of sustainability encompasses concerns such as poverty, cultural preservation, and empowerment. The overarching objective is to ensure equity within one generation (intra-generational equity) while also promoting equitable relations between the current and next generation (inter-generational equity). [26] In the economic dimension, the focus is on efficiency, growth, and stability to ensure the sustainable use of resources while achieving economic success. Concurrently, ecological costs must be assessed and integrated into economic decisions. The ecological dimension is also a fundamental component of this multifaceted approach. This involves the conservation of biodiversity, natural resources, and the mitigation of environmental pollution to ensure the long-term resilience of ecosystems. Achieving sustainable development necessitates a comprehensive approach, ensuring that no dimension is prioritized over another. [28,29]

2.4 Sustainability frameworks

The multidimensional nature of sustainability provides a substantial framework for addressing global challenges. However, the translation of these principles into actionable strategies necessitates a more structured and unified approach. One such approach is the Sustainable Development Goals (SDGs), a universal agreement designed to end poverty, protect the planet, and ensure peace and prosperity for both present and future generations. [30] The 17 goals (divided into five areas of critical importance) (**Table 1**) were

adopted in 2015 by all member states of the United Nations for the period from 2016 to 2030 in response to scientific and empirical evidence that the world needs a much more sustainable approach. [30]

Table 1. Summary of the UN's 17 Sustainable Development Goals, [30] which are associated with the five Areas of Critical Importance.

Area	Goal
People	Goal 1 - No Poverty
	Goal 2 - Zero Hunger
	Goal 3 - Good Health and Well-being
	Goal 4 - Quality Education
	Goal 5 - Gender Equality
	Goal 6 - Clean Water and Sanitation
Prosperity	Goal 7 - Affordable Clean Energy
	Goal 8 - Decent Work and Economic Development
	Goal 9 - Industry, Innovation and Infrastructure
	Goal 10 - Reduce Inequalities
	Goal 11 - Sustainable Cities and Communities
	Goal 12 - Responsible Consumption and Production
Planet	Goal 13 - Climate Action
	Goal 14 - Life below Water
	Goal 15 - Life on Land
Peace and partnerships	Goal 16 - Peace, Justice and Strong Institutions
	Goal 17 - Partnerships for the Goals

The SDGs offer a meticulously formulated and empirically substantiated framework that is politically viable and readily comprehensible to the public. This ensures the necessary collaboration and alignment required to implement global strategies to ensure a just, healthy, and prosperous future. [30] Goal 17 underscores the need for contributions from various academic disciplines to achieve the sustainability objectives. Chemistry plays a pivotal role in this endeavor. As the central science for material and energy transformations, chemistry has the potential to drive sustainable innovations that are in line with the SDGs. However, this potential can only be fully realized if the principles of sustainable and environmentally conscious practices are followed. In 1991, Paul Anastas and John Warner introduced the 12 Principles of *Green Chemistry* (**Table 2**) as a foundational framework for environmentally conscious chemical practices. [6] Key principles include the prevention of waste (Principle 1), the development of safer chemicals and products (Principle 4), the improvement of energy efficiency (Principle 6), and the use of renewable raw materials (Principle 7).

Table 2. The twelve principles of *Green Chemistry*. [6]

	Principle
1	Prevention
2	Atomic Economy
3	Less Hazardous Chemical Synthesis
4	Designing Safer Chemicals
5	Safer Solvents and Auxiliaries
6	Design for Energy Efficiency
7	Use of Renewable Feedstocks
8	Reduce Derivates
9	Catalysis
10	Design for Degradation
11	Real-Time Analysis for Pollution Prevention
12	Inherently Safer Chemistry for Accident Prevention

2.5 Biomass as a sustainable solution

Green Chemistry's seventh principle, "Use of Renewable Feedstocks", underscores the potential of biomass as a viable solution to mitigate environmental impacts and reduce reliance on finite fossil fuels. While oil, gas, and coal are limited resources, photosynthesis in nature produces approximately 170 billion tons of biomass annually. [31] CO_2, a major contributor to global warming, is converted into carbohydrates, which are essential to life on Earth. [2] Despite its immense potential, only about 3.5% of these raw materials are currently utilized. [2] A broad array of natural resources, including plants, trees, flowers, fruits, grains, and vegetables, can be classified as "renewable". [2] However, certain natural substances serve a dual purpose as both industrial raw materials and food sources, underscoring the need for strategic management in the utilization of these resources in the face of expanding human populations, especially in terms of their use as food. Non-food biomass comprises a variety of organic materials, including plants, wood, agricultural waste, and animal by-products such as beef tallow. These resources can be used as materials, *e.g.,* for the production of chemicals, or as energy, *e.g.*, for biofuels. [2]

2.6 Advantages and challenges of biomass utilization

Biomass offers numerous advantages; however, it also presents certain challenges. Its most salient benefit is its renewability, as it is continuously produced by natural processes such as photosynthesis. The utilization of biomass is nearly CO_2-neutral, as the released CO_2 can be bio-sequestered and subsequently converted back into biomass. However, the process of cultivating, harvesting, and processing these raw materials often require fossil

energy, thereby increasing the overall carbon footprint. [2] The inherent complexity of sustainable raw materials offers potential for chemical synthesis, potentially reducing the need for the extensive synthesis steps that are characteristic of the petrochemical industry. However, these structures also present challenges as well, as many biomolecules contain additional elements, such as oxygen and nitrogen, which must be removed before processing. [2] A significant challenge arises in the logistics of extraction and processing, which are often more complex and costly than those associated with fossil fuels. In contrast to fossil raw materials, which can be readily extracted and transported, sustainable raw materials such as wood or crops require collection from extensive areas and result in substantial transportation costs. Moreover, the economic viability of their utilization is not guaranteed, as the high costs associated with their production may not be offset by the prices of the end products. [2] While sustainable raw materials hold considerable promise for *Green Chemistry*, innovative approaches are necessary to counterbalance their inherent disadvantages and fully leverage their advantages.

2.7 Lignocellulose

Lignocellulose, a prevalent form of biomass, can be derived from various plant materials, including agricultural residues, forestry residues, and special energy crops. [3] It is composed of three primary macromolecular components: cellulose, hemicellulose, and lignin. [3] Cellulose, a polymer of glucose molecules arranged in linear chains, adopts a ribbon-like structure with a flat configuration. [32] The repeating unit, designated as the anhydroglucose unit (AGU), comprises two anhydroglucose rings $(C_6H_{12}O_6)_n$, with the value of n contingent on the cellulose source. [32] The glucose rings are interconnected by a covalent β-(1→4)-glycosidic bond between the C1 atom of one ring and the C4 atom of the neighboring ring (**Figure 1**). [32]

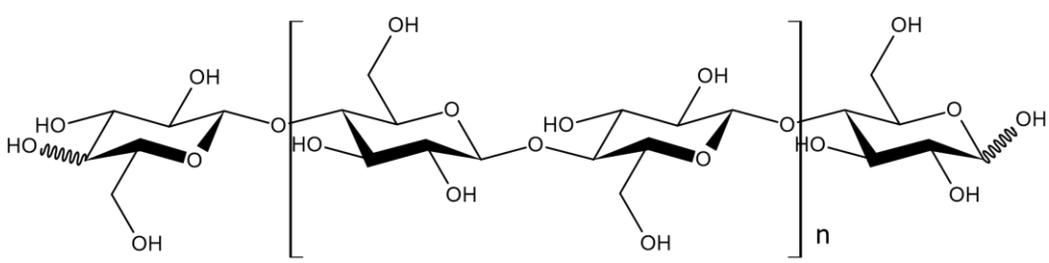

Figure 1. Chemical structure of cellulose consisting of β-(1→4)-linked D-glucose units.

The cellulose chain's stability is reinforced by intramolecular hydrogen bonds between the hydroxyl groups and oxygen atoms of the neighboring rings. Furthermore, a network of intra- and intermolecular hydrogen bonds ensures the high axial rigidity of the cellulose fibrils, thereby making cellulose a stable polymer. [33]

Hemicelluloses are complex polysaccharides that comprise a significant component of plant cell walls, where they form a stable matrix in conjunction with cellulose and lignin. [3] This contributes to the plant's mechanical strength, protection against pathogens, and the facilitation of water and nutrient transport. [34,35] Notable hemicelluloses include xylans, mannans, arabinans, and galactans, whose composition varies according to the plant species (**Figure 2**). [35]

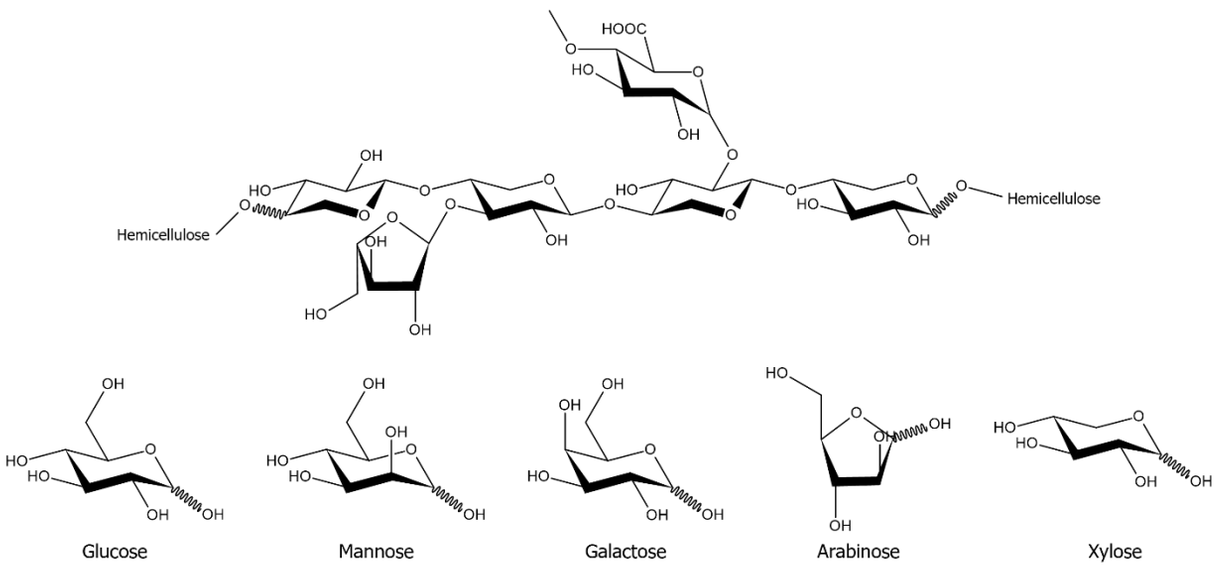

Figure 2. Chemical structure of hemicellulose and of the main sugar units present in hemicellulose.

The industrial applications of hemicelluloses are diverse. [35–38] They serve as the basis for biodegradable films [39,40] and coatings [41] suitable for environmentally friendly food packaging, and their biocompatibility makes them important components in hydrogels and biomaterials for drug delivery, [42,43] tissue engineering, [44,45] and wound healing [46]. Certain hemicelluloses, such as arabinoxylans, also act as prebiotics, promoting the growth of beneficial intestinal bacteria and contributing to gut health. [47–49] In biorefineries, hemicelluloses undergo hydrolysis, resulting in the production of fermentable sugars that serve as raw materials for biofuels, such as ethanol. [50,51] Lignin, also referred to as protolignin in its natural form, is a three-dimensional, highly branched, and non-crystalline macromolecule. [52,53] It is the second most abundant natural material after cellulose and comprises approximately 30% of the organic carbon in the biosphere. The inherent insolubility of lignin in water serves to maintain structural stability and facilitate the transport of water and nutrients within the plant. [52,53] Lignin is composed of aromatic and aliphatic groups, containing substituted phenylpropane rings. [52,54] These rings are linked together by different types of bonds, such as ether and carbon-carbon bonds, [52,54] and have a variety of functional groups that enable chemical and biological interactions. [52,54,55] Essentially, lignin consists of three hydroxycinnamyl alcohols: *p*-coumaryl alcohol, coniferyl alcohol, and sinapyl alcohol (**Figure 3**). [3]

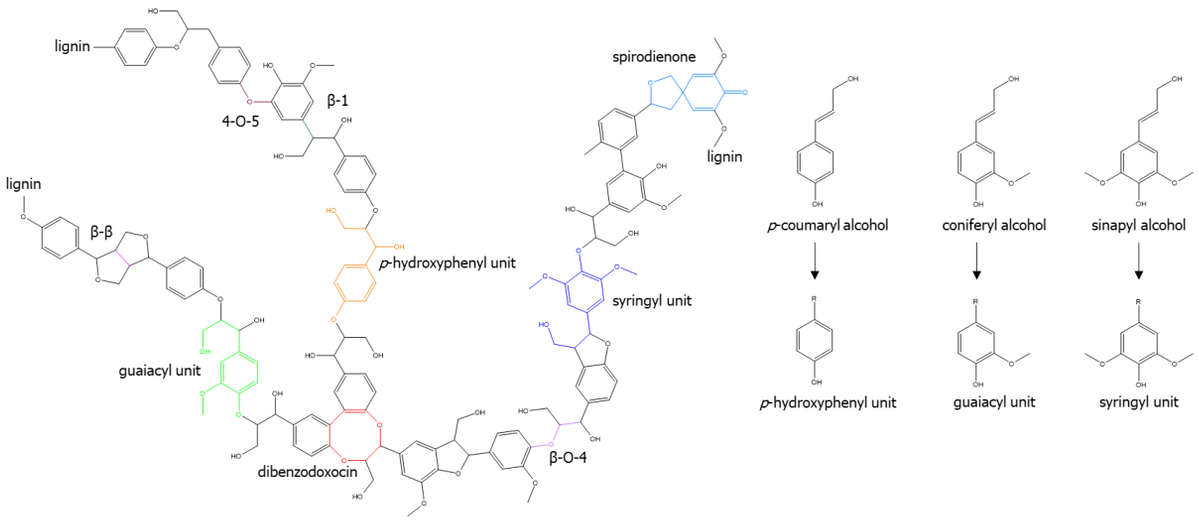

Figure 3. Example of lignin structure, based on Djakovitch *et al.* [56], highlighting the diversity of constituting units and interunit bonds and monomeric precursors of lignin.

The precise composition of lignin varies depending on the specific plant species, and it is also influenced by the extraction method employed. [52,57,58] In contrast to cellulose or hemicellulose, lignin is not a "regular polymer". Its structural formation is initiated by enzymatically mediated phenolic coupling reactions, wherein free radicals serve as initiators for chain polymerization (**Figure 4**). [54,59] The random reaction mechanisms that underpin this process give rise to a substantial variety of lignin macromolecules, which complicates the precise description of its structure. [3] Consequently, it is implausible that two lignin molecules are identical. [3]

2.8 Lignin

Conventionally, lignin has been regarded as a low-value waste product. In the current context, the utilization of lignin holds considerable potential in reducing our reliance on fossil fuels, thereby facilitating a more expeditious transition to a sustainable, bio-based economy due to its abundance, structural complexity, and chemical versatility. Its aromatic and aliphatic structures, rich in phenylpropane units, provide a valuable source to produce aromatic chemicals and advanced materials that are difficult to obtain from other renewable resources. In addition, lignin's properties, such as water insolubility and resistance to biodegradation, make it an excellent candidate for applications that require durability and stability. [3]

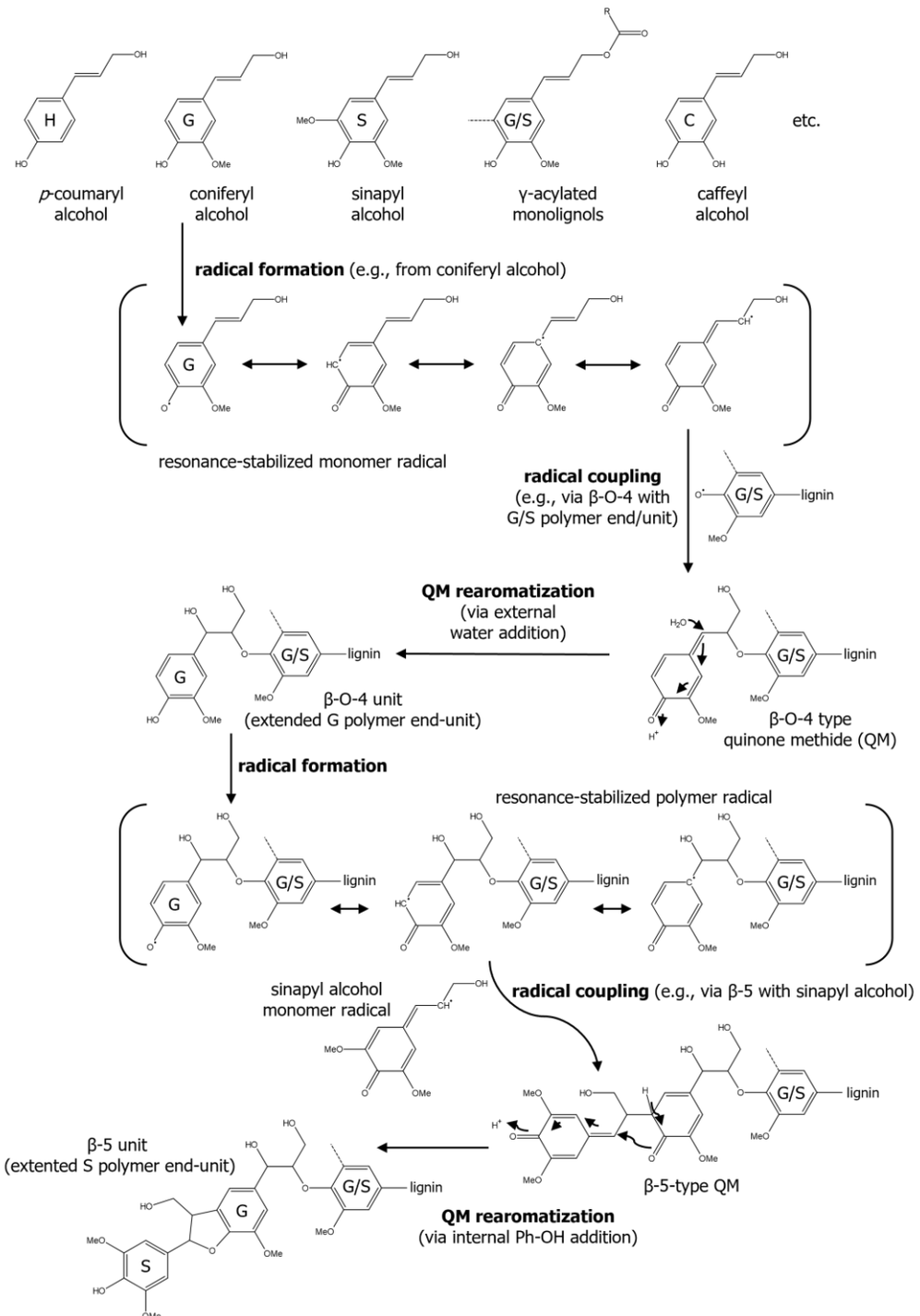

Figure 4. Monolignols and their polymerization, based on Tobimatsu and Schuetz [59]. The polymerization of lignin is predominantly facilitated by the "end-wise" polymerization process, wherein an oxidized monolignol radical undergoes a cross-coupling reaction with a radical that is formed on the free-phenolic termini of a growing lignin polymer. As a demonstration, sequential polymer chain extension reactions *via* β-O-4 and β-5 radical coupling reactions with coniferyl and sinapyl alcohols are shown.

The utilization of lignin offers a promising solution to the pressing infrastructure challenges associated with biomass. Lignin is a by-product of the paper and ethanol manufacturing processes, and the required infrastructure is already established. The pulp and paper industry produces approximately 70 million tons [60,61] of lignin per year, with

only a negligible percentage (<2%) [4] being utilized for high-value applications. It is estimated that annual lignin production will increase by 225 million tons by 2030. [62] This estimate is based on the fact that the Renewable Fuel Standard (RFS) program has mandated the production of 60 billion gallons of biofuel. [62] This amount of biofuel will require 0.75 billion tons of biomass, resulting in 0.225 billion tons of a lignin-rich by-products. [62] Consequently, there is a pressing need to develop cost-effective valorization technologies to ensure the long-term stability and vitality of biorefineries.

Lignins can be categorized into two distinct classes: those that contain sulfur and those that do not (**Table 3**). The production of lignin that contains sulfur occurs predominantly within the paper and pulp industry. This type of lignin contains inorganic sulfur, which is introduced during the extraction process, resulting in a distinctive odor and limiting its applications. Lignin, extracted by boiling wood chips in sodium hydroxide and sodium sulfide, is known as Kraft lignin. It contains 0.5-3.0% ash and 3.0-7.0% sulfur. LignoBoost® technology facilitates the extraction of Kraft lignin from black liquor on an industrial scale. In contrast, lignosulfonate, extracted using sulfur dioxide and bases such as calcium, sodium, magnesium, or ammonium bases, exhibits a higher sulfur content of 3.5-8.0% and an ash content of 4.0-8.0% compared to Kraft lignin. [63] Lignin persists as an insoluble residual product during the enzymatic hydrolysis process, a method designed to disintegrate cellulose. However, this process concurrently generates 7.0-8.0% carbohydrates, which remain inseparable, even by repeated treatment methods. [62]

Sulfur-free lignin is regarded as the more versatile and environmentally friendly alternative to the sulfur-containing variant. Organosolv lignin is extracted using organic solvents such as ethanol or acetic acid and has low ash content (~1.75%). It is insoluble in water but soluble in organic solvents. [63] The Soda boiling of plants such as straw, flax, or hardwood produces the so-called Soda lignin, which has a higher ash content of 0.7–2.3%. [63] Furthermore, sulfur-free lignin can also be obtained as a by-product from biorefineries during the hydrolytic pre-treatment of biomass. [64]

Table 3. Overview about different types of lignin.

Lignin Type	Sulfur Content (%)	Ash Content (%)
Kraft	3.0-7.0	0.5-3.0
Lignosulfonate	3.5-8.0	4.0-8.0
Organosolv	0	~1.75
Soda	0	0.7-2.3
Biorefinery	0	N/A

2.9 Applications of lignin

Currently, lignin is predominantly utilized as a fuel, burned to generate of heat and electricity, with an average calorific value of approximately 25 MJ/kg. [62] Coal, by comparison, has an energy density of 24-30 MJ/kg. [62] Research has demonstrated that the co-firing of lignin with coal can enhance the efficiency of boilers by 38% [65] and curtail carbon emissions by 60% [66]. The market value of the released heat ranges from 6 to 10 USD/BTU (from 0.00569 USD/J to 0.00948 USD/J). [62] While energy generation remains the primary use of lignin, its unique chemical structure presents opportunities for higher-value applications beyond combustion.

2.9.1 Direct technical applications

A notable approach involves the gasification of lignin. [62] Through pyrolysis, varying thermal treatment conditions can yield a diverse range of products from a single lignin source. Utilizing elevated temperatures, extended residence times, and reduced heating rates can optimize the gas yield. [67] The gasification process yields a mixture of hydrogen (H_2), carbon monoxide (CO), and a trace amount of CO_2. The resulting synthesis gas can be used in numerous processes, including the production of methanol, dimethyl ether (DME), and in the Fischer-Tropsch synthesis for *green* diesel. [62] Additionally, synthesis gas can be utilized for heating, cooking, and electricity generation. [62] Water-soluble lignin salts have been employed as binders in water-based pigment printing compositions. [62] Inexpensive binders made from lignosulfonates can also be used for coal briquettes or ceramics, briquetting of mineral dust (fine dust, chips) and wood-like materials such as plywood or chipboard. [68] Lignin can also be utilized as an economical and efficient additive for cement. [69,70] The addition of lignin in small amounts has been demonstrated to enhance the performance of concrete by increasing strength, facilitating grinding, and reducing damage to exterior walls from moisture and acid rain. [62]

2.9.2 Examples of formulations without chemical modification of lignin

Lignin has been found to enhance the biodegradation of polyolefins, such as polypropylene (PP) and polyethylene (PE), through its incorporation into these materials. Adding 30% lignin powder has been shown to modify the mechanical properties of these polymers, [68] protecting them from photochemical oxidation and enhancing their durability. Lignin-based thermoplastic copolyesters can be synthesized by polymerizing Kraft lignin with sebacoyl chloride, resulting in materials that are more environmentally friendly and thermally stable up to 200 °C. [71] The Fraunhofer Institute has developed ARBOFORM, a bioplastic made from sulfur-free lignin, plant fibers, and natural additives such as wax. [68]

This material is waterproof, moldable like conventional plastic, and highly recyclable. The final product exhibits a resemblance to polished wood or matte plastic and is suitable for various applications, including toys and household items. [68]

2.9.3 Examples of formulations with chemical modification of lignin

Epoxy resins are a class of well-established and well-known polymers. [72] The production of most resins involves the use of epichlorohydrin as the primary raw material for polymerization, which subsequently reacts with other molecules, such as bisphenol A, to form linear polymers. Adding modified lignin can enhance cross-linking, thereby improving the properties of the final product. This modification, which aims to improve reactivity, is achieved by reacting lignosulphonate with phenol and sulfuric acid. The newly formed phenolic units can be integrated into the lignin matrix and partially hydrolyze the lignin, enabling polymerization along with epichlorohydrin and bisphenol A. [73,74] Another possibility is the modification of phenol-formaldehyde resins by partially replacing the phenol with lignin. The utilization of such resins as adhesives for plywood has already been demonstrated. [75] However, for this application, it is essential to modify the lignin beforehand by introducing additional reaction sites for formaldehyde. Two approaches are currently under consideration for this purpose. [68] The initial approach entails the reaction with phenol to augment the number of phenolic units, while the secondary approach involves the enhancement of free hydroxyl groups, such as through treatment with molten pyridinium chloride. [68]

2.9.4 High-value products though lignin depolymerization

Lignin boasts a multitude of technical applications, but its intricate and heterogeneous structure imposes limitations on its utilization for high-quality products. To capitalize on the full potential of lignin as a sustainable raw material source for the production of fine chemicals and value-added products, depolymerization emerges as a rational approach. Depolymerization effectively dismantles the intricate lignin structure, yielding smaller, reactive aromatic and aliphatic compounds. These monomers and oligomers, by virtue of their enhanced reactivity, possess a considerably higher market value and can serve as precursors for a range of chemicals, materials, and biofuels. [76–85]

2.10 Methods for depolymerization

To facilitate the efficient conversion of lignin into high-quality compounds, a variety of depolymerization methods can be employed, each of which has distinct advantages and challenges. These methods can be broadly categorized into three distinct classes: biocatalytic, chemocatalytic, and electrochemical techniques. The primary distinguishing

factors among these categories are energy consumption, reaction conditions, and the nature of the catalysts utilized.

2.10.1 Biocatalytic methods

Before biomass can be depolymerized into high-quality products, it must first undergo pretreatment to make cellulose, hemicelluloses, and lignin more accessible. [3] One method of disrupting the cell wall components is biological treatment using microorganisms. [3] This approach is distinguished by its low energy consumption, its independence from chemicals, and its alignment with the principles of *Green Chemistry*, as it does not yield harmful by-products and is conducted under mild conditions. [86] However, it is important to acknowledge that this method also has significant drawbacks: Biological pre-treatments require extended incubation times and exhibit reduced efficiency compared to thermochemical processes, necessitating further optimization to compete with alternative methods. [87] Microorganisms such as bacteria and fungi play a pivotal role in biological pretreatment by employing ligninolytic enzyme systems to degrade lignin, thereby enhancing biomass accessibility. These enzyme systems encompass laccases and peroxidases, which either directly oxidize lignin or utilize mediators to penetrate the cell wall and attack its structure. [88] In addition to enhanced enzymatic digestibility, biological processes offer the possibility of utilizing lignin derivatives, by-products produced during treatment, as platform chemicals. [89] However, the variability in the properties of the starting material, the formation of inhibitors during degradation, and the need for process optimization can impose limitations on efficiency. [90] Furthermore, the high recalcitrance of biomass constitutes a substantial challenge, as plants have evolved barriers that impede the penetration of microorganisms. [91]

2.10.2 Chemocatalytic methods

Chemical depolymerization of lignocellulose has demonstrated high selectivity and effective reaction control. In contrast to biological depolymerization, this method enables the targeted cleavage of the complex structures of lignocellulose into valuable products such as biofuels and aromatic chemicals. [3,92] The depolymerization process is typically carried out at elevated temperatures and pressures, using either homogeneous or heterogeneous catalysts. [93] Homogeneous depolymerization is well established and relatively easy to control. [92,93] Liquid catalysts such as caustic Soda, ammonia, or acids (*e.g.*, HCl) are used. [94,95] Hydrolysis with HBr can lead to the production of phenolic resins with improved properties. [96] However, these processes often require elevated pressures and temperatures, and the utilization of substantial amounts of catalysts generates

considerable amounts of waste, which curtails the sustainability of the processes. [97] Heterogeneous depolymerization employs solid catalysts, such as zeolites, mesoporous materials, or metal oxides. [98] This method has the advantage that it can be carried out under milder reaction conditions, which reduces the formation of undesirable by-products. [99–101] Nevertheless, the development of durable and highly active catalysts capable of withstanding employed conditions remains a significant challenge. [102]

2.10.3 Electrochemical methods

Electrochemical depolymerization of lignin represents a promising and sustainable approach that aligns with the principles of *Green Chemistry*. [6] In comparison to alternative methods, electrochemical depolymerization offers several advantages, including the ability to be carried out at ambient pressure and room temperature. This is due to the fact that the kinetic barriers are overcome by the applied electric potential rather than by thermal energy. [7] The utilization of hydrogen and oxygen as redox reagents is particularly advantageous due to their safe *in-situ* generation through electrochemistry during water splitting, eliminating the need for pressurized tanks. [8]

A notable benefit of electrochemical processes is the ease with which product and catalyst can be separated, as the electrodes can be simply removed. [8] The selectivity of the products and the reaction rate can be effectively controlled by adjusting the potential or the current density, obviating the need for catalyst or solvent modification. [8] The flexibility of the process is further enhanced by the ability to adjust parameters such as solvents, electrolytes, additives, electrode materials, and temperature to optimize the reaction yield. [9] The utilization of electrical energy instead of stoichiometric amounts of reducing or oxidizing agents offers both ecological and economic advantages. [9] Direct electrolysis does not necessitate the use of additional reagents, while indirect electrolysis only requires catalytic quantities of a mediator that is continuously regenerated. A notable advantage of paired electrolysis is the simultaneous production of an oxidation product at the anode and a reduction product at the cathode, enhancing the energy efficiency of the process. [9]

Electrochemical depolymerization can occur *via* oxidative or reductive pathways. Oxidative processes, such as electrocatalytic oxidation (ECO), are frequently utilized for lignin degradation due to their capacity to introduce carbonyl groups into the lignin chain. This hinders condensation reactions and facilitates bond cleavage. [8] Reductive approaches, exemplified by electrocatalytic hydrogenation (ECH), yield products with reduced oxygen content, a property that is advantageous when the hydrogen evolution reaction (HER) can be minimized. [8]

Despite the advantages, there are also challenges. For instance, over-oxidation in oxidative processes can result in the formation of undesirable by-products, such as CO_2. [103] Similarly, in reductive processes, competition from HER can hinder the efficiency. [104]

2.11 Sustainable potential of electrochemical lignin depolymerization

The electrochemical lignin depolymerization approach, a relatively novel technique that has garnered significant interest from the industrial sector, is poised to contribute to SDG 9 ("Industry, Innovation and Infrastructure"). Lignin aligns with the principle of preventing waste, as its utilization through the electrochemical depolymerization process is both resource-efficient and environmentally friendly. This approach fulfills Principle 2 ("Atomic Economy"). A significant benefit of lignin is its potential to serve as a German raw material, presenting a notable advantage over oil imports, which are both expensive and politically risky. The domestic utilization of lignin from the paper industry has the potential to reduce reliance on foreign sources, thereby contributing to the realization of SDG 10 ("Reduce Inequalities"). This method aligns with SDG 12 ("Responsible Consumption and Production") as it promotes sustainable production patterns. The utilization of lignin as a renewable raw material is in accordance with Principle 7 ("Use of Renewable Feedstocks"). Furthermore, the approach minimizes toxicity by circumventing the use of hazardous solvents, aligning with Principles 3 and 5 ("Less Hazardous Chemical Syntheses" and "Safer Solvents and Auxiliaries"). The utilization of lignin has the potential to contribute to a reduction in the CO_2 footprint and greenhouse gas emissions over time, thereby aligning with SDG 13 ("Climate Action"). The use of catalysts in electrochemical reactions has been shown to enhance efficiency and reduce energy consumption, aligning with Principle 9 ("Catalysis"). The development of environmentally friendly, lignin-based products and the avoidance of harmful chemicals reduces the impact on marine ecosystems and protects biodiversity on land, which corresponds to SDG 14 ("Life below Water") and SDG 15 ("Life on Land"). Finally, the utilization of lignin also contributes to SDG 17 ("Partnerships for the Goals"). Achieving the SDGs and implementing *Green Chemistry* necessitates close collaboration among research institutions, industry, and international partners.

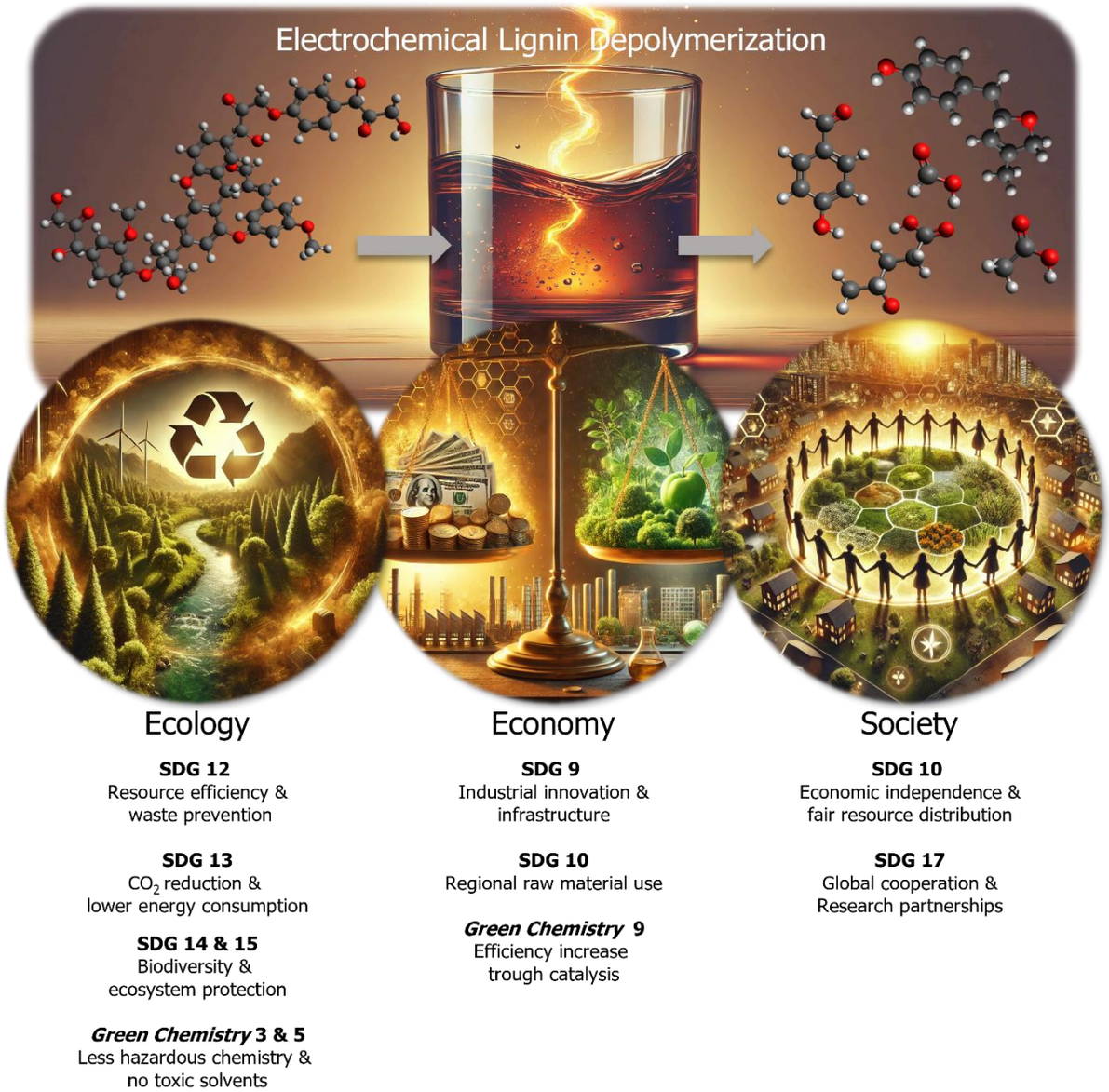

Figure 5. Classification of electrochemical lignin depolymerization in the context of Sustainable Development Goals (SDG) and the principles of *Green Chemistry*, with a comprehensive justification.

2.12 Analytical techniques for catalyst characterization

Catalysts are pivotal components of *Green Chemistry*, playing a substantial role in enhancing resource efficiency, reducing energy consumption, and preventing waste. The use of catalysts aligns directly with the SDGs, particularly Goals 12 ("Responsible Production and Consumption") and 13 ("Climate Action"). Therefore, precise characterization of catalysts facilitates the development of more efficient and durable materials. This approach aligns with the fundamental principles of sustainable chemistry, particularly the promotion of catalysis (Principle 9) and the avoidance of waste (Principle 1 and 2). Analytical techniques facilitate a deep comprehension of the structural and

chemical properties of catalysts. This in-depth knowledge is indispensable for the optimization of their efficiency. The employment of sophisticated characterization techniques is instrumental in fostering the development of more sustainable chemical processes, including the assessment of catalyst reusability.

2.12.1 X-ray diffraction

X-ray diffraction (XRD) is a widely used technique for analyzing crystalline materials. It is used to determine crystal structures, identify and quantify phases, and determine lattice constants. Furthermore, the use of this technique facilitates the investigation of textures, internal stresses, grain and particle sizes. [105] The distinct diffraction patterns produced by each crystalline phase serve as a "fingerprint" for unambiguous material identification. The principle of XRD was discovered in 1912 by Max von Laue and the physicists Friedrich and Knipping and is based on the interference of X-rays at the crystal's lattice planes. In a XRD diffractometer, a monochromatic X-ray beam is directed with precision onto the specimen. The radiation reflected and scattered by the crystallites is then recorded by the detector. According to Bragg's equation, constructive interference occurs if the angle of incidence, denoted by the symbol θ, and the grid plane distance, denoted by the symbol d, of the sample fulfill certain conditions (**Figure 6**).

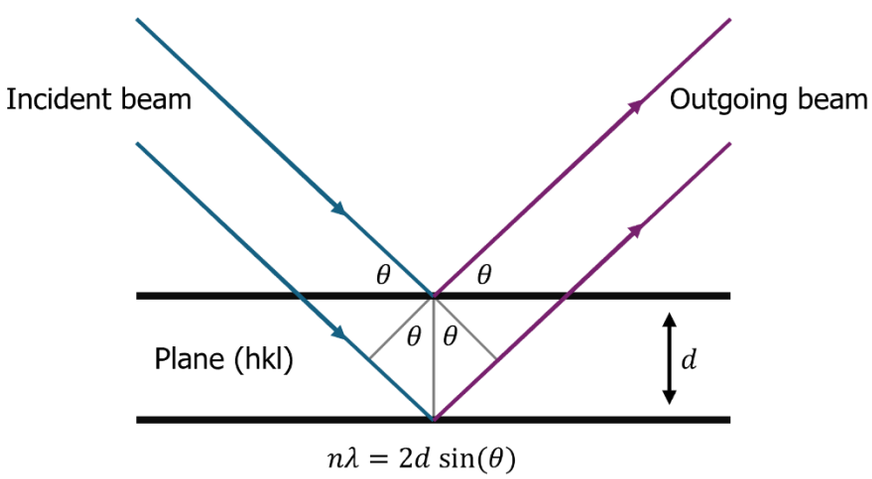

Figure 6. Graphical representation of the Bragg equation.

By measuring the reflection angle (typically 2θ), the lattice plane spacing can be calculated, thereby enabling the determination of the crystallographic structure of the material. These measurements are typically performed in Bragg-Brentano geometry, where the sample is positioned in a specific focusing configuration to obtain optimal diffraction signals. [105] The spatial resolution, which is contingent on the optics employed, can reach a maximum of 30 µm. In addition to the analysis of crystalline materials, XRD facilitates the estimation of the amorphous portion of a given sample. The detection limit

for crystalline phases is approximately 1% by volume. [105] However, it should be noted that reflection overlays can have a deleterious effect on the accuracy of the analysis. A potential interference factor is the fluorescence excitation by the primary radiation, which leads to increased background noise in the case of iron in combination with a copper anode, for example. [105] Sample preparation is a relatively straightforward process. However, the presence of interfering cover or processing layers can compromise the accuracy of the analysis. The instrumentation encompasses a range of detector types, including classic proportional counter tubes and scintillation counters (0D), modern area detectors (2D), and energy-dispersive detectors. [105]

2.12.2 Scanning electron microscopy

Scanning Electron Microscopy (SEM) is a highly versatile technique that allows for high-resolution imaging and analysis of samples at the micro- and nanometer scale. [105] Beyond mere imaging, analytical SEM, in conjunction with supplementary systems such as EDX (energy dispersive X-ray spectroscopy), facilitates the determination of chemical composition and crystal orientation. The process entails the direction of a finely focused electron beam (less than 1 nm) onto the sample surface at voltages of up to 30 kV, which in turn generates secondary electrons (SE) and backscattered electrons (BSE). [105] The resulting interactions offer insights into the topography, material composition, and atomic number contrasts of the specimen. The electron beam is guided with sub-nanometer precision over the sample surface by scanning coils, while a detector captures the reflected signal and generates a high-resolution image. It is crucial to note that a vacuum is necessary for the measurements to avoid interference from air molecules. SEM, when utilized with field emission cathodes, can achieve a resolution of up to 0.6 nm and can produce micrographs with a magnification range of 100 to 500000 times. [105] The method of sample preparation is contingent upon the material's composition. Metallic and conductive samples can be examined directly, while insulating materials must be coated with a conductive layer of carbon or precious metals (vapor deposition or sputtering), such as Au and Pt, before analysis. [105]

2.12.3 Transmission electron microscopy

Transmission electron microscopy (TEM) is a powerful technique for examining materials at the atomic level. It facilitates high-resolution imaging of structures, analysis of crystal orientations, defects, and chemical bonding ratios, as well as determination of elemental composition using electron energy loss spectroscopy (EELS) and EDX. [105] TEM operates at acceleration voltages ranging from 80 to 400 kV, with specialized instruments reaching up

to 3 MV. [105] This ensures high stability for precise imaging and analysis. The underlying principle of TEM is based on the irradiation of ultra-thin samples with high-energy electrons. Due to their short de Broglie wavelength, these electrons achieve a resolution far below atomic distance. The resulting image contrasts are attributable to disparities in material density, crystal structure, and diffraction effects. In addition to classical imaging, the STEM (Scanning Transmission Electron Microscope) mode facilitates the use of a grid pattern to direct the electron beam over the specimen, thereby enabling detailed chemical and structural analysis with nanometer resolution. [105] With a resolution as high as 50 pm, TEM is regarded as one of the most precise imaging techniques for material analysis. [105]

High-angle annular dark-field scanning transmission electron microscopy (HAADF-STEM) is a powerful technique for the observation of catalyst morphologies and the investigation of catalyst properties at the atomic level. When high-energy electrons are accelerated toward the catalyst surface, they interact with the atoms in various ways. Elastically scattered electrons are distributed over wide angles, while inelastically scattered electrons pass through the sample at smaller angles. By collecting only the elastically scattered electrons at wide angles, HAADF-STEM produces dark-field images, where brighter spots correspond to atoms with higher atomic numbers. [106]

It is vital to obtain deeper insights into the mechanisms of chemical reactions when characterizing more complex catalysts, such as nanoparticles or SACs. *In-situ* or *in-operando* techniques are indispensable tools for this purpose. The aberration-corrected TEM is a powerful instrument for nano-material characterization with sensitivity to detect single-atoms. [107] The environmental TEM (ETEM) facilitates *in-situ* characterization of the structural evolution of SACs under gaseous and operational conditions, representing a prevalent, efficacious approach for visualizing the dynamic state of atoms in real space and time. [108]

Gai and Boyes initially reported the *in-situ* TEM for direct probing of gas-solid reactions at elevated temperatures (2000 °C). [109] This pioneering work laid the foundation for *in-situ* studies of SACs dynamics. Subsequent studies have utilized *in-situ* TEM to demonstrate the migration of single platinum atoms from particles on a carbon support under reduction and oxidation environments. [110] Liu *et al.* have provided further confirmation of the dynamic and reversible transformation of single platinum atoms, clusters, and nanoparticles under redox conditions. [111]

2.12.4 Energy dispersive X-ray spectroscopy

Energy-dispersive X-ray spectroscopy (EDX) is a widely used method for the analysis of elements in solids at the micro- and nanometer scale. This analytical technique facilitates both qualitative and quantitative analyses. Furthermore, the chemical compositions of materials can be elucidated through the use of element distribution images (mapping). [105] The method utilizes the characteristic X-ray radiation that is produced when a high-energy electron beam strikes a sample. This process involves the removal of electrons from energy levels near the nucleus, causing higher electrons to migrate in and emit the excess energy as X-ray quanta. A semiconductor detector is employed to detect this element-typical X-ray radiation, which is subsequently converted into electrical pulses for analysis. The intensity of the detected X-ray signals is then used to quantitatively determine the elements present. [105] The EDX spectrometer offers a spatial resolution of less than 1 µm in a SEM and less than 2 nm in a TEM. The energy resolution of the EDX is approximately 120-130 eV. The method's utility extends to the detection of all elements from atomic number $Z > 10$, though it is not applicable to the analysis of chemical compounds. The detection limit is approximately 0.1%, with light elements presenting a greater analytical challenge. [105] To ensure precise quantification, the specimen must be homogeneous and flat, with an analyzed area of at least 3 µm in the SEM and at least 3 nm in the TEM. A notable challenge associated with EDX is the inherent low selectivity of neighboring X-ray lines, particularly for elements with comparable energy levels. Despite the utilization of mathematical deconvolution methods, this limitation can impede the precision of quantitative analysis. [105]

The identification of single atoms can be facilitated by a combination of EDX for elemental composition analysis and HAADF-STEM for high-resolution imaging. EDX mapping reveals the spatial distribution of elements, while HAADF-STEM confirms the presence of isolated single atomic sites. [106]

2.12.5 Electron energy loss spectroscopy

Electron energy loss spectroscopy (EELS) is a high-precision method for determining the local chemical composition of materials in the nanometer range. [105] The process is based on the interaction of high-energy electrons (10-100 keV) with a thin sample (< 100 nm). During this process, a portion of the electrons undergo inelastic scattering, thereby releasing energy. This process enables the extraction of information regarding the chemical composition, stoichiometry, energy levels and electronic structure of the material under investigation. [105,112,113] The energy losses can be attributed to various processes, including ionization, interband transitions, and plasmon excitations. The energy losses generate

element-specific edges in the EELS spectrum, enabling the identification of chemical elements and the analysis of their fine structure. A distinction is made between the near-edge region (ELNES), which provides information about oxidation states and electronic states, and the far-edge EXELFS region, which allows conclusions to be drawn about bond lengths and structural properties. The method exhibits a high degree of sensitivity to light elements, transition metals, and rare earth elements, while the detection of hydrogen, helium, and certain heavier elements (Rh-Bi) can present more challenges. The energy resolution, while approximately 0.5 eV, can be enhanced to 0.15 eV using monochromators. The analysis is rapid, with an estimated time of 10 seconds per measurement point. [105]

The energy loss of a single-atom state is distinct from that of other chemical states, thereby enabling the identification of a single-atom. [106]

2.12.6 X-ray absorption spectroscopy

X-ray absorption spectroscopy (XAS) is comprised of two methods: EXAFS (Extended X-ray Absorption Fine Structure) and XANES (X-ray Absorption Near Edge Structure). [105] These methods enable detailed investigations of the chemical environment of a specific element in solid, liquid, and gaseous samples. Specifically, EXAFS offers insights into the structural characteristics of the immediate environment surrounding an absorber atom, encompassing the distance, type, and number of neighboring atoms. In contrast, XANES facilitates a more precise analysis of the chemical state and electronic structure of an element. [105] This capability is instrumental in determining oxidation states and investigating unoccupied electron states. The underlying physical principle is based on the absorption of X-rays at energies specific to the element under investigation. In the context of XANES, the absorption of photons by a sample is only possible if their energy is sufficient to release an electron from the atom. This process results in the emission of a photoelectron, which in turn creates an absorption edge in the resulting spectrum. The interaction of the photoelectron with the surrounding atomic structure leads to periodic fluctuations in the absorption coefficient, known as EXAFS. [105] These oscillations are attributed to interference effects between the outgoing electron wave and neighboring atoms, facilitating the extraction of detailed information regarding the local structure of the absorber atom. [105] The region immediately adjacent to the absorption edge, which extends up to approximately 30 eV above the edge, is referred to as XANES. This region exhibits a higher signal intensity compared to EXAFS, attributable to its enhanced interactions with the surrounding environment. XANES is predominantly employed for the analysis of oxidation states and chemical bonds. [105] A salient benefit of X-ray absorption spectroscopy is its independence from the crystallinity of a specimen, thereby enabling its

application in the analysis of amorphous materials, liquids, and gases. The method allows for measurements in various spatial resolutions, ranging from large-volume bulk samples to micro investigations in the μm^3 range. While EXAFS typically operates within the energy range from 30 eV to approximately 2000 eV above the absorption edge and necessitates prior information regarding the sample (*e.g.*, molecular formula or structural model). A notable advantage of XANES is its relatively straightforward sample preparation. [105] For solid samples, a common procedure involves processing them into pellets, while for liquid and gas samples, specialized cells with thin windows are employed for examination. For *in-situ* experiments, closed sample cells with suitable materials, such as Kapton, are employed. Ensuring uniform sample homogeneity and optimal sample thickness is paramount to ensure reliable measurement outcomes. Due to the stringent requirements for EXAFS and XANES analysis, these methods are predominantly performed at synchrotron radiation sources, given the necessity for precise X-ray energy calibration. The experimental setup is relatively straightforward, but it requires a stable and tunable X-ray monochromator, as well as suitable detectors such as ionization chambers or energy-dispersive semiconductor detectors (HPGe, SDD, PIPS). [105]

XAS has the potential to offer the most compelling evidence for the existence of single atoms. [106] A pronounced discrepancy has been identified in the XANES characteristics exhibited by metal single-atom sites, metal foils, and metal nanoparticles. The absence of the peak attributed to the metal-metal bond within the r-space spectrum of the single-atom catalyst serves as a salient corroboration of the singly dispersed state of the metal atoms. [106,114] XAS can be utilized *in-situ* to ascertain the structure of SACs under realistic reaction conditions. [115–119] For instance, Wei *et al.* employed *in-situ* XAS to monitor the evolution of catalytic active sites in Co SACs during the alkaline hydrogen evolution reaction. [116] Their study revealed that the unsaturated singly dispersed Co sites undergo structural and valence state changes in the reaction environment. Upon the adsorption of hydroxyl groups, the Co sites transform into an HO–Co_1–N_2 moiety, which subsequently evolves into H_2O–(HO–Co_1–N_2) through the adsorption of water molecules. [116]

2.12.7 X-ray photoelectron spectroscopy

X-ray photoelectron spectroscopy (XPS) is an analytical method that is used to investigate the composition and electronic state of the elements on the surface. [120,121] It enables the determination of oxidation states, chemical bonds, and electronic structures at interfaces and surfaces. Furthermore, the band structure can be determined, and layer thicknesses can be analyzed by determining the absorption length using angle-resolved XPS (AR-XPS). [105] The underlying physical principle of XPS is rooted in the external photoelectric

effect, which was initially observed by Heinrich Hertz and subsequently elucidated through theoretical frameworks by Albert Einstein. The experimental setup involves irradiating a specimen with monochromatic X-rays, whose energy exceeds the work function of the material under investigation. This process leads to the emission of electrons from occupied energy levels into the vacuum. These photoelectrons, originating from regions near the specimen's surface, are detected by a spectrometer, which operates on an energy-dispersive basis. The excitation radiation typically originates from magnesium Kα (1253.6 eV) or aluminum Kα (1486.6 eV) sources, though synchrotron radiation can also be employed for higher energy ranges. The kinetic energy of the emitted electrons is measured, and the binding energy relative to the Fermi level is calculated, taking into account the excitation energy. [105] As the work function of the sample material is irrelevant, conclusions can be drawn about the chemical environment of the atoms. The information depth of XPS ranges from 0.5 to 5 nm and is contingent upon the excitation energy and the detection angle. It is necessary to maintain an ultra-high vacuum environment (at least 10^{-7} Pa) to circumvent surface contamination. XPS possesses the capability to analyze nearly all elements, with a detection limit ranging from approximately 0.1 to 1 atomic percent (element-dependent). However, hydrogen and helium exhibit indirect detectability due to their diminutive cross-section. The lateral resolution of these devices is contingent upon the measurement mode employed, with options including multipoint, small area, and line scan analysis. This flexibility enables resolutions ranging from 10 µm to 1 mm, depending on the specific device utilized. [105]

The provision of suitable reactants and reaction temperatures to the XPS chamber enables the enhancement of XPS to ambient pressure XPS (AP-XPS). This modification facilitates the characterization of catalysts within the reaction atmosphere. [122–124] It has been demonstrated that singly dispersed atoms exhibit elevated levels of unsaturation and interact with support, resulting in a distinct structure and electronic state for the single atoms when compared to their metal or metal oxide counterparts. The application of AP-XPS has emerged as a valuable tool for the study of the properties exhibited by singly dispersed sites, given the established presence of single atoms on the surface of catalysts. [123–125]

2.12.8 Low energy ion scattering

Low energy ion scattering (LEIS) is a method of ion beam spectroscopy that is used to analyze surface and deep structures with high atomic resolution. [105] It enables the determination of the chemical composition of surface layers of almost all elements as well as the investigation of ultra-thin multilayers. Furthermore, it offers the possibility of

analyzing element depth distributions with high precision, for example in implantation profiles. A notable advantage of LEIS over other analysis techniques, such as XPS, is its capacity for standard-free quantitative analysis without the influence of matrix effects. [105] The analysis is conducted by subjecting the sample, maintained in a vacuum, to ion beams. LEIS utilizes low-energy ions, such as He^+, Ne^+, or Ar^+ with energies ranging from 1 to 10 keV, which undergo elastic scattering on the atoms of the uppermost monolayer. By measuring the energy and the scattering angle of the reflected ions, conclusions can be drawn about the mass of the scattered atoms and thus about the composition of the sample. Additionally, the surface structure can be determined from the angular dependence of the backscattered intensity. [105]

The discussed techniques are summarized in **Table 4** and highlight the diverse range of information that can be obtained through different characterization methods.

Table 4. Different techniques for catalyst characterization.

Techniques	Information obtained	Merits and limitations
XAS	Valence state; electronic structure; coordination number	Atomic level sensitivity; *in-situ* recognition of adsorption process; it is sensitive to chemical groups, local structures and spatial coordination; the test time is short and the damage to the sample is small; complex data processing
HAADF-STEM	Atomic distribution state; morphology structure	Atomic level sensitivity; *in-situ* recognition of adsorption process; thick and low contrast specimens can be observed; micro diffraction can be realized; imaging is limited to selected areas
EDX	Element type analysis	Atomic level sensitivity; *in-situ* recognition of adsorption process; used with HAADF-STEM; low energy resolution
EELS	Element and chemical state analysis	Atomic level sensitivity; *in-situ* recognition of adsorption process; high electronic structure sensitivity; insensitive to high number atoms
XPS	Element analysis; chemical state	Atomic level resolution; it can detect detailed electronic structure and geometric information; *in-situ* detection process; the information is not persuasive
SEM	Morphology; surface topology	High spatial resolution; provides detailed images of surface structures; suitable for a wide range of materials; limited chemical information
LEIS	Surface composition analysis	Extreme surface sensitivity (top atomic layers); provides quantitative elemental depth profiling; limited penetration depth; requires ultra-high vacuum conditions

Abstract:

Replacing fossil resources as the primary source of carbon-based chemicals by alternative feedstocks, while implementing more sustainable production routes, has become imperative for environmental and resource sustainability. In this context, lignin, often treated as a biomass waste, emerges as an appealing candidate, considering the principles of circular economy. For this pursuit, depolymerization methods offer potential strategies to harness lignin to produce valuable organic chemicals, while electrocatalysis processes stand out especially in the context of sustainability, as they can be powered by electricity from renewable sources. This minireview article explores the pivotal role of various electrocatalysts in lignin depolymerization, investigating both oxidative and reductive pathways. Emphasizing recent advancements, the review delves into the diverse nature of electrocatalysts and their influence on lignin valorization. Highlighting current trends, the discussion encompasses the catalytic mechanisms and selectivity of electrochemical processes employed for lignin breakdown. Additionally, we also offer some insights into emerging technologies, emphasizing the need for sustainable and efficient strategies. By providing an overview of the field, this minireview aims to guide future research endeavors toward innovative electrocatalytic approaches for lignin depolymerization, paving the way for sustainable biorefinery processes.

Chapter 3

Revisiting the Electrocatalyst Role on Lignin Depolymerization

Based on:

Lucie M. Lindenbeck, Vanessa C. Barra, Björn B. Beele, Bruno V. M. Rodrigues, and Adam Slabon

Advanced Energy and Sustainability Research, **2024**, *5* (10), 2400130.

DOI: 10.1002/aesr.202400130

Biomass valorization · Depolymerization · Electrocatalysis · Lignin

Chapter 3 - Revisiting the electrocatalyst role on lignin depolymerization

3.1 Introduction

Phenomena in nature can reveal parallels between human actions and decisions in a remarkable way. In their search for food, processionary moths move in a row one behind the other. [126] If the first caterpillar happens to meet the last caterpillar or is placed behind it, this leads to a circular arrangement of these caterpillars. From then on, they would wander endlessly in a circle. Metaphorically, this scenario can also be found in the history of human use of oil.

In the 19th century, mankind began to use crude oil as a central resource for the chemical industry. German chemist Justus von Liebig set the first milestone in this direction when he extracted benzene from a tar product. When the British chemist Sir James Young then developed various processes for distilling petroleum and extracting useful chemical products, such as kerosene wax and kerosene, petrochemistry became increasingly central. [127] However, rather than continuing to search for sustainable alternatives, society as a whole has followed this path, resulting in an endless cycle of consuming finite resources. Dependence on oil has led to environmental and social challenges and has created a cycle that urgently needs to be broken. Analogous to nature, where breaking the caterpillar cycle frees it from its endless cycle, innovative ideas and scientific approaches have been always welcome to steer the chemical industry toward a more sustainable path.

The availability of fossil fuels, such as oil, gas, and coal, is limited. However, nature produces 170 billion tons of renewable raw materials every year through photosynthesis, including plants, trees, flowers, fruits, cereals, grasses, and vegetables. [2] Renewable raw materials can be used as both chemical raw materials and food, and their use as food should be prioritized because of the increasing world population. Renewable raw materials are thus defined as follows: “Renewable raw materials are any organic materials that grow back and are thus available repeatedly. They are produced by agriculture or forestry and are predominantly used in the non-food sector. They can be used for both materials and energy.” [2] Within the biomass, cellulose and lignin are particularly noteworthy. Together, these two components constitute approximately 69% of all biomass, as they are the main components of plant walls. [2]

Lignin is a structurally complex biomacromolecule found in the cell walls of plants that holds immense potential as a renewable resource for the chemical industry. [128–130] While being responsible for providing the framework of plants, lignin also provides vessels for water and prevents microbial infections. This complex plant polyphenol consists mostly of the three phenylpropane units p-hydroxyphenyl (H), guaiacyl (G), and syringyl (S) (see **Figure 7**). [131,132] Due to its irregularly branching structure and multiple bonds between monomers, lignin has a high level of structural diversity and complexity. The heterogeneity aspect presents considerable problems in depolymerization processes because it is aimed at reducing lignin into its basic monomeric or oligomeric units that can be applied as substrates for biofuels, chemicals and materials production. Because of the robust C-C and C-O bonds available in it, efficient depolymerization becomes difficult due to this recalcitrance that arises from intricate construction. Thus, knowledge about these characteristic structural units of lignin and the challenges they pose to depolymerization is essential to devise appropriate approaches necessary for optimization of this large renewable resource. [100,133]

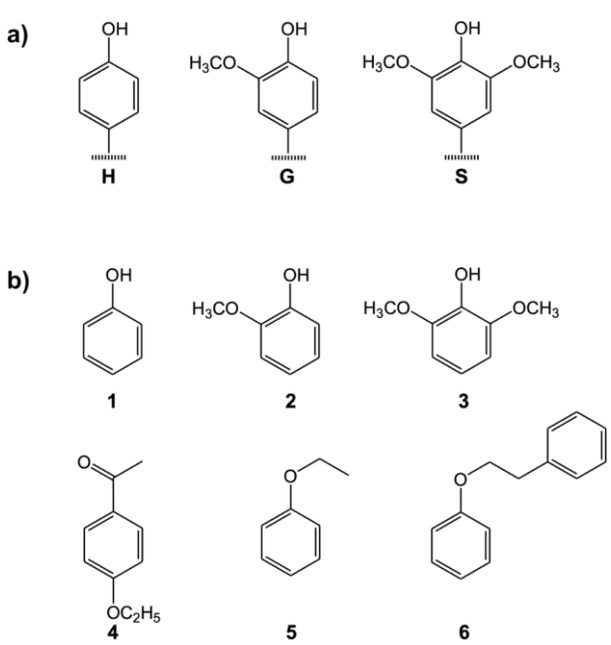

Figure 7. (a) Three typical substructures found in lignin: p-hydroxyphenyl (H), guaiacyl (G), and syringyl (S). (b) Some selected and widely used lignin model compounds phenol (1), guaiacol (2), syringol (3), p-ethoxy-acetophenone (4), phenetole (5), 2-phenoxy-1-phenylethane (6).

The structural units of lignin differ significantly in their reactivity and ease of depolymerization due to their distinct chemical compositions and bonding patterns. Guaiacyl and syringyl units, derived from coniferyl and sinapyl alcohols respectively, are the most common in hardwood lignins, whereas softwood lignins are primarily composed of guaiacyl units. [131,132,134] The presence of methoxy groups in guaiacyl and syringyl units

enhances their electron density, influencing the types of linkages formed and their susceptibility to cleavage. Guaiacyl units tend to form more recalcitrant carbon-carbon (C-C) bonds, which are harder to break compared to the ether bonds (C-O) commonly found in syringyl units. Consequently, syringyl-rich lignins generally undergo more efficient depolymerization than guaiacyl-rich lignins. The simpler structure of *p*-hydroxyphenyl units, predominant in grasses and some softwoods, further influences depolymerization dynamics. [131,132,134] Understanding these structural differences is crucial for tailoring depolymerization strategies, [135] optimizing catalyst selection, and improving the overall efficiency of lignin valorization processes.

In the quest for sustainable solutions, electrocatalysis emerges as a promising avenue for lignin valorization. [8,136] Electrochemical methods offer precise control over reaction parameters, enabling selective bond cleavage and product formation. Moreover, the tunability of electrocatalysts presents a versatile platform for tailored lignin transformations, ranging from depolymerization to value-added product synthesis. [8,136] In this context, scientists are on the brink of transforming how we use lignin, by tapping into the potential of electrochemistry. This breakthrough could lead to a major shift toward *greener* chemistry practices and more sustainable ways of using our natural resources.

The electrochemical depolymerization of lignin stands at the forefront of sustainable biomass utilization, holding significant promise to produce high-value chemicals and fuels. [8,136] As the most abundant aromatic macromolecule in nature, lignin presents a vast resource for renewable feedstock; however, its complex and recalcitrant structure poses a formidable challenge for efficient conversion processes. In this scenario, catalysts emerge as pivotal agents, wielding the power to orchestrate intricate chemical transformations and unlock the latent potential of lignin. The choice of catalyst in electrochemical depolymerization represents a critical determinant of process efficiency, selectivity, and product yield. Catalysts play multifaceted roles, acting as facilitators of electron transfer, mediators of chemical reactions, and regulators of reaction pathways. They serve to mitigate kinetic barriers, promote desired bond cleavage, and suppress unwanted side reactions, thereby steering the transformation of lignin towards targeted molecular products.

The nature of catalysts employed in electrochemical depolymerization spans a diverse spectrum, ranging from metal-based nanoparticles to organic ligands and complex molecular complexes. Each catalyst type offers distinct advantages and functionalities, tailored to address specific challenges inherent to lignin depolymerization. Metal catalysts, such as transition metals and their oxides, exhibit redox activity crucial for electron

transfer processes, while organic catalysts provide molecular recognition and substrate specificity, enabling selective bond cleavage. Furthermore, the design and engineering of catalysts extend beyond mere catalytic activity, encompassing considerations of stability, reusability, and compatibility with electrochemical systems. Catalyst immobilization strategies, electrode surface modifications, and synergistic catalyst combinations further enhance the performance and robustness of electrochemical depolymerization processes.

In this minireview, we revisit the electrocatalyst's role in lignin depolymerization, exploring recent advancements, challenges, and prospects. By delving into the intricate interplay between catalyst design, reaction mechanisms, and process optimization, we aim to elucidate the key principles driving electrochemical lignin valorization. Through a comprehensive analysis of current literature and emerging trends, we endeavor to provide insights that inspire innovation and propel the chemical industry towards a *greener*, more sustainable future.

3.2 Catalytic electrochemical lignin depolymerization mechanisms

Electrochemical lignin depolymerization is a process that involves electrochemical reactions to break down the complex structure of lignin *via* oxidative or reductive pathways, *e.g.*, by dissociation of β-O-4 bonds (**Figure 8**). The transfer of electrons between the electrode and the lignin substrate at the electrode interfaces causes molecular rearrangements and bond cleavages. Dissociation of O-H or C-C bonds, for example, yields differently substituted benzoquinones, side-chain oxidations give access to phenolic aldehydes, ketones, or acids, and opening aromatic rings yields different aliphatic acids or their salts. [137,138] Oxidation reactions occur at the anode and reduction reactions at the cathode when an electrical voltage is applied, which initiates lignin degradation. In the combination of electrochemistry and lignin chemistry, there are various methods for depolymerization that are determined by different mechanistic principles.

Knowledge about these reaction mechanisms can decisively optimize a successful reaction and the formation of the desired products. As C-C bonds generally have a higher dissociation energy than C=O bonds in lignin, a selective cleavage of C-C bonds consequently poses a challenge for lignin degradation. [137] Numerous research groups are tackling the task of understanding electrochemical decomplexation pathways using experimental methods like HPLC, UV/Vis-, IR- or NMR spectroscopy, mass spectrometry or theoretical studies. Due to the naturally wide and varying structure of lignin most mechanistic studies are carried out using lignin model compounds like phenol, guaiacol, syringol or differently substituted acetophenones or ethers as they are cheap, safe and easy

to handle and represent building blocks of the relevant lignin substructures. [139] Some of the most widely utilized model compounds are shown in **Figure 7**.

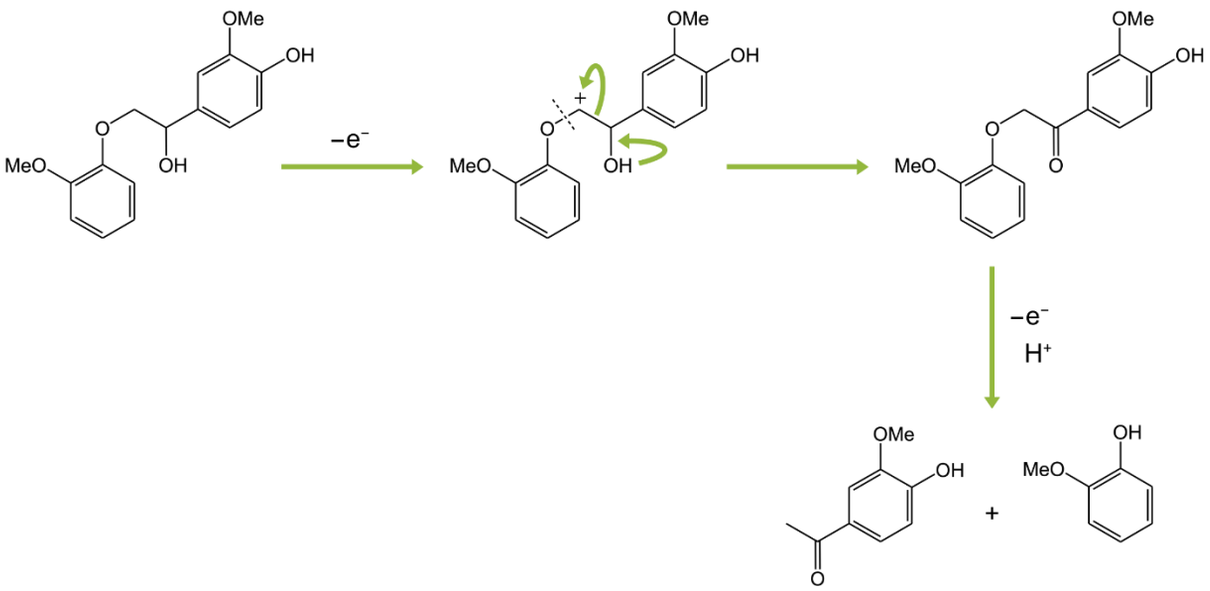

Figure 8. Dissociation of β-O-4 bonds by oxidation. [78]

3.2.1 Depolymerization using homogeneous catalysis

Homogeneous catalysis refers to a type of catalysis in which the catalyst and the reacting substances are in the same physical state. This means that the catalyst and reactants are in a solution or gaseous state and are therefore free to move. During the reaction, the catalyst interacts with the starting materials, accelerating the reaction rate and thus enabling the conversion of the starting materials into the desired products.

Main advantages of homogeneous catalysis are comparable high reaction rate as catalyst and reactants are in the same physical state and the possibility to apply mild conditions for the reaction. [140] Homogeneous catalysts based on metal complexes with Pd, Pt, Ru and Ir, for example, are generally highly selective and efficient while enable reactions under mild reaction conditions.

Electrochemical oxidations can be homogeneously catalyzed by a series of classical oxidizing agents like quinones [141,142] or chromates [143]. Most intensively studied are two stable radical molecules: 2,2,6,6-tetramethylpiperidine-N-oxyl (TEMPO) [144] and different N-hydroxyphthalimides among which phthalifmide-N-oxyl (PINO) is the most thoroughly studied [145]. TEMPO shows two redox transitions between −2 and +2 V *vs.* SCE, indicating a possibility of acting as an electrocatalyst with multiple redox states. It can furthermore be used as a catalyst precursor by generating active oxidizing species. The first TEMPO-catalyzed electrochemical oxidation of a series of alcohols, including the monomeric lignin model compound anisyl alcohol was published in 1983. [146] Using 5 mol% TEMPO as a

precursor, anisyl alcohol was converted to anisyl aldehyde in 83% yield. PINO is short-lived and is often generated in situ by an oxidation of its precursor N-hydroxyphthalimide (NHPI) in the presence of a base. Due to a high bond dissociation energy of 88 kcal/mol [147] PINO is a useful hydrogen atom transfer catalyst used for oxidations particularly for weak C-H bonds. A review by S. Stahl and co-workers summarized the benefits and limitations of N-Oxyl radical oxidizers and their use in electrochemical oxidations. [148]

In 2011 Sedai *et al.* studied the aerobic oxidation of the lignin model compound 1,2-diphenyl-2-methoxyethanol using TEMPO and Cu^{I} and V^{V} catalysts. [149] Products resulting from *β*-O-4 bond cleavage were characterized with NMR spectroscopy and different selectivities were found for the two metal catalysts. The studied vanadium catalyst produced 85% benzoic acid and 84% methyl benzoate as the major products *via* the intermediate product benzoin methyl ether. The copper catalyst yielded 84% benzaldehyde and 88% methyl benzoate without intermediate formation. Although the authors did not perform calculations, they described their findings with literature known proton-coupled electron transfer mechanism for the copper catalyzed reaction [150] and a one electron pathway for the vanadium catalyzed reaction [151]. Most research focusing on homogeneous electrochemical oxidation or reduction of lignin using peroxides, TEMPO- or PINO-mediated systems follow the reaction scheme shown in **Figure 9** (middle) in which the catalyzing agent is recovered electrochemically on an electrode surface. 2021 Yang *et al.* summarized advances in this field of electrochemical lignin oxidation in a detailed review article. [145] Recently Li *et al.* used a recoverable polyoxometalate catalyst to convert different *β*-O-4 lignin model compounds into aromatic acids and phenols under mild homogeneous conditions. [152] At 1 bar oxygen pressure and 130 °C the catalyst achieved yields of 96% for benzoic acid and 80% for phenol in 12 h. Due to its property as ionic liquid the catalyst can easily be recovered by precipitation with ethyl acetate and subsequently reused. In a widely studied and discussed oxidation mechanism first an oxidation occurs in *α*-position to an ether oxygen atom. Afterwards a C-O bond dissociation yields smaller carbonyl- and alcohol products. This oxidation can be initialized by the above mentioned radical compounds, small oxidizing compounds or metal complexes. Further mechanisms like depolymerization *via* pyrolysis, microwave-assisted depolymerizations or reactions using bacteria or fungi are described in a recently published and well-organized review article [153] and an article also dealing with utilization of products from different types of lignin [78].

3.2.2 Depolymerization using heterogenous catalysis

Intensive research efforts are being made developing heterogeneous catalysts, as in such catalytic systems, the catalyst and product are easier to separate. [154] Heterogeneous oxidation catalysts have already played a substantial role in paper industry for removing lignin and other compounds from wood pulp. [134]

Three main pathways for heterogeneous electrochemical depolymerization are discussed in literature. [155] These three pathways are: 1) an electron transfer from lignin directly to the electrode surface (see **Figure 9**, left); 2) Electrolysis of a small molecule on the anode surface. Subsequently this molecule serves as redox partner by conversing the lignin substrate while being regenerated on the metal surface (see **Figure 9**, middle); 3) The catalytic cycle and the electron transfer step from 2) are interlinked by another catalytic active species (often noted as an enzymatic catalytic cycle, see **Figure 9**, right).

The direct electron transfer at the electrode surface is the most common approach for the electrochemical conversion of lignin. This process is limited by the surface area of the anode material. As in this mechanism a direct electron abstraction from lignin is involved, offering a good electrolyte for the reaction and sufficient solubility of lignin are dominating challenges. [156]

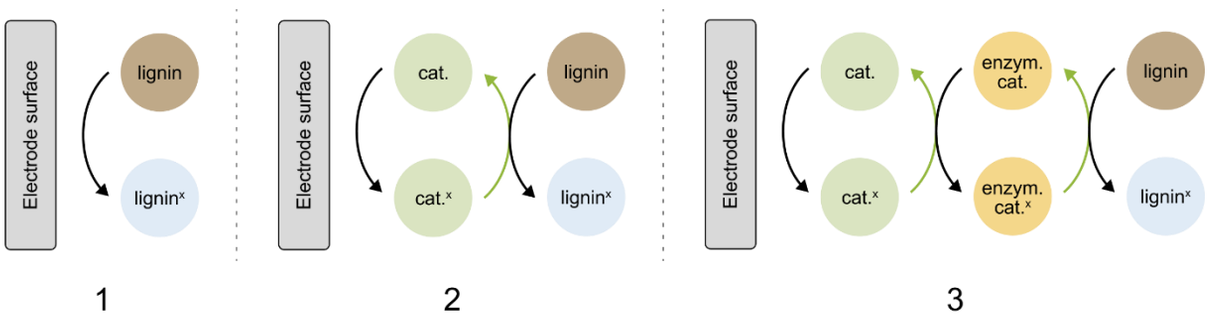

Figure 9. Possibilities for electron transfer during an electrochemical reaction.

Electrocatalytic hydrogenation (ECH) and deoxygenation occur at the cathode in the reductive pathway. The first step ((1) and (2)) is the chemisorption of hydrogen at the electrode surface. This is followed by the substrate reaction ((3) to (5)), as shown in **Figure 10A**. [8] In competition with these reactions, the hydrogen evolution reaction (HER) ((7) and (8)) also occurs at the cathode. [8] However, not only double bonds but also carbonyl compounds can be hydrogenated by ECH (**Figure 10B**). [3] In the oxidative pathway, the electrocatalytic oxidation reaction (ECO) occurs at the anode, which includes the chemisorption of hydroxyl radicals ((8)), the formation of metal oxides ((9)), and the subsequent oxidation of the substrate ((10) and (11)). The oxygen evolution reaction (OER), which is described by (12) and (13), also occurs at the anode. [8]

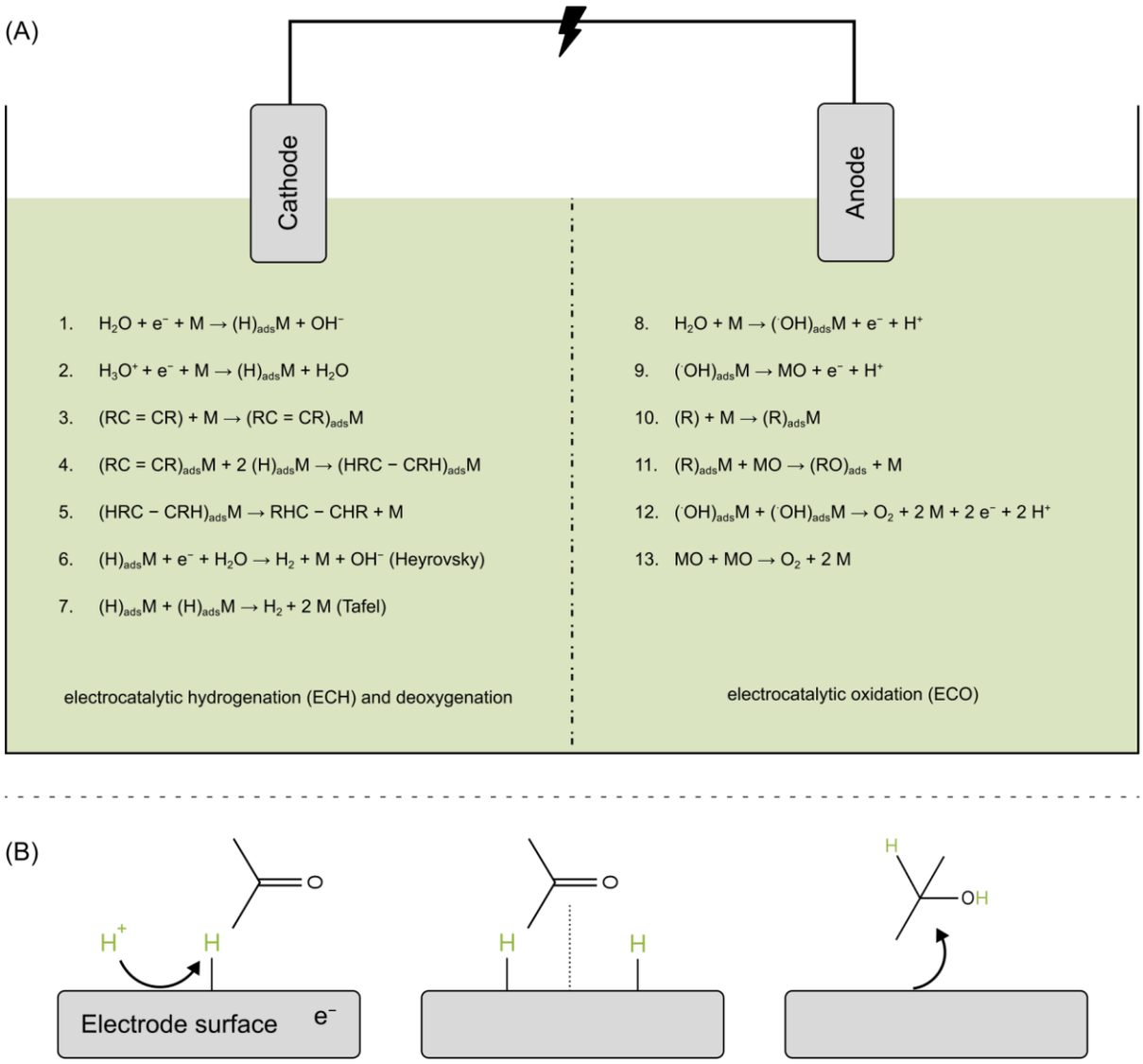

Figure 10. (A) Electrocatalytic Hydrogenation (ECH) and Deoxygenation and Electrocatalytic Oxidation (ECO). In ECH, water protons are reduced on the metal surface (M), leading to their adsorption ((H)adsM). Subsequent adsorption of the organic substrate (RC=CR) forms a metal–substrate complex ((RC=CR)adsM), followed by adjacent adsorption resulting in the hydrogenation of the organic substrate ((HRC-CRH)adsM). The desorption phase releases the hydrogenated product (HRC-CRH) and elemental hydrogen. In ECO, hydroxyl radicals from water electrolysis and organic species (R) adsorb onto the metal surface, initiating oxidation through interactions with the adsorbed organic substrate (R)ads, metal oxide (MO), and adsorbed hydroxyl radicals (·OH)adsR. Simultaneously, dioxygen is formed *via* the Oxygen Evolution Reaction (OER). (B) Process of carbonyl compound hydrogenation in the context of Electrocatalytic Hydrogenation (ECH).

Jiang *et al*. described the depolymerization of lignin by reactive oxygen species (ROS) generated through the water-oxygen reaction (WOR) at the anode and the oxygen reduction reaction (ORR) at the cathode. ·OH and H_2O_2, formed at the anode, participated in lignin degradation. The ORR pathways at the cathode also produce H_2O_2. Electrochemical oxidation using ROS from ORR can efficiently degrade lignin in aqueous electrolytes, while the use of electrochemical membrane reactors can enhance product selectivity by isolating the degradation products from the oxidizing environment. [157]

Mechanistic studies involve detailed analyses regarding the cleavage of *β*-O-4 aryl ether bonds [158] as well as C−C bonds [159,160]. Some articles focus on the investigation of the lignin decomposition and the subsequent oxidation mechanism. By studying the relationship between depolymerization rate and formation of phenol products Almada *et al.* were able to identify the deprotonation of the lignin phenolic units as a first step. Two reaction paths are possible: The first and predominant reaction path involves the degradation of the aromatic units through ring-opening reactions to form small aliphatic molecules, such as oxalic acid or acetic acid. The second reaction pathway is probably the cleavage of lignin subunits and thus leads to compounds with small molecular weight (oligomers, vanillin). [161–164] These steps are summarized schematically in mechanistic studies involve detailed analyses regarding the cleavage of *β*-O-4 aryl ether bonds as well as C-C bonds. Some articles focus on the investigation of the lignin decomposition and the subsequent oxidation mechanism. By studying the relationship between depolymerization rate and formation of phenol products Almada *et al.* were able to identify the deprotonation of the lignin phenolic units as a first step. Two reaction paths are possible: The primary and most common reaction pathway involves breaking open the aromatic ring unit to produce small aliphatic molecules like oxalic acid or acetic acid. The second reaction pathway relies on the possible cleavage of lignin subunits, leading to compounds with small molecular weight (oligomers, vanillin). These steps are summarized schematically in **Figure 11**.

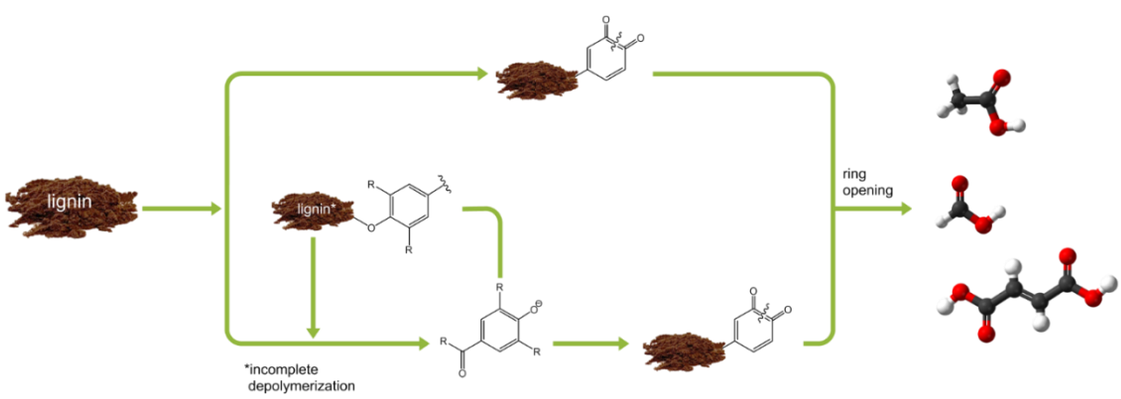

Figure 11. Lignin oxidation steps according to ref. [161].

In a thorough analysis Chen *et al.* studied the mechanism of electrochemical oxidation of non-phenolic alkyl aryl ethers and *β*-O-4 dimer model compounds both experimentally using IR- and UV/Vis spectroscopy, CV, GC-MS and theoretically by DFT calculations. [165] Reactions were performed using Pt sheet working and counter electrodes and an Ag/Ag^+ reference electrode using 0.025 mol l^{-1} substrate concentration and 2.0 V for 8 h and additionally followed oxidation reactions in situ using a Pt grid working electrode and 0.1 mol l^{-1} substrate concentration. The authors showed that the tested alkyl

aryl ethers first undergo a C_α carbonylation followed by a subsequent cascade of electron transfers and chemical transformations yielding carbonylic compounds. [160] Presence of C_α-hydroxy groups are found to be crucial for the formation of new aldehyde products and benzoic acid through a different mechanism in contrast to the C_α=O group in the β-O-4 dimer due to the electrochemical oxidation. The authors proposed a possible oxidation mechanism and plausible oxidation products arising from 2-phenoxy-1-phenethanol, 2-phenoxyacetophenone and 2-phenoxy-1-phenylethane (**Figure 12**). Breaking of C_β-O and C_α-C_β bonds in dimer molecules was attributed to delocalization of HOMOs.

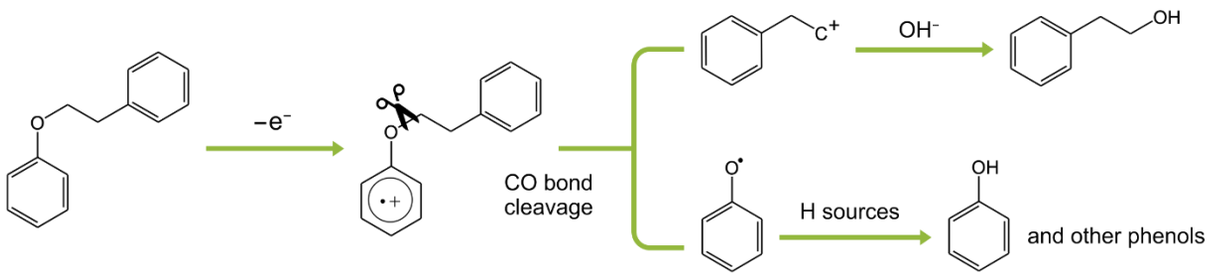

Figure 12. Possible oxidation mechanism of 2-phenoxy-1-phenylethane according to ref. [165]. Mechanisms for oxidation of β-hydroxy ethers and β-keto ethers are also given in ref. [165].

In a recent work Hasan *et al.* carried out thorough NMR-, IR- and CV investigations on combined electrooxidation and electroreduction for selective cleavage of the β-O-4 bonds in lignin using a Pt coil electrode. [166] Oxidations were carried out using a potential of +0.45 V, reductions using a potential of −0.2 V. The absorbance peaks in the ATR-FTIR spectra show that during oxidative potential, new signals stemming from the C-O aryl ethers and aldehyde due to the production of vanillin and its derivatives emerge. Using a reductive potential, signals from aromatic C-O moieties in β-O-4 linkages disappear during the experiment. Quantitative 2D HSQC NMR spectra clearly show that, using an oxidative potential, the presence of β-O-4 alkyl-aryl ethers decrease significantly and the presence of *p*-hydroxy cinnamyl alcohol end groups increase. The ratio of most aromatic structural components decreases while a reductive potential is applied, due to the dissociation of C-C bonds in the aromatic ring.

Bawareth *et al.* investigated the kinetics of lignin depolymerization using an electrochemical batch reactor. Two primary depolymerization reactions were identified: random degradation/recombination, where larger polymers are broken down into smaller units, and specific degradation, which focuses on cleaving polymer chains at specific points. The study monitored the depolymerization kinetics by observing the degradation rate of aromatic compounds, including vanillin and vanillic acid. The results showed that vanillin can undergo various reactions, leading to the formation of different aromatics or organic acids through the opening of its aromatic ring. The focus of the study was mainly on the

degradation of aromatic products into organic acids, which release carbon dioxide and water. [167]

α-O-4 bonds can easily be broken by acid *via* protonation of the O-H function and subsequent dissociation of the C-O bond yielding an alcohol and a carbocation. In non-aqueous alcohol mixtures the nature of the product is highly dependent on the temperature, solvent acidity and polarity. The acidity of the reaction media had a minor effect. [168]

Electrochemically Lin *et al.* carried out an experimental and theoretical study on electrochemical cleavage of the *α*-O-4 bond in benzyl phenyl ether as model compound for lignin. [169] The authors performed a series of Ni-catalyzed electroreductive *α*-O-4 bond cleaving experiments in methanol using divided cells for a time of 5 h and under argon atmosphere to prevent oxidation of the electrode. In this reaction argon atmosphere was found to be crucial for a good conversion. Deuterium labelling experiments and DFT calculations showed that the mechanism of the *α*-O-4 bond dissociation resembles a Pd/C catalyzed hydrogenation. The benzyl ring of the model compound approaches the catalytic surface on which an adsorbed H atom is transferred to the carbon atom in a splitting the *α*-O-4 bond.

3.3 Depolymerization electrocatalysts

3.3.1 Carbon based materials

Carbon based materials can be employed in two distinct ways: as catalyst supports, common practice in the production of fine chemicals, or directly as catalysts, [170] where they have the potential to serve as an alternative to metal catalysts due to numerous advantages, including high availability, low cost, tolerance to acidic/alkaline conditions, [171] and high electronic conductivity. [172] Carbon-based electrodes have a clear advantage in terms of sustainability. *Green Chemistry* requires the use of all harmful or rare resources in a closed material cycle, which can be achieved with biomass-based electrodes (**Figure 13**). These electrodes can be produced from biomass, which is created by the conversion of CO_2 by the sun. The sun also produces energy that can be used for the electrochemical depolymerization of lignin, where carbon electrodes are utilized. The CO_2 released during the depolymerization process can be converted back into biomass. [173]

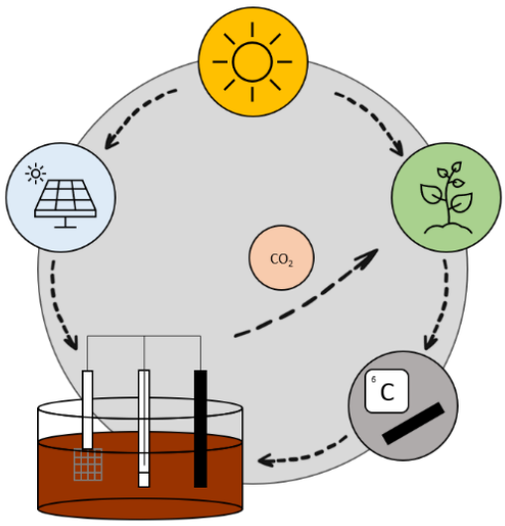

Figure 13. The closed carbon cycle is formed when the sun converts CO_2 into biomass, which can be used to produce electrodes, and generates solar energy that can be utilized for electrochemical lignin depolymerization.

Building upon the idea of a closed carbon cycle, in 2023, Park and Kim demonstrated a sustainable method for producing porous carbon electrodes using mandarin peel waste. This method aligns with the ethos of biomass-based electrode production. The process involved washing and drying the peels, followed by grinding and sieving to obtain mandarin peel powder (DMP), which was then carbonized. [174] The concept of a closed carbon cycle in which CO_2 is converted into biomass and used to produce electrodes is promising. However, questions remain about the efficiency and practicality of this cycle on a large scale. The energy costs and carbon footprint of the entire process chain (from biomass production to electrode production and CO_2 recycling) must be evaluated. Furthermore, the process may not be scalable. There is a need to investigate the availability of biomass sources and the efficiency of the conversion process. Additionally, the entire conversion process, including drying, grinding, sieving, and carbonization, requires energy and chemicals, which can affect the overall environmental balance.

Carbon materials can exist in three different allotropes: amorphous carbon, diamond, and graphite. [175,176] Graphite consists of multilayer graphene sheets with conjugated sp^2 carbon hexagons, which are held together by weak van der Waals forces. [172] Graphene nanosheets (NSs), which are composed of a single layer of graphite and carbon nanotubes (CNTs), share a common building block with conjugated alternating bonds C-C and C=C, which leads to the delocalization of π-electrons. [172,177]

Despite the diversity of carbon's molecular structures, this commonality allows for unique properties, including high specific surface area, [178] electrical conductivity, [179] thermal conductivity, [180] Young's modulus, [181] and charge mobility [179]. CNTs are formed by

rolled-up graphite sheets and can exist as either single-walled (SWCNT) or multi-walled (MWCNT) structures. [182,183] CNTs have garnered significant interest as a support material for electrocatalysts due to their exceptional mechanical and electrical properties. [184] Oh *et al.* introduced an oxidative technique for enhancing lignin depolymerization using phosphomolybdic acid as both catalyst and mediator alongside a carbon nanotube (CNT) paper as the active electrode. This strategy facilitated the generation of valuable compounds such as CO and vanillin, as well as an effective means for (photo)chemical hydrogen production, exhibiting a Faraday efficiency nearing unity under acidic pH conditions. [185] MWCNTs serve as highly conductive support materials, providing enhanced mass transport and interaction with the support for various chemical reactions, [186] including methanol oxidation [187]. Furthermore, the utilization of catalytic particles on MWNTs is often superior to that on conventional carbon black powders. [188] Bateni *et al.* investigated the use of non-precious β-PbO_2/MWNTs nanocomposites (deposited on a Pt rotating disk electrode (RDE)) for the electrochemical depolymerization of lignin. The catalyst's increased surface area and stability suggest a promising approach for efficient lignin depolymerization. GC-MS measurements detected the main oxidation products for constant potential experiments at 0.5 V *vs.* SHE under two different oxidation durations of 24 and 48 h. These products include vanillin, methyl salicylate, 1,3-bis(1,1-dimethylethyl)-benzene, and 2,4-bis(1,1-dimethylethyl)-phenol. [189] CNTs are therefore promising candidates for lignin depolymerization, but they also pose a potential risk to human health. [190] In particular, the toxic effects of CNTs on the lungs, skin, cardiovascular system, and cytotoxicity have been investigated. The different sizes of nanoparticles and impurities can influence the toxicity of CNTs. In particular, metal impurities, which are often present in the production of CNTs, are considered to be the main cause of toxic effects. [190] Pulskamp *et al.* [191] and Kagan *et al.* [192] posit that the acute toxic effects are caused by heavy metals rather than by the CNTs themselves. Conversely, there are studies that document direct pathological effects of CNTs themselves. CNTs increase the production of reactive oxygen species, which can shorten the viability of cells. [190] CNTs can also lead to inflammatory reactions and cell damage. [193,194]

Human lung cells show reduced cell viability and increased inflammatory markers when exposed to CNTs. [195,196] Contact of CNTs with the skin can lead to morphological changes and pro-inflammatory reactions. [194,197] During the handling of CNTs, they can be released in the form of aerosols, leading to skin and respiratory tract exposure. Furthermore, CNTs are difficult to degrade and can therefore accumulate in the environment and become part of the food chain. [190]

Carbon quantum dots (CQDs) are a class of carbon-based materials that can be synthesized through two basic routes: top-down and bottom-up. [198] Top-down synthesis involves breaking down larger carbon structures (such as carbon nanotubes, carbon fibers, graphite rods, carbon ash, and activated carbon) into smaller CQDs using processes like arc discharge or laser ablation. [198] The use of the top-down method results in CQDs with high crystallinity and an intact nanostructure, leading to excellent photochemical and electrochemical performance. [198] In contrast, the bottom-up process polymerizes and carbonizes small organic molecules, resulting in carbon quantum dots (CQDs) with an amorphous structure, numerous surface groups, and doping sites. [198] Citric acid, glucose, polyethylene glycol, urea, ionic liquids are common carbon sources for this. [199] CQDs have attracted significant attention in the field of electrocatalysis due to their favorable properties. These include a large surface area, high conductivity, and excellent charge transfer properties. Additionally, CQDs are rich in surface functional groups, like -OH, $-NH_2$, etc., providing numerous favorable sites for constructing highly active electrocatalysts. The strong interactions within CQDs-based composites facilitate intermolecular electron transfer. The electronic properties of CQDs can be further improved by introducing doped heteroatoms such as N, P, S, and B. [198] Despite the outstanding properties and potential for modification, and the usefulness for photocatalytic depolymerization of lignin, [200] to our knowledge, there have been no publications on the use for electrochemical lignin depolymerization.

Reticulated vitreous carbon (RVC) is a suitable electrode material due to its low density, low thermal expansion, high corrosion resistance, and high thermal and electrical conductivity. It is composed of an open-cell foam, resulting in a high pore count, large surface area, stable structure, low resistance to fluid flow, and very high temperature resistance in non-oxidizing environments. It can be used for applications requiring high current densities, low electrical/liquid resistance, minimal volume loss at electrodes and controlled pore sizes for infused materials. [201] Fang *et al.* investigated the influence of different pre-oxidized lignin samples, under otherwise identical conditions, on the selectivity and yield of products soluble in ethyl acetate. For this study, they used an H-cell separated with a Nafion membrane. The anodic cell was equipped with a platinum wire and a pH 8 phosphate buffer and the cathodic cell with an RVC electrode in a NaOH/methanol mixture. Reactions were carried out for 6 h at 20 mA. Kraft and Soda lignin showed low depolymerization rates due to their strong cross-linking, while GVL lignin showed improved depolymerization. Cu-AHP lignin gave the best results with the highest yield. Syringic acid, vanillin, *p*-OH-benzoic acid, acetosyringone and propiosyringone were identified as the main products. [202]

Lindenbeck *et al.* [138] conducted a recent study on the reductive electrochemical depolymerization of Soda lignin in aqueous medium using carbon catalysis. They employed a non-modified glassy carbon electrode. After testing various reaction times (up to 25 h) and currents (up to −200 mA), the researchers reported −175 mA and a reaction time of 20 h produced the best results for this reaction. Remarkably, these conditions not only depolymerized the lignin, but also completely dearomatized it, resulting in the selective production of short aliphatic compounds such as levulinic acid, 4-hydroxyvaleric acid, acetic acid, and formic acid. In another study, Lindenbeck *et al.* replaced the sodium carbonate-water solvent mixture with an aqueous GVL solution (with sodium carbonate as the electrolyte), while retaining the electrode configuration. They were able to show that the same products could be obtained despite the change in solvent and that the yield of the final product could be further increased by the targeted base-catalyzed ring opening of the GVL to 4-hydroxyvalerate. [203]

Carbon-based materials offer significant advantages as catalysts and catalyst supports due to their high availability, low cost, and excellent conductivity. Their use in sustainable processes, such as biomass-derived electrodes, supports *Green Chemistry* principles by enabling a closed carbon cycle. Innovations such as mandarin peel waste-derived porous carbon electrodes and the application of CNTs and CQDs enhance electrocatalysis. Nevertheless, further investigation is required to address the challenges associated with efficiency, scalability, and environmental impact, as well as the health risks associated for example with CNTs. Those seeking to employ a carbon-based electrode for lignin depolymerization may find it beneficial to examine other applications of similar electrodes, such as the production of hydrogen peroxide, in order to gain insight into the challenges encountered therein and to be able to address them directly. In the synthesis of hydrogen peroxide, the high porosity of the carbon electrodes can impede the release of H_2O_2 and thus reduce the efficiency of the process. [204] This phenomenon might also be observed in depolymerized lignin fragments. According to the literature, the electrodes are stable in acidic and basic environments. [171]

However, they are not stable against hydrogen peroxide, for example. [204] They may also not be stable against the products of depolymerization, which could affect the lifetime and consistency of the process. Therefore, further investigation into the stability of the electrodes in reactive environments is warranted. Furthermore, it has been demonstrated that the incorporation of foreign elements into the carbon electrodes can influence the electron transfer rates in both positive and negative ways. [204] To achieve the desired catalytic properties, it is necessary to implement structural adjustments, such as the introduction of defects or morphology tuning, which require precise control.

Despite these challenges, carbon-based materials offer significant potential for sustainable catalytic applications (**Table 5**).

Table 5. Summary of the parameters of current publications on the electrochemical depolymerization of lignin using carbon-based electrodes.

Electrode material	Lignin	Solvent	Oxidative/ reductive	Electro-catalytic performance	Main products	Ref.
CNT-paper	not specified	PMA	oxidative	0.95 V *vs.* RHE, 10 mA cm^{-2}	CO, vanillin	185
β-PbO_2/ MWNTs	Biorefinery	H_2O/NaOH	oxidative	0.5 V *vs.* SHE	Vanillin, methyl salicylate, 1,3-bis(1,1-dimethylethyl)-benzene, 2,4-bis(1,1-dimethylethyl)-phenol	189
RVC	Kraft	H_2O/NaOH	reductive	10 mA cm^{-2}	Vanillin	202
RVC	Soda	H_2O/NaOH	reductive	10 mA cm^{-2}	Vanillin	202
RVC	GVL	H_2O/NaOH	reductive	10 mA cm^{-2}	Syringic acid, vanillin, *p*-OH-benzoic acid, acetosyringone, propiosyringone	202
RVC	Cu-AHP	H_2O/NaOH	reductive	10 mA cm^{-2}	Syringic acid, vanillin, *p*-OH-benzoic acid, acetosyringone, propiosyringone	202
Glassy carbon	Soda	H_2O/ Na_2CO_3	reductive	−175 mA	Sodium levulinate, sodium 4-hydroxyvalerate, sodium acetate, sodium formate	138
Glassy carbon	Soda	H_2O/GVL	reductive	−18 mA cm^{-2}	Sodium levulinate, sodium 4-hydroxyvalerate, sodium acetate, sodium formate	203

3.3.2 Nickel based materials

Nickel is often used as good-conducting and catalytically active electrode material in various applications due to some unique properties of this metal. The standard potential of nickel (Ni^{2+}/Ni) (−0.236 V *vs.* SHE) [205] is significantly lower compared to noble metals like the coinage metals, platinum or palladium, but still nickel is electrochemically a very stable element. As it is much more abundant compared to many noble metals producing nickel electrode materials is consequently more cost-efficient while possessing similar properties. Furthermore, nickel is ductile allowing it to be easily shaped and formed into different electrode configurations. It is resistant to corrosion in acidic and alkaline environments. In the latter, it forms NiOOH layers which are conducting and are continuously regenerated, improving the oxidative performance of the electrode. [8] Those layers are known to be very selective for alcohol oxidation. [206] One drawback using nickel

as electrode material is that certain nickel catalysts may require high reaction temperatures to achieve optimal activity.

Besides electrodes manufactured from pure nickel metal some nickel-containing materials like NiO also have remarkable properties. NiO for example is a semiconductor with a wide band gap of 3.6–4.0 eV [207] which properties can be changed significantly in dependance of the degree of defects in the lattice. It is used in many applications such as catalyst, in fuel cells or as comparable *green* and cost-efficient super conductor. [208]

Over the last decade, many different research groups have contributed on clarifying the mechanisms behind heterogeneous, Ni-catalyzed decomplexation of lignin model compounds (see for example [209–211]). The suggested mechanism of catalytic dissociation of *β*-O-4 bonds is shown in **Figure 2**. [78] Song *et al.* indicated that nickel electrodes serve as potent catalysts for production of small phenolic compounds *via* selective dissociation of ether C-O-C bonds and subsequent hydrolyzation of carbon-hydroxyl linkers. [212] Anastas and co-workers recently added a new theoretical and experimental study on the electrochemical cleavage of the *α*-O-4 bond in benzyl phenyl ether as model compound for lignin in 2023. [169] The mechanism was found to be similar to Pd/C-catalyzed hydrogenation in which the benzylic side of the model compound first approaches the surface in the adsorption step before new chemical bonds are formed. NiOOH was proven to be the active site during electrooxidative depolymerization reactions of *β*-O-4 model compounds utilizing different metal catalysts on nickel foam. Different plausible reaction routes were considered and NiOOH showed higher catalytic activity compared to other metal oxyhydroxides. [213]

Here we focus rather on recent findings on formation of valuable compounds and building blocks from lignin using electrocatalysis than on mechanistic studies or work on model compounds. In 2021, a series of highly useful compounds like vanillin, vanillic acid, syringic acid was obtained from Soda lignin with Ni-catalyzed oxidative depolymerization and identified and quantified by UPLC-MS. [214]

Carkner *et al.* focused in a recent work on understanding the impact of a series of parameters like temperature, electric potential, lignin concentration, cell type and others on the yield of small oxidation product in electrocatalytic lignin depolymerization. [215] They found for example an order of magnitude higher impact of the reaction temperature on the formation rate of vanillin in comparison to the effect of the electric potential.

A series of valuable monoaromatic compounds (vanillin, syringaldehyde, corresponding ketones and guaiacol) were obtained from technical organosolv lignin in a combined yield of 7.8 wt% as published 2023 by Breiner *et al.*. Depolymerization products

were characterized very detailed using NMR- and IR methods. [216] The same group reported a heterocatalytic electrochemical depolymerization of lignosulfonate yielded 9.7 wt% vanillin relative to the dry mass in 5 h at elevated pressure using Ni sheet electrodes in a two-step process. [217]

Nickel offers the opportunity to be used as foam which benefits from higher surface are and consequently higher turnover numbers yielding a more effective set up for heterogenous catalysis.[218] Yan *et al.* exploited low-cost nickel foam as anode under alkaline conditions and obtained vanillin and syringaldehyde with a combined maximum yield of 17.5% by electrochemical depolymerization. [219]

In 2023, Aguillon-Rodríguez *et al.* synthesized novel Ni nano particles from $Ni(OAc)_2$ and 1,10-phenanthroline followed by pyrolysis at 600 °C for 2 h and acidic work-up. Resulting nano particles were thoroughly characterized using TEM, pXRD and EPR spectroscopy and used in hydrogenolysis of Dioxasolv lignin and Kraft lignin at 150 °C and a reaction time of 2 h. Resulting monomer products guaiacol and isoeugenol were separated by GPC and products characterized using NMR spectroscopy. [220]

In a departure from previous discussed research articles, Ouyang *et al.* [221] conducted a study in 2023 that focused on converting lignin into electricity rather than valuable chemicals. They introduced an innovative liquid flow fuel cell (LFFC) utilizing nickel foam anodes with solid metal sulfide electrocatalysts, enabling the direct conversion of lignin to electricity under mild conditions. This technology achieved a peak power density of 176 mW cm^{-2}, with the anode demonstrating high stability. The process primarily involved depolymerizing lignin by cleaving the β-O-4 aryl-ether bond and partially mineralizing it to CO_2. These findings demonstrate the LFFC's potential for efficient and sustainable biomass-based power generation. **Table 6** summarizes the parameters of current publications on the electrochemical depolymerization of lignin using nickel-based electrodes.

Table 6. Summary of the parameters of current publications on the electrochemical depolymerization of lignin using nickel-based electrodes. * extrapolated from fig. 1 in [219].

Electrode material	Lignin	Solvent	Oxidative/ reductive	Electro-catalytic performance	Main products	Ref.
Ni/NiOOH	Ligno-sulfonate	3 M NaOH	oxidative	6 mA cm^{-2}	Vanillin, acetovanillone	[217]
Ni	Organosolv	H_2O/ KOH	oxidative	7.5 mA*	Acetovanillone, syringaldehyde, acetylsyringone, others	[215]
Ni/NiOOH	Different organosolv lignins	3 M NaOH	oxidative	15 mA cm^{-2}	Vanillin, acetovanillone, syringaldehyde, acetylsyringone guaiacol, other aromatic monomers	[216]
Ni nano-particles	Kraft, Dioxasolv	H_2O/ EtOH	reductive	n/a	Guaiacol, isoeugenol	[220]
Ni/NiOOH	Soda	1.0 M NaOH	oxidative	2 mA cm^{-2}	Vanillin, acetovanillone, syringaldehyde,sinapic acid	[214]

3.3.3 Lead based materials

Similar to nickel, lead is a soft and malleable metal that usually can be handled easily and that shows high chemical stability in aggressive media or when used with high overpotentials. [222] Prices for lead materials are usually significantly lower compared to nickel and noble metals making it the more cost-efficient material for oxidation electrode production. The use of lead as electrode material, however, is for some applications discouraged due to the potential health risks covering effects on the hematopoietic, renal, reproductive, and central nervous system. [223] In addition to health issues, the use of Pb/PbO_2 electrodes was first inhibited by corrosion or catalyst deactivation caused by the leaching of Pb^{2+} ions. [224] Research efforts focusing on the production of stable PbO_2 layers has alleviated this disadvantage and thus Pb/PbO_2 anodes are used in numerous applications such as the field of wastewater treatment. Wang *et al.* see in their review article great potential for PbO_2-based catalysts (especially modern nano materials or lead containing alloys) in future for environmental applications like. PbO_2-based sensors or ozone generation. [225]

Pb/PbO_2 electrodes have been widely used as anode materials for oxidative lignin depolymerization. [189,222] The first Pb-catalyzed oxidation of lignin were already carried out in 1946, where Bailey *et al.* obtained a series of ketones and acids from lignin using a Pb electrode in sodium hydroxide and a substantial current density of 2 A/dm^2. [226] Pan *et al.* used PbO_2 nanoparticles supported on TiO_2 nanotubes for the electrooxidative depolymerization of Kraft lignin. The nanotubes were used to obtain a higher PbO_2 loading per area and hence, a higher catalytic efficiency. The prepared electrode produced vanillin

and vanillic acid from Kraft lignin. These products were identified by IR and HPLC. Yields were not given in this work. [227]

By C-C bond oxidation using a Pb/PbO_2 catalyst, Wang *et al.* obtained 4-methylanisole from lignin in 1 mol/L NaOH solution. [228] Electrodes were thoroughly analyzed using XRD and SEM. In this work, the authors showed that C-C bonds are first broken by •OH radicals oxidation, and then hydrogenated by H atoms. Using optimized conditions (lignin content: 40 g/L, current density: 50 mA/cm^2, temperature 50 °C), a cumulative yield of 4-methylanisole reached 343.3 g/kg lignin at a reaction time of 8 h.

Lan *et al.* presented an oxidative depolymerization of cornstalk lignin in alkaline solution using a Pb/PbO_2 anode. Different valuable small hydrocarbons, like toluene and xylenes, were detected and identified using HPLC and GC-MS methods. Optimized reaction conditions for the production of aromatic hydrocarbons were stablished at a concentration of 40 g lignin/L NaOH (1 mol/L), a current density 30 mA/cm^2, and a reaction time of 10 h at 30 °C. [229] Pb/PbO_2 anodes were able to generate different lignin-derived products, such as vanillin (5.83 g/kg lignin) and syringaldehyde (9.30 g/kg lignin), *via* electrocatalyzed oxidation of bamboo-derived lignin when used with Cu cathodes in 1 M NaOH solution. [230]

One interesting approach is using radicals stemming from allyl halides, a Pb/PbO_2 anode, and a Cu cathode to produce allyl-substituted aromatic molecules from lignin. [231] Overviewing the development of Pb/PbO_2 catalysts with time it is anticipated that using lead-based materials in heterogeneous catalysis will develop from pure Pb/PbO_2 electrodes more in direction of intermetallic nanoparticles or alloy materials that are fine-taylored for the desired application. Due to the non-negligible health concerns, we note that in the current literature mainly carbon and platinum electrodes are used in the electrocatalytic conversion of lignin. With increasing interest in the above mentioned newly designed nano and alloy materials this is anticipated to change in future. **Figure 14** illustrates the electrocatalytic oxidation products obtained recently using Pb/PbO_2 catalysts.

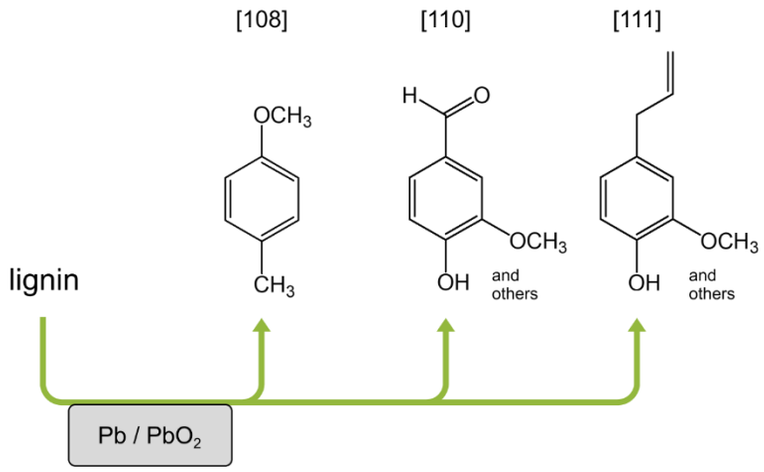

Figure 14. Electrocatalytic oxidation products realized recently using Pb/PbO_2 catalysts. *[108] = [228]; [110] = [230]; [111] = [231]

3.3.4 Platinum based materials

Platinum is a precious and ductile metal that is often used as an electrocatalyst due to its resistance to oxidizing agents and stability in various acids and bases. [232] Additionally, platinum is biocompatible. [233] However, its high cost is a significant drawback compared to other commonly used electrode materials, like nickel and copper. In addition to being used as an electrocatalyst, Pt has been commonly used as a counter electrode in electrochemical depolymerization. [234]

M. Hasan *et al.* presented a method for selectively cleaving the β-O-4 linkage of dealkaline lignin through combined electrocatalytic oxidation and reduction. The reaction was conducted in tetrahydrofuran with the addition of sulfuric acid to promote hydrolysis of the interlink bonds. A standard Ag/AgCl electrode could not be used in this set up. This standard reference electrode may develop a liquid junction potential at the junction between the background solution and the reference electrode solution. Therefore, a pseudo-Ag^+ reference electrode was used. Quantitative calculations from NMR-spectroscopy revealed that the presence of aromatic components of the lignin polymer increased by 28.67% during the controlled holding of the oxidative potential while aliphatic structural components decreased by 32.73%. Similarly, during controlled reductive potentials the presence of aromatic structural compounds decreased by 33.50%, and aliphatic structural compounds decreased by 78.43%. [166]

In 2021, Di Fidio *et al.* investigated the effects of various reaction parameters on the oxidative depolymerization of Soda technical lignin Protobindt 1000 (P1000). For that purpose, the authors tested different electrocatalysts, including platinum, nickel oxide hydroxide, and graphite. The results showed that the platinum electrode had the lowest current density at the maximum oxidative potential value compared to the other electrode

materials. The best reaction conditions among those tested were NiOOH, pH 14, 20 g lignin, and 0.4 V. [214]

As already mentioned, the high price is one of the negative aspects of using platinum as an electrode material. One way to reduce costs is to use platinum not only in its pure form, but also in combination with other materials. In a recent study, Xiao *et al.* utilized Pt@CeO_2 as an electrocatalyst for the oxidation of lignin. CeO_2-based materials are well suited catalysts for electrocatalytic reactions due to their exceptional electrochemical redox performance and high resistance to corrosion in alkaline media. [235] They loaded a small amount of Pt nanoparticles on CeO_2 and employed industrial alkali lignin as a substrate. Their results demonstrated that Pt@CeO_2 effectively cleaved C(OH)-C bonds. The experiment resulted in the production of G-type and S-type phenolic structures, along with other aldehydes and carboxylic acid derivatives. Additionally, benzoic acid was obtained at low currents using PPE as a lignin model compound. [236] Electrocatalytic reactions have not been only investigated for lignin, but also for model compounds. [236–239]

Although platinum is occasionally utilized as a working electrode in various studies, it is more commonly employed as a counter electrode for the electrochemical depolymerization of lignin. This preference is primarily attributed to its inertness to oxidation. [240] A significant limitation of using platinum as an electrocatalyst is its high cost. Platinum can be combined with other materials to mitigate these expenses, potentially enhancing its performance while reducing overall costs.

Table 7 summarizes the parameters of current publications on the electrochemical depolymerization of lignin using platinum-based electrodes.

Table 7. Summary of the parameters of current publications on the electrochemical depolymerization of lignin using platinum-based electrodes.

Electrode material	Lignin	Solvent	Oxidative/ reductive	Electrocatalytic performance	Main products	Ref.
Pt coil	Dealkaline	Tetrahydro-furan	both	CV from −0.7 V to +1.0 V *vs.* pseudo $Ag\|Ag^+$	Aromatic and aliphatic compounds	[166]
Pt wire	Soda Protobindt 1000 (P1000)	H_2O/NaOH	Oxidative	CV from −1.0 V to +0.8 V *vs.* Ag/AgCl	n/a	[214]
Pt@CeO_2	Alkali	H_2O/HCl	Oxidative	35 mA	G-type, S-type phenolic compounds, other aldehydes	[236]

3.3.5 Copper based materials

Copper is a soft metal with high ductility and malleability. Compared to precious metals like platinum, silver, and gold, copper exhibits lower activity towards HER. [241] It is also cheaper and widely accessible.

Da Cruz *et al.* reported on the reductive electrochemical depolymerization of Kraft lignin in a 5.17 M aqueous solution of levulinic acid using copper foil as an electrocatalyst. The reaction was carried out for 20 h at −1.7 V *vs*. Ag/AgCl. The resulting compounds were predominantly composed of aryl ether and phenol groups, including 4-ethylguaiacol, paracoumaryl alcohol, and apocynin. [104]

In a previous article from 2022, Da Cruz *et al.* demonstrated the reductive cleavage of 2-phenoxyacetophenone, a lignin model compound with utilization of copper foil as an electrocatalyst. They used a deep eutectic solvent composed of choline chloride and ethylene glycol in a 1:2 molar ratio. Two types of cells were employed: an undivided cell and a membrane cell. In both setups, the electrochemical reaction was carried out at −1.7 V *vs*. Ag/AgCl for 20 h. The choice of reactor influenced the products obtained. The membrane cell products contain a higher amount of carbonyl groups, whereas the open cell products have a higher concentration of hydroxyl groups. [242]

Klein *et al.* investigated the degradation of lignosulfonates to different aldehydes using various electrocatalysts, including a copper-silver compound. [217] In particular, the yields of vanillin and acetovanillone obtained were analyzed. In the case of the copper-silver electrode, a vanillin yield of 1.9 wt% and an acetovanillone yield of 0.6 wt% was obtained.

In a recently published article, Dourado *et al.* compared thermo- and electrochemical catalysis to valorize lignin using CuO catalysts. In the case of electrocatalysis, a glassy carbon disk was coated with CuO. They showed a similar oxidative behavior of lignin on CuO catalysts between thermo- and electrocatalysis. Under mild oxidative conditions, more aldehydes were obtained with both methods. Mainly monophenolic aldehydes and ketones were identified by GC-FID. [243]

In 2023, Han *et al.* used various catalysts for lignin oxidation, including a copper catalyst. They identified various aromatic compounds such as vanillin, vanillic acid. In the case of vanillin and vanillic acid, it was found that Ni, Ag, Al and Cu resulted in a higher or similar yield of these components compared to carbon paper. [244] **Table 8** summarizes the parameters of current publications on the electrochemical depolymerization of lignin using copper-based electrodes.

Table 8. Summary of the parameters of current publications on the electrochemical depolymerization of lignin using copper-based electrodes.

Electrode material	Lignin	Solvent	Oxidative/ reductive	Electro-catalytic performance	Main products	Ref.
Copper foil	Kraft	H_2O/ levulinic acid	Reductive	−1.7 V *vs.* Ag/AgCl 4.5−9 mA/cm^2	Monomers and dimers with mainly ether and phenol groups	104
Copper foil	2-phenoxyaceto-phenone	1:2 choline chloride/ ethylene glycol	Reductive	−1.7 V *vs.* Ag/AgCl	Aliphatic compounds, monomers and dimers with mainly ether and phenol groups	242
Cuprosilver (Ag 62.5% Cu 37.5%)	Ligno-sulfonate	H_2O/NaOH	Oxidative	12.5 mA/cm^2	Vanillin, acetovanillone	217
Glassy carbon disk coated with CuO	Pepper	H_2O/NaOH	Oxidative	Various	Monophenolic aldehydes/ ketones	243
Carbon Paper coated with copper	Kraft	H_2O/KOH	Oxidative	−1.0 V *vs.* Ag/AgCl	Vanillin, vanillic acid and other aromatic monomers	244

3.4 Future and outlook

In the pursuit of a *greener* and more sustainable future, electrocatalytic lignin depolymerization may play a pivotal role in the transition to bio-based chemical production. However, for this to become a reality, it is essential to critically examine the concept of "sustainable" biomass conversion. While biomass offers numerous advantages, its disadvantages must not be overlooked. The most important advantage of biomass over fossil fuels is that biomass is always available because it is constantly being regenerated. The logistics involved in harvesting and transporting biomass present unique challenges compared to fossil raw materials. Unlike crude oil and natural gas, which can be extracted and transported through pipelines, biomass requires harvesting from widespread areas and transportation *via* trucks, trains, or ships. However, the energy required for this process often comes from non-renewable sources rather than renewable ones.

Transitioning all transportation modes to renewable energy sources like solar power is imperative to enhance the sustainability of biomass logistics. Nevertheless, implementing this transition on a large scale presents significant challenges, such as the need for extensive infrastructure upgrades. Highways and rail systems, for instance, are not optimized for handling the volumes required to replace pipelines.

One promising solution lies in repurposing biomass waste. By repurposing waste biomass, we can circumvent additional logistical hurdles associated with harvesting and

transportation. As discussed in our review, lignin is a plentiful biomass waste currently primarily burned for energy generation. However, a more sustainable approach would involve converting lignin into valuable products rather than incinerating it. This shift represents a significant step towards sustainability, but addressing several key factors is necessary. Enhancing the selectivity and yield of lignin depolymerization processes is essential to maximize resource utilization and minimize waste. This requires further advancements in electrode materials, particularly in terms of conductivity and stability, to enhance the efficiency of these reactions. Additionally, it is urgent to explore and advance catalyst systems. While we reviewed the latest advances on carbon, nickel, lead, platinum, and copper-based electrodes, there is a clear gap when it comes to exploring other metal-based systems for lignin depolymerization, such as silver-based and gold-based electrodes, for example.

Gold has an excellent conductivity, stability, and catalytic properties, while its surface can be readily modified to optimize its catalytic activity for specific reactions, thanks to its propensity for forming diverse surface structures and binding configurations with reactants. Its high conductivity allows efficient electron transfer, facilitating redox reactions with exceptional precision. [245–247] However, despite all these remarkable features, apart from studies involving lignin model compounds, there are only a few works published in the literature addressing gold and gold-based electrodes for the electrochemical depolymerization of lignin. A good example is the investigation reported by Song *et al.*, [248] which focused on a novel heterogeneous catalyst system for the aerobic oxidation and depolymerization of lignin, focusing on the β-aryl ether fragment. This system utilized gold nanoparticles (Au) supported on a basic Li–Al LDH30 under atmospheric pressure with molecular oxygen. Notably, the Au/Li–Al LDH catalyst exhibits high oxidation activity across various lignin model compounds. Through oxidation experiments targeting the β-O-4 linkage dimers, the catalyst effectively cleaves the linkage after selective benzylic alcohol oxidation, yielding ester moieties amenable to depolymerization *via* hydrolysis. NMR analysis of oxidized Kraft lignin and guaiacol lignin confirms the formation of esters, evidenced by the disappearance of benzylic alcohol groups. Subsequent hydrolysis of the oxidized lignin samples yields significant aromatic monomer yields, with guaiacol lignin producing 40 wt% monomers and Kraft lignin yielding 10 wt%.

The use of bifunctional catalysts may also become a promising avenue of research in the future, as they have the potential to enhance the efficiency and economy of chemical processes by enabling multiple reactions simultaneously. In 2023, Qi *et al.* [249] described the development of a phosphorus-doped $CoMoO_4$ (P-$CoMoO_4$) electrocatalyst that functions in a bifunctional manner, enabling the oxidative cleavage of lignin and the reduction of

furfural simultaneously. The catalyst exhibited high efficiency, with a lignin conversion of 99% and a monomer selectivity of 56%. Additionally, it demonstrated a reduction selectivity for 2-furaldehyde of 73%. [249]

Similarly, Du *et al.* [250] described 2017 an electrochemical method for the cleavage of lignin and the simultaneous production of hydrogen using proton-exchange membrane electrolysis. Lignin served as the hydrogen source at the anode, where polyoxometalates (POM) or $FeCl_3$ were employed as catalysts and charge transfer agents. This method achieved over 90% Faraday efficiency and reduced energy consumption by up to 40% compared to conventional water electrolysis. In addition to the production of hydrogen, the depolymerization of lignin into valuable aromatic chemicals was also observed. [250]

Another innovative approach that could potentially guide future developments in electrochemical lignin depolymerization is the integration of photocatalysis, electrocatalysis, and biocatalysis for the efficient conversion of lignin, as described by Ko *et al.* in 2019. The system employed a TiO_2 photocatalyst, a cobalt-based electrocatalyst, and biocatalysts separated by Nafion and cellulose membranes to achieve high selectivity (98.7%) and yield. The utilization of solar energy as a power source and the elimination of the necessity for external electricity or chemical additives render the process particularly sustainable and cost-effective. [251]

Developing innovative electrode materials requires comprehensive characterization, especially regarding their stability and potential changes during reactions. Prioritizing comprehensive characterization enables a deeper understanding of electrode behavior and stability throughout reactions. In this regard, X-ray absorption spectroscopy (XAS), particularly *in-situ* measurements, emerges as a powerful tool. To date, no *in-situ* measurements have been conducted on electrodes for lignin electrocatalytic depolymerization, representing a significant gap in research. *In-situ* measurements offer real-time insights into electrode behavior and structural changes during electrochemical processes, providing data to enhance electrode stability and optimize reaction conditions. Additionally, there is a critical need to delve into the mechanisms underlying lignin depolymerization for better control over selectivity.

Additionally, extensive research on the electrocatalytic depolymerization of lignin has primarily focused on oxidative pathways, with less emphasis on reductive pathways. However, most of these studies were conducted on a laboratory scale, limiting their applicability to industrial settings. To overcome these challenges and facilitate upscaling, interdisciplinary collaboration among research groups specializing in catalyst design, reactor engineering, and process optimization is crucial. Collaboration between groups

specializing in these aspects is essential for developing scalable and efficient depolymerization systems. Additionally, establishing close partnerships with industry stakeholders is paramount. By fostering collaboration and communication between academia and industry, researchers can address challenges more effectively and develop tailored solutions for scaling up lignin depolymerization processes.

3.5 Acknowledgements

We would like to thank the University of Wuppertal for the research support and Philipp Grassow for his contribution to the graphic design. Additional financial support within the COMET InTribology 2 project (FFG No. 872176, project coordinator: AC2T research GmbH).

3.6 Conflict of interest

The authors declare no conflict of interest.

3.7 Author contributions

Conceptualization, L.M.L., A.S., and B.V.M.R.; writing—original draft preparation, L.M.L., V.C.B., B.B.B., and B.V.M.R.; writing—review and editing, L.M.L., B.V.M.R., and A.S.; supervision, B.V.M.R. and A.S.

Abstract:

Replacing crude oil as the primary industrial source of carbon-based chemicals has become crucial for both environmental and resource sustainability reasons. In this scenario, wood arises as an excellent candidate, whilst depolymerization approaches have emerged as promising strategies to unlock the lignin potential as a resource in the production of high-value organic chemicals. However, many drawbacks, such as toxic solvents, expensive catalysts, high energy inputs, and poor product selectivity have represented major challenges to this task. Herein, we present an unprecedented approach using electrocatalysis for the simultaneous depolymerization and dearomatization of lignin in aqueous medium under ambient conditions. By employing water/sodium carbonate as a solvent system, we demonstrated a pathway for selectively depolymerizing lignin under reductive electrochemical conditions using carbon as an electrocatalyst. After reductive electrocatalysis, the presence of aromatic compounds was no longer detected via nuclear magnetic resonance (NMR) spectroscopy. Further characterization by NMR, FTIR spectroscopy, and mass spectrometry revealed the major presences of sodium levulinate, sodium 4-hydroxyvalerate, sodium formate, and sodium acetate as products. By achieving a complete dearomatization, valuable aliphatic intermediates with enhanced reactivity were selectively obtained, opening new avenues for further synthesis of many different organic chemicals, and contributing to a more sustainable and circular economy.

Chapter 4

Organic Chemicals from Wood: Selective Depolymerization and Dearomatization of Lignin via Aqueous Electrocatalysis

Based on:

Lucie M. Lindenbeck, Vanessa C. Barra, Sira Dahlhaus, Silas Brand, Luca M. Wende, Björn B. Beele, Nils. H. Schebb, Bruno V. M. Rodrigues, and Adam Slabon

ChemSusChem, **2024**, *17* (9), e202301617.

DOI: 10.1002/cssc.202301617

Biomass · Dearomatization · Depolymerization · Electrochemistry · Lignin

Preface to Chapter 4

Electrocatalytic depolymerization has emerged as a promising method for the conversion of lignin into valuable chemical platform molecules. [5] While the majority of research in this field aims to obtain aromatics through depolymerization, [3,252–254] this study adopts a divergent approach by simultaneous depolymerization and dearomatization of Soda lignin to selectively obtain aliphatic compounds. This novel strategy opens up new avenues for sustainable platform chemicals, which can serve as building blocks for a variety of organic syntheses.

The selection of an appropriate solvent is crucial for this reaction, given the poor solubility of Soda lignin. A previous study employed levulinic acid as a solvent for Kraft lignin, [104] but this approach resulted in challenges during product isolation. During liquid-liquid extraction, levulinic acid also dissolved along with the target products, complicating complete isolation. This issue was circumvented by using an aqueous sodium carbonate (Na_2CO_3) solution. It was found that Soda lignin is already soluble under alkaline conditions, thereby eliminating the need for an additional organic solvent. The role of an electrolyte in ensuring the flow of electricity during electrochemical reactions is also crucial. Instead of sodium hydroxide (NaOH), which is frequently used as an electrolyte for lignin-related electrochemical processes, [252] this study employed Na_2CO_3. This choice offers two primary advantages. Firstly, Soda lignin is already soluble in Na_2CO_3, eliminating the need for an additional solvent. Secondly, Na_2CO_3 is significantly more environmentally friendly than NaOH in both its production and disposal. The production of NaOH is associated with the energy-intensive chlor-alkali electrolysis process, which has been observed to generate chlorine gas as a byproduct. [255] This process leads to significant environmental pollution, including greenhouse gas emissions and high aquatic toxicity. [256] In contrast, the Solvay process, [257] despite its own environmental considerations, generally has a lower ecological footprint and results in the production of Na_2CO_3. This approach is not only a chemically effective alternative, but also a more ecologically sustainable one. Another key aspect is the choice of electrocatalyst. The decision was made in favor of an unmodified carbon electrode, which offers several advantages: it is inexpensive, chemically stable, [171,172] and showed no signs of wear even after multiple uses. This stability is particularly relevant for later technical implementation, since material losses and catalyst degradation represent major challenges in electrochemical processes.

The electrochemical reaction was carried out in an open beaker, which, while allowing for potential interference from atmospheric oxygen, also had the advantage of

simplifying the apparatus requirements. Despite the relatively simple conditions, the method demonstrated high efficiency, negating the need for separation of the electrodes or a closed system. Another aspect influencing selectivity is the potential for products reduced at the carbon electrode to be oxidized again at the platinum electrode. However, this effect did not have a negative impact on product formation in practice, and it even facilitated the selective production of desired target products. The depolymerization was carried out under constant current, with the potential changing during the reaction. By systematically varying the current, it was demonstrated that an intensity of −175 mA over a duration of 20 h provides optimal conditions for the reaction. The utilization of a constant current approach offers the benefit of ensuring uniform charge transfer, facilitating the selective transformation of reactants. Aromatic compounds were detected even at lower current strengths of −25 mA, while complete dearomatization was only achieved at currents below −100 mA. These observations underscore the pivotal role of sufficient electron transfer in the complete breakdown of the aromatic structure of lignin, ultimately converting it into aliphatic compounds. At the working electrode, the carbon electrode, a series of electrochemical partial reactions unfold, culminating in depolymerization and dearomatization. Under reductive conditions, the initial hydrogenation of aromatic units leads to the formation of acyclic olefins as intermediate products. These intermediate compounds persist in the NMR spectra, particularly at medium reaction times (*e.g.*, after 13 h). However, at longer reaction times, these olefins undergo complete reduction to saturated aliphatic compounds. Under optimal conditions, the predominant reaction products are sodium levulinate, sodium 4-hydroxyvalerate, sodium formate, and sodium acetate. These compounds hold significant potential as platform chemicals, offering a foundation for diverse organic syntheses.

The kinetic studies demonstrated that the reaction progresses rapidly during the initial hours, exhibiting a substantial increase in product formation between 1 and 6 h. After 6 h, the product yield increased gradually and reached its maximum at 58% after 20 h. However, an extension of the reaction time to 25 h did not result in an increased yield; instead, a slight decrease was observed. This observation suggests the possibility of degradation of certain products under these conditions or their conversion into other volatile by-products, *e.g.* CO_2. It was notable that traces of aromatic intermediates were still present during the first 10 h, but then completely disappeared. This observation supports the hypothesis that the reaction involves acyclic olefins as intermediates, which are only fully reduced with a longer reaction time.

The electrochemical depolymerization of Soda lignin under these conditions can be utilized for the targeted synthesis of aliphatic compounds. The combination of a

sustainable solution system, a cost-efficient electrode, and a comparatively simple reaction control in an open system renders the process technically attractive.

Chapter 4 - Organic chemicals from wood: selective depolymerization and dearomatization of lignin via aqueous electrocatalysis

4.1 Introduction

Organic chemicals, on an industrial scale, originate from carbon compounds primarily derived from crude oil, a fossil fuel. Comprising a mixture of relatively small molecules, these can be separated through petrochemical distillation and further processed into various organic compounds. Replacing crude oil as a source of organic chemicals has become imperative for both environmental and resource sustainability reasons. As a non-renewable fossil resource, its extraction and processing have substantial environmental impacts, including greenhouse gas emissions and habitat disruption. Additionally, the finite nature of crude oil reserves urgently calls for the exploration of alternative and renewable sources for organic chemicals. In this context, wood emerges as an excellent candidate to replace crude oil for several reasons.

Being a renewable and biodegradable source, trees absorb carbon dioxide from the atmosphere as they grow. By considering wood as a potential source of organic chemicals, the carbon released during processing is offset by the carbon sequestered during tree growth, making it a potentially carbon-neutral process. All the main components of wood, namely cellulose, hemicellulose, and lignin, can potentially be broken down into various chemical building blocks, providing a wide range of options for organic chemical production. Nevertheless, accomplishing this remains a notable challenge.

Lignin, a wood-related and one of the most abundant biomacromolecules on Earth, has garnered substantial attention in recent years as a sustainable and renewable resource in the production of high-value chemicals and materials. [130,252,258,259] Successful valorization of this polyphenol has the potential to revolutionize the *Green Chemistry* landscape by reducing the reliance on fossil fuels and minimizing environmental impacts. [6,130] Nevertheless, because of its complex and highly aromatic structure, comprised of phenolic and non-phenolic units linked through various ether and carbon-carbon bonds, the efficient and selective breakage of this macromolecule is rather challenging. [3,253]

To enhance value-added processes for lignin conversion, researchers have explored several depolymerization techniques aimed at producing functionalized aromatic compounds at ambient temperature with high yields. [3,252–254]

In this pursuit, electrocatalysis (EC) has emerged as a noteworthy approach due to its alignment with sustainable principles. [8,104,242] Additionally, EC enables precise control of cell potential, thereby improving catalyst selectivity and activity, while allowing the adoption of mild reaction conditions, including room temperature and environmentally friendly solvents. [139,254] In this way, electrochemical depolymerization of lignin in a wide variety of *green* solvents, such as levulinic acid, [104] ionic liquids (1-ethyl-3-methylimidazolium trifluoromethanesulfonate and triethylammonium methanesulfonate), [260] and deep eutectic solvents (DES), [261] has been reported.

It is widely recognized that the process of depolymerizing lignin lacks selectivity, resulting in the formation of mixtures containing monomers, dimers, and oligomers, rather than producing single compounds. The presence of a diverse mixture of molecules makes the separation and purification processes energy-intensive and expensive. [254,262] Therefore, selective separation of valuable lignin-derived compounds from undesirable by-products can be demanding, increasing the cost of lignin valorization processes. In a commercial point of view, this low selectivity results in inconsistent product quality, making it challenging to meet industry standards and specifications. As consequence, there is a major barrier to commercial adoption, as industries often require reliable and predictable feedstock quality for their operations. Hence, many efforts have been employed to address the issue of low selectivity in lignin depolymerization processes, [263,264] while researches into more selective catalysts and process optimization techniques aim to improve product yields and reduce the formation of unwanted by-products.

Aromaticity is a hallmark feature of lignin, and selectively disrupting this aromatic network is a key step towards facilitating its conversion into valuable products. In pursuit of this goal, numerous strategies can be explored to breakdown lignin's intricate structure, one of which is dearomatization. [265] As we delve into this field, our study introduces an innovative and selective approach to the simultaneous depolymerization and dearomatization of lignin *via* electrocatalysis, using an aqueous sodium carbonate solution as a solvent system (**Scheme 1**). The choice of aqueous electrocatalysis, comparatively to traditional harsh chemical treatments, offers significant advantages since it is an environmentally friendly process that operates under relatively mild conditions. [8,104,139] In the meanwhile, electrochemical techniques provide precise control over reactions and enable the use of readily available water as a reaction medium, making it a promising candidate for lignin depolymerization. The key advantage of this method is the absence of additional solvents, as the sodium carbonate solution creates an alkaline environment where lignin can be successfully dissolved, thus circumventing the need for other potentially environmentally impactful solvents. Although sodium hydroxide has been often

chosen for oxidative depolymerization of lignin, [252] this base presents many disadvantages compared to sodium carbonate, including significant environmental repercussions associated with its production. Significant environmental impacts arise from the production of one kilogram of sodium hydroxide. These impacts encompass fossil energy usage (3.5 MJ), global warming potential (0.6329 kg of CO_2 equivalents), influence on aquatic ecotoxicity (1.298 g of 1,4-dichlorobenzene equivalents), contribution to acidification (0.706 SO_2 equivalents), and potential for human toxicity (specifically carcinogenicity) (0.4927 g of 1,4-dichlorobenzene equivalents). [266]

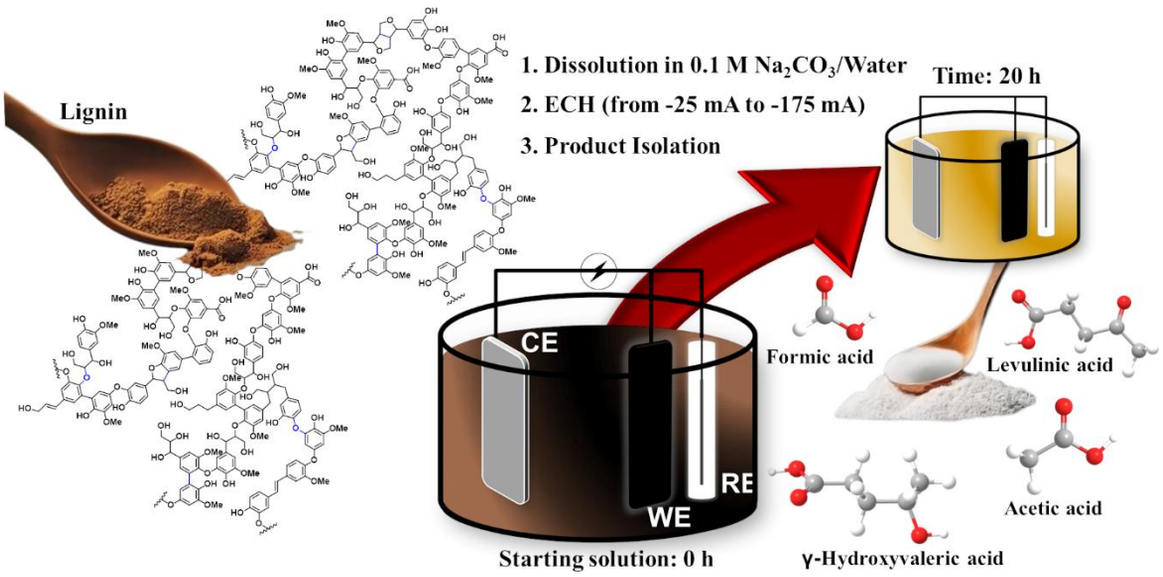

Scheme 1. Scheme showing the electrochemical depolymerization of Soda lignin in water/Na_2CO_3 system *via* ECH.

This study has introduced an unprecedent, sustainable, and straightforward approach to selectively convert lignin into valuable chemical compounds. By achieving a complete dearomatization, a significant milestone in lignin valorization has been reached. This process yields valuable chemical intermediates with enhanced reactivity (**Scheme 1**), opening new avenues for further utilization and contributing to a more sustainable and circular economy. Furthermore, the high cost of noble metal electrodes, which poses as one of the main limitations in the scaling-up of electrochemical processes, was overcome by choosing carbon as the electrocatalyst due to the economic feasibility.

4.2 Results and discussion

Here, we explored a novel approach for the electrochemical reductive depolymerization of lignin, by using Soda lignin as starting material. This process involved the dissolution of lignin in an aqueous sodium carbonate solution, followed by an electrocatalytic reaction aiming the complete depolymerization and dearomatization of lignin along with a selective conversion into valuable aliphatic products.

The electrochemical depolymerization was conducted using a three-electrode setup, with carbon (⌀: 6 mm; length: 65 mm) serving as the electrocatalyst. An Ag/AgCl (satd. KCl) electrode was employed as the reference electrode, and a platinum mesh acted as the counter electrode.

4.2.1 Influence of different currents

Through a systematic investigation, we established a current of −175 mA and a reaction time of 20 h as the optimal parameters for the Soda lignin depolymerization in our system (−175mA/20h).

The selection of these parameters was based on several factors, including the observed color change of the solution, yields, and resulting products. The color change of the solution during the reaction served as an indirect indicator of the success of the depolymerization process. [261,265] Notably, the dissolution of lignin in aqueous sodium carbonate solution initially resulted in a deep brown solution, which gradually became clearer through the reaction course (**Figure 15**). While −175 mA and −200 mA led to a transparent and yellowish solution after 20 h, lower currents such as −25 mA and −100 mA still retained a brown hue, pointing out the incompleteness breakdown of lignin in the medium (**Figure 15**).

Figure 15. The color change of the solution during the reaction is dependent on the applied current, whilst the solution becomes clearer as the applied current rises. This phenomenon serves as an indirect indicator of the degree of depolymerization.

The reaction yields (**Table 9**) further underscores the efficiency of −175 mA for this depolymerization process. An increase in yield was observed as the current increased from 0 mA to −175 mA. However, further increasing the current to −200 mA resulted in a lower yield. In this case, yield represents the fraction of products of depolymerization (DL) ethanol-soluble relative to the mass of starting Soda lignin. Notably, in the reference reactions (Soda lignin powder and 0mA/20h), products could also be extracted with ethanol, but their yields were significantly lower compared to the reaction where electrocatalysis was employed.

Table 9. Yields of depolymerization products (DL) related to the mass of products obtained after extraction with ethanol compared to the mass of starting Soda lignin. All reactions (0mA/20h, −25mA/20h, −100mA/20h, −175mA/20h, and −200mA/20h) were carried out for 20 h. The yield of Soda lignin is related to the ethanol fraction from pure Soda lignin without electrocatalysis. The yield of 0 mA/20h is related to the ethanol fraction after Soda lignin was dissolved in water/sodium carbonate system and left aside for 20 h without electrocatalysis.

	Soda Lignin	0mA/20h	−25mA/20h	−100mA/20h	−175mA/20h	−200mA/20h
Yield [wt%]	7	6	18	46	58	44

With aid of NMR spectroscopy (**Figure 16**), four major depolymerization products could be identified for −175mA/20h: sodium levulinate, sodium 4-hydroxyvalerate, sodium formate, and sodium acetate. The last two could be further confirmed by comparing to the NMR spectra of pure sodium acetate and sodium formate compounds (**Figure S 1**). The ^{1}H-^{1}H COSY NMR spectra in **Figure 17** clearly show the presence of 4-hydroxyvalerate and levulinate are present as products in −175mA/20h. No methanol was detected in these experiments, indicating that the depolymerization does not follow the Kolbe pathways [267,268] in our catalyst system.

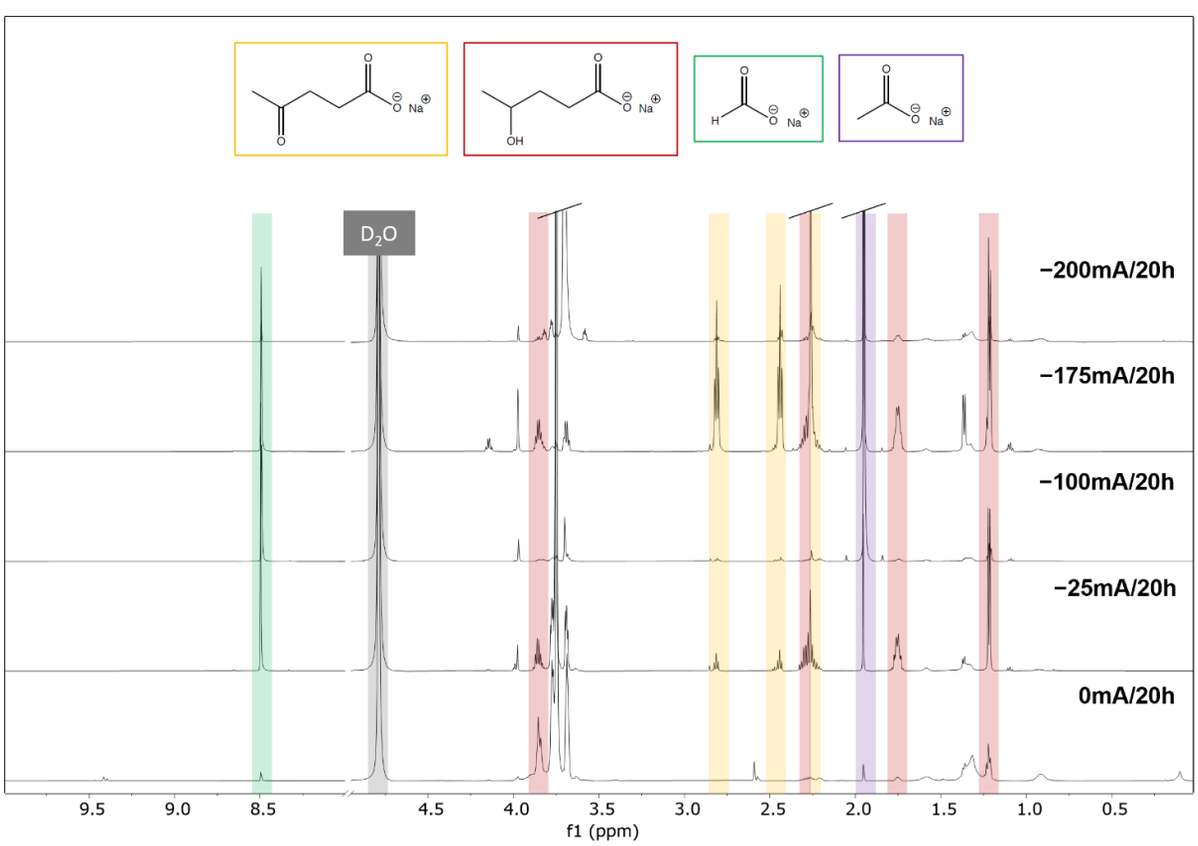

Figure 16. ^{1}H NMR spectra (D_2O, 600.13 MHz) of DL for different applied currents: 0mA/20h, −25mA/20h, −100mA/20h, −175mA/20h, and −200mA/20h. Levulinate (yellow), 4-hydroxyvalerate (red), formate (green), and acetate (purple) could be identified as the main products of Soda lignin depolymerization.

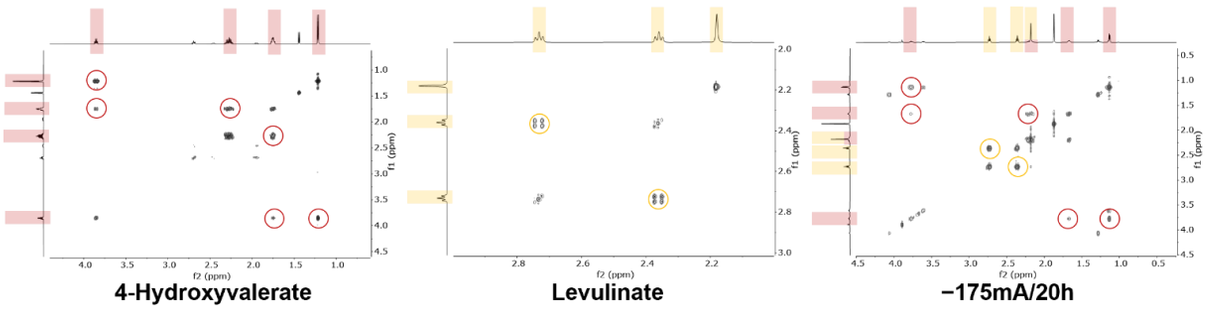

Figure 17. ^{1}H-^{1}H COSY NMR spectra (D_2O, 600.13 MHz) of 4-hydroxyvalerate, levulinate and −175mA/20h. 4-Hydroxyvalerate and γ-valerolactone exist in equilibrium in water. [269] For this reason, signals of γ-valerolactone are also visible in the spectrum of 4-hydroxyvalerate.

Figure 16 also illustrates the dependence of depolymerization process on the applied current (0, −25, −100, −175, and −200 mA) at a constant reaction time (20 h). In the absence of an electrochemical potential (0mA/20h), the products observed included sodium formate, sodium acetate, and sodium 4-hydroxyvalerate, suggesting that in a reaction period of 20 h sodium carbonate already leads to partial depolymerization of lignin.

Nonetheless, a considerable increase in the intensity of sodium formate and sodium acetate signals can already be detected at a current of −25 mA compared to 0mA/20h. Sodium levulinate is introduced as a new product when electrocatalysis was applied, even at low currents such as −25 mA. Chen and Kanan report on the electrochemical reduction of CO_2 to CO and HCO_2H. [270] Their observation led to the suspicion that formate is not a product of the depolymerization of lignin but is formed by the reduction of sodium carbonate. To verify this, control experiments were conducted without lignin, with only sodium carbonate and water, but under otherwise identical conditions. In these instances, no significant signals were observed in the NMR spectrum, except for those corresponding to the solvent, confirming that the depolymerization products indeed stem from lignin breakage and not from the reduction of sodium carbonate as it could be expected. Furthermore, it is important to highlight that the presence of aromatic products persisted at −25mA/20h, while from −100mA/20h upwards, they were no longer detectable *via* NMR spectroscopy (**Figure 18**). Instead, the NMR spectra for −100mA/20h, −175mA/20h, and −200mA/20h exhibited acyclic olefins with very low intensity.

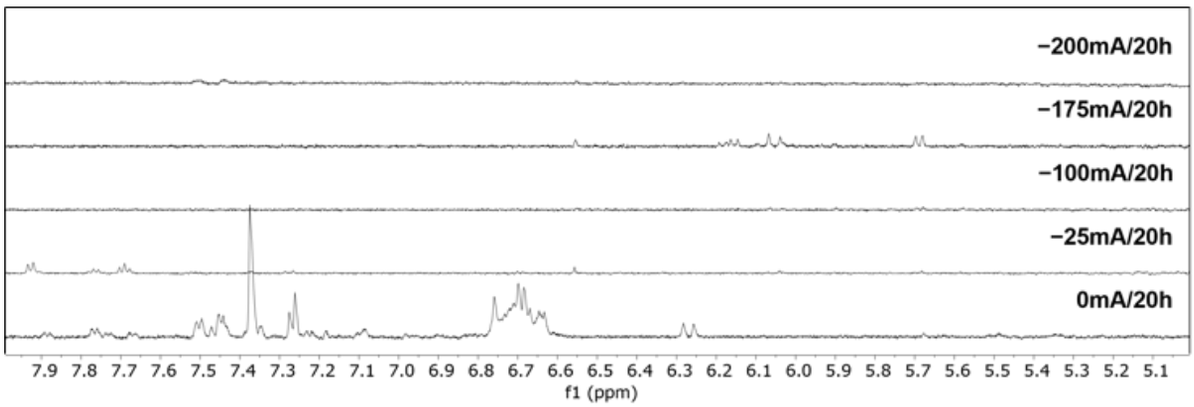

Figure 18. ^{1}H NMR spectra (D_2O, 600.13 MHz) of DL at different applied currents – enlarged section from 5 to 8 ppm. Aromatic compounds were detectable in 0mA/20h and −25mA/20h, whilst up from −100mA/20h a complete dearomatization can be assumed.

The identification of four major products challenges the conventional understanding that lignin depolymerization is a low-selectivity process, [104] thereby adding a new dimension to the discourse surrounding lignin breakdown. The extraction with ethanol reveals that the products, except for 4-hydroxyvaleric acid in a very low intensity, are not initially present in pure Soda lignin, while ^{1}H NMR spectrum mainly shows γ-valerolactone (GVL) signals. The spectrum also confirms the presence of aromatics, as expected for lignin (**Figure S 2**). It can be assumed that GVL is present as an impurity in the starting Soda lignin, since this solvent has been often used for the extraction of lignin from wood. [271] In contrast to pure lignin, the spectrum of 0mA/0h mainly shows the signals of 4-hydroxyvalerate, and only at lower intensities the signals of GVL (**Figure S 3**). This can be explained by the alkaline-catalyzed ring-opening of GVL (**Figure 19**). [269]

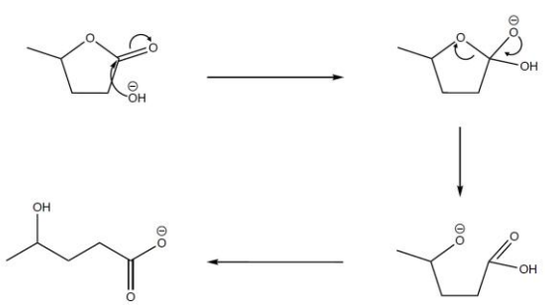

Figure 19. Mechanism of ring opening of GVL in alkaline environment. The hydroxide ion from a strong base acts as a nucleophile and attacks the electropositive carbon of the ester unit creating a carboxylate ion that is stabilized by a positive counterion. [269]

The influence of the applied current on the depolymerization process is also evident *via* FTIR analysis, as demonstrated in **Figure 20**. With increasing the applied current, the intensity of the hydroxy group signal decreases. The greatest differences are observable between 1800 and 1200 cm^{-1}: The signals at 1560 and 1407 cm^{-1} increase with increasing the applied current. The peak at 1560 cm^{-1} can be attributed to the asymmetric and

1407 cm^{-1} to the symmetric vibration of the carboxylate group. [272] This demonstrates the increase in the concentration of levulinate, 4-hydroxyvalerate, formate, and acetate. The shoulder signal at 1652 cm^{-1} in −25mA/20h can be attributed to stretching vibrations of non-conjugate carbonyl and conjugate carbonate from carboxylic acid and ketone groups, respectively. [273] The spectra of −100mA/20h and −175mA/20h are very similar. The main difference is that in −175mA/20h the carbonyl stretching vibration at 1710 cm^{-1} is clearly visible, which can be attributed to the ketone group of levulinate.

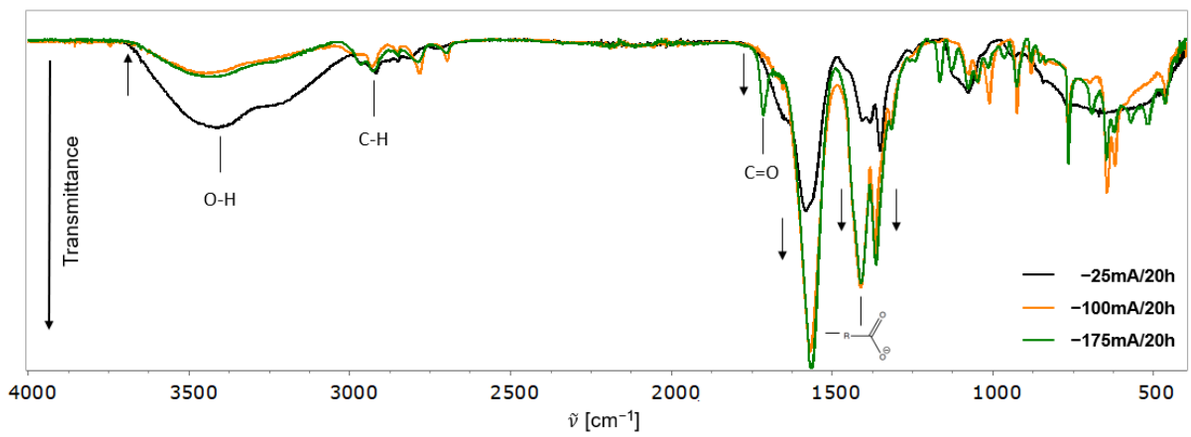

Figure 20. FTIR spectra of DL at different applied currents (−25mA/20h, −100mA/20h, and −175mA/20h). The characteristic oscillations of the O-H, CH, C=O, and COO^- groups can be observed. The intensity of the carboxylate band also increases, which is due to the higher concentration of levulinate, 4-hydroxyvalerate, formate, and acetate.

4.2.2 Influence of different reaction times

Since applying a current of −175 mA for 20 h has proven to be the optimal parameter for the depolymerization of Soda lignin, it is essential to explore the kinetic aspects of this process. To gain deeper insights into the reaction kinetics, a series of experiments was carried out in which the reaction times were systematically varied while maintaining −175 mA as the applied current. Reactions were carried out for 1, 3, 6, 10, 13, 20, and 25 h, and the respective ethanol-soluble fractions were compared over these time intervals. This time-dependent study not only provides a more detailed understanding on the kinetics of the depolymerization, process but also provides important information on the evolution of the product profiles as a function of reaction time. Furthermore, this temporal analysis allows to determine the optimal reaction time required to maximize both the yield and selectivity of the desired products, thereby improving the efficiency and sustainability of the depolymerization process. **Table 10** reveals that the DL achieved the highest yield after 20 h. Initially, at the outset of the reaction (0mA/0h), the yield was 8%, signifying the baseline state of the reaction. After a reaction time of 20 h, the highest yield achieved was 58%. Extending the reaction time does not increase the yield; instead, it leads to a decrease

in ethanol-soluble products. This temporal evolution of the yield underscores the time-dependent nature of the depolymerization process. Of particular interest is the substantial increase in yield from the early stages (−175mA/1h) to intermediate times, such as 6 h, indicating a rapid transformation of Soda lignin into valuable aliphatic products during this period. It is worth noting that after reaching its peak at 6 h (36%), the yield experienced a slight decline at 10 and 13 h, before ultimately rebounding to 58% at 20 h and then drops to 44% after 25 h.

Table 10. Yields of DL related to the mass of products obtained from the ethanol fraction compared to the mass of starting Soda lignin. All reactions (except for 0mA/0h) were carried out at −175 mA.

Duration	0mA/0h	−175mA/ 1h	−175mA/ 3h	−175mA/ 6h	−175mA/ 10h	−175mA/ 13h	−175mA/ 20h	−200mA/ 25h
Yield [wt%]	8	18	23	36	19	18	58	44

Thirty years ago, the *E-factor* (mass of waste/mass of product) was introduced to evaluate the efficiency of chemical processes. [274] In the case of −175mA/20h, the *E-factor* was 17.15, which is within the range for the production of fine chemicals in the chemical industry. [274]

Throughout the course of the kinetic experiments, there is an increase in the concentration of the four main products: levulinate, 4-hydroxyvalerate, acetate, and formate. In parallel with the trends observed in the yield data, the NMR spectra (**Figure 21**) reveal temporal nuances within the kinetics. A discernible progression in the formation of the product is evident from the initial hour up to 6 h. However, after 10 h, there is a deviation from this pattern.

Among all collected spectra, the −175mA/20h spectrum emerges as the most selective, boasting the highest product intensities. This reaffirms the prior determination that −175 mA for a 20 h reaction represents the optimal parameters for achieving a heightened selectivity in product formation during Soda lignin depolymerization.

One of the most important findings from the NMR spectra (**Figure 22**) is the conversion of aromatics into acyclic olefins. This transition is particularly evident at hour 13 and becomes even more pronounced at hour 20, where the presence of aromatics is no longer detectable. Furthermore, the appearance of acyclic olefins from 13 h suggests that aromatics are converted to these intermediates, which are subsequently reduced to aliphatic products. This mechanistic interpretation is consistent with the reductive conditions inherent in the experimental setup.

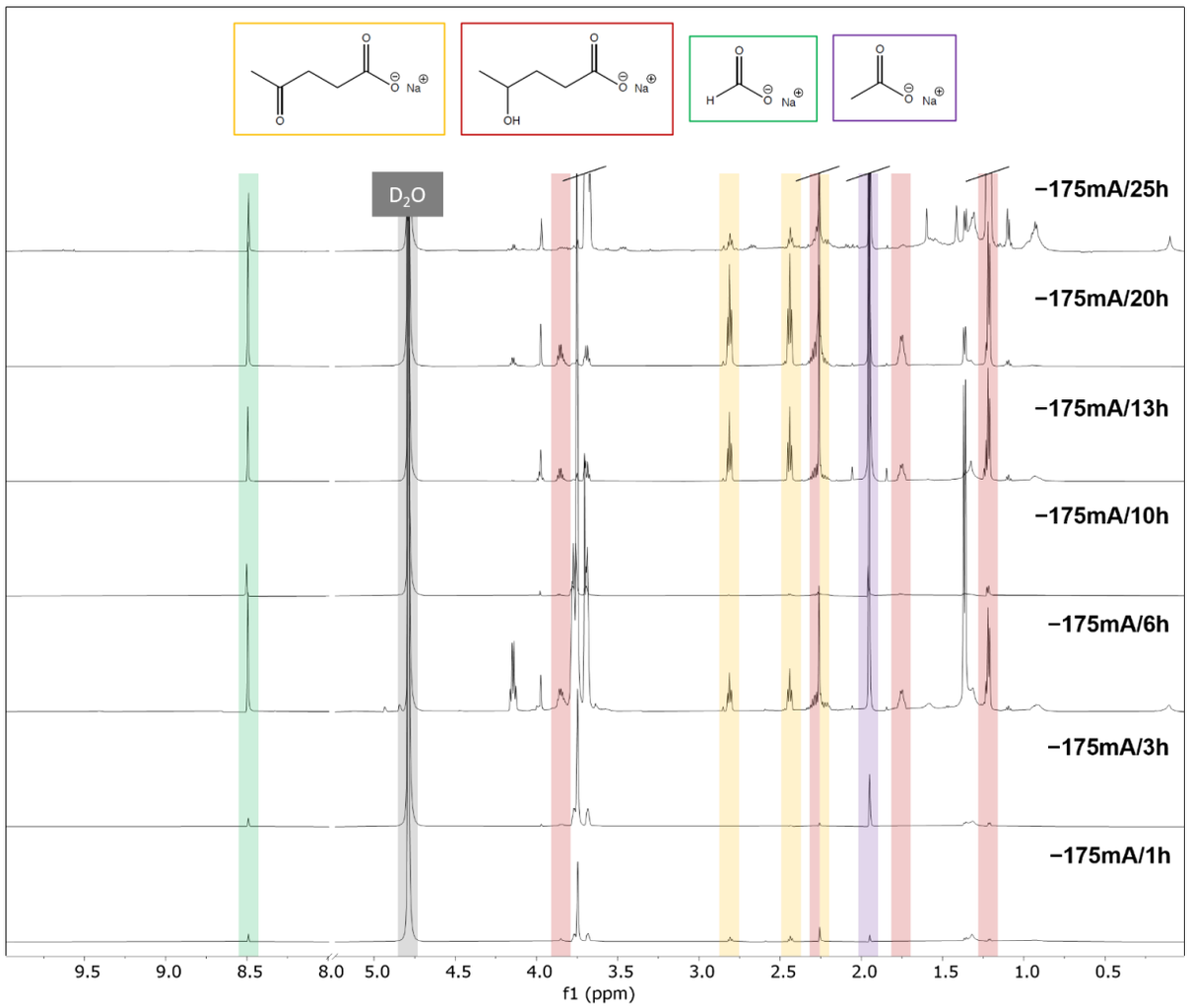

Figure 21. ^{1}H NMR spectra (D_2O, 600.13 MHz) of DL for different reaction times: 1 h, 3 h, 6 h, 10 h, 13 h, 20 h, and 25 h. Levulinate (yellow), 4-hydroxyvalerate (red), formate (green), and acetate (purple) can be identified as the main products. For reasons of clarity, only the products in the first and last reaction are color coded. An increase in intensity of the main products over time is clearly visible.

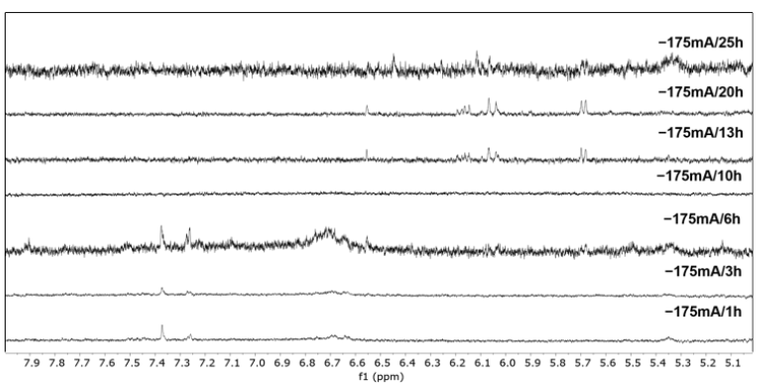

Figure 22. ^{1}H NMR spectra (D_2O, 600.13 MHz) of DL for different reaction times: 1 h, 3 h, 6 h, 10 h, 13 h, 20 h, and 25 h – enlarged section from 5 to 8 ppm. The process of dearomatization can be followed kinetically.

The FTIR spectra for 0mA/0h, −175mA/10h, and −175mA/20h are presented in **Figure 23**. Even in 0mA/0h, the spectrum reveals distinct signals (1558 and 1411 cm^{-1}) associated with the carboxylate group. [272] However, a noteworthy trend emerges as the

reaction progresses, with the intensity of these signals steadily increasing over time. This heightened intensity directly correlates with the greater presence of the products, namely levulinate, 4-hydroxyvalerate, acetate, and formate. Furthermore, the FTIR spectra exhibit a subtle yet crucial detail in the form of a shoulder in the signal for the asymmetric stretching oscillation of the carbonyl group in 0mA/0h. This shoulder is attributed to the signal emanating from the C-C oscillation within the aromatic compounds. This observation underscores the presence of aromatic compounds in the initial reaction mixture which was expected. However, the most significant variations are discernible within the region associated with the carbonyl groups. In 0mA/0h, a signal at 1770 cm^{-1} is evident, which can be attributed to conjugated ester groups. [275] In stark contrast, in −175mA/20h, a distinct signal at 1714 cm^{-1} emerges, signifying the presence of the keto group in sodium levulinate.

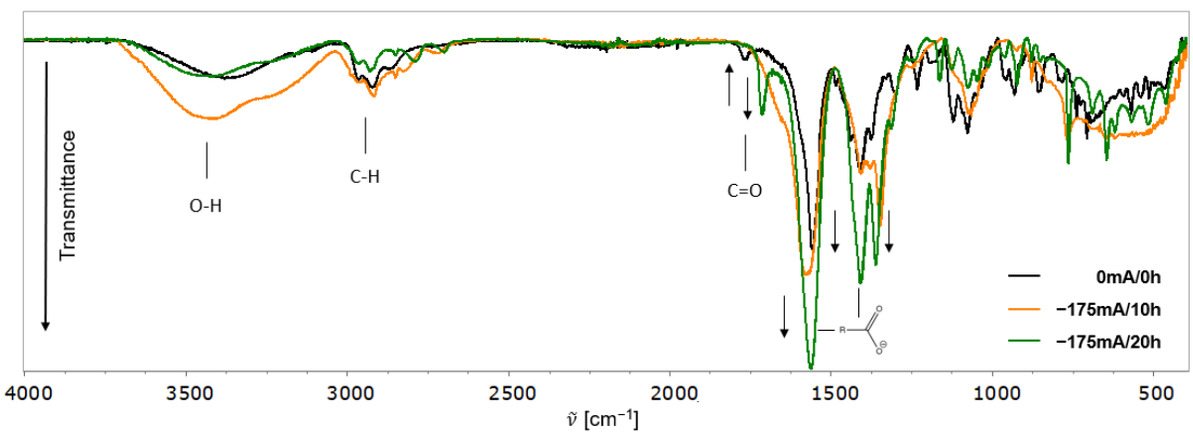

Figure 23. FTIR spectra of DL for different reaction durations (0 h, 10 h, and 20 h). The characteristic oscillations of the O-H, C-H, C=O, and COO^- groups can be found in the IR spectra. With increasing reaction duration, the band of the C-C vibration disappears in aromatics, which proves the dearomatization. The intensity of the carboxylate band also increases, which is due to the higher concentration of levulinate, 4-hydroxyvalerate, formate, and acetate.

Two compounds were detected in the DL sample (−175mA/20h) by liquid chromatography electrospray ionization mass spectrometry (LC-ESI-MS). A peak at 1.27 min (DL product 1) was detected in DL corresponding to the $[M\text{-}H^+]^-$ ion of 4-hydroxyvaleric acid. The peak showed in LC-ESI(−)-MS analysis intense signals at m/z 117.0557. Retention time, precursor m/z as well as fragment spectra match with a synthesized standard of 4-hydroxyvaleric acid (**Figure 24**).

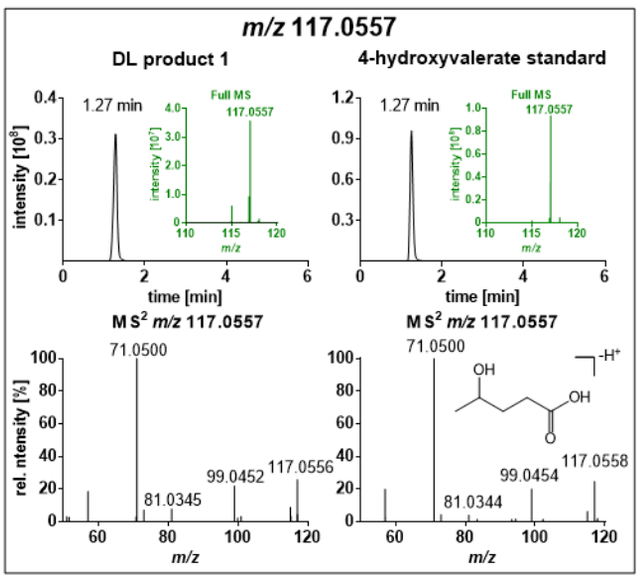

Figure 24. Detection of 4-hydroxyvalerate in DL (−175mA/20h) using LC-ESI(−)-MS. Top: extracted ion chromatogram at *m/z* 117.0557 and Full MS at 1.27 min, bottom: corresponding fragment spectra. The peak at 1.27 min (DL product 1) could be identified as $[M\text{-}H^+]^-$ ion of 4-hydroxyvalerate at *m/z* 117.0577 based on comparison of retention time and fragment spectra to an authentic synthetic standard compound.

Two compounds were detected in the DL sample (−175mA/20h) by liquid chromatography electrospray ionization mass spectrometry (LC-ESI-MS). A peak at 1.27 min (DL product 1) was detected in DL corresponding to the $[M\text{-}H^+]^-$ ion of 4-hydroxyvaleric acid. The peak showed in LC-ESI(−)-MS analysis intense signals at *m/z* 117.0557. Retention time, precursor *m/z* as well as fragment spectra match with a synthesized standard of 4-hydroxyvaleric acid (**Figure 25**).

A second peak was detected at 1.33 min with intense ions at *m/z* 115.0400. Based on comparison with an authentic reference compound this peak could be identified as $[M\text{-}H^+]^-$ ion of levulinic acid (**Figure 25**). No aromatic compounds could be detected based on LC-UV signals (280 nm).

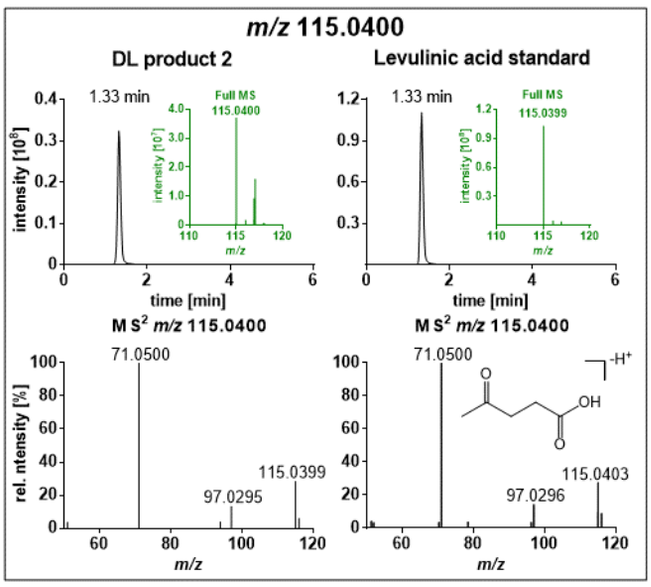

Figure 25. Detection of levulinate in DL (−175mA/20h) using LC-ESI(−)-MS. Top: extracted ion chromatogram at *m/z* 115.0400 and full MS at 1.33 min, bottom: corresponding fragment spectra. The peak at 1.33 min (DL product 2) could be identified as $[M\text{-}H^+]^-$ ion of levulinate at *m/z* 115.0400 based on comparison of retention time and fragment spectra to an authentic standard compound.

To evaluate the chemical and electrochemical stabilities of the primary products, namely sodium acetate, sodium formate, sodium levulinate, and sodium 4-hydroxyvalerate, under the experimental conditions employed in this investigation, a mixed aqueous solution comprising these compounds underwent electrochemical testing employing identical parameters (including electrolyte concentration). Following a 20 h reaction at an applied current of −175 mA, the observed outcomes indicate that these compounds remained stable over the course of the experiment. This stability is discernible through a comparative analysis of the NMR spectra (**Figure S4**) before and after the electrochemical reaction.

4.3 Conclusion

The novel electrocatalytic approach presented in this investigation has shattered the barriers that have long hindered the effective depolymerization of lignin, allowing considering wood as replacement for crude oil in the production of organic compounds on industrial scale. By harnessing the power of reductive electrochemistry in an aqueous medium using carbon as electrocatalyst, we have not only overcome the challenges of toxic solvents, expensive catalysts, and excessive energy inputs but have also achieved unparalleled selectivity in the conversion of a complex polyphenol into valuable aliphatic intermediates. The absence of aromatic compounds after electrocatalysis signals a transformative breakthrough and milestone in lignin valorization. With the emergence of sodium levulinate, sodium 4-hydroxyvalerate, sodium formate, and sodium acetate as the

primary products, we pave the way for a more sustainable and circular economy, where lignin can finally become a cornerstone of innovation for the generation of high-value added products.

4.4 Acknowledgements

We would like to thank University of Wuppertal for the research support. We also would like to thank Prof. Christian Kloc and Dr. Serhiy Budnyk for valuable discussions and comments that helped on the writing of this manuscript. L. M. L. thanks the networking program 'Sustainable Chemical Synthesis 2.0' (*SusChemSys* 2.0) for the support and fruitful discussions across disciplines.

4.5 Conflict of interests

The authors declare no conflict of interest.

4.6 Data availability statement

The data that support the findings of this study are available from the corresponding author upon reasonable request.

4.7 Author contributions

Conceptualization, L.L., A.S., and B.V.M.R.; Methodology, L.L., V.C.B., S.D., and S.B.; Investigation, L.L., V.C.B., S.D., and S.B.; Data Curation, L.L., B.B.B, and L.M.W.; Formal Analysis, L.L. and L.M.W.; Writing – Original Draft, L.L.; Writing – Review & Editing, L.L., B.V.M.R., and A.S.; Supervision, N.H.S, B.V.M.R., and A.S.

Abstract:

This study builds upon our experience with electrocatalyzed dearomatization of lignin in aqueous systems, which has shown to produce sodium levulinate, sodium 4-hydroxyvalerate, sodium acetate, and sodium formate as major depolymerization products. Here, we extend this investigation by exploring a water/γ-valerolactone (GVL) solvent system for electrochemical depolymerization and dearomatization of lignin, using Na_2CO_3 as electrolyte. GVL, derived from biomass, has frequently been employed as a solvent for biomass treatment, notably in the Organosolv process. Consequently, various biorefinery strategies have emerged utilizing GVL as a green platform, primarily for its potential in delignifying lignocellulosic biomass when combined with water and dilute acid. This study proposes electrochemical depolymerization of lignin in GVL as a step toward the concept of a bioelectrorefinery, aiming to convert lignin into aliphatic organic chemicals. Consistent with our prior work in aqueous systems, applying a current of −100 mA over 8 h yielded sodium levulinate, sodium 4-hydroxyvalerate, sodium acetate, and sodium formate. Confirmation was provided by liquid chromatography electrospray ionization high-resolution mass spectrometry, nuclear magnetic resonance, and infrared spectroscopy. These findings advance our understanding of GVL as a biomass-based platform, highlighting its potential not only for biomass treatment but also as a medium for converting lignin into valuable aliphatic organic chemicals.

Chapter 5

Breaking down Lignin in Gamma-Valerolactone: Advances into a Bioelectrorefinery

Based on:

Lucie M. Lindenbeck, Sira Dahlhaus, Luca M. Wende, Björn B. Beele, Marcella Frauscher, Nils Helge Schebb, Christian W. Lehmann, Julia Bornhorst, Adam Slabon, and Bruno V. M. Rodrigues

Green Chemistry Letters and Reviews, **2024**, *17* (1), 2390867.

DOI: 10.1080/17518253.2024.2390867

Gamma-valerolactone · Lignin · Biomass · Bioelectrorefinery

Depolymerization · Electrocatalysis

Preface to Chapter 5

Biomass can be converted into fuels and chemicals in a manner analogous to that of petroleum. [276] In biorefineries, biomass that has historically been regarded as "worthless" is converted into valuable platform chemicals that serve as starting materials for fuels, chemicals, and materials through thermal, biochemical, or catalytic processes. [276] The prerequisite for this process is the separation of the biomass into cellulose, hemicellulose, and lignin by suitable pretreatment steps, without destroying the components. [276] Established methods include catalytic processes, steam explosion, acidic or alkaline pretreatment, and enzymatic steps. [276] The Organosolv process uses organic solvents such as ethanol and water at 170-200 °C for efficient lignin extraction [277] and can be performed under alkaline and acidic conditions. [276] Although it offers economic advantages such as easy solvent recovery, challenges remain in lignin separation and scaling. [276]

Lignin-first approaches prioritize the targeted extraction of lignin prior to further biomass processing, [278] with gamma-valerolactone (GVL) being considered a promising solvent. [276] Adjusting the GVL/water ratio allows lignin to be separated by filtration in an energy-efficient manner, while the addition of salts, co-solvents, or liquid CO_2 facilitates the formation of a biphasic system and optimizes the downstream process. In combination with phenolic solvents or formaldehyde, GVL has been shown to enhance lignin yield and quality by preventing lignin condensation. [279–281] GVL recovery is imperative due its comparatively high cost.

Various methods have been developed to concentrate GVL in a water-insoluble phase. While CO_2-based or phenolic extraction processes offer high recovery rates, they are cost-intensive. A more economical alternative is co-solvent extraction, which enables efficient GVL recovery at lower investment costs under moderate conditions. Liquid-liquid extraction is particularly promising because it allows for low-energy and cost-efficient solvent recovery. [282]

However, the question arises as to whether these elaborate separation steps are necessary at all. A more promising approach is to use the lignin-GVL solution directly as feedstock for electrochemical lignin depolymerization. This approach eliminates the need for energy-intensive solvent recovery and lignin separation, simplifying the process and potentially enhancing the efficiency of recyclable material recovery from biomass. Moreover, this strategy could position electrochemical depolymerization as a pivotal method in biorefinery processes, contributing to a more sustainable utilization of biomass.

The successful electrochemical depolymerization of lignin in GVL, facilitated by the addition of water and sodium carbonate (Na_2CO_3) as an electrolyte, underscores the potential for direct depolymerization immediately following extraction. The economic advantages of carbon electrodes, particularly their stability and cost efficiency, further enable the scalability of the process.

A notable aspect pertains to the documented base-catalyzed ring-opening reaction of GVL to 4-hydroxyvalerate, [269,283] a lignin depolymerization product that has been previously identified. To elucidate the factors influencing this reaction, systematic tests were conducted prior to the electrochemical depolymerization. Parameters such as reaction time, water content, electrolyte, temperature, and electrochemical factors like current and reaction time were analyzed. In addition to Na_2CO_3, sodium chloride (NaCl) was also tested as an electrolyte, which demonstrated that NaCl, compared to Na_2CO_3, can reduce ring opening of GVL. Nevertheless, Na_2CO_3 was used as the depolymerization electrolyte to avoid the potential formation of persistent organic pollutants. Chlorinated compounds are recognized for their high persistence and bioaccumulation potential, and organochlorinated by-products such as polychlorinated dibenzo-dioxins and dibenzofurans (PCDDs and PCDFs) are the focus of international regulations. [284] The selection of Na_2CO_3 contributes to the environmental compatibility of the process.

Test results indicate that GVL maintains electrochemically stable under conditions up to a current of −100 mA for 8 h, during which time Na_2CO_3 is the exclusive agent responsible for ring opening. The Na_2CO_3 solvent system yielded optimal results, characterized by the highest yield and most selective product distribution, at a current of −175 mA and a reaction time of 20 h. Complete depolymerization was achieved after a reaction time of 10 h at −175 mA or after 20 h at −100 mA. The GVL/H_2O solvent system also yields products such as sodium levulinate, sodium 4-hydroxyvalerate, sodium acetate, and sodium formate. Notably, the product 4-hydroxyvalerate exhibited an enrichment of GVL ring opening. Despite employing a shorter reaction time and a lower current intensity compared to the other solvent system, complete dearomatization was attained. This outcome suggests that the process is less energy-intensive and has the potential for future industrial applications.

A techno-economic analysis has revealed that electrochemical processes in biorefineries still face economic challenges, particularly due to high investment costs and the limited efficiency of electrochemical reactors. Notwithstanding these challenges, the process demonstrates considerable promise, particularly in terms of its capacity to yield

higher productivities and the comparatively low cost of the raw materials in comparison to the value of the end products, such as sodium 4-hydroxyvalerate and sodium levulinate.

A salient benefit of GVL is its dual functionality, which enables its utilization in both lignin extraction and direct depolymerization. This characteristic eliminates the necessity for additional purification and recycling processes, leading to enhanced efficiency. Moreover, GVL's multifaceted role as both a solvent and a reactant contributes to an increase in productivity.

Chapter 5 - Breaking down lignin in gamma-valerolactone: advances into a bioelectrorefinery

5.1 Introduction

The prevailing climate crisis is compelling industries to adopt more sustainable processes. These processes must ensure efficient resource utilization, minimize waste production, and substitute fossil fuels with renewable energy sources. Although the chemical industry is vital for pharmaceuticals and polymers, traditional processes are often not aligned with environmental concerns. [285] Historically, the industry has relied heavily on oil and gas due to their availability and cost-effectiveness. [286] However, with fossil fuels depleting and energy demand rising, the focus has shifted to renewable sources such as wind, solar, geothermal, hydropower, and biomass - a readily available organic carbon source of high interest. [287]

The conversion of biomass and biomass waste into fuels and chemicals is a promising route toward a more sustainable economy. About 170 billion tons of renewable resources are generated on Earth every year, but only 3.5% of this amount is accounted for human use. [2] Concerning lignocellulosic biomass, lignin, one of its main components, has emerged as a valuable raw material for the production of chemicals and fuels. [254] As a complex biomacromolecule found in plant cell walls, lignin provides structural support to plants and is highly abundant in lignocellulosic biomass, particularly in wood. It can be sourced from various materials, including hardwood, softwood, and agricultural residues. The highly crosslinked molecular structure of this polyphenol involves three primary phenylpropane units interconnected by ether and carbon-carbon linkages, along with hydroxyl and methoxy groups, which accounts for its recalcitrant characteristic. [288,289] Therefore, the selective and efficient breakdown of this macromolecule into high-value added products is rather challenging. [254]

Depolymerizing lignin requires efficient catalysts and optimized reaction conditions. Precise adjustment of parameters such as temperature, pressure, and choice of solvent is critical to achieving high product yields. [288,290–293]

In electrochemical approaches, the selectivity and speed of the reaction can be improved by adjusting the potential or current density, as well as other parameters such as solvents, electrolytes, and electrode materials. [9,104,138,185,216,294] Various sustainable conversion approaches, including biological, [295–300] thermal, [290] chemical, [291–293] and electrochemical [104,138,185,216,217,294,301] pathways have been explored to attempt to break down

lignin into smaller (aromatic) compounds. [3] In this context, electrochemical processes have gained a significant recognition in recent decades, [302,303,304] due to the possibility of using milder conditions while being atom efficient. [305] Electrochemical biomass depolymerization aligns with *Green Chemistry* principles introduced in the early 1990s as the "design of chemical products and processes to reduce or eliminate the use and generation of hazardous substances". [6] Electrocatalysis can operate at ambient temperature and pressure, overcoming kinetic barriers through an applied potential rather than thermal energy, [7] with the advantage of using hydrogen and oxygen produced from water splitting. [8] The sustainability aspect can be further increased by using biomass-derived electrodes, such as carbon, and renewable energy sources, such as solar energy. [173] In addition, heterogeneous catalysis enables simple product-catalyst separation.

Lignin depolymerization through electrochemical processes has been recently documented using many eco-friendly solvents, such as levulinic acid, [104] ionic liquids (*e.g.*, 1-ethyl-3-methylimidazolium trifluoromethanesulfonate and triethylammonium methanesulfonate), [260,306] deep eutectic solvents (DES), [261] and an aqueous sodium carbonate (Na_2CO_3) solvent system [138]. After a 20 h depolymerization reaction of lignin at −1.7 V with a copper electrocatalyst in levulinic acid, monomers and dimers could be obtained in which aryl ether and phenol groups predominated. [104] Using triethylammonium methanesulfonate as a protic ionic liquid and a $Ru_{0.25}V_{0.05}Ti_{0.7}O_x$ mixed oxide electrode, various oxidation products, including aldehydes (benzaldehyde, 3-furaldehyde, m-tolualdehyde, vanillin, and acetovanillon) and ketones, were obtained at potentials ranging from 1.0 V to 1.5 V. A yield of 6 wt.% of the original lignin mass was achieved. [306] During the electrochemical depolymerization of lignin in a DES at different potentials (0.5 V and 1 V), guaicol, vanillin, acetovanillon, and syringaldehyde were obtained as the main products. Compared with the amount of lignin used, a yield of 2 wt.% was obtained. [261] In the process of depolymerizing with simultaneous dearomatization of lignin within an aqueous Na_2CO_3 solvent system, four aliphatic main products were identified: sodium levulinate, sodium 4-hydroxyvalerate, sodium acetate, and sodium formate. These products were obtained after 20 h at a current of −175 mA under reductive conditions. A yield of 58 wt.%, relative to the initial mass of lignin, was achieved. [138]

Solvent choice is a crucial aspect of *Green Chemistry*. [307,308] In this context, biomass-derived γ-valerolactone (GVL) has been proved to be a sustainable solvent, since it boasts favorable physical and chemical properties and can be stored and transported in large quantities with ease and safety, thanks to its low melting (−31 °C), high boiling (207 °C) and flash (96 °C) points. GVL has a distinct odor, aiding leak detection, and excellent miscibility with water, promoting biodegradation. While serving as a polar aprotic solvent,

GVL plays a pivotal role in stabilizing acidic protons derived from protonated transition states. This property accelerates the rates of acid-catalyzed biomass conversion reactions. [309] Utilized either as a primary solvent or co-solvent, GVL demonstrates its versatility in generating higher-value products from diverse sources such as lignin, carbohydrates, sugars, and smaller molecules. The combination of GVL with water creates arrangements at the surface that effectively promote hydrolysis reactions. [310] An intriguing application of GVL lies in its role as a solvent for the Organosolv treatment. This application not only prevents the re-precipitation of lignin by-products on cellulose surfaces but also augments chemical modifications at the cellulose surface, including bond cleavage. [310] Positioned as a promising solvent within a biorefinery aspiring for circularity, GVL's widespread adoption hinges on the feasibility of large-scale production to drive down costs. [311] Noteworthy initiatives in this direction are emerging from various European countries. [312]

This study builds upon our experience in the electrocatalyzed depolymerization and dearomatization of lignin in an aqueous system using Na_2CO_3 as an electrolyte, [138] which generates sodium levulinate, sodium 4-hydroxyvalerate, sodium acetate, and sodium formate as the major depolymerization products (DL). [138] At the same time, given that GVL has been often used for the delignification and pretreatment of the lignocellulosic biomass, [313] the utilization of this solvent as medium for the electrocatalytic depolymerization of lignin becomes appealing. As long as GVL recycling remains a challenge, [314] it is highly advisable to prioritize “one-pot” GVL/water processes for efficient biomass conversion. The dual utilization of GVL for the initial extraction of lignin from biomass and its possible subsequent direct application in electrochemical depolymerization can reduce the need for supplementary chemical agents and solvents. Furthermore, it circumvents the need for intricate recycling procedures, thereby addressing current limitations and propelling the advancement of GVL-based biorefinery technologies. It is known that GVL undergoes a ring-opening reaction to 4-hydroxyvalerate under basic conditions. [283,315] This could for instance result in an overlap between the products of lignin depolymerization in water/Na_2CO_3 and the ring-opening product of GVL. The main goal of this study was to increase the overall yield of the reaction by selectively inducing the ring opening of GVL to enrich the depolymerization products with 4-hydroxyvalerate (**Scheme 2**).

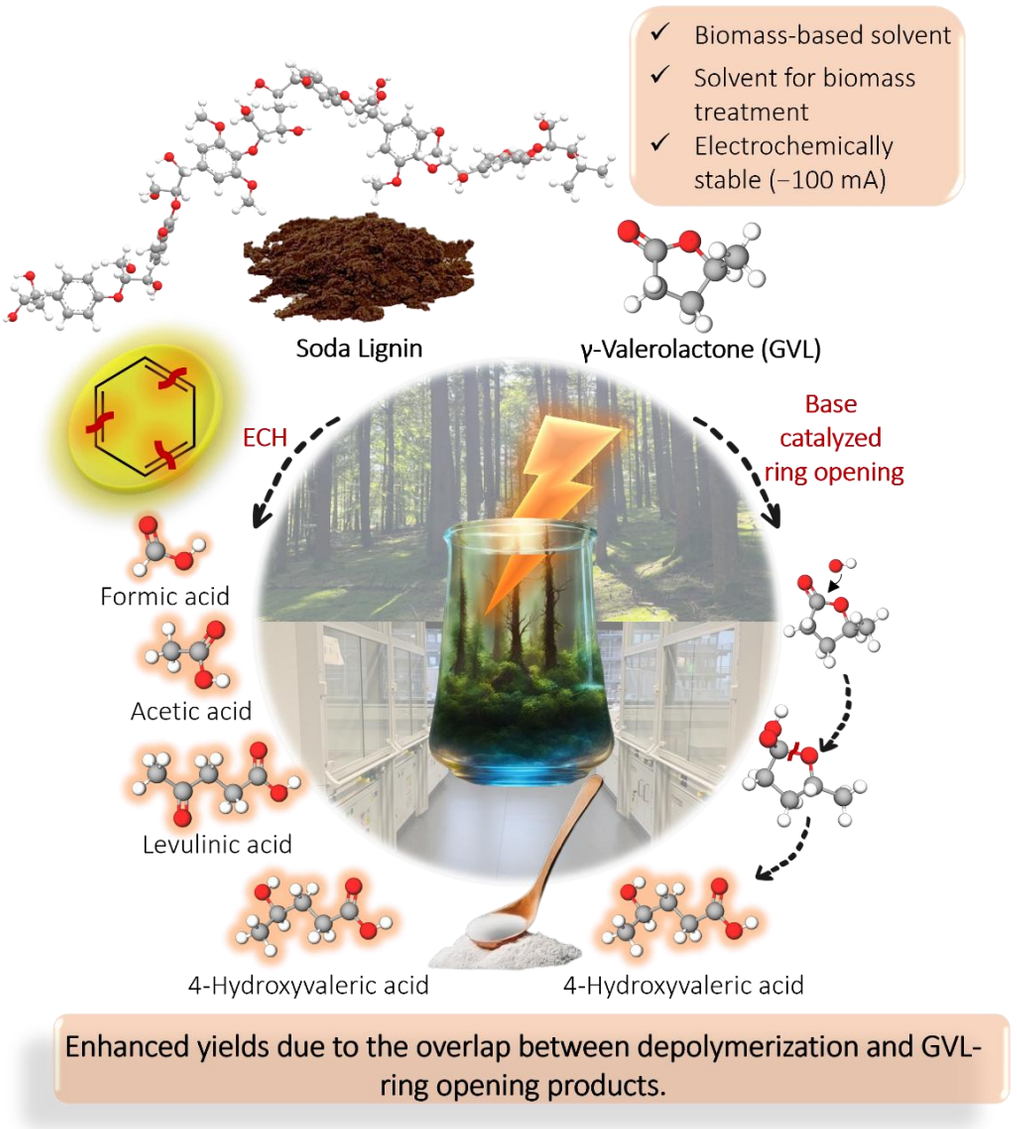

Scheme 2. Scheme of the electrochemical depolymerization of Soda lignin in a water/GVL system using electrocatalytic hydrogenation (ECH). The main depolymerization products (DL) of this process are levulinic acid, 4-hydroxyvaleric acid, formic acid, and acetic acid. Additionally, 4-hydroxyvaleric acid is synthesized by the ring-opening reaction of the GVL, which enriches the products of depolymerization and increases the reaction yield.

The transformation of GVL into 4-hydroxyvalerate has the potential to offset some of the costs and challenges associated with solvent recovery. The generation of a commercially valuable product from the solvent allows for the creation of supplementary revenue streams, thereby enhancing the overall economic feasibility of the process. These discoveries deepen our comprehension of GVL's role as a biomass-derived platform, highlighting its capacity as a medium for transforming lignin into valuable aliphatic organic chemicals. This research not only propels the bioelectrorefinery concept forward but also paves the way for harnessing renewable resources, foreseeing a plausible shift

from crude oil to become the predominant industrial source for carbon-based chemicals in the future.

5.2 Materials and methods

5.2.1 Materials

γ-Valerolactone (GVL, thermo scientific) (98 %), $Na_2CO_3 \times 10\ H_2O$ (Grüssing GmbH), and levulinic acid (Merck KGaA) (98%) were used as received. The Soda lignin used originates from the hardwood black liquor of a sulfur-free pulp production in a pilot plant (WAT Venture Sp. z o.o., Poland). All aqueous solutions were prepared with ultrapure water obtained from a Millipore system.

5.2.2 Electrochemical depolymerization of Soda lignin

Soda lignin was dissolved at 3 $g \cdot L^{-1}$ in 50 mL of a 5 M GVL aqueous solution by magnetic stirring. Electrochemical depolymerization was conducted using a three-electrode setup on an ATLAS 1131 Electrochemical Unit & Impedance Analyser (Atlas-Sollich, Rebiechow). The three-electrode set-up consisted of a carbon working electrode, a platinum wire counter electrode, and an Ag/AgCl (saturated KCl) reference electrode. 5 mL of a sodium carbonate solution (1 M) was added to the solution as an electrolyte. Chronopotentiometry was performed using an applied current of −100 mA for 8 h at room temperature. After the reaction, a brown, but slightly transparent solution remained. Water was removed from the mixture under reduced-pressure conditions, leaving behind a solid and liquid, which were separated from each other by filtration. The solid was then redissolved in water, which was once again removed under reduced pressure. This procedure was repeated several times. The resulting brown solid was dried at 60 °C in a drying oven.

^{1}H NMR (600.13 MHz, D_2O) δ 8.49 (s, formate), 4.89 – 4.81 (m, GVL), 3.85 (h, 4-hydroxyvalerate), 2.81 (t, levulinate), 2.74 – 2.62 (m, GVL), 2.49 – 2.39 (m, GVL), 2.44 (t, levulinate), 2.34 – 2.21 (m, 4-hydroxyvalerate), 2.26 (s, levulinate), 1.95 (s, acetate), 1.75 (dtd, 4-HVA), 1.43 (d, GVL), 1.21 (d, 4-hydroxyvalerate).

^{13}C NMR (150.94 MHz, D_2O) δ 215.0 (C=O, levulinate)*, 184.19 (COO^-, 4-hydroxyvalerate), 182.2 (COO^-, levulinate)*, 181.0 (COO^-, acetate)*, 167.7 (C=O, GVL)*, 163.2 (HCOO, formate)*, 81.0 (CH, GVL)*, 68.85 (CH, 4-hydroxyvalerate), 63.5 (CH, 4-hydroxyvalerate)*, 40.76 (CH_2, levulinate), 35.97 (CH_2, 4-hydroxyvalerate), 35.19 (CH_2, 4-hydroxyvalerate), 32.56 (CH_2, levulinate), 30.35 (CH_3, levulinate), 31.8 (CH_2, GVL)*, 30.2 (CH_2, GVL)*, 24.1 (CH_3, acetate)*, 22.91 (CH_3, 4-hydroxyvalerate).

*: assignment *via* ^{1}H,^{13}C HSQC and ^{1}H,^{13}C HMBC NMR spectra

FTIR (Diamond-ATR): ν [cm^{-1}] = 3381 (OH, w), 3201 (OH, w), 2962 (CH, w), 2930 (CH, w), 2916 (CH, w), 2872 (CH, w), 1773 (C=O, w), 1707 (C=O, w), 1561 (COO^-, vs), 1406 (COO^-, s), 1367 (m), 1312 (m), 1296 (w), 1193 (w), 1127 (m), 1073 (m), 1051 (w), 938 (w), 920 (w), 873, 846 (w), 796, 781 (w), 766 (w), 691 (w), 649 (w), 621 (w), 593 (w), 551 (w), 516 (w), 467 (w), 433 (w).

5.2.3 Synthesis of sodium 4-hydroxyvalerate

Sodium 4-hydroxyvalerate was synthesized according to previous works. [138]

^{1}H NMR (600.13 MHz, DMSO-d^6) δ 6.27 (s, 1H, OH), 3.60 (h, $^3J_{HH}$ = 6.0 Hz, 1H, C(OH)H), 2.10 (dt, $^2J_{HH}$ = 15.6, $^3J_{HH}$ = 6.4 Hz, 1H, CH_2), 2.03 (dt, $^2J_{HH}$ = 15.2, $^3J_{HH}$ = 7.1 Hz, 1H, CH_2), 1.50 (q, $^3J_{HH}$ = 6.3 Hz, 2H, CH_2), 1.00 (d, $^3J_{HH}$ = 6.2 Hz, 3H, CH_3).

^{13}C NMR (151 MHz, DMSO-d^6) δ 178.43 (COO^-), 66.99 (C(OH)H), 35.67 (CH_2), 35.31 (CH_2), 24.04 (CH_3).

FTIR (Diamond-ATR): ν [cm^{-1}] = 3383 (OH, w), 3236 (OH, w), 3151 (OH, w), 2962 (CH, w), 2930 (CH, w), 2916 (CH, w), 2884 (CH, w), 1562 (COO^-, s), 1406 (COO^-, s), 1367 (m), 1313 (m), 1295 (m), 1223 (w), 1194 (w), 1128 (m), 1073 (s), 1051 (m), 950 (m), 938 (m), 920 (m), 873 (m), 845 (w), 796 (w), 760 (w), 737 (w), 722 (w), 680 (w), 622 (w), 592 (w), 551 (w), 477 (w), 433 (w).

5.2.4 Material characterization

Vibrational spectroscopy. FTIR spectra were measured using a diamond 7 ATR unit on a Nicolet ID5 in the range of 4000-400 cm^{-1}.

Nuclear magnetic resonance spectroscopy. Nuclear magnetic resonance (NMR) measurements were performed on a BRUKER Avance 400 MHz spectrometer and on a BRUKER Avance III 600 MHz spectrometer. The following probe heads were used: 5 mm broadband inverse probe with automatic frequency determination, 5 mm QNP probe, and 5 mm broadband inverse probe. Chemical shifts were referenced with respect to Me_4Si.

Direct infusion (DI) ESI-HRMS. Depolymerized lignin samples were dissolved in methanol, ultrasonicated for 30 min and centrifuged for 10 min (14000 rpm). High-resolution mass spectrometry (HRMS) was used as an advanced analytical method to gain the structure information of degradation products of lignin. MS and MS^n spectra were obtained using an Orbitrap-IQX high-resolution mass spectrometer (ThermoFisher Scientific, Bremen, Germany), equipped with an ESI source. ESI-MS analyses were carried out in ESI(-) and ESI(+) mode. The solutions were infused into the ESI source *via* direct infusion (DI) at a rate of 5 μL min^{-1}. Typical spray and ion optics for negative mode

conditions were the following: source voltage, 3.0 kV; sheath gas flow rate, 8 arb; capillary temperature, 275 °C; capillary voltage, −50 V; tube lens voltage, −130 V. Fragmentation and interpretation was done based on negative ionization mode, positive ionization mode was used for additional confirmation. Xcalibur version 2.0.7 and Mass Frontier version 8.0 (ThermoFisher Scientific, Bremen, Germany) software were used for data processing and evaluation.

LC-ESI-HRMS. Samples were dissolved in H_2O/ACN 50/50 (*v*/*v*) (1 µg mL^{-1}) and injected (5 µL) into the LC-ESI-HRMS system. Standard compounds were injected in a concentration of 1 µM. Chromatographic separation was carried out using a ZORBAX Eclipse Plus C18 column (2.1x150 mm; 1.8 µm) and A: H_2O/ ACN/HAc (95/5/0.1) (*v*/*v*/*v*) and B: ACN + 0.1% HAc as eluents at a flow rate of 300 µL min^{-1}. The LC-System was coupled to a QExactive HF Orbitrap mass spectrometer (Thermo, Schwerte, Germany) equipped with a HESI II ionization source operating in ESI(−) and ESI(+) mode with the following settings: sheath gas flow rate 48 psi; aux gas flow rate 11 arb; sweep gas flow rate 2 psi; spray voltage ±4.5 kV; capillary temperature 256 °C; S-lens RF level 75; aux gas heater temperature 413 °C. Data was acquired in Full MS/data dependent MS^2 mode with the following settings: Full MS: Resolution 120,000; AGC target 1x10^6 ; Maximum IT 160 ms; Scan range *m*/*z* 80-1000. $DdMS^2$; Resolution setting 15,000; AGC target 5x10^4; Maximum IT 100 ms; Top N 10; NCE 30.

Scanning electron microscopy (SEM). Micrographs of the electrodes were taken using a Hitachi TM3030 PLUS tabletop scanning electron microscope operated at an acceleration voltage of 15 kV. Backscattered electrons (BSE) and secondary electrons (SE) were detected to obtain both compositional distribution and topographic information.

Thermogravimetric analysis (TGA). Thermogravimetric analysis (TGA) data were obtained using a Netzsch STA 449 F5 Jupiter instrument. Samples were placed in 40 µL aluminum crucibles closed with aluminum lids and heated from 20 °C to 600 °C (10 °C/min) under a nitrogen flow (25 mL/min).

5.3 Results and discussion

In two recent investigations from our research group, the electrochemical depolymerization of technical lignins in different aqueous solvent systems have been reported, one comprising levulinic acid [104] and another based on a sodium carbonate (Na_2CO_3) aqueous solution. [138] Although γ-valerolactone (GVL) has been faced as a promising sustainable platform for biomass treatment and dissolution, this solvent undergoes a ring-opening reaction depending on the temperature and presence of acids or bases. [269,283] Wong *et al.* [283] investigated the stability of GVL under neutral, acidic, and basic conditions and

Granatier *et al.* [269] studied its stability under pulping conditions. In our investigation, before using GVL as a solvent for electrochemical depolymerization, its stability was assessed. For this purpose, the stability of GVL in combination with Na_2CO_3 as electrolyte was tested under different conditions - room temperature and 60 °C and during electrochemical reactions at different applied currents. It was confirmed that GVL, in combination with Na_2CO_3, undergoes a ring-opening reaction leading to sodium 4-hydroxyvalerate (**Figure S 14**, **Table S 3**), in further discussion referred to as 4-hydroxyvalerate). The percentage of 4-hydroxyvalerate increased by increasing the temperature (**Figure S 15**, **Table S 3**).

At an applied current of −100 mA for 8 h, the ring opening reaction was caused exclusively by the presence of Na_2CO_3 and not by the applied current (**Figure S 16**, **Table S 4**). With longer reaction times (20 and 24 h) and higher currents (reductive ones, such as −150 mA, −200 mA, and oxidative ones such as +200 mA), the concentration of 4-hydroxyvalerate increased (**Figure S 17 - Figure S 19**, **Table S 4**). The highest concentration of 10.0 mol% was achieved after 20 h at an applied current of −100 mA (**Figure S 18**, **Table S 4**). A detailed analysis of the stability is provided in the Supporting Information (SI).

In a previous study conducted by our group, the electrocatalyzed depolymerization of Soda lignin in an aqueous Na_2CO_3 solution resulted in four main products: sodium levulinate, sodium 4-hydroxyvalerate, sodium acetate, and sodium formate. [138] This study served as the basis for our current research, where we strategically utilized the overlap between the depolymerization products and the products from the GLV ring-opening reaction. The aim was to enhance the overall yield of the reaction by selectively inducing the ring opening of GVL, thereby enriching the depolymerization products with 4-hydroxyvalerate. An important observation from the investigation into the electrochemical stability of GVL is the molar ratio of 4-hydroxyvalerate to GVL after 8 h at −100 mA. This ratio was identical to that of the reference reaction conducted without electrochemical intervention, which stands at 2.5 mol%. This equivalence suggests that the ring-opening process of GVL is exclusively attributed to base catalysis under these conditions.

The molar ratio of 4-hydroxyvalerate surpassed that of the reference reaction only when subjected to higher currents or prolonged reaction times. Therefore, we judiciously chose the parameters of −100 mA and an 8 h reaction time for the depolymerization process, since higher currents and/or longer reaction times would excessively promote the

formation of sodium 4-hydroxyvalerate, reducing the influence of depolymerized products in the final product.

The electrochemical depolymerization of Soda lignin in GVL was carried out using a carbon working electrode, platinum counter electrode, and Ag/AgCl (satd. KCl) reference electrode. The reaction setup and possible mechanisms of electron transfer in ECH reaction on the carbon surface are shown in **Figure 26**.

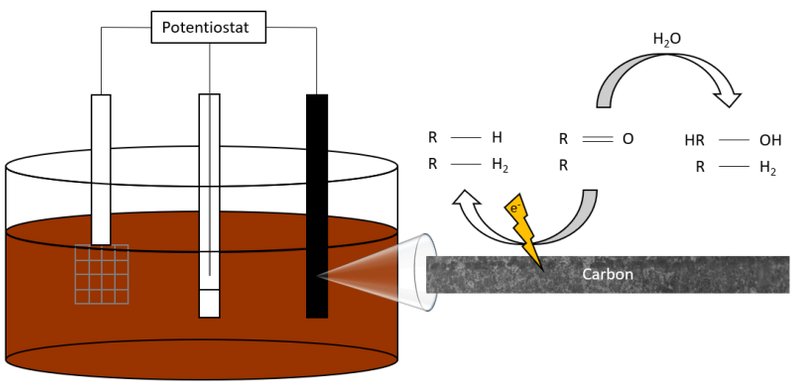

Figure 26. Reaction setup and possible mechanisms of electron transfer in ECH reaction on the carbon surface: electronation–protonation and electrocatalytic hydrogenation. A three-electrode setup consisting of a carbon working electrode, a platinum counter electrode, and Ag/AgCl (saturated KCl) is used for the reaction. The reaction solution consists of 5 M GVL, with a Soda lignin concentration of 3 g L^{-1}. As electrolyte, 1 M Na_2CO_3 is added to the reaction solution.

A current of −100 mA corresponded to a current density of −18 mA/cm^2. However, when observing the SEM micrographs of the carbon electrode (**Figure 27**), the actual surface area was assumed to be significantly larger due to intrinsic porosity.

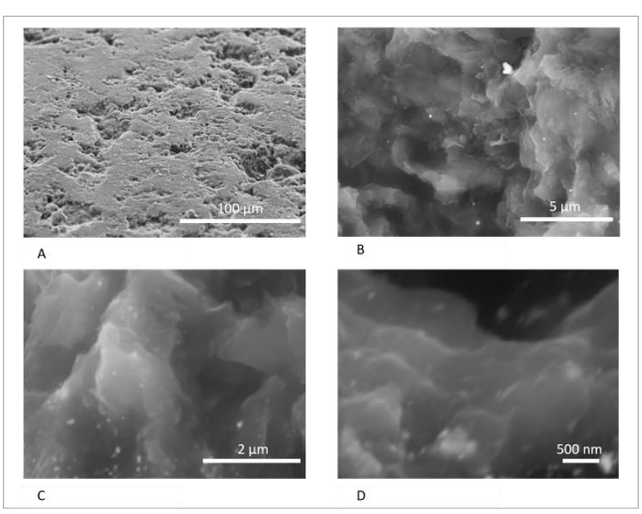

Figure 27. SEM micrographs of the carbon electrode at different areas and magnifications: A x1.0k, B x15.0k, C x40.0k, D x60.0k. The micrographs show an enlarged surface of the electrode, which is caused by its highly porous character.

The chronopotentiometry course at −100 mA is shown in **Figure 28**. At the beginning of the reaction, a potential of −4.1 V was present which was reduced to an average potential of −3.7 V during the reaction. In the first hour, the potential dropped to −3.6 V, slowly increasing to −3.8 V afterwards until the end of the reaction. This indicates that either part of the solvent began to evaporate, or the components of the reaction solution settled on the electrode. Both lead to the fact that a higher potential is necessary to maintain a constant current of −100 mA. During the reaction, the volume of the solution gradually decreased. The water electrolysis process explains this phenomenon, which occurs at high working voltages of E >1.23 V *vs.* RHE and results in formation of hydrogen at the cathode and oxygen at the anode. [316] The remaining water was removed under reduced pressure after the reaction resulting in 1030 mg of a brown solid and 16.5 mL of a remaining liquid. The mass of products after depolymerization was seven times greater than the starting Soda lignin. Accordingly, it can be assumed that the product was a mixture of the depolymerization products of Soda lignin (DL) and the sodium 4-hydroxyvalerate, also generated by the lignin depolymerization process. This hypothesis was further supported by NMR, FTIR, and mass spectrometry.

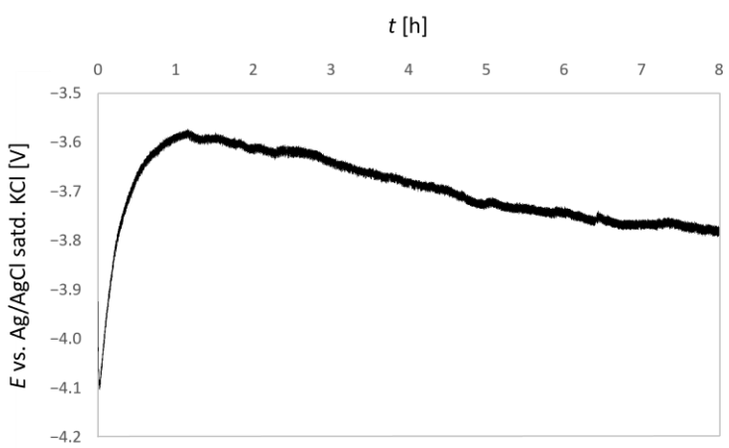

Figure 28. Potential (Ag/AgCl (saturated KCl)) *vs.* time during depolymerization of Soda lignin in GVL at a constant current of −100 mA over a period of 8 h. Within the first hour, the potential decreases, whereupon it constantly increases over the next seven hours.

The starting material Soda lignin was characterized by ^{1}H NMR spectroscopy (**Figure S 4**) and FTIR spectroscopy (**Figure S 5**). The ^{1}H NMR spectrum of the DL (**Figure 29, Figure 30**) shows mainly the signals of 4-hydroxyvalerate and GVL. The ring opening and closing of GVL is an equilibrium reaction in water. For this reason, GVL can also be detected in ^{1}H NMR in D_2O (**Figure 31**). In addition, levulinate signals are observed at 2.81, 2.44, and 2.26 ppm. [138] Moreover, two more singlets at 1.95 ppm and

8.49 ppm can be assigned to acetate and formate. [138] It is assumed that the products are the sodium salts of the carboxylic acids due to the use of Na_2CO_3 as electrolyte since no proton signals are recognizable in the ^1H NMR. These results are consistent with those of our previous study on the depolymerization and dearomatization of lignin in an aqueous Na_2CO_3 medium. [138] The use of an internal standard (100 µL, deuterated methanol (99.8%)) enabled the quantification of the depolymerized products (**Figure S 23**). The composition of the obtained product was found to be 85 mol% sodium 4-hydroxyvalerate, 8 mol% sodium levulinate, 6 mol% sodium acetate, and 1mol% sodium formate.

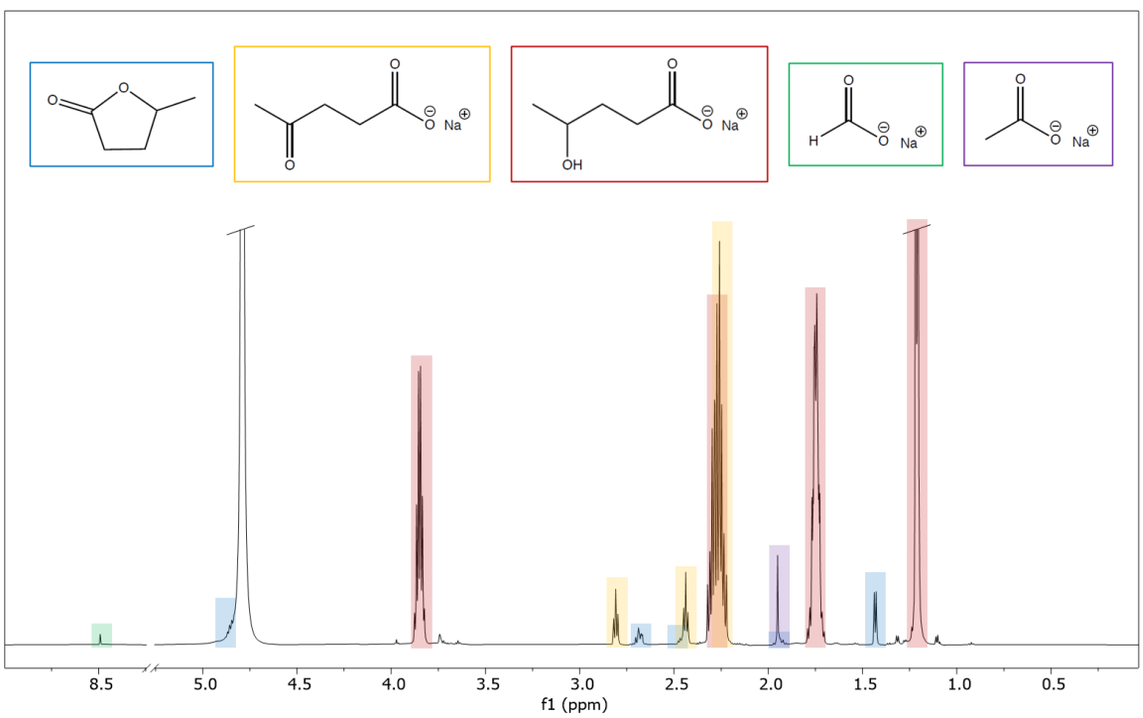

Figure 29. ^1H NMR spectrum (D_2O, 600.13 MHz) of the depolymerization products (DL). Levulinate (yellow), 4-hydroxyvalerate (red), formate (green), and acetate (purple) can be identified as the main products of Soda lignin depolymerization. GVL (blue) is also recognizable because of its equilibrium with 4-hydroxyvalerate in water.

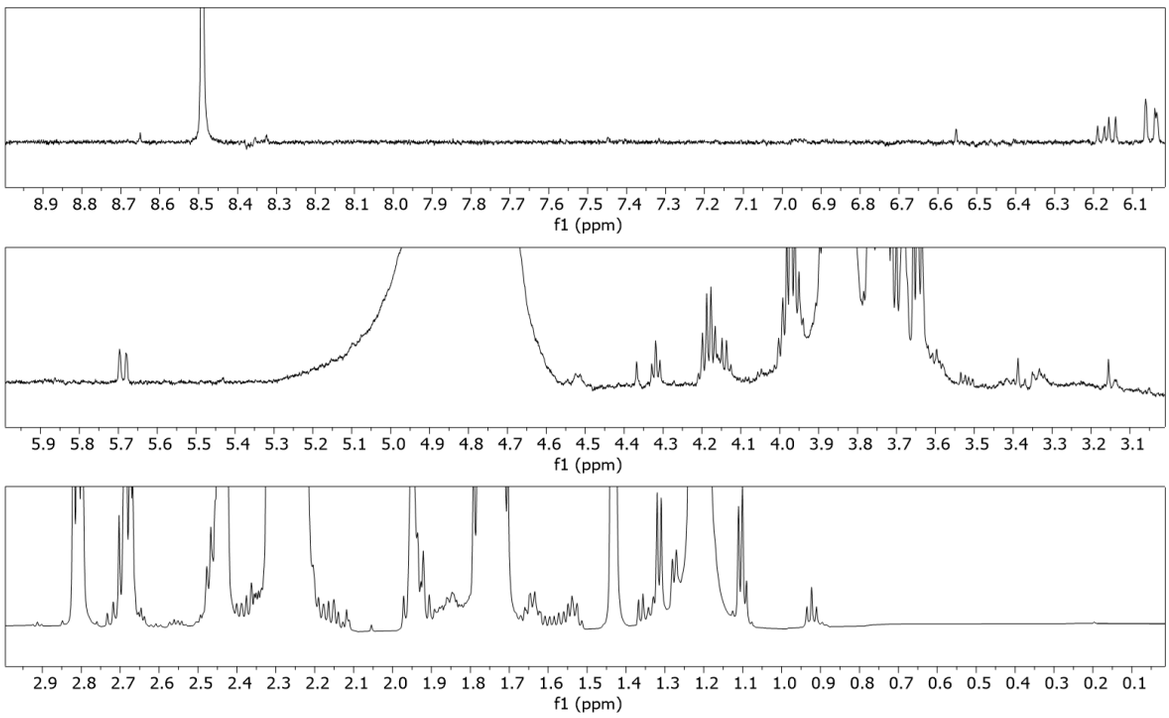

Figure 30. ^{1}H NMR spectrum (D_2O, 600.13 MHz) of the DL - higher magnification.

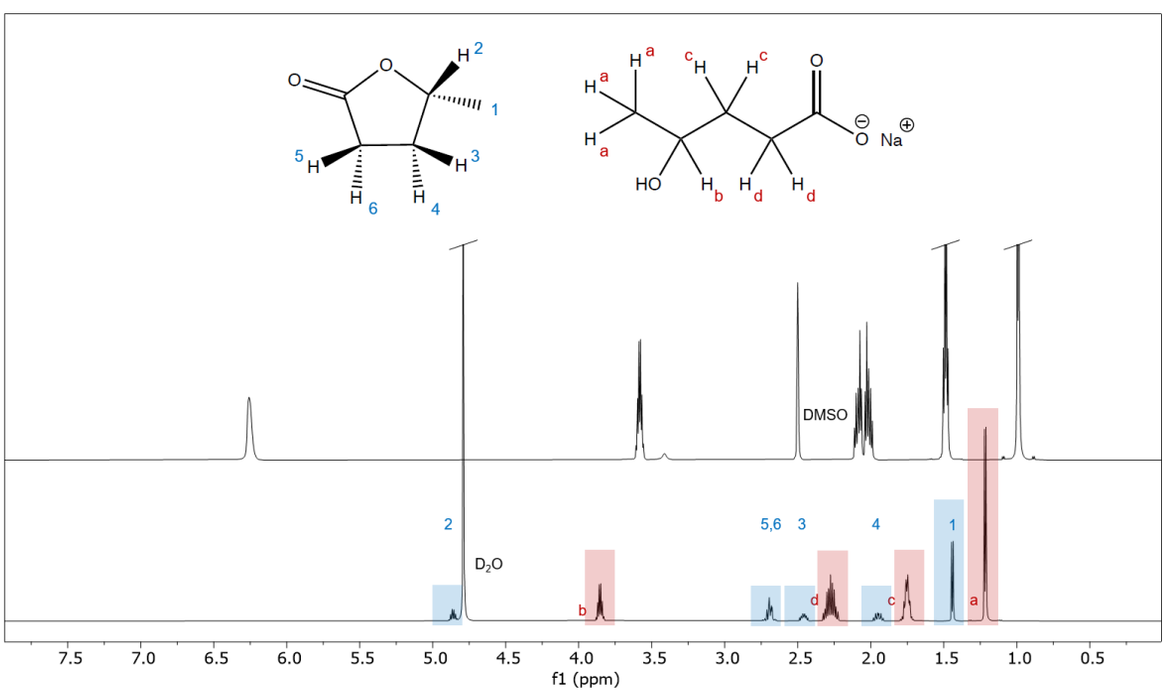

Figure 31. ^{1}H NMR spectra (D_2O (below) and DMSO–d^6 (above), 600.13 MHz) of 4-hydroxyvalerate. A comparison of the measurements of the same product in two different solvents shows the equilibrium reaction between GVL and 4-hydroxyvalerate. In DMSO-d^6, only the signals of 4-hydroxyvalerate (red) are present. In D_2O, on the other hand, GVL (blue) signals are also present. Thus, the ring of GVL is closed again in equilibrium by dissolving sodium 4-hydroxyvalerate in water.

The FTIR spectra of sodium 4-hydroxyvalerate and DL provide insights into their molecular structure. In the FTIR spectrum of sodium 4-hydroxyvalerate (**Figure 32**), OH vibration signals are evident between 3400-3100 cm^{-1}. CH vibration signals are observed

at 2962, 2930, 2916, and 2884 cm^{-1}. Signals at 1562 (antisymmetric stretch vibration) and 1406 cm^{-1} (symmetric stretching vibration) can be associated to the carboxylate group. [272]

This pattern aligns with the trends observed in the ^{1}H NMR spectrum. Similarly, the FTIR spectrum of DL (**Figure 32**) displays OH vibration signals between 3400 and 3200 cm^{-1}, CH vibration signals at 2962, 2930, 2916 and 2872 cm^{-1}, and carboxylate group signals at 1561 and 1406 cm^{-1}. [272] Although the concentration of sodium 4-hydroxyvalerate is higher than the concentration of depolymerization products in DL, additional signals at 1773 and 1707 cm^{-1} indicate the presence of depolymerization products. The signal at 1770 cm^{-1} can be attributed to conjugated ester groups [275] and the signal at 1707 cm^{-1} can be attributed to the carbonyl group of sodium levulinate, indicating that sodium levulinate is the primary product of lignin depolymerization. The remaining functional groups of levulinate correspond to those of 4-hydroxyvalerate.

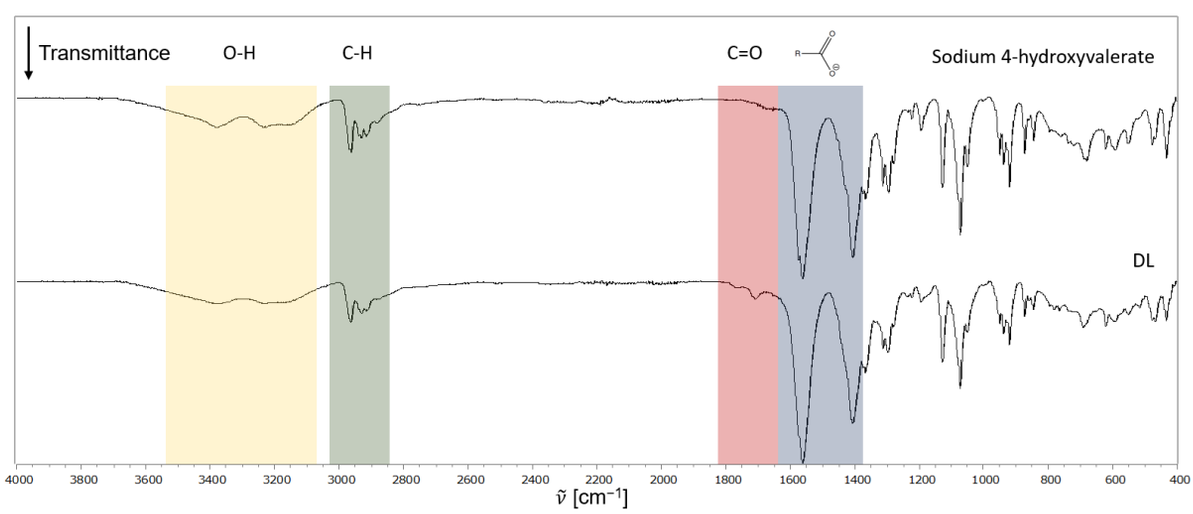

Figure 32. FTIR spectra of sodium 4-hydroxyvalerate and the DL. In the spectrum of sodium 4-hydroxyvalerate the characteristic bands (-OH, -CH and -COO^{-}) are present. The spectrum of the DL shows the characteristic vibrations of the O-H, C-H, C=O, and COO^{-} groups. Sodium levulinate can also be identified as one of the main products contributing to the carbonyl vibration at 1707 cm^{-1}.

Differential scanning calorimetry (DSC) measurements of sodium 4-hydroxyvalerate and DL revealed distinct thermal behaviors. Sodium 4-hydroxyvalerate exhibits a melting point of 146.8 °C, as illustrated in **Figure S 24(A)**. The corresponding thermogravimetric (TG) curve shows two significant steps: a first-stage mass loss of 20.7% (calculated: −20.7 %) attributed to the elimination of -CHO and a subsequent second-stage mass loss of 31.8% (calculated: −31.4%) associated with the release of CO_2. Upon heating to 600 °C, the residual mass of 43.0% (calculated: −44.2%) corresponded to Na_2O. Contrastingly, the DSC measurement of DL (**Figure S 24(B)**) indicates a lower melting point of 127.3 °C. Beyond 250 °C, a series of successive processes was observed, suggesting a complex

decomposition. Simultaneous TGA measurements revealed that after heating to 600 °C, a mass of 45.6% remains.

In the analysis of DL *via* DI-ESI-HRMS in the negative ionization mode, the main product is 4-hydroxyvaleric acid (**Figure S 25(A)**) *m/z* 117.0550, *i.e.* sodium 4-hydroxyvalerate (confirmed in positive mode, not shown).

Levulinic acid (*m/z* 115.0400) was also detected but in a significantly lower intensity (**Figure S 25(B)**). In addition to 4-hydroxyvaleric acid, the dimer (*m/z* 257.0997), trimer (*m/z* 397.1442), and tetramer (*m/z* 537.1883) of 4-hydroxyvaleric acid can be seen on the total ion current spectrum (**Figure S 25(A)**). The peak at *m/z* 99.0447 is identified as GVL, corresponding to the residual solvent.

Subsequent characterization of the hydrolysis product (sodium 4-hydroxyvalerate) and DL products was conducted using liquid chromatography coupled with electrospray ionization high resolution mass spectrometry (LC-ESI(-)-HRMS). The resulting chromatogram (XIC) of the hydrolysis product (**Figure 33(A)**) shows the signal of the 5 µM GVL standard and the product at *m/z* 101.0597 (±5 ppm) in positive mode. The GVL standard showed a peak at 1.51 min which could not be detected in the product. Instead, another peak with the same *m/z* at 1.25 min was observed matching to the $[M\text{-}H_2O]^+$ ion of 4-hydroxyvaleric acid (4-HVA) with <5 ppm. The absence of the peak of GVL in the product indicated a high conversion rate to the product. The $[M\text{-}H^+]^-$ ion of GVL was not detectible in ESI(−) (**Figure 33 (B)**). In contrast a prominent peak in ESI(−) at *m/z* 117.0557 was observed in the product, which accurately matches the molecular mass of 4-HVA ($[M\text{-}H^+]^-$) with a mass deviation <1 ppm (**Figure 33 (C)**). The resulting extracted ion chromatogram (XIC) of the product of depolymerization shows the signal of the $[M\text{-}H^+]^-$ ion of a standard of levulinic acid and the product at *m/z* 115.0400 (±5 ppm) in negative ionization mode (**Figure 34A**).

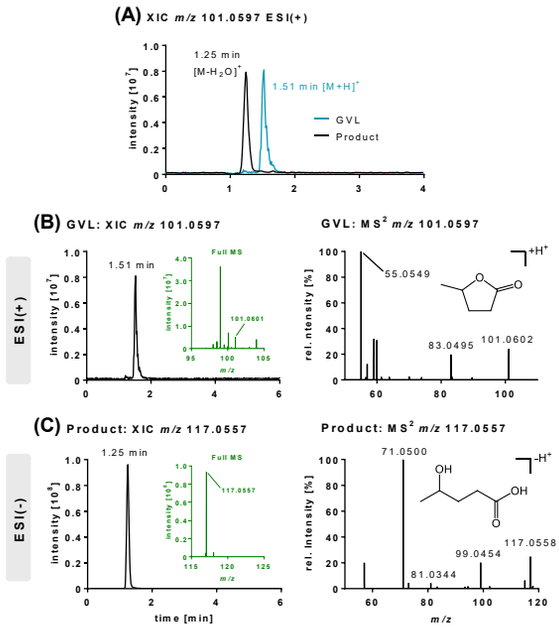

Figure 33. Characterization of GVL and its hydrolysis product 4-hydroxvalerate using LC-MS. (A): Extracted ion chromatogram (XIC) at *m/z* 101.0597 of the $[M+H]^+$ ion of GVL (blue) and the $[M+H-H_2O]^+$ ion of the hydrolysis product in LC-ESI(+)-MS. (B): XIC at *m/z* 101.0597 showing the signal of GVL in addition to its Full MS and MS^2 spectra obtained in ESI(+). (C): XIC at *m/z* 117.0557 showing the signal of the $[M-H^+]^-$ ion of 4-HVA in the hydrolysis product and its Full MS and MS^2 spectra in LC-ESI(−)-MS.

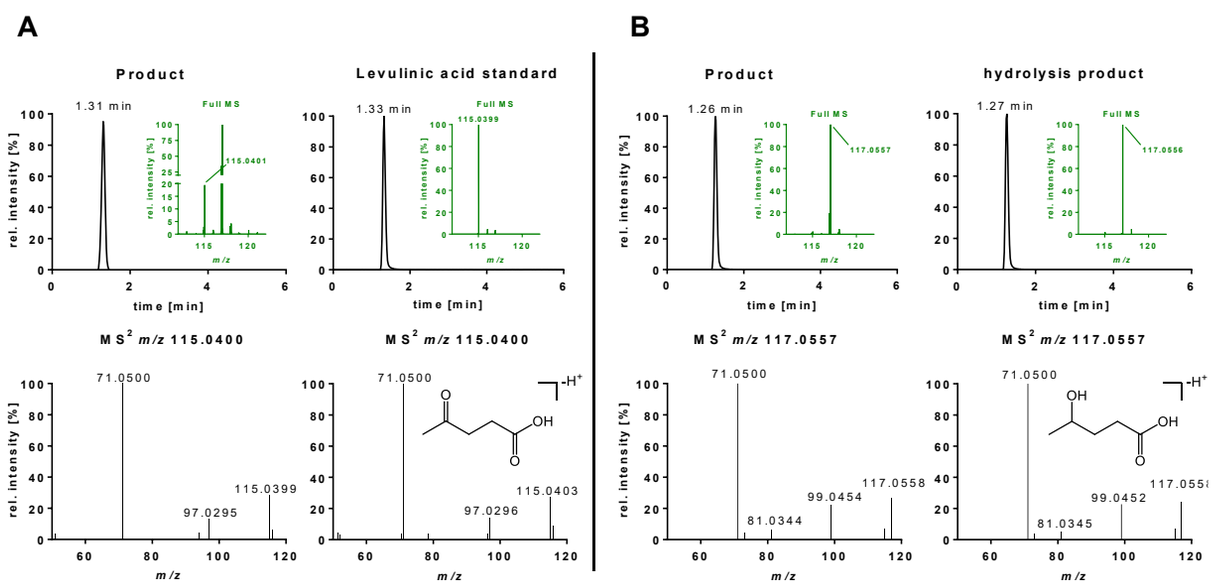

Figure 34. Detection of levulinic acid (A) and 4-hydroxyvalerate (B) in the depolymerization product using LC-ESI(−)-HRMS. Top: extracted ion chromatogram and MS spectrum of A: the depolymerization product and a levulinic acid standard compound at *m/z* 115.0400 and B: the depolymerization product and the hydrolysis product of GVL which was tentatively identified as 4-hydroxyvalerate at *m/z* 117.0557. Bottom: corresponding fragment spectra. The peaks at 1.31 min and 1.26 min in the depolymerization product could be identified as $[M-H^+]^-$ ion of levulinic acid at *m/z* 115.0400 and 4-HVA at *m/z* 117.0557 based on comparison of retention time and fragment spectra to an authentic standard compound or to the hydrolysis product of GVL.

The displayed peak in the product matches with the retention time of the levulinic acid standard. The detection of levulinic acid in the product was supported by comparison of the fragmentation spectra between product and standard. The presence of

4-hydroxyvalerate could also be confirmed by LC-MS (**Figure 34B**) using the hydrolysis product of GVL as reference which was tentatively identified as 4-hydroxvalerate (**Figure 33**). No aromatic compounds could be detected by LC-UV (280 nm).

Sodium levulinate could not be detected in any NMR experiment investigating the stability of GVL (**Figure S 9-Figure S 11** and **Figure S 14-Figure S 19***).* However, with the aid of mass spectrometry, it was possible to detect a small amount of sodium levulinate in the absence of lignin (**Figure 33**). Since sodium levulinate has already been detected as a product during the depolymerization of Soda lignin in an aqueous Na_2CO_3 solution, [138] it can be assumed that in this case, the component is formed from both GVL and Soda lignin. Compared to the other signals of the DL, those of the sodium levulinate are clearly more intense. Hence, sodium levulinate is assumed as the main product of the depolymerization of Soda lignin in GVL and Na_2CO_3 with the help of a carbon working electrode.

Furthermore, it can be assumed that 4-hydroxyvalerate is formed from Soda lignin in addition to levulinate. Hence, both GVL and Soda lignin are sources of 4-hydroxyvalerate, [138] which means that the concentration of 4-hydroxyvalerate from the Soda lignin can be enriched by the solvent GVL.

A techno-economic analysis (TEA) of electrochemical methods for biorefineries has shown that adopting these approaches faces significant economic challenges. In addition to the costs of electricity, starting materials, and solvents, other factors must be considered, including the purchase costs of the reactor, capital costs, depreciation, taxes, and return on investment. [317] Studies like those conducted by Naderi Nasrabadi *et al.*, [317] have shown that electrochemical reactors have not yet achieved the economic efficiency needed for widespread implementation. Nevertheless, there is potential for future growth, particularly through further increases in yield.

Although the recycling of GVL remains a challenge at present, [314] further research is expected to enable its efficient recycling in the future. The potential dual use of GVL in biorefineries – first to extract lignin from biomass and then to depolymerize lignin in the same solution – will enhance overall efficiency. This is because additional purification steps, solvent recycling, and the use of extra solvents and chemicals will no longer be necessary. Furthermore, GVL is advantageous as it can function as both a solvent and a reactant, increasing the yield of 4-hydroxyvalerate and maintaining a more balanced process. To address these economic challenges and achieve up-scaling, it is crucial for research groups in biomass conversion, reactor engineering, and process optimization to collaborate. Equally important is establishing strong partnerships with industry stakeholders. Enhanced collaboration and communication between academic and

industrial partners will facilitate the efficient resolution of obstacles and the development of scalable, economic solutions for lignin depolymerization. [5]

5.4 Conclusion

Biorefinery and electrocatalysis are combined in the bioelectrorefinery concept creating a potential source for valuable bio-based platform chemicals. One possible approach is to use renewable energy to convert lignin into aliphatic organic chemicals, while valorizing γ-valerolactone (GVL) as a *green* solvent medium. This study explored the reductive depolymerization and dearomatization of Soda lignin in GVL, built upon our previous experience with electrocatalyzed dearomatization of lignin in aqueous systems. In a recent work, we have shown that feasibility of dearomatizing lignin in aqueous Na_2CO_3 solutions to produce sodium levulinate, sodium 4-hydroxyvalerate, sodium acetate, and sodium formate as major depolymerization products. Although GVL does not strictly qualify as a reaction-inert solvent, its specific application in ring-opening reactions was emphasized. We observed a pronounced ring opening with increasing temperature, reaction time, and Na_2CO_3 concentration, while GVL remained stable under the applied electrochemical conditions. Ring opening was solely initialized by the Na_2CO_3 electrolyte. In the present work, electrochemical depolymerization and dearomatization of Soda lignin in GVL produced key compounds like sodium levulinate and sodium 4-hydroxyvalerate, in agreement with our previous investigation. The production of 4-hydroxyvalerate out of lignin was particularly interesting and one of the main goals, since we could simultaneously increase the overall yield of this compound by selectively inducing the ring opening of GVL. The successful synthesis of bulk chemicals through lignin depolymerization showcases the methodology's potential in chemical manufacturing, contributing to the expansion of *Green Chemistry* and offering innovative pathways for renewable resource utilization, thus promoting the sustainable evolution of the chemical industry. The obtained products are thoroughly characterized using a broad range of spectroscopic methods like NMR, FTIR and HR-LC MS. NMR spectra furthermore gave access to a quantitative insight into the composition of the products obtained by electrocatalytic depolymerization and dearomatization. This study enhances the bioelectrorefinery concept, offering novel prospects for harnessing renewable resources and contemplating a viable shift away from crude oil as the predominant source of carbon-based chemicals in industries.

5.5 Acknowledgement

We would like to thank University of Wuppertal for the research support. L. M. L. thanks the networking program ‘Sustainable Chemical Synthesis 2.0’ (*SusChemSys 2.0*) for the

support and fruitful discussions across disciplines. Parts of the presented results were realized in research projects with financial support from the participating project partners and the Austrian COMET program (Project InTribology2, No. 906860). The COMET program is funded by the Austrian Federal Government and concerning InTribology by the provinces of Lower Austria and Vorarlberg. We thank Andjelka Ristic for her significant contribution to the DI-ESI-HRMS measurement.

5.6 Disclosure statement

No potential conflict of interest was reported by the author(s).

5.7 Author contributions

Conceptualization, L.M.L., A.S., and B.V.M.R.; Methodology, L.M.L. and S.D.; Investigation, L.M.L. and S.D.; Data Curation, L.M.L., L.M.W, B.B.B, and M.F.; Formal Analysis, L.M.L., L.M.W and M.F.; Writing – Original Draft, L.M.L.; Writing – Review & Editing, L.M.L., B.V.M.R., and A.S.; Supervision, N.H.S, C.W.L, J.B., B.V.M.R. and A.S.

Abstract:

Transitioning from crude oil to renewable sources for carbon-based chemicals is critical for advancing sustainable development. Lignin, a wood-derived biomacromolecule, holds great potential as a renewable feedstock, but efficient depolymerization and dearomatization methods are required to fully unlock its potential. In this investigation, we present a silver-catalyzed aqueous electrocatalytic method for the selective depolymerization and partial dearomatization of Soda lignin under mild, ambient conditions. Utilizing a water/sodium carbonate solvent system and a silver electrode to mediate the electrochemical reduction, we achieved significant lignin depolymerization over reaction times ranging from 5 to 20 h. Analysis by nuclear magnetic resonance (NMR) and high-resolution mass spectrometry (HRMS) revealed sodium levulinate, sodium acetate, and sodium formate as main aliphatic products, alongside various aromatic species in the depolymerized lignin products (DL). This selective conversion of lignin into both valuable aromatic compounds and reactive aliphatic intermediates offers promising opportunities for further synthesis of a wide range of organic chemicals, contributing to the development of a more sustainable and circular economy.

Chapter 6

Silver-Catalyzed Aqueous Electrochemical Valorization of Soda Lignin into Aliphatics and Phenolics

Based on:

Lucie M. Lindenbeck, Silas Brand, Franka Stallmann, Vanessa Barra, Marcella Frauscher, Björn B. Beele, Adam Slabon, and Bruno V. M. Rodrigues

Polymers, **2024**, *16* (23), 3325.

DOI: 10.3390/polym16233325

Electrocatalysis · Lignin · Silver · Depolymerization · Dearomatization

Preface to Chapter 6

Following the demonstration of the electrochemical depolymerization of Soda lignin with a carbon working electrode in both an aqueous sodium carbonate solution (Na_2CO_3/H_2O) [138] and an aqueous gamma-valerolactone (GVL/H_2O) [203] system, the influence of the working electrode on the product distribution was investigated. The Na_2CO_3/H_2O system was deliberately chosen for this purpose to exclude the influence of the GVL ring-opening product 4-hydroxyvalerate.

While carbon, copper, nickel, lead, and platinum have been identified as electrocatalysts for lignin depolymerization, [5] silver has received comparatively less investigation, despite its potential benefits. Silver's high conductivity, catalytic efficiency, and stability make it a promising candidate for electrocatalytic applications. [318–323] Its selective activation of oxygen-containing groups, catalysis of both oxidative and reductive reactions, and facilitation of depolymerization and dearomatization of lignin make it a valuable electrocatalyst. [323] Its low overvoltage potential enables more energy-efficient reactions compared to carbon or copper. [136,324] For the direct investigation of the catalytic effect, the reaction conditions optimized for carbon (highest selectivity, maximum yield) were retained. Soda lignin was dissolved in a 0.1 M Na_2CO_3 solution and depolymerized at a constant current of −175 mA for 20 h. It was observed that the lignin solution underwent complete decolorization when reacting with silver, while carbon exhibited a similar decolorization trend, albeit with retention of a yellowish tone. This color change serves as an indirect indicator of the change in the average molecular weight, with complete decolorization indicating a stronger depolymerization and thus a stronger fragmentation of the lignin structure. This suggests that silver catalyzes depolymerization at a faster rate compared to carbon. Product analysis revealed clear differences between the two catalysts. The utilization of FTIR and DI-HRMS facilitated the discernment of aromatic compounds in the silver-catalyzed products, while carbon promoted complete dearomatization. In the ^1H NMR spectrum (in D_2O) only marginal aromatic signals were perceptible amidst the noise when silver was employed, attributable to the diminished solubility of aromatics in D_2O. While levulinate, acetate, and formate were detected in the presence of silver, 4-hydroxyvalerate formation was not observed. The product yield was also lower than with carbon.

The strong discoloration of the reaction solution with silver suggests that a shorter reaction time might already enable comparable depolymerization. Therefore, the reaction was repeated for 5, 10, and 15 h. This demonstrated that dearomatization occurs over time.

While a reference reaction, without applied current, exhibited the presence of numerous aromatic compounds with high intensity, these compounds underwent a decrease in intensity over time. This outcome demonstrates that silver induces partial dearomatization, a process that can be modulated by the duration of the reaction.

The catalyst selected and the reaction time exert a substantial influence on the product distribution. Complete dearomatization can be accomplished with a carbon electrode, whereas silver facilitates targeted partial dearomatization, a process that can be regulated by adjusting the reaction time.

However, given the lower product yield in silver-catalyzed depolymerization, it may be advantageous to test alternative work-up methods to optimize the efficiency of product isolation and recovery.

Chapter 6 - Silver-catalyzed aqueous electrochemical valorization of Soda lignin into aliphatics and phenolics

6.1 Introduction

The quest for sustainable and renewable sources of organic chemicals has directed significant research attention toward lignin, an abundant macromolecule found in the cell walls of plants. This complex polyphenol is one of the most abundant natural macromolecules, constituting approximately 15–30% of the biomass in vascular plants. Despite its potential as a renewable source of aromatic compounds, its complex and intricate structure presents a major challenge in its depolymerization and subsequent conversion into valuable chemicals [76,254]. Unlike cellulose or hemicellulose, lignin has a highly crosslinked network, which hinders its breakdown using conventional thermal or chemical processes. These challenges have historically limited lignin's industrial application to low value uses such as combustion for energy production in pulp mills, but advances in catalysis are now cracking new pathways for its valorization [76,138,254,325].

Traditionally considered a waste product in the pulp and paper industry, lignin holds vast potential as a feedstock for valuable aromatic compounds [76,104,254]. In this context, electrocatalysis has emerged as a promising approach for lignin valorization, most specifically its depolymerization, offering significant advantages over traditional methods [104,138,145,325,326]. Conventional methods for lignin depolymerization, such as pyrolysis and hydrogenolysis, operate under extreme conditions of temperature and pressure, which often lead to a wide distribution of products with limited selectivity. As a result, there is growing interest in developing milder, more selective processes, such as Soxhlet extraction and reflux, [327] and planetary ball milling, [324] which also offer the potential to produce more desirable products with targeted compositions. Similarly, electrocatalysis is another technique that enables lignin depolymerization under milder conditions, [104,138] with the potential for greater control over reaction pathways. This method minimizes energy input and reduces the likelihood of side reactions that lead to high-molecular-weight byproducts, enabling more selective conversion of lignin into smaller, more valuable molecules [76,104,136,254].

One of the key benefits of electrocatalysis is its ability to operate at lower temperatures and pressures compared to conventional thermal or chemical processes, which often require harsh conditions and can lead to unwanted by-products. [325] The

successful valorization of lignin would represent a dual opportunity: reducing reliance on fossil-based feedstocks for chemical production while also creating economic value from what is currently considered a low-value byproduct of the pulp and paper industry. Converting lignin into high-value chemicals aligns with the principles of a circular bioeconomy, addressing the need for sustainable and renewable sources of carbon-based materials. [326] Additionally, electrocatalytic methods can be finely tuned by adjusting parameters, allowing for greater control over the reaction pathways and product selectivity. The use of renewable electricity further enhances the sustainability of this approach, reducing reliance on fossil fuels and minimizing the environmental impact. Consequently, electrocatalysis holds great potential for transforming lignin into a range of useful chemicals and fuels in a more efficient and eco-friendly manner. [325,326]

In a recent study, we demonstrated the efficacy of carbon as an electrocatalyst in achieving selective depolymerization and full dearomatization of lignin in aqueous medium under reductive conditions, leading to valuable aliphatic compounds instead of aromatics. [138] Through a systematic investigation, a current of −175 mA and a reaction time of 20 h were established as the optimal parameters for Soda lignin depolymerization/dearomatization, when carbon was used as an electrocatalyst. This previous work not only highlighted the feasibility of utilizing lignin as a resource for aliphatic organic chemicals but also set the stage for exploring alternative electrocatalysts to further enhance the process. Building on this foundation, we have turned our attention to silver as a potential electrocatalyst. This transition metal has garnered significant attention as an electrocatalyst due to its exceptional electrical conductivity, catalytic efficiency, and relatively low cost compared to other noble metals like platinum. [318–323] Silver stands out among electrocatalysts due to its unique ability to selectively activate oxygen-containing functional groups while maintaining stability across a variety of electrochemical conditions. Its ability to engage in both reductive and oxidative transformations makes it particularly suited for biomass conversions where complex multifunctional molecules, like lignin, are involved. [323] Compared to other materials, silver's interaction with aromatic groups in lignin may facilitate not only depolymerization but also selective partial dearomatization, a crucial step in producing valuable aliphatic intermediates. Furthermore, its relatively low overpotential for electrochemical reductions suggests it can drive these reactions with greater energy efficiency compared to other catalysts like carbon or copper. [136,324] Mechanistic studies on silver containing catalysts for lignin depolymerization however are scarce and limited for example to silver-copper oxide [328] or Ag_2S@CdS redox catalysts used in photodegradation of lignin [329]. Regardless of that, its unique surface properties facilitate various electrochemical reactions, making it a

versatile material for applications in fuel cells [330–332], batteries [333,334], and the reduction of carbon dioxide to valuable chemicals [333,335]. The high surface area of nanostructured silver enhances its catalytic performance, providing a larger number of active sites for reactions [319,336].

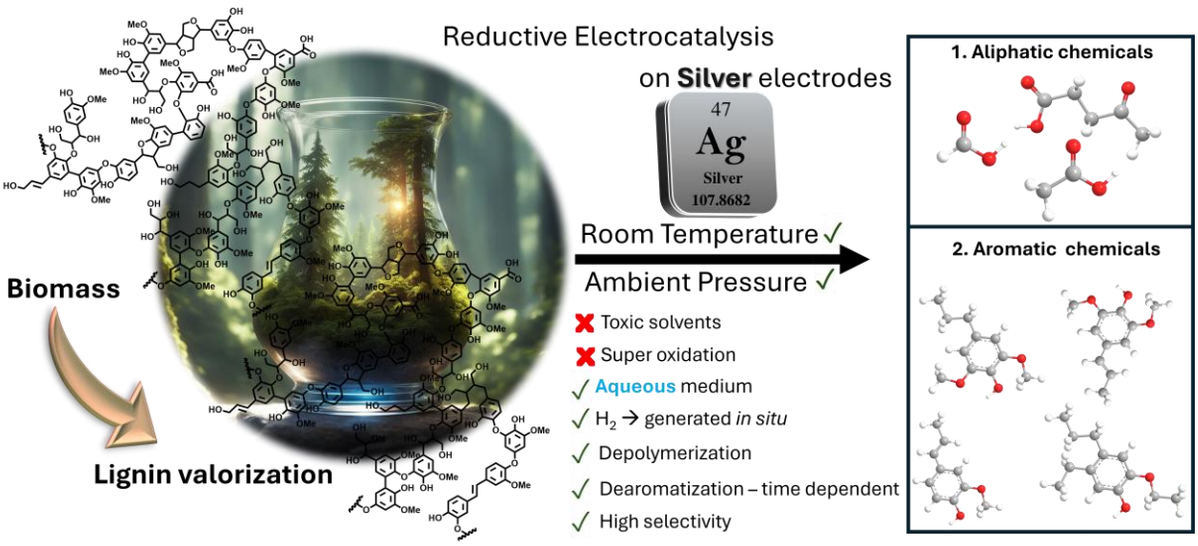

Scheme 3. Schematic representation of the silver-catalyzed electrocatalytic depolymerization and partial dearomatization of Soda lignin in an aqueous sodium carbonate medium. The process involves the application of a constant current (−175 mA), driving the electrochemical reduction of lignin at ambient temperature and pressure. The selective cleavage of lignin results in the formation of both aliphatic compounds (*e.g.*, sodium levulinate, sodium formate, and sodium acetate) and aromatic species, which are extracted using ethanol as a solvent. The mechanism highlights the role of silver as an electrocatalyst in enhancing product distribution and selectivity compared to previous systems.

In this follow-up study, we investigate the use of silver as an electrocatalyst in the reductive depolymerization of lignin towards organic chemicals, both aliphatics and phenolics (**Scheme 3**). Our objectives centered on the comparison between the obtained products using a silver electrode with those obtained from carbon electrodes [138,203], while assessing the influence of silver on the product distribution and setting the grounds to understand the underlying mechanisms driving the enhanced reactivity. By leveraging the catalytic properties of silver, we aimed to achieve higher yields of valuable organic chemicals and further our understanding of the fundamental processes involved in lignin electrocatalysis.

6.2 Materials and methods

6.2.1 Materials

Soda lignin was obtained from WAT Venture Sp. z o.o., Poland, which was extracted from the hardwood black liquor of a sulfur-free pulp production in a pilot plant. A silver wire (0.5 mm diameter, 99.9% purity) from AlfaAesar was used as working electrode. Sodium carbonate (≥99.5%, ACS reagent, Merck (Darmstadt, Germany)), Methanol (MeOH, LC-

MS grade, Fisher Scientific (Schwerte, Germany)), and ethanol (puriss. p.a., absolute, ≥99.8% (GC), Sigma Aldrich) were used as received. All aqueous solutions were prepared with ultrapure water obtained from a Millipore system.

6.2.2 Lignin depolymerization

All electrochemical reactions were carried out using an ATLAS 1131 Electrochemical Unit & Impedance Analyser (Atlas Sollich). In a standard experiment, Soda lignin was initially dissolved at a concentration of 3 $g \cdot L^{-1}$ in 5 mL of a 1 M aqueous sodium carbonate solution. Subsequently, 45 mL of water was added to this mixture. The electrochemical depolymerization process was conducted with a three-electrode system: a silver wire working electrode, a platinum wire counter electrode, and an Ag/AgCl (satd. KCl) reference electrode. Chronopotentiometry was performed with a constant current of −175 mA for different reaction times (up to 20 h). All experiments were conducted at room temperature and ambient pressure. Post-reaction, water was removed under reduced pressure, and the resulting solid was dried under the same conditions. The dried solid was then suspended in ethanol and stirred vigorously for 1 h. The remaining residue was filtered off, and ethanol was evaporated from the filtrate under reduced pressure, yielding a white solid.

0 h: FTIR (Diamond-ATR): ν [cm^{-1}] = 3313 (O-H, w), 2961 (C-H, w), 2918 (C-H, w), 2873 (C-H, w), 2850 (C-H, w), 1717 (C=O, m), 1700 (C=O, m), 1652 (m), 1594 (C=C, m), 1443 (C=C, m), 1346 (s), 1258 (C-O, s), 1015 (C-O-C, C-O-H, s), 877 (m), 866 (m), 835 (C-H, s), 798 (CH, s), 668 (s), 400 (m).

5 h: FTIR (Diamond-ATR): ν [cm^{-1}] = 3566 (O-H, w), 2918 (C-H, w), 2873 (C-H, w), 2851 (C-H, w), 1772 (w), 1733 (C=O, m), 1717 (C=O, m), 1700 (C=O, m), 1652 (m), 1589 (C=C, m), 1521 (C=C, m), 1374 (s), 1349 (s), 1249 (C-O, m), 948 (m), 878 (m), 837 (C-H, s), 767 (m), 700 (C-H, m), 668 (s), 420 (s).

10 h: FTIR (Diamond-ATR): ν [cm^{-1}] = 3310 (OH, w), 2917 (CH, m), 2850 (CH, m), 1728 (C=O, m), 1595 (C=C, m), 1565 (m), 1347 (C-H, s), 1260 (C-O, s), 1076 (C-O, s), 1049 (s), 982 (s), 833 (C-H, s), 767 (m), 654 (s), 569 (s).

15 h: FTIR (Diamond-ATR): ν [cm^{-1}] = 3350 (O-H, w), 2954 (C-H, w), 2916 (C-H, w), 2872 (C-H, w), 2850 (C-H, w), 1733 (C=O, m), 1717 (C=O, m), 1700 (C=O, m), 1652 (m), 1635 (m), 1564 (C=C, m), 1456 (C-H, m), 1048 (s), 1012 (C-O-C, C-O-H, s), 833 (C-H, s), 781 (m), 668 (s), 400 (m).

20 h: FTIR (Diamond-ATR): ν [cm^{-1}] = 3399 (O-H, w), 2962 (C-H, w), 2917 (C-H, w), 1717 (C=O, m), 1700 (C=O, m), 1591 (C=C, m), 1564 (C=C, m), 1441 (C-H, m), 1259 (C-O, s), 1078 (s), 1015 (C-O-C, C-O-H, s), 832 (C-H, s), 798 (C-H, s), 668 (s), 404 (m).

6.2.3 Characterization

Nuclear magnetic resonance spectroscopy (NMR). ^{1}H NMR spectra were obtained using a Bruker Avance III 600 NMR instrument at a temperature of 300 K in deuterium oxide (D_2O). The following sample probes were employed: a 5 mm broadband inverse probe with automatic frequency determination, a 5 mm QNP probe, and a 5 mm broadband inverse probe. Chemical shifts were referenced against tetramethylsilane (Me_4Si). Unless otherwise specified, 16 scans were recorded with a 1.0-second delay between each scan for the ^{1}H NMR spectra.

Vibrational spectroscopy (FTIR). Fourier-transform infrared (FTIR) spectra were measured using a Nicolet iS5 spectrometer, equipped with an iD5 diamond attenuated total reflection (ATR) unit.

Direct infusion (DI) ESI-HRMS. Depolymerized lignin samples were dissolved in methanol, ultrasonicated for 30 min and centrifuged for 10 min (14,000 rpm). High-resolution mass spectrometry (HRMS) was used as an advanced analytical method to gain the structure information of degradation products of lignin. MS and MS^n spectra were obtained using an Orbitrap-IQX high-resolution mass spectrometer (ThermoFisher Scientific, Bremen, Germany), equipped with an ESI source. ESI-MS analyses were carried out in ESI(−) and ESI(+) mode. The solutions were infused into the ESI source *via* direct infusion (DI) at a rate of 5 μL min^{-1}. Typical spray and ion optics for negative mode conditions were the following: source voltage, 3.0 kV; sheath gas flow rate, 8 arb; capillary temperature, 275 °C; capillary voltage, –50 V; tube lens voltage, –130 V. Fragmentation and interpretation was done based on negative ionization mode, positive ionization mode was used for additional confirmation. Xcalibur version 2.0.7 and Mass Frontier version 8.0 (ThermoFisher Scientific, Bremen, Germany) software were used for data processing and evaluation.

6.3 Results and discussions

In this work, we extended our investigation toward the electrochemical reductive depolymerization of Soda lignin [138,203], by using silver as an electrocatalyst. This process involved dissolving Soda lignin in an aqueous sodium carbonate solution, followed by an electrocatalytic reaction aimed at the simultaneous depolymerization and partial dearomatization of lignin to produce valuable aliphatic products. Prior to its utilization as an electrocatalyst, the stability of the electrode was evaluated through cyclic voltammetry (CV) (**Figure S 26**) in a lignin solution. No evidence of electrode oxidation was discerned, thereby indicating that the electrode remains stable under the chosen conditions. The choice of −175 mA as the applied current was based on previous work, where this current

was shown to be the optimal one. [138] Following the depolymerization process, the resulting depolymerized lignin (DL) products were extracted through solid–liquid extraction using ethanol as the extractant. Ethanol was carefully chosen due to its specific incompatibility with our electrolyte, sodium carbonate. This selection minimized unwanted interactions between the extractant and the electrolyte, facilitating a cleaner separation of the products. Additionally, ethanol offers several practical benefits for our extraction process. One key advantage is its potential for reuse, allowing for repeated extractions without significant loss of efficacy. Moreover, ethanol is regarded as a safe and environmentally friendly solvent, recognized by CHEM21 for its sustainable profile in chemical processes. [337]

The dissolution of lignin in an aqueous sodium carbonate solution results in the formation of a dark brown solution (**Figure 35**, 0 h). It is well established that the reaction time and applied current exert a significant influence on the decolorization of the lignin solution during the process. [138] In earlier studies, the extent of decolorization was employed as an indirect indicator of depolymerization. [138,261] The decolorization of the lignin solution during the reaction is readily apparent. At the completion of the reaction, a solution that is entirely devoid of color and transparent is observed. Additionally, the volume of the reaction mixture undergoes a reduction over the course of the reaction, which can be attributed to water splitting (E >1.23 V *vs.* RHE). [316]

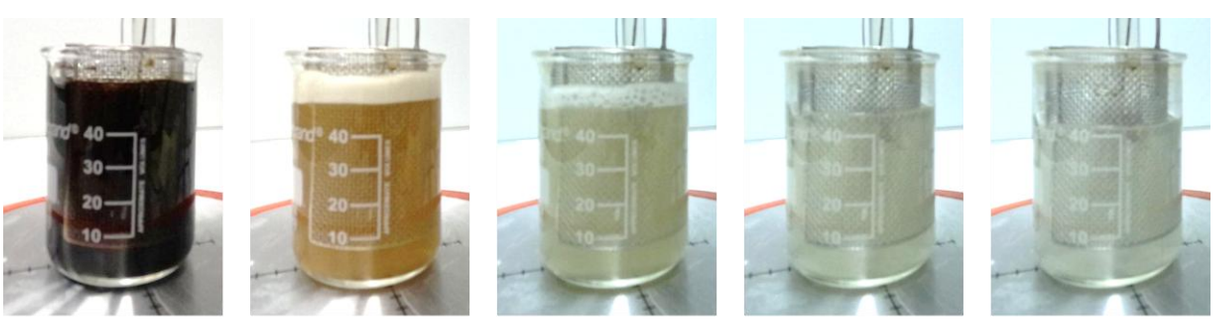

Figure 35. The color of the solution changes during the depolymerization process in a time-dependent manner, becoming clearer as the reaction progresses. This observation serves as an indirect indicator of the extent of depolymerization.

The time-dependent reaction yields (**Table 11**) showed an increase throughout the depolymerization process, from 5 to 20 h. In this case, the yield represents the fraction of depolymerization products (DL) that are ethanol-soluble, relative to the mass of the starting Soda lignin. Notably, in the reference reactions (Soda lignin powder and 0 h), products could also be extracted with ethanol, but their yields were significantly lower compared to the reactions where electrocatalysis was employed.

Table 11. Yields of depolymerization products (DL) relative to the mass of products obtained after ethanol extraction, compared to the initial mass of Soda lignin. All reactions were carried out at room temperature and ambient pressure with a constant current of −175 mA. The yield from Soda lignin corresponds to the ethanol-soluble fraction of untreated Soda lignin (*i.e.*, without electrocatalysis). The yield at 0 h refers to the ethanol-soluble fraction of Soda lignin dissolved in a water/sodium carbonate solution and left for 20 h without undergoing electrocatalysis.

Duration	Soda Lignin	0 h	5 h	10 h	15 h	20 h
Yield [wt%]	7	6	13.4	21.8	18.33	18.35

After 10 h a slight decline in yield is observed. It is postulated that this phenomenon may be attributed to the extensive depolymerization of lignin, which may result in the formation of small volatile products. Given that the reaction is conducted in an open system, these volatile products may be lost, which may explain the observed decrease in yield after 10 h.

NMR spectroscopy is established as a non-invasive and fast spectroscopic method for characterizing both lignin structural motifs [263,338–341] and valuable depolymerization products. [104,138,203] Using ^{1}H NMR spectroscopy we observe a decrease of aromatic product with time as well as occurrence of characteristic resonances of three main depolymerization components: sodium levulinate, sodium formate, and sodium acetate (**Figure 36**).

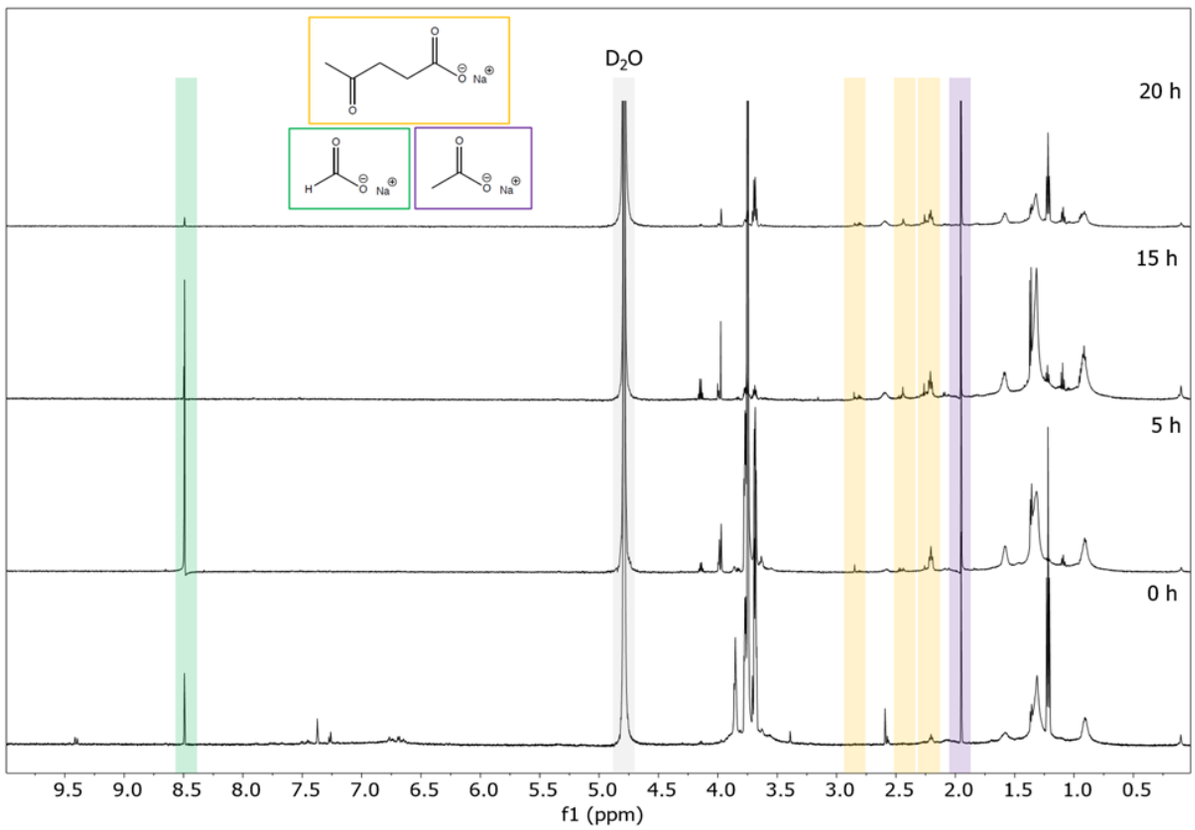

Figure 36. ^{1}H NMR spectra (D_2O, 600.13 MHz) of DL for different reaction times: 0 h, 5 h, 15 h, and 20 h. Levulinate (yellow), formate (green), and acetate (purple) could be identified as main aliphatic components.

In our previous work, in which carbon was used as an electrocatalyst for the depolymerization of Soda lignin, sodium 4-hydroxyvalerate was also identified as a major organic aliphatic product. [138] It was assumed that gamma-valerolactone (GVL) was present as an impurity in the starting lignin, as this solvent is often used to extract lignin from wood [271]. Therefore, sodium 4-hydroxyvalerate would result from the alkaline-catalyzed ring-opening of GVL. The absence of this product in the DL products indicates that silver, as an electrocatalyst, may have played a role throughout the reaction, not preserving this aliphatic compound in the final products but instead converting it into smaller fractions. Since no methanol was detected in these experiments, we can confirm that the depolymerization does not follow the Kolbe pathway in our catalyst system. [268]

FTIR spectroscopy is a versatile, non-destructive analytical technique that provides information on functional groups with in a sample. It is widely used in various scientific fields, such as characterizing modern nanocomposite materials [342], elucidating structural motifs in different lignin types [343], and serving as a rapid method for monitoring lignin decomplexation reactions [138,203,344–346].

Figure 37 and **Figure 38** exhibit the FTIR spectra of the DL products obtained through different depolymerization times. The full range Spectrum (**Figure 37**) shows that

O-H stretching vibrations are evident between 3600 and 3100 cm^{-1}, while C-H stretching vibrations are observed at 2961, 2918, 2873, and 2850 cm^{-1}. Most of the signals in the spectrum appear below 1800 cm^{-1} (**Figure 38**). A signal at 1730 cm^{-1} is attributed to carbonyl (C=O) stretching vibrations. Peaks at 1590 and 1443 cm^{-1} could indicate the presence of C=C double bonds. The signal at 1113 cm^{-1}, assignable to C-O stretching vibrations, originates from ether bonds. Prominent signals around 1015 cm^{-1} suggest C-O-H and C-O-C stretching vibrations. C-H deformation vibrations at 833 cm^{-1} point to the presence of aromatic compounds which are present in DL as well as in the reference reaction. [275]

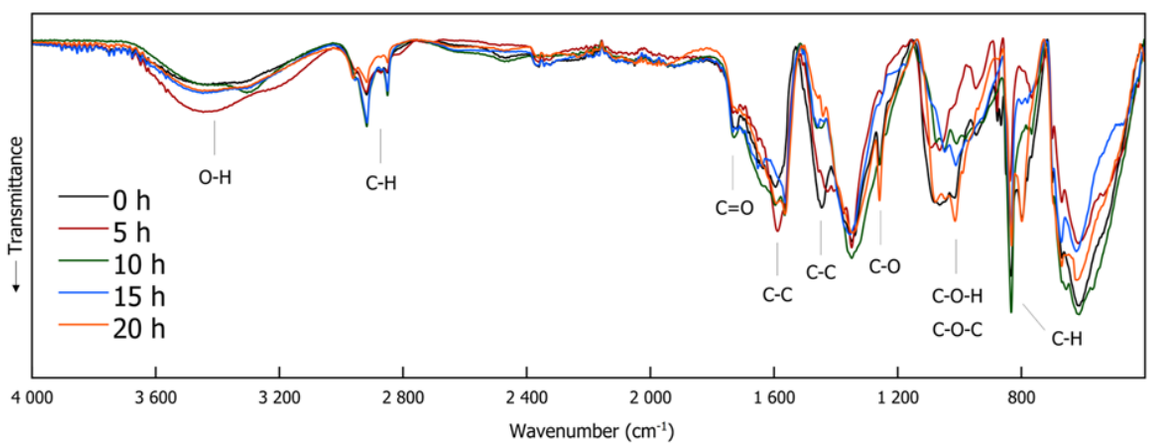

Figure 37. FTIR spectra of DL for different reaction durations (0 h, 5 h, 10 h, 15 h, and 20 h).

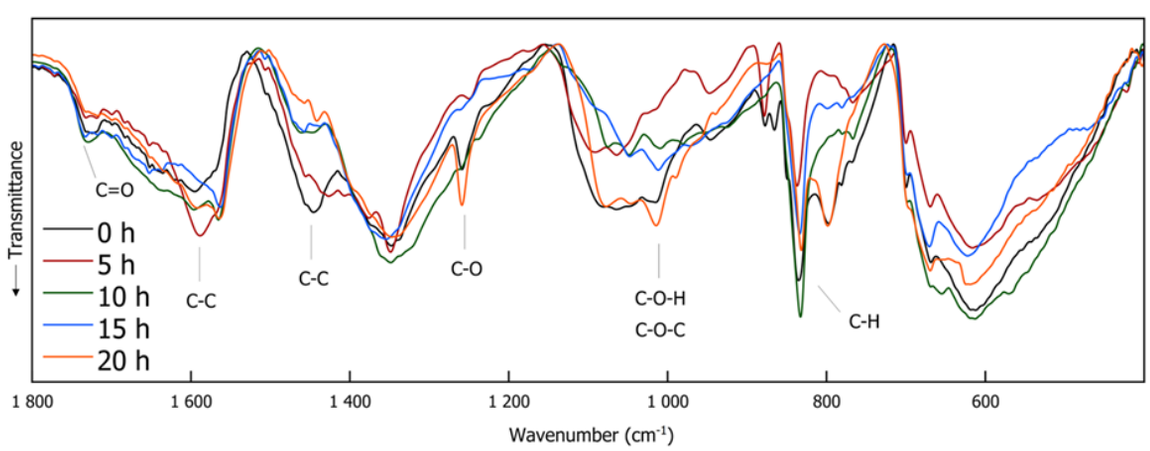

Figure 38. FTIR spectra of DL for different reaction durations zoomed in the region between 1800-400 cm^{-1} (0 h, 5 h, 10 h, 15 h, and 20 h).

Lignin depolymerization is widely acknowledged to be a process with inherently low selectivity, producing a broad array of products [10]. As a result, the characterization of the extracted compounds often reveals a diverse spectrum of chemical species. This complexity also poses challenges in the precise quantification of the individual compounds, which in

turn complicates the determination of critical reaction parameters such as yield and selectivity toward specific target molecules. The heterogeneity of the product mixture makes it difficult to pinpoint exact quantities and proportions of each compound, limiting our ability to fully optimize the depolymerization process. To gain a deeper understanding of the composition of the DL products, high-resolution mass spectrometry was employed for direct injection analysis. This technique allowed for the identification of the major aromatic compounds (**Table 12**). One of the primary motivations for utilizing reductive fractionation in this study was to avoid overoxidation and undesirable condensation reactions, which can occur during lignin depolymerization [104,136,347].

Table 12. Main phenolic products of depolymerization identified by direct infusion (DI) ESI-HRMS.

m/z	121.0292	137.0272	149.0605	151.0400	165.0193
Chemical Structure	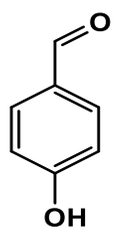	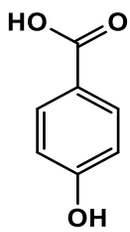	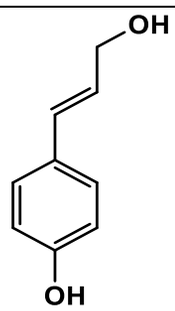	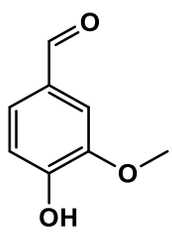	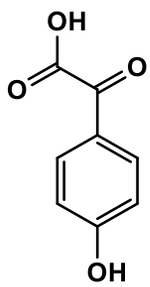
Name	4-hydroxy-benzaldehyde	4-hydroxy-benzoic acid	(E)-4-(3-hydroxyprop-1-en-1-yl)phenol	4-hydroxy-3-methoxybenz-aldehyde	2-(4-hydroxy-3-methoxyphenyl) -2-oxoacetic acid
m/z	165.0552	189.0915	193.0504	195.0297	195.0661
Chemical Structure	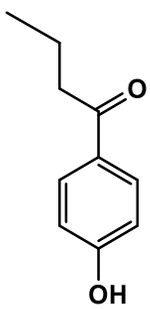	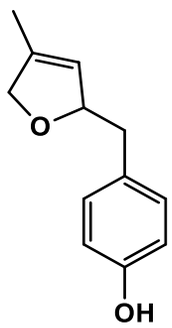	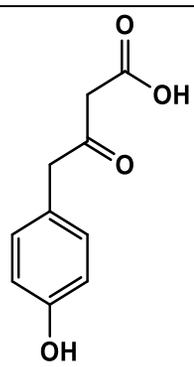	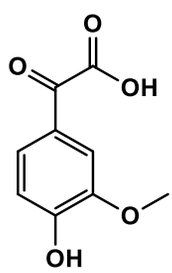	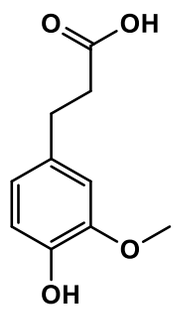
Name	1-(4-hydroxyphenyl) butan-1-one	4-((4-methyl-2,5-dihydro-furan-2-yl)-methyl)phenol	4-(4-hydroxyphenyl)-3-oxobutanoic acid	2-(4-hydroxy-3-methoxyphenyl) -2-oxoacetic acid	3-(4-hydroxy-3-methoxyphenyl) propanoic acid

These side reactions often lead to the formation of recalcitrant, high-molecular-weight by-products that are difficult to valorize. By applying a reductive approach, we were able to mitigate these issues and primarily obtained products rich in aryl ether and phenolic functional groups (**Table 12**).

Silver-catalyzed aqueous electrochemical valorization of Soda lignin into aliphatics and phenolics

Previous studies have demonstrated that in the *late-stage catalytic conversion* of lignin, the lignin structure undergoes targeted breakdown toward the end of the depolymerization process, often resulting in the formation of a higher yield of monomeric and dimeric compounds. [104] This stage typically involves catalytic strategies that suppress undesired re-polymerization and condensation reactions, which can otherwise limit the yield and functionality of the resulting lignin-based feedstock. In alignment with these findings, our approach resulted in the production of not only lignin monomers but also lignin dimers (**Table 12**). These compounds closely resemble those typically obtained from reductive catalytic fractionation (RCF), which is known to produce a low-molecular-weight, highly functional lignin oil. [348,349] The presence of such a product profile suggests that our process avoids excessive condensation, yielding a lignin oil that is both chemically versatile and amenable to further refinement.

Table 13 presents the relative intensity of phenolic products as a function of depolymerization time.

Table 13. Relative intensity of phenolic products as a function of depolymerization time.

m/z	0 h	5 h	10 h	15 h	20 h
121.0292					
137.0272					
149.0605					
151.0400					
165.0193					
165.0552					
189.0915					
193.0504					
195.0297					
195.0661		-	-	-	-
Intensity	maximum	medium	low	-	-

It can be observed that both the intensity and the presence of certain aromatic compounds decrease as the reaction progresses, indicating that lignin dearomatization is time-dependent. This result is consistent with our previous work [138], which showed that dearomatization is influenced not only by time but also by the applied current.

Figure 39 provides a comparison between the DL products obtained in this work to previous one where Soda lignin, as well as Kraft lignin, have been also depolymerized under electrochemical reductive conditions.

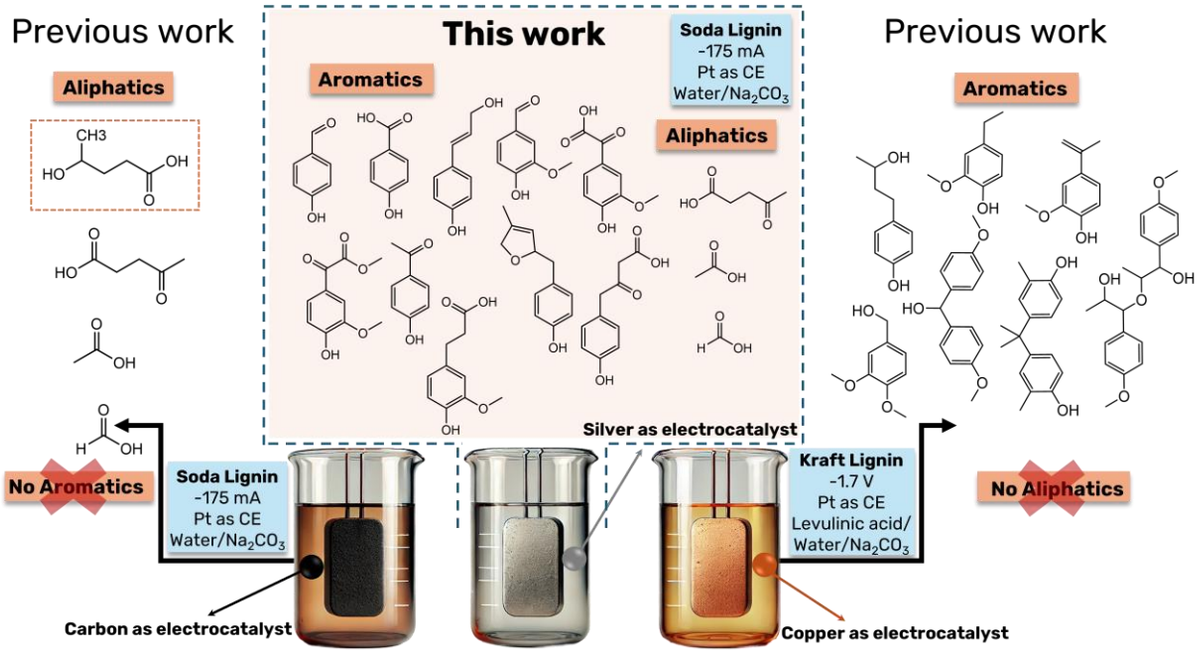

Figure 39. Comparison DL products obtained in the current study with those from previous experiments, where Soda lignin and Kraft lignin were subjected to electrochemical reductive depolymerization under varying conditions [104,138]. This figure highlights the impact of using different electrocatalysts (silver, carbon, copper) and reaction parameters (current, time, and electrolyte composition) on the product distribution. The comparison illustrates how the choice of electrocatalyst significantly influences the selectivity towards aliphatic and aromatic compounds, with silver showing a broader range of products compared to previous studies using carbon and copper.

In our pioneering work on the electrochemical depolymerization of lignin under reductive conditions, copper was employed as the electrocatalyst, with Kraft lignin as the substrate and a solvent system composed of levulinic acid and water. [104] The electrolyte, Na_2CO_3, was the same as in the present study. Unlike the current work, which utilizes chronopotentiometry, the previous study used chronoamperometry at a fixed potential of −1.7 V for 20 h. For comparison, the resulting current density in that study was 9 mA cm^{-2}, considerably lower than the −175 mA employed here. The earlier study primarily identified aryl ether and phenolic groups in the depolymerized lignin (DL) products, with no aliphatic compounds detected (**Figure 39**). In contrast, in another earlier work, using carbon as the electrocatalyst and Soda lignin as the substrate, no aromatic compounds were observed after 20 h of depolymerization at −175 mA in a water/sodium carbonate solvent system. [138] Instead, the reaction was highly selective towards four major aliphatic products: sodium levulinate, sodium 4-hydroxyvalerate, sodium formate, and sodium acetate. Except for sodium 4-hydroxyvalerate, all these aliphatic compounds have also been identified in the present work. However, the presence of aromatic compounds in the present work suggests reduced selectivity when silver was employed as the electrocatalyst.

The observed differences in product distribution when copper, carbon, or silver are employed as electrocatalysts could be attributed to the distinct catalytic properties and surface interactions of these materials. Copper, known for its strong catalytic activity in reductive processes, tends to favor the cleavage of aryl ether bonds, leading to a higher yield of phenolic compounds in the depolymerized lignin. [104] Although silver is often associated with high selectivity in catalytic reactions [350,351] due to its unique electronic properties, it seems to facilitate both aromatic and aliphatic product formation in this case. This could be attributed to silver's affinity for oxygen-containing functional groups, [352] which would favor the simultaneous cleavage of different bond types within lignin. Thus, the choice of electrocatalyst significantly impacts product distribution, with silver showing a broader range of products, including both aromatic and aliphatic compounds.

6.4 Conclusions

This study successfully demonstrates a silver-catalyzed electrochemical method for selective depolymerization and partial dearomatization of soda lignin under ambient, mild conditions, representing a significant advance in lignin valorization. Utilizing a sodium carbonate-based solvent system, the process achieved conversion of lignin into valuable aliphatic and aromatic compounds, as evidenced by yields up to 21.8 wt% of depolymerization products over a reaction time of 10 h. NMR and HRMS analyses identified sodium levulinate, sodium acetate, and sodium formate as principal aliphatic products, while various phenolic compounds were identified in the aromatic fraction *via* Direct infusion (DI) ESI-HRMS. The use of silver as an electrocatalyst enabled a broader range of product formation than previous studies with copper and carbon, though with lower selectivity toward aliphatic products. This process not only optimizes lignin depolymerization under mild conditions but also highlights silver's potential to drive sustainable bio-based chemical production, contributing to circular economy goals by reducing reliance on fossil-based resources. Further optimizations in catalyst design and reaction parameters could refine the selectivity and yield, paving the way for scalable applications in sustainable bio-refining.

6.5 Author contributions

Conceptualization, A.S. and B.V.M.R.; methodology, L.M.L., S.B., F.S. and V.B.; validation, M.F., B.B.B. and B.V.M.R.; formal analysis, L.M.L., B.B.B., M.F. and B.V.M.R.; investigation, L.M.L., S.B., F.S. and V.B.; data curation, L.M.L. and M.F.; writing—original draft preparation, L.M.L. and B.V.M.R.; writing—review and editing, A.S., L.M.L., B.B.B. and B.V.M.R.; supervision, A.S. and B.V.M.R.; project administration, A.S. and

B.V.M.R.; funding acquisition, A.S. and M.F. All authors have read and agreed to the published version of the manuscript.

6.6 Funding

We acknowledge financial support from the COMET InTribology project (FFG No. 872176, project coordinator: AC2T research GmbH).

6.7 Institutional review board statement

Not applicable.

6.8 Data availability statement

The original contributions presented in the study are included in the article; further inquiries can be directed to the corresponding author.

6.9 Acknowledgments

We would like to thank University of Wuppertal for the research support. L. M. L. thanks the networking program 'Sustainable Chemical Synthesis 2.0' (*SusChemSys* 2.0) for the support and fruitful discussions across disciplines. The authors would also like to acknowledge Andjelka Ristic fort the HRMS measurements.

6.10 Conflicts of interest

Author Marcella Frauscher was employed by AC2T Research GmbH. The remaining authors declare that the research was conducted in the absence of any commercial or financial relationships that could be construed as a potential conflict of interest. The authors declare the study received fundings from COMET InTribology project (FFG No. 872176,347 project coordinator: AC2T research GmbH). The funder was not involved in the study design, collection, analysis, interpretation of data, the writing of this article or the decision to submit it.

Abstract:

This investigation presents a one-pot electrochemical depolymerization of lignin, coupled with *in-situ* extraction, to enhance product recovery and process efficiency. Kraft lignin was dissolved in an aqueous sodium carbonate solution and covered with a methyl isobutyl ketone (MIBK) layer. The electrocatalytic reaction, conducted at −350 mA, facilitated lignin depolymerization, yielding a lignin-based bio-oil (LO) composed of a mixture of aromatic compounds, smaller aliphatic molecules such as alcohols, ketones, and acids, as well as sugar derivatives. MIBK was chosen as an effective solvent for *in-situ* extraction due to its proven efficacy, reusability, and compliance with sustainable solvent guidelines. Preliminary tribological assessments demonstrated that, despite a higher coefficient of friction (COF) compared to conventional ester oils, LO provided comparable wear resistance, with minimal surface damage observed. Wear imaging further revealed stronger, more resilient surface interactions, suggesting LO's potential as an eco-friendly lubricant with enhanced durability. These findings mark a critical advancement in lignin valorization, successfully overcoming challenges in product recovery from depolymerization processes and demonstrating its viability as a sustainable alternative to petroleum-based lubricants. Future studies will focus on optimizing formulation and fine-tuning performance to expand LO's application potential in industrial lubrication.

Chapter 7

One-Pot Electrocatalytic Lignin Depolymerization with *In-Situ* Extraction: A Feasible Approach Toward Biomass-Based Oils

Based on:

Lucie M. Lindenbeck, Silas Brand, Finn Schatz, Franka Stallmann, Nele Petersen, Björn B. Beele, Jessica Pichler, Marcella Frauscher, Serhiy Budnyk, Adam Slabon, and Bruno V. M. Rodrigues

This chapter is based on a preprint version of the manuscript that had not undergone peer review at the time of the thesis submission. The content included here is a slightly modified version of the preprint.

DOI (Preprint): 10.26434/chemrxiv-2025-1jl0d

After the thesis submission, the manuscript was revised according to reviewer comments and subsequently accepted and published in *Green Chemistry*:

Green Chemistry, **2025**, *27*, 9927-9936

DOI (Published article): 10.1039/D5GC01810B

Lignin Depolymerization · Biorefinery · Green Chemistry

Biomass Valorization · Electrocatalysis

Preface to Chapter 7

After demonstrating its efficacy as a catalyst for Soda lignin, the potential of silver for depolymerization of Kraft lignin is a subject that merits exploration. The structural disparities between Soda lignin and Kraft lignin may exert a direct influence on their depolymerization process. The higher proportion of phenylglycerol structures in Soda lignin results in less condensed intermolecular bonds, [353] thereby facilitating cleavage. The higher prevalence of β-O-4 bonds in Soda lignin [353] renders it more amenable to cleavage through catalytic methods. In contrast, Kraft lignin, subjected to Kraft pulping, exhibits a greater degree of modification, with numerous β-O-4 bonds already broken and an increased prevalence of C-C fused structures. [353] These bonds exhibit significantly higher stability, making depolymerization less efficient. Additionally, the lower content of functional hydroxyl groups in Kraft lignin [353] contributes to its reduced solubility, further complicating the reaction conditions.

These differences in reactivity are evident in the experimental results. While a 0.1 M sodium carbonate (Na_2CO_3) solution was sufficient for Soda lignin, a 0.2 M solution is required to dissolve Kraft lignin. To initiate upscaling, the volume of the lignin solution was increased from 50 mL to 100 mL. Consequently, the applied current was increased from −175 to −300 mA. The reaction time was left unchanged. The yield of 18% when using Soda lignin is already low. When changing from Soda lignin to Kraft lignin, the yield decreased further to 3%. It was also observed that the solution turned yellow, but that complete decolorization did not occur as it did with silver and Soda lignin. This observation underscores the notion that Kraft lignin is more recalcitrant and less susceptible to depolymerization, a property that can be attributed to the presence of C-C-condensed structures. The low yield obtained underscores the necessity for the expeditious establishment of a novel approach to enhance the product yield and thereby improve the efficiency of the overall process. Consequently, a novel two-phase system was employed. This system incorporates an additional methyl isobutyl ketone (MIBK) phase, which, due to its inability to mix with the aqueous Na_2CO_3 solution during the reaction, just comes into direct contact with the phase boundary. MIBK, classified as a safer and recommended organic solvent by CHEM21, [337] is a non-conductive medium. Na_2CO_3 exhibits insolubility in MIBK. Consequently, products of depolymerization that migrate from the aqueous phase into the organic phase are not further depolymerized and remain as they are. The insolubility of Na_2CO_3 in MIBK also signifies that the products from the organic phase are pure products and not sodium salts, contrasting with previous studies.

The transition of the products takes place at the phase boundary. Water splitting at the electrodes leads to gas formation, which subsequently escapes from the reaction vessel through the organic phase. The gas bubbles take some of the solution with them as they escape, which leads to greater contact with the organic phase. After the reaction, the organic and aqueous phases were separated. The solvent was removed from the organic phase under reduced pressure, and the aqueous phase was processed with ethanol in a known manner [138,354] (solid-liquid extraction). The combined fractions yielded a yield exceeding 100%, attributable to the sodium content of the ethanol-soluble products derived from the aqueous phase.

Notably, this method attained a yield that surpassed the levels observed in previous studies, thereby enhancing the efficiency of the process and rendering it more suitable for future industrial applications. Moreover, the organic phase has yielded a novel array of products, including small aliphatic compounds, aromatic monomers, dimers, and sugar molecules. These compounds, in their role as feedstock, exhibit considerable promise for future applications, such as in the field of lubricants.

Chapter 7 - One-pot electrocatalytic lignin depolymerization with *in-situ* extraction: a feasible approach toward biomass-based oils

7.1 Introduction

In the 19th century, crude oil became a fundamental component of the chemical industry, with significant developments such as Sir James Young's pioneering distillation of petroleum to produce valuable products like kerosene. [5,127] This reliance on petrochemicals has resulted in a cycle of consuming finite resources, which has in turn contributed to a number of environmental and social challenges. [5] It is therefore imperative to pursue a strategic shift away from this dependency in order to achieve long-term sustainability. [5] While fossil fuels are limited in their availability, nature produces 170 billion tons of renewable raw materials on an annual basis through photosynthesis. [2] Renewable resources, such as cellulose and lignin, which together account for 69% of biomass, [2] offer significant potential as sustainable alternatives in the chemical industry.

In this scenario, there is an urgent need for a shift from fossil-based resources to renewable feedstocks. Among potential alternatives, lignin—a major component of lignocellulosic biomass and the second most abundant natural macromolecule after cellulose—presents a unique opportunity. [355–357] Lignin is a complex polyphenol that accounts for up to 30% of the biomass in vascular plants, making it a highly available yet underutilized resource. Despite its potential, its complex, heterogeneous, and recalcitrant structure has posed significant challenges for its conversion into high-value chemicals, [76,79,355,358] relegating lignin to low-value applications such as combustion for energy recovery.

Efforts to valorize lignin have focused on its depolymerization, [76,79,355,358] a process that involves breaking its intricate network of ether and carbon-carbon linkages to release valuable aromatic [104,354] or even aliphatic [138,354] compounds. Among the various methods explored—thermal, chemical, biological, and catalytic—electrocatalysis has emerged as a promising approach. [8,138,166,359] While aligning with the principles of *Green Chemistry* by operating under mild conditions, electrochemical depolymerization offers precise reaction control, and enables the use of renewable electricity. This technique minimizes the environmental footprint while maximizing the potential to produce a wide array of lignin-derived products, thus providing a viable pathway toward a circular bioeconomy.

Despite these advantages, challenges still remain. Conventional lignin depolymerization processes often suffer from low selectivity, complex product mixtures, and energy-intensive separation steps, which hinder their scalability and economic feasibility. [360] Integrating efficient product recovery methods into the depolymerization process is essential to overcome these limitations. [262,361,362] In this direction, the potential of using *in-situ* extraction techniques to simplify downstream processing and improve overall process efficiency appears as a simple and cost-efficient alternative. Such strategies could enable simultaneous depolymerization and separation, reducing energy consumption and solvent waste, while enhancing the recovery of valuable products.

The efficacy of integrating electrochemical lignin depolymerization with *in-situ* extraction has been previously demonstrated. Di Marino *et al.* employed an electrochemical emulsion oxidation process, wherein lignin was dissolved in a deep eutectic solvent (DES) and depolymerized under oxidative conditions, with simultaneous *in-situ* extraction into a methyl isobutyl ketone (MIBK) phase. [363] Their work underscored the potential of such hybrid approaches for enhanced product recovery. Building on this concept, we present in this investigation a modified one-pot strategy that replaces the oxidative depolymerization with a reductive approach, uses an aqueous sodium carbonate solution instead of DES, and employs a two-phase system with MIBK instead of an emulsion. These modifications aim to further streamline the process and improve the scalability of the method.

The process involves dissolving lignin in an aqueous sodium carbonate solution, overlaying the solution with methyl isobutyl ketone (MIBK) as an extracting solvent, and applying reductive electrocatalytic conditions to depolymerize lignin into a bio-based oil (**Scheme 4**). The MIBK layer facilitates the selective extraction of depolymerized lignin products, which are subsequently recovered by solvent removal under reduced pressure. MIBK was chosen for its established efficiency extraction, its potential for reuse, and its recognition as a *green* solvent. [337] This integrated approach addresses the dual challenges of depolymerization and product recovery, paving the way for more efficient and scalable lignin valorization processes. Beyond its chemical significance, this study also explores the tribological properties of the resulting lignin-based oil (LO) as a sustainable lubricant.

By integrating advanced electrochemical techniques with practical extraction strategies, this work contributes to the development of *greener* and more efficient biorefinery technologies. It demonstrates the feasibility of producing high-value products from lignin while addressing key challenges in process optimization and product recovery. Ultimately, this study underscores the potential of lignin as a cornerstone for sustainable chemistry and industrial innovation.

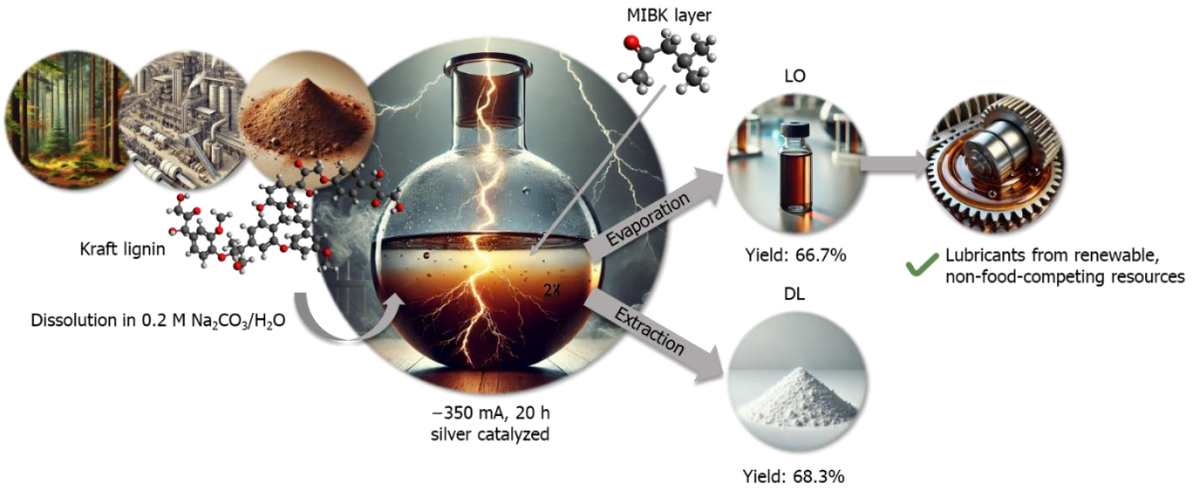

Scheme 4. Schematic representation of the silver-catalyzed one-pot electrochemical depolymerization of lignin, coupled with in-situ extraction to enhance product recovery and process efficiency. For this purpose, Kraft lignin was dissolved in an aqueous sodium carbonate solution and covered with a methyl isobutyl ketone (MIBK) layer. The process involved applying a constant current of −350 mA for 20 h, which facilitated lignin depolymerization and resulted in a lignin-based bio-oil (LO). The MIBK layer served as an effective solvent for the in-situ extraction of the depolymerized lignin products. The resulting lignin-based oil was further tested as a sustainable alternative lubricant.

7.2 Materials and methods

Materials. The Kraft lignin used in this work originates from the hardwood black liquor of a pulp production in a pilot plant (WAT Venture Sp. z o.o., Poland). All aqueous solutions were prepared with ultrapure water obtained from a Millipore system. Ester oil from Klüber (Klüber Lubrication Deutschland GmbH & Co. KG, München, Deutschland) was used for comparison in tribological investigations.

Electrochemical depolymerization of Kraft lignin. All electrochemical reactions were performed using an ATLAS 1131 Electrochemical Unit & Impedance Analyzer (Atlas Sollich). In a standard experiment, Kraft lignin at a concentration of 3 $g \cdot L^{-1}$ was first dissolved in 10 mL of a 2 M aqueous sodium carbonate solution. Then 90 mL of water was added to this mixture. The mixture was transferred to a 250 mL four-necked flask and covered with 100 mL of methyl isobutyl ketone (MIBK). The electrochemical depolymerization process was performed using a three-electrode system: a silver wire working electrode, a platinum wire counter electrode, and an Ag/AgCl (saturated KCl) reference electrode placed in the necks of the flask. The fourth neck was equipped with a reflux condenser. Chronopotentiometry was performed with a constant current of −350 mA. All experiments were performed at room temperature and ambient pressure. After the reaction, the organic MIBK phase was separated from the aqueous phase and dried over sodium sulfate. The MIBK was removed under reduced pressure, leaving a

brown oil. Water was removed from the water/sodium carbonate phase under reduced pressure and the resulting solid was dried under the same conditions. The dried solid was then suspended in ethanol and stirred vigorously for 1 h. The remaining residue was filtered, and ethanol was evaporated from the filtrate under reduced pressure to give a white solid.

Vibrational spectroscopy. FTIR spectra were measured using a diamond 7 ATR unit on a Nicolet ID5 in the range of 4000-400 cm^{-1}.

Nuclear magnetic resonance spectroscopy. Nuclear magnetic resonance (NMR) measurements were performed on a BRUKER Avance 400 MHz spectrometer and on a BRUKER Avance III 600 MHz spectrometer. The following probe heads were used: 5 mm broadband inverse probe with automatic frequency determination, 5 mm QNP probe, and 5 mm broadband inverse probe. Chemical shifts were referenced with respect to Me_4Si. For NMR analysis of the organic phase the brown oil after MIBK removal was extracted with 0.5 ml DMSO-d^6. 16 scans were accumulated for ^1H NMR analysis and 1024 scans for ^{13}C NMR analysis.

Direct infusion (DI) ESI-HRMS. Depolymerized lignin samples were dissolved in methanol, ultrasonicated for 30 min and centrifuged for 10 min (14000 rpm). High-resolution mass spectrometry (HRMS) was used as an advanced analytical method to gain the structure information of degradation products of lignin. MS and MS^n spectra were obtained using an Orbitrap-IQX high-resolution mass spectrometer (ThermoFisher Scientific, Bremen, Germany), equipped with an ESI source. ESI-MS analyses were carried out in ESI(−) and ESI(+) mode. The solutions were infused into the ESI source *via* direct infusion (DI) at a rate of 5 µL min^{-1}. Typical spray and ion optics for negative mode conditions were the following: source voltage, 3.0 kV; sheath gas flow rate, 8 arb; capillary temperature, 275 °C; capillary voltage, −50 V; tube lens voltage, −130 V. Fragmentation and interpretation was done based on negative ionization mode, positive ionization mode was used for additional confirmation. Xcalibur version 2.0.7 and Mass Frontier version 8.0 (ThermoFisher Scientific, Bremen, Germany) software were used for data processing and evaluation.

Thermogravimetric measurements. Thermogravimetric (TG) measurements were conducted using a Netzsch STA F5 Jupiter instrument in 80 µL aluminium crucibles, closed with aluminium lids. LO samples were heated from 25 to 600 °C with a heating rate of 10 $K \cdot min^{-1}$ in a nitrogen atmosphere applying a constant nitrogen flow of 25 $ml \cdot min^{-1}$.

Tribological investigation Friction and wear were analyzed using an SRV3® reciprocating test rig (Optimol Instruments Prüftechnik GmbH, München, Deutschland)

in a ball-on-disc configuration (both 100Cr6) in an oscillating motion, with a ball of 10 mm diameter. A load of 30 N, frequency of 30 Hz, and stroke length of 2 mm were applied. The temperature was kept at room temperature. Each test, with a duration of 2 h, was carried out three times. The wear scar width on the ball and disc was measured using a stereo microscope (SZX16, digital sensor DP23, and objective SDF PLAPO 1XPF, all Olympus Corporation, Tokyo, Japan). The wear area was measured on three microscopic images of balls and discs, based on the width and length of the wear scar. The results are presented as the mean with standard deviation (SD).

7.3 Results and discussion

In our previous research, we investigated the electrochemical reductive depolymerization of technical lignins, including Soda lignin [138,203,354] and Kraft lignin [104], using a range of bulk electrocatalysts, including copper, [104] carbon, [138,203] and silver [354]. In this study, we expanded our approach by incorporating an *in-situ* extraction step during the depolymerization process, with the objective of enhancing product recovery and process efficiency. The process entailed the dissolution of Kraft lignin in an aqueous sodium carbonate solution, subsequent coverage of the solution with a methyl isobutyl ketone (MIBK) layer, and finally, an electrocatalytic reaction designed to facilitate the depolymerization of lignin, thereby producing a lignin-based oil. The selection of −350 mA as the applied current was based on the findings of previous research. [138] The depolymerized lignin (DL) products were subsequently extracted by separating the MIBK phase from the aqueous phase and then removing the solvent MIBK under reduced pressure. MIBK was selected as the extractant due to its established efficacy in the extraction of lignin depolymerization products. [104] A significant benefit of utilizing MIBK is its potential for reuse in subsequent extractions, in addition to its designation as a safe and recommended solvent by CHEM21. [337]

To ascertain the suitability of the solvent MIBK in our context, a series of reference reactions were conducted. First, a reaction devoid of lignin was conducted, employing solely the Na_2CO_3/H_2O solution with a MIBK layer (−350mA/20h/WM/NL; *WM = with MIBK*, *NL = no lignin*). This was done to evaluate the stability of MIBK throughout the electrochemical experiment, which involved a current of −350 mA and a duration of 20 h. The solvent's stability was assessed using NMR spectroscopy (**Figure S 27**), which did not reveal any alterations in the solvent. Thus, it can be concluded that the solvent remains stable. Moreover, Kraft lignin was stirred in MIBK for 20 h and then separated from MIBK by filtration, serving as a reference (0mA/20h/LS; *LS = lignin solubility test*) for the solubility of lignin in MIBK. The MIBK was subsequently removed under reduced

pressure, resulting in a 7.7% yield of a brown solid, which represents the MIBK-soluble fraction of lignin (**Table 14, Figure S 28**). Two additional reference reactions were conducted without applied current, but otherwise under the same conditions as the standard reaction. The first was initiated directly after the reactants were combined (after 0 h) (0mA/0h/WM, **Table 14, Figure S 29**), and the second was initiated after 20 h of stirring (0mA/20h/WM, **Table 14, Figure S 30**). As a final reference reaction (−350mA/20h/NM; *NM = no MBIK*), electrochemical depolymerization was carried out in accordance with the established procedure, [138,354] excluding MIBK. The yield obtained from the aqueous phase was 3.0% DL (NMR spectrum can be found in SI (**Figure S 31**)).

Table 14. Yields of the products obtained from the MIBK phase.

Sample	0mA/20h/LS	0mA/0h/WM	0mA/20h/WM	LO
Yield [wt%]	7.7	3.0	7.7	66.7

** LS = lignin solubility test; WM = with MBIK; LO = lignin-based oil.*

While the aqueous-phase products (DL) are not the primary focus of this study, it is nevertheless important to highlight the significantly higher yield observed in the present study compared to that of the reference reaction conducted without MIBK. The incorporation of an MIBK layer resulted in a notable enhancement in the yield of the aqueous phase, increasing from 3.0% (−350mA/20h/NM) to 68.3% (calculated based on the mass of the products relative to the lignin input) (NMR can be found in the Supporting Information). The organic phase yielded 66.7% (LO, **Table 14**), However, it should be noted that a direct summation of these values does not reflect a true material balance, as the products in the aqueous and organic phases differ significantly in composition. Specifically, the depolymerized lignin (DL) in the aqueous phase consists predominantly of sodium salts, which contribute to the measured mass but do not directly correspond to the organic LO fraction in the MIBK phase. The LO products in the organic phase represent neutral organic molecules, whereas the DL products include ionized species that retain sodium [138,354] from the reaction medium. As a result, the reported values should not be interpreted as additive but rather as indicative of the efficiency of extraction and separation.

Dissolving lignin in an aqueous sodium carbonate solution result in a dark brown solution, while the MIBK solvent is colorless. During the reaction, the MIBK phase turns brownish, indicating that the depolymerization products are passing into the organic phase (**Figure 40**).

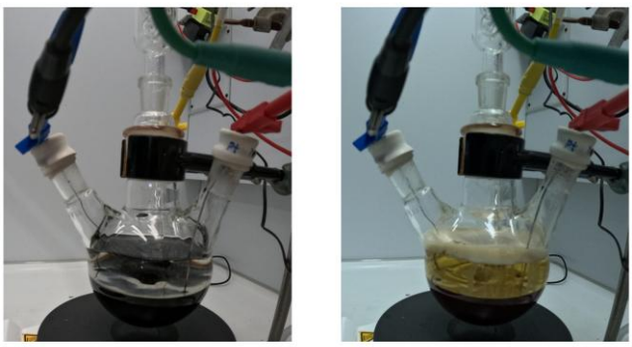

Figure 40. Color change of the MIBK phase during the electrochemical reaction.

The color change is therefore an indirect indicator of the success of the reaction. It is noteworthy that although the aqueous phase becomes more transparent, it still exhibits a brownish hue and only a slight decolorization occurs. In our earlier work, when using Soda lignin and silver as the electrocatalyst, the solution decolorized to a yellowish tone. [354] The solution also decolorized in the reference reaction with Kraft lignin (**Figure S 32**). It can therefore be assumed that the additional organic phase influences the depolymerization and alters the inherent equilibrium of the reaction.

Figure 41 illustrates the FTIR spectra of LO and Kraft lignin, and **Table 15** summarizes the assignments. A broad band at 3445 cm^{-1} in the LO spectrum and 3491 cm^{-1} in the spectrum of Kraft lignin is attributed to O-H stretching vibrations, which are associated with both phenolic and aliphatic hydroxyl groups. The unaltered position of this peak suggests that the hydroxyl functionality remains intact throughout the conversion of Kraft lignin to LO. The C-H stretching vibrations assigned to the CH_3 and CH_2 groups exhibit a peak at 2936 cm^{-1} in the Kraft lignin spectrum, which is shifted to 2964 cm^{-1} in the LO spectrum. This is accompanied by an increased intensity, which indicates a larger number of methyl (CH_3) and methylene (CH_2) groups in the LO. Additionally, a peak at 2840 cm^{-1}, indicative of OCH_3 stretching vibrations in Kraft lignin, shifts to 2874 cm^{-1} in LO and exhibits an increase in intensity. A peak at 1699 cm^{-1} in the Kraft lignin, assigned to the C=O stretching vibrations (*e.g.*, ketones, carbonyl groups, or esters), shifts to 1710 cm^{-1} in the LO and shows an increase in intensity. This suggests that the formation of carbonyl-containing groups in LO is more pronounced, which is likely a consequence of depolymerization processes. The alterations in the aromatic C-C stretching vibrations are especially noteworthy. The bands at 1596 cm^{-1} and 1512 cm^{-1} in the Kraft lignin spectrum shift to 1634 cm^{-1} and 1516 cm^{-1}, respectively, in LO. The diminished intensity of these peaks suggests that the aromatic character of the lignin is reduced due to cleavage within the aromatic backbone during depolymerization. The band at 1367 cm^{-1} in the Kraft lignin spectrum, which corresponds to the C-H stretching

vibrations of aliphatic CH_3 groups, exhibits a slight shift to 1362 cm^{-1} in the LO spectrum and displays an increase in intensity, also indicating an increase in aliphatic CH_3 groups. The FTIR spectra demonstrate clear structural alterations, including a reduction in the aromatic backbone and an increase in aliphatic groups, throughout the conversion of Kraft lignin to LO.

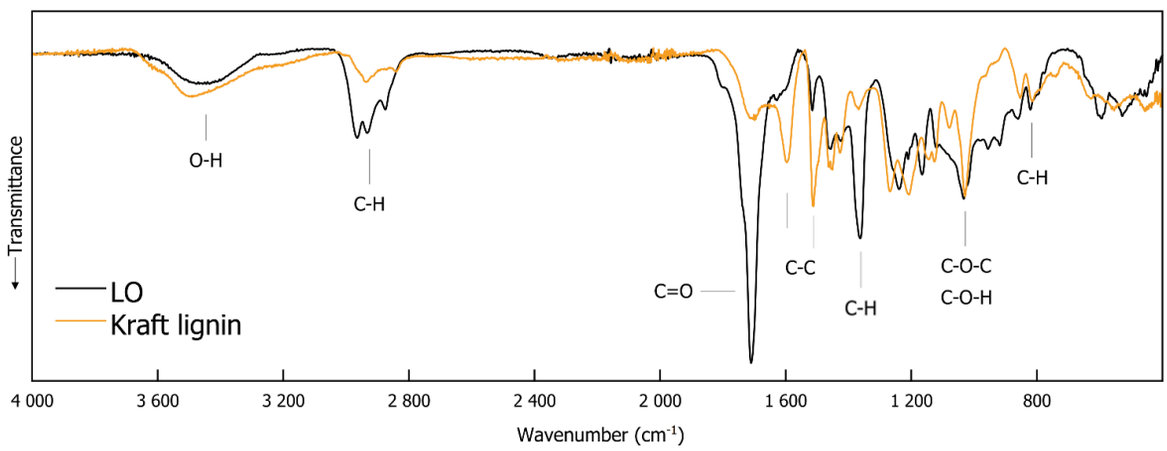

Figure 41. FTIR spectra of Kraft lignin and LO, which is obtained by electrochemical depolymerization of Kraft lignin in a two-phase system comprised by an aqueous sodium carbonate solution and a MIBK layer on top.

Table 15. FTIR absorption bands and assignments, based on [364,365], for Kraft lignin and lignin-based oil (LO).

Assignments	Frequency (cm^{-1})		Intensity Trend (Kraft lignin to LO)
	Kraft lignin	LO	
O-H stretching (phenolic OH and aliphatic OH)	3491	3445	~
C-H stretching (CH_3 and CH_2 groups)	2936	2964 2933	⇧
C-H stretching (OCH_3)	2840	2874	⇧
C=O stretching (unconjugated ketone, carbonyl and ester groups)	1699	1710	⇧
C-C stretching (aromatic skeleton)	1596	1634	⇩
C-C stretching (aromatic skeleton)	1512	1516	⇩
C-H deformation (asymmetric in CH_3 and CH_2)	1462	1452	~
C-C stretching (aromatic skeleton)	1427	1423	~
C-H stretching (aliphatic CH_3)	1367	1362	⇧
C-O stretching vibration of secondary alcohol	1268	-	⇩
Ar-CH in plane (syringyl)	1126	1119	~
C-O(H) + C-O(C) (first order aliphatic OH and ether)	1029	1033	~
C-H out of plane (aromatic ring)	813	821	~

The depolymerization of lignin has been demonstrated to exhibit a low degree of selectivity. [10] As shown by the ^{1}H NMR spectrum (**Figure 42**), a broad range of signals across various chemical shift regions indicates the complex mixture of products generated during lignin depolymerization. In the aromatic region (6–9 ppm), the presence of several signals points to the occurrence of aromatic compounds, likely derived from phenolic monomers and dimers, which are typical products of lignin breakdown. The aliphatic region (0.5–4 ppm) is characterized by multiple intense signals, indicating the presence of aliphatic chains. The high signal intensity in this region highlights the significant contribution of aliphatic fragments to the product mixture. Weak signals in the carboxylic/carbonyl region (10–12 ppm) suggest the presence of aldehydes, carboxylic acids, or other oxygen-containing carbonyl compounds, reflecting the oxygen-rich nature of the depolymerization products.

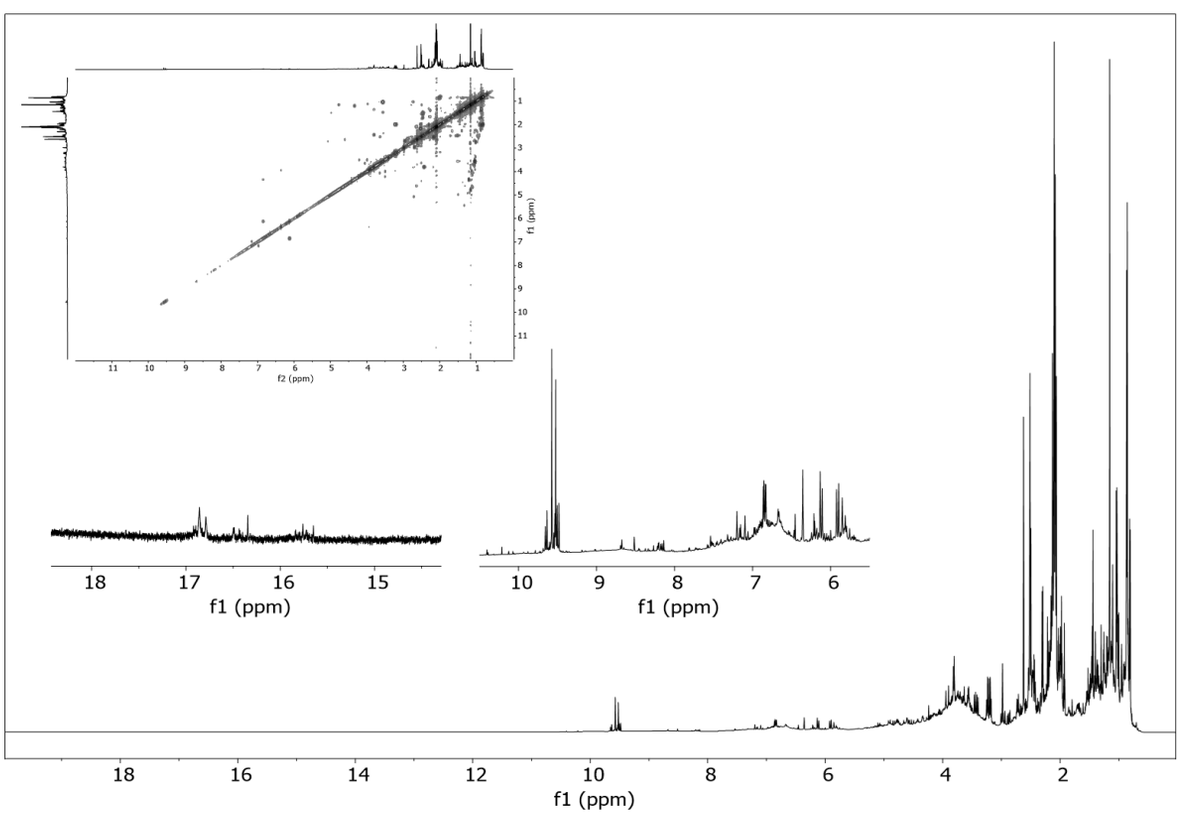

Figure 42. ^{1}H NMR spectra (DMSO-d^{6}, 600.13 MHz) of LO, which is obtained by the electrochemical depolymerization of Kraft lignin in a two-phase system of an aqueous sodium carbonate solution and MIBK. The electrochemical depolymerization of lignin produces a complex mixture of compounds, including both aromatic and aliphatic compounds.

Additionally, the spectrum reveals signals in the range of 4.5–6 ppm, which can be attributed to unsaturated olefinic protons. The ^{1}H,^{1}H COSY NMR (**Figure 3**), ^{13}C NMR (**Figure S9**), and ^{1}H ^{13}C-HSQC NMR (**Figure S10**) spectra provide further information on molecular connectivities of the depolymerization products. Despite its capacity to provide

insights into the functional groups present, NMR analysis does not allow for the precise identification of individual molecules due to the high complexity and diversity of the product mixture.

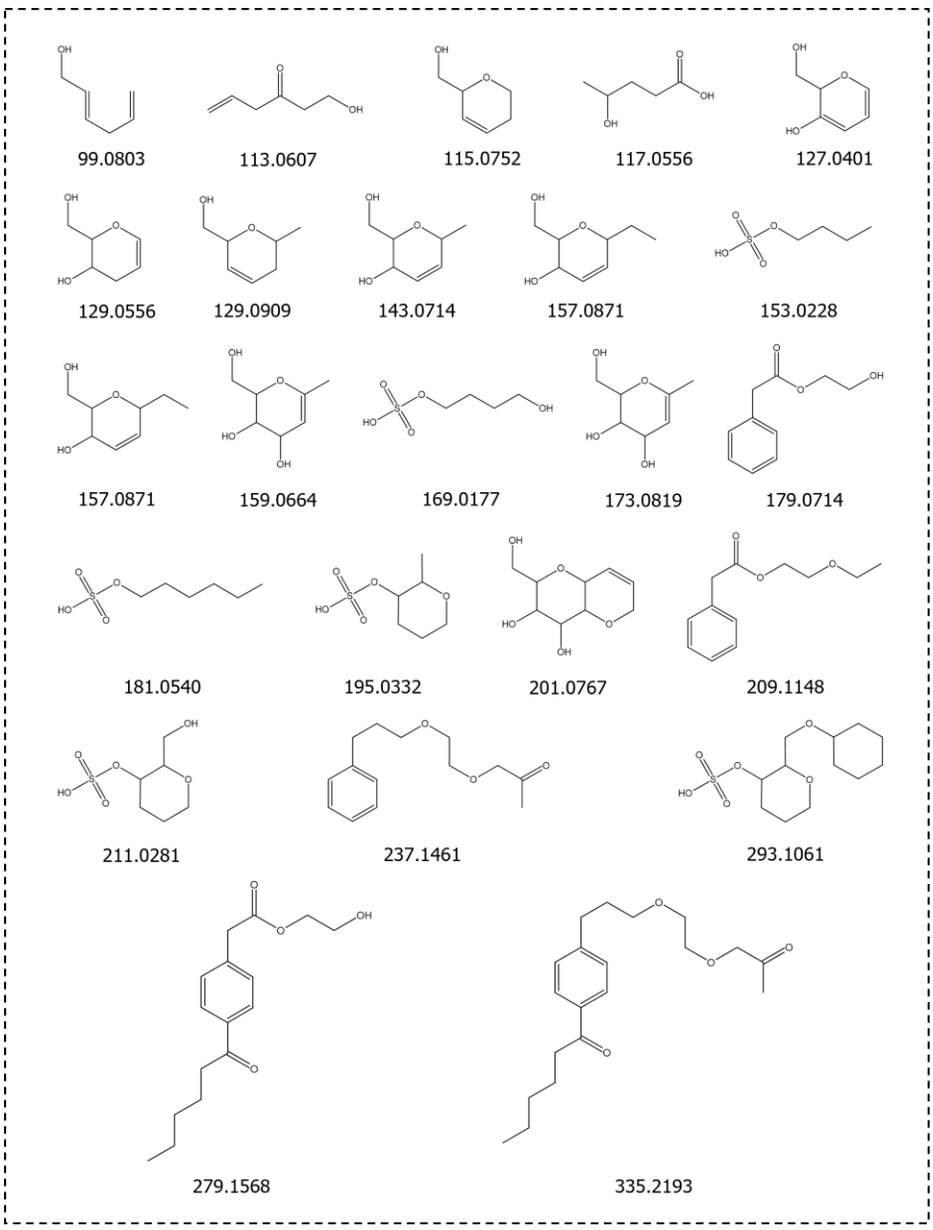

Figure 43. Main products of lignin depolymerization in LO identified *via* (DI) ESI-HRMS with their respective experimental *m/z* values.

Direct infusion high-resolution mass spectrometry (DI ESI-HRMS) provides a more detailed perspective on the molecular composition of the lignin depolymerization products, while their quantification remains a significant challenge. Nevertheless, DI ESI-HRMS enabled the identification of several lignin-derived monomers and dimers. The products (**Figure 43**) include aromatic compounds (*e.g.*, *m/z* 179.0714, *m/z* 237.1461) and smaller

aliphatic molecules such as alcohols, ketones, or acids (*e.g.*, *m/z* 99.0803, *m/z* 113.0607, *m/z* 115.0752), as well as sugar derivatives (*e.g.*, *m/z* 115.0752, *m/z* 129.0909).

The analyses from nuclear magnetic resonance (NMR) and mass spectrometry (MS) reveal a complex mixture of lignin depolymerization products with diverse functional groups. Rather than necessitating costly separation processes, this mixture can be directly utilized as a feedstock for applications such as lubricants.

Thermogravimetric (TG) analysis provided us with more information on the thermal behavior of LO (**Figure 5A**), showing its thermal stability up to 111.7 °C. At this temperature, a continuous mass loss begins, leading to a residual mass of 8.8% at 600 °C, indicating almost complete decomposition and evaporation of volatile compounds by this temperature. The first derivative of the TG curve (DTG, *Differential Thermogravimetry*, **Figure 5B**) shows the mass loss rate as a function of temperature.

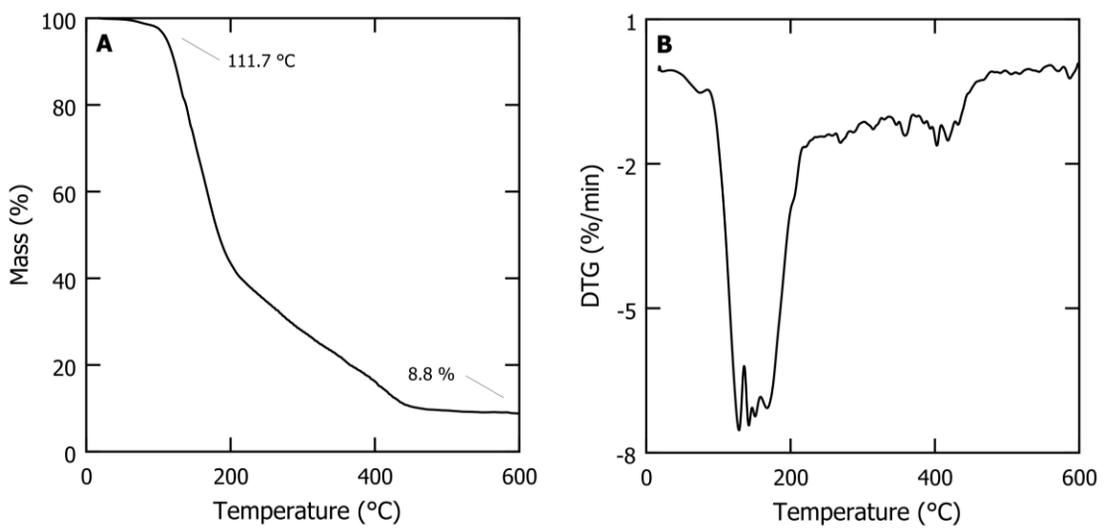

Figure 44. Thermogravimetric analyses for LO: (A) TGA, (B) DTG. Samples were heated from 20 °C to 600 °C (10 °C·min^{-1}) under a N_2 flow (25 mL·min^{-1}).

Between the onset temperature and 215 °C, a high mass loss rate of nearly 8% min^{-1} is observed, which decreases to approximately 1.2% min^{-1} in the temperature range of 215-410 °C. Kraft lignin in comparison shows a significantly higher thermal stability with an onset degradation temperature of 156 °C and a residual mass of 50% at a temperature of 498 °C. [366] Due to the complex mixture of the LO sample, mass loss steps in the TG and DTG curves cannot be attributed to distinct processes.

Compared to common ester oil, LO has a higher coefficient of friction (COF) (**Figure 45A**), likely due to its greater molecular complexity, with viscosity differences being a possible contributing factor. Furthermore, 2D wear measurements were

challenging for LO (**Figure 45D&E**), as the wear scar is very subtle, and the area is not clearly defined, leading to a higher standard deviation in measurements. However, the wear measurements appear comparable between ester oil (**Figure 45B&C**) and LO (**Table 16**). Additionally, wear images reveal more surface scratching with ester oil. This suggests that LO may offer a stronger, more resilient surface interaction than ester oil.

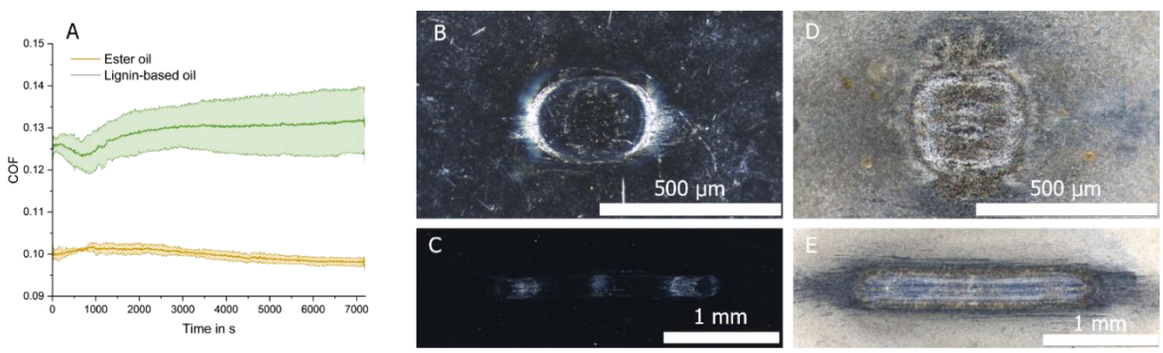

Figure 45. Tribological investigation of LO compared to ester oil. A: friction values (coefficient of friction, COF) of SRV® experiments of LO and ester oil given with standard deviation between data sets (n = 3); B & C: Light microscopic wear scar surface images of ester oil on ball (top) and disc (bottom) after SRV® experiments; D & E: Light microscopic wear scar surface images of LO on ball (top) and disc (bottom) after SRV® experiments. The exposure of the microscope was adjusted for the best representation of wear scars.

Table 16. Wear track characterization of ester oil and lignin-based oil after SRV® experiments giving the mean area and standard deviation of three measurements.

Sample	Ball		Disc	
	Area, mm²	SD	Area, mm²	SD
Ester oil	0.07	0.00	0.50	0.03
Lignin-based oil (LO)	0.08	0.03	0.89	0.40

7.4 Conclusion

This investigation demonstrated a simple one-pot electrocatalytic approach for lignin depolymerization, integrating *in-situ* extraction to enhance both product recovery and process efficiency. By using MIBK as an effective extractant, we achieved a substantial increase in yield, streamlining downstream separation steps while improving process sustainability. Unlike conventional approaches, this integrated strategy minimizes energy-intensive purification processes, bringing lignin valorization closer to industrial feasibility. The resulting lignin-based oil (LO) exhibited distinct physicochemical

properties, with FTIR, NMR, and mass spectrometry analyses confirming significant structural alterations from Kraft lignin.

Further tribological assessments indicated that while LO exhibits a higher coefficient of friction (COF) than conventional ester oils, it offers comparable wear protection. The reduced surface scratching observed in wear imaging highlights the formation of robust surface interactions, positioning LO as a promising next-generation bio-based lubricant. These findings emphasize lignin electrocatalytic valorization as a scalable and eco-friendly approach to producing high-value bio-based products. By addressing key limitations of prior depolymerization methods - inefficient recovery, and complex separation steps - this study marks a significant step forward in the sustainable utilization of lignin-based oils.

Future research will focus on optimizing reaction parameters, exploring molecular tailoring strategies to fine-tune performance, and benchmarking against commercial lubricants to ensure its industrial competitiveness. Additionally, catalyst tailoring and advanced extraction methodologies will further refine selectivity and economic viability. Ultimately, this study contributes to the growing efforts to replace fossil-based lubricants with renewable, lignin-derived alternatives, supporting the broader vision of a circular bioeconomy and sustainable chemical industry.

7.5 Acknowledgement

We would like to express our gratitude to the University of Wuppertal for their research support. L. M. L. acknowledges the networking program 'Sustainable Chemical Synthesis 2.0' (*SusChemSys* 2.0) for the support and interdisciplinary discussions. Parts of the results presented were achieved through research projects financially supported by the participating project partners and the Austrian COMET program (Project InTribology2, No. 906860). The COMET program is funded by the Austrian Federal Government, as well as the provinces of Lower Austria and Vorarlberg in the case of InTribology. We also extend our thanks to Andjelka Ristic for her significant contribution to the DI-ESI-HRMS measurements.

7.6 Author contributions

Conceptualization, L.M.L., A.S. and B.V.M.R.; methodology, L.M.L., S.B., F.S., F.St., and N.P.; formal analysis, L.M.L., B.B.B., M.F., and B.V.M.R.; investigation, L.M.L., S.B., F.S., and F.St.; data curation, L.M.L. and M.F.; writing—original draft preparation, L.M.L. and B.V.M.R.; writing—review and editing, A.S., L.M.L., B.B.B., and B.V.M.R.; supervision, A.S. and B.V.M.R.; project administration, A.S. and B.V.M.R.; funding acquisition, A.S. and M.F.

Abstract:

In this perspective, we propose a conversation towards the future of sustainable chemical industry through the lens of electrochemical biomass depolymerization. Despite the chemical industry's extensive history and established processes, the discovery of new materials remains crucial. This perspective highlights the limitations of current bulk and thin-film electrocatalysts for biomass depolymerization, which have not matched the advancements seen in electrochemical CO_2 reduction. We propose a paradigm shift toward the use of complex catalysts, including transition metal borides (TMBs), transition metal nitrides (TMNs), transition metal carbides (TMCs), MXenes, transition metal phosphides (TMPs), nanoparticles, and single atom catalysts (SACs), to enhance product selectivity, *i.e.*, Faradaic efficiency, in biomass depolymerization. By leveraging the dynamic structural features and superior catalytic properties observed in electrocatalysts for CO_2 reduction, we aim to achieve high selectivity for specific bond cleavages in biobased feedstocks. This shift promises to unlock new pathways in biomass valorization, underscoring the ongoing need for innovative materials to drive sustainable technologies. The development of such catalysts not only advances our scientific understanding but also holds the potential to shape a truly *green* future, reaffirming the vital role of solid-state chemistry in the 21st century.

Chapter 8

Electrochemical Biomass Depolymerization: Will Complex Catalysts Trigger High Product Selectivity?

Based on:

Lucie M. Lindenbeck, Björn B. Beele, Dirk F. Lützenkirchen-Hecht, Bruno V. M. Rodrigues, and Adam Slabon

Chemistry of Materials, **2024**, *36* (19), 9173-9188.

DOI: 10.1021/acs.chemmater.4c02078

Biomass · Catalysts · Depolymerization · Materials · Metals

Chapter 8 - Electrochemical biomass depolymerization: will complex catalysts trigger high product selectivity?

8.1 Introduction

We would like to emphasize that it is an honor to contribute to the special issue in memory of Prof. Francis DiSalvo, whose pioneering research across the chemistry-physics interface has been inspirational in our understanding of structure-property relationships of solids. The latter points toward to the question *why it is still necessary to discover new materials or catalysts in a time, where the chemical industry is a well-established industrial branch with approximately 170 years of experience?* Despite the fact that major large-scale chemical processes are already set up in combination with the accompanying engineering know-how, we would argue in favor on the vision that the future sustainable chemical industry will rely on new materials, bridging both the bulk and nanoscale, *i.e.*, the scale where nature performs chemical processes across interfaces. Electrochemical biomass depolymerization, which aims to break down complex biomass into valuable smaller molecules, is poised to become a key component of this future. In opposite to electrochemical reduction of small molecules, *e.g.*, CO_2 to C_1 building blocks, where major advances in product-specific Faradaic efficiency (FE) and current densities have been triggered by studies on structure-sensitive features, including particle size and exposed crystallographic facets, electrochemical biomass depolymerization on heterogenous electrocatalysts has somewhat remained in its infancy. As such, the complexity of these catalysts has been often limited to the choice of the chemical element to be used as electrode, *e.g.* carbon, copper, and nickel electrodes for depolymerization of lignin.

We draw a parallel between electrochemical biomass depolymerization and the electrochemical CO_2 reduction reaction (CO_2RR) because both processes are critical in addressing the global carbon challenge. While CO_2RR directly reduces atmospheric CO_2 concentrations by converting it into useful chemicals, biomass depolymerization serves a complementary role. Biomass, as a renewable carbon resource, captures CO_2 through photosynthesis and stores it in complex polymers. Efficient depolymerization of biomass not only valorizes this renewable carbon source but also plays a pivotal role in achieving carbon neutrality by integrating bio-based carbon into the circular economy, thus reducing dependence on fossil resources. The comparison with CO_2RR is particularly relevant because both processes require the development of advanced, selective electrocatalysts that can operate efficiently under industrial conditions. However, while CO_2RR has seen

significant strides, biomass depolymerization remains relatively underexplored, especially in terms of catalyst design and product selectivity. Thus, this perspective primarily aims to raise the question whether the development of complex catalysts could similarly trigger high product selectivity in biomass depolymerization, paralleling the successes observed in CO_2RR, and paving the way for new materials to drive future sustainable chemical processes.

In light of the analogous challenges and opportunities inherent to catalyst development for both CO_2RR and biomass depolymerization, it becomes evident that certain catalysts initially designed for CO_2RR have also demonstrated efficacy in biomass depolymerization (**Table 17**). This indicates that other catalysts that have proven successful in CO_2RR could similarly be effective for biomass depolymerization, offering avenues for cross-application and innovation in catalyst design.

Table 17. Selected catalysts used for CO_2RR and biomass depolymerization, highlighting potential cross-application of catalysts between these two processes.

	CO_2RR			Biomass Depolymerization			Notes
	Catalyst	**Main Products**	**Ref.**	**Catalyst / Biomass**	**Main Products**	**Ref.**	
Cu	Cu single crystals: Cu(111), Cu(100), Cu(S)-[*n*(100)x(111)]	Cu(111): Methane Cu(100): Ethylene Cu(S)-[*n*(100)x(111)]: Ethylene	367	Cu foil / Kraft lignin	Monomers and dimers with mainly ether and phenol groups	104	Cost-effective and widely accessible, highly ductile and malleable, low activity towards HER
	Prism-shaped Cu	Ethylene	368	Glassy carbon disk coated with CuO / Pepper lignin	Monophenolic aldehydes/ ketones	243	
	Cu nanoparticles	Ethylene, ethanol, and n-propanol	369	Carbon Paper coated with Cu / Kraft lignin	Vanillin, vanillic acid and other aromatic monomers	244	
Pt	Pt/CNT	Formic acid, methane, CO, methanol	370	Pt coil / Dealkaline lignin	Aromatic and aliphatic compounds	166	Precious and highly ductile, resistant to oxidizing agents, stable in various acids and bases
	Carbon-supported Pt nanoparticle	Methane	371	Pt wire / Soda lignin Protobindt 1000 (P1000)	n/a	214	
Ni	Ni@MicroPNC	CO	372	Ni / Organosolv lignin	Acetovanillone, syringaldehyde, acetylsyringone and others	215	Good conductor, low standard potential, highly ductile
	Ni dual-atom catalysts	CO	373	Ni NP / Kraft-, Dioxasolv lignin	Guaiacol and isoeugenol	220	
	Single-nickel-atomic dispersed N-doped carbon framework	CO	374	Ni/NiOOH	Vanillin, acetovanillone, syringaldehyde, sinapic acid	214	
Pb	Pb/CNT	Formic acid, CO, methane, methanol	375	Pb/PbO_2 / Cellulose	Depolymerized cotton cellulose, soluble sugar such as monosaccharide and oligosaccharides	376	Soft and highly malleable, stable in aggressive media, cost-effective

8.2 Electrochemical biomass depolymerization *vs.* electrochemical CO_2 reduction reaction (CO_2RR)

It is well known and reported that air capture deals with an extremely low CO_2 concentration (ca. 400 ppm today). First, let us consider the thermodynamic aspects in the reduction reaction of 6 CO_2 molecules to one sugar molecule $C_6H_{12}O_6$ according to reaction (1), using the available thermodynamic data [377] from **Table 18**:

$$6\ CO_2 + 6\ H_2O \rightarrow C_6H_{12}O_6 + 6\ O_2 \quad (1)$$

Calculating the free *Gibbs* enthalpy that corresponds to this equation, we arrive consequently at $\Delta G_{\text{process}} = \Delta G^0_{f,C6H12O6} + 6\ \Delta G^0_{f,O2} - 6\ \Delta G^0_{f,CO2} - \Delta G^0_{f,H2O} = +2872$ kJ/mol. In words, this amount of energy has to be provided if 6 CO_2 molecules shall be valorized to higher value chemicals, such as sugars by a reduction reaction. Despite this high demand in energy, this scenario, in the form of the electrochemical CO_2RR to C_1 building blocks or higher, may be considered nowadays as industrially relevant if sufficient high CO_2 concentration is ensured to saturate the corresponding electrolyte. Having both the required energy demand and high local CO_2 concentration in the electrolyzer as system constraints, efficient materials as electrocatalysts are known today that can generate for example C_1 chemicals at excellent FE, *i.e.,* amount of product relative to the amount that could be produced from the total charge passed during CO_2RR.

Table 18. Thermodynamic data of molecules involved in the reduction of CO_2 to sugars. [377]

	M	**ΔH**	**ΔS**	**ΔG = ΔH − TΔS**
Units	g/mol	kJ/mol	kJ/mol K	kJ/mol T = 298 K
CO_2	44	−394.1	0.0009	−394.36
H_2O	18	−286	−0.1638	−237.18
$C_6H_{12}O_6$	180	−1264	−0.1637	−917.22
O_2	32	0	0	0

Only recently, a complex electrocatalyst in the form of nickel nanoparticles supported on nitrogen-substituted carbon, often referred as nitrogen-doped carbon, has been disclosed to generated a high FE of 92.8% for CO with a high partial current density (j_{CO}) of 22.4 mA cm^{-2} and outstanding current density stability at −0.81 V *vs.* RHE for 10 h. [372] The origin of the exceptional electrocatalytic activity is a synergistic interaction between the nickel center and the glycine-derived N-substituted porous carbon material, reflecting

the importance of materials complexity across interfaces that are addressed at the level of chemical synthesis. Given the abovementioned considerations, we would argument that the major advantage of biomass is its continuous reproduction from CO_2, where nature addresses the outlined energy demand by solar energy conversion while simultaneously performing CO_2 capture (**Scheme 5**). Similar to the electrochemical CO_2RR, biomass could be depolymerized by selective cleaving C-C or C-O bonds in aqueous electrolytes if solubility is possible.

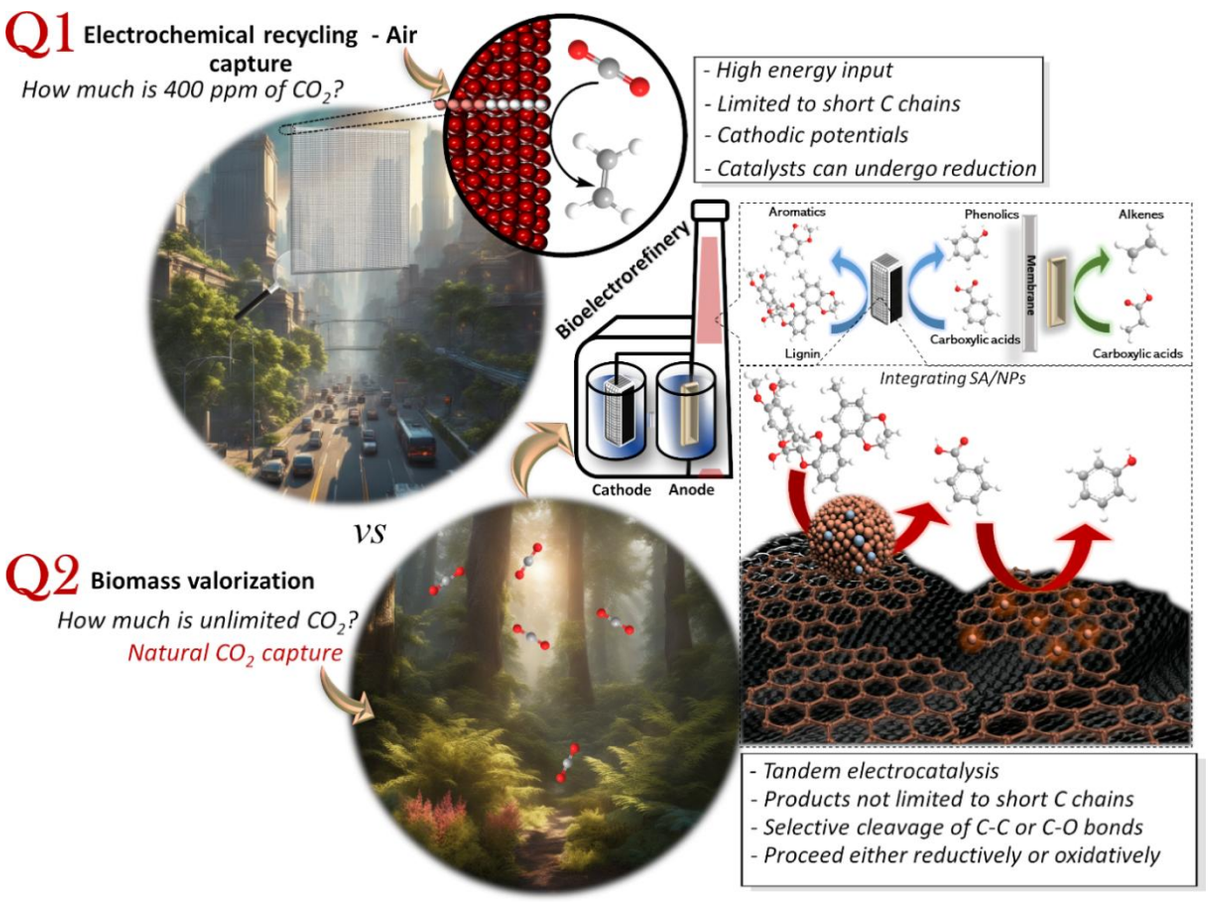

Scheme 5. A schematic illustration depicting a comparison between the electrochemical recycling of CO_2 *via* air capture (Q1) with biomass valorization in the natural CO_2 recycling cycle (Q2), leading to the concept of bioelectrorefinery.

Biomass is not limited to the naturally occurring polymers or oligomers, *e.g.* cellulose, hemicellulose, starch, or lignin, but spans into biomass-derived materials that are processed in biorefineries. For instance, spent sulfite liquor, a side-stream from the pulp and paper industry, is an abundantly available carbon source for bio-based platform chemicals. This side-stream contains aldonic acids, where the latter cannot be biotechnologically metabolized, making thus biotechnological valorization impossible. Using gold and silver, being elements driving also the electrochemical CO_2RR toward CO,

as thin film electrocatalyst, spent sulfite liquor as bio-derived side-stream is valorized *via* the electrochemical reduction of aldonic acids toward sugar. [322,378]

Research on the valorization of CO_2 *via* the electrochemical CO_2RR has shown several breakthroughs in the last decade, which have been based on the understanding of the dynamic structural changes of the catalyst by applying *in operando* and *in situ* methodologies. For the electrochemical CO_2RR, copper is the only electrocatalyst able to yield multicarbon products at acceptable rates, but its mechanistic aspects on the corresponding nanoparticles' surfaces have been debated. It has been disclosed using that 7 nm copper nanoparticles undergo substantial structural changes during CO_2RR into significantly larger metallic copper nanograins, followed by oxidation to single-crystalline Cu_2O nanocubes upon contact with air after electrolysis. [369,379] Whereas CO_2RR is performed at cathodic potentials and the catalytic materials are potentially also exposed to reduction, being equivalent to reduction of metal oxides to metallic form, the electrochemical depolymerization of biomass can occur either the reductive (cathodic) or oxidative (anodic) pathway.

8.3 Complex electrocatalysts for biomass valorization

The electrochemical conversion of biomass represents an approach to the production of valuable chemicals, yet most catalyst studies have primarily focused on bulk electrodes with limited structural and chemical diversity. For instance, these electrodes lack the necessary selectivity, resulting in a complex mixture of depolymerization products. To overcome this challenge, we ask whether more sophisticated catalysts—those exhibiting enhanced structural and chemical diversity—could be the key to product selectivity.

By 'complex catalysts', we refer to materials that either i) contain multiple active sites, ii) consist of binary compounds or higher, or iii) are a combination of surface structural features that enable them to engage in specific interactions with biomass-derived intermediates. These catalysts are not merely multi-component or multi-phase materials; they are designed with precise control over their composition and architecture to tailor their catalytic behavior at the molecular level. For example, catalysts such as transition metal borides (TMBs), transition metal nitrides (TMNs), transition metal carbides (TMCs), MXenes, transition metal phosphides (TMPs), single-atom catalysts (SACs), and high-entropy alloys (HEAs) exhibit unique electronic properties, multiple active sites, or phase boundaries that contribute to their catalytic performance.

Although some of these materials, like SACs, are often single-phase, their catalytic complexity arises from the atomic-level dispersion of active sites, which can create a unique environment for biomass conversion. Others, like HEAs, combine multiple metallic

elements in a solid solution, providing a rich diversity of active sites and both novel synergistic effects, either of geometric or electronic origin, which can enhance catalytic performance. The potential of these materials to improve the efficiency and selectivity of biomass conversion processes remains underexplored, particularly in the context of electrochemical depolymerization. Thus, we advocate for further investigation into how these complex catalysts could be engineered to optimize product selectivity and overall process efficiency in biomass conversion.

Conversion of biomass into smaller molecules includes activating C–C and C–O bonds, which are robust and hard to dissociate. Especially a selective dissociation of C–C bonds is a substantial challenge. [137] For selective electrocatalytic processes a good understanding of C–O and C–C bond breaking is very important. Splitting C–C bonds leads to carbocations and O–C · radicals and dissociation of β–O–4 bonds to carbocations and oxygen radicals that form alcohols, carbonyls or new C–C bonds depending on the reaction conditions and the following work-up. [5] Crucial factor for the cleavage of ß–O–4 and C–C bonds is the delocalization of HOMOs by the catalyst. [165] Reduction processes generally cleave C–O bonds using for example copper, nickel, platinum, and palladium [5,165], C–C bonds can be dissociated for example in lead containing catalysts [5,228]. Theoretic and experimental work focusing on activation of C–C and C–O bonds by TMBs [380], TMNs [381], TMCs [382] and TMPs [383] are becoming increasingly subject of research. Still, concise insights in the relationship of the above-mentioned catalysts structural and electronical properties on the dissociation selectivity are still highly demanded. Besides efficient bond breaking reactants and products also have to be effectively transported to and from catalytically active sites. An important improvement in catalyst effectiveness of porous catalysts is consequently attributed to raised diffusivity. [384] To optimize diffusion porous structures can be custom-tailored for example by the annealing temperature [385] or by the template content as recently shown on nickel containing carbon nanosheet based electrocatalysts [386]. Du *et al.* modulated the pore structures of nanoparticle-loaded carbon material observing enhanced OER activity while not hampering the electronic structures of metal species at the same time. [387] The authors furthermore emphasize the importance of a universal control of pore size distributions in porous catalyst systems in order to accelerate electrocatalytic performance.

Transition metal borides (TMBs) represent a class of materials that have a long history, with the first report about iron boride dating back to 1835. [388,389] This class is renowned for its high superconductivity, [390–392] magnetism, [393–397] ultra-hardness, [398–402] thermoelectric properties, [403,404] and catalytic activity [405–410] (**Figure 46**). However, even if the development of nanostructured materials is not a relatively new area of research, their

application on biomass conversion is still in an early stage. In the field of electrocatalysis, a number of M_xB_y compounds (including Ni_xB_y, Co_xB, Mo_xB_y, Fe_xB, NiCoB, NiFeB, CoMoB, CoFeB, MoAlB, FeCoNiB) have been identified as catalysts for water splitting. [406,410–417] The effectiveness of TMBs in the processes of hydrogen evolution (HER) and oxygen evolution (OER) at low overpotentials to reach 10 mA cm^{-2} has been demonstrated. For instance, Ni_3B (Fe_3C-type structure, space group *Pnma*) has been shown to exhibit excellent performance in both HER and OER, with overpotentials of only 79 mV and 290 mV, respectively. [418,419] Amorphous M_xB_y compounds have been observed to exhibit higher activity than pure metals in the electrochemical reduction of water. [411] In 2017, Fokwa *et al.* [420] investigated the potential of bulk binary polycrystalline molybdenum borides as HER electrocatalysts. Their findings demonstrated that these materials possess promising HER activity. Nevertheless, they postulated that the catalytic performance could be further enhanced by nanoscaling, due to the irregular shape and large size of the particles.

Despite extensive research on the utilization of TMBs as catalysts, a comprehensive understanding of the structural and electronic properties of these borides that elucidates their enhanced catalytic performance remains elusive. [411] One proposed mechanism is the reverse electron transfer, in which electrons are transferred from the metal to the boron. [411] However, studies, such as those by Okamoto *et al.*, indicate that boron is positively charged in the metal boride structure, suggesting that electrons are transferred from boron to the metal. [421] This theory is supported by a number of measurements and simulations which indicate the filling of the metal 3d bands. [411] The reverse electron transfer has frequently been proposed as an explanation for the enhanced catalytic activity observed in amorphous M_xB_y. The metal sites of these materials display an increased electronic enrichment and exhibit elevated resistance to oxidation. [405,422] In spite of that, to gain insight into the catalyst's behavior during the reaction, *in operando* analytical techniques are essential.

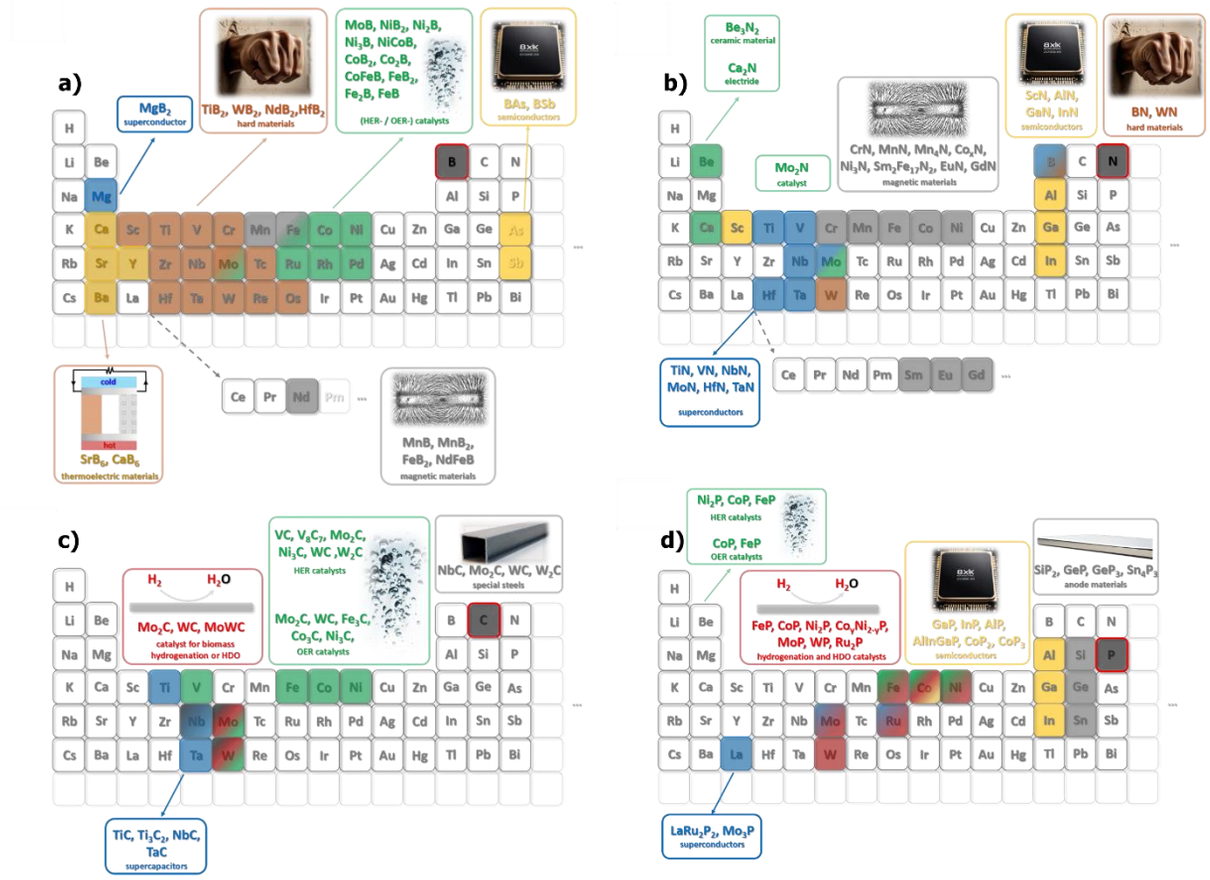

Figure 46. Some applications of a) metal borides,[411] b) metal nitrides,[423] c) metal carbides[424] and d) metal phosphides[425] compiled across the periodic table.

Copper is a well-established catalyst for the conversion of CO_2 into hydrocarbons with multiple carbon atoms. [426] Additionally, copper has been employed in the conversion of biomass, including the electrochemical depolymerization of lignin, as detailed by our research group in 2022. [104] Nevertheless, the catalytic efficiency of copper in the conversion of CO_2 to C_2 compounds remains constrained. DFT simulations have demonstrated that the local electronic structure of copper can be tailored with positive valence sites, thereby increasing the conversion of CO_2 to C_2 products. [426] It was demonstrated that the ratio of active $Cu^{\delta+}$ to Cu^0 sites can be modified with boron. *In situ* XANES electrochemical measurements revealed a copper valence state of +0.32 in boron-doped copper electrocatalysts. [427] The catalyst demonstrated high Faraday yields (approximately 80%), high current density, and excellent stability for C_2 hydrocarbons. [427] The notable enhancement in catalytic efficiency through the transition from copper bulk electrodes to nanostructured boron-doped copper electrodes reinforces the necessity of this alteration in the electrochemical conversion of biomass.

The formation of bonds between nitrogen and the least electronegative elements, such as transition metals, results in the creation of stable compounds in the form of

nitrides. [428] Transition metal nitrides (TMNs), which possess a rich electron bonding, exhibit remarkable electronic, catalytic, and magnetic properties (**Figure 46**). [428] These properties render them potential candidates for the conversion of biomass. Nitrides can be classified according to the type of bonding present. Ionic bonds with metals of groups I and II (*e.g.*, Li_3N (space group $P6/mmm$)), covalent bonds with metals of groups III and IV (*e.g.*, semiconductors), and mixed bonds with transition metals, which offer versatile physical and chemical properties, are the three main types of metal nitrides. [428]

TMNs modify the d-band of the parent metal, increase the density of states near the Fermi level, and promote catalytic activities similar to those of noble metals, [428] rendering them attractive candidates for the electrochemical conversion of biomass. The utilization of TMNs has already been the subject of research in the context of biomass conversion. [429] However, this field of study is still in its infancy. One of the initial stages in the conversion of biomass is de-functionalization. TMNs have demonstrated considerable potential as catalysts for the removal of heteroatoms, including oxygen, nitrogen, and sulfur, through hydrotreatment reactions. [430] Selective bond cleavage is a requisite step in a multitude of biomass refining processes. Upstream reactions, such as lignin pyrolysis, necessitate the cleavage of C–O bonds while maintaining the C–C bonds to guarantee sufficient oxygen removal, followed by the selective cleavage of C–O, C–C, or C–H bonds. [430] In order to optimize the selectivity and activity of these catalysts, it is necessary to develop a comprehensive understanding of the active species, the intermediates, and the reaction pathways. [430] It is therefore essential to prioritize the investigation of model surfaces, probe molecules, and computational studies. [430] Ethanol is a simple model compound that nevertheless contains all the intersaturated bonds, including C–O, C–C, C–H, and O–H. As a result, it is an appropriate subject for investigation into the selectivity and the active catalytic sites. Machine learning models were employed to predict that a Pt/Mo_2N catalyst would exhibit threefold higher reforming activity and comparable selectivity relative to a pure platinum surface. [431]

Transition metal carbides (TMCs) are interstitial alloys composed of carbon atoms and a transition metal element. [424,432] Since the advancement of layered materials in 2004, TMCs have regained significant attention due to their remarkable properties, which vary with their dimensionality and structure. [432] TMCs have been known for their bifunctional capabilities, effectively facilitating both direct deoxygenation (DDO) and hydrodeoxygenation (HD) processes within the context of biomass conversion and catalytic hydrotreatment of bio-oils (**Figure 46**). Additionally, they exhibit catalytic properties akin to those of noble metal-based catalysts, but with significantly lower production costs. [433]

Numerous studies have been published utilizing TMCs as catalysts, addressing both first-generation and second-generation biomass sources. In the case of second-generation biomass, several investigations have focused on the use of TMCs in the transformation of cellulose, hemicellulose, and lignin feedstocks. [434,435] In a study by Mai *et al.*, [436] the hydrogenation of levulinic acid (LA) —often obtained from the acid-catalyzed hydrolysis of cellulose—to γ-valerolactone (GVL) was examined over molybdenum carbide supported on active carbon and carbon nanotubes. GVL is another platform molecule that finds a plethora of applications, including fuel, fuel additives and is also known as an excellent precursor for chemicals. This investigation aimed to explore cost-effective and readily available alternatives to noble metal-based catalysts, which are typically employed in GVL production due to their superior catalytic properties. Molybdenum carbide was selected for its catalytic efficiency comparable to that of noble metals, as well as for its notable mechanical strength, and excellent electrical and thermal conductivity. The experiments were conducted at various temperatures (100 °C, 150 °C, and 200 °C) to assess the impact of the support material on the reaction efficiency. Results demonstrated that higher temperatures significantly enhanced LA conversion rates for both supported catalysts, achieving approximately 95% conversion with Mo_2C/CNT and over 99% with Mo_2C/AC at the highest temperature tested. Specifically, the Mo_2C/CNT catalyst showed remarkable performance, achieving over 99% conversion at 200 °C, compared to just 15% at 100 °C, and maintaining stable conversion rates over a 6-hour period at all tested temperatures.

Ma *et al*. investigated the conversion of Kraft lignin into valuable chemicals using a molybdenum carbide catalyst in supercritical ethanol. [437] The reaction products included a variety of aliphatic alcohols, esters, monophenols, benzyl alcohols, and arenes, with esters being the most abundant, yielding 947 mg per gram of lignin. In a separate study, Ma *et al*. [438] also converted Kraft lignin into C_6-C_{10} chemicals at high yields without producing tar or char, utilizing a nanostructured *α*-molybdenum carbide catalyst. This ethanolysis process, conducted in supercritical ethanol without added gaseous hydrogen, employed an activated carbon-supported *α*-molybdenum carbide (*α*-MoC_{1-x}/AC) catalyst. The reaction yielded various aliphatic compounds, including C_6 alcohols and C_8–C_{10} esters, as well as aromatic compounds such as C_8–C_{10} arenes, phenols, and benzyl alcohols. A total of 25 products were identified and quantified. These examples underscore the extensive range of possibilities that TMCs offer in catalysis. However, these studies also highlight a significant challenge: the lack of product selectivity. While TMCs can drive a variety of reactions and produce a wide spectrum of chemical products, the ability to precisely control and target specific products remains a critical area for further research and development. Despite the advantages of TMCs in promoting hydrodeoxygenation (HDO) products with

higher carbon efficiency, a significant obstacle to their large-scale application is the deactivation resulting from surface oxidation during extended reactions. Additionally, there is a lack of comprehensive understanding regarding the nature of active sites under various synthesis and reaction conditions, as well as the surface reaction mechanisms when dealing with more complex bio-oil compounds.

Metal nitrides and metal carbides are viable candidates for consideration. It is therefore pertinent to comment on the potential utility of MXenes, exfoliated and as such two-dimensional (2D) metal nitrides, with extensive studies published on this topic, for example by Jeitschko *et al.* (for reference, see *e.g.* [439,440]), and metal carbides, which have already been the subject of detailed discussion, for example by Pöttgen *et al.* beginning in the early 1990s (for reference, see *e.g.* [441–443]). MXenes represent a relatively novel class of functional materials, with the initial discovery of $Ti_3C_2T_x$ occurring in 2021. [444] This class of materials, which has recently attracted considerable academic interest, can be described as a two-dimensional flake comprising one additional layer of an early transition metal (M, n+1(n=1−3)) interleaved with n layers of carbon or nitrogen (X). This results in a general formula of $M_{n+1}X_nT_x$, where T_x represents the surface terminations, such as O, OH, F, and/or Cl, which are bonded to the outer M layers. [445] A minimum of 100 stoichiometric MXene compositions and an infinite number of solid solutions provide not only distinctive combinations of properties but also a means of tuning these properties by varying the ratios of M or X elements. [445] In a study conducted in 2020, Jin *et al.* employed DFT calculations to investigate the thermodynamic stability and HER performance of 24 distinct ordered double transition metal carbides under conditions relevant to the HER. [446] The authors demonstrated that 18 of the 24 transition metal carbide MXenes possess the potential to function as effective HER catalysts. The lowest overpotential was observed for Mo_2NbC_2O. Furthermore, they were able to demonstrated that the HER performance of MXenes can be enhanced by modulating the O-termination charge, M′-O bond strength, and M′ species. [446] This suggests that MXenes can be readily adapted and optimized for diverse applications, including biomass conversion. The initial progress in the conversion of biomass by MXene catalysis has already been documented. [447] On a technical scale, alcohols can be derived from the fermentation of biomass, which can then undergo oxidation to aldehydes to yield crucial intermediates. Despite the fact that methanol oxidation is already established on an industrial scale, the catalyst used tends to deactivate. The utilization of $V_4C_3T_x$ MXene aerogel under oxidative dehydrogenation (ODH) conditions resulted in partial oxidation, leading to the formation of nanorods containing an exceptionally active and selective mixture of vanadium oxides, including

VO_2, V_6O_{13}, V_3O_7, and V_2O_5. The oxides derived from the MXene aerogel exhibited high alcohol ODH activity and a remarkable degree of selectivity and stability. [447]

Transition metal phosphides (TMPs) are a group of compounds with metal atoms bonded to phosphorus atoms. Even though the discovery of artificial TMPs date to the 18th century, their exploration did not start until mid-20th century when initial studies laid much emphasis on their structural and electronic properties. [448] TMPs have been of much interest due to their distinctive physical and chemical properties like high electrical conductivity and thermal stability and notable catalytic activity. [425] The synthesis and study of TMPs has been going on for a few decades now and its current applications have already been shaped by significant recent developments in this area, particularly in the fields of electrochemistry and electrocatalysis (**Figure 46**). [425,449,450] There is an array of crystal structures exhibited by TMPs, ranging from basic binary compounds to more complex ternary or quaternary ones. Some of the frequently studied metal phosphides include those of transition metals such as nickel (Ni), cobalt (Co), iron (Fe), and molybdenum (Mo). These compounds are highly stable due to the strong covalent bonds between metal atoms and phosphorus atoms. On top of that, these compounds are metallic in nature with excellent electrical conductivity so that they could be employed in electronics.

The use of TMPs in electrochemistry and electrocatalysis has experienced a significant increase due to their superior catalytic properties. MPs have come up as highly efficient HER catalysts, including Ni_2P, CoP, and FeP which have been found to be highly active and stable across different pH values. [451,452] Their improved performance comes from favorable electronic structure that enhances proton adsorption and reduction to form H_2 gas. In addition to HER, MPs are also promising materials for OER [452–454] and ORR [452,455]. These reactions are critical for the functioning of metal-air batteries and fuel cells. Take cobalt phosphide (CoP) or iron phosphide (FeP) for example; they have been widely studied in terms of OER with high catalytic activity and sustainability being among their main advantages. Similarly, nickel phosphides are investigated for ORR based on their stability and conductivity characteristics.

In a recent and extensive review by Lu *et al.*, [450] it was nicely approached that the metal-acid bifunctional properties of TMPs render them highly effective catalysts for biomass hydrogenation and hydrodeoxygenation (HDO) upgrading reactions. MPs like FeP, [456] CoP, [456] Ni_2P, [456,457] MoP, [456] WP, [456,458] and Ru_2P exhibit these beneficial bifunctional properties. During biomass hydrogenation and HDO processes, the primary active phases in these TMPs are $M^{\delta+}$ and PO−H, which are formed through the partial

reduction of phosphate precursors. The $M^{\delta+}$ ions act as Lewis's acid sites, facilitating hydrogenation, hydrolysis, and demethylation reactions, while PO−H serves as a Brønsted acid site, aiding in the formation of active hydrogen species and promoting hydrogenolysis. [450,459] A notable example is the selective conversion of biofuranic aldehydes to diketones using Ni_2P nanoparticles, first reported by Fujita *et al.* [460] Ni_2P displays unique catalytic properties compared to traditional NiO and Ni(0) NPs and other MPs. Without any additives, Ni_2P nanoparticles efficiently convert biomass furfural in water. Spectroscopic analyses have confirmed that Ni_2P nanoparticles possess metal-acid bifunctional characteristics, with P−OH as surface acidic sites and Ni−Ni species as H_2-activated sites. This bifunctional nature is crucial for the successful conversion of biomass into diketones, offering a new, efficient, and cost-effective method for synthesizing diketones from biofuranic aldehydes.

More efficient TMPs can be achieved by adjusting their composition, structure, and chemical properties to create multicomponent alloy-like structures. [461] For instance, Xu *et al.* [461] designed an yttrium-doped Co−Ni−P catalyst ($(YPO_4)_x/Co_yNi_{2-y}P$) for the hydrogenation of biomass-derived furfural (FAL) and levulinic acid (LA) in water. The $(YPO_4)_{0.2}/Co_{1.0}Ni_{1.0}P$ catalyst demonstrated superior performance, achieving yields of up to 98.1% for GVL and 92.7% for cyclopentanone at lower reaction pressures (0.1–0.5 MPa). The Co ratio and YPO_4 content were critical in optimizing hydrogen activation and acid catalytic performance, with kinetic studies showing that $(YPO_4)_{0.2}/Co_{1.0}Ni_{1.0}P$ had lower activation energy than $Co_{1.0}Ni_{1.0}P$.

In summary, the unique physicochemical properties, stability, and high catalytic activity of TMPs make them highly advantageous for biomass conversion. However, the field of TMPs-driven catalysis is still in its infancy, with synthesis strategies, structure-property relationships, and catalytic performance modulation not yet fully understood. While many synthesis methods exist, there is a critical need to develop *green* and cost-effective approaches for large-scale TMPs production. Currently, most catalysts used in biomass conversion are monometallic TMPs, highlighting the need for future research into doped and multimetallic TMPs. These advanced materials could enhance catalytic performance through the synergistic effects of different metals. Additionally, TMPs possess robust hydrogenation capabilities, enabling *in situ* hydrogen generation during reactions, which can eliminate the need for external hydrogen sources.

The transition from bulk metal particles to nanoparticles has already resulted in a notable enhancement in reactivity. [462] The final step in optimizing reactivity has to be the utilization of single atoms. SACs are composed of individual, isolated metal atoms

dispersed on a support material. This configuration enables nearly every metal atom to act as an active catalyst, which can result in markedly high efficiency up to 100% (**Scheme 5**). [463]

The single-atom structure enables precise control of the electronic environment of the active centers. SACs can be developed to preferentially activate or cleave specific chemical bonds, thereby achieving high selectivity for specific reactions. [462] The strong binding of the individual atoms to the support results in greater stability and a reduced propensity for aggregation compared to conventional catalysts. It is necessary to question whether the designation "single-atom catalyst" is an accurate and precise term in light of the strong binding of single atoms on a support. It is plausible that the support structure, for example a carbon matrix, which is already used unmodified in electrochemical lignin depolymerization, [138,203] may already exhibit intrinsic catalytic properties. This could render the term "single-atom catalyst" a misnomer. In recent years, preliminary studies have been conducted to investigate the potential of SAC for biomass conversion and CO_2RR.

Wu *et al.* described a pretreatment method using choline chloride-lactic acid deep eutectic solvent (ChCl-LA) and niobium-based single-atom catalyst (Nb/CN), which achieved 96.5% lignin removal and high glucose (92.7%) and xylose (67.5%) yields from corn straw. The high yields of fractions and monosaccharides were attributed to the preliminary fractionation by deep eutectic solvent (DES) and the deep fractionation by Nb/CN. [464]

Yang *et al.* investigated the structure and catalytic activity of a single-atom nickel(I) CO_2RR catalyst with an outstanding FE of 97% at −0.61 V (*vs.* RHE). [465] The CO_2 reduction performance is found to be highly dependent on variables like roughness and porosity of the material and addition of heteroatoms stabilizing the active sites. [372] It is unambiguously shown by DFT calculations that the nitrogen atoms interacted with the nickel sites, lowering the energy barriers of transition states in the reaction pathway. Unravelling the identity and structure-performance relationships of SAC catalysts will be crucial for a deep understanding and optimization of future CO_2RR catalytic systems. To reach this goal it is of fundamental importance to ensure that single-atom materials are studied and that no aggregation results in the formation and growth of nanostructures.

This aggregation is one possible pathway reducing a catalysts lifetime. Each electrocatalyst used for biomass valorization offers distinct advantages and functionalities, but also shows potential vulnerabilities towards different deactivation mechanisms. [466] Understanding these for catalytic systems suitable for biomass conversion technologies is

especially demanding because processes can consist of multiple steps or take place in aqueous environments potentially containing poisoning impurities. Deactivation mechanisms can for example be deposition of impurities on the catalytic sites, thermal degradation, poisoning by dissolved impurities such as sulfur, collapsing of porous catalytic material or particle agglomeration. [466] These deactivation mechanisms are thoroughly discussed in a series of excellently written review articles [347–349].

Especially using catalytic materials supported on nanostructures operating at high pressure or temperature deactivation occurs *via* formation of organic deposits on the catalytic sites [469] or by collapse of the catalysts structure leading to a loss of active surface. [466,467] Addressing these problems can be achieved by developing tolerant catalytic systems and designing supports with a robust architecture. [466]

Removing all containing contaminants producing deposits is not foreseeable and consequently research in the field of developing efficient catalyst regeneration methods is and will be ongoing. [466,470] Advanced nano electrocatalysts with a robust structure for example do not show deactivation over a longer time and elevated temperatures and work excellently for example in tandem catalyzed conversion of CO_2 to valuable C_2-C_4 hydrocarbons. [471]

High Entropy Alloys (HEAs) are materials in which aggregation is explicitly desired. They represent an extraordinarily innovative class of metallic alloys that are characterized by an exceptional composition and fascinating properties. Unlike traditional alloys, consisting of a main metal and smaller amounts of other elements, HEAs are composed of five or more main elements (*e.g.* iron, nickel, cobalt, manganese, molybdenum or noble metals from the coinage or platinum metal row) in approximately equal proportions synthesized by laser-, grinding-, pyrolysis-, sol-gel- or dealloying methods. [472] Usually, high temperatures are needed for the synthesis of high entropy materials and low temperature methods remain remarkable exceptions. [473] **Figure 47** shows schematically the proposed growth of HEA nano particles on a solid support as discussed in ref. [474].

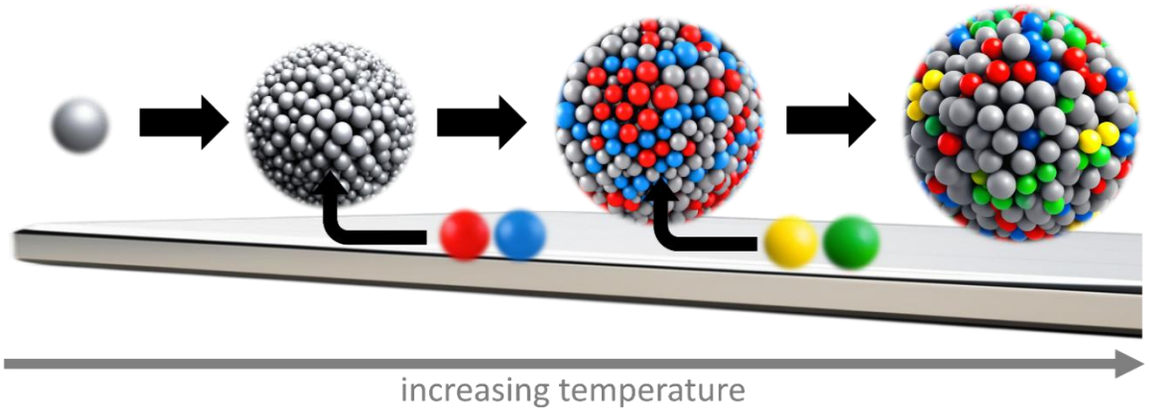

Figure 47. Thermodynamically favored growth of HEA nano particles on a solid support as discussed in [474]. Gray, red, blue, yellow and green spheres are representatives for different metals forming the HEA nano particle upon elevated temperatures.

HEAs high configurational entropy contributes to the stability of these materials [475] giving them remarkable properties such as high mechanic strength, thermal stability, hardness and ductility, both potentially at room temperature and at high temperatures [476]. Many HEAs show excellent corrosion and oxidation resistance and retain their mechanical properties even at high temperatures, making them ideal for high-temperature applications. HEAs however sometimes face problems with internal oxidation reducing the otherwise advantageous properties. [477] The number of metal combinations and shapes creates a nearly unlimited pool of possibilities for HEAs compositions and hence, their applications. Moving from pure metal catalysts towards HEA results in highly innovative materials like FeCoNiMnRu HEA nano particles which are already successfully utilized for water splitting at 1.65 V at a stable current density of 1 A cm^{-2} continuously over a time of more than 600 h. [474] High entropy nitrides (HENs) and borides (HEBs) represent special groups within high entropy alloys accessible starting from HEAs *via* surfactant-assisted hydrothermal synthesis using urea or ammonia as nitrogen sources [474] or boron carbide as boron source [478]. In HENs and HEBs positions in the structure are occupied by nitrogen or boron as non-metallic element instead of a metal and were first mostly known as thin films and very sensitive materials. Nowadays more and more compounds of different structural motifs are synthesized and exhibit high thermal stability and corrosion resistance. [479] Their applications vary from desulfurization from fuels [480], electrocatalytic oxygen evolution [481] to electrochemical reduction of potentially hazardous nitrate to the highly versatile ammonia molecule using the exceptional efficient HEB $(TiVCrMo)B_2$. [482] Due to the versatile properties of HEAs it is not surprising that catalytic capabilities have caught attention for volatilization of biomass like lignin or (hemi)cellulose. [483] Genuinely high surface area of nanoparticle sized materials and individual applicability of each

element are very useful to control bond cleavages of lignin and other natural macromolecules. [483] HEA materials can utilize biomass by activation of both C–C and C–O bonds. [483,484] When it is desired to preserve aromatic structures introducing tungsten in HEA is beneficial as it accelerates dissociation of *β*–O–4 and *α*–O–4 bonds and limits hydrogenation. [485] Selective cleavage of C–C and C–O bonds using HEA is furthermore discussed by Tong *et al.* [483]

A nickel foam-based anode modified with five different metals was tested in the oxidative lignin depolymerization using a flow-through cell setup. [486] A composition of $Cu_{44}Co_{41}Pd_{15}$ on the nickel foam electrode and applying two different pulses of 0.40 V and 0.55 V *vs.* Ag/AgCl respectively showed best catalytic results for formation of vanillin and two other highly useful products in the chosen setup.

The catalytic performance can be further enhanced bringing benefits from high-entropy materials to single-atom catalysts designing high-entropy single-atom catalysts (HESACs) as multi-functional catalytically active materials with several active metal sites. While a rational design and thorough characterization of HESACs is essential innovative work is found in the field of ORR using a FeCoNiRu HESAC [487] or desulfurization using a Mo high-entropy perovskite oxide catalyst [488].

Bringing palladium in a high entropy $(CeZrHfTiLa)O_x$ environment yields a highly stable HESAC catalyst exhibiting higher low-temperature CO oxidation activity and resistance to thermal and hydrothermal degradation. [489]

8.4 Electrode characterization using *in-operando* methods

Investigation of active sites of HEA and HEN materials while serving as a catalyst material can nowadays be carried out using *in-operando* Raman spectroscopy. [474] This cutting-edge modification of a well-established technique allows characterization of materials and processes in real time and under operational conditions. [490,491] Hence it is possible to observe the structural and chemical changes in materials as they are “at work” in a non-invasive way without disturbing or altering the system [492] as schematically shown in **Figure 48** for *in-operando* Raman and XAS while performing electro-catalyzed reactions.

In-operando Raman studies follow changes in Raman-active vibrations on catalytically-active materials like electrodes and were already successfully employed characterizing F^- intercalation in graphite used as electrode material. [493] While being intercalated in electrode graphene layers the force constant of E_{2g} vibration modes change giving access to following intercalation processes during charging or de-charging processes. Recently, *in-operando* Raman spectra have shown the formation of the Co-Mo-N interfaces

accelerating the free water adsorption and dissociation in electro-catalyzed water splitting reactions. [494] In the growing field of CO_2RR [372,495–498], *in-operando* Raman spectroscopy gives access to follow CO adsorption on Fe in CuFe single-atom catalysts and in catalysts made of elemental copper. This observation suggests the crucial role of iron sites in binding and converting CO_2 to CO using potentials of −1.1 V *vs.* RHE and more negative. [499] Most of the used *in operando* Raman cells are still custom-tailored to the scientific question being dealt with and commercially available set-ups are still scarce.

In-operando methods can span further into high energy density X-ray methods like *in-operando* X-ray absorption spectroscopy (XAS) experiments. XAS, including both the near edge (XANES, X-ray absorption near edge structure) and far above the edge (EXAFS, extended X-ray absorption fine structure) is inherently sensitive towards the atomic short-range order environment around the X-ray absorbing atom (see *e.g.* [500]) and thus ideally suited to investigate the atomic structure and the electronic structure of nanomaterials, in particular, *i.e.*, SACs or nanoparticles ([501–504] and references therein). As a hard X-ray photon-in – photon-out probe, the used radiation may easily transmit through any used electrolyte, and thus, XAS experiments are feasible for operando conditions (for reference, see *e.g.* [505–507]).

Moreover, the time resolution available at current X-ray spectroscopy beamlines allow to follow the dynamics of the reaction on timescales from milliseconds to minutes and hours. [508–511] The main difficulty is the construction of a suited operando cell, that is on one hand compatible with the (electro-) chemistry, *e.g.* the mass transfer of the solution to the investigated catalysts and possible gas evolution, and on the other with the energy of the X-rays used. In the case of X-ray absorption spectroscopy, the energy band used for the experiment is simply determined by the edge energy of the X-ray absorbing element, which poses difficulties for the X-ray transmission through the windows and in particular the electrolyte.

For example, 1 mm of an aqueous electrolyte absorb more than 99% of the incident X-ray intensity at the Ti K-edge (4966 eV), while this parasitic absorption decreases to about 50% at the Cu K-edge, so that a thicker electrolyte layer may be tolerated here. Other opportunities are to make use of a very thin layer of the active material only, and to investigate the structural changes from the backside by detecting the fluorescence radiation emitted from the sample [512] as schematically sketched in **Figure 48**. Recent examples using *in-operando* XAS techniques characterizing different electrode materials include the investigation of mono-, bi- or trimetallic CO_2 hydrogenation catalysts on SiO_2 support [513] or highly versatile copper thin film catalysts on glassy carbon electrodes [514].

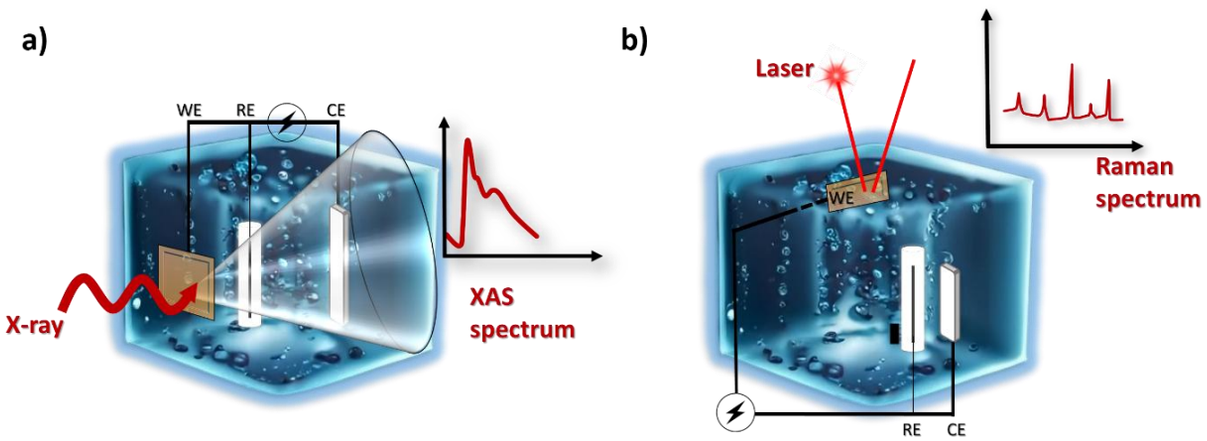

Figure 48. Schematic illustration of a) *in-operando* XAS and b) *in-operando* Raman spectroscopy during an electro-catalyzed reaction.

In order to illustrate the opportunities and the capabilities of the XAS technique for the investigation of catalysts, we show a comparison of normalized Fourier-transforms (FT) of the EXAFS fine structure oscillations c(k)*k^3 from different Fe-based electrocatalysts in **Figure 49**. Data, taken at beamline 10 at the DELTA storage ring, [515] are from a single-atom catalyst, in this particular case from single, N-coordinated Fe atoms incorporated in graphene sheets as schematically depicted in **Figure 49**. The FT of this material depicts a strong nearest neighbor peak at about 1.5 Å radial distance, which is related to the 4 nearest nitrogen-neighbors in a distance of ca. 2.02 ± 0.03 Å. Smaller peaks related to backscattering atoms from the carbon framework in larger distances and multiple scattering events characteristic for the environment around the X-ray absorbing Fe atom are detected at about 2.5 – 3.5 Å. In contrast, for a similar material with larger Fe content, a substantially stronger peak related to a Fe backscattering atom is detected at about 2.6 Å, and for a third catalyst containing both Fe and Se atoms, a third peak is detected at about 2.0 Å. In comparison to the FT of an iron metal foil, it can clearly be seen that the shortest Fe-Fe distances in the catalysts are observed in larger distances of about 2.69 ± 0.03 Å (while the first Fe-Fe coordination is at only 2.46 ± 0.02 Å for metallic body-centered cubic iron with 8 nearest neighbors), corresponding to the available sites in the graphene host lattice. The metallic Fe-Fe peaks at larger distances of up to 5 Å are entirely absent for the catalysts, suggesting the absence of smaller Fe clusters accordingly, and the presence of Fe dimers and Fe-Se coordinations instead.

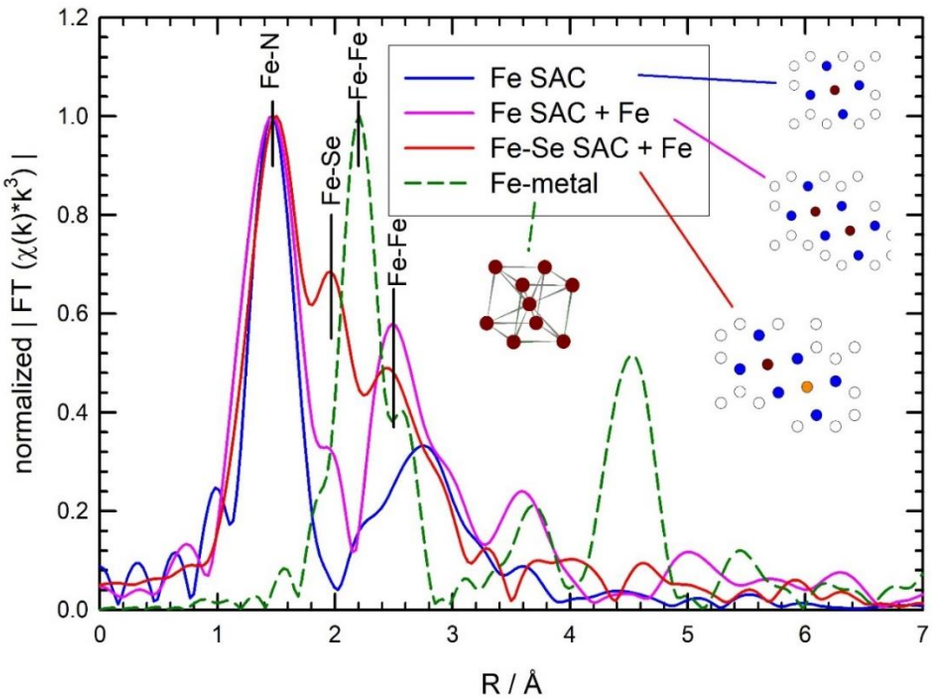

Figure 49. Distinguishing between metal NPs and SACs: Comparison of the normalized magnitude of the Fourier-transform of the k^3-weighted EXAFS fine structures $c(k)*k^3$ for different Fe-based single-atom catalyst materials (full lines) in comparison to metallic iron (dashed line). While the first coordination shell of the catalysts is related to a fourfold Fe-N environment, the second and third shell originate from Fe-Fe and Fe-Se coordinations at larger distances, for catalysts with larger Fe concentration and Se contributions, as indicated. Structural motifs for the different materials are depicted with iron (●), nitrogen (●), carbon (o), and selenium atoms (●), respectively.

It is important to note that also the Fe-Fe and Fe-Se coordination numbers determined by EXAFS fits are equal to » 1, what can also qualitatively be deduced from the non-normalized magnitude of the catalysts Fourier-transforms in comparison to Fe metal, with a coordination number of 8 in the first shell and 6 in the second. Thus, the presence of Fe dimers is very likely for the selected catalyst materials here.

We are convinced that *in-operando* analytical methods, in particular photon-based techniques, open a gate towards a highly important insight into understanding and further optimization of innovative new materials for a series of highly important catalytic reaction types, such as electrochemical biomass depolymerization. They give chemists tools for observing *electrochemistry on duty* which is crucial for further improvement for electrocatalysts for all sorts of applications.

8.5 Conclusion

The current approach to electrocatalysts for biomass depolymerization, predominantly focused on bulk or thin-film electrodes, has reached a *plateau* in terms of selectivity and efficiency. In contrast, recent advancements in electrochemical CO_2 reduction (CO_2RR) and

water splitting have demonstrated that dynamic changes in the shape and size of nanoparticle catalysts under operational conditions can significantly enhance catalytic performance. This observation suggests a new direction for electrocatalyst design in biomass depolymerization: the incorporation of complex nanostructured catalysts, including single-atom catalysts (SACs) and nanoparticles, capable of dynamic evolution during the reaction process. To drive this field forward, research should focus on the following potential directions:

***In-situ* and *operando* characterization:** Developing advanced *in-situ* and *operando* techniques to monitor the structural and electronic changes of nanoparticle catalysts during biomass depolymerization. Understanding these dynamic transformations will be crucial for designing catalysts that can selectively target specific chemical linkages, such as C-O or C-C bonds.

Rational design of hybrid catalysts: Exploring the synergistic effects of SACs anchored to carbon-based supports in combination with transition metal-based nanoparticles. These hybrid systems could offer a dual catalytic function—improving both the stability of the catalyst and its selectivity towards desired products. Such catalysts may be particularly effective in tandem processes where sequential reactions are needed to achieve complete depolymerization and product valorization.

Exploration of transition metal catalysts beyond CO_2RR: Investigating the catalytic potential of transition metal-based catalysts, including those not traditionally associated with CO_2RR, such as iron or manganese-based SACs, for biomass depolymerization. These materials could introduce new reaction pathways or improve the efficiency of existing processes.

Integration of computational and experimental approaches: Employing computational methods, such as density functional theory (DFT), to predict and screen novel catalyst materials, which can then be validated experimentally. This integrated approach will accelerate the discovery of materials with optimal catalytic properties for biomass depolymerization.

Sustainability and scalability considerations: Addressing the challenges of catalyst stability, recyclability, and scalability, which are critical for the industrial application of these advanced catalysts. Emphasizing the development of sustainable and cost-effective synthesis methods for these materials will be essential for their practical deployment.

By pursuing these directions, the field can move beyond the limitations of bulk electrode systems and harness the potential of nanostructured and single-atom catalysts

to achieve higher selectivity, efficiency, and sustainability in biomass depolymerization. As we continue to push the boundaries of solid-state chemistry, these efforts will not only advance our understanding of catalytic processes but also contribute to the development of *greener* technologies that are essential for a sustainable future.

This brings us back to the initial question of this perspective article why we still need to study new materials today. If we can depolymerize and dearomatize lignin with bulk carbon electrodes toward four major products despite the relatively low yield, [138] then adding complexity to catalyst design could be the game-changer in biomass valorization. Despite the 170 years old history of the chemical industry, we believe that sustainable technologies will be triggered by discovery of new inorganic materials. Having the synthetic and analytical toolkit for discoveries of electrocatalysts for biomass depolymerization, these are exciting times for the solid-state chemist to shape a truly *green* future.

8.6 Acknowledgement

We would like to thank the University of Wuppertal for the research support. Parts of the presented results were realized in research projects with financial support from the participating project partners and the Austrian COMET program (Project InTribology2, No. 906860). The COMET program is funded by the Austrian Federal Government and concerning InTribology by the provinces of Lower Austria and Vorarlberg. Additionally, we acknowledge the provision of beamtime by the DELTA synchrotron (Dortmund, Germany)

8.7 Author contributions

Conceptualization, L.M.L., A.S., and B.V.M.R.; writing—original draft preparation, L.M.L., B.B.B., D.F.L.H., and B.V.M.R.; writing—review and editing, L.M.L., B.V.M.R., and A.S.; supervision, B.V.M.R. and A.S.

Abstract:

Transitioning from crude oil to renewable carbon sources is crucial for a circular economy. Lignin, a by-product of the paper industry, has significant potential as a renewable feedstock, but its efficient depolymerization remains challenging. This study presents an iron dual-atom catalyst (DAC) supported on biochar derived from spent coffee grounds for the selective electrochemical depolymerization of Kraft lignin under ambient conditions. The catalyst was synthesized via pyrolysis and characterized using X-ray absorption spectroscopy (XAS), low-energy ion scattering (LEIS), and X-ray photoelectron spectroscopy (XPS). These techniques confirmed the DAC's atomic dispersion and chemical composition. The DAC's in-operando stability was confirmed through XAS under varying electrochemical potentials. In a water/sodium carbonate electrolyte, the DAC achieved lignin depolymerization within 20 h. Nuclear magnetic resonance (NMR) and high-resolution mass spectrometry (HRMS) analyses identified aliphatic products such as sodium acetate and formate, alongside phenolic monomers and dimers. This work demonstrates the potential of DACs for the valorization of biomass while establishing a framework for the monitoring of catalyst behavior at an atomic level during electrochemical biomass depolymerization, thus contributing to the development of advanced catalytic processes.

Chapter 9

Electrocatalytic Lignin Depolymerization enabled by a Biomass-derived Iron Dual-Atom Catalyst: from Synthesis to an *In-Operando* X-Ray Absorption Spectroscopy Study

Based on:

Lucie M. Lindenbeck, Anuja P. Nawadkar, Dirk F. Lützenkirchen-Hecht, Andreas Drichel, Marcella Frauscher, Björn B. Beele, Piotr Kuśtrowski, Prathamesh Patil, Christian M. Pichler, Yu Chen, Yi Yu, Christian W. Lehmann, Jiayin Yuan, Bruno V. M. Rodrigues, and Adam Slabon

This chapter is based on a preprint version of the manuscript that had not undergone peer review at the time of the thesis submission. The content included here is a slightly modified version of the preprint.

DOI (Preprint): 10.26434/chemrxiv-2025-jnt4c

After the thesis submission, the manuscript was revised according to reviewer comments and subsequently accepted and published in *Green Chemistry Letters and Reviews*.

Electrocatalysis · Depolymerization · *in-operando* XAS

atomically dispersed Catalyst · Structure Determination

Preface to Chapter 9

The previous studies of this work about electrochemical lignin depolymerization focused on bulk electrodes made of carbon and silver. In the domain of electrochemical CO_2 reduction, it has been demonstrated that transitioning from bulk electrodes to nanostructured and atomically dispersed catalysts can result in a substantial enhancement in selectivity and efficiency. [10] Moreover, numerous studies have indicated that catalysts that have demonstrated efficacy in CO_2 reduction are also applicable for lignin depolymerization. [10]

On this foundation, an atomically dispersed iron catalyst was developed on a coffee biochar matrix for the purpose of electrochemical lignin depolymerization. Iron was chosen because, like silver, it has not been widely researched in this area. The use of used coffee grounds as a carrier material not only promotes reuse but also enhances the process's sustainability by repurposing a waste product to efficiently valorize another waste product, lignin.

Metal catalysts play a crucial role in accelerating chemical reactions by binding reactants or intermediates to their surface. [516] Transition metals exhibit remarkable activity in this regard. However, they are encumbered by high costs, limited availability, and restricted stability. [516] To address these challenges and enhance the cost-effectiveness and effectiveness of catalysts, research has shifted toward single-atom catalysts (SACs). [516] In this approach, individual metal atoms are dispersed on a support material, enabling each atom to function as an active center. [463] SACs offer a combination of the benefits of homogeneous (isolated active sites) and heterogeneous (stable and easy to separate) catalysis, exhibiting high activity, selectivity, and stability. [517]

However, SACs also present challenges, including the tendency of individual metal atoms to aggregate, which can diminish their efficiency. [518] Additionally, their flexibility is often constrained by a fixed relationship between the adsorption forces of various reaction intermediates. [518] Dual-atom catalysts (DACs) present a promising alternative in this regard. With two neighboring metal centers, DACs enable higher metal loading and more flexible reaction mechanisms. DACs can more specifically control interactions with reaction intermediates, optimize the electronic structure, and overcome the limitations of SACs. [518]

Three main approaches have been developed for the synthesis of DACs. [518] The first method utilizes binuclear metal complexes that are anchored on a carbon support and subsequently pyrolyzed, enabling precise placement of the metal atoms. [519–521] However,

this approach is limited in metal loading and prone to aggregation. An alternative strategy is potential-driven adsorption, which employs electrochemical interactions to synthesize DACs with oxygen bridges in a targeted manner. [522,523]

In this study, the bottom-up approach was selected, which is based on the synthesis of SACs and offers a particularly simple and scalable synthesis method. In this process, metal salts are combined with organic precursors, resulting in higher metal loadings and favoring the formation of adjacent metal centers. [373,524,525] Although single atoms and different coordination structures can also arise, this approach is convincing due to its uncomplicated implementation.

The characterization of atomically dispersed catalysts poses significant challenges due to the necessity of employing divergent methodologies compared to those utilized for bulk electrodes. The detection of SACs or DACs necessitates the integration of multiple analytical techniques.

After the synthesis, X-ray diffraction (XRD) can be employed. In the presence of iron atoms within the coffee matrix, the XRD diffractogram should just exhibit reflections originating from the carbon present in the coffee. XRD can not permit the identification of individual atoms. The presence of metallic reflections indicates the formation of nanoparticles or clusters and excludes the presence of individual atoms.

If no additional reflections are visible, a scanning electron microscopy (SEM) examination can be carried out to identify visible particles or agglomerates on the catalyst surface. If no particles can be detected, energy dispersive X-ray spectroscopy (EDX) can be performed to verify the presence of metals, in this particular case iron, in the catalyst. If iron is present but no particles are visible, this indicates atomically dispersed iron atoms.

A high-resolution transmission electron microscope (HR-STEM) with spherical aberration correction enables the direct visualization of individual metal atoms. In the HAADF mode, atoms with higher atomic numbers appear as bright spots, [106] allowing SACs and DACs to be distinguished. However, metal atoms on a carbon matrix tend to agglomerate under electron irradiation, which can complicate the analysis.

Subsequent investigation can utilize X-ray absorption spectroscopy (XAS), a synchrotron-based technique for analyzing the chemical environment of the metal centers. Two primary types of XAS exist: extended X-ray absorption fine structure (EXAFS) and X-ray absorption near-edge structure (XANES). EXAFS provides information on atomic distances, coordination numbers, and adsorbed atoms, while XANES provides insights into the oxidation state. [105] *In-operando* XAS during electrochemical lignin depolymerization allows for the assessment of the stability of the DAC, [10] with the absorption edges and

oscillations across different potentials remaining unchanged indicating high stability of the catalyst.

Additional analytical techniques such as XPS and LEIS can be used to study the catalyst surface. Analysis of the reference sample, carbonized coffee grounds with melamine but without added iron, showed that iron was detectable on the surface. For this reference, coffee grounds from a filter coffee machine were used, for which ground coffee was purchased. Surprisingly, the iron concentration was so high that it interfered with the XPS analysis, suggesting that the iron was enriched on the surface by the grinding process in a steel mill. This effect could only be eliminated by using a bean-to-cup coffee machine with a ceramic mill that processes whole beans.

The subsequent analyses substantiated the effective synthesis of an iron dual-atom catalyst on a coffee biochar matrix. This catalyst exhibited remarkable efficacy in the electrochemical lignin depolymerization process, demonstrating superior performance compared to the reference catalysts.

These findings offer a compelling foundation for the utilization of atomically dispersed catalysts in electrochemical lignin depolymerization processes.

Chapter 9 - Electrocatalytic lignin depolymerization enabled by a biomass-derived iron dual-atom catalyst: from synthesis to an *in-operando* X-ray absorption spectroscopy study

9.1 Introduction

When employing heterogeneous electrocatalysts, it is imperative to consider potential changes in their structure and chemical environment throughout the course of a reaction. [10] X-ray absorption spectroscopy (XAS) methods, including X-ray absorption near-edge structure (XANES) and extended X-ray absorption fine structure (EXAFS), are highly effective for investigating the atomic and electronic structure of atomically dispersed catalytic metal sites, such as single-atom catalysts (SACs) and dual-atom catalysts (DACs), or nanoparticles. [500–504] These hard X-ray techniques permit studies to be conducted under conditions that more closely resemble those that would be encountered in a realistic setting; in other words, the catalyst structure can be studied "on duty". [505–507] Improvements in time-resolved XAS have enabled the tracking of reaction dynamics over a timescale that extends from milliseconds to hours. [508–511]

CO_2RR and the electrochemical biomass depolymerization are two processes that share a common objective: addressing global carbon challenges. While CO_2RR directly reduces atmospheric or captured CO_2 by converting it into useful chemicals, biomass depolymerization complements this process by unlocking the potential of renewable carbon stored in complex lignocellulosic polymers. [10] Lignin, a significant component of lignocellulosic biomass and the most substantial natural source of aromatic compounds, is produced on an industrial scale of about 70 million tons [60] as a by-product of the pulp and paper industry. However, the utilization of lignin for high-value applications remains limited, with only a small percentage (<2%) [4] being employed for such purposes. The majority of lignin is currently incinerated for energy recovery. Lignin's highly crosslinked molecular structure, composed of three primary phenylpropane units by ether and carbon-carbon bonds, along with hydroxyl and methoxy groups, renders it highly resistant to breakdown, [288,289] what makes the selective and efficient depolymerization into high-value added products challenging. [254] The abundance and inherent aromaticity of lignin make it a promising candidate for the sustainable production of value-added chemicals.

Lignin depolymerization can be achieved through oxidative and reductive electrochemical approaches. While oxidative methods, which break down lignin *via* anodic

reactions, have been more extensively explored, reductive electrochemical depolymerization remains still heavily unexplored. In a previous study, we demonstrated the first reductive depolymerization of lignin using electrochemical methods under mild conditions. [104]

The majority of studies on electrocatalysts for lignin valorization have focused on bulk electrodes, including carbon, [138,185,202,203] nickel, [214,215,217] platinum, [166] lead, [228,230,231] and copper. [104] Yet, the structural and chemical diversity of these electrodes is rather limited. [10] So far, studies have focused on bulk, *i.e.* macroscopic, materials whereas nanoscopic or atomically-dispersed catalysts for the reductive depolymerization of lignin, to the best of our knowledge, have not been reported so far. The progress in the eCO_2RR has successfully demonstrated the application of such catalysts to achieve high *Faradaic Efficiencies* (FE) and current densities. Electrocatalytic lignin depolymerization has been so far heavily under-researched within this respect. [462]

The progress in catalyst discovery for eCO_2RR and water-splitting using nanostructured materials can be attributed to the increased surface area of nanostructured materials, which provides more active and low-coordinated catalytic sites, and their ability to precisely tailor electronic properties to favor specific reaction pathways. The subsequent evolution from nanoparticular to atomically structured electrodes, such as SACs and DACs, offers promise for further improvement. SACs are composed of discrete metal atoms dispersed across a support material. This configuration enables nearly every metal atom to function as an active site, with the potential to achieve efficiencies as high as 100%. [463] The single-atom configuration permits precise control over the electronic environment surrounding the active sites. SACs can be designed to selectively activate or break specific chemical bonds, thereby enabling high selectivity for targeted reactions. [462] The robust attachment of individual atoms to the support structure confers enhanced stability and mitigates the proclivity for aggregation, thereby outperforming conventional catalysts in these aspects.

Despite the significant strides made in the design of the coordination environment of SACs, they are confronted with a pivotal challenge in the optimization of the adsorption of all reaction intermediates, which is constrained by thermodynamics. [518] This limitation significantly restricts SACs in catalyzing reactions that require the synergistic activation of multiple molecules and intermediates. To address this issue, the concept of DACs has been introduced. The presence of adjacent active sites in DACs offers additional positions for molecule activation and intermediate adsorption, thereby providing an extra level of flexibility for catalytic control. [518]

The selection of the matrix is of critical importance to SACs and DACs. Commonly used matrices, such as ZnO, [526] poly(ionic liquid) surface-coated filter paper, [527] bipyridine-based two-dimensional conjugate covalent-organic frameworks, [528] porous nitrogen-substituted carbon, [529] hollow carbon–nitrogen spheres**,** [530] and nitrogen-substituted carbon nanofibers [531], are predominantly composed of carbon and nitrogen in various commercially available modifications. Since carbon is a major component of biomass, it is logical to use biomass as a carbon source for the matrix. Carbon as a bulk catalyst has already been used for the electrochemical depolymerization of lignin, the substrate of interest in the present study. [138,185,202,203] The recent surge in interest surrounding biochar, a material produced through the thermochemical conversion of biomass, can be attributed to its versatility in a multitude of applications. Primarily utilized as a soil amendment, biochar has demonstrated efficacy in reducing greenhouse gas emissions and enhancing soil quality. [532] Additionally, biochar is being employed as a precursor in the synthesis of catalysts and adsorbents for contaminant removal, underscoring its growing utility in various fields. [532] Yet, the use of biomass also presents logistical challenges, such as the need for large-scale harvesting and transportation, which often rely on non-renewable energy sources. These challenges can be mitigated by using biomass waste, as is the case with lignin, which does not require any additional logistical changes as the existing infrastructure can efficiently accommodate its use. [5]

Coffee is among the most extensively traded agricultural commodities globally, with an estimated annual production of approximately 8 billion kilograms. [533] The commercial production of coffee beverages generates vast amounts of spent coffee grounds, which require effective waste management. These by-products present a significant challenge due to their high oxygen demand during decomposition and the potential release of environmental pollutants, including residual caffeine, tannins, and polyphenols. [534] Nonetheless, novel strategies for the valorization of spent coffee grounds present a sustainable alternative. [533,535,536]

While the application of SACs has demonstrated remarkable advancement as efficient catalysts, the use of DACs in biomass conversion remains largely unexplored. While bulk electrodes composed *e.g.* of carbon, [138,203] copper, [104] silver, [354] and nickel [214,215,220] have gained recognition for their application in electrochemical lignin depolymerization, to the best of our knowledge, iron has not yet been utilized in this context. Iron-based DACs have been predominantly studied for other reactions, such as the oxygen reduction reaction [537,538] (ORR), oxygen evolution reaction (OER), [523] and CO_2RR [539]. However, most of these DACs consist of mixed dual-atoms, such as iron-nickel [537,539] or iron-cobalt [523,540,541] combinations, rather than purely iron-based systems. This highlights both a significant

gap in current research and the as yet untapped potential of DACs, particularly iron-only DACs, for the electrochemical depolymerization of lignin.

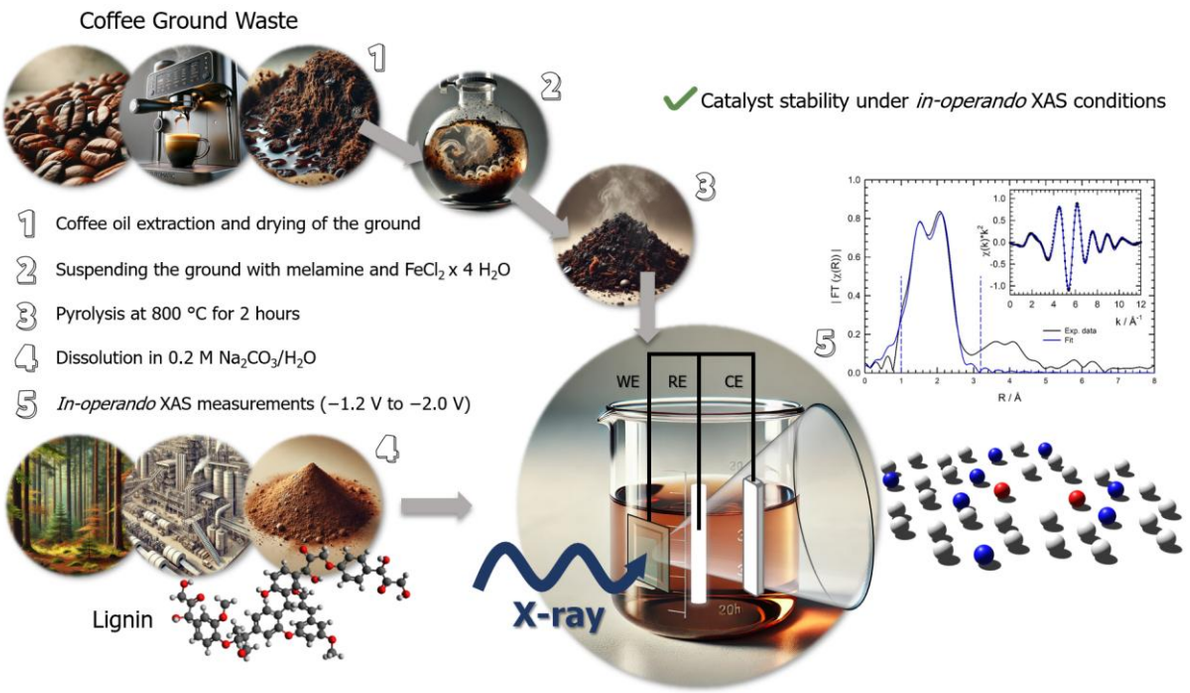

Scheme 6. Schematic representation of the preparation process for the iron DAC, followed by *in-operando* XAS measurements conducted in an aqueous lignin/sodium carbonate medium under varying potentials to evaluate the catalyst's stability.

In this study, we disclose an iron dual-atom catalyst on coffee waste biochar as electrocatalyst for the reductive depolymerization of Kraft lignin towards organic chemicals, both aliphatics and phenolics. This represents a significant advance in the development of atomically structured catalysts, marking a departure from the use of bulk catalysts, such as copper, [104] silver, [354] and carbon, [138,203] which have been the focus of our previous investigations. In this study, our objective is twofold: first, to characterize the catalyst and test its performance and stability under *in-operando* conditions, and second, to examine the electrochemical depolymerization of lignin (**Scheme 6**).

9.2 Materials and methods

Materials. The coffee grounds were collected by a fully automated machine with a ceramic grinder and subsequently kept at −18 °C until required for use. Kraft lignin obtained from industrial pulping spent liquor was used as starting material for the lignin depolymerization. All other chemicals were purchased from commercial suppliers and employed in their original, unpurified state. All aqueous solutions were prepared with ultrapure water, obtained from a Millipore system.

Preparation of coffee grounds. The ground coffee waste (30 g) was subjected to three cycles of washing with ultrapure water and subsequent drying at 105 °C for 48 h. The coffee was mixed with n-hexane (50 mL) and heated overnight at 80 °C under reflux. The coffee was separated from the n-hexane by filtration, after which the coffee powder was washed with water and ethanol and dried for 48 h at 105 °C. The n-hexane was removed from the filtrate under reduced pressure, resulting in the isolation of coffee oil with a yield of 8.3% (based on the total weight of the coffee).

Catalyst preparation. First, 2.0 g of coffee ground waste, 0.5 g of melamine, and 150 mg of $FeCl_2$ x 4 H_2O powder were combined in 30 mL of ethanol and stirred for 1 h, followed by 10 min of sonication in an ultrasonic bath. The ethanol was subsequently removed under reduced pressure, and the residue mixture was subjected to drying at 60 °C over night. Subsequently, the catalyst was synthesized by pyrolyzing the as-prepared material at 800 °C with a heating rate of 5 °C min^{-1} under a nitrogen atmosphere for 2 h. Subsequently, the furnace was permitted to cool to room temperature. The catalyst was then ground with concentrated hydrochloric acid to remove any excess metallic species. The catalyst was separated from the hydrochloric acid by vacuum filtration and subsequently washed to a pH of 7 with ultrapure water. Finally, the catalyst was washed three times with ethanol and dried overnight at 60 °C. The synthesis process of the control sample (BC) was similar to that of the catalyst, with the exception of the addition of $FeCl_2$ x 4 H_2O during the process.

Electrode preparation. The electrodes were prepared by first combining 100 mg of the catalyst with 0.8 mL of Nafion™ solution, following by the addition of 0.6 mL of ethanol and 0.6 mL of ultrapure water. Subsequently, the suspension was subjected to ultrasonication for 5 min. Carbon paper (2 cm x 5 cm) was coated with a catalyst suspension (~5 mg·cm^{-1}) on both sides and dried overnight at 60 °C.

Electrochemical depolymerization of Kraft lignin. In a standard experiment, Kraft lignin was initially dissolved at a concentration of 3 g·L^{-1} in 5 mL of a 2 M aqueous sodium carbonate solution. Subsequently, 45 mL of water was added to this mixture. The electrochemical depolymerization process was conducted with a three-electrode system: a working electrode (carbon paper (CP), biochar coated on carbon paper (BC), dual-atom catalyst coated on carbon paper (DAC)), a platinum mesh counter electrode, and an Ag/AgCl (saturated KCl) reference electrode. Chronoamperometry was performed with a constant potential of −1.6 V. All experiments were conducted at room temperature and ambient pressure. After each reaction, water was removed under reduced pressure, and the resulting solid was dried under the same conditions. The dried solid was then

suspended in ethanol and stirred vigorously for 1 h. The remaining residue was filtered off, and ethanol was evaporated from the filtrate under reduced pressure, yielding a white solid.

Nuclear magnetic resonance spectroscopy. Nuclear magnetic resonance (NMR) measurements were performed on a BRUKER Avance 400 MHz spectrometer and on a BRUKER Avance III 600 MHz spectrometer. The following probe heads were used: 5 mm broadband inverse probe with automatic frequency determination, 5 mm QNP probe, and 5 mm broadband inverse probe. Chemical shifts were referenced with respect to Me_4Si.

Direct infusion (DI) ESI-HRMS. Depolymerized lignin samples were dissolved in methanol, ultrasonicated for 30 min and centrifuged for 10 min (14000 rpm). High-resolution mass spectrometry (HRMS) was used as an advanced analytical method to gain the structure information of degradation products of lignin. MS and MS^n spectra were obtained using an Orbitrap-IQX high-resolution mass spectrometer (ThermoFisher Scientific, Bremen, Germany), equipped with an ESI source. ESI-MS analyses were carried out in ESI(−) and ESI(+) mode. The solutions were infused into the ESI source *via* direct infusion (DI) at a rate of 5 μL min^{-1}. Typical spray and ion optics for negative mode conditions were the following: source voltage, 3.0 kV; sheath gas flow rate, 8 arb; capillary temperature, 275 °C; capillary voltage, −50 V; tube lens voltage, −130 V. Fragmentation and interpretation was done based on negative ionization mode, positive ionization mode was used for additional confirmation. Xcalibur version 2.0.7 and Mass Frontier version 8.0 (ThermoFisher Scientific, Bremen, Germany) software were used for data processing and evaluation.

Differential scanning calorimetry and thermogravimetric analysis (DSC/TGA). Differential scanning calorimetry (DSC) and thermogravimetric analysis (TGA) data were obtained using a Netzsch STA 449 F5 Jupiter instrument. Samples were placed in 40 μL Al_2O_3 crucibles closed with Al_2O_3 lids and heated from 20 °C to 800 °C (5 °C·min^{-1}), followed by a period of 2 h during which the sample was maintained at 800 °C, under a nitrogen flow (25 mL·min^{-1}).

X−ray spectroscopy (XAS). Extended X−ray absorption fine structure (EXAFS) experiments were carried out at the materials science beamline 10 at the DELTA storage ring (TU Dortmund / Germany) operating with 1.5 GeV electrons and a stored current of 100−130 mA [515] (Range: 4−14 keV). A Si (111) channel−cut monochromator was employed, and the intensity of the incident beam on the sample was measured using a nitrogen−gas filled ionization chamber, while the X−ray fluorescence from the sample was collected using a large−area PIPS® photodiode (Passivated Implanted Planar Silicon). The energy

range measured covered the X−ray absorption edge of Fe (7112 eV). Fluorescence mode EXAFS data were collected on the fly in the quick−scanning EXAFS mode, in which the Bragg−angle of the monochromator was continuously decreased while each data point in the spectrum is collected within a small integration time of typically 50−100 ms. [542]

***In-operando* X−ray spectroscopy (XAS).** A small reactor was built for *in-operando* synchrotron radiation measurements. With the catalyst (DAC) coated carbon paper was attached to the front with epoxy resin. Kapton® tape was used to seal the front and back, creating a compartment for the electrolyte. The counter and reference electrodes were fixed in separate chambers. To ensure stable electrochemical conditions before data collection, each potential was applied for 10 min before the quick-scan XAS measurement was conducted.

Low-energy ion scattering spectroscopy (LEIS). Low-energy ion scattering spectroscopy was performed using an ION-TOF Qtac100 spectrometer (IonTOF, Germany). The residual pressure of the LEIS chamber is maintained at 10^{-8} mbar. LEIS experiments were performed using He^+ ions with an energy of 3 keV as the primary beam at an incident angle of 0° and a scattering angle of 145°. The measurement area was 2 mm x 2 mm. A beam of 2 keV Ar^+ ions at an incident angle of 59° was used as sputter cleaning beam to clean the sample from residual contaminations. The flux of primary He^+ ions was maintained approximately $1 \cdot 10^{14}$ ion s^{-1}. The total measurement time was $1.1 \cdot 10^4$ s. The time-of-flight (ToF) filter was switched on while measuring the scattered ions. This filters out low-energy ions, which contributes to reducing the background. The charge compensation was switched to minimize charging of the electrically insulating catalyst samples. The samples were prepared by pressing onto a copper tape with a spatula until firm and then introduced into the chamber.

X-ray powder diffraction (XRD). XRD experiments were carried out employing the Bragg-Brentano parafocusing geometry on an X'Pert Pro multi-purpose diffractometer (PanAnalytical, Almelo, The Netherlands). Non-monochromatized Cu Kα radiation (40 kV, 40 mA) was used for irradiation of the powder samples on a rotating zero-background holder, and the scattered intensities were collected with a multi-strip X'celerator detector in an angular range from 2θ=10 to 110°. The incident beam path was comprised of a vertical divergence slit with an opening angle of 0.5°, a 0.04 rad Soller slit and a fixed horizontal mask (10 mm), respectively. In the diffracted beam path, a 0.02 mm Ni Kβ-filter, a 0.02 Soller slit and an anti-scatter slit were installed.

X-ray photoelectron spectroscopy (XPS). XPS spectra were collected in a Prevac photoelectron spectrometer equipped with a hemispherical analyzer (VG SCIENTA R3000)

using monochromatized aluminum Al K*α* radiation (E = 1486.6 eV). The binding energy scale was calibrated to the position of XPS C 1s peak at 285.0 eV attributed to adventitious carbon. The data were processed in the Casa XPS software.

Scanning electron microscopy with energy dispersive X-ray spectroscopy (SEM-EDX). Energy-dispersive X-ray (EDX) spectroscopy was employed to analyze the catalyst, utilizing a Hitachi TM3030 PLUS tabletop scanning electron microscope with an Oxford EDX detector.

Inductively coupled plasma optical emission spectrometry (ICP-OES). The samples were digested in an HNO_3/HCl mixture (1 mL ddH_2O, 250 µL HNO_3, 250 µL HCl) and the iron content was measured using inductively coupled plasma-optical emission spectrometry (ICP-OES; Avio 220 Max, PerkinElmer).

High-resolution transmission electron microscopy (HR-TEM). HR-TEM images were performed on a JEOL JEM-F200 microscope (Cs: ~1 mm), operated at 200 kV with a field-emission gun and a Gatan Rio16 camera.

9.3 Results and discussion

We employed a supported iron dual-atom catalyst (DAC) synthesized from coffee waste biochar for the reductive electrochemical depolymerization of Kraft lignin. For the preparation of the catalyst matrix, the coffee oil has been removed from the coffee grounds using n-hexane. This approach presents two major advantages. First, the coffee oil does not interfere with the pyrolysis process, where it could otherwise vaporize and subsequently condense in the furnace. Second, the coffee oil can be reused, aligning with the principles of *Green Chemistry* by converting a waste product into a valuable resource. For instance, it could serve as a *green* lubricant. [535] It should be noted that the focus of this study was not on characterizing the oil. The relevant data can be found in the Supporting Information, which includes ^{1}H, ^{13}C, ^{1}H ^{1}H-COSY, and ^{1}H ^{13}C-HSQC NMR (**Figure S 1-4**).

To simulate and gain a deeper understanding of the pyrolysis conditions within the furnace, the mixture of coffee residues, melamine, and iron chloride, which had not yet undergone carbonization, was subjected to a thermogravimetric analysis (TGA) (**Figure S 41**). At the onset of the heating process, up to 254 °C, the TGA curve exhibits a minimal loss of mass (~ −6%), predominantly attributable to the evaporation of residual moisture and the initial evaporation of highly volatile organic constituents within the coffee ground and melamine. In the primary decomposition phase, between 254 °C and 600 °C, there is a pronounced reduction in mass as organic compounds are thermally decomposed, yielding smaller, volatile molecules. These processes contribute to the formation of a carbon-rich structure in the sample. Upon reaching 800 °C, the sample was

maintained at this temperature for 2 h to facilitate the formation of a stable, carbon-rich structure. At this stage, the TGA curve exhibits only minimal additional mass loss, indicating that most of the volatile components have already been released. Carbonization at even higher temperature was not tested as the previous study indicated an iron-catalyzed graphitization step occurring rapidly above 850 °C. [543] The final mass stabilized at approximately 31.6%, reflecting the catalyst yield after pyrolysis and confirming the efficacy of the pyrolysis conditions in producing the desired product.

Low-energy ion scattering spectroscopy (LEIS) measurements were performed on the DAC (**Figure S 42**). Coffee is known to contain major amounts of caffeine, but it is also rich in numerous phytochemicals, including phenols (such as chlorogenic acid and caffeic acid), diterpenes (such as cafestol and kahweol), lactones, niacin, and trigonelline, which is the precursor of niacin. [544–546] In total, there are almost 1000 defined phytochemicals in coffee. [547] The peaks observed in the LEIS spectrum can be attributed to the presence of carbon, nitrogen, and oxygen, which can be explained by the addition of melamine and the above-mentioned components of coffee. The successful doping of the coffee by the iron species is corroborated by the presence of a peak that can be assigned to iron. Furthermore, magnesium, sodium, potassium and chloride have been identified as minor constituents of coffee. [544,548,549] It is plausible that the chloride present is augmented by the introduction of $FeCl_2$.

Similarly to the LEIS measurement, a SEM-EDX measurement (**Figure S 43**) enabled the detection of carbon, nitrogen, oxygen, iron, sodium, potassium, and chlorine. Furthermore, the sample exhibited the presence of calcium, magnesium, aluminum, phosphorus, and sulfur, which are also known components of coffee. [548,550]

The iron content of the DAC was determined to be 2.81% by inductively coupled plasma optical emission spectrometry (ICP-OES). Additionally, the iron content of a biochar (BC) sample, which did not undergo the $FeCl_2$ addition, was also quantified as a reference. A negligible quantity of iron (0.01%) was identified in this sample, as iron is a known component of coffee. [548]

The picture of the surface composition given by LEIS was supplemented by X-ray photoelectron spectroscopy (XPS), another technique well-suited for surface analysis, but also providing additional information about the chemical state of elements. In addition to carbon and oxygen, which are the main components of the surface of DAC, the presence of significant amounts of N was identified. The XPS N 1s spectrum (**Figure 50A**) shows three components at 398.3 eV, 399.7 eV, and 400.9 eV assigned to pyridinic, pyrrolic, and quaternary nitrogen species, respectively. [551,552] In the case of the component at 399.7 eV,

the contribution of Fe-N_x bonds resulting from the interaction between the d-orbitals of Fe and p-orbitals of N cannot be excluded. [553]

Conversely, the analysis of the XPS Fe 2p spectrum (**Figure 50B**) discloses that Fe^{3+} is a dominant iron-containing form on the studied surface. Its presence is confirmed by the position and multiplet structure of the main peak at 710.6 eV in the Fe $2p_{3/2}$ region. [554] Still, a very weak peak at 706.9 eV is observed on the shoulder on the side of lower binding energies, indicating the occurrence of traces of strongly reduced species, most probably metallic Fe.

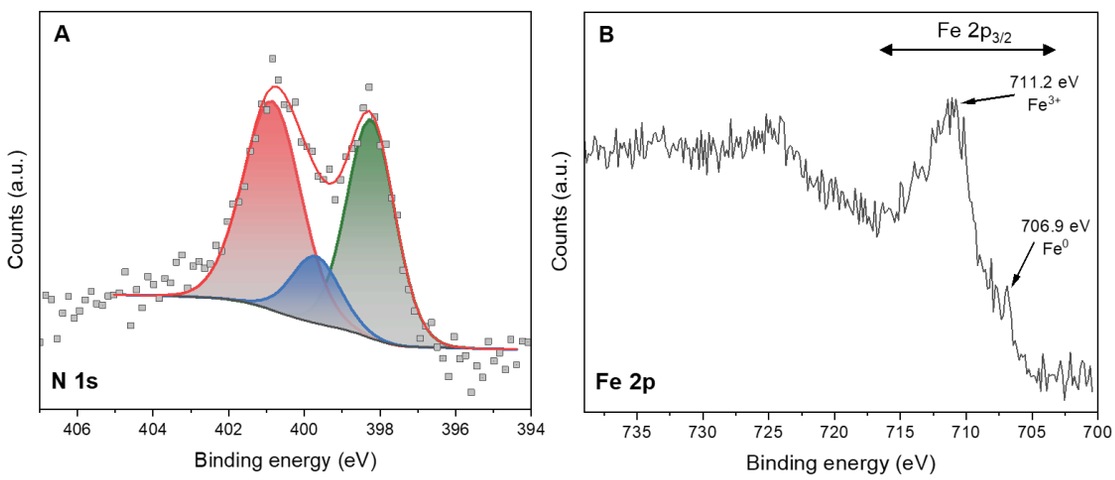

Figure 50. XPS N 1s (A) and Fe 2p (B) core level spectra of DAC. The XPS N 1s spectrum reveals peaks attributed to pyridinic (green), pyrrolic (blue), and quaternary (red) nitrogen species, indicating successful nitrogen doping of the biochar matrix. Furthermore, the Fe 2p spectrum validates the presence of Fe^{3+} as the predominant oxidation state, accompanied by a negligible contribution from metallic Fe.

High-resolution transmission electron microscopy (HR-TEM) was utilized to examine the structure of the catalyst. As documented in literature, atomically dispersed metal atoms, particularly those supported on carbon materials, are potentially vulnerable to high-energy electron irradiation, which can result in the structural collapse of the support and the aggregation of originally dispersed metal atoms during TEM analysis. [555] In a similar manner, in this study, the coffee waste biochar and iron atoms exhibited sensitivity to electron irradiation, complicating the analysis and leading to iron aggregation. A representative image is provided in the Supporting Information (**Figure S 44**).

In order to achieve a more profound comprehension of the structure of DAC, X-ray powder diffraction experiments (**Figure S 45**) were conducted on DAC and BC as a reference. The XRD patterns of DAC and BC, both exhibit two prominent broad reflection peaks at 23° and 43°, corresponding to the (002) and (101) reflections of the graphitic phase, respectively. [527] Furthermore, the presence of a weak reflection peak around 80°, attributed

to the (112) reflection, suggests the occurrence of long-range graphitic stacking, thereby indicating that DAC and BC can be classified as turbostratic carbons. [527]

To gain insight into the coordination structure of the iron atoms in DAC, X-ray absorption (XAS) measurements, that may provide a detailed picture of the atomic environment around the metal centers [556,557] were conducted. The Fourier-transformed (FT) X-ray absorption fine structure (EXAFS) spectrum of DAC (**Figure 51A**) exhibits two peaks at about 1.5 Å and 2.1 Å, indicative of the presence of a Fe-N (1.99 ± 0.03 Å) and a Fe-Fe (2.63 ± 0.03 Å) bond. Note that the determined Fe-Fe bond distance is slightly larger compared to bulk bcc iron with R(Fe-Fe)= 2.48 Å. Furthermore, also carbon from the matrix is detectable in a distance of 2.55 ± 0.05 Å. Most important, compared to metallic Fe in a body-centered cubic structure with 8 iron neighbors in the first shell, the magnitude of the peak at 2.1 Å belonging to Fe-Fe interactions in the first shell is a factor of about ≈ 5 smaller (see **Figure S 46**), a strong indication for a substantially reduced Fe-Fe coordination number. Accordingly, a Fe-Fe coordination number of about 1.6 can already be anticipated for sample DAC from the inspection of the Fourier-transformed data, which is confirmed by the quantitative fits (**Figure 51A**), giving a value of N(Fe-Fe)=1.53 ± 0.23. Second, the second Fe-Fe shell, expected at a radial distance of about 2.9 Å, is absent in the raw data. If such a shell is included in the fit model, the resulting amplitude is zero, *i.e.*, there are no small iron clusters in the sample, which would also reveal Fe second nearest neighbor and even more distant Fe atoms. The fitting results (**Figure 51A**) thus suggested a structural model for DAC comprising a N_2-Fe-Fe-N_2 motif (**Figure 52**, **Figure S 48**). Assuming that iron and nitrogen are incorporated in graphene sheets of the carbon matrix, a simple 2-dimensional model appears sufficient here. Coordination numbers determined for Fe-N (N(Fe-N) ≈ 3.2 ± 0.3) and Fe-C (N(Fe-C) ≈ 3.1 ± 0.3) bonds are compatible with the presented structural motif within the errors of the fits. Detailed fit results are provided in **Table S 5** and **Table S 6** of the Supplement. To ascertain the stability of the catalyst, the measurement was repeated post-reaction (after lignin depolymerization: −1.6 V (*vs.* Ag/AgCl (satd. KCl) for 20 h). The same structural motif (N_2-Fe-Fe-N_2) was observed to fit (**Figure 51B**) after the reaction, with identical Fe-N and Fe-Fe bond distances of and only slightly changed coordination numbers, indicating that the catalyst remains stable throughout the course of the reaction.

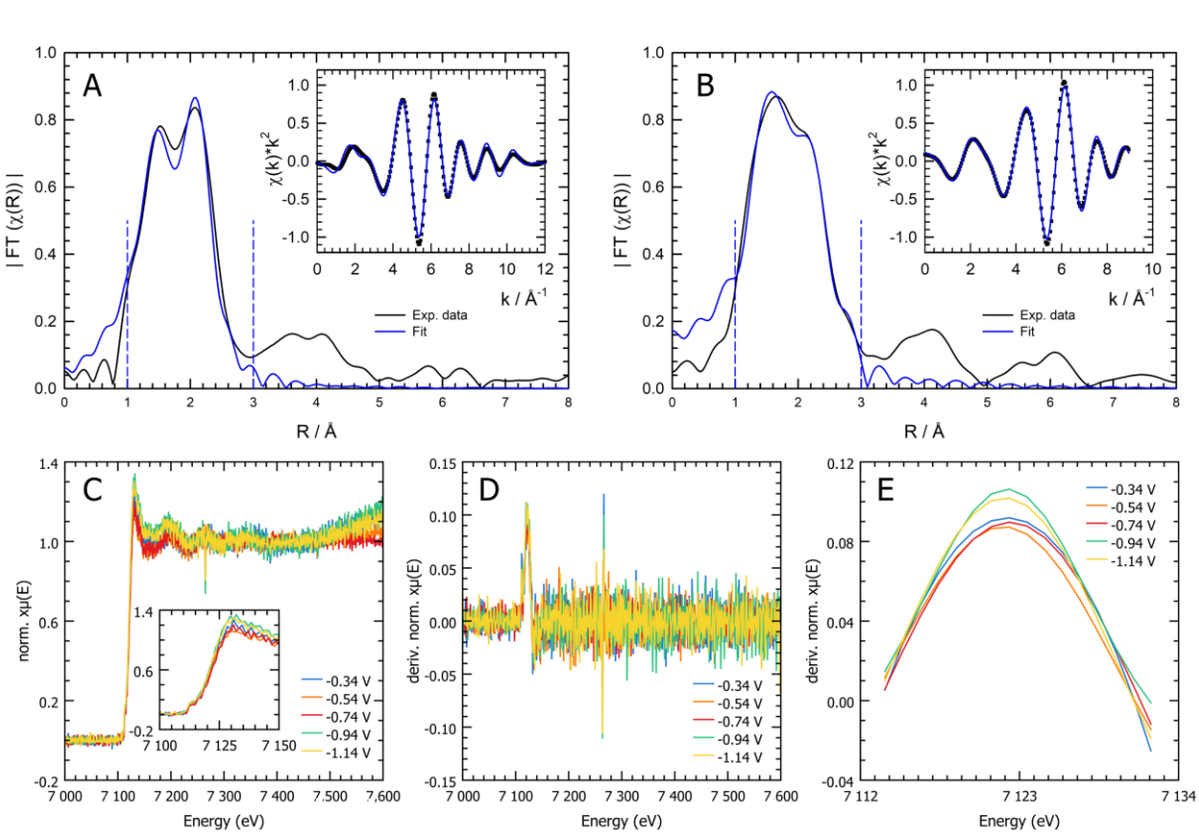

Figure 51. Coordination structure and stability of DAC. **A** Fourier transform (FT) of the Fe K-edge EXAFS spectrum of DAC pre-reaction and corresponding fitting curve (k-range for the FT 1.3 $Å^{-1}$ < k < 11.6 $Å^{-1}$). The inset depicts the back-transformed data from 1.0 Å < R < 3.2 Å according to the dashed vertical lines. **B** Fourier transformation of the Fe K-edge EXAFS spectrum of DAC post-reaction and corresponding fitting curve, again the range from 1.0 Å < R < 3.2 Å was back-transformed into k-space and is depicted in the inset. **C** Normalized Fe K-edge XAS spectra measured *in-operando* for different potentials (*vs.* RHE) as indicated. **D** First derivation of the normalized Fe K-edge XAS spectra. **E** Gaussian fit for the first derivative in the edge region (7112 eV < E < 7143 eV) of the normalized Fe K-edge XAS spectra. No systematic shift of the edge positive is observed.

For stability assessment of the catalyst, *in-operando* XAS measurements were conducted, contingent on the potential. To this end, a reactor was designed in which the electrochemical lignin depolymerization could be conducted concurrently with the XAS measurement. The theoretical (**Figure S 50**) and practical (**Figure S 51**) configuration of the reactor is detailed in the Supporting Information. Due to the high absorbance of the lignin solution, only fluorescence XAS-data could be detected. **Figure 51C** depicts the normalized Fe K-edge XAS spectra at applied potentials of −1.2, −1.4, −1.6, −1.8, and −2.0 V (*vs.* Ag/AgCl (satd. KCl)) (−0.34, −0.54, −0.74, −0.94, and −1.14 V (*vs.* RHE)), respectively. Although the *in-operando* data is noisier than the *ex-situ* measurements due to the significantly lower fluorescence intensity under *in-operando* conditions, all spectra exhibit identical edge positions as well as post-edge absorption minima and maxima. This indicates that the catalyst does not undergo substantial alterations as a function of potential. To verify this assertion with greater precision, the absorption edge was observed

and examined for energy shifts, that would be a sensitive indicator, *e.g.*, for potential-induced changes of the Fe-valence. **Figure 51D** depicts the first derivative of the spectra. Due to the inherent noise in the spectra, a Gaussian fit was performed for the first derivative of the absorption edge (**Figure 51E**). No discernible shifts are evident, confirming that the catalyst maintains stability across a range of potentials.

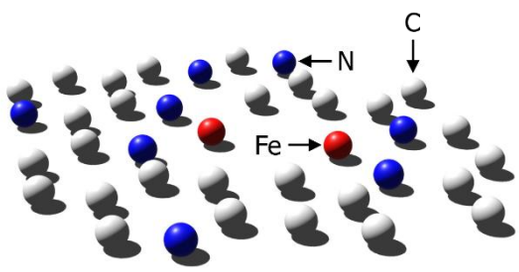

Figure 52. Structural model, based on fitting results, for DAC comprising a N_2-Fe-Fe-N_2 motif. The model illustrates the coordination environment of the dual-atom active sites in the DAC. Fitting results from XAS and extended EXAFS analysis confirm the presence of Fe-N and Fe-Fe bonds, along with carbon interactions from the biochar matrix.

Although DACs have demonstrated efficacy in other catalytic processes due to their synergistic active sites, their potential in addressing the structural complexity of biomass, such as lignin and cellulose, has yet to be fully realized. To address this gap, the performance the DAC was evaluated using the reductive depolymerization of Kraft lignin as a representative reaction. This model reaction was selected to substantiate the catalytic activity and stability of the DAC under realistic electrochemical conditions. The principal aim of this study was not to optimize the depolymerization process but to demonstrate the DAC's capacity to facilitate biomass valorization while maintaining structural integrity.

The DAC was successful in enabling lignin depolymerization, resulting in the production of both aliphatic and phenolic compounds. Qualitative observations, such as the decolorization of the lignin solution, provided visual evidence of the reaction's progress (**Figure 53, Figure S 12**). The selection −1.6 V as the potential (*vs.* Ag/AgCl (satd. KCl)) (−0.74 V *vs.* RHE) was based on the premise of maintaining a potential below that required for water splitting (E > 1.23 V *vs.* RHE) [316] throughout the reaction, irrespective of pH fluctuations.

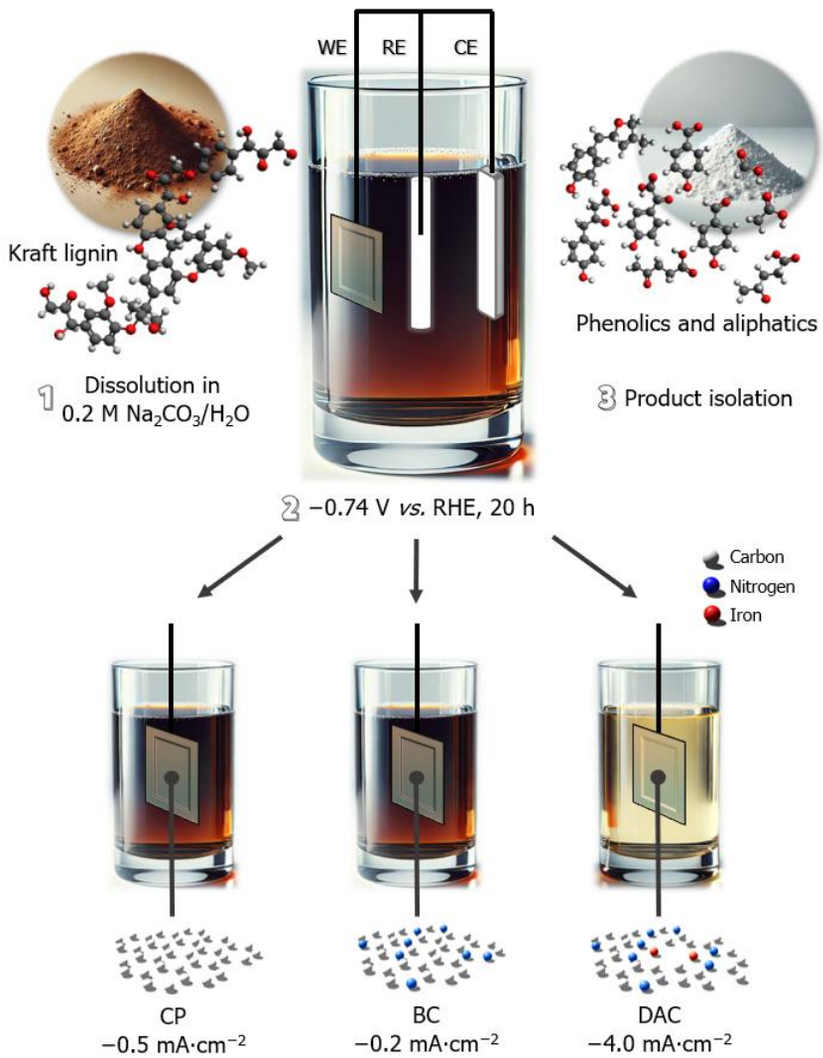

Figure 53. Representation of electrocatalytic depolymerization and partial dearomatization of Kraft lignin (3 g L^{-1}) in an aqueous sodium carbonate medium catalyzed by carbon paper (CP), biochar without Fe-doping (BC) or DAC. The process involves the application of a constant potential (−0.74 V *vs.* RHE), driving the electrochemical reduction of lignin. The selective cleavage of lignin results in the formation of both aliphatic compounds (*e.g.*, sodium levulinate, sodium 4-hydroxyvalerate sodium formate, sodium hexanoate, and sodium acetate) and aromatic species, which are selectively extracted using ethanol as a solvent.

The electrochemically active surface area (ECSA) was determined to be 58.35 cm^2 for the Fe DAC (**Figure S 49**). However, we used the geometric current instead of the ECSA-normalized current to ensure comparability with literature-reported catalysts for lignin depolymerization.

Figure 54 illustrates the current course during the 20-hour reaction for DAC and CP and BC for comparison. The DAC exhibits the highest and most sustained current, reaching −48.4 mA (−4.0 mA cm^{-2}) at the completion of the reaction, which is significantly higher than that observed for the other materials. In contrast, the CP and BC electrodes demonstrate much lower currents, with CP maintaining a consistent but weak

performance (−6.4 mA, −0.5 mA cm^{-2}) and BC exhibiting minimal activity throughout the reaction (−2.8 mA, −0.2 mA cm^{-2}). These results underscore the superior catalytic activity of the DAC.

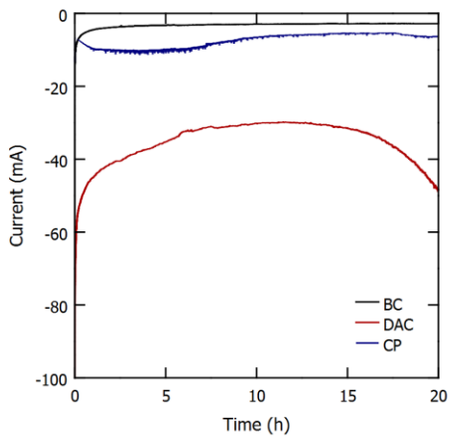

Figure 54. Constant potential electrocatalytic depolymerization at −0.74 V *vs.* RHE of Kraft lignin in 0.2 M Na_2CO_3/H_2O. The DAC demonstrates the highest and most stable current throughout the reaction, reaching −48.4 mA (−4.0 mA cm^{-2}) by the reaction's completion, thereby exhibiting a significant performance level that surpasses that of CP and BC. The CP electrode displays a consistent but low current of −6.4 mA (−0.5 mA cm^{-2}), while BC exhibits minimal catalytic activity with a current of −2.8 mA (−0.2 mA cm^{-2}).

Following the depolymerization reaction, the lignin products (DL) were extracted *via* solid–liquid extraction using ethanol as the solvent. The selection of ethanol was based on its incompatibility with the electrolyte, sodium carbonate, which ensures minimal interaction and a cleaner product separation. Furthermore, ethanol's reusability and status as a safe, sustainable solvent, endorsed by CHEM21, make it an ideal choice for this process. [354]

Table 19 presents a list of the phenolic monomers and dimers that can be identified in DL through DI ESI-HRMS analysis. **Table 20** illustrates the relative intensity of the resulting phenolic products as a function of the employed electrocatalyst, demonstrating the impact of catalyst selection on the observed product distribution.

Table 19. Identified phenolic products of depolymerization identified by direct infusion (DI) ESI-HRMS.

m/z	121.0292	137.0272	149.0605	151.0400	165.0193
Chemical Structure	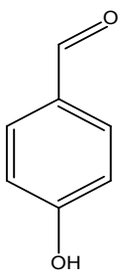	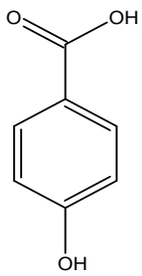	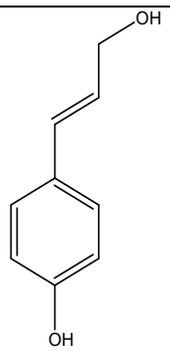	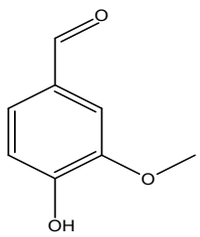	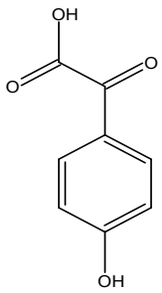
Name	4-hydroxybenz-aldehyde	4-hydroxy-benzoic acid	(E)-4-(3-hydroxyprop-1-en-1-yl)phenol	4-hydroxy-3 methoxybenz-aldehyde	2-(4-hydroxyphenyl)-2 oxoacetic acid
m/z	165.0552	189.0915	193.0504	195.0297	195.0661
Chemical Structure	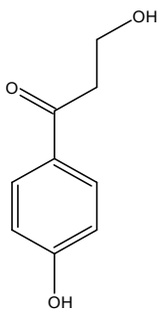	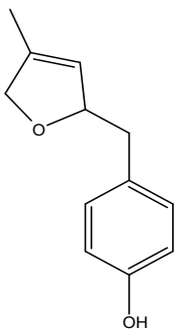	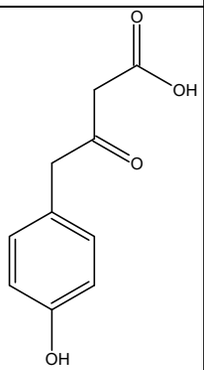	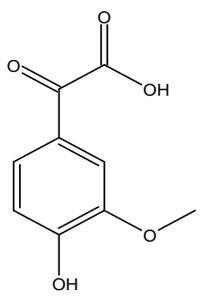	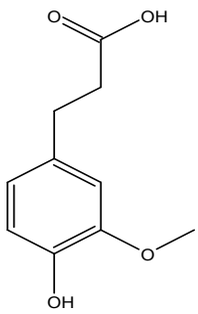
Name	3-hydroxy-1-(4-hydroxyphenyl) propan-1-one	4-((4-methyl-2,5-dihydrofuran-2-yl)methyl)-phenol	4-(4-hydroxyphenyl)-3-oxobutanoic acid	2-(4-hydroxy-3-methoxyphenyl) -2-oxoacetic acid	3-(4-hydroxy-3 methoxyphenyl) propanoic acid

Table 20. Relative intensity of the phenolic products in the depolymerization products as a function of the electrocatalyst.

m/z	**CP**	**BC**	**DAC**
121.0292			
137.0272			
149.0605			
151.0400			
165.0193			
165.0552			
189.0915			
193.0504			
195.0297			
195.0661			
Intensity	maximum	medium	low

The DI ESI-HRMS analysis revealed the presence of aliphatic compounds, including the products known for lignin depolymerization, [138,203] levulinic acid (m/z 115.0400) and 4-hydroxyvaleric acid (m/z 117.0556), in low intensity. Additionally, hexanoic acid (m/z 115.0763) was identified. Furthermore, formic acid and acetic acid, which are also known aliphatic products of lignin depolymerization, [138,203,354] were detected with the help of a nuclear magnetic resonance (NMR) analysis.

Further analyses and discussions are presented in the SI, as well as a table comparing previously reported bulk catalysts with the Fe-DAC to provide context for its performance.

9.4 Conclusion

This study introduces an iron dual-atom catalyst (DAC) supported on biochar derived from spent coffee grounds for the electrochemical reductive depolymerization and partial dearomatization of Kraft lignin. The DAC's atomically dispersed iron sites exhibited high catalytic efficiency and selectivity under ambient conditions. *In-operando* XAS confirmed the catalyst's structural stability across varying electrochemical potentials, thereby ensuring consistent performance throughout the reaction. Building on the demonstrated stability and effective depolymerization of lignin into aliphatic and phenolic products, this study highlights the potential of the DAC for innovative biomass valorization. By integrating innovative catalyst design with *in-operando* characterization, a framework for the broader application of dual-atom catalysts is established, and a model for exploring structure-performance relationships in electrochemical systems is provided. These findings pave the way for new opportunities in the rational design and optimization of catalysts tailored to efficient and scalable biomass conversion processes.

9.5 Acknowledgement

We would like to thank the University of Wuppertal and the Stockholm University for their research support. Parts of the results presented here have been achieved through collaborative research projects made possible by the financial support of our project partners and the Austrian COMET program (Project InTribology2, No. 906860). The COMET program is funded by the Austrian federal government and, specifically for InTribology, by the provinces of Lower Austria and Vorarlberg. The XPS study was carried out using research infrastructure funded by the European Union in the framework of the Smart Growth Operational Programme, Measure 4.2; Grant No. POIR.04.02.00-00-D001/20, "ATOMIN 2.0 – Center for materials research on ATOMic scale for the INnovative economy". The financial support of the Strategic Programme Excellence

Initiative at Jagiellonian University, used for servicing measurement systems, is also appreciated. We thank the Gesellschaft für Forschungsförderung Niederösterreich (Project FTI21-D002) and the European Regional Development Fund under grant number WST3-F-542638/004-2021 for financial support. A.N. and J.Y. thank the Swedish Research Council for Sustainable Development (FORMAS) for financial support. We thank Andjelka Ristic for her significant contribution to the DI-ESI-HRMS measurement and Julia Bornhorst and Vivien Michaelis for their support with the ICP-OES measurement. In addition, we are grateful for the beam time provided by the DELTA synchrotron (Dortmund, Germany). We would also like to express our appreciation to Madlin Spiewak for her support with the XAS measurements and Franka Stallmann for her support throughout the whole project. We thank Dr. Serhiy Budnyk for the fruitful discussions. L. M. L. appreciates the support and enriching interdisciplinary discussions provided by the 'Sustainable Chemical Synthesis 2.0' (*SusChemSys* 2.0) networking program.

9.6 Author contributions

Conceptualization, L.M.L., A.S., and B.V.M.R.; Methodology, L.M.L. and A.P.N.; Investigation, L.M.L. and A.P.N.; Data Curation, L.M.L., D.L.H., A.D., M.F., P.P., B.B.B., P.K., and Y.C.; Formal Analysis, L.M.L., D.L.H., B.B.B., M.F., and P.K.; Writing – Original Draft, L.M.L.; Writing – Review & Editing, L.M.L., B.B.B., B.V.M.R., and A.S.; Supervision, C.M.P., Y.Y., C.W.L., J.Y., B.V.M.R., and A.S.

Chapter 10

Overview and Future Perspective

Chapter 10 - Overview and future perspective

10.1 Overview

In this dissertation, three different electrocatalysts were examined, and three novel work-up methods were developed. Initial investigations focused on the utilization of bulk catalysts, comprising carbon and silver, prior to the transition to an atomically dispersed catalyst comprising iron atoms on a carbon-nitrogen matrix.

An unmodified carbon electrode was initially employed for the reductive electrochemical depolymerization of Soda lignin in an aqueous sodium carbonate solution. The selection of carbon as an electrocatalyst is predicated on numerous advantages: i) carbon materials can be used either as a support medium for catalysts or as a direct catalyst; [170] they are regarded as a sustainable alternative to metallic catalysts due to their cost-effectiveness, chemical stability, resistance to acidic and alkaline conditions, and high electronic conductivity, [171,172] which is imperative for electrochemical processes. In this approach, the electrical current and reaction time were varied with otherwise identical parameters to ascertain the optimal reaction conditions. After the reaction, water was removed under reduced pressure, and the ethanol-soluble fraction of the depolymerization products were extracted. Ethanol was selected as the solvent due to its incompatibility with sodium carbonate, thereby preventing unwanted interactions and enabling a more efficient product separation. Its reusability contributes to its efficiency, enabling multiple extractions with minimal efficacy loss. Furthermore, ethanol is acknowledged by CHEM21 for its sustainability, thereby affirming its aptitude as an environmentally friendly solvent within the stipulated process. [337]

It was ascertained that a current of −175 mA over 20 h achieved the most selective product distribution and, concomitantly, the highest yield. However, a clear correlation between current and yield could not be established. At higher currents than −175 mA, the yield decreased, indicating that either volatile depolymerization products escaped or the reaction was inhibited by a competing reaction, such as water splitting.

It is well established that the characterization of products resulting from lignin depolymerization is challenging. This complexity arises from the fact that a substantial number of products are generated during the depolymerization process, despite the never-ending search for “selective” methodologies. This inherent ambiguity hinders the interpretation of nuclear magnetic resonance (NMR) spectra, as the signals from numerous products frequently overlap, obscuring the distinct spectral characteristics of each

individual compound. Nevertheless, the choice of a carbon electrode, operating at −175 mA for 20 h, facilitated the identification of four predominant aliphatic compounds from lignin depolymerization: sodium levulinate, sodium 4-hydroxyvalerate, sodium acetate, and sodium formate. This identification was achieved through the utilization of ^{1}H and ^{1}H-^{1}H COSY NMR spectroscopy, complemented by a comparison with reference substances. The presence of sodium levulinate and sodium 4-hydroxyvalerate was additionally confirmed by liquid chromatography-electrospray ionization-mass spectrometry (LC-ESI-MS). It is noteworthy that aromatic signals could no longer be detected using NMR spectroscopy (in D_2O) from a current of −100 mA (with a reaction time of 20 h) or a reaction time of 10 h (with a constant current of −175 mA). An examination of the products with LC-UV (280 nm) also showed the complete dearomatization of the lignin.

The majority of research on lignin depolymerization has primarily centered on the generation of aromatic compounds. [3,252–254] This study underscores the potential for complete dearomatization of lignin to yield aliphatic precursors through a simple electrochemical depolymerization. While the present study did not prioritize elucidating the depolymerization mechanisms, initial mechanistic trends can be discerned through NMR spectroscopy. An examination of the NMR spectra reveals the presence of aromatic signals at hours 1, 3, and 6. However, olefinic signals become discernible at hour 6, which were not visible before. From hour 10 onwards, olefinic signals become predominant, with no aromatic signals being identified. This suggests that hydrogenation of the aromatic compounds occurs over time, which leads to ring-opening. The olefins are presumably further reduced to aliphatic compounds. Similar trends can also be observed when other values of current are used.

In a subsequent study, the unmodified carbon electrode was substituted with a silver wire to assess the impact of the electrocatalyst on depolymerization. The electrocatalytic depolymerization of lignin using silver as an electrocatalyst has received limited attention in the research community, resulting in a significant research gap that this study aimed to address. [5] This noble metal has emerged as a promising candidate for electrocatalysis due to its exceptional electrical conductivity, high catalytic activity, and excellent cost-effectiveness compared to platinum. [318–323] A notable advantage of silver is its capacity to selectively activate oxygen-containing functional groups while maintaining stability under electrochemical conditions. This property makes silver particularly suitable for biomass conversions, where complex, multifunctional macromolecules such as lignin undergo transformation. [323] Furthermore, silver's interaction with aromatic groups in lignin not only facilitates depolymerization but also promotes targeted dearomatization, a crucial step in the formation of valuable aliphatic intermediates.

Soda lignin, Na_2CO_3/H_2O as a solvent system, and a constant current of −175 mA were selected for direct comparison, with only the reaction time being varied. Previous studies, such as the carbon-catalyzed depolymerization, have already demonstrated that the degree of decolorization of the lignin solution is an indicator of the degree of depolymerization. While the solution became significantly more transparent after 20 h and took on a yellowish tone, the silver reaction reached the same degree of decolorization after only 5 h and was completely decolorized after 20 h. At the same time, a volume loss of about 10 mL (−20%) was observed when silver was used as the electrocatalyst, indicating that either water splitting or the formation of volatile depolymerization products had taken place. This initial finding suggests that silver catalyzes the depolymerization of Soda lignin more rapidly than carbon. A direct comparison of the catalysts revealed a substantial discrepancy in the yield, with the carbon electrode yielding 58% and the silver electrode yielding 18%. NMR spectroscopy analysis revealed the presence of three aliphatic compounds: sodium levulinate, sodium acetate, and sodium formate. However, sodium 4-hydroxyvalerate could not be identified as a product, in contrast to when carbon was used as an electrocatalyst. When employing carbon (−175 mA, 20 h), no aromatic compounds could be detected in the NMR, a finding that was also confirmed by LC-UV (280 nm). The presence of aromatic compounds is not discernible within the NMR spectrum when silver is utilized as the electrocatalyst. However, aromatic compounds were detected using DI-HRMS, indicating that D_2O may not be the most suitable solvent for their detection. This observation indicates that, despite the apparent dissolution of the compounds, they may in fact be present as a fine suspension. Consequently, the consideration of alternative solvents becomes imperative for achieving more precise analytical results.

The findings of both studies clearly demonstrate that the choice of catalyst has a significant impact on depolymerization, while the reaction can be effectively controlled by adjusting the current and reaction time to obtain the desired products. Silver has been identified as an effective catalyst to produce both aromatic and aliphatic compounds, while carbon is particularly suitable for achieving complete dearomatization of lignin.

When silver was utilized, a comparatively low yield was attained under otherwise identical conditions (−175 mA, 20 h) (carbon 58%, silver 18%). Substituting Soda lignin with Kraft lignin, which possesses distinct properties such as a higher degree of modification and an increased prevalence of C-C fused structures, [353] resulted in a further decline of the yield to 3%. This observation suggests that a more detailed characterization of the starting lignins would be beneficial to fully understand their influence on the reaction outcome.

In light of the suboptimal yield, there is an imperative for an alternative processing method that can enhance efficiency and yield. To enhance the efficiency of depolymerization product recovery, the previous solvent system (Na_2CO_3/H_2O) was modified to incorporate an organic phase as top layer. A previous study demonstrated that methyl isobutyl ketone (MIBK) is a suitable solvent, though it has been utilized primarily for subsequent extraction of the products. [104] To the best of the authors knowledge, this is the first documented *in-situ* two-phase extraction for electrochemical lignin depolymerization. The utilization of an electrochemical emulsion oxidation process, as pioneered by Di Marino *et al.*, involves the dissolution of lignin in a deep eutectic solvent (DES), followed by *in-situ* emulsification with MIBK and depolymerization under oxidative conditions. [363] This approach laid the foundation for enhanced product recovery through hybrid methodologies. Reference reactions have demonstrated the stability of MIBK during the reaction, a finding that offers two distinct advantages. Firstly, it can be excluded that MIBK contributes to the final product mixture, and secondly, it enables the reusability of MIBK. Preliminary tests were done to assess the solubility of lignin in MIBK. Specifically, Kraft lignin was stirred in MIBK for 20 h at room temperature, resulting in 8% lignin dissolution. Subsequent tests involved a two-phase system, wherein lignin was initially dissolved in Na_2CO_3 and H_2O, followed by a 0-hour and 20-hour stirring process with MIBK, yielding 3% and 8% lignin, respectively. By applying a current of −350 mA (double volume, double current), the electrochemical depolymerization process increased the MIBK-soluble fraction, yielding a 67% oil-like brown product.

In earlier studies, the term “yield” was defined as the mass of the products divided by the mass of the lignin utilized. [138,354] However, in the instance of products obtained from the ethanol-soluble fraction, the “real yield” was found to be affected due to the inclusion of sodium originating from the electrolyte (Na_2CO_3) in the calculation. In the reference reaction to assess MIBK stability, the organic solvent could be evaporated without any electrolyte residue, indicating that Na_2CO_3 is not soluble in MIBK. Consequently, the products from the MIBK phase are pure compounds rather than sodium salts, thereby emphasizing the high yield compared to previous work. However, to unequivocally confirm the absence of sodium, an additional ICP analysis would be beneficial. After the reaction, the aqueous and MIBK phases were separated, while the aqueous one was subjected to standard processing using ethanol, yielding a white solid. Remarkably, the yield increased from 3% to 68% when a MIBK phase was present, suggesting that the organic phase has a great influence on the reaction equilibrium. The underlying reason for this substantial discrepancy remains to be examined. One hypothesis posits that this increase may be attributed to the absence of contact between the aqueous phase and the atmosphere. The

yield of the MIBK phase and that of the aqueous phase collectively exceed 100%, a phenomenon that can be attributed to the sodium content of the aqueous phase. Notably, this yield significantly surpasses that of the previous method.

It is important to note that achieving high selectivity in lignin depolymerization should not always be the optimal objective, as a broad product spectrum can offer economic and technological advantages. [360] The comprehensive analysis of the aqueous and organic phases of the reaction products revealed the formation of numerous compounds during the reaction, which underscores the need for a reevaluation of lignin valorization strategies.

The NMR spectrum of the aqueous phase suggests the presence of sodium levulinate, sodium acetate, and sodium formate. Additionally, the spectrum displays a greater variety of signals, some of which overlap, suggesting an expanded product range. Signals from aliphatic compounds are predominantly identifiable in the spectrum, though aromatic and olefinic signals are also present, albeit with lower intensity. The NMR spectrum of the organic phase reveals a distinct distribution. In addition to aliphatic signals, a variety of aromatic, olefinic compounds, and carboxylic acids are discernible. Supported by DI-HRMS analyses, it was determined that larger monomers, dimers, or oligomers tend to transition into the MIBK phase during the reaction, while smaller aliphatic products prefer to remain in the aqueous phase. Therefore, once again it should be noted that conventional strategy of highly selective depolymerization towards single aromatic monomers is not necessarily the optimal approach. The intricate nature of lignin presents significant challenges in achieving complete selective cleavage to a single monomer. [360] A more advantageous approach might involve the conversion to a chemically heterogeneous product mixture, particularly within the context of a liquefy-first strategy. [360] This strategy would not only enhance scalability and industrial feasibility but also facilitate the broader utilization of lignin fractions. The concept of converting lignin into liquid, versatile feedstocks aligns with existing refinery processes and could therefore serve as a viable alternative to traditional depolymerization methods.

The oil-like product obtained from the MIBK phase was utilized in preliminary application-related tests. A considerable portion of global energy consumption (23%, equivalent to 103 EJ) is attributable to tribological contacts, particularly friction. [558] Zinc dialkyl dithiophosphate (ZDDP) is frequently employed to mitigate wear, as it forms protective films on metal surfaces through *in-situ* decomposition. [559] However, ZDDP releases zinc vapors (<1 µm) during decomposition, which can cause metal fume fever, skin irritation, and even fatality if swallowed. [559,560] A more environmentally friendly alternative are traditional ester oils, which are biodegradable and less toxic. [561] However,

they compete with the food industry, which limits their long-term availability and sustainability. Due to these challenges, interest in renewable, environmentally friendly tribological solutions is growing. Although the use of this lignin-based oil as a lubricant exhibited a higher coefficient of friction (COF) than conventional ester oils, a comparable wear protection was observed. The reduced surface scratching observed in the wear demonstration highlights the formation of robust surface interactions and positions lignin as a promising raw material to the next generation bio-based lubricants.

The selection of an appropriate solvent is a pivotal factor in advancing the electrochemical depolymerization of lignin, as it directly influences both process efficiency and economic viability. A particularly promising approach with regard to future biorefineries involves the use of γ-valerolactone (GVL) as a solvent for lignin. GVL has already proven to be suitable for lignin extraction, [276] so that the combination of extraction and depolymerization in one medium could eliminate the need for costly solvent changes. This could avoid energy- and resource-intensive processing steps and significantly increase the efficiency of the overall process.

The electrochemical depolymerization of Soda lignin in GVL was achieved through the use of an unmodified carbon electrode, offering an alternative to the previous approach that used Na_2CO_3/H_2O as the solvent system. The novel method involves substituting half of the water with GVL, while maintaining Na_2CO_3 as an integral component due to its role in providing the necessary conductivity as an electrolyte. The selection of a carbon electrode was predicated on the findings of prior research demonstrating its effectiveness in catalyzing the depolymerization. This electrode has demonstrated stability, cost-effectiveness, and suitability for future upscaling, making it a favorable option. It is well-documented in the existing literature that GVL, in conjunction with bases such as Na_2CO_3, undergoes a ring-opening reaction to yield 4-hydroxyvaleric acid or 4-hydroxyvalerate salts, [269,283] which is a main product of lignin depolymerization. While the ring opening of the solvent may appear disadvantageous at first glance, it can also be viewed positively, as the solvent can be used to further enrich the depolymerization products. The selection of a constant current of −100 mA and an 8-hour reaction time was based on preliminary tests, which demonstrated that under these conditions, ring opening is exclusively base-catalyzed and not caused by the applied current. However, at higher currents and longer reaction times, GVL becomes electrochemically unstable, leading to a more significant degree of ring opening. In addition to 4-hydroxyvalerate, the other products identified in previous studies were also detected in this approach when using carbon as a catalyst. With the aid of an internal standard (deuterated methanol), NMR spectroscopy revealed a ratio of 85% 4-hydroxyvalerate, 8% levulinate, 6% acetate, and 1% formate. Notably, no

aromatic signals were detected in the NMR spectrum. Complete depolymerization was further confirmed by LC-UV (280 nm).

It is noteworthy that in this approach with GVL, complete depolymerization could be achieved at a current of −100 mA and a reaction time of 8 h, whereas in the Na_2CO_3/H_2O system, complete depolymerization only occurred at −175 mA and 10 h or −100 mA and 20 h. This finding indicates that the utilization of GVL can expedite the depolymerization process towards aliphatic products, consequently reducing the energy demand. Moreover, the elimination of additional processing steps and the direct extraction of lignin holds promise for further biorefineries in the future. The enrichment of the product mixture by the solvent has been shown to enhance the overall yield of the process, thereby promoting economic efficiency.

The transition from bulk to atomically dispersed catalysts signifies a notable advancement in the field of heterogeneous electrocatalysis. While conventional bulk catalysts, such as carbon, [138,203] silver, [354] and copper, [104] have been utilized for the electrochemical depolymerization of lignin, their catalytic efficiency is frequently constrained by a limited number of active sites and less precise control of the reaction pathways. Initial research endeavors focused on nanostructured and atomically dispersed catalysts for the electrochemical reduction of CO_2 (eCO_2RR). [369,371,373,374,465] It was demonstrated that by augmenting the specific surface area and reducing the coordination number of individual metal atoms, selective and efficient reaction pathways could be achieved. The present moment marks the transition of these findings to the electrocatalysis of biomass, with a particular focus on the electrochemical depolymerization of lignin. In contrast to conventional bulk catalysts, atomically dispersed catalysts (single-atom catalysts, SACs) and dual-atom catalysts (dual-atom catalysts, DACs) exhibit enhanced efficiency and control over reaction pathways, and improved mass utilization, since nearly every metal atom functions as an active center. [463,518] The iron dual-atom catalyst (Fe DAC) is dispersed on a carbon matrix that was synthesized by the pyrolysis of biochar derived from coffee grounds. This material serves as a support for the atomic distribution of the iron atoms. To investigate the structure and chemical environment of these active sites, the catalyst was characterized by various spectroscopic methods. X-ray absorption spectroscopy (XAS), including X-ray absorption near-edge structure (XANES) and extended X-ray absorption fine structure (EXAFS), confirmed the dual-atom configuration of the iron atoms (N_2-Fe-Fe-N_2 motif). Furthermore, the use of low-energy ion scattering (LEIS) and X-ray photoelectron spectroscopy (XPS) enabled a comprehensive analysis of the catalyst's chemical composition.

A critical consideration for industrial implementation pertains to the stability of the catalyst under the aimed reaction conditions.[10] To validate this, *in-operando* XAS measurements were conducted during the electrochemical depolymerization of lignin in an aqueous sodium carbonate solution. The spectra obtained at different electrochemical potentials exhibited no substantial alterations in the electronic structure of the iron atoms, suggesting that the catalyst is stable across different potentials (−0.34, −0.54, −0.74, −0.94, and −1.14 V (*vs.* RHE)). Further EXAFS measurements before and after catalysis (−0.74 V for 20 h) demonstrated that the same structural motif (N_2-Fe-Fe-N_2 motif) could be fitted after the reaction, thereby confirming the stability of the catalyst throughout the entire reaction period. In contrast to previous studies, the electrochemical depolymerization of Kraft lignin was carried out at a constant potential of −0.74 V *vs.* RHE instead of a constant current. This was done to suppress water splitting (E > 1.23 V *vs.* RHE) as a reference reaction. The system using Fe DAC as electrocatalyst showed the highest current compared to two reference catalysts, with a final value of −48.4 mA (−4.0 mA·cm^{-1}) after a reaction time of 20 h. In comparison, the currents exhibited by carbon paper (CP, −0.5 mA cm^{-2}) and non-doped biochar (BC, −0.2 mA cm^{-2}) were considerably lower, thereby underscoring the superior catalytic efficacy of the Fe DAC (−4.0 mA cm^{-2}). After the completion of the reaction, the depolymerization products were characterized *via* NMR spectroscopy and DI-HRMS, which confirmed the presence of aliphatic compounds, including sodium levulinate, sodium acetate, and sodium formate, as well as phenolic monomers and dimers.

Although the Fe DAC yielded only 5%, this result was nevertheless higher than the 3% obtained with a silver electrode when using Kraft lignin. This outcome underscores the notion that depolymerization is more efficacious with soda lignin than with Kraft lignin, thereby impacting the efficiency of ethanol extraction. As such, this finding underscores the necessity for alternative processing methodologies, such as a MIBK 2-phase system, which may warrant further investigation.

A comparison of Fe DAC with conventional catalysts reveals that the dual-atom structure allows for more efficient utilization of metal sites, leading to a reduction in the amount of metal required and a substantial enhancement in the sustainability and cost-effectiveness of the process.

These findings underscore the pivotal role of catalyst selection, solvent system, and extraction strategy in determining lignin depolymerization efficiency, product selectivity, and industrial viability. As illustrated in **Table 21**, a comparative analysis reveals that while carbon-based electrodes offer sustainability and stability, silver electrodes enable

more selective depolymerization while exhibiting diminished yields in a Na_2CO_3/H_2O solvent system. The integration of an *in-situ* extraction phase has been shown to enhance product recovery, and the Fe-Dual-Atom Catalyst has been shown to achieve the highest atomic efficiency and confirmed *in-operando* stability. These findings demonstrate the potential of advanced catalyst design for sustainable biomass valorization.

Table 21. Comparison of Electrocatalytic Lignin Depolymerization Methods: Catalyst Performance, Product Distribution, and Industrial Relevance.

Catalyst	Carbon	Carbon	Silver	Silver	Iron Dual-Atoms on Coffee Waste Biochar
Solvent	Na_2CO_3/H_2O	GVL/H_2O	Na_2CO_3/H_2O	Na_2CO_3/H_2O MIBK layer	Na_2CO_3/H_2O
Lignin	Soda	Soda	Soda	Kraft	Kraft
Current [mA]	−175	−100	−175	−350	−48
Potential [V *vs.* Ag/AgCl (satd. KCl)]	-	−3.7	-	-	−1.6
Time [h]	20	8	20	20	20
Main aliphatic products	Levulinate, 4-hydroxyvalerate, acetate, formate	Levulinate, 4-hydroxy-valerate, acetate, formate	Levulinate, acetate, formate	WP: Levulinate, acetate, formate OP: 4-hydroxyvaleric acid, 1-hydroxyhex-5-en-3-one, Hexa-2,5-dien-1-ol	Levulinate, acetate, formate
Complete dearomatization	Yes	Yes	No	No	No
Yield [wt%]	58	-*	18	WP: 68 OP: 67	5
Industrial relevance	Sustainable and stable electrode material, no toxic solvents required	Potential for direct integration into biorefineries through combined extraction and depolymer-ization process	Electrode material stable under reductive conditions, but relatively low yield	High efficiency and yield through *in-situ* extraction, potential industrial applications as feedstock	Highest atomic efficiency, high sustainability by utilizing two different types of biomass waste

*The yield of the depolymerization cannot be precisely determined, as the product mixture includes contributions from the GVL ring-opening reaction.

10.2 Future perspective

The pressing challenges of our time—including climate change, a rapidly growing global population, dwindling fossil fuel reserves, and the increasing demand for food and energy—have brought humanity to a point where a paradigm shift is urgently needed.

While it may be difficult to visualize exceeding the 1.5 °C limit for the first time in 2024, the increasing frequency of natural disasters, such as the wildfires in California in January 2025, makes the severe consequences of human-induced climate change since the Industrial Revolution increasingly tangible to the public. These devastating events confront humanity with the harsh reality of the crisis, yet in their severity lies an opportunity. Media attention on natural disasters has the potential to challenge entrenched systems, break habitual patterns, and serve as a catalyst for the urgent changes that are needed.

These global challenges require not only international collaboration but also interdisciplinary cooperation within the scientific community (Sustainable Development Goal (SDG) 17). In the coming years, it will be crucial to strengthen partnerships between universities, research institutions, and industry to accelerate the transition from laboratory innovations to real-world applications.

10.2.1 Biomass as a key resource for a more sustainable future

The efficient utilization of biomass has already proven to be a valuable approach to addressing modern challenges. Although a complete replacement of fossil fuels with biomass may not be feasible, biomass can serve as a sustainable alternative for at least a portion of them.

One key reason why biomass alone is unlikely to be a fully sufficient solution is the distinction between first-generation (1G) and second-generation (2G) biomass feedstocks. 1G feedstocks are primarily derived from food crops such as grains, sugarcane, and vegetable oils, while 2G feedstocks come from lignocellulosic sources like miscanthus, willow, wood and wood waste, as well as agricultural and forestry residues or co-products such as wheat straw and corn stover. [562] Given the growing global population and the objectives of SDG 2, which emphasizes ensuring food security for all, it is essential to prioritize the valorization of 2G biomass to avoid competition with food production. Additionally, the global infrastructure is not designed to handle the vast quantities of biomass required to fully replace fossil fuels, which could be easily extracted from concentrated sources and transported *via* pipelines. To increase the availability of usable

biomass, it is not only essential to focus on 2G feedstocks but also to utilize food waste and by-products generated during food production, such as coffee grounds.

In the coming years, researchers should focus not only on developing novel, more complex, and *in-operando* stable catalysts for biomass valorization but also on exploring new biomass sources and potential applications for the resulting products. This holistic approach will be crucial in facilitating the transition from laboratory research to industrial implementation.

10.2.2 Advancing catalyst development for biomass depolymerization

Bulk catalysts play a valuable role in lignin depolymerization, offering advantages such as ease of handling, commercial availability, and straightforward cleaning, making them well-suited for future implementation in biorefineries. However, to the best of the authors knowledge, this study is the first to employ a dual-atom catalyst (DAC) for electrochemical lignin depolymerization, paving the way for further exploration of atom-dispersed catalysts in this field.

Nanoparticles share some advantages with single-atom catalysts (SACs) and DACs, albeit to a lesser extent. While their higher surface area enables more efficient catalyst utilization, they do not reach the atomic efficiency of SACs and DACs. However, they offer the additional benefit of allowing precise control over alloy composition and structural architecture through tailored synthesis processes. [537] Although metal nanoparticles have been explored for electrochemical lignin depolymerization (*e.g.* [189,563]), they remain under-researched, leaving a significant gap in the field that warrants further investigation.

Copper has already demonstrated its effectiveness as a catalyst for reductive lignin depolymerization, [104] making copper nanoparticles a worthwhile next step. Given that used coffee has proven to be a suitable matrix, it also holds promise as a support material for copper nanoparticles. Initial experiments have demonstrated that copper nanoparticles can be synthesized *in-situ* on coffee powder, followed by carbonization of the resulting material (**Figure 55**), thereby creating a novel copper-based catalyst that has already proven effective in lignin depolymerization.

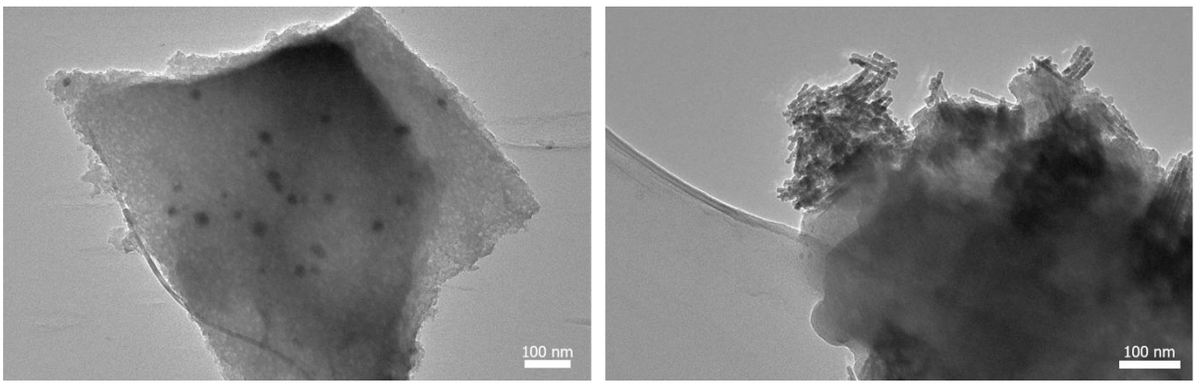

Figure 55. TEM micrographs of a coffee waste biochar catalyst decorated with copper nanoparticles.

This catalyst can be reused multiple times while maintaining a consistent product distribution. Copper nanoparticles are known to undergo oxidation state transitions in different solvents [564] and exhibit morphological changes under electrochemical conditions [369]. However, it is important to note that, if these transformations occur in this system, they do not appear to affect the catalyst's overall performance (**Figure 56**). Nonetheless, *in-operando* studies, such as *in-operando* X-ray absorption spectroscopy (XAS), are crucial for gaining deeper insights into structural and electronic changes during the reaction and for achieving a complete understanding of the catalyst's behavior under operational conditions.

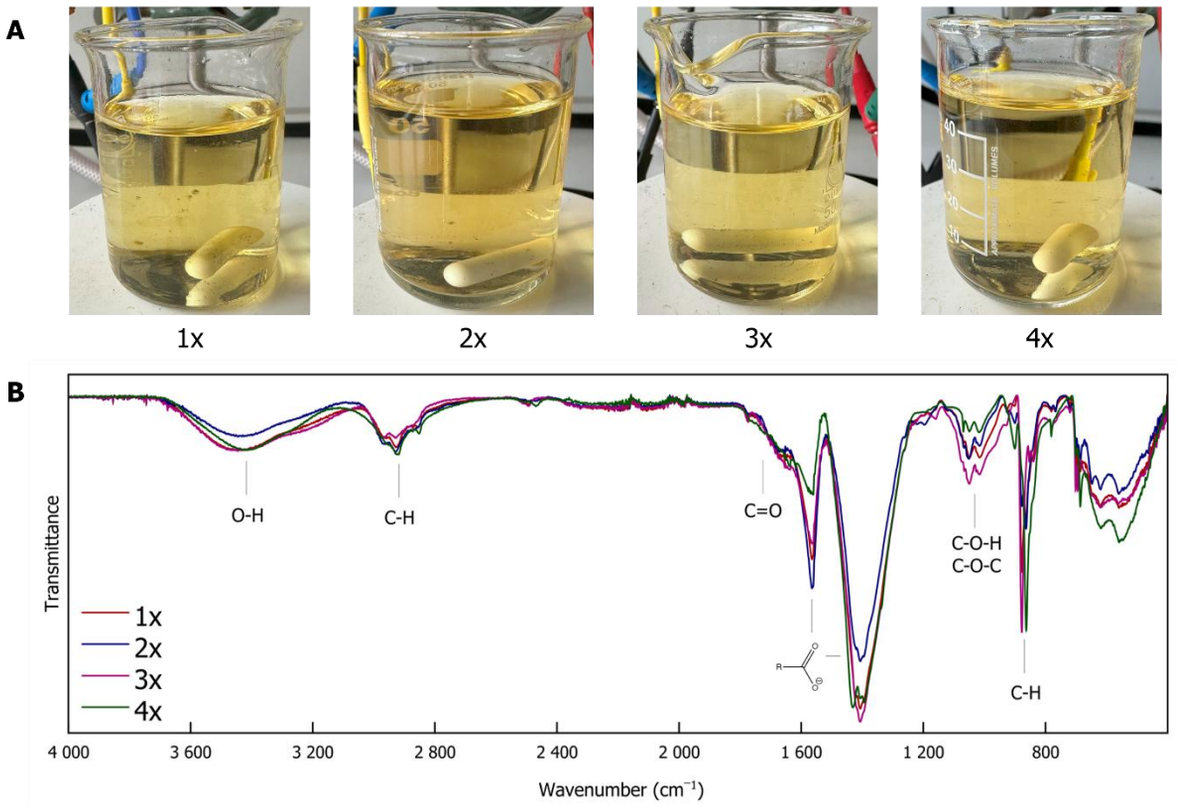

Figure 56. A Color change observed in the solution during the reaction, which remains constant even after four uses of the catalyst. **B** FTIR spectra of the ethanol soluble fraction of depolymerized lignin after repeated electrode use (1x, 2x, 3x, and 4x). Characteristic vibrational bands corresponding to O–H, C–H, C=O, and COO^- groups can be observed, indicating the preservation of key functional groups throughout the reaction cycles.

The continued utilization of copper, albeit transitioning to a different food industry by-product, signifies the prospective lignin depolymerization catalyst that targets copper atoms present on a biochar substrate derived from spent grains. Brewers' spent grains, a lignocellulosic material, constitute the predominant by-product (85%) of the brewing industry, comprising approximately 17% cellulose, 28% non-cellulosic polysaccharides, predominantly arabinoxylans, and 28% lignin. [565] Additionally spent grains are characterized by their high fiber and protein content. [566] To date, the primary application of this by-product has been as an animal feed, [566] with a market value of ~€35 per ton [567]. On average, the global production of beer is estimated to be 39 million tons per year. Of this total, approximately 3.4 million tons are produced in the European Union, with Germany accounting for 2 million tons of that total. [568,569] Furthermore, it has been determined that approximately 20 kilograms of wet spent grains are produced per 100 liters of brewed beer. [565] Due to economic and environmental factors, spent grains have primarily been used as animal feed, but this option is becoming increasingly problematic. The centralization of farming and brewing has led to logistical challenges, especially for large breweries producing over one million hL of beer, where oversupply and declining agricultural demand complicate disposal. While spent grains are microbiologically stable

during production, the prolonged storage can lead to spoilage due to microbial activity, thus limiting the application in the food and feed industries. [569] Consequently, there is an urgent need to identify additional applications for spent grains. Presently, the applications of spent grains are mainly limited to the domains of biogas production, biochar, and composite material. [570] However, it is imperative to acknowledge the potential of spent grains as a matrix material for catalysis. In this context, highly active brewers' grain biochar coated with Ag-Cu nanocrystals has been reported for the mineralization of methyl orange and methylene blue dye mixtures. [571] Meanwhile, preliminary tests on potential copper atomically dispersed catalysts (**Figure 57**), which still require further characterization, have already shown promising activity in electrochemical lignin depolymerization.

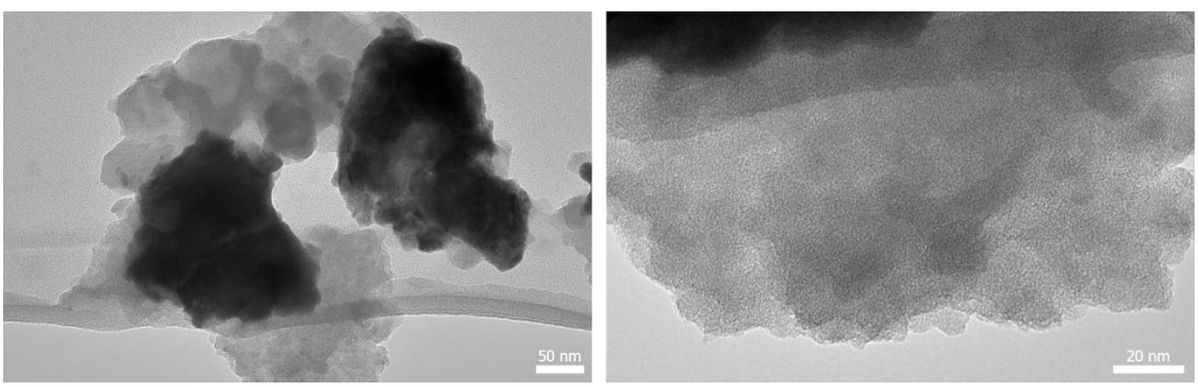

Figure 57. TEM micrographs of a copper-doped spent grains biochar catalyst, indicating atomic dispersion due to the absence of visible copper nanoparticles.

A future research direction that should be prioritized is the investigation of tandem and cascade catalysts, which have the potential to streamline chemical transformations by integrating multiple reaction steps into a single system. [572] This approach could result in a significant reduction in energy consumption, processing time, and material loss, enhancing efficiency, selectivity, and scalability. The elimination of intermediate isolation is a crucial aspect of these approaches, making them highly pertinent for industrial applications. These methods also enable precise bond activation through the combination of different catalysts, such as SACs and nanoparticles, facilitating the synthesis of complex products. [572]

Beyond SACs, DACs, and nanoparticles, a variety of more complex catalytic materials have been identified as promising candidates for biomass depolymerization. These include transition metal borides (TMBs), transition metal nitrides (TMNs), transition metal carbides (TMCs), MXenes, and transition metal phosphides (TMPs). [10] The unique electronic properties, stability, and tunability of these materials render them

attractive for improving selectivity and efficiency in lignin valorization. However, as these systems have already been extensively discussed in the perspective **Chapter 8**, they will not be further elaborated upon here.

10.2.3 Invasive plants as a sustainable feedstock for biomass valorization

In addition to utilizing biomass waste, the range of non-competing biomass sources can be expanded to include invasive plant species, which pose a threat to ecosystems and human health due to their high environmental adaptability, rapid reproduction, and aggressive spread. [573] As a result, their management has gained increasing attention in recent years. Initial studies have already demonstrated their potential for valorization, for example, in biochar production or as a matrix for catalysts. [573–577]

One example for an invasive plant is Japanese knotweed, which is one of the most invasive and problematic plant species of the world. [578] Japanese knotweed was introduced to Europe from Japan in 1848 [579] for the purpose of horticultural experimentation. Following its initial introduction, the species proliferated and disseminated extensively within its introduced range. [580] It is often spreading rapidly along riparian zones and transportation corridors, where it often forms dense stands that can span several hundred square meters. [581,582] Due to its rapid spread and ability to outcompete native plants, controlling or removing Japanese knotweed is necessary. This makes it an ideal, sustainable source of cellulose and lignin, turning an ecological challenge into a valuable resource.

Initial experiments have demonstrated that Japanese knotweed can be effectively processed in order to extract and isolate its main components, enabling the selective extraction of cellulose and lignin (**Figure 58**). This is achieved using a modified method based on the treatment of biomass with formic acid, acetic acid, and hydrogen peroxide, as described by Watkins *et al.* [583]

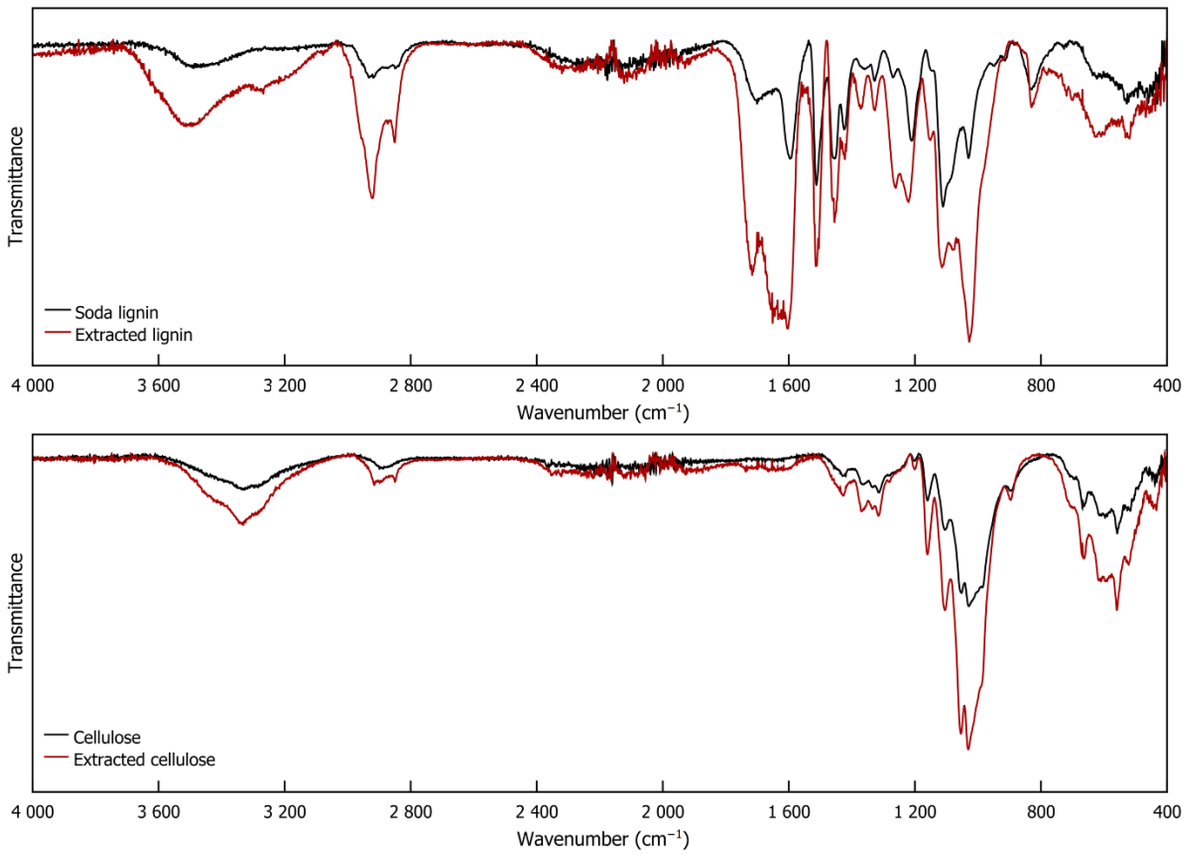

Figure 58. FTIR spectra of Soda lignin and lignin extracted from Japanese knotweed (top), as well as commercial cellulose and cellulose extracted from Japanese knotweed (bottom). The similarity in functional groups confirms the successful extraction of lignin and cellulose from Japanese knotweed.

This process has the potential to use this plant in a closed-loop system. The extracted cellulose can be impregnated with metal salts while wet-pressed into a filter paper-like form. Initial experiments indicate that the cellulose remains dimensionally stable after pyrolysis and can be used directly as an electrode, similar to carbon paper. This electrode can then be used in electrochemical lignin depolymerization, effectively allowing Japanese knotweed to serve as the starting material in a self-depolymerizing process (**Figure 59**).

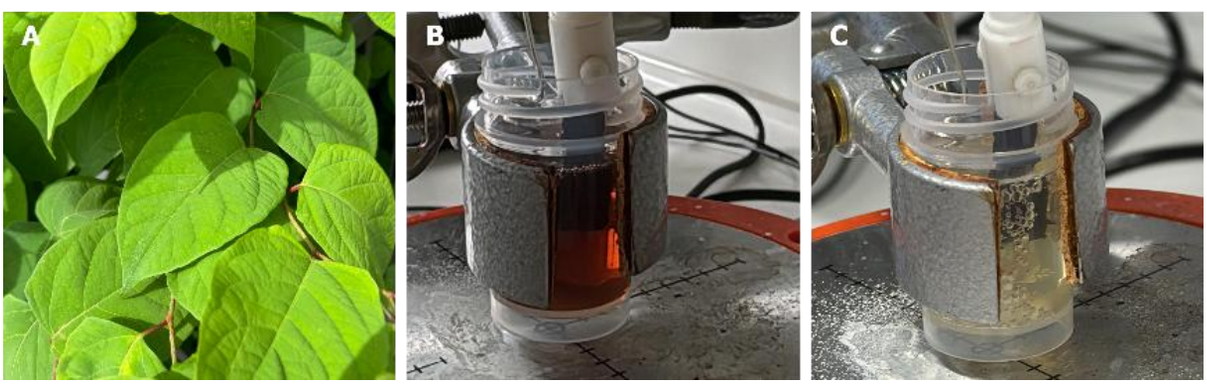

Figure 59. A Japanese knotweed harvested at 51°10'49.4"N 7°09'59.6"E. **B** Initial state before depolymerization: lignin from Japanese knotweed with a carbonized cellulose electrode, extracted from Japanese knotweed and decorated with copper and nickel. **C** Same reaction after 20 h, showing decolorization of the solution as the first indicator of reaction success.

In addition to the depolymerization of lignin, the depolymerization of cellulose should be given more attention in the future. There are already approaches to convert cellulose into valuable products such as levulinic acid,[584–587] but electrochemical cellulose depolymerization remains largely unexplored, with only a few studies (*e.g.* [376,588]) conducted to date. Compared to lignin, cellulose has the major drawback of being a highly demanded resource, particularly in the paper industry, rather than a widely available waste product. Therefore, using cellulose derived from invasive plants as a feedstock for depolymerization presents a sustainable alternative. To further enhance the closed-loop concept, electrodes made from carbonized cellulose or a lignin-based electrode matrix extracted from Japanese knotweed could also be explored for cellulose depolymerization.

A significant challenge in the electrochemical depolymerization of cellulose is the low solubility, which in most cases necessitates pretreatment (see *e.g.* [589]). A study by Han *et al.* demonstrated that cellulose becomes physically soluble in GVL after undergoing thermal treatment at 200 °C for 2 h.[585] In light of these findings, it is reasonable to hypothesize that cellulose depolymerization could be integrated with lignin depolymerization in GVL [203]. Subjecting biomass, including invasive plants, to thermal treatment in GVL prior to depolymerization suggests the potential for both cellulose and lignin to be dissolved in the same solvent, thereby facilitating simultaneous depolymerization.

10.2.4 Understanding the mechanism of depolymerization

In future studies, greater emphasis should be placed on a more comprehensive understanding of the mechanistic pathways involved in lignin depolymerization. This enhanced knowledge will facilitate the optimization of reaction conditions and the improvement of catalyst performance. The discussed research did not resolve the question of whether the depolymerization process primarily follows a reductive mechanism on the working electrode, an oxidative mechanism on the platinum counter electrode, or a mixed mechanism, which directly impacts the product selectivity. In this regard, transitioning to a split H-cell configuration (**Figure 60**), wherein the cathode and anode cells are separated by a membrane, could be advantageous. Such a setup would allow for the selective control (oxidatively or reductively) of depolymerization processes and help determine whether a combination of both mechanisms is required. However, this approach remains to be explored in future investigations.

Figure 60. Example setup of an H-cell for lignin depolymerization. The cathode compartment (left) holds the lignin solution, working electrode, and reference electrode, facilitating reductive lignin depolymerization. The anode compartment (right) contains only the counter electrode and electrolyte. Gas formation at the anode indicates the electrochemical oxygen evolution reaction.

Furthermore, there is a need for more focused studies on catalyst characterization during operation. *In-situ* and *in-operando* characterization techniques are instrumental in studying catalysts under real reaction conditions, offering valuable insights into reaction kinetics, the nature of active sites, and underlying mechanistic pathways. [590–593] The term *in-situ* refers to the collection of spectral data of a catalyst while it is exposed to relevant treatment or operating conditions. [594] Conversely, *in-operando* characterization involves the simultaneous analysis of a working catalyst under actual reaction conditions, allowing for direct correlation of its catalytic activity and selectivity. [594,595] Future research endeavors should prioritize the extension of these techniques from *in-situ* to *in-operando*, leveraging methodologies [107] such as *in-operando* transmission electron microscopy (TEM), scanning tunneling microscopy (STM), Fourier-transform infrared spectroscopy (FTIR), X-ray absorption spectroscopy (XAS), ambient-pressure X-ray photoelectron spectroscopy (AP-XPS), and time-of-flight mass spectrometry (TOF-MS), among others. The incorporation of these techniques will facilitate the design of more efficient catalytic systems.

10.2.5 Rethinking plastic valorization

Plastics are versatile materials that are used daily by society and play a crucial role in various industries. Nevertheless, plastic consumption is steadily increasing, whereas recycling rate remains critically low. Only approximately 8% of the plastic waste produced is recycled, whereas less than 12% is incinerated. The majority (approximately 79%) remain in use, ending up in landfills or the environment, often due to inadequate disposal methods. [596] Every year, between 5 and 13 million tons of plastic end up in the ocean. [597] The floating plastic is concentrated in garbage eddies, where microplastic concentrations

are higher than in the rest of the oceans. [598] In 1997, the first garbage eddy, the "*Great Pacific Garbage Patch*", was discovered by oceanographer and captain Charles Moore. [598] Particularly threatening is the proliferation of microplastics, which are tiny plastic particles that can enter the food chain while containing harmful additives. [596] The presence of microplastics in the human body has been documented, with instances including fecal matter, blood, the placenta, the lower respiratory tract, and the lungs. [599] Microplastics can arise from both purposefully produced primary and secondary microplastics that are unintentionally released during the use and disposal of plastics. [596] Although various innovative approaches exist to combat microplastic problems, such as using bacterium *Ideonella sakaiensis*, which expresses enzymes for plastic degradation, [600] collecting neptune grass washed ashore, which physically binds microplastics; [601] or nanotubes, which produce strongly oxidize radicals that can degrade plastic, [602] measures to prevent the formation of microplastics are more promising.

So far, there is no silver bullet to solve the pervasive problem of plastic pollution. While novel recycling technologies are urgently needed, their impact will only be truly transformative with global coordination, such as the World Plastics Treaty, and the implementation of an upper limit on plastic production. [603]

In the future, tackling the plastic problem will require a multi-faceted approach, addressing it from at least three directions. Recycling processes must be improved, biodegradable alternatives need to be developed and adopted, and waste materials should be repurposed to minimize plastic waste. The biggest challenge in plastic recycling lies in the complexity and diversity of plastic compositions, which is further compounded by the addition of chemical additives that enhance versatility. [603] Recycling mixed plastic types often leads to a degradation of material properties. [604] Even when processing a single type of plastic, such as PET, which is typically 100% recyclable, [605] variations like different colors can result in low-quality recyclates. [606,607] As a consequence, pigmented plastics are often discarded rather than recycled. [603] Even though recycling mixed plastics is challenging, finding an alternative to disposal is urgent. In this context, it could be a useful approach to learn from the previous milestones in lignin depolymerization and to adapt principles for the valorization of plastic waste.

Like mixed plastics, lignin cannot be broken down into a single monomer due to its complex and diverse non-polymeric structure. To address this, Slabon and Rodrigues recently proposed the "liquefy-first" approach, which prioritizes industrial applicability over maximum selectivity. [360] This strategy converts industrial lignin waste into chemically diverse liquid feedstocks through processes like electro- or photocatalytic

liquefaction. Instead of isolating specific monomers, it leverages lignin's heterogeneity, allowing integration into existing industrial refining processes, with a focus on scalability and flexibility.

Liquefied lignin feedstocks can be used directly as lubricants, as demonstrated in the study about *in-situ* methyl isobutyl ketone (MIBK) extraction (**Chapter 7**). Additionally, liquefied biomass intermediates can be further refined into fuels or chemicals or integrated into hydrodeoxygenation and refining processes. [608–610] The "liquefy-first" approach, along with findings from the study using *in-situ* extraction with MIBK, highlights that separating individual monomers after depolymerization is not essential. Instead, the resulting feedstocks can serve as intermediates or can be used directly in industrial applications. Therefore, a paradigm shift should take place from the unrealistic goal of recycling mixed plastics back into high-quality plastics to a "plastic-to-feedstock" approach. In this envisioned strategy, mixed plastics could be depolymerized, for example, electrochemically, into monomers or intermediates that may serve as feedstock for various industrial applications. Both lignin ("liquefy-first") and plastic ("plastic-to-feedstock") feedstocks have the potential to be converted into e-fuels using electrochemical methods in the near future, thus providing an alternative to fossil raw materials and biomass that competes with the food industry. The oxygen content of lignin derivatives is notably higher than that of petroleum and petroleum by-product streams. [611] This characteristic poses a substantial challenge to the utilization of lignin in conventional fuel processing unit operations. Consequently, deoxygenation and hydrotreating are essential steps in the process of obtaining a refinery feedstock blend. [611] The issue persists in the context of plastic feedstocks. However, this obstacle can be surmounted in both contexts through the application of electrochemical hydrodeoxygenation. [612,613]

The electrochemical depolymerization of plastic waste aligns with the principles of *Green Chemistry*, although energy input remains essential. Combining two different reactions, such as lignin and plastic depolymerization, could help to reduce the overall energy consumption. A split H-cell could enable this process by separating the two depolymerization reactions: lignin depolymerization, which can occur under reductive conditions, [104,138,203,354] in the cathodic compartment, and plastic depolymerization, which can operate under oxidative conditions, [614–616] in the anodic compartment.

However, a major challenge is the solubilization of plastic waste. [616,617] Ideally, both lignin and plastic should dissolve in the same solvent to enable efficient processing. Alternatively, the electrochemical depolymerization of plastic suspensions or emulsions could offer a way to bypass the solubility challenge. [614]

10.2.6 Tackling food waste through sustainable materials

It is not only plastic pollution, but also food waste that is a pressing global issue. Globally, 1.3 billion tons of food are wasted annually, contributing significantly to pollution. [618] Food loss occurs at various stages of the production chain: 24% during production, 24% postharvest, and 35% at the consumption stage, [619] resulting from decisions by retailers, food services, and consumers. [620] The extension of shelf life for perishable foods stands as a pivotal strategy for mitigating waste. Fruit coatings emerge as a promising solution to ensure the maintenance of product quality during storage by impeding microbial growth, enzymatic browning, and moisture loss. [621] An efficacious strategy for the reduction of waste is the repurposing of waste materials. Chitosan, a biopolymer derived from crustacean shell waste, [622] has demonstrated potential as an antimicrobial and antioxidant coating. [623–625] Its use in food packaging is increasing due to its biodegradability. [626] However, its high water sensitivity limits its broader applications. [627,628]

Preliminary tests have demonstrated that the incorporation of 25 wt% depolymerized lignin (DL), derived from the electrochemical Soda lignin depolymerization in GVL, into chitosan-based films not only addresses the inherent limitations of pure chitosan, such as excessive water solubility (decreasing from 76.5 ± 2.5% to 38.4 ± 2.0%) and moisture sensitivity, rendering them highly durable under humid conditions, but still soluble enough to be removed from fruit shells through washing. Furthermore, the results of biodegradation tests demonstrated that chitosan-DL films disintegrate within a period of three weeks, thereby signifying a substantial ecological benefit in comparison to conventional plastic packaging, which exhibits resistance to degradation. The rate of decomposition observed was found to be faster than that of non-modified chitosan films. A toxicity assessment employing *Caenorhabditis elegans* as a model organism indicated the potential for safe use. The assessment revealed no significant effect on the survival of *C. elegans*, though further testing is necessary to confirm its suitability for food-related applications. Furthermore, the potential of chitosan-DL films to extend the shelf life of apples by preventing spoilage could be demonstrated (**Figure 61**).

Figure 61. Preservation of an apple with a chitosan-DL coating (left) compared to an uncoated reference apple (right). Initially, both apples appeared fresh. After 29 days, the uncoated apple showed significant decomposition, whereas the coated apple exhibited minimal spoilage and retained its structural integrity.

Algae biomass represents another marine biomass that is both highly underexploited and largely unrecognized. [629] The alginate industry processes more than one hundred thousand tons per year of algae in Europe. [630] Alginate, a primary component of the cell wall in various brown seaweeds, possesses gelling, emulsifying, and film-forming properties, rendering it a widely utilized ingredient in numerous sectors, including pharmaceuticals, cosmetics, textiles, and food production. [631] In comparison to the low solubility of chitosan in pure water in its original form prior to processing into films or coatings, the sodium salt of alginic acid, which is produced during the extraction of alginic acid from algae, [629] is water-soluble, [632] thereby facilitating more efficient processing compared to chitosan. Furthermore, given that alginic acid is derived from fast-growing algae rather than crustaceans, it is considered a more sustainable and vegan-friendly alternative.

According to initial tests, unmodified alginate films have demonstrated a notable deficiency in terms of irritation resistance and elasticity, which considerably restricts their practical applications. However, the incorporation of DL, derived from depolymerization in GVL, has been shown to enhance the irritation resistance of alginate films. Nevertheless, the alginate-DL films demonstrated limited elasticity, which could be enhanced by incorporating glycerine as a plasticizer. Compared to chitosan, determining the water solubility of alginate films is not feasible, as they immediately disintegrate upon contact with water. This property allows for easy, residue-free removal from apples by washing, but it may pose challenges during storage and transportation under high humidity. Under normal storage conditions, however, this effect appears negligible. Even after four months, the apple coated with an alginate-DL film remains visually fresh, whereas both the uncoated reference apple and the apple coated only with alginate are completely decomposed (**Figure 62**).

Figure 62. Preservation of an apple with an alginate-DL coating (right) is demonstrated in comparison to an uncoated reference apple (left) and an alginate-coated apple (middle). After a period of four months, both reference apples exhibited significant decomposition, whereas the alginate-DL apple demonstrated minimal spoilage and maintained its structural integrity.

These biodegradable coatings made from chitosan or alginate and lignin-derived aliphatic compounds have the potential to extend fruit shelf life. Preventing food spoilage supports SDG 2 (“Zero Hunger”), ensuring food availability and minimizing waste along the supply chain. The use of renewable, locally available resources like chitosan and lignin aligns with SDG 12 (“Responsible Consumption and Production”) by promoting sustainable material cycles. Using biodegradable materials contributes to SDG 14 (“Life Below Water”) and SDG 15 (“Life on Land”), helping to protect ecosystems from pollution. Additionally, the focus on biomass-based materials fosters SDG 10 (“Reduced Inequalities”) by decreasing dependence on fossil resources, promoting resource independence for countries without domestic fossil fuel production.

10.2.7 Summary of future research directions

To advance this field, research should concentrate on the following potential directions:

1) **Strengthening collaboration between academia and industry.**

   Close collaboration is imperative to bridge the gap between laboratory research and real-world applications. Industry partners should proactively communicate their needs and market demands to academia, ensuring that research is aligned with practical applications. By designing reactions with scalability in mind from the outset, processes can be developed in an industry-oriented manner, making them easily transferable to industrial settings without extensive modifications.

2) **Expanding biomass sources.**

   To enhance sustainability and resource efficiency, future research should explore the potential of invasive plant species and food industry by-products as viable biomass sources.

3) **Integrating cellulose depolymerization for biorefinery advancement.**

   Future research endeavors should extend beyond lignin to encompass cellulose depolymerization, either in isolation or in conjunction, with the objective of enhancing efficiency and scalability. This approach is expected to further propel the advancement of biorefinery concepts.

4) **Development of advanced catalysts for biomass depolymerization.**

   The exploration of more complex catalysts, including single-atom catalysts (SACs), dual-atom catalysts (DACs), and nanoparticles, transition metal borides (TMBs), nitrides (TMNs), carbides (TMCs), MXenes, and phosphides (TMPs), is recommended.

5) **Designing tandem catalysts for multi-step reactions into a single system.**

   Hybrid catalysts, combining *e.g.* SACs with nanoparticles, could target different bonds in lignin, leading to a broader product spectrum. Furthermore, the development of tandem reactor systems has the potential to enable the concurrent execution of complementary reactions, such as lignin depolymerization in conjunction with cellulose degradation or plastic depolymerization. This could further enhance process efficiency and resource utilization.

6) **Deeper understanding of reaction mechanisms.**

   The utilization of H-cells has the potential to facilitate the discernment of whether lignin depolymerization transpires through a reduction, oxidation, or a combination of these mechanisms.

7) ***In-operando* catalyst characterization.**

   Greater emphasis should be placed on *in-operando* studies to understand catalyst dynamics during reactions, which will help to improve knowledge about stability, deactivation mechanisms, and long-term performance.

8) **Shifting focus to the "liquefy-first" strategy.**

   Rather than prioritizing maximum selectivity, research should explore direct practical applications for lignin-derived feedstocks, such as lubricants and e-fuels.

9) **Using waste to prevent waste.**

   The utilization of waste materials, including but not limited to chitosan, lignin, and alginate, holds significant potential in the development of biodegradable coatings and packaging. This approach is particularly salient in addressing the pressing issue of food loss.

10) **Transferring insights from lignin depolymerization to plastic depolymerization.**

    Lessons learned in lignin depolymerization should be applied to plastic waste valorization, adapting similar catalytic and process strategies.

Appendix – Supplementary Material

Appendix – Supplementary material

Supplementary material for Chapter 4

Organic chemicals from wood: selective depolymerization and dearomatization of lignin via aqueous electrocatalysis

Experimental procedures

Materials

Soda lignin obtained from the hardwood black liquor of a sulfur-free pulp production in a pilot plant (WAT Venture Sp. z o.o., Poland) was used as starting material. Sodium carbonate decahydrate (Grüssing GmbH (Filsum, Germany), sodium acetate trihydrate (VWR (Darmstadt, Germany)), sodium formate (RIEDEL-DE HAËN AG (Hannover, Germany)), levulinic acid (Merck (Darmstadt, Germany)), γ-valerolactone (Fisher Scientific (Schwerte, Germany), 98%), Methanol (MeOH, LC-MS grade, Fisher Scientific (Schwerte, Germany)), acetic acid (Hac, Fisher Scientific (Schwerte, Germany)), acetonitrile (ACN, VWR (Darmstadt, Germany) and ethanol (puriss. p.a., absolute, ≥99.8% (GC), Sigma Aldrich) were used as received. A carbon electrode was purchased from WAT Venture (Poland) and used as working electrode. All aqueous solutions were prepared with ultrapure water, obtained from a Millipore system.

Lignin depolymerization

An ATLAS 1131 Electrochemical Unit & Impedance Analyser (Atlas Sollich) was used for all electrochemical reactions. In a typical experiment, Soda lignin was first dissolved at 3 $g \cdot L^{-1}$ in 5 mL of a 1 M aqueous solution of sodium carbonate. Next, 45 mL of water was added to the solution. The electrochemical depolymerization was conducted with a three-electrode setup consisting of a carbon working electrode a platinum wire counter electrode, and an Ag/AgCl (saturated KCl) reference electrode. Chronopotentiometry was performed using different currents, ranging from −25 mA to −200 mA, for 20 h. The course of the depolymerization at −175 mA was observed kinetically. For this purpose, the reactions were carried out for 1, 3, 6, 10, 13, 20 and 25 h. All experiments were performed at ambient conditions. After all reactions, water was removed under reduced-pressure conditions, whilst the resulting solid was also dried under reduced pressure. The solid obtained was

suspended in ethanol and the suspension was stirred vigorously for 1 h. The remaining residue was filtered off and the ethanol was removed from the filtrate under reduced pressure. Thus, a white solid was obtained.

To corroborate the results from the electrochemical depolymerization, three reference reactions were considered: the first reference reaction involved suspending pure Soda lignin in ethanol for 1 h, with subsequent removal of the remaining lignin, and evaporation of the ethanol under reduced pressure, resulting in a brownish solid. As a further reference reaction (named 0mA/0h), Soda lignin was dissolved in an aqueous sodium carbonate solution in the same proportions as in the electrochemical experiments but then the work up was done directly (no applied current). The last reference reaction (named 0mA/20h) followed a similar procedure from the electrochemical reactions, but without the application of an electrical current and with a stirring duration of 20 h, followed by subsequent work up.

Synthesis of sodium 4-hydroxyvalerate

To a solution of GVL (50 mL, 0.51 mol), 73.53 g of $Na_2CO_3 \times 10\ H_2O$ (0.26 mol, 0.5 eq.) dissolved in 400 mL of warm water was added. The final solution was heated and stirred at 140 °C for 6 h. The remaining solution was removed under reduced pressure. A white hygroscopic solid was obtained after drying under reduced pressure on a vacuum line with a yield of 98% (70.64 g).

Synthesis of sodium levulinate

To a solution of levulinic acid (10 mL, 0.097 mol), 13.96 g of $Na_2CO_3 \times 10\ H_2O$ (0.049 mol, 0.5 eq.) dissolved in 50 mL of water were added. The remaining solution was removed under reduced pressure. A white solid was obtained after drying under reduced pressure on a vacuum line with a yield of 95% (12.81 g).

Stability tests

Sodium levulinate, sodium 4-hydroxyvalerate, sodium formate, or sodium acetate were dissolved at 3 $g \cdot L^{-1}$ in 5 mL of a 1 M aqueous solution of sodium carbonate. Then 45 mL of water was added to the solution. An ATLAS 1131 Electrochemical Unit & Impedance Analyser (Atlas Sollich) was used for the electrochemical reaction. The electrochemical reaction was conducted with a three-electrode setup consisting of a carbon working electrode, a platinum wire counter electrode, and an Ag/AgCl (saturated KCl) reference electrode. Chronopotentiometry was performed at −175 mA for 20 h. The experiment was performed at ambient conditions. Afterward, water was removed under reduced-pressure

conditions, whilst the resulting solid was also dried under reduced pressure. The solid obtained was suspended in ethanol and the suspension was stirred vigorously for 1 h. The remaining residue was filtered off and the ethanol removed from the filtrate under reduced pressure. Thus, a white solid was obtained.

Table S 1. Yield of the products from the stability tests related to the mass of products obtained after extraction with ethanol compared to the mass of starting material.

	Sodium levulinate	Sodium 4-hydroxyvalerate	Sodium formate	Sodium acetate
Yield [wt%]	72	68	84	81

Characterization

Nuclear magnetic resonance spectroscopy (NMR): ^{1}H NMR spectra were recorded on a Bruker Avance III 600 and a Bruker Avance 400 NMR instrument at 300K in D_2O. The following sample heads were used: 5 mm broadband inverse probe with automatic frequency determination, 5 mm QNP probe, and 5 mm broadband inverse probe. Chemical shifts are given with respect to Me_4Si (^{1}H, ^{13}C). If not noted differently, 16 scans were accumulated with a 1.0 s delay between each scan for ^{1}H NMR spectra.

Vibrational spectroscopy (FTIR): FTIR spectra were recorded using a Nicolet iS5 spectrometer equipped with an iD5 diamond ATR unit.

Liquid chromatography-electrospray ionization-mass spectrometry (LC-ESI-MS): The dried product was solved in ethanol and the solution evaporated to dryness and was reconstituted in methanol. This solution was diluted in the LC-MS eluent (H_2O/ACN 50/50) to a concentration of 14 µg/mL for injection (5 µL) into the LC-ESI-MS system. Standard compounds solved in H_2O/ACN 50/50 (v/v) were diluted to 1 µM or 1 µg/ml for 4-hydroxyvalerate. Chromatographic separation was carried out using a RP column (ZORBAX Eclipse Plus C18, Agilent, Waldbronn, Germany) with the dimensions 2.1x150 mm, 1.8 µm particle. The following eluents were used A: H_2O/ACN/HAc 95/5/0.1 (v/v/v); B: ACN + 0.1% HAc at a flow rate of 300 µL/min. The LC-System was coupled to a QExactive HF Orbitrap mass spectrometer (Thermo, Schwerte, Germany) equipped with a HESI II ionization source operating in ESI(−) mode with the following settings: sheath gas flow rate 48 psi; aux gas flow rate 11 arb; sweep gas flow rate 2 psi; spray voltage −4.5 kV; capillary temperature 256 °C; S-lens RF level 75; aux gas heater temperature 413 °C. Data was acquired in Full MS/data dependent MS2 mode with the following settings: Full MS: Resolution 120,000; AGC target 1x106 ; Maximum IT 160 ms; Scan range m/z 80-1000. ddMS2 : Resolution 15,000; AGC target 5x104 ; Maximum IT 100 ms; Top N 10; NCE 30.

Results and discussion

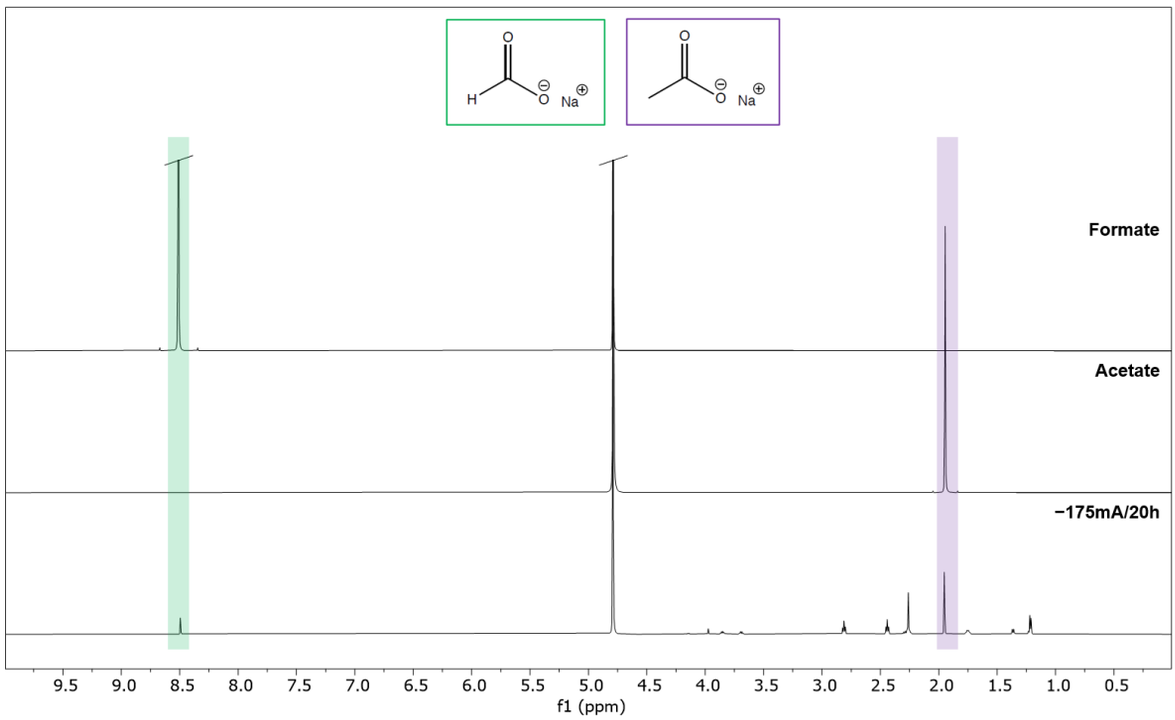

Figure S 1. ^{1}H NMR spectra (D_2O, 600.13 MHz) of −175mA/20h, acetate and formate.

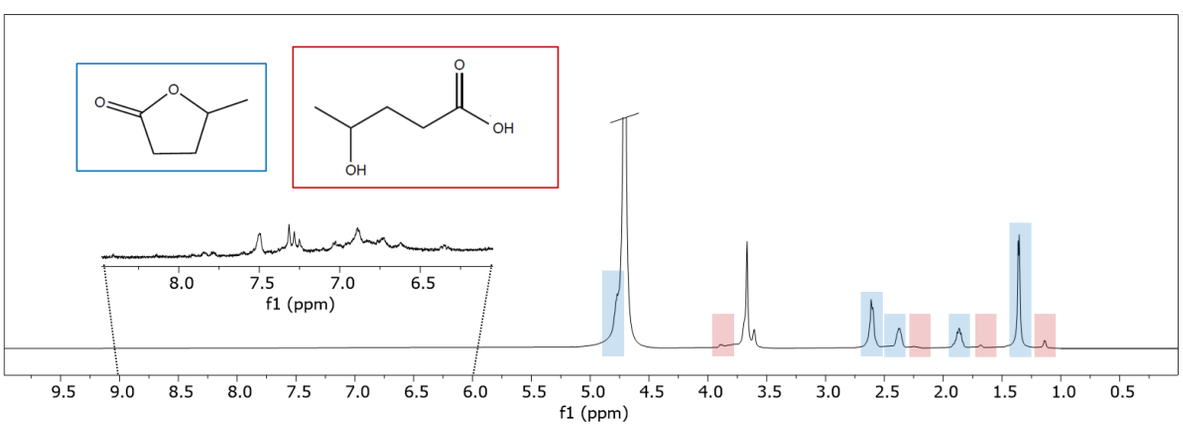

Figure S 2. ^{1}H NMR spectrum of products of ethanol extraction of pure Soda lignin (600.13 MHz) in D_2O.

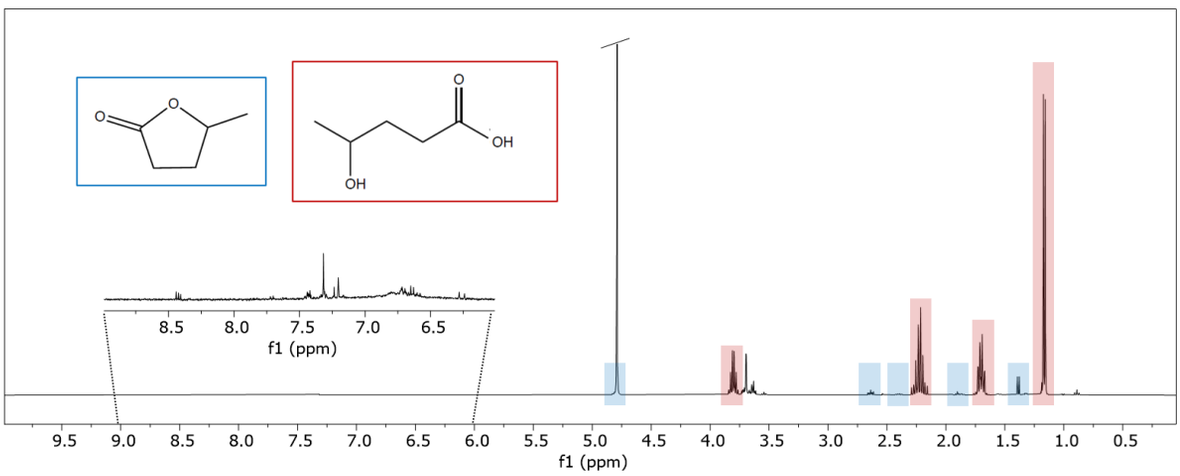

Figure S 3. ^{1}H NMR spectrum of 0mA/0h (400.13 MHz) in D_2O.

Supplementary material for Chapter 5

Breaking down lignin in gamma-valerolactone: advances into a bioelectrorefinery

Materials and methods

NMR experiments

Several NMR experiments were conducted to evaluate the stability of the solvent system. First, we evaluated the stability of pure γ-valerolactone (GVL) and aqueous GVL solutions. For this, 0.25 mL of pure GVL (10.28 M) and 0.25 mL of a 5 M GVL solution were separately dissolved in DMSO-d_6 (0.25 mL). To evaluate the influence of sodium carbonate (Na_2CO_3) in a 5 M GVL solution (50 mL), 5 mL of 1 M Na_2CO_3 were added, and the final solution was stirred at room temperature for 1 min. Afterwards 0.25 mL of the solution and 0.25 mL DMSO-d_6 were transferred into a NMR tube. In all experiments, NMR tubes were closed and immediately used for ^{1}H-NMR, ^{13}C-NMR, ^{1}H ^{1}H-COSY, ^{1}H ^{13}C-HSQC and ^{1}H ^{13}C-HMBC measurements. ^{1}H and ^{13}C NMR measurements were performed every hour for several hours. During the last measurement additionally ^{1}H ^{1}H COSY, ^{1}H ^{13}C HSQC and ^{1}H ^{13}C-HMBC spectra were recorded. When necessary, NMR experiments were also carried out at 60 °C.

Electrochemical stability

An ATLAS 1131 Electrochemical Unit & Impedance Analyser (Atlas Sollich) was used for all electrochemical experiments. The electrochemical stability of 50 mL of an aqueous GVL solution (5 M) was tested using a three-electrode setup, consisting of a carbon working electrode, a platinum wire counter electrode, and an Ag/AgCl reference electrode (saturated KCl). 5 mL of an aqueous solution of sodium carbonate (1 M) were added to the solution as an electrolyte. The reaction conditions of all experiments are summarized in **Table S 2**.

Table S 2. Summary of the reaction conditions for the experiments to evaluate the electrochemical stability of the solvent system.

Electrolyte	Applied Current [mA]	Time [h]
Na_2CO_3	0	8
Na_2CO_3	−100	8
Na_2CO_3	−100	20
Na_2CO_3	−150	8
Na_2CO_3	−200	8
Na_2CO_3	0	24
Na_2CO_3	−200	24
Na_2CO_3	−200	24

Results and discussion

Characterization of the starting material

Due to limited solubility a characterization of the used Soda lignin is carried out by ^{1}H NMR spectroscopy (**Figure S 4**) in DMSO–d^6 and FTIR spectroscopy (**Figure S 5***)*.

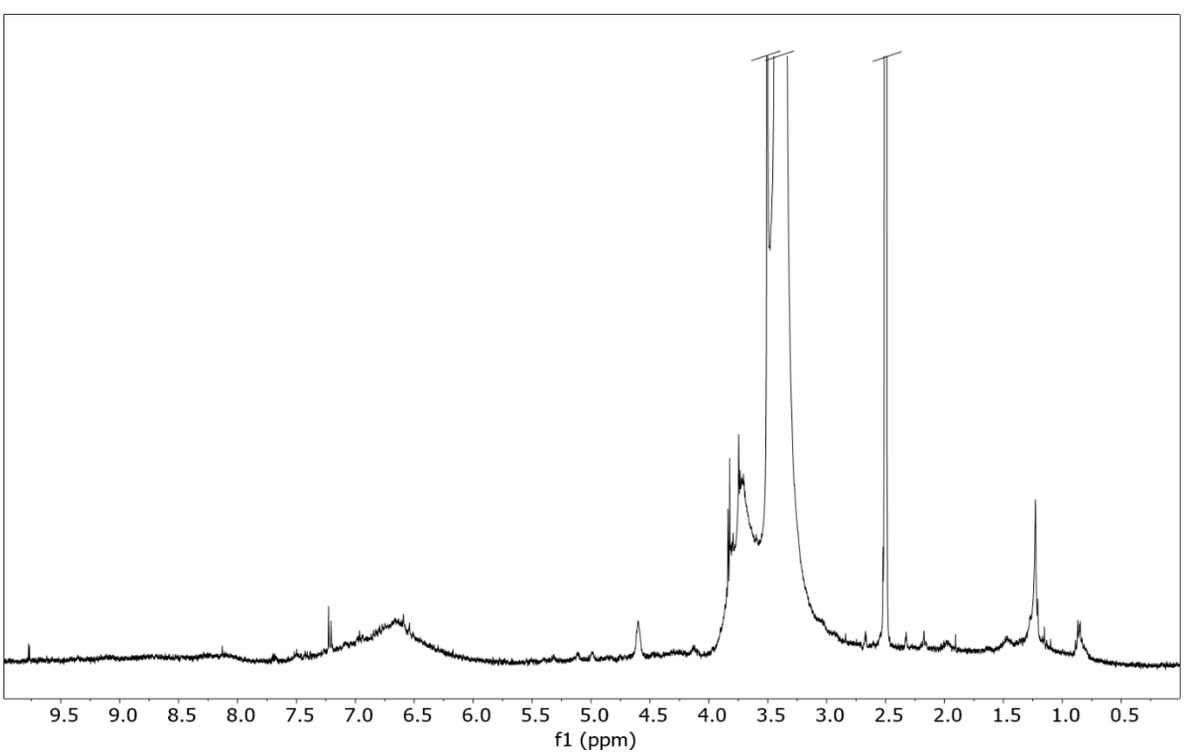

Figure S 4. ^{1}H NMR spectrum (DMSO–d^6, 600.13 MHz) of Soda lignin.

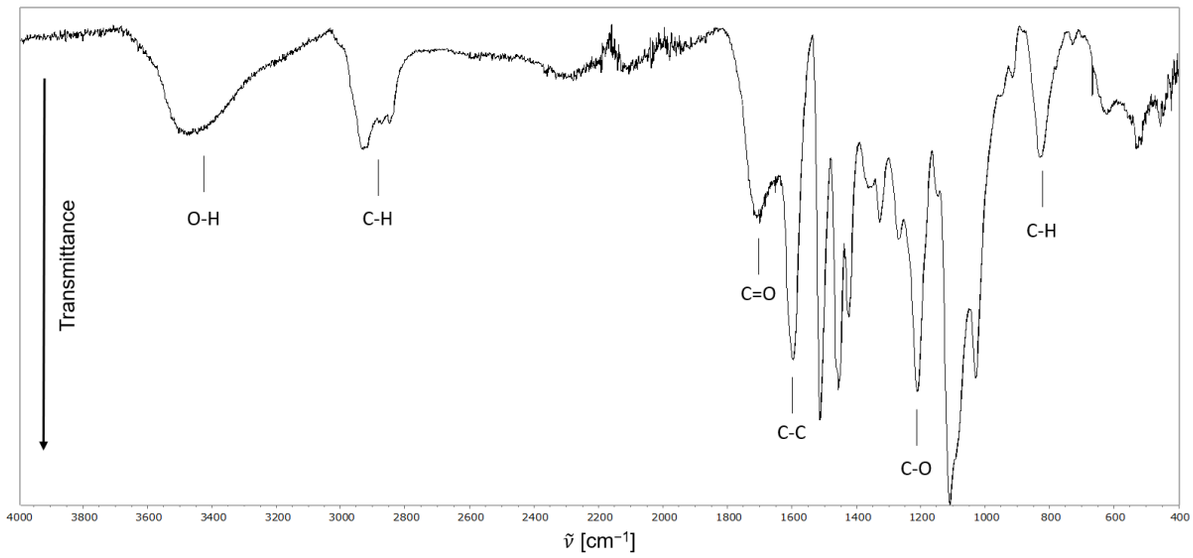

Figure S 5. FTIR spectrum of Soda lignin. The broad and intensive band at 3475 cm^{-1} is characteristic for alkyl or phenolic –OH groups. The distinct absorbance between 2929 and 2847 cm^{-1} are assigned to CH stretching of methyl or methylene groups. A broad band of medium intensity at 1699 cm^{-1} is due to the conjugated carbonyl stretching. Two bands at 1513 cm^{-1} and 1595 cm^{-1} are characteristic of aromatic rings due to the aromatic vibrations and the band at 1211 cm^{-1} is due to the C–O stretching in ether moieties. An absorbance at 831 cm^{-1} is present due to C–H deformation and ring vibrations.

Stability of GVL under different influences

The stability of pure γ-valerolactone (GVL), in combination with water and sodium carbonate (Na_2CO_3), was evaluated both at room temperature and at 60 °C, as well as the electrochemical stability. Furthermore, the stability observed during the electrochemical reactions were compared with reference reactions without applied electrochemical potential (same reaction time, 0 V).

Characterization and stability of "pure" GVL

To verify the stability of "pure" GVL, a portion of GVL was taken directly from the solvent bottle and characterized by ^{1}H NMR spectroscopy. In addition to the signals of GVL, the ^{1}H NMR spectrum (**Figure S 6**), shows a doublet at 0.99 ppm belonging to the methyl group of 4-hydroxyvaleric acid (4-HVA). By integrating the signals of the methyl groups of GVL and 4-HVA, their relative ratios can be inferred. Thus, it can be shown that a small fraction of 4-HVA (approx. 0.1 mol%) is present in "pure" GVL from the bottle, even at room temperature storage. Because of such low concentration, other signals related to 4-HVA are not detectable in the spectrum. Only the signals of GVL are identified in the ^{13}C NMR spectrum (**Figure S 7**).

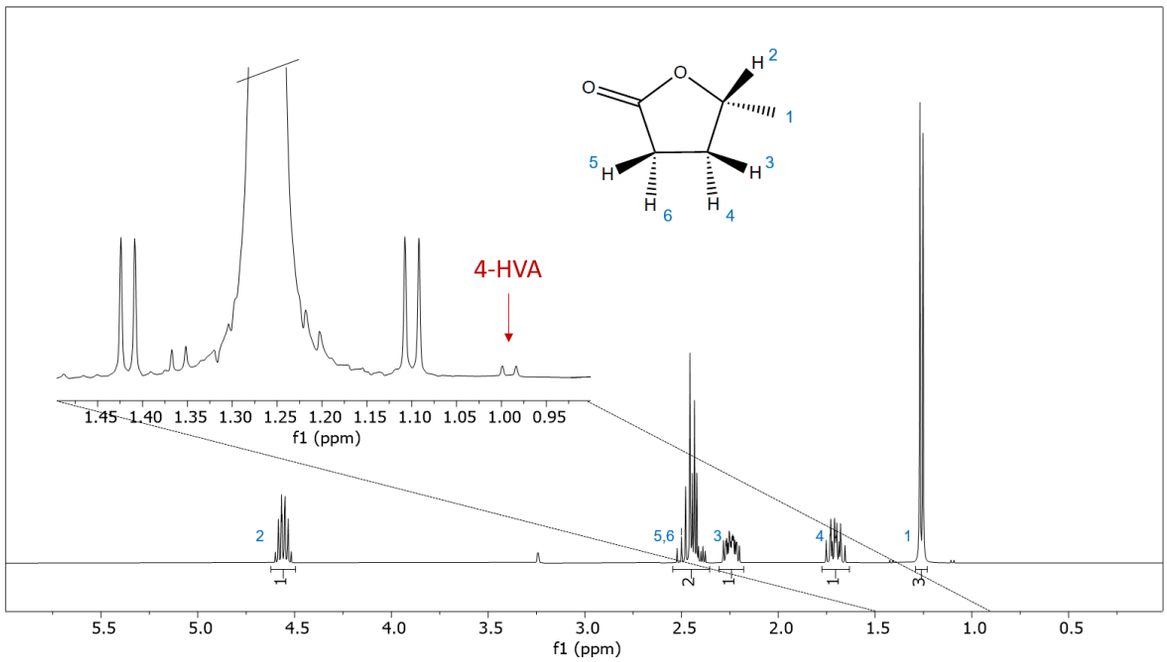

Figure S 6. ^{1}H NMR spectrum (DMSO–d^{6}, 400.13 MHz) of pure GVL at room temperature. The spectrum shows characteristic GVL signals (blue). In addition, a doublet of 4-HVA (red) is visible at 0.99 ppm. 4-HVA is present in a small amount (approx. 0.1 mol%) relatively to GVL.

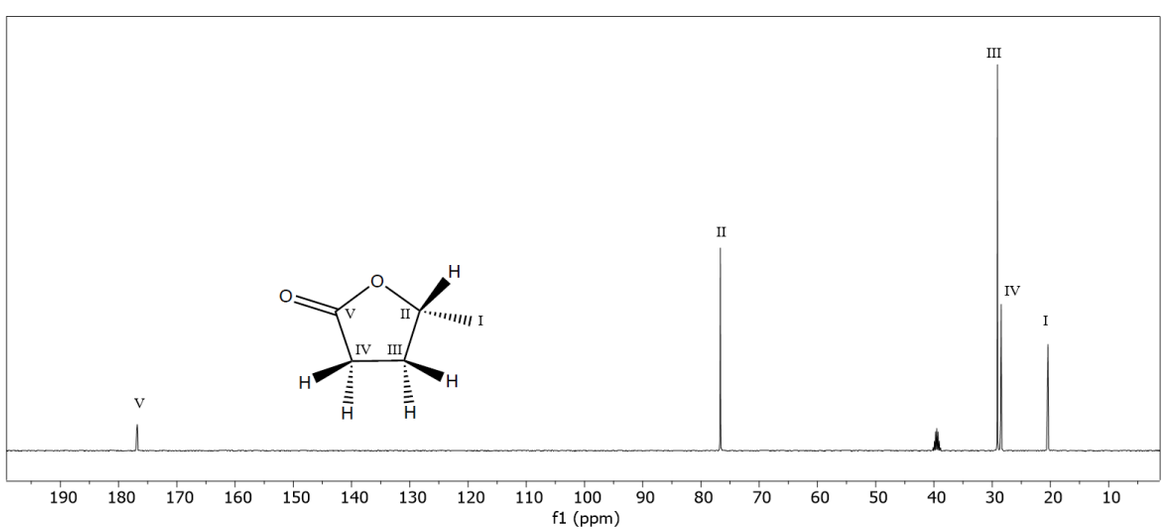

Figure S 7. ^{13}C NMR spectrum (DMSO–d^{6}, 101.62 MHz) of pure GVL at room temperature. The spectrum shows only characteristic GVL signals.

In the FTIR spectrum (**Figure S 8**), both C-H valence vibration signals (2979, 2936, and 2874 cm^{-1}) and the intense signal of the C=O valence oscillation at 1764 cm^{-1} are clearly visible. The signal at 1558 cm^{-1} cannot be assigned to any functional group of the GVL. For instance, this signal can be attributed to carboxylate groups. [272] Thus, the IR spectrum also reveals an equilibrium between the closed ring (GVL) and its open form (4-HVA). The carboxylate signal shows that 4-HVA is deprotonated in solution.

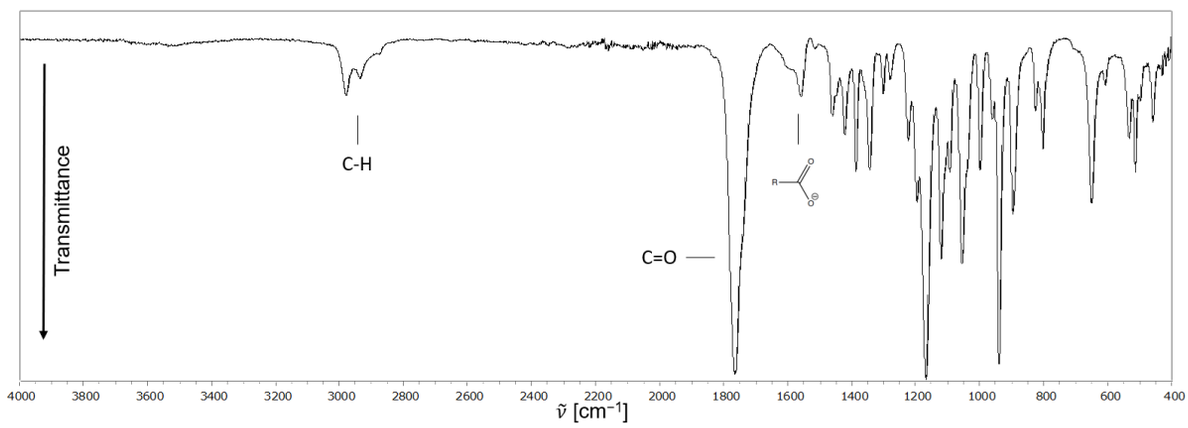

Figure S 8. FTIR spectrum of pure GVL at room temperature. The spectrum shows the characteristic oscillations of the C-H and C=O groups. These can be attributed to GVL. Additionally, the oscillation at 1558 cm^{-1} is recognizable, which belongs to the antisymmetric stretching oscillation of the carboxylate group in 4-HVA. Thus, the IR spectrum also shows equilibrium between GVL and 4-HVA.

GVL remained stable when heated to 60 °C over a 15-hour period (see **Figure S 9**). The concentration of 4-HVA remained constant (0.1 mol%) through the whole experiment.

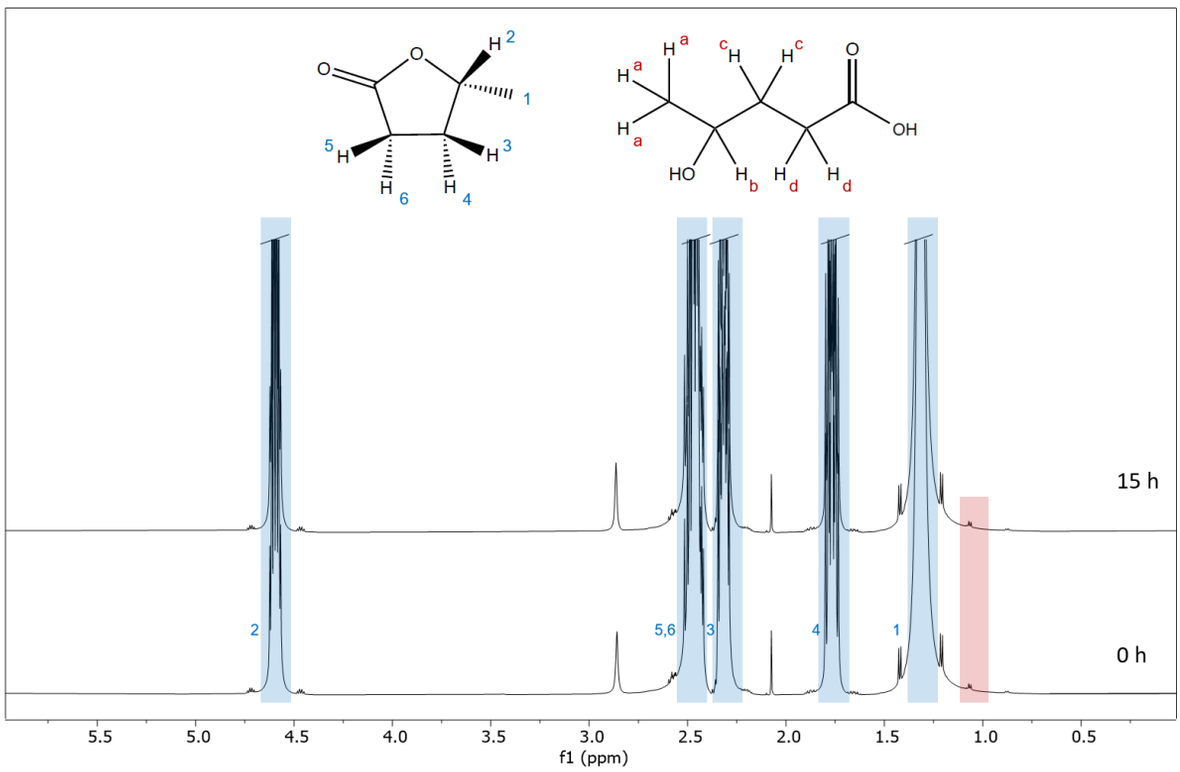

Figure S 9. ^{1}H NMR spectra (DMSO–d^{6}, 600.13 MHz) of pure GVL after 0 and 15 h at 60 °C.

Stability of 5 M GVL

Wong *et al*. reported that GVL is stable for several weeks up to 60 °C when combined with water. [283] Using NMR spectroscopy it can be shown that after the addition of water, the concentration of 4-HVA was identical to that in the pure GVL (**Figure S 10**).

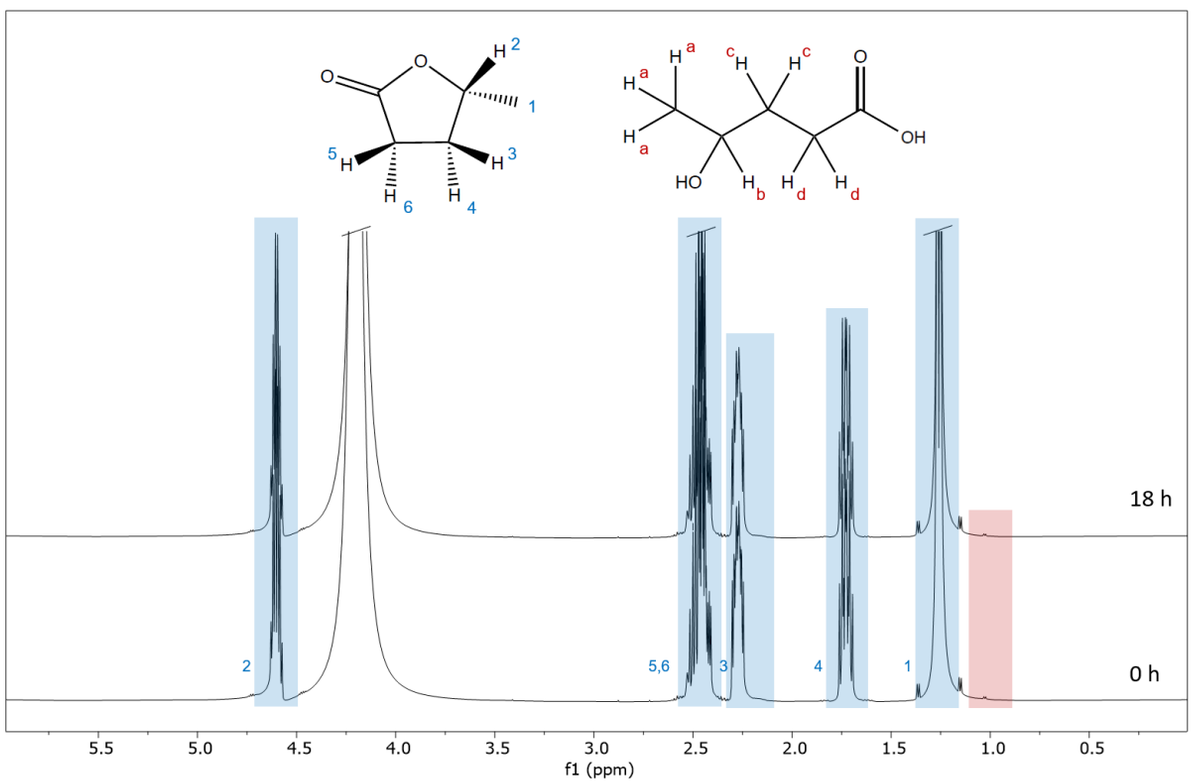

Figure S 10. ^{1}H NMR spectra (DMSO–d^{6}, 600.13 MHz) of 5 M GVL after 0 and 18 h at room temperature.

NMR investigations (**Figure S 11**) employing GVL in the presence of water demonstrated that ring-opening occurred after subjecting the system to 60 °C for 16 h. The concentration of 4-HVA was determined to be 1.4 mol% at the end of the NMR experiments. Notably, elevated-temperature NMR experiments revealed variations in the signal intensity of 4-HVA.

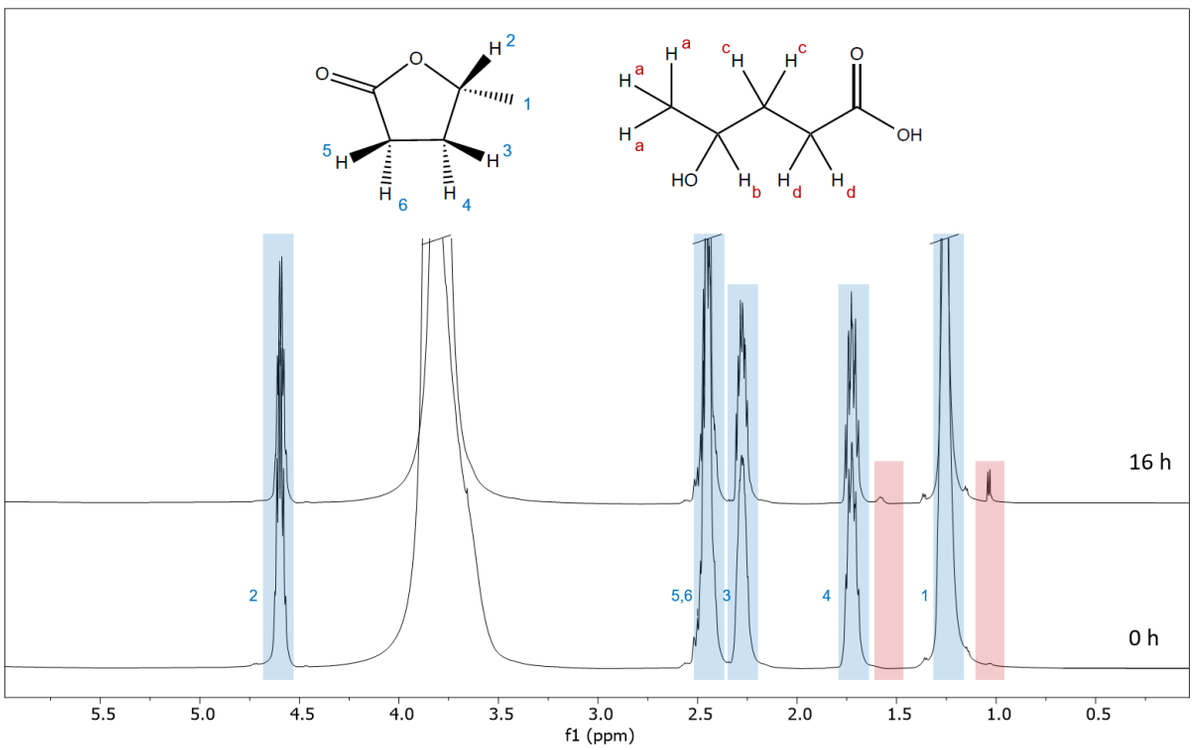

Figure S 11. ^{1}H NMR spectra (DMSO–d^{6}, 600.13 MHz) of 5 M GVL after 0 and 16 h at 60 °C.

Figure S 12 portrays the equilibrium reaction in water involving GVL and 4-HVA.

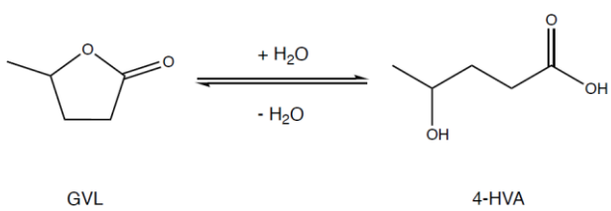

Figure S 12. Equilibrium reaction between GVL and its open form (4-HVA).

Stability of 5 M GVL under the influence of sodium carbonate

Na_2CO_3 is often chosen as a standard electrolyte for electrochemical experiments. For this purpose, we proposed to evaluate any possible effect of this electrolyte on the stability of GVL. Adding a 1 M Na_2CO_3 solution to a 5 M GVL solution (1:10 ratio) triggers the ring-opening reaction. The mechanism involves the nucleophilic attack of the hydroxide ion, leading to a stabilized carboxylate ion (**Figure S 13**). [269]

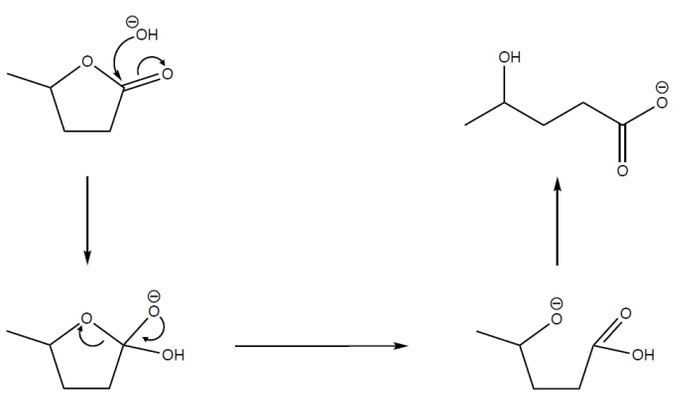

Figure S 13. Mechanism of ring opening of GVL in alkaline environment. The hydroxide ion from a strong base acts as nucleophile and attacks the positively polarized carbon atom of the ester unit creating a carboxylate ion that is stabilized by a positive counterion.

The corresponding ^{1}H NMR spectra (**Figure S 14**) highlights both GVL and 4-hydroxyvalerate signals, with the latter present at 2.1 mol% relative to GVL.

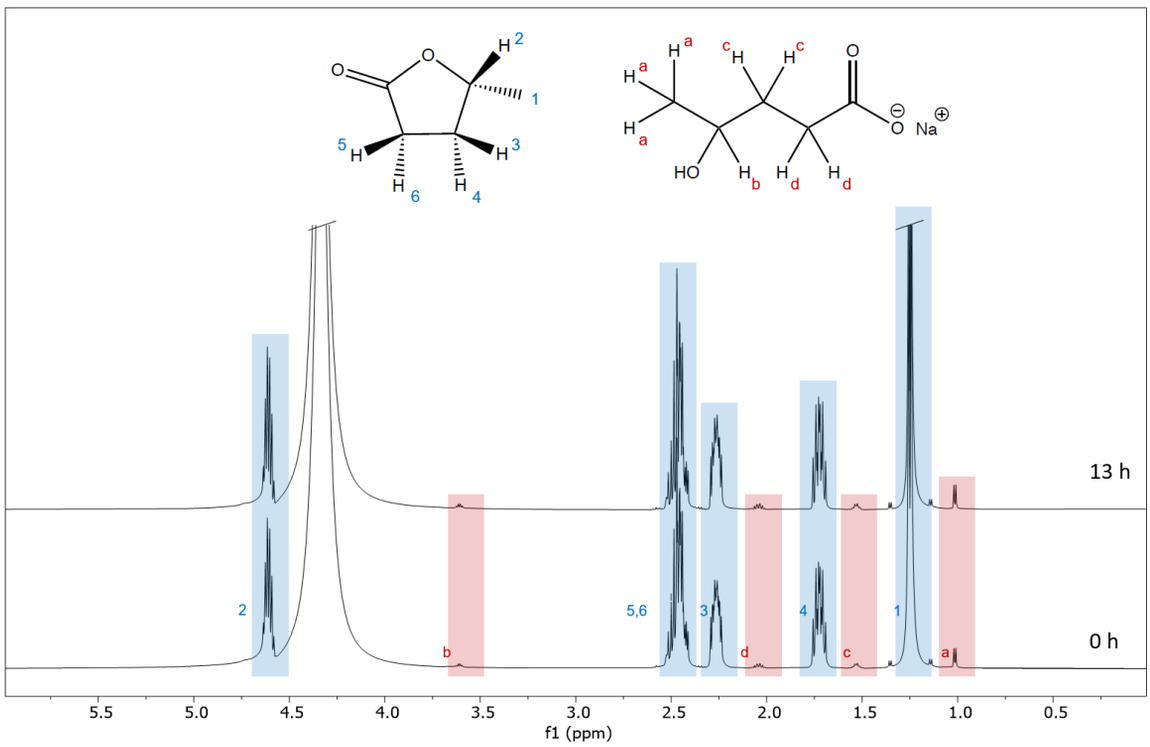

Figure S 14. ^{1}H NMR spectra (DMSO–d^{6}, 600.13 MHz) of a mixed (10:1) 5 M GVL/aqueous Na_2CO_3 solution (1 M) after 0 and 13 h at room temperature. The spectra primarily show the GVL signals (blue). In addition, 4-hydroxyvalerate (red) signals are also visible. 4-hydroxyvalerate is present at a concentration of 2.1 mol% relative to GVL.

Analysis of the ^{1}H NMR spectra (**Figure S 15**) of water and an aqueous solution of Na_2CO_3 at 60 °C indicated that an equilibrium between GVL and 4-hydroxyvalerate was established after 9 h. At this equilibrium point, the concentration of 4-hydroxyvalerate reached 4.1 mol%.

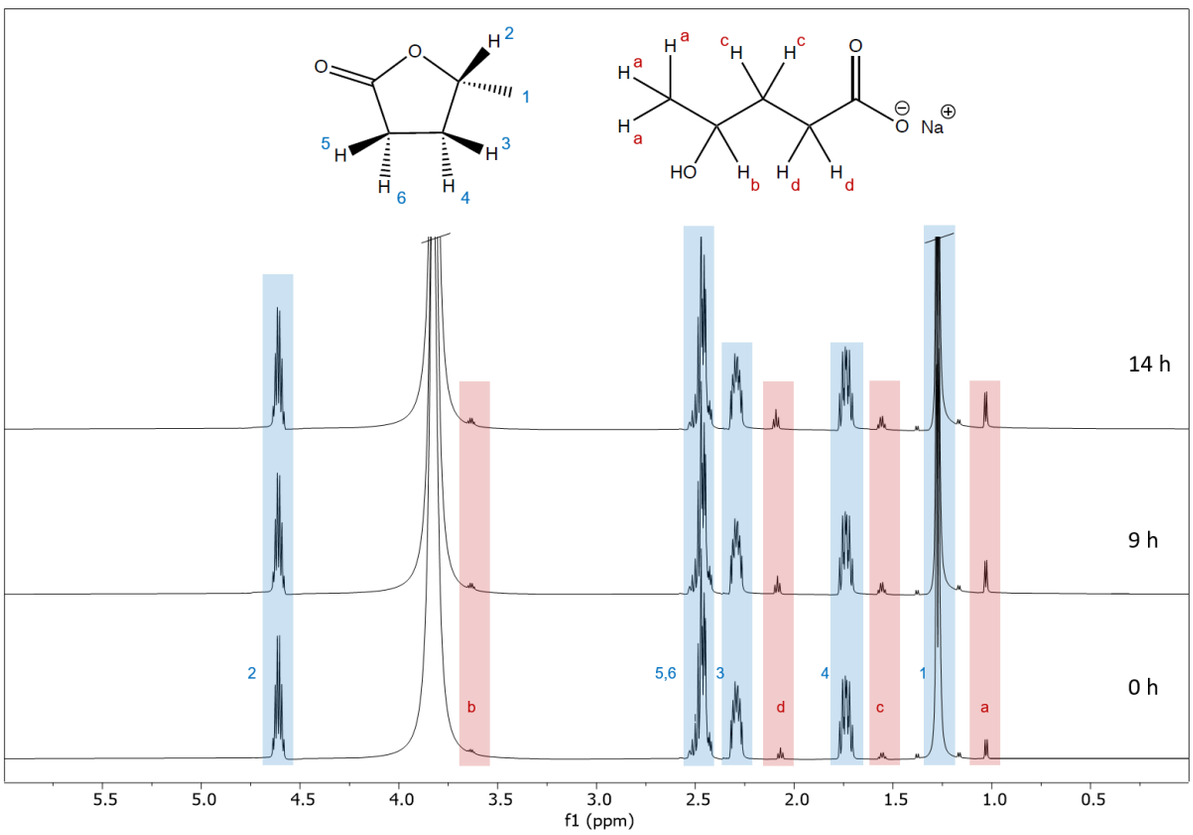

Figure S 15. ^{1}H NMR spectra (DMSO–d^{6}, 600.13 MHz) of 5 M GVL and an aqueous solution of Na_2CO_3 after 0, 9 and 14 h at 60 °C.

The relative concentrations of 4-hydroxyvalerate compared to GVL at the different influences are summarized in **Table S 3**.

Table S 3. Summary of the relative concentrations of 4-hydroxyvalerate compared to GVL at different influences in mol%.

Influence	60 °C	H_2O	60 °C H_2O	H_2O Na_2CO_3	60 °C H_2O Na_2CO_3
mol% [4-hydroxyvalerate]	0.1	0.2	1.4	2.1	4.1

Stability of GVL during electrochemical reactions

To assess the potential of GVL as a solvent for electrochemical reactions, we investigated its electrochemical stability in conjunction with Na_2CO_3. During electrochemical reactions, the presence of electrolytes is desired for better conductivity and thus an adequate current flow. Therefore, when assessing stability in the presence of an applied current, it is imperative to acknowledge the pre-existing impact of the electrolyte on the stability of GVL. To probe the specific influence of the current during the electrochemical experiment, a reference reaction was conducted without the application of a current, ensuring that all other conditions remained identical.

The electrochemical experiments were carried out under reductive conditions. 50 mL GVL (5 M) was mixed with 5 mL of the electrolyte Na_2CO_3 (1 M). The reaction was performed at room temperature and −100 mA for 8 h. NMR measurements (**Figure S 16**) show that the concentration of 4-hydroxyvalerate was 2.5 mol% after 8 h at −100 mA. In the reference reaction (no applied current), the 4-hydroxyvalerate concentration was also 2.5 mol%. Therefore, it can be concluded that GVL is stable at the considered electrochemical conditions and that the ring opening was caused exclusively by sodium carbonate.

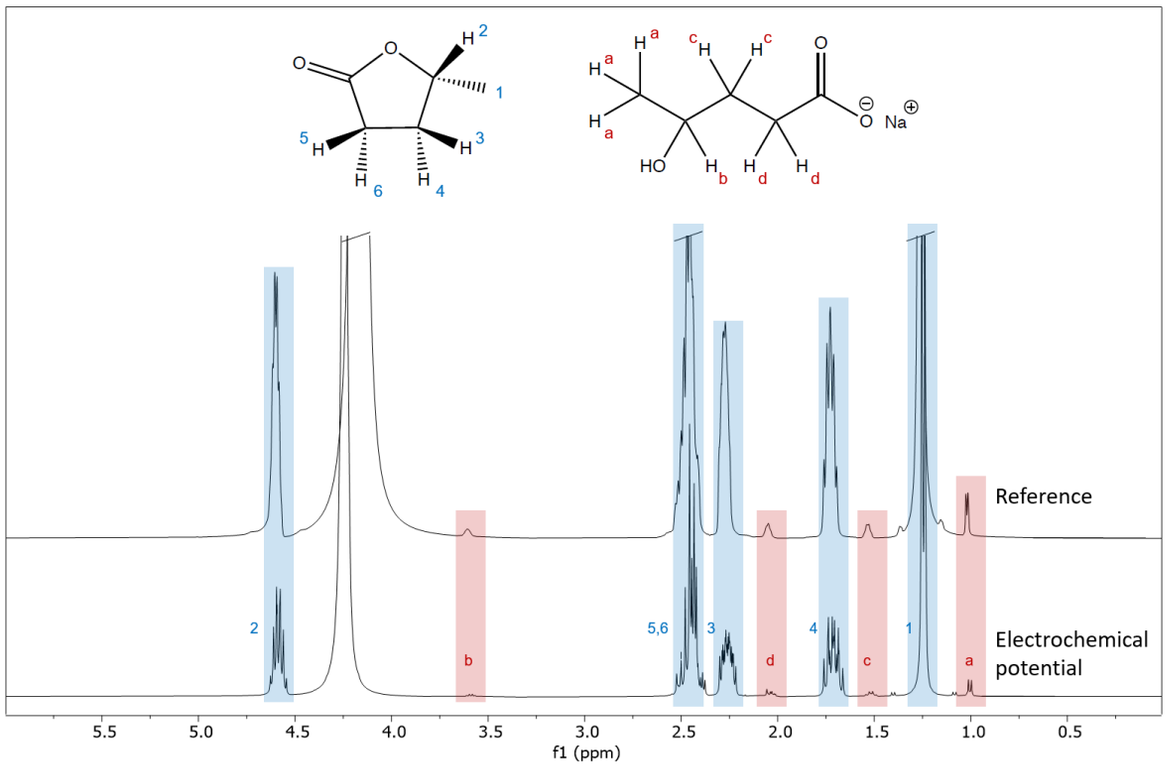

Figure S 16. ^{1}H NMR spectra (DMSO–d^{6}, 600.13 MHz) of the solution of 5 M GVL and an aqueous solution of Na_2CO_3 after 8 h at −100 mA and of a reference solution after 8 h stirring. In both spectra, the signals of the GVL (blue) as well as of the 4-hydroxyvalerate (red) are recognizable. The relative concentration in the reference solution and in the reaction solution is identical at 2.5 mol%. Thus, a current of −100 mA has no influence on the ring opening of the GVL.

To scrutinize the prospect of ring opening at higher currents, the reaction with sodium carbonate was repeated for 8 h at −150 mA and −200 mA (**Figure S 17**). Upon inspection, the 4-hydroxyvalerate concentration increased with increasing current. The concentration of the reference solution was 2.5 mol%. At −100 mA, the concentration was 2.5 mol%, at −150 mA 3.5 mol% and −200 mA 4.6 mol%. Thus, it is obvious that higher applied currents affect ring opening, and GVL remains stable only at current densities smaller or equal to −100 mA in a period of eight h. To verify the influence of time, the reaction was performed for 20 h at −100 mA. After 20 h, the 4-hydroxyvalerate concentration was 10.0 mol% (**Figure S 18**). The series of electrochemical experiments to verify the stability of GVL was completed with two reactions at −200 mA and +200 mA for 24 h (**Figure S 19**). This was done to monitor whether ring opening in GVL occurs only reductively or also oxidatively. With the oxidative variant, the concentration increases to 3.7 mol% and with the reductive variant to 6.8 mol%. Thus, it can be shown that ring opening of GVL occurs in both oxidative and reductive electrochemical reactions.

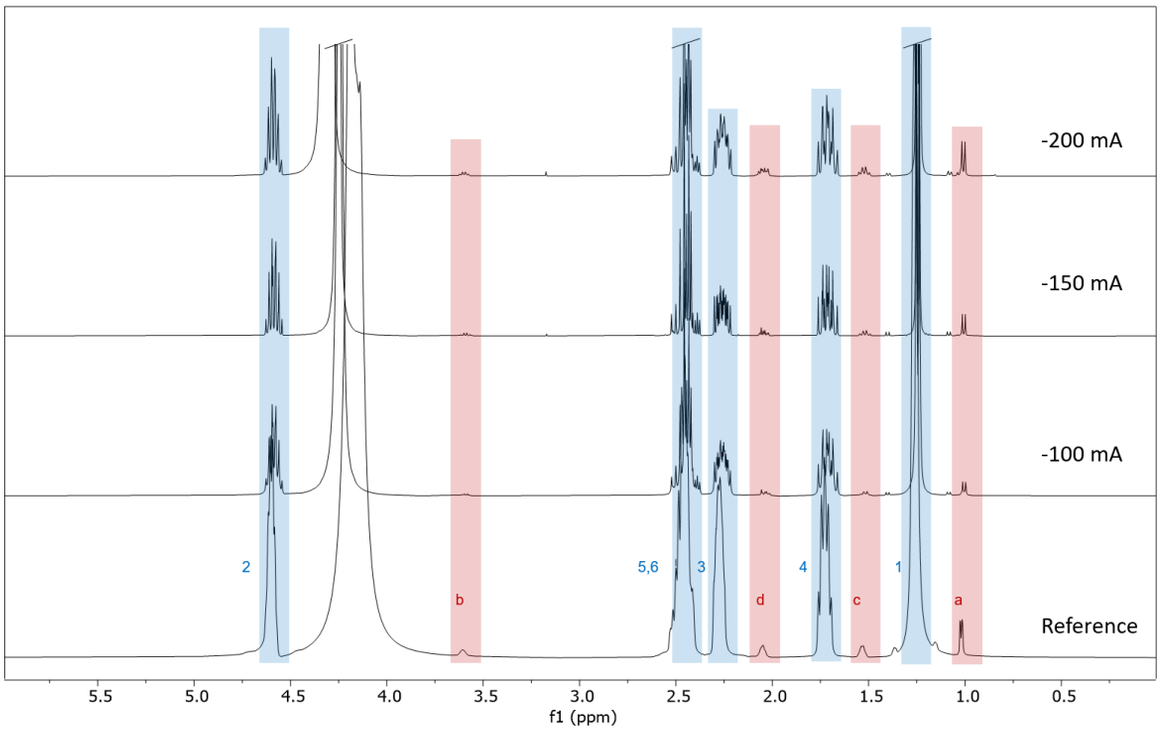

Figure S 17. ^{1}H NMR spectra (DMSO–d^{6}) of the solution of 5 M GVL and an aqueous solution of Na_2CO_3 after 8 h at −100 mA (400.13 MHz), −150 mA (600.13 MHz), −200 mA (600.13 MHz) and of a reference solution after 8 h stirring (600.13 MHz).

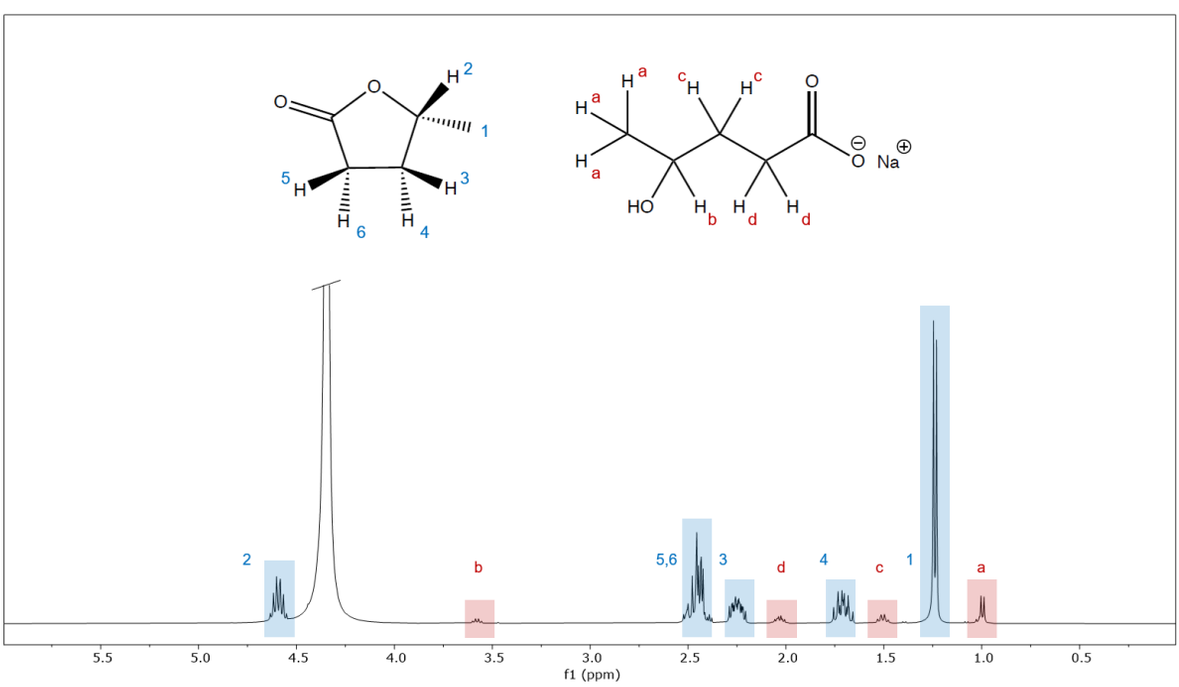

Figure S 18. ^{1}H NMR spectrum (DMSO–d^{6}, 400.13 MHz) of the solution of 5 M GVL and an aqueous solution of Na_2CO_3 after 20 h at −100 mA.

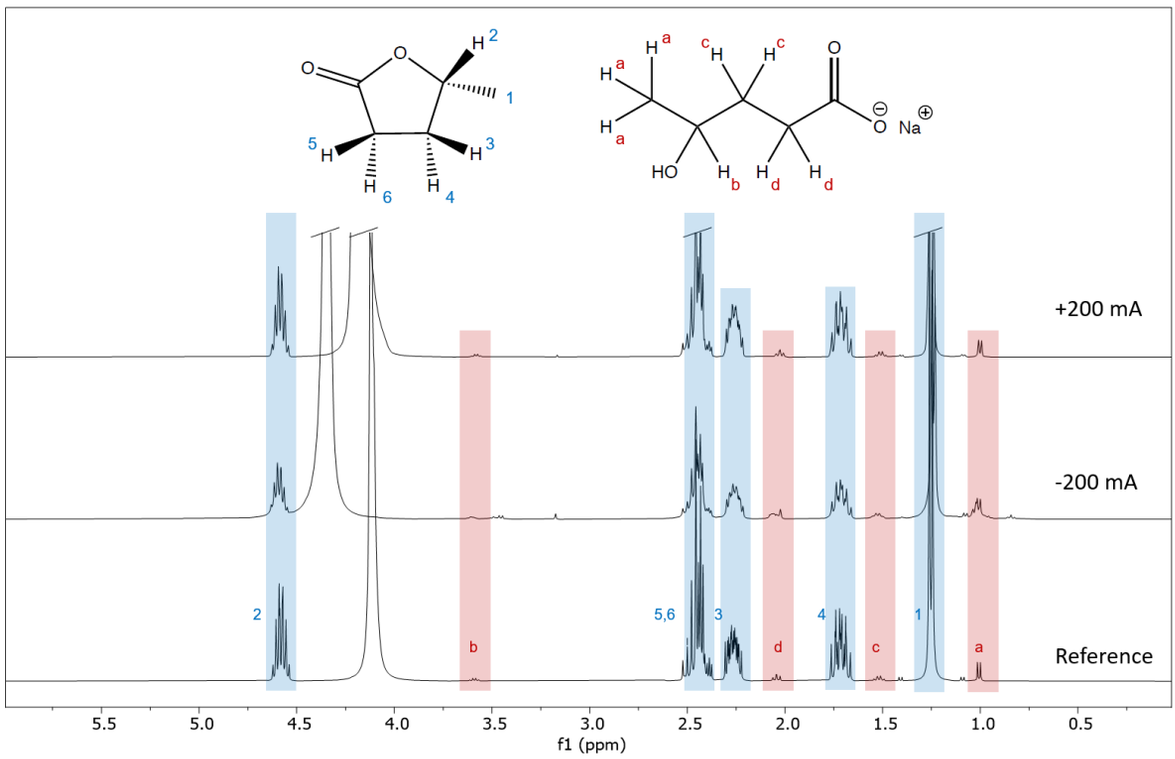

Figure S 19. ^{1}H NMR spectra (DMSO–d^{6}, 400.13 MHz) of the solution of 5 M GVL and an aqueous solution of Na_2CO_3 after 24 h at −200 mA, +200 mA of a reference solution after 24 h stirring.

The relative concentrations of 4-HVA compared to GVL at the different electrochemical influences are summarized in **Table S 4**.

Table S 4. Summary of the relative concentrations of 4-hydroxyvalerate compared to GVL at different electrochemical influences in mol%. All experiments were carried out in aqueous solution.

Influence	Na_2CO_3 8 h	Na_2CO_3 8 h −100 mA	Na_2CO_3 8 h −150 mA	Na_2CO_3 8 h −200 mA	Na_2CO_3 20 h −100 mA	Na_2CO_3 24 h	Na_2CO_3 24 h +200 mA	Na_2CO_3 24 h −200 mA
mol% [4-hydroxy-valerate]	2.5	2.5	3.5	4.6	10.0	2.5	3.7	6.8

NMR-spectroscopic characterization of the depolymerized products

In addition to the recorded ^{1}H NMR spectrum depolymerized products were characterized by ^{13}C-NMR (**Figure S 20**), ^{1}H ^{13}C-HSQC (**Figure S 21**) and ^{1}H ^{13}C-HMBC (**Figure S 22**) measurements and signals assigned to the obtained products (see experimental section). After addition of an internal standard (deuterated methanol) we were able to quantify the depolymerized products within the limitations of the method (**Figure S 23**). Because of solubility reasons we chose 100 µl deuterated methanol (99.8%).

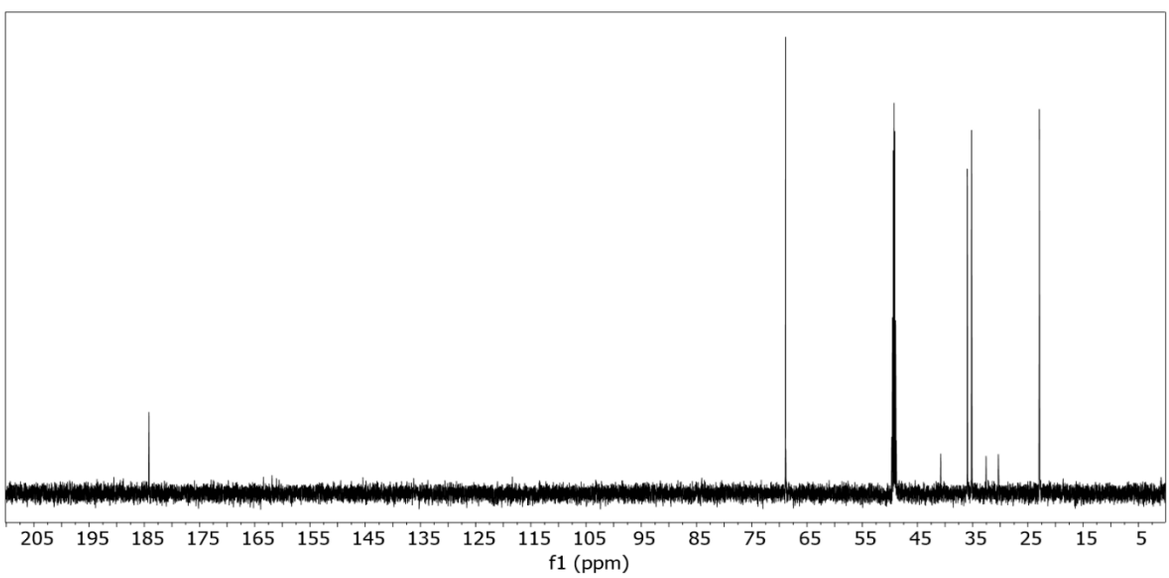

Figure S 20. ^{13}C NMR spectrum (D_2O, 150.94 MHz) of the depolymerized products after addition of 100 µl deuterated methanol (99.8%).

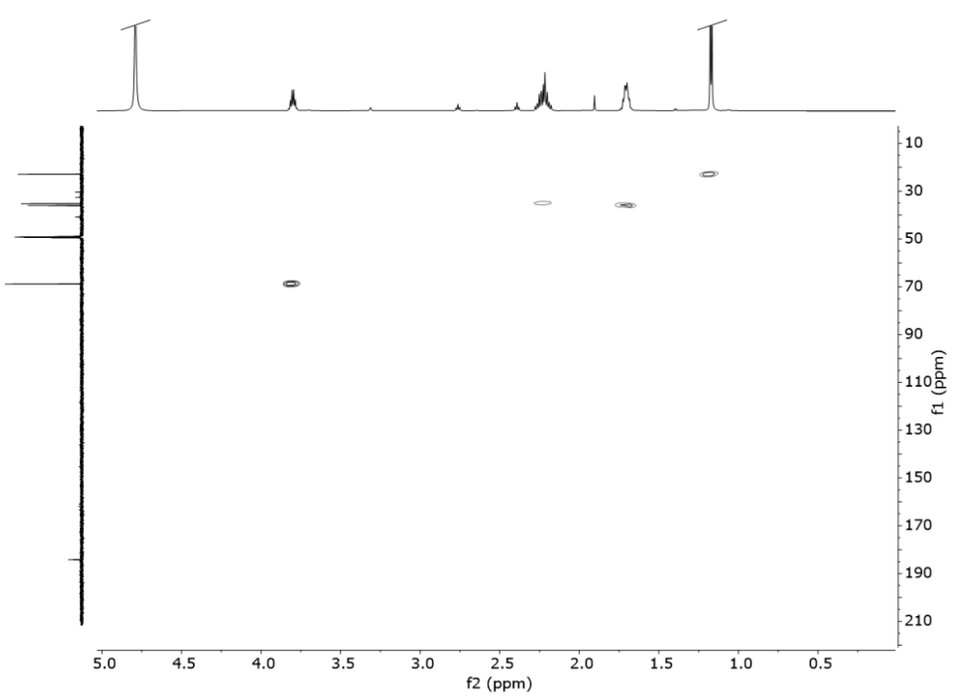

Figure S 21. ^{1}H ^{13}C-HSQC spectrum (D_2O, 600.12/150.94 MHz) of the depolymerized products after addition of 100 µl deuterated methanol (99.8%).

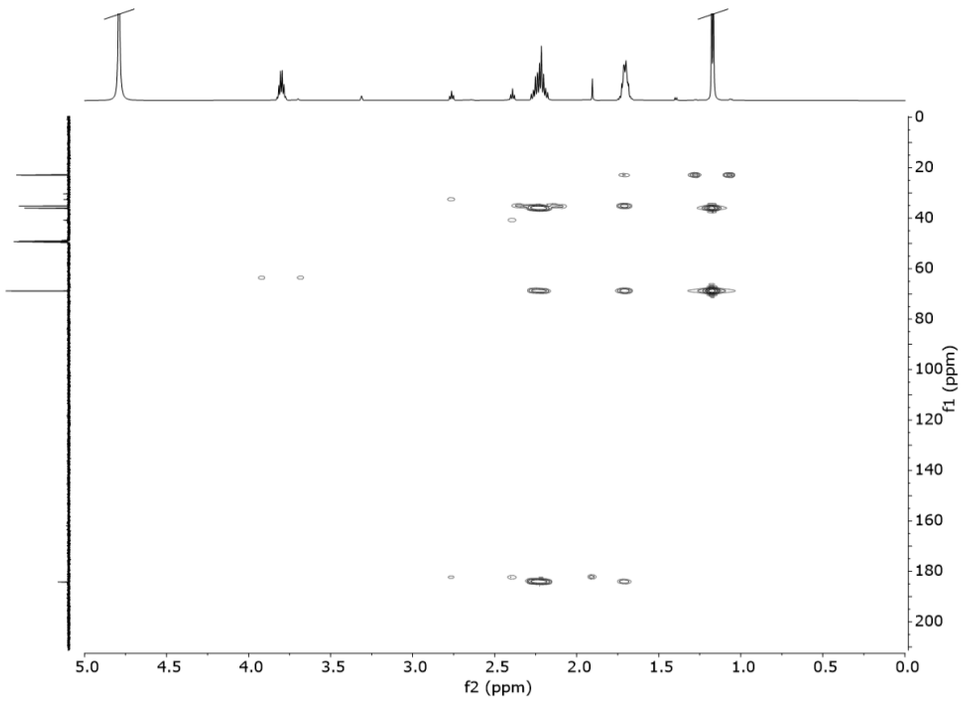

Figure S 22. ^{1}H ^{13}C-HMBC spectrum (D_2O, 600.12/150.94 MHz) of the depolymerized products after addition of 100 µl deuterated methanol (99.8%).

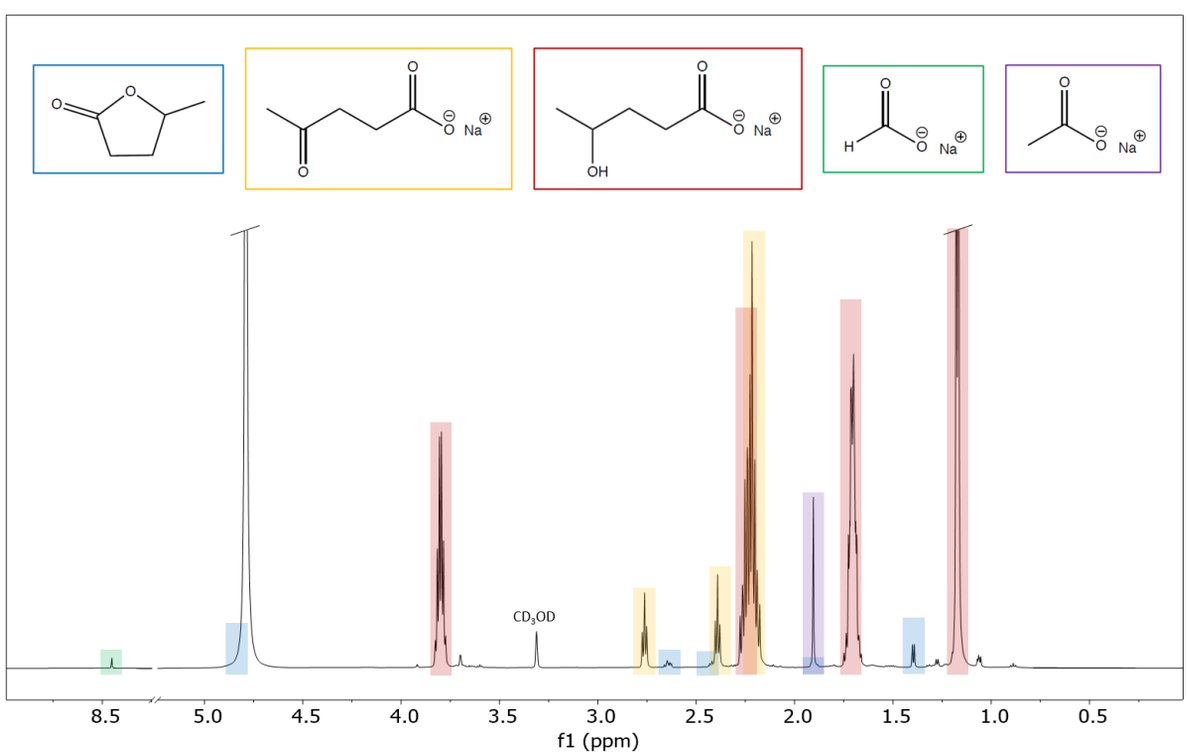

Figure S 23. ^{1}H NMR spectrum (D_2O, 600.12 MHz) of the depolymerized products after addition of 100 µl deuterated methanol (99.8%). We obtained a composition of 85 mol% sodium 4-hydroxovalerate, 8 mol% sodium levulinate, 6 mol% sodium acetate and 1 mol% sodium formate.

DSC/TGA characterization of the depolymerized products

The different heating characteristics of sodium 4-hydroxyvalerate and depolymerized products (DL) were investigated by DSC/TGA (**Figure S 24**).

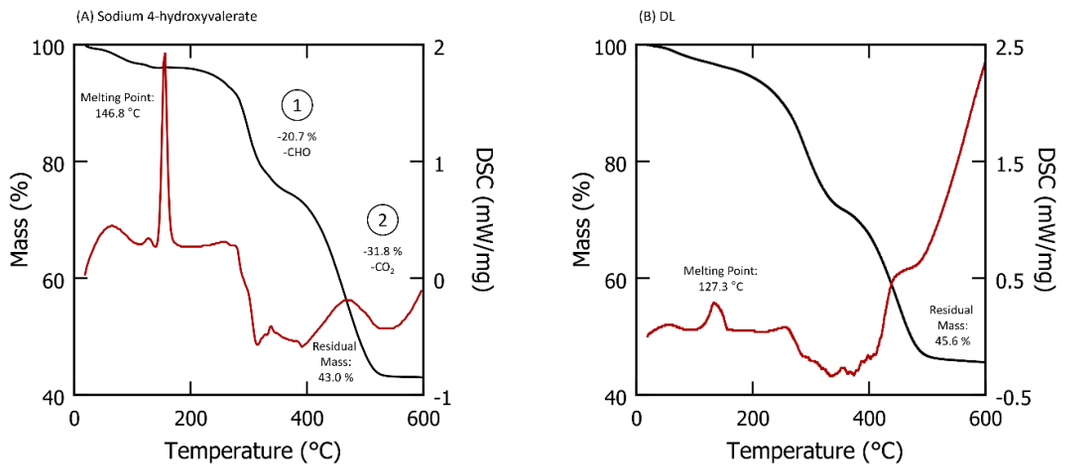

Figure S 24. DSC (red) / TGA (black) measurements of (A) sodium 4-hydroxyvalerate and (B) DL in a range between 20 °C and 600 °C. Using the DSC curves, the melting points can be determined to 146.8 °C for sodium 4-hydroxyvalerate and 127.3 °C for DL. The TG curve of sodium 4-hydroxyvalerate shows two assignable steps. The first step is the elimination of -CHO (–20.7 %) and the second step is the elimination of CO_2 (–31.8 %). The residual mass of 43.0 % belongs to Na_2O.

DI-ESI-HRMS characterization of the depolymerized products

To obtain a clear structure elucidation of the depolymerization products, direct injection electrospray ionization high-resolution mass spectrometry (DI-ESI-HR-MS) (**Figure S 25**) was used.

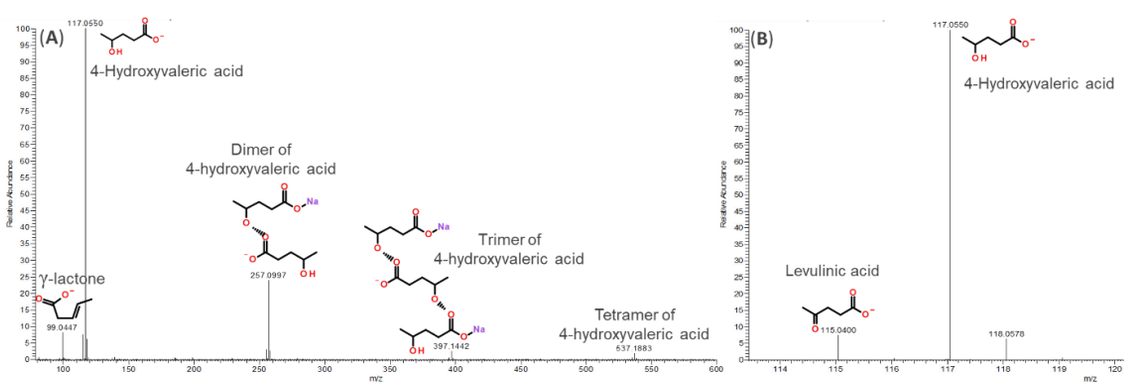

Figure S 25. Detection of γ-lactone, levulinic acid and 4-hydroxyvaleric acid in the depolymerization product using DI-ESI(–)-HRMS. (A) total ion current mass range m/z 80 – 600 and (B) zoom to mass range m/z 113 – 120.

Supplementary material for Chapter 6

Silver-catalyzed aqueous electrochemical valorization of Soda lignin into aliphatics and phenolics

Stability of the silver electrode

To determine the stability of the electrode material, a cyclic voltammetry (CV) experiment was conducted in a lignin solution (3 g·L^{-1}). The potential range was set to −1.5 to −2.5 V *vs.* Ag/AgCl (satd. KCl), and no peaks corresponding to reduction or oxidation were observed. This indicates that the electrode material exhibited high stability under these reaction conditions.

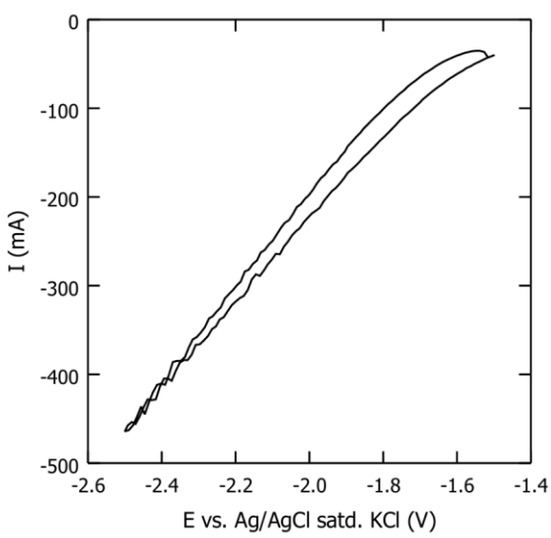

Figure S 26. Cyclic voltammogram assess the stability of the silver electrode in lignin solution during the electrochemical reaction.

Supplementary material for Chapter 7

One-pot electrocatalytic lignin depolymerization with in-situ extraction: a feasible approach toward biomass-based oils

Reference reactions

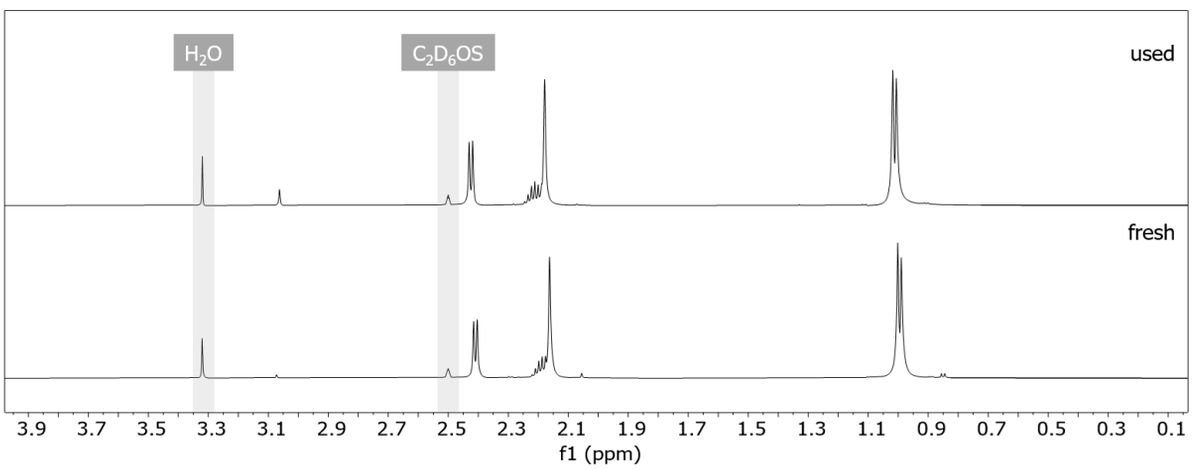

Figure S 27. ^{1}H NMR spectrum (DMSO-d^{6}, 600.13 MHz) of MIBK (–350 mA/20h/WM/NL) before (fresh) and after (used) reaction.

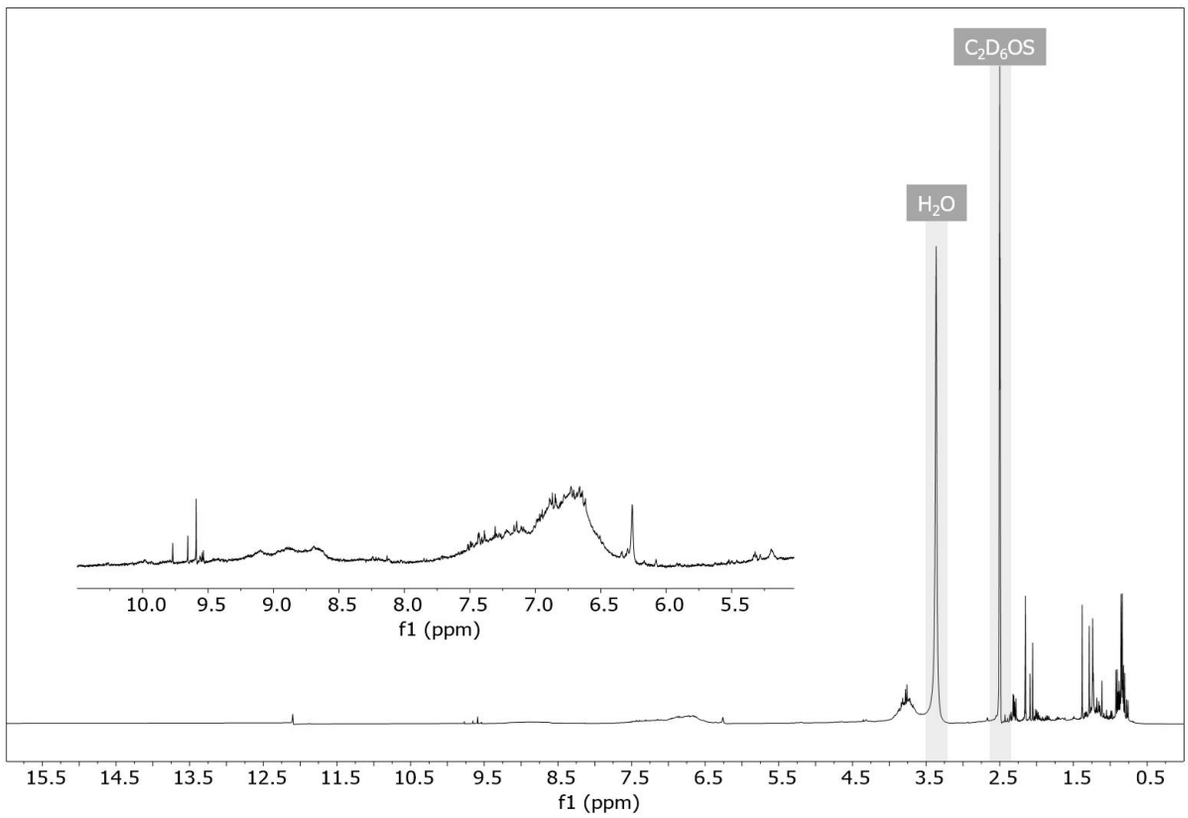

Figure S 28. ^{1}H NMR spectrum (DMSO-d^{6}, 400.13 MHz) of the MIBK-soluble fraction of lignin (0 mA/20h/LS).

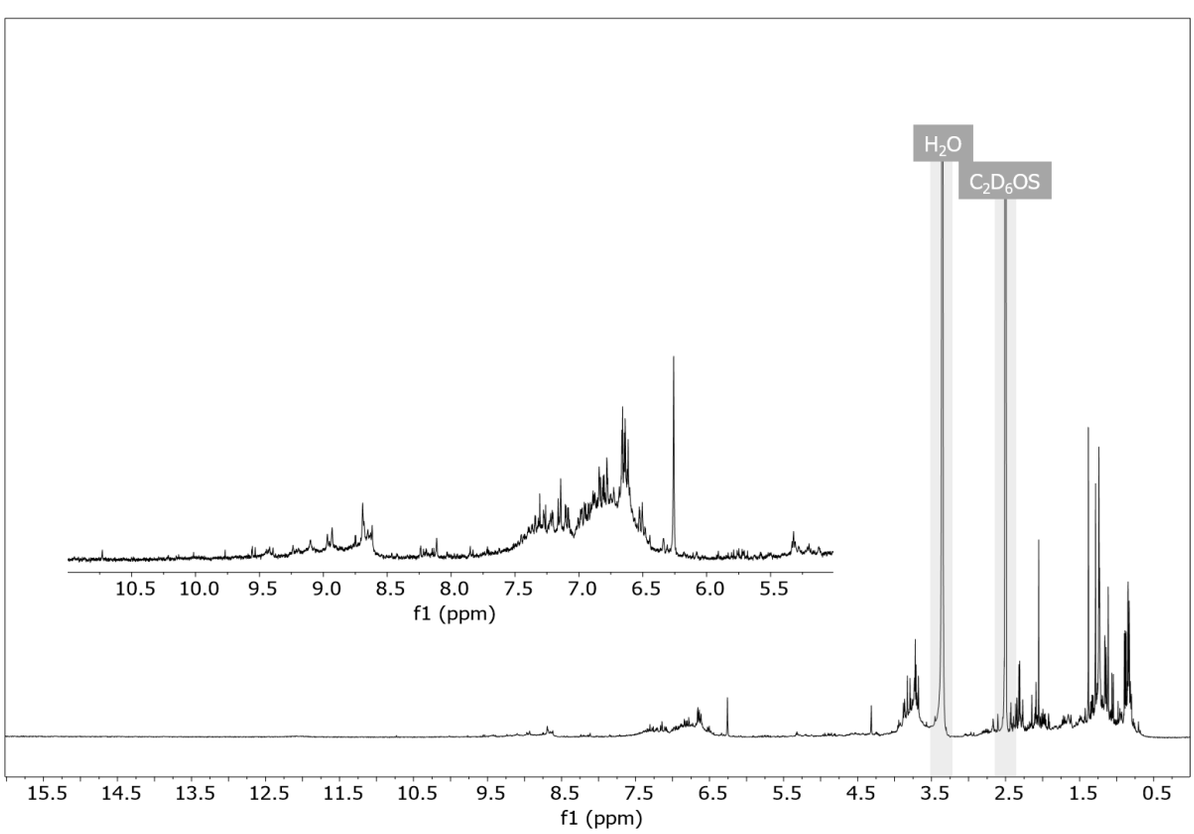

Figure S 29. ^{1}H NMR spectrum (DMSO-d^{6}, 400.13 MHz) of the MIBK-soluble fraction of lignin without the application of current and directly following the combination of reactants (0 mA/0h/WM).

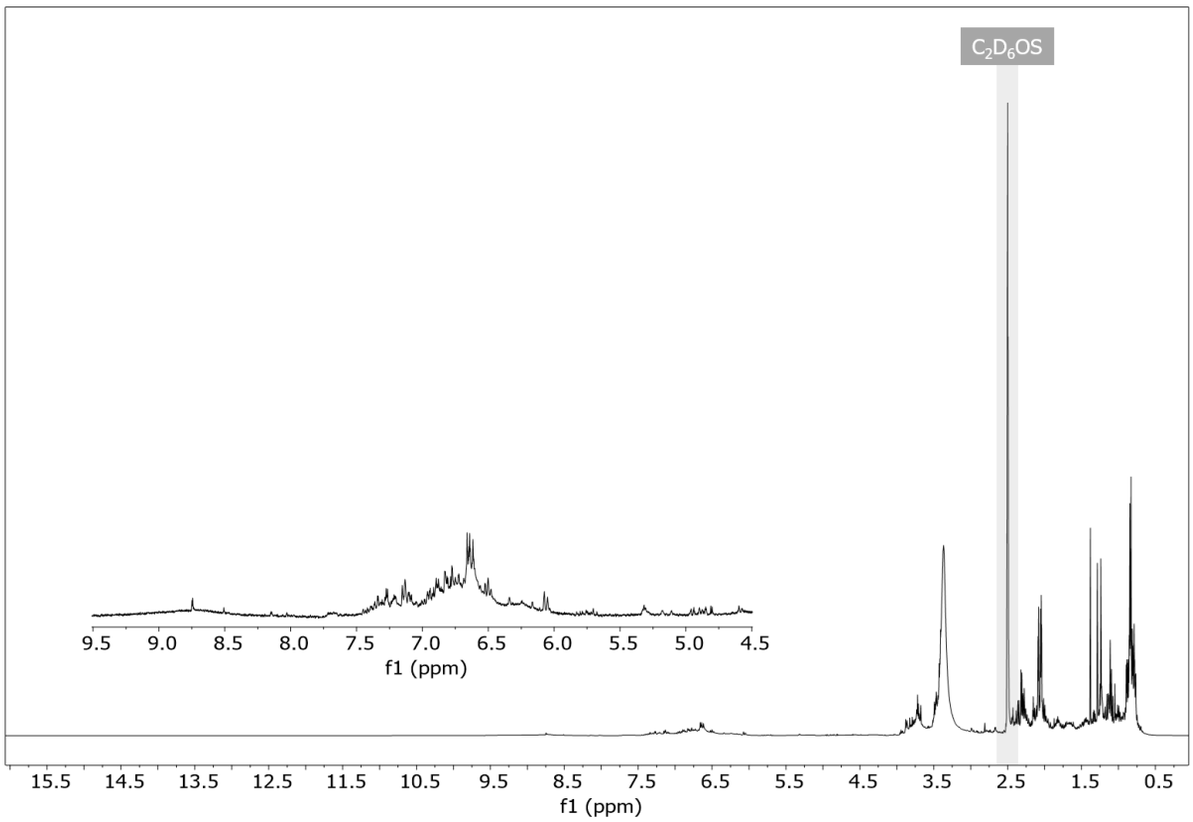

Figure S 30. ^{1}H NMR spectrum (DMSO-d^{6}, 400.13 MHz) of the MIBK-soluble fraction of lignin without the application of current and after 20 h stirring (0 mA/20h/WM).

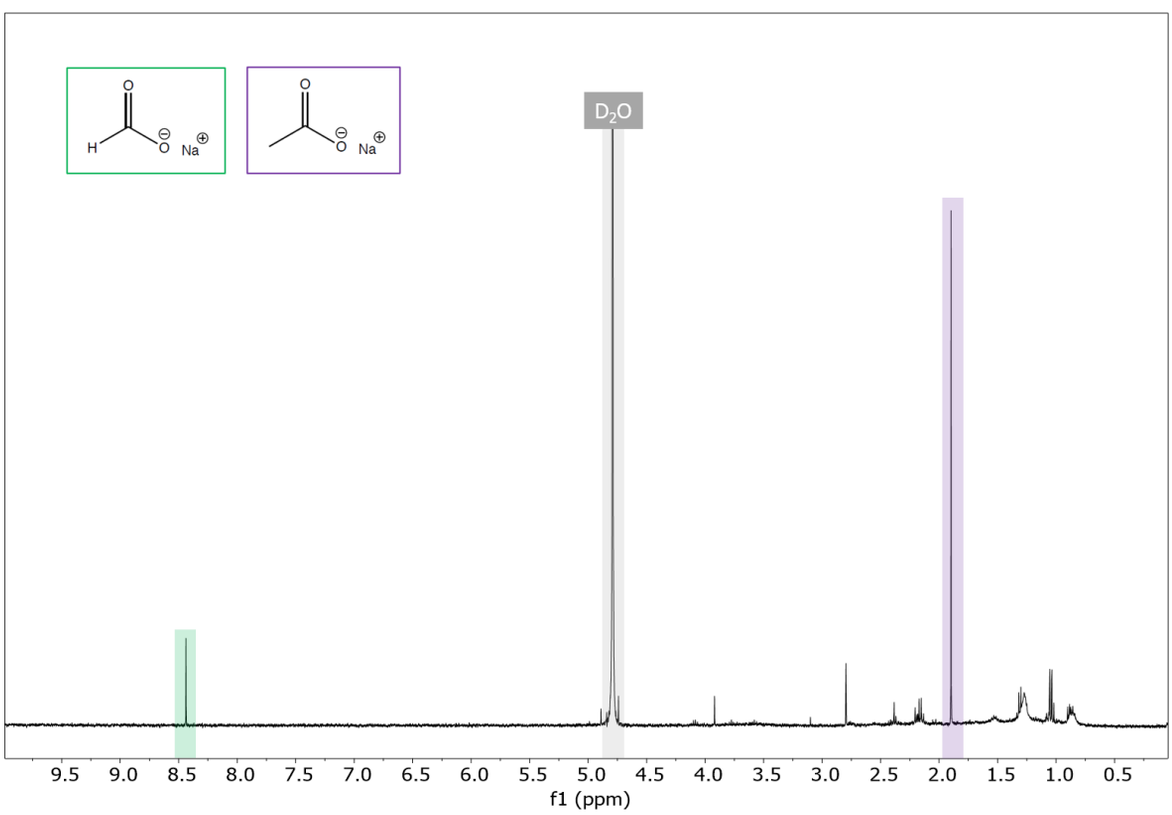

Figure S 31. ^{1}H NMR spectrum (D_2O, 400.13 MHz) of DL without a MIBK layer (–350 mA/20h/NM).

Figure S 32. Decolorization of the reference reaction (−350mA/20h/NM) subsequent to 20 h of depolymerization.

Characterization of depolymerization products derived from the aqueous phase

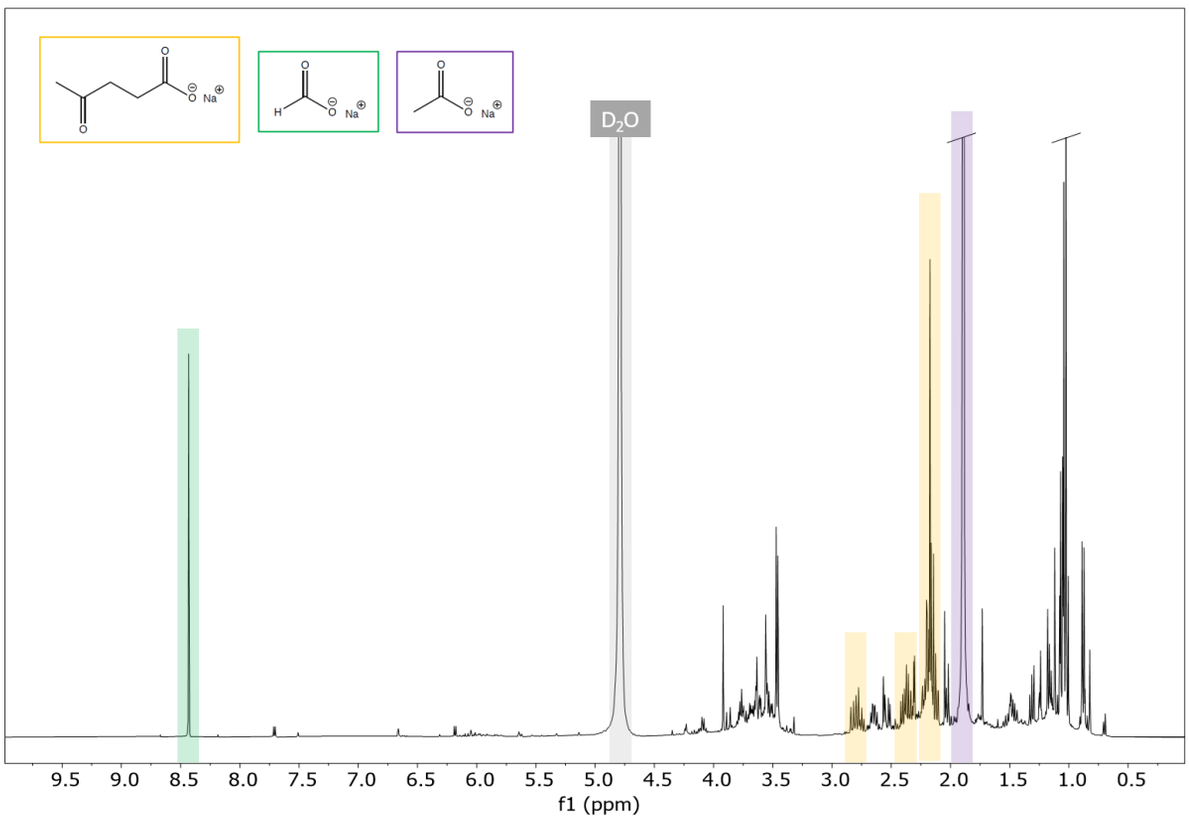

Figure S 33. ^{1}H NMR spectrum (D_2O, 400.13 MHz) of DL.

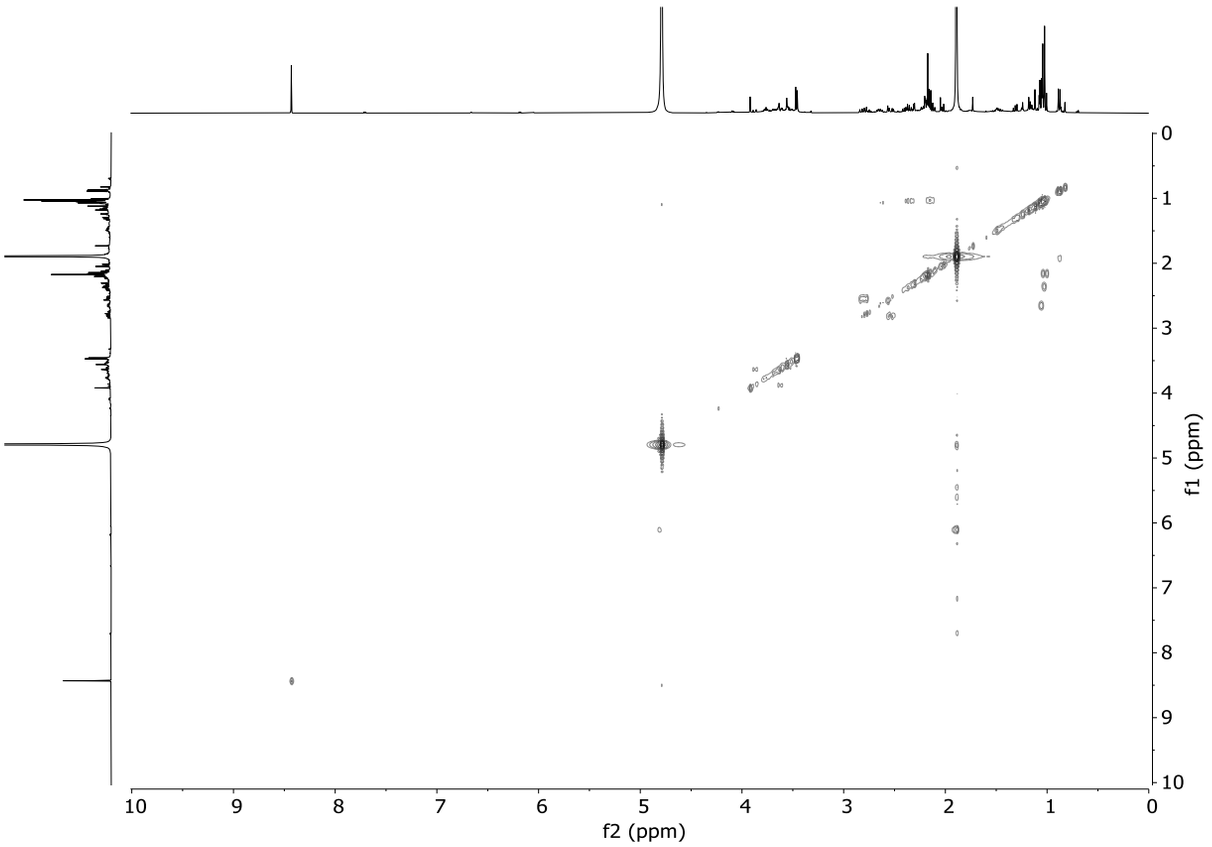

Figure S 34. ^{1}H ^{1}H-COSY NMR spectrum (D_2O, 400.13 MHz) of DL.

Characterization of depolymerization products derived from the MIBK phase

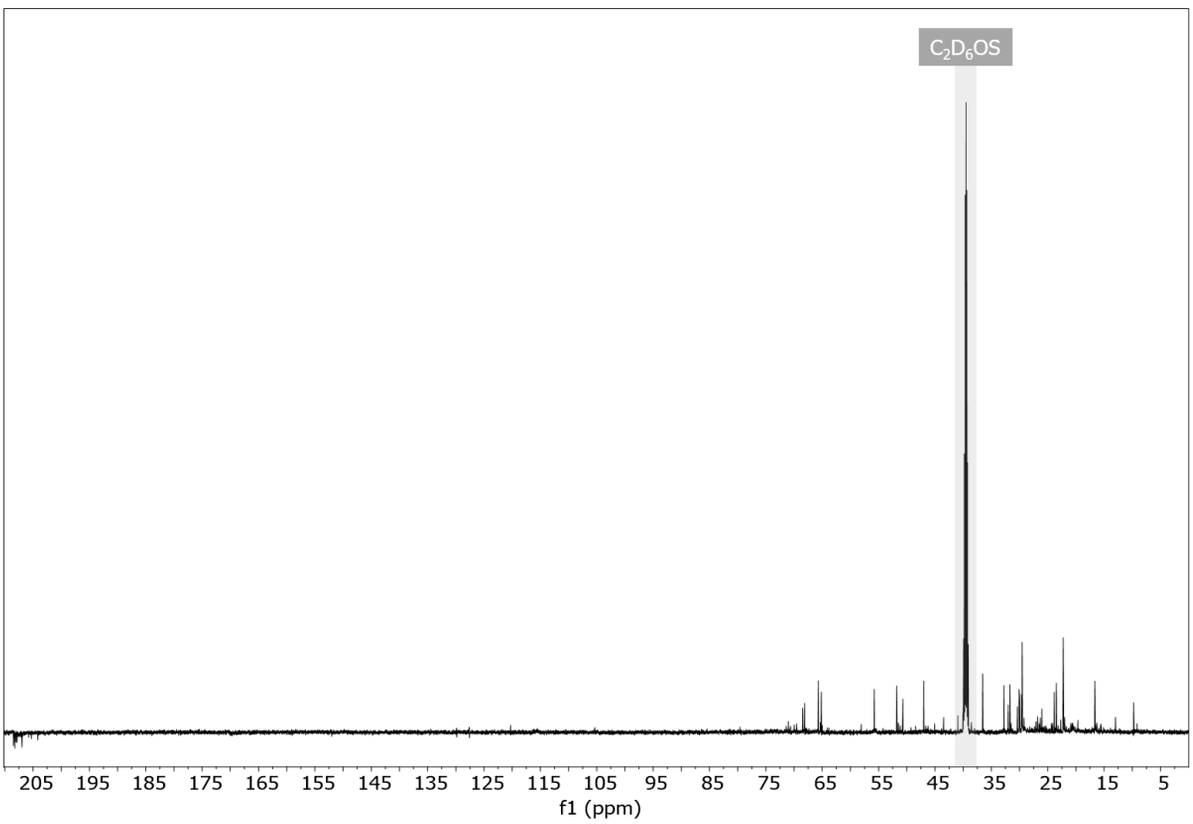

Figure S 35. ^{13}C NMR spectrum (DMSO-d^6, 150.94 MHz) of LO.

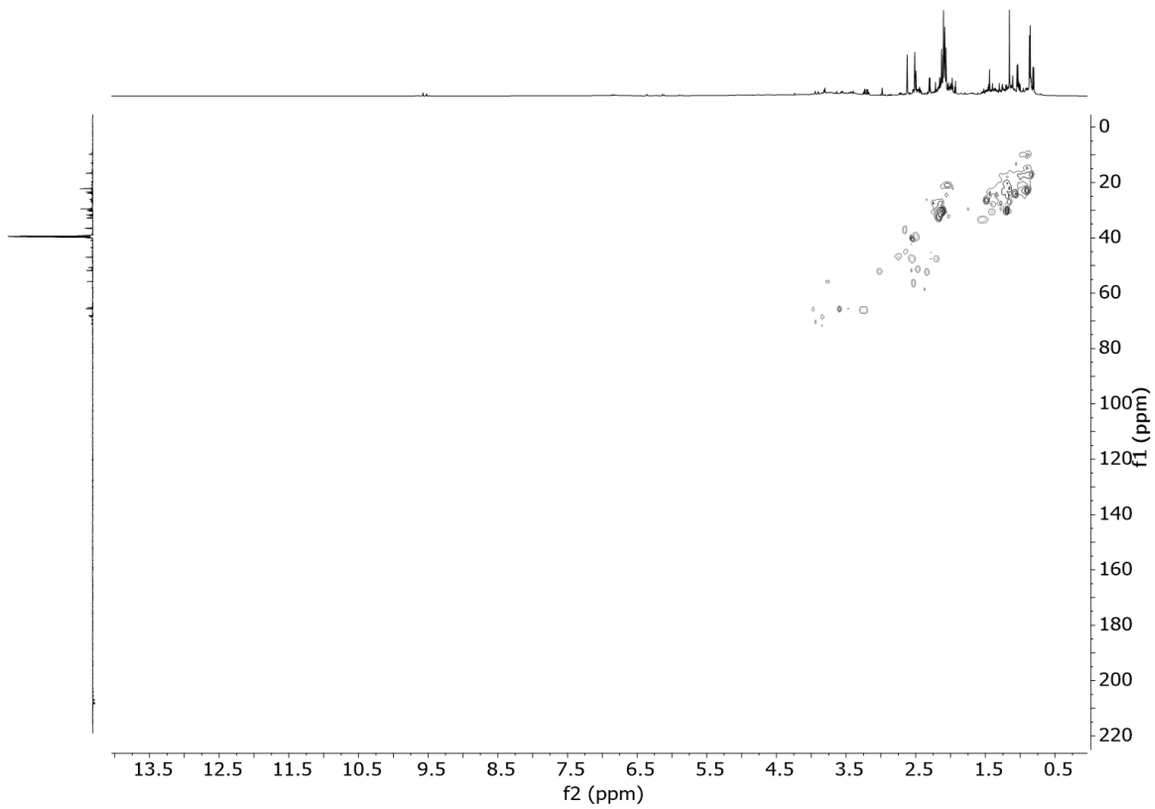

Figure S 36. ^{1}H ^{13}C-HSQC NMR spectrum (DMSO-d^6, 600.13/150.94 MHz) of LO.

Supplementary material for Chapter 8

Electrocatalytic lignin depolymerization enabled by a biomass-derived iron dual-atom catalyst: from synthesis to an *in-operando* X-ray absorption spectroscopy study

Characterization of the coffee oil

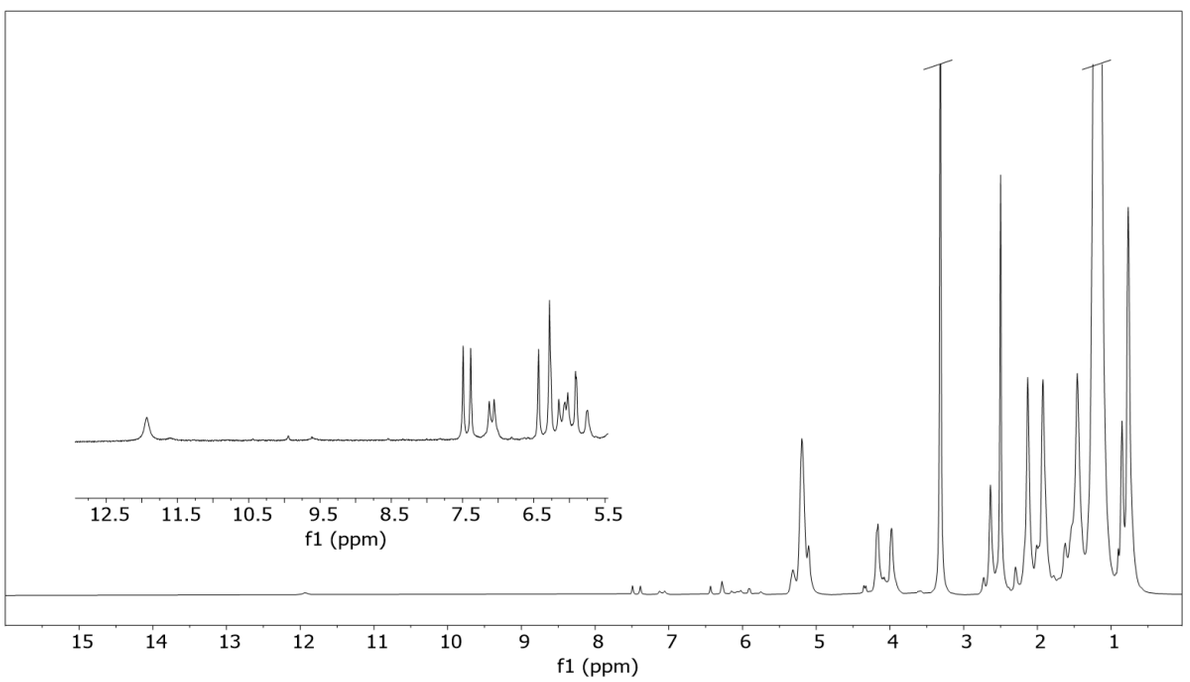

Figure S 37. ^{1}H NMR spectrum (DMSO–d^{6}, 600.13 MHz) of coffee oil.

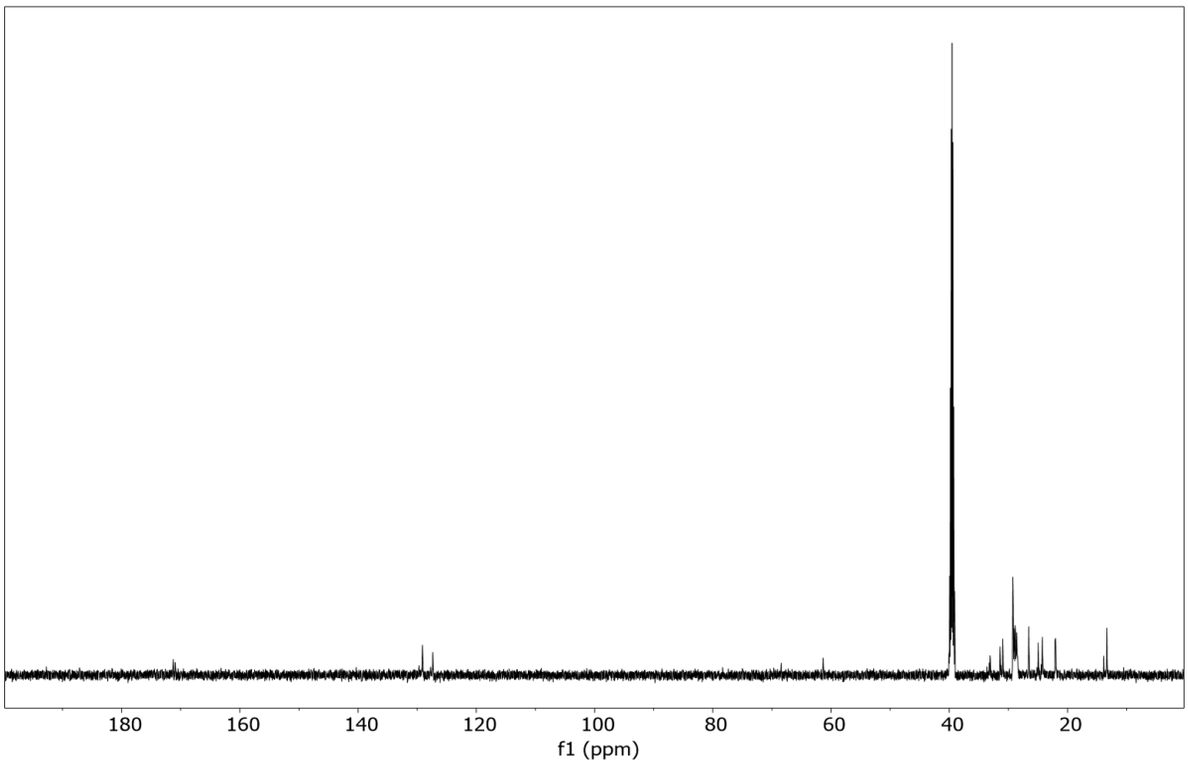

Figure S 38. ^{13}C NMR spectrum (DMSO–d^6, 150.94 MHz) of coffee oil.

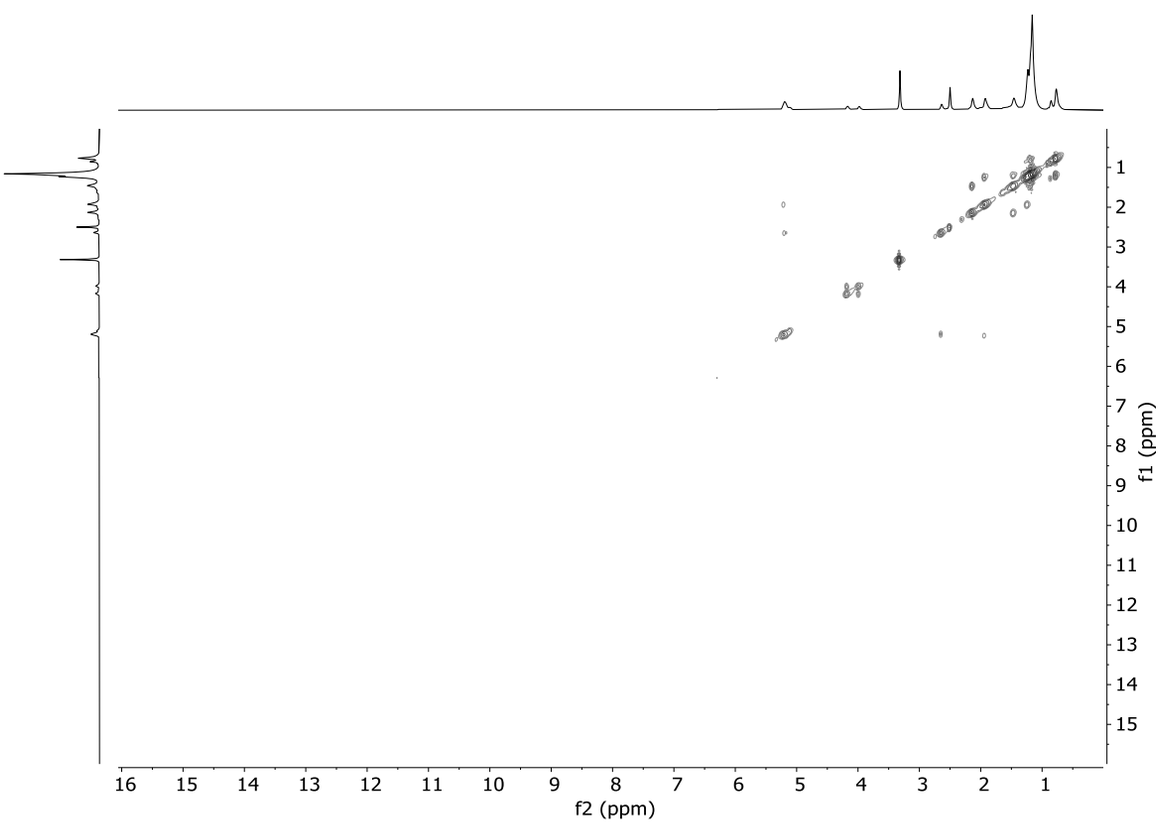

Figure S 39. ^{1}H ^{1}H-COSY NMR spectrum (DMSO–d^6, 600.13 MHz) of coffee oil.

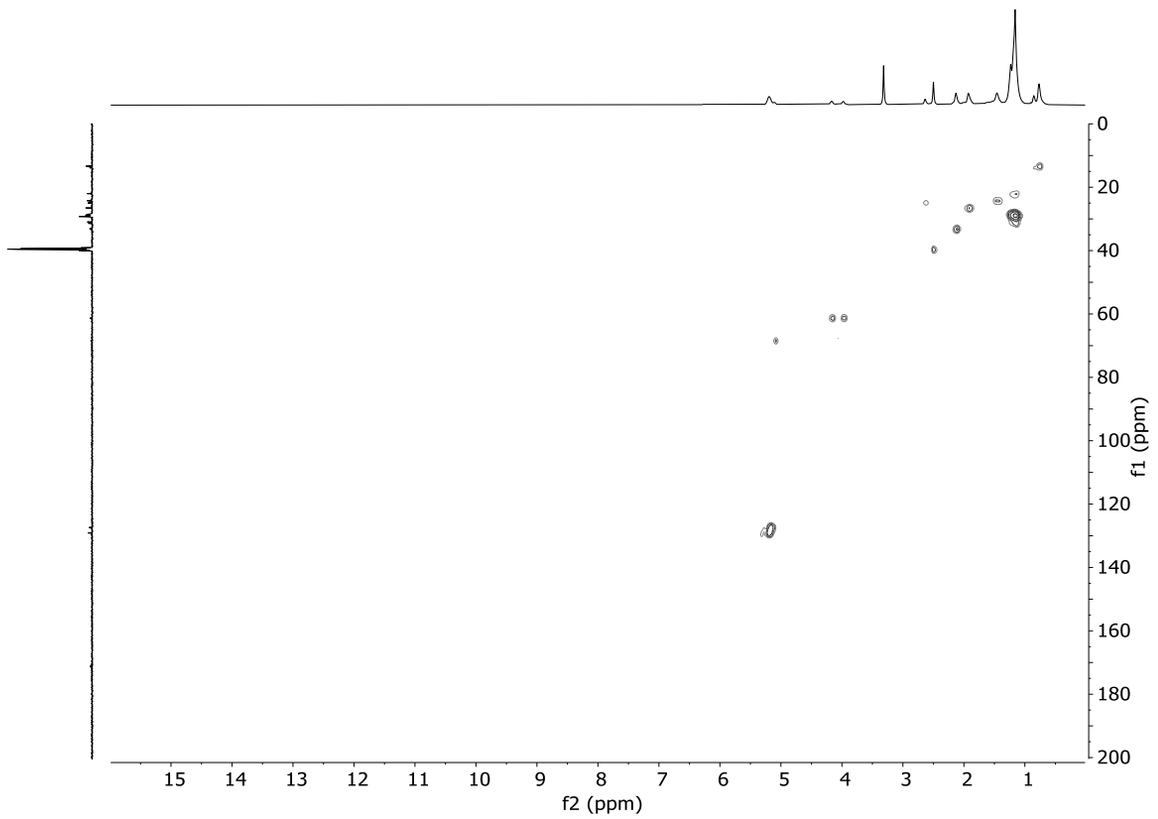

Figure S 40. ^{1}H ^{13}C-HSQC spectrum (DMSO–d^{6}, 600.12/150.94 MHz) of coffee oil.

Characterization of the catalyst

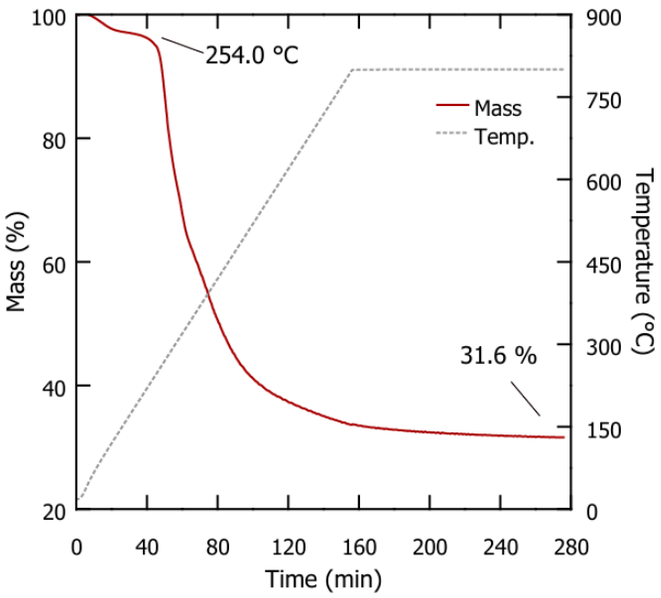

Figure S 41. Thermogravimetric analysis (TGA) for the mixture of coffee ground, melamine, and iron chloride. The sample was heated from 20 °C to 800 °C, at a rate of 5 °C·min^{-1}. Next, the sample was maintained at 800 °C for 2 h under a nitrogen flow (25 mL·min^{-1}), which was sufficient to simulate the pyrolysis process occurring within the furnace.

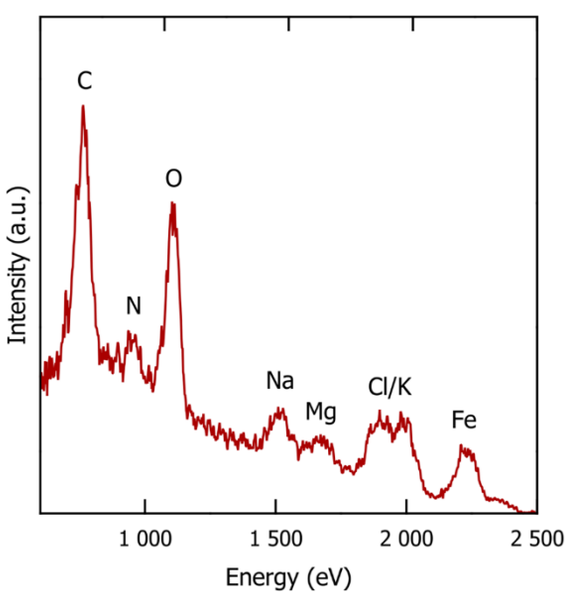

Figure S 42. Low-energy ion scattering (LEIS) spectrum of DAC. The spectrum provides confirmation of the surface composition of the DAC, exhibiting peaks for carbon, nitrogen, and oxygen derived from the biochar matrix and melamine, in addition to iron peaks, which are indicative of successful doping. Furthermore, trace elements such as magnesium, sodium, potassium, and chlorine are detected, originating from the coffee precursor and $FeCl_2$.

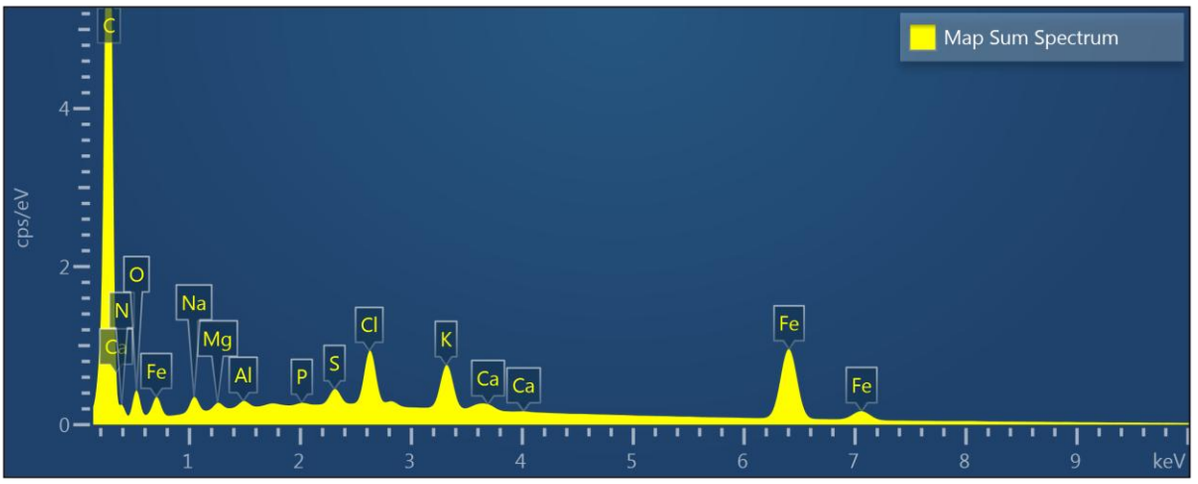

Figure S 43. Energy-dispersive X-ray spectroscopy (EDX) spectrum showing the elemental composition of the iron dual-atom catalyst (DAC). The peaks correspond to characteristic X-ray emissions of the detected elements, with their intensities indicating relative abundance.

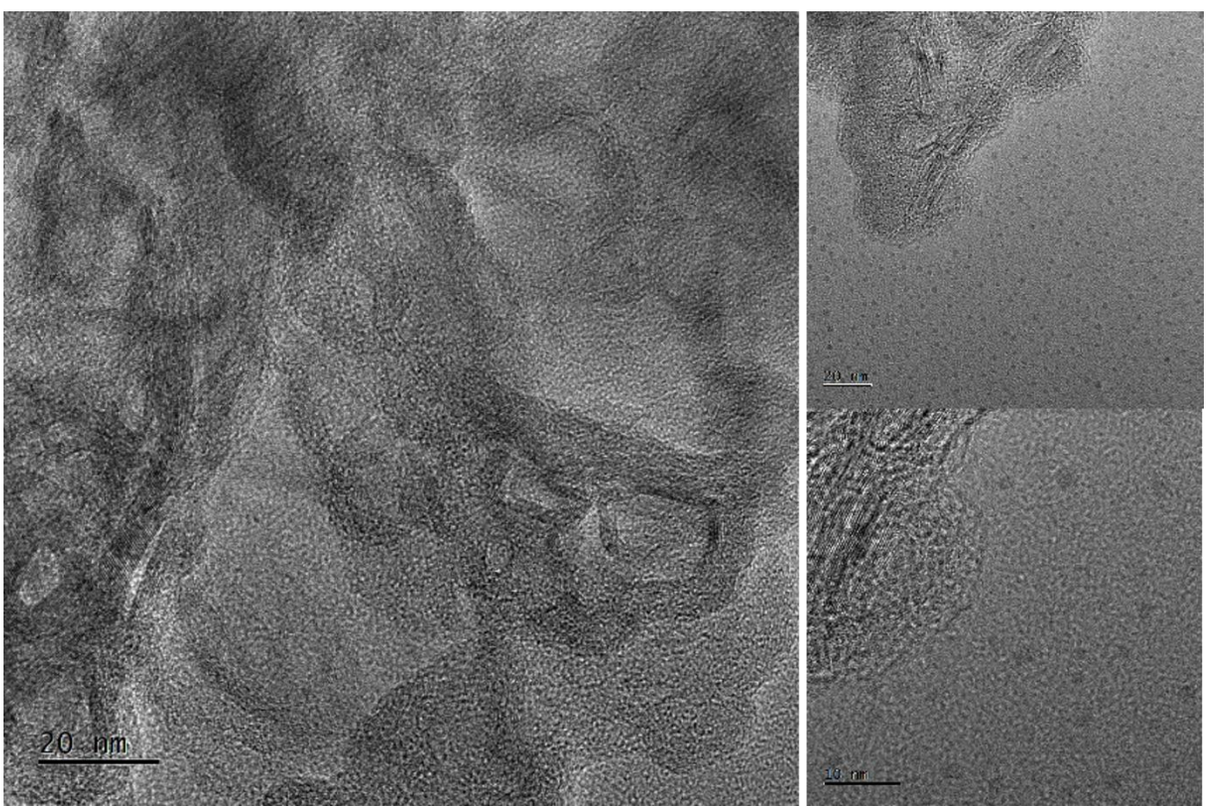

Figure S 44. High-resolution transmission electron microscopy images (HR-TEM) of DAC.

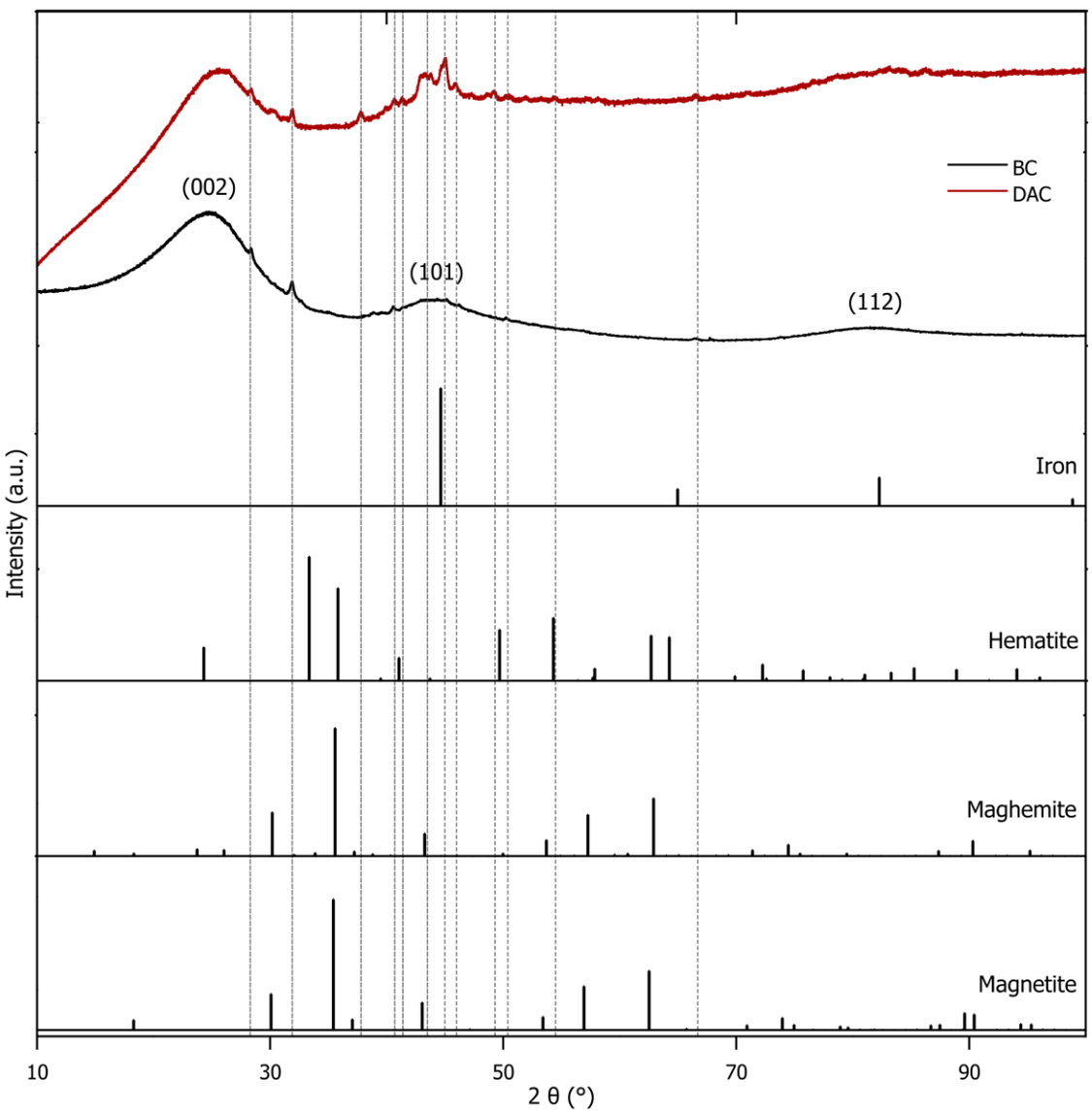

Figure S 45. X-ray powder diffraction (XRD) analysis of DAC and BC (biochar without Fe-doping) as a control sample and reference patterns of iron, hematite, maghemite, and magnetite. The XRD patterns demonstrate the presence of characteristic broad reflection peaks at 23° and 44° for both DAC and BC, corresponding to the (002) and (101) reflections of the graphitic carbon phase, respectively. Additionally, a weak reflection peak at approximately 80°, attributed to the (112) reflection, is observed in both samples. Furthermore, small reflection peaks appear in both DAC and BC, which does not contain iron. Consequently, it can be deduced that these reflections originate from the coffee-derived biochar matrix rather than the iron sites. [633] The DAC sample does not exhibit additional reflection peaks corresponding to crystalline iron species, such as iron, hematite, maghemite, or magnetite, suggesting the absence of larger iron particles or clusters, supporting the hypothesis that the iron species in the DAC are atomically dispersed.

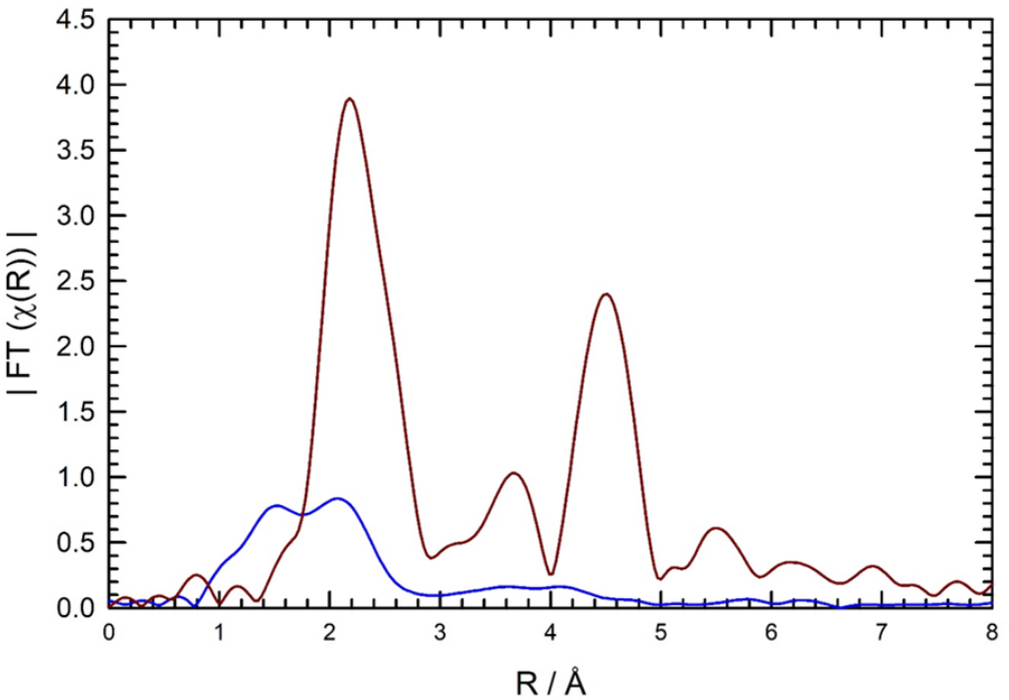

Figure S 46. Fourier transform (FT) of the Fe K-edge EXAFS spectra of DAC pre-reaction (blue) and iron metal foil (red).

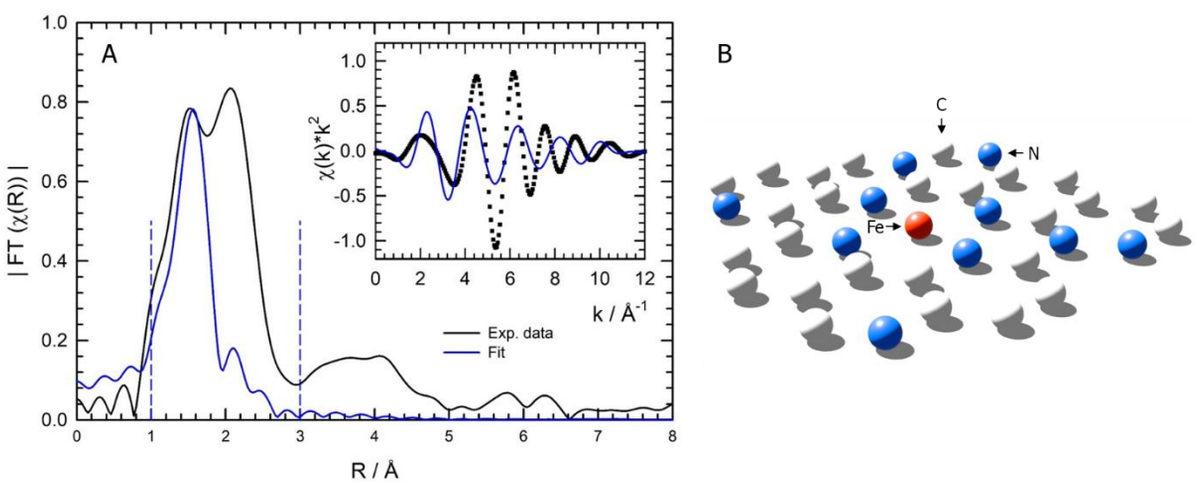

Figure S 47. A Fourier transform (FT) of the Fe K-edge EXAFS spectrum of DAC pre-reaction and fitting curve (k-range for the FT 1.3 $Å^{-1}$ < k < 11.6 $Å^{-1}$) for an iron single-atom catalyst, demonstrating that the fitting does not align with the expected coordination environment of a single-atom catalyst, indicating the presence of dual-atom active sites. B Structural model of an iron SAC that does not align with the experimental data.

Table S 5. Fit parameters determined for the quantitative fitting of the fresh Fe-containing DAC catalyst. A global inner potential shift ΔE_0 with a fitted value of ΔE_0= -1.17 eV ± 0.50 eV was used for all coordination shells. From the k-range used for the Fourier-transform and the R-range used for the fit, a total number of 12 fit parameters was allowed according to the Nyquist criterion [634]. For the Fe DAC sample, in total 4 different scattering paths were taken into account as follow. Besides the first Fe-N nearest neighbor (R_1, N_1), also the nearest carbon (R_2, N_2) and two Fe-Fe shells (R_3, N_3, R_4, N_4) were considered. R_3 and R_4 were fitted with only one parameter, that scales the actual fitted distances to those of the body-centered-cubic Fe metal reference. Each shell is fitted with a disorder parameter (σ_i^2), so that in total 12 fit parameters resulted, making the fit with an R - factor of R = 0.02 statistically sound.

	R_i / Å	N_i	σ_i^2 / 10^{-3} Å^2	ΔE_0 / eV
Fe – N	1.99 ± 0.03	3.2 ± 0.3	11.5 ± 1.50	−1.17 ± 0.50
Fe – C	2.55 ± 0.05	3.1 ± 0.3	2.14 ± 0.60	−1.17 ± 0.50
Fe – Fe	2.63 ± 0.03	1.53 ± 0.40	7.42 ± 1.20	−1.17 ± 0.50
Fe – Fe	3.04 ± 0.04	0.0 ± 0.0	16.6 ± 2.40	−1.17 ± 0.50

Table S 6. Fit parameters determined for the quantitative fitting of the used Fe-containing DAC catalyst. A global inner potential shift ΔE_0 with a fitted value of ΔE_0= 6.05 eV ± 0.75 eV was used for all coordination shells. From the k-range used for the Fourier-transform and the R-range used for the fit, a total number of 12 fit parameters was allowed according to the Nyquist criterion [634]. For the Fe DAC sample, in total 4 different scattering paths were taken into account as follow. Besides the first Fe-N nearest neighbor (R_1, N_1), also the nearest carbon (R_2, N_2) and two Fe-Fe shells (R_3, N_3, R_4, N_4) were considered. R_3 and R_4 were fitted with only one parameter, that scales the actual fitted distances to those of the body-centered-cubic Fe metal reference. Each shell is fitted with a disorder parameter (σ_i^2), so that in total 12 fit parameters resulted, making the fit with an R - factor of R = 0.01 statistically sound.

	R_i / Å	N_i	σ_i^2 / 10^{-3} Å^2	ΔE_0 / eV
Fe – N	2.07 ± 0.07	3.2 ± 0.3	8.09 ± 1.11	6.05 ± 0.75
Fe – C	2.66 ± 0.09	3.1 ± 0.3	3.86 ± 0.56	6.05 ± 0.75
Fe – Fe	2.66 ± 0.05	1.92 ± 0.45	8.83 ± 1.20	6.05 ± 0.75
Fe – Fe	3.07 ± 0.06	0.03 ± 0.03	72.2 ± 24.0	6.05 ± 0.75

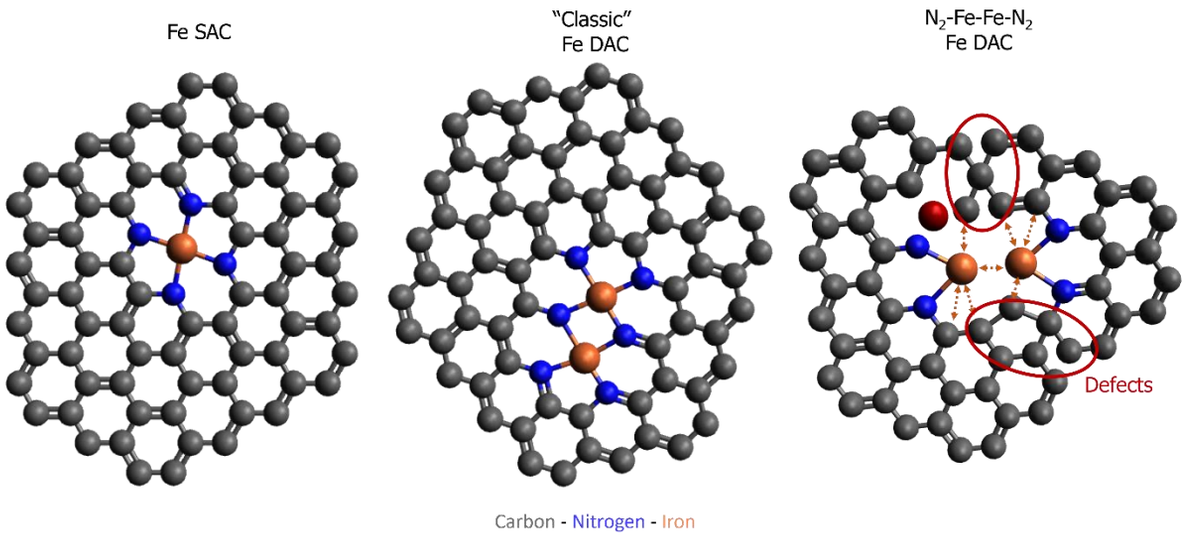

Figure S 48. EXAFS analysis reveals a first-shell Fe-Fe interaction at 2.63 Å, which would not be present in a purely atomic dispersion (Fe SAC). In a conventional DAC, metal centers are typically isolated and fully coordinated by nitrogen ("Classic" Fe DAC). For Fe in graphene, $N_N = 4$ and $N_C = 4$ would be expected, but EXAFS fits show reduced values. To reconcile this, the two "shared" nitrogen atoms are removed. Additionally, carbon rearranges to form more regular motifs, leaving each Fe with three carbon neighbors further adjusting the coordination environment.

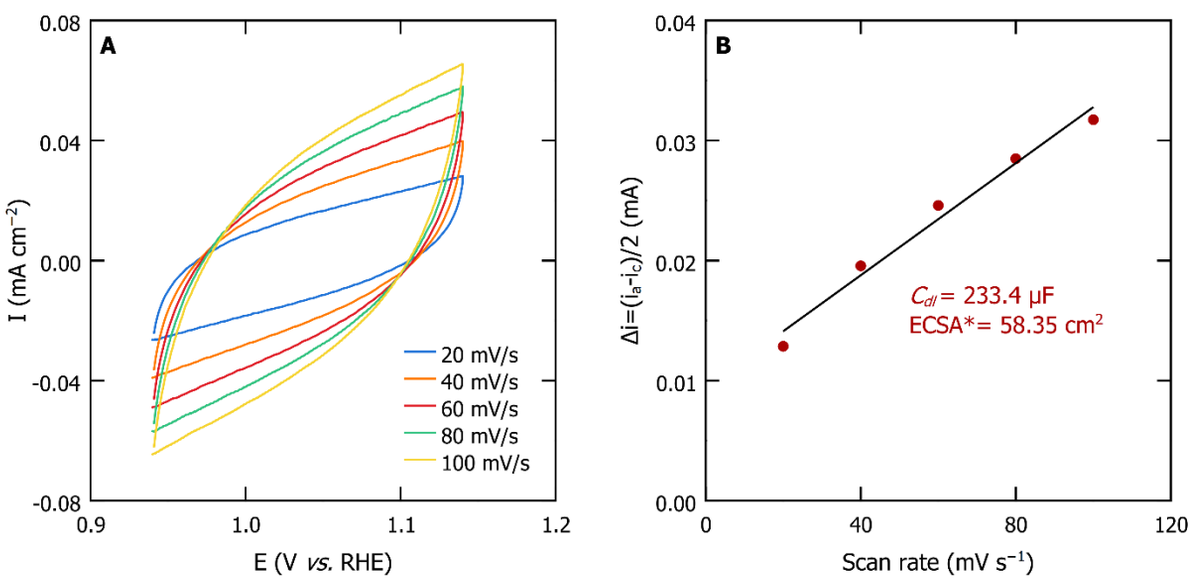

Figure S 49. (A) CV curves of Fe DAC in a 0.01 M Na_2CO_3 solution at various scan rates within a potential window from 0.94 V to 1.14 V (vs. RHE) without Faradaic process. (B) Average variance between the anodic and cathodic current at 1.09 V against the scan rate. * ECSA was calculated using a specific capacitance of $C_s = 4$ µF cm^{-2}, based on literature values for carbon-based materials. [635]

In-operando characterization of the catalyst

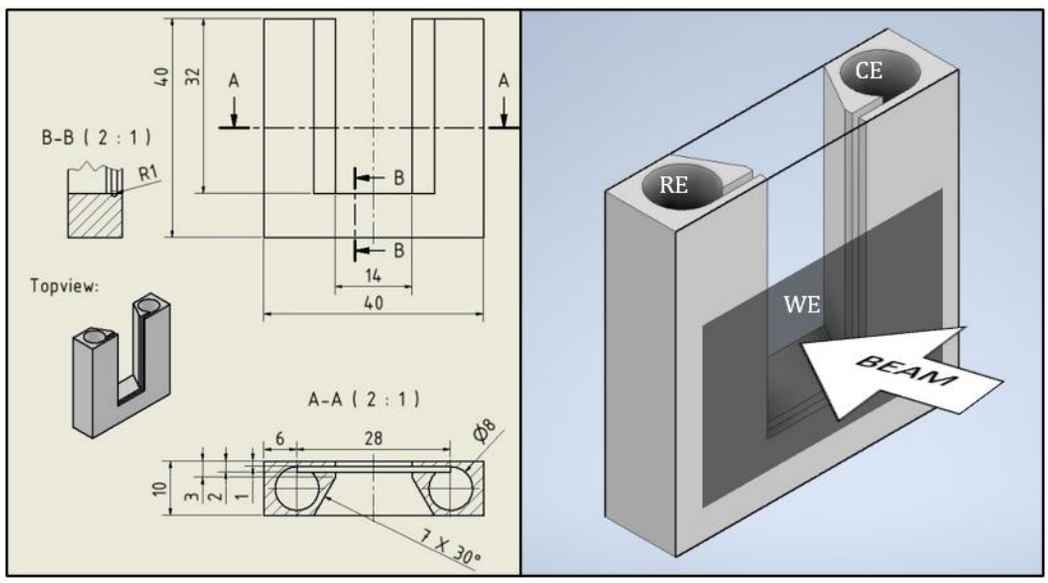

Figure S 50. The technical schematic depicts the *in-operando* reactor utilized for synchrotron radiation measurements during electrochemical lignin depolymerization.

Figure S 51. Photograph of the *in-operando* experimental setup during synchrotron radiation measurements.

Electrochemical depolymerization of Kraft lignin

Dissolving lignin in an aqueous solution of sodium carbonate results in a dark brown solution (**Figure S 52**). It is established that the selection of reaction times and currents or potentials has an impact on the decolorization of the lignin solution during the reaction. [138] In previous studies, the degree of decolorization was identified as an indirect indicator of the degree of depolymerization. [138,261,265,354] It can be demonstrated that the selection of catalyst, under otherwise identical conditions (potential of −1.6 V *vs.* Ag/AgCl (satd. KCl) and reaction time of 20 h), also has a pronounced effect on decolorization (**Figure S 52**).

As a comparison, the depolymerization reactions were also performed using carbon paper (CP) and biochar (BC) (coffee grounds and melamine, without Fe-doping).

The use of CP as an electrocatalyst results in a slight increase in solution transparency, although the brown color remains largely unchanged. Similarly, when using BC, the solution's appearance remains identical to its pre-reaction state, exhibiting no noticeable change after the reaction. In contrast, the reaction solution achieves near complete decolorization when the DAC is employed, highlighting the enhanced catalytic efficacy of the iron species.

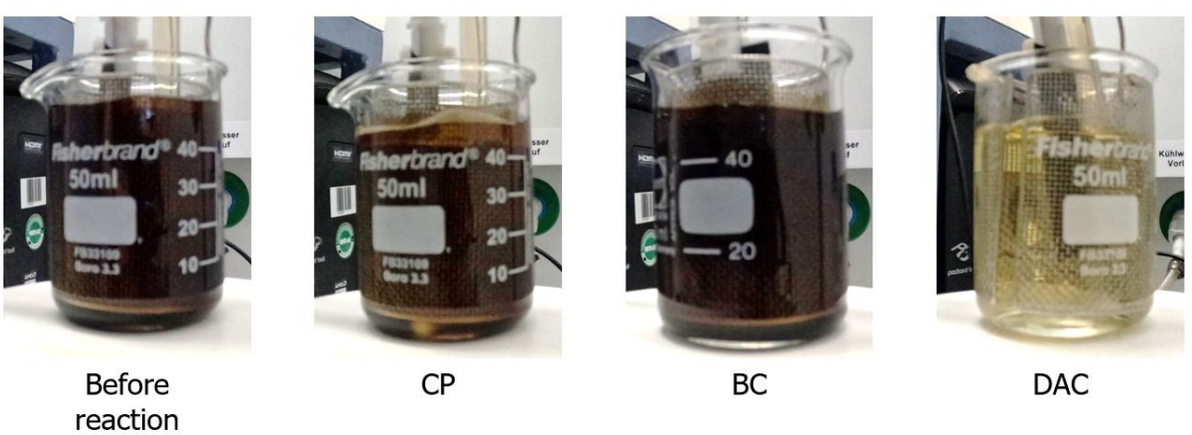

Figure S 52. The color change observed in the solution during the course of the reaction is contingent upon the specific electrocatalyst that is employed.

A comparison of the yields of depolymerization products (DL) (**Table S 7**) also demonstrates that DAC, with a yield of 4.6 wt%, is the most effective catalyst under these conditions. In this case, the yield represents the fraction of (DL) that is soluble in ethanol relative to the mass of the starting Kraft lignin.

Table S 7. Yields of depolymerization products (DL) related to the mass of products obtained after extraction with ethanol compared to the mass of starting Kraft lignin.

	CP	BC	DAC
Yield [wt%]	2.6	1.3	4.6

The ethanol-soluble fraction of DL was subjected to nuclear magnetic resonance (NMR) analysis (**Figure S 53**). Formate (8.45 ppm) and acetate (1.90 ppm), which are known products of lignin depolymerization, [138,203] were detected after the use of all three electrodes (CP, BC, DAC). In the range of 0-4.5 ppm, the signals appear to be nearly identical, exhibiting only slight variations in intensity when different catalysts are employed. Notable discrepancies are evident in the aromatic range (6-9 ppm). The signals with the highest intensity are observed between 7.0 and 7.5 ppm when CP is used, while the main signals between 7.2 and 8.2 ppm can be found with DAC. Notably, when BC is employed, only signals with low intensity, which are obscured by background noise, are discernible. Consequently, the NMR analysis also indicates that the selectivity is influenced by the choice of the catalyst. The same trends observed in the NMR analysis can also be demonstrated through a Direct Infusion Electrospray Ionization High-Resolution Mass Spectrometry (DI ESI-HRMS) analysis.

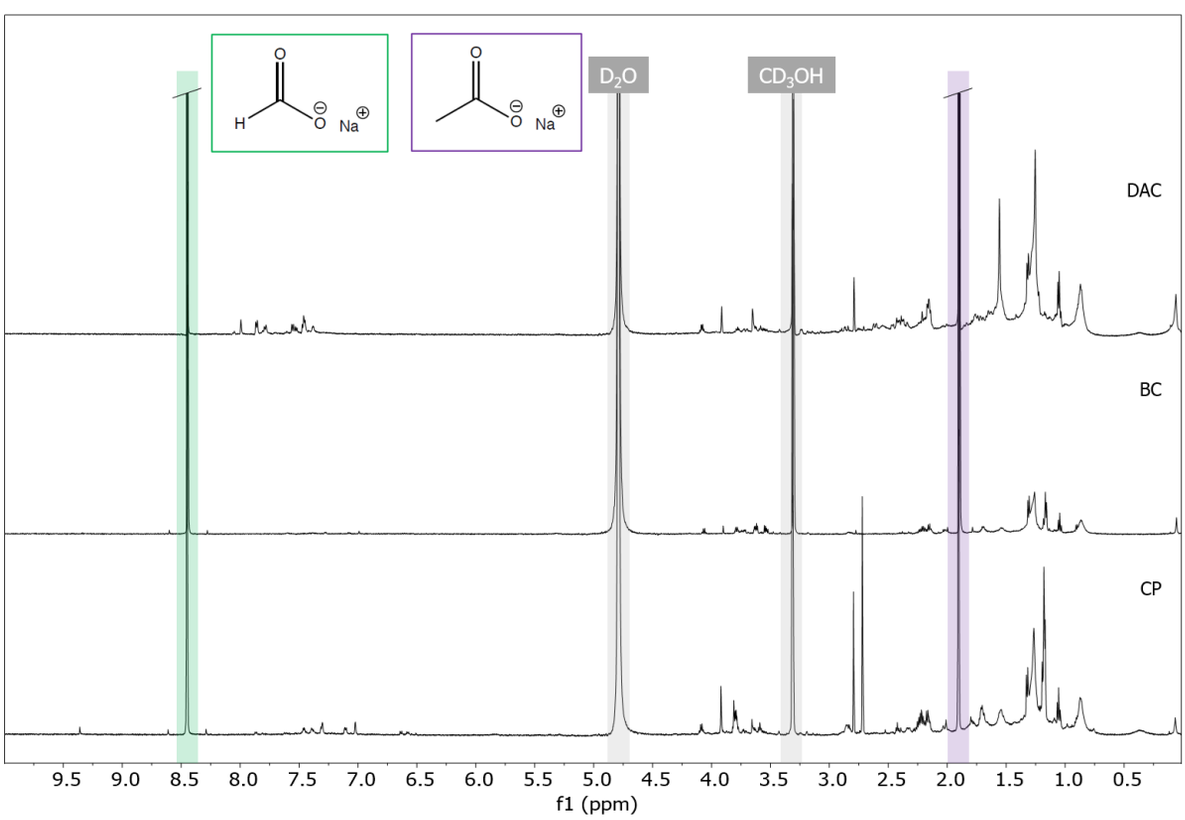

Figure S 53. ^{1}H NMR spectra (D_2O/CD_3OD 50/50, 600.12 MHz) of the depolymerized products using CP, BC and DAC as electrocatalysts.

Table S 8. Comparison of Electrocatalytic Lignin Depolymerization Methods.

Catalyst	Copper	Carbon	Silver	Fe DAC
Solvent	Levulinic Acid/H_2O	Na_2CO_3/H_2O	Na_2CO_3/H_2O	Na_2CO_3/H_2O
Lignin	Kraft	Soda	Soda	Kraft
Current [mA]	−9	−175	−175	−48
Potential [V *vs.* Ag/AgCl (satd. KCl)]	−1.7	-	-	−1.6
Time [h]	20	20	20	20
Main aliphatic products	none	levulinate, 4-hydroxyvalerate, acetate, formate	levulinate, acetate, formate	levulinate, acetate, formate
Complete dearomatization?	No	Yes	No	No
Yield [wt%]	-	58	18	5
Reference	[104]	[138]	[354]	-

References

References

(1) Copernicus Climate Change Service (C3S). *Global Climate Highlights 2024*; Copernicus Climate Change Service (C3S) / ECMWF, 2025. https://climate.copernicus.eu/global-climate-highlights-2024 (accessed 2025-02-05).

(2) Behr, A.; Seidensticker, T. *Einführung in die Chemie nachwachsender Rohstoffe: Vorkommen, Konversion, Verwendung*; Springer Berlin Heidelberg: Berlin, Heidelberg, 2018. https://doi.org/10.1007/978-3-662-55255-1.

(3) Lindenbeck, L.; Liu, Y.; Beele, B. B.; Slabon, A.; Rodrigues, B. V. M. Sustainable Routes for the Depolymerization of Lignocellulosic Biomass. In *Encyclopedia of Inorganic and Bioinorganic Chemistry*; Scott, R. A., Ed.; Wiley, 2023; pp 1–19. https://doi.org/10.1002/9781119951438.eibc2862.

(4) Davis, K.; Rover, M.; Brown, R.; Bai, X.; Wen, Z.; Jarboe, L. Recovery and Utilization of Lignin Monomers as Part of the Biorefinery Approach. *Energies* **2016**, *9* (10), 808–836. https://doi.org/10.3390/en9100808.

(5) Lindenbeck, L. M.; Barra, V. C.; Beele, B. B.; Rodrigues, B. V. M.; Slabon, A. Revisiting the Electrocatalyst Role on Lignin Depolymerization. *Adv. Energy Sustainability Res.* **2024**, *5* (10), 2400130. https://doi.org/10.1002/aesr.202400130.

(6) Anastas, P.; Eghbali, N. Green Chemistry: Principles and Practice. *Chem. Soc. Rev.* **2009**, *39* (1), 301–312. https://doi.org/10.1039/B918763B.

(7) May, A. S.; Biddinger, E. J. Strategies to Control Electrochemical Hydrogenation and Hydrogenolysis of Furfural and Minimize Undesired Side Reactions. *ACS Catal.* **2020**, *10* (5), 3212–3221. https://doi.org/10.1021/acscatal.9b05531.

(8) Garedew, M.; Lin, F.; Song, B.; DeWinter, T. M.; Jackson, J. E.; Saffron, C. M.; Lam, C. H.; Anastas, P. T. Greener Routes to Biomass Waste Valorization: Lignin Transformation Through Electrocatalysis for Renewable Chemicals and Fuels Production. *ChemSusChem* **2020**, *13* (17), 4214–4237. https://doi.org/10.1002/cssc.202000987.

(9) Latsuzbaia, R.; Bisselink, R. J. M.; Crockatt, M.; van der Waal, J. C.; Goetheer, E. L. V. Biomass Processing via Electrochemical Means. In *Biomass Valorization*; John Wiley & Sons, Ltd, 2021; pp 225–264. https://doi.org/10.1002/9783527825028.ch8.

(10) Lindenbeck, L. M.; Beele, B. B.; Lützenkirchen-Hecht, D. F.; Rodrigues, B. V. M.; Slabon, A. Electrochemical Biomass Depolymerization: Will Complex Catalysts Trigger High Product Selectivity? *Chem. Mater.* **2024**, *36* (19), 9173–9188. https://doi.org/10.1021/acs.chemmater.4c02078.

(11) Ripple, W. J.; Wolf, C.; Newsome, T. M.; Gregg, J. W.; Lenton, T. M.; Palomo, I.; Eikelboom, J. A. J.; Law, B. E.; Huq, S.; Duffy, P. B.; Rockström, J. World Scientists' Warning of a Climate Emergency 2021. *BioScience* **2021**, *71* (9), 894–898. https://doi.org/10.1093/biosci/biab079.

(12) Ripple, W. J.; Wolf, C.; Newsome, T. M.; Galetti, M.; Alamgir, M.; Crist, E.; Mahmoud, M. I.; Laurance, W. F.; 15,364 scientist signatories from 184 countries. World Scientists' Warning to Humanity: A Second Notice. *BioScience* **2017**, *67* (12), 1026–1028. https://doi.org/10.1093/biosci/bix125.

(13) Holechek, J. L.; Geli, H. M. E.; Sawalhah, M. N.; Valdez, R. A Global Assessment: Can Renewable Energy Replace Fossil Fuels by 2050? *Sustainability* **2022**, *14* (8), 4792. https://doi.org/10.3390/su14084792.

(14) Mercer, J. H. West Antarctic Ice Sheet and CO2 Greenhouse Effect: A Threat of Disaster. *Nature* **1978**, *271* (5643), 321–325. https://doi.org/10.1038/271321a0.

(15) Cassia, R.; Nocioni, M.; Correa-Aragunde, N.; Lamattina, L. Climate Change and the Impact of Greenhouse Gasses: CO2 and NO, Friends and Foes of Plant Oxidative Stress. *Front. Plant Sci.* **2018**, *9*, 273. https://doi.org/10.3389/fpls.2018.00273.
(16) Romm, J. J. *Climate Change: What Everyone Needs to Know*, Third edition.; What everyone needs to know; Oxford University Press: New York, 2022.
(17) Steffen, W.; Rockström, J.; Richardson, K.; Lenton, T. M.; Folke, C.; Liverman, D.; Summerhayes, C. P.; Barnosky, A. D.; Cornell, S. E.; Crucifix, M.; Donges, J. F.; Fetzer, I.; Lade, S. J.; Scheffer, M.; Winkelmann, R.; Schellnhuber, H. J. Trajectories of the Earth System in the Anthropocene. *Proc. Natl. Acad. Sci. U.S.A.* **2018**, *115* (33), 8252–8259. https://doi.org/10.1073/pnas.1810141115.
(18) Gonzalez, P. Energy Use, Human. In *Encyclopedia of Biodiversity*; Elsevier, 2013; pp 250–266. https://doi.org/10.1016/B978-0-12-384719-5.00242-2.
(19) West, T. O.; Marland, G. A Synthesis of Carbon Sequestration, Carbon Emissions, and Net Carbon Flux in Agriculture: Comparing Tillage Practices in the United States. *Agric. Ecosyst. Environ.* **2002**, *91* (1–3), 217–232. https://doi.org/10.1016/S0167-8809(01)00233-X.
(20) Howarth, R. W. A Bridge to Nowhere: Methane Emissions and the Greenhouse Gas Footprint of Natural Gas. *Energy Sci. Eng.* **2014**, *2* (2), 47–60. https://doi.org/10.1002/ese3.35.
(21) Yoon, S.; Song, B.; Phillips, R. L.; Chang, J.; Song, M. J. Ecological and Physiological Implications of Nitrogen Oxide Reduction Pathways on Greenhouse Gas Emissions in Agroecosystems. *FEMS Microbiol. Ecol.* **2019**, *95* (6), fiz066. https://doi.org/10.1093/femsec/fiz066.
(22) Wang, J.; Azam, W. Natural Resource Scarcity, Fossil Fuel Energy Consumption, and Total Greenhouse Gas Emissions in Top Emitting Countries. *Geosci. Front.* **2024**, *15* (2), 101757. https://doi.org/10.1016/j.gsf.2023.101757.
(23) Qu, X.; Li, X.; Bardgett, R. D.; Kuzyakov, Y.; Revillini, D.; Sonne, C.; Xia, C.; Ruan, H.; Liu, Y.; Cao, F.; Reich, P. B.; Delgado-Baquerizo, M. Deforestation Impacts Soil Biodiversity and Ecosystem Services Worldwide. *Proc. Natl. Acad. Sci. U.S.A.* **2024**, *121* (13), e2318475121. https://doi.org/10.1073/pnas.2318475121.
(24) Shivanna, K. R. Climate Change and Its Impact on Biodiversity and Human Welfare. *Proc.Indian Natl. Sci. Acad.* **2022**, *88* (2), 160–171. https://doi.org/10.1007/s43538-022-00073-6.
(25) Pistone, K.; Eisenman, I.; Ramanathan, V. Observational Determination of Albedo Decrease Caused by Vanishing Arctic Sea Ice. *Proc. Natl. Acad. Sci. U.S.A.* **2014**, *111* (9), 3322–3326. https://doi.org/10.1073/pnas.1318201111.
(26) Ruggerio, C. A. Sustainability and Sustainable Development: A Review of Principles and Definitions. *Sci. Total Environ.* **2021**, *786*, 147481. https://doi.org/10.1016/j.scitotenv.2021.147481.
(27) *Sustainability and the U.S. EPA*; National Academies Press: Washington, D.C., 2011; p 13152. https://doi.org/10.17226/13152.
(28) Spangenberg, J. H. Environmental Space and the Prism of Sustainability: Frameworks for Indicators Measuring Sustainable Development. *Ecol. Indic.* **2002**, *2* (3), 295–309. https://doi.org/10.1016/S1470-160X(02)00065-1.
(29) Valentin, A.; Spangenberg, J. H. A Guide to Community Sustainability Indicators. *Environ. Impact Assess. Rev.* **2000**, *20* (3), 381–392. https://doi.org/10.1016/S0195-9255(00)00049-4.
(30) Morton, S.; Pencheon, D.; Squires, N. Sustainable Development Goals (SDGs), and Their Implementation. *Br. Med. Bull.* **2017**, *124* (1), 1–10. https://doi.org/10.1093/bmb/ldx031.

(31) *Perspektiven nachwachsender Rohstoffe in der Chemie*; Eierdanz, H., Wiley InterScience (Online service), Eds.; VCH: Weinheim New York, 1996. https://doi.org/10.1002/9783527624720.
(32) Gardner, K. H.; Blackwell, J. The Structure of Native Cellulose. *Biopolymers* **1974**, *13* (10), 1975–2001. https://doi.org/10.1002/bip.1974.360131005.
(33) Tashiro, K.; Kobayashi, M. Theoretical Evaluation of Three-Dimensional Elastic Constants of Native and Regenerated Celluloses: Role of Hydrogen Bonds. *Polymer* **1991**, *32* (8), 1516–1526. https://doi.org/10.1016/0032-3861(91)90435-L.
(34) Rao, J.; Lv, Z.; Chen, G.; Peng, F. Hemicellulose: Structure, Chemical Modification, and Application. *Prog. Polym. Sci.* **2023**, *140*, 101675. https://doi.org/10.1016/j.progpolymsci.2023.101675.
(35) Spiridon, I.; Popa, V. I. Hemicelluloses: Major Sources, Properties and Applications. In *Monomers, Polymers and Composites from Renewable Resources*; Elsevier, 2008; pp 289–304. https://doi.org/10.1016/B978-0-08-045316-3.00013-2.
(36) Ma, M.; Ji, X. Extraction, Purification, and Applications of Hemicellulose. *Paper and Biomaterials* **2021**, *6* (3), 47–60. https://doi.org/10.1213/j.issn.2096-2355.2021.03.006.
(37) Hu, L.; Fang, X.; Du, M.; Luo, F.; Guo, S. Hemicellulose-Based Polymers Processing and Application. *AJPS* **2020**, *11* (12), 2066–2079. https://doi.org/10.4236/ajps.2020.1112146.
(38) Huang, L.-Z.; Ma, M.-G.; Ji, X.-X.; Choi, S.-E.; Si, C. Recent Developments and Applications of Hemicellulose From Wheat Straw: A Review. *Front. Bioeng. Biotechnol.* **2021**, *9*, 690773. https://doi.org/10.3389/fbioe.2021.690773.
(39) Sabiha-Hanim, S.; Siti-Norsafurah, A. M. Physical Properties of Hemicellulose Films from Sugarcane Bagasse. *Procedia Eng.* **2012**, *42*, 1390–1395. https://doi.org/10.1016/j.proeng.2012.07.532.
(40) Zhao, Y.; Sun, H.; Yang, B.; Weng, Y. Hemicellulose-Based Film: Potential Green Films for Food Packaging. *Polymers* **2020**, *12* (8), 1775. https://doi.org/10.3390/polym12081775.
(41) Hansen, N. M. L.; Plackett, D. Sustainable Films and Coatings from Hemicelluloses: A Review. *Biomacromolecules* **2008**, *9* (6), 1493–1505. https://doi.org/10.1021/bm800053z.
(42) Sun, X.-F.; Wang, H.; Jing, Z.; Mohanathas, R. Hemicellulose-Based pH-Sensitive and Biodegradable Hydrogel for Controlled Drug Delivery. *Carbohydr. Polym.* **2013**, *92* (2), 1357–1366. https://doi.org/10.1016/j.carbpol.2012.10.032.
(43) Zhao, W.; Odelius, K.; Edlund, U.; Zhao, C.; Albertsson, A.-C. In Situ Synthesis of Magnetic Field-Responsive Hemicellulose Hydrogels for Drug Delivery. *Biomacromolecules* **2015**, *16* (8), 2522–2528. https://doi.org/10.1021/acs.biomac.5b00801.
(44) Xu, W.; Wang, X.; Sandler, N.; Willför, S.; Xu, C. Three-Dimensional Printing of Wood-Derived Biopolymers: A Review Focused on Biomedical Applications. *ACS Sustainable Chem. Eng.* **2018**, *6* (5), 5663–5680. https://doi.org/10.1021/acssuschemeng.7b03924.
(45) Liu, H.; Chen, T.; Dong, C.; Pan, X. Biomedical Applications of Hemicellulose-Based Hydrogels. *Curr. Med. Chem.* **2020**, *27* (28), 4647–4659. https://doi.org/10.2174/0929867327666200408115817.
(46) Liu, J.; Chinga-Carrasco, G.; Cheng, F.; Xu, W.; Willför, S.; Syverud, K.; Xu, C. Hemicellulose-Reinforced Nanocellulose Hydrogels for Wound Healing Application. *Cellulose* **2016**, *23* (5), 3129–3143. https://doi.org/10.1007/s10570-016-1038-3.
(47) Yossa, R.; Levesque, S.; Groman, D. B.; Lora, J. H. Preliminary Evaluation of Purified Lignin and Hemicellulose as Prebiotics Candidates for Atlantic Salmon, *Salmo Salar* L.

J. Appl. Aquacult. **2018**, *30* (3), 256–271. https://doi.org/10.1080/10454438.2018.1439795.

(48) Jana, U. K.; Kango, N.; Pletschke, B. Hemicellulose-Derived Oligosaccharides: Emerging Prebiotics in Disease Alleviation. *Front. Nutr.* **2021**, *8*, 670817. https://doi.org/10.3389/fnut.2021.670817.

(49) Deloule, V.; Boisset, C.; Hannani, D.; Suau, A.; Le Gouellec, A.; Chroboczek, J.; Botté, C.; Yamaryo-Botté, Y.; Chirat, C.; Toussaint, B. Prebiotic Role of Softwood Hemicellulose in Healthy Mice Model. *J. Funct. Foods* **2020**, *64*, 103688. https://doi.org/10.1016/j.jff.2019.103688.

(50) Sun, Y.; Cheng, J. Hydrolysis of Lignocellulosic Materials for Ethanol Production: A Review. *Bioresour. Technol.* **2002**, *83* (1), 1–11. https://doi.org/10.1016/S0960-8524(01)00212-7.

(51) Méndez, J.; Passos, D. D. F.; Wischral, D.; Modesto, L. F.; Pereira, N. Second-Generation Ethanol Production by Separate Hydrolysis and Fermentation from Sugarcane Bagasse with Cellulose Hydrolysis Using a Customized Enzyme Cocktail. *Biofuels* **2021**, *12* (10), 1225–1231. https://doi.org/10.1080/17597269.2019.1608034.

(52) Ralph, J.; Lapierre, C.; Boerjan, W. Lignin Structure and Its Engineering. *Curr. Opin. Biotechnol.* **2019**, *56*, 240–249. https://doi.org/10.1016/j.copbio.2019.02.019.

(53) Ponnusamy, V. K.; Nguyen, D. D.; Dharmaraja, J.; Shobana, S.; Banu, J. R.; Saratale, R. G.; Chang, S. W.; Kumar, G. A Review on Lignin Structure, Pretreatments, Fermentation Reactions and Biorefinery Potential. *Bioresour. Technol.* **2019**, *271*, 462–472. https://doi.org/10.1016/j.biortech.2018.09.070.

(54) Higuchi, T. Lignin Biochemistry: Biosynthesis and Biodegradation. *Wood Sci. Technol.* **1990**, *24* (1), 23–63. https://doi.org/10.1007/BF00225306.

(55) Spiridon, I. BIOLOGICAL AND PHARMACEUTICAL APPLICATIONS OF LIGNIN AND ITS DERIVATIVES: A MINI-REVIEW. *Cellulose Chem. Technol.* **2018**, *52* (7–8), 543–550.

(56) Djakovitch, L.; Essayem, N.; Eternot, M.; Rataboul, F. A Landscape of Lignocellulosic Biopolymer Transformations into Valuable Molecules by Heterogeneous Catalysis in C'Durable Team at IRCELYON. *Molecules* **2021**, *26* (22), 6796. https://doi.org/10.3390/molecules26226796.

(57) Tribot, A.; Amer, G.; Abdou Alio, M.; De Baynast, H.; Delattre, C.; Pons, A.; Mathias, J.-D.; Callois, J.-M.; Vial, C.; Michaud, P.; Dussap, C.-G. Wood-Lignin: Supply, Extraction Processes and Use as Bio-Based Material. *Eur. Polym. J.* **2019**, *112*, 228–240. https://doi.org/10.1016/j.eurpolymj.2019.01.007.

(58) Xu, J.; Kong, Y.; Du, B.; Wang, X.; Zhou, J. Exploration of Mechanisms of Lignin Extraction by Different Methods. *Environ. Prog. Sustainable Energy* **2021**, e13785. https://doi.org/10.1002/ep.13785.

(59) Tobimatsu, Y.; Schuetz, M. Lignin Polymerization: How Do Plants Manage the Chemistry so Well? *Curr. Opin. Biotechnol.* **2019**, *56*, 75–81. https://doi.org/10.1016/j.copbio.2018.10.001.

(60) Berlin, A.; Balakshin, M. Industrial Lignins. In *Bioenergy Research: Advances and Applications*; Elsevier, 2014; pp 315–336. https://doi.org/10.1016/B978-0-444-59561-4.00018-8.

(61) Luo, H.; Abu-Omar, M. M. Chemicals From Lignin. In *Encyclopedia of Sustainable Technologies*; Elsevier, 2017; pp 573–585. https://doi.org/10.1016/B978-0-12-409548-9.10235-0.

(62) Bajwa, D. S.; Pourhashem, G.; Ullah, A. H.; Bajwa, S. G. A Concise Review of Current Lignin Production, Applications, Products and Their Environmental Impact. *Ind. Crops Prod.* **2019**, *139*, 111526. https://doi.org/10.1016/j.indcrop.2019.111526.

(63) Mandlekar, N.; Cayla, A.; Rault, F.; Giraud, S.; Salaün, F.; Malucelli, G.; Guan, J.-P. An Overview on the Use of Lignin and Its Derivatives in Fire Retardant Polymer Systems. In *Lignin - Trends and Applications*; Poletto, M., Ed.; InTech, 2018. https://doi.org/10.5772/intechopen.72963.
(64) Cotana, F.; Cavalaglio, G.; Nicolini, A.; Gelosia, M.; Coccia, V.; Petrozzi, A.; Brinchi, L. Lignin as Co-Product of Second Generation Bioethanol Production from Ligno-Cellulosic Biomass. *Energy Procedia* **2014**, *45*, 52–60. https://doi.org/10.1016/j.egypro.2014.01.007.
(65) Khitrin, K. S.; Fuks, S. L.; Khitrin, S. V.; Kazienkov, S. A.; Meteleva, D. S. Lignin Utilization Options and Methods. *Russ. J. Gen. Chem.* **2012**, *82* (5), 977–984. https://doi.org/10.1134/S1070363212050313.
(66) Scown, C. D.; Gokhale, A. A.; Willems, P. A.; Horvath, A.; McKone, T. E. Role of Lignin in Reducing Life-Cycle Carbon Emissions, Water Use, and Cost for United States Cellulosic Biofuels. *Environ. Sci. Technol.* **2014**, *48* (15), 8446–8455. https://doi.org/10.1021/es5012753.
(67) Demirbas, A. Progress and Recent Trends in Biofuels. *Prog. Energy Combust. Sci.* **2007**, *33* (1), 1–18. https://doi.org/10.1016/j.pecs.2006.06.001.
(68) Calvo-Flores, F. G.; Dobado, J. A. Lignin as Renewable Raw Material. *ChemSusChem* **2010**, *3* (11), 1227–1235. https://doi.org/10.1002/cssc.201000157.
(69) Aso, T.; Koda, K.; Kubo, S.; Yamada, T.; Nakajima, I.; Uraki, Y. Preparation of Novel Lignin-Based Cement Dispersants from Isolated Lignins. *J. Wood Chem. Technol.* **2013**, *33* (4), 286–298. https://doi.org/10.1080/02773813.2013.794841.
(70) Ouyang, X.; Ke, L.; Qiu, X.; Guo, Y.; Pang, Y. Sulfonation of Alkali Lignin and Its Potential Use in Dispersant for Cement. *J. Dispersion Sci. Technol.* **2009**, *30* (1), 1–6. https://doi.org/10.1080/01932690802473560.
(71) Thanh Binh, N. T.; Luong, N. D.; Kim, D. O.; Lee, S. H.; Kim, B. J.; Lee, Y. S.; Nam, J.-D. Synthesis of Lignin-Based Thermoplastic Copolyester Using Kraft Lignin as a Macromonomer. *Compos. Interfaces* **2009**, *16* (7–9), 923–935. https://doi.org/10.1163/092764409X12477479344485.
(72) *Epoxy Resins: Chemistry and Technology*, 2nd ed.; May, C. A., Ed.; Routledge, 2018. https://doi.org/10.1201/9780203756713.
(73) Zhao, B.; Chen, G.; Liu, Y.; Hu, K.; Wu, R. Synthesis of Lignin Base Epoxy Resin and Its Characterization. *J. Mater. Sci. Lett.* **2001**, *20* (9), 859–862. https://doi.org/10.1023/A:1010975132530.
(74) Liu, Y.; Li, K. Preparation and Characterization of Demethylated Lignin-Polyethylenimine Adhesives. *The Journal of Adhesion* **2006**, *82* (6), 593–605. https://doi.org/10.1080/00218460600766632.
(75) *Wood Adhesives: Chemistry and Technology*, 1st ed.; Pizzi, A., Ed.; CRC Press, 2018. https://doi.org/10.1201/9780203733721.
(76) Zhou, N.; Thilakarathna, W. P. D. W.; He, Q. S.; Rupasinghe, H. P. V. A Review: Depolymerization of Lignin to Generate High-Value Bio-Products: Opportunities, Challenges, and Prospects. *Front. Energy Res.* **2022**, *9*, 758744. https://doi.org/10.3389/fenrg.2021.758744.
(77) Zhang, C.; Wang, F. Catalytic Lignin Depolymerization to Aromatic Chemicals. *Acc. Chem. Res.* **2020**, *53* (2), 470–484. https://doi.org/10.1021/acs.accounts.9b00573.
(78) Chio, C.; Sain, M.; Qin, W. Lignin Utilization: A Review of Lignin Depolymerization from Various Aspects. *Renewable Sustainable Energy Rev.* **2019**, *107*, 232–249. https://doi.org/10.1016/j.rser.2019.03.008.
(79) Ji, D.; Wang, Y.; Peng, J.; Yuan, D.; Li, Z.; Ji, D.; Wu, H. Recent Advances in Depolymerization and High-Value Utilization of Lignin: A Review. *Ind. Eng. Chem. Res.* **2024**, *63* (46), 19916–19935. https://doi.org/10.1021/acs.iecr.4c02617.

(80) Lopez Camas, K.; Ullah, A. Depolymerization of Lignin into High-Value Products. *Biocatal. Agric. Biotechnol.* **2022**, *40*, 102306. https://doi.org/10.1016/j.bcab.2022.102306.
(81) Tian, Q.; Xu, P.; Huang, D.; Wang, H.; Wang, Z.; Qin, H.; He, Y.; Li, R.; Yin, L.; Chen, S.; Zhao, Y. The Driving Force of Biomass Value-Addition: Selective Catalytic Depolymerization of Lignin to High-Value Chemicals. *J. Environ. Chem. Eng.* **2023**, *11* (3), 109719. https://doi.org/10.1016/j.jece.2023.109719.
(82) Agarwal, A.; Rana, M.; Park, J.-H. Advancement in Technologies for the Depolymerization of Lignin. *Fuel Process. Technol.* **2018**, *181*, 115–132. https://doi.org/10.1016/j.fuproc.2018.09.017.
(83) Zeng, J.; Yoo, C. G.; Wang, F.; Pan, X.; Vermerris, W.; Tong, Z. Biomimetic Fenton-Catalyzed Lignin Depolymerization to High-Value Aromatics and Dicarboxylic Acids. *ChemSusChem* **2015**, *8* (5), 861–871. https://doi.org/10.1002/cssc.201403128.
(84) Pandey, M. P.; Kim, C. S. Lignin Depolymerization and Conversion: A Review of Thermochemical Methods. *Chem. Eng. Technol.* **2011**, *34* (1), 29–41. https://doi.org/10.1002/ceat.201000270.
(85) Ren, T.; Qi, W.; Su, R.; He, Z. Promising Techniques for Depolymerization of Lignin into Value-added Chemicals. *ChemCatChem* **2019**, *11* (2), 639–654. https://doi.org/10.1002/cctc.201801428.
(86) Ummalyma, S. B.; Supriya, R. D.; Sindhu, R.; Binod, P.; Nair, R. B.; Pandey, A.; Gnansounou, E. Biological Pretreatment of Lignocellulosic Biomass—Current Trends and Future Perspectives. In *Second and Third Generation of Feedstocks*; Elsevier, 2019; pp 197–212. https://doi.org/10.1016/B978-0-12-815162-4.00007-0.
(87) Wan, C.; Li, Y. Fungal Pretreatment of Lignocellulosic Biomass. *Biotechnol. Adv.* **2012**, *30* (6), 1447–1457. https://doi.org/10.1016/j.biotechadv.2012.03.003.
(88) Martínez, Á. T.; Speranza, M.; Ruiz-Dueñas, F. J.; Ferreira, P.; Camarero, S.; Guillén, F.; Martínez, M. J.; Gutiérrez, A.; Río, J. C. del. Biodegradation of Lignocellulosics: Microbial, Chemical, and Enzymatic Aspects of the Fungal Attack of Lignin. *Int. Microbiol.* **2005**, *8*, 195–204.
(89) Chen, S.; Zhang, X.; Singh, D.; Yu, H.; Yang, X. Biological Pretreatment of Lignocellulosics: Potential, Progress and Challenges. *Biofuels* **2010**, *1* (1), 177–199. https://doi.org/10.4155/bfs.09.13.
(90) Chae, T. U.; Ahn, J. H.; Ko, Y.-S.; Kim, J. W.; Lee, J. A.; Lee, E. H.; Lee, S. Y. Metabolic Engineering for the Production of Dicarboxylic Acids and Diamines. *Metab. Eng.* **2020**, *58*, 2–16. https://doi.org/10.1016/j.ymben.2019.03.005.
(91) Gupta, V. K.; Kubicek, C. P.; Berrin, J.-G.; Wilson, D. W.; Couturier, M.; Berlin, A.; Filho, E. X. F.; Ezeji, T. Fungal Enzymes for Bio-Products from Sustainable and Waste Biomass. *Trends Biochem. Sci* **2016**, *41* (7), 633–645. https://doi.org/10.1016/j.tibs.2016.04.006.
(92) Luo, X.; Wu, H.; Li, C.; Li, Z.; Li, H.; Zhang, H.; Li, Y.; Su, Y.; Yang, S. Heteropoly Acid-Based Catalysts for Hydrolytic Depolymerization of Cellulosic Biomass. *Front. Chem.* **2020**, *8*, 580146. https://doi.org/10.3389/fchem.2020.580146.
(93) Questell-Santiago, Y. M.; Galkin, M. V.; Barta, K.; Luterbacher, J. S. Stabilization Strategies in Biomass Depolymerization Using Chemical Functionalization. *Nat. Rev. Chem.* **2020**, *4* (6), 311–330. https://doi.org/10.1038/s41570-020-0187-y.
(94) Zhu, Z.; Toor, S. S.; Rosendahl, L.; Yu, D.; Chen, G. Influence of Alkali Catalyst on Product Yield and Properties via Hydrothermal Liquefaction of Barley Straw. *Energy* **2015**, *80*, 284–292. https://doi.org/10.1016/j.energy.2014.11.071.
(95) Faith, W. L. Development of the Scholler Process in the United States. *Ind. Eng. Chem.* **1945**, *37* (1), 9–11. https://doi.org/10.1021/ie50421a004.

(96) Gao, C.; Li, M.; Zhu, C.; Hu, Y.; Shen, T.; Li, M.; Ji, X.; Lyu, G.; Zhuang, W. One-Pot Depolymerization, Demethylation and Phenolation of Lignin Catalyzed by HBr under Microwave Irradiation for Phenolic Foam Preparation. *Composites, Part B* **2021**, *205*, 108530. https://doi.org/10.1016/j.compositesb.2020.108530.
(97) Zhou, S.; Zhang, M.; Zhu, L.; Zhao, X.; Chen, J.; Chen, W.; Chang, C. Hydrolysis of Lignocellulose to Succinic Acid: A Review of Treatment Methods and Succinic Acid Applications. *Biotechnol. Biofuels Bioprod.* **2023**, *16* (1), 1. https://doi.org/10.1186/s13068-022-02244-5.
(98) Wan, Z.; Zhang, H.; Guo, Y.; Li, H. Advances in Catalytic Depolymerization of Lignin. *ChemistrySelect* **2022**, *7* (40), e202202582. https://doi.org/10.1002/slct.202202582.
(99) Du, B.; Liu, C.; Wang, X.; Han, Y.; Guo, Y.; Li, H.; Zhou, J. Renewable Lignin-Based Carbon Nanofiber as Ni Catalyst Support for Depolymerization of Lignin to Phenols in Supercritical Ethanol/Water. *Renewable Energy* **2020**, *147*, 1331–1339. https://doi.org/10.1016/j.renene.2019.09.108.
(100) Liu, X.; Bouxin, F. P.; Fan, J.; Budarin, V. L.; Hu, C.; Clark, J. H. Recent Advances in the Catalytic Depolymerization of Lignin towards Phenolic Chemicals: A Review. *ChemSusChem* **2020**, *13* (17), 4296–4317. https://doi.org/10.1002/cssc.202001213.
(101) Chen, M.; Shi, J.; Wang, Y.; Tang, Z.; Yang, Z.; Wang, J.; Zhang, H. Conversion of Kraft Lignin to Phenol Monomers and Liquid Fuel over Trimetallic Catalyst W-Ni-Mo/Sepiolite under Supercritical Ethanol. *Fuel* **2021**, *303*, 121332. https://doi.org/10.1016/j.fuel.2021.121332.
(102) Yuan, Z.; Dai, W.; Zhang, S.; Wang, F.; Jian, J.; Zeng, J.; Zhou, H. Heterogeneous Strategies for Selective Conversion of Lignocellulosic Polysaccharides. *Cellulose* **2022**, *29* (6), 3059–3077. https://doi.org/10.1007/s10570-022-04434-8.
(103) Di Marino, D.; Jestel, T.; Marks, C.; Viell, J.; Blindert, M.; Kriescher, S. M. A.; Spiess, A. C.; Wessling, M. Carboxylic Acids Production via Electrochemical Depolymerization of Lignin. *ChemElectroChem* **2019**, *6* (5), 1434–1442. https://doi.org/10.1002/celc.201801676.
(104) Da Cruz, M. G. A.; Gueret, R.; Chen, J.; Piątek, J.; Beele, B.; Sipponen, M. H.; Frauscher, M.; Budnyk, S.; Rodrigues, B. V. M.; Slabon, A. Electrochemical Depolymerization of Lignin in a Biomass-based Solvent. *ChemSusChem* **2022**, *15* (15), e202201246. https://doi.org/10.1002/cssc.202201246.
(105) Bauch, J.; Rosenkranz, R. *Physikalische Werkstoffdiagnostik: Ein Kompendium wichtiger Analytikmethoden für Ingenieure und Physiker*; Springer Berlin Heidelberg: Berlin, Heidelberg, 2017. https://doi.org/10.1007/978-3-662-53952-1.
(106) Qi, P.; Wang, J.; Djitcheu, X.; He, D.; Liu, H.; Zhang, Q. Techniques for the Characterization of Single Atom Catalysts. *RSC Adv.* **2022**, *12* (2), 1216–1227. https://doi.org/10.1039/D1RA07799F.
(107) Li, X.; Yang, X.; Zhang, J.; Huang, Y.; Liu, B. In Situ/Operando Techniques for Characterization of Single-Atom Catalysts. *ACS Catal.* **2019**, *9* (3), 2521–2531. https://doi.org/10.1021/acscatal.8b04937.
(108) Jinschek, J. R. Advances in the Environmental Transmission Electron Microscope (ETEM) for Nanoscale in Situ Studies of Gas–Solid Interactions. *Chem. Commun.* **2014**, *50* (21), 2696–2706. https://doi.org/10.1039/C3CC49092K.
(109) Gai, P. L.; Boyes, E. D. Advances in Atomic Resolution in Situ Environmental Transmission Electron Microscopy and 1Å Aberration Corrected in Situ Electron Microscopy. *Microsc. Res. Tech.* **2009**, *72* (3), 153–164. https://doi.org/10.1002/jemt.20668.
(110) Gai, P. L.; Lari, L.; Ward, M. R.; Boyes, E. D. Visualisation of Single Atom Dynamics and Their Role in Nanocatalysts under Controlled Reaction Environments. *Chem. Phys. Lett.* **2014**, *592*, 355–359. https://doi.org/10.1016/j.cplett.2013.12.038.

(111) Liu, L.; Zakharov, D. N.; Arenal, R.; Concepcion, P.; Stach, E. A.; Corma, A. Evolution and Stabilization of Subnanometric Metal Species in Confined Space by in Situ TEM. *Nat. Commun.* **2018**, *9* (1), 574. https://doi.org/10.1038/s41467-018-03012-6.
(112) Koshy, D. M.; Landers, A. T.; Cullen, D. A.; Ievlev, A. V.; Meyer, H. M.; Hahn, C.; Bao, Z.; Jaramillo, T. F. Direct Characterization of Atomically Dispersed Catalysts: Nitrogen-Coordinated Ni Sites in Carbon-Based Materials for CO_2 Electroreduction. *Adv. Energy Mater.* **2020**, *10* (39), 2001836. https://doi.org/10.1002/aenm.202001836.
(113) Piao, Y.; Jiang, Q.; Li, H.; Matsumoto, H.; Liang, J.; Liu, W.; Pham-Huu, C.; Liu, Y.; Wang, F. Identify Zr Promotion Effects in Atomic Scale for Co-Based Catalysts in Fischer–Tropsch Synthesis. *ACS Catal.* **2020**, *10* (14), 7894–7906. https://doi.org/10.1021/acscatal.0c01874.
(114) Chen, Z.; Zhang, Q.; Chen, W.; Dong, J.; Yao, H.; Zhang, X.; Tong, X.; Wang, D.; Peng, Q.; Chen, C.; He, W.; Li, Y. Single-Site Au^I Catalyst for Silane Oxidation with Water. *Adv. Mater.* **2018**, *30* (5), 1704720. https://doi.org/10.1002/adma.201704720.
(115) Simonovis, J. P.; Hunt, A.; Palomino, R. M.; Senanayake, S. D.; Waluyo, I. Enhanced Stability of Pt-Cu Single-Atom Alloy Catalysts: In Situ Characterization of the Pt/Cu(111) Surface in an Ambient Pressure of CO. *J. Phys. Chem. C* **2018**, *122* (8), 4488–4495. https://doi.org/10.1021/acs.jpcc.8b00078.
(116) Cao, L.; Luo, Q.; Liu, W.; Lin, Y.; Liu, X.; Cao, Y.; Zhang, W.; Wu, Y.; Yang, J.; Yao, T.; Wei, S. Identification of Single-Atom Active Sites in Carbon-Based Cobalt Catalysts during Electrocatalytic Hydrogen Evolution. *Nat. Catal.* **2018**, *2* (2), 134–141. https://doi.org/10.1038/s41929-018-0203-5.
(117) Bafaqeer, A.; Tahir, M.; Amin, N. A. S. Synthesis of Hierarchical ZnV_2O_6 Nanosheets with Enhanced Activity and Stability for Visible Light Driven CO_2 Reduction to Solar Fuels. *Appl. Surf. Sci.* **2018**, *435*, 953–962. https://doi.org/10.1016/j.apsusc.2017.11.116.
(118) Abbas, I.; Kim, H.; Shin, C.-H.; Yoon, S.; Jung, K.-D. Differences in Bifunctionality of ZnO and ZrO_2 in $Cu/ZnO/ZrO_2/Al_2O_3$ Catalysts in Hydrogenation of Carbon Oxides for Methanol Synthesis. *Appl. Catal., B* **2019**, *258*, 117971. https://doi.org/10.1016/j.apcatb.2019.117971.
(119) Feng, X.; Song, Z.; Liu, Y.; Chen, X.; Jin, X.; Yan, W.; Yang, C.; Luo, J.; Zhou, X.; Chen, D. Manipulating Gold Spatial Location on Titanium Silicalite-1 To Enhance the Catalytic Performance for Direct Propene Epoxidation with H_2 and O_2. *ACS Catal.* **2018**, *8* (11), 10649–10657. https://doi.org/10.1021/acscatal.8b02836.
(120) Chen, Y.; Zou, L.; Liu, H.; Chen, C.; Wang, Q.; Gu, M.; Yang, B.; Zou, Z.; Fang, J.; Yang, H. Fe and N Co-Doped Porous Carbon Nanospheres with High Density of Active Sites for Efficient CO_2 Electroreduction. *J. Phys. Chem. C* **2019**, *123* (27), 16651–16659. https://doi.org/10.1021/acs.jpcc.9b02195.
(121) Jung, J. Y.; Hong, Y. L.; Kim, J.-G.; Kim, M. J.; Kim, Y.-K.; Kim, N. D. New Insight of Tailor-Made Graphene Oxide for the Formation of Atomic Co-N Sites toward Hydrogen Evolution Reaction. *Appl. Surf. Sci.* **2021**, *563*, 150254. https://doi.org/10.1016/j.apsusc.2021.150254.
(122) Qiao, Y.; Yang, H.; Chang, Z.; Deng, H.; Li, X.; Zhou, H. A High-Energy-Density and Long-Life Initial-Anode-Free Lithium Battery Enabled by a Li_2O Sacrificial Agent. *Nat. Energy* **2021**, *6* (6), 653–662. https://doi.org/10.1038/s41560-021-00839-0.
(123) Schilling, A. C.; Groden, K.; Simonovis, J. P.; Hunt, A.; Hannagan, R. T.; Çınar, V.; McEwen, J.-S.; Sykes, E. C. H.; Waluyo, I. Accelerated Cu_2 O Reduction by Single Pt Atoms at the Metal-Oxide Interface. *ACS Catal.* **2020**, *10* (7), 4215–4226. https://doi.org/10.1021/acscatal.9b05270.
(124) Bruix, A.; Füchtbauer, H. G.; Tuxen, A. K.; Walton, A. S.; Andersen, M.; Porsgaard, S.; Besenbacher, F.; Hammer, B.; Lauritsen, J. V. *In Situ* Detection of Active Edge Sites in

Single-Layer MoS_2 Catalysts. *ACS Nano* **2015**, *9* (9), 9322–9330. https://doi.org/10.1021/acsnano.5b03199.
(125) Lin, J.; Wang, A.; Qiao, B.; Liu, X.; Yang, X.; Wang, X.; Liang, J.; Li, J.; Liu, J.; Zhang, T. Remarkable Performance of Ir_1/FeO_x Single-Atom Catalyst in Water Gas Shift Reaction. *J. Am. Chem. Soc.* **2013**, *135* (41), 15314–15317. https://doi.org/10.1021/ja408574m.
(126) De Boer, J.; Harvey, J. Range-Expansion in Processionary Moths and Biological Control. *Insects* **2020**, *11* (5), 267. https://doi.org/10.3390/insects11050267.
(127) Lea, C. Derbyshire's Oil and Refining History: The James 'Paraffin' Young Connection. *Geol. Soc.* **2018**, *465* (1), 71–76. https://doi.org/10.1144/SP465.4.
(128) Rishikesh, M. S.; Harish, S.; Mahendran Prasanth, S.; Gnana Prakash, D. A Comprehensive Review on Lignin Obtained from Agro-Residues: Potential Source of Useful Chemicals. *Biomass Conv. Bioref.* **2023**, *13* (7), 5533–5556. https://doi.org/10.1007/s13399-021-01637-0.
(129) Poveda-Giraldo, J. A.; Solarte-Toro, J. C.; Cardona Alzate, C. A. The Potential Use of Lignin as a Platform Product in Biorefineries: A Review. *Renewable Sustainable Energy Rev.* **2021**, *138*, 110688. https://doi.org/10.1016/j.rser.2020.110688.
(130) Zevallos Torres, L. A.; Lorenci Woiciechowski, A.; De Andrade Tanobe, V. O.; Karp, S. G.; Guimarães Lorenci, L. C.; Faulds, C.; Soccol, C. R. Lignin as a Potential Source of High-Added Value Compounds: A Review. *J. Cleaner Prod.* **2020**, *263*, 121499. https://doi.org/10.1016/j.jclepro.2020.121499.
(131) Vanholme, R.; Demedts, B.; Morreel, K.; Ralph, J.; Boerjan, W. Lignin Biosynthesis and Structure. *Plant Physiol.* **2010**, *153* (3), 895–905. https://doi.org/10.1104/pp.110.155119.
(132) Boerjan, W.; Ralph, J.; Baucher, M. Lignin Biosynthesis. *Annu. Rev. Plant Biol.* **2003**, *54* (1), 519–546. https://doi.org/10.1146/annurev.arplant.54.031902.134938.
(133) Ročnik, T.; Likozar, B.; Jasiukaitytė-Grojzdek, E.; Grilc, M. Catalytic Lignin Valorisation by Depolymerisation, Hydrogenation, Demethylation and Hydrodeoxygenation: Mechanism, Chemical Reaction Kinetics and Transport Phenomena. *Chem. Eng. J.* **2022**, *448*, 137309. https://doi.org/10.1016/j.cej.2022.137309.
(134) Zakzeski, J.; Bruijnincx, P. C. A.; Jongerius, A. L.; Weckhuysen, B. M. The Catalytic Valorization of Lignin for the Production of Renewable Chemicals. *Chem. Rev.* **2010**, *110* (6), 3552–3599. https://doi.org/10.1021/cr900354u.
(135) Galkin, M. V.; Samec, J. S. M. Lignin Valorization through Catalytic Lignocellulose Fractionation: A Fundamental Platform for the Future Biorefinery. *ChemSusChem* **2016**, *9* (13), 1544–1558. https://doi.org/10.1002/cssc.201600237.
(136) Wijaya, Y. P.; Smith, K. J.; Kim, C. S.; Gyenge, E. L. Electrocatalytic Hydrogenation and Depolymerization Pathways for Lignin Valorization: Toward Mild Synthesis of Chemicals and Fuels from Biomass. *Green Chem.* **2020**, *22* (21), 7233–7264. https://doi.org/10.1039/D0GC02782K.
(137) Gao, D.; Ouyang, D.; Zhao, X. Electro-Oxidative Depolymerization of Lignin for Production of Value-Added Chemicals. *Green Chem.* **2022**, *24* (22), 8585–8605. https://doi.org/10.1039/D2GC02660K.
(138) Lindenbeck, L. M.; Barra, V. C.; Dahlhaus, S.; Brand, S.; Wende, L.; Beele, B. B.; Schebb, Nils. H.; Rodrigues, B. V. M.; Slabon, A. Organic Chemicals from Wood: Selective Depolymerization and Dearomatization of Lignin via Aqueous Electrocatalysis. *ChemSusChem* **2024**, e202301617. https://doi.org/10.1002/cssc.202301617.
(139) Garedew, M.; Lam, C. H.; Petitjean, L.; Huang, S.; Song, B.; Lin, F.; Jackson, J. E.; Saffron, C. M.; Anastas, P. T. Electrochemical Upgrading of Depolymerized Lignin: A

Review of Model Compound Studies. *Green Chem.* **2021**, *23* (8), 2868–2899. https://doi.org/10.1039/D0GC04127K.
(140) Kumar, A.; Daw, P.; Milstein, D. Homogeneous Catalysis for Sustainable Energy: Hydrogen and Methanol Economies, Fuels from Biomass, and Related Topics. *Chem. Rev.* **2022**, *122* (1), 385–441. https://doi.org/10.1021/acs.chemrev.1c00412.
(141) Gierer, J.; Norén, I. Oxidative Pretreatment of Pine Wood to Facilitate Delignification during Kraft Pulping. *Holzforschung* **1982**, *36* (3), 123–130. https://doi.org/10.1515/hfsg.1982.36.3.123.
(142) Zhang, C.; Li, H.; Lu, J.; Zhang, X.; MacArthur, K. E.; Heggen, M.; Wang, F. Promoting Lignin Depolymerization and Restraining the Condensation via an Oxidation−Hydrogenation Strategy. *ACS Catal.* **2017**, *7* (5), 3419–3429. https://doi.org/10.1021/acscatal.7b00148.
(143) Ljunggren, S.; Olsson, A. The Specificity in Oxidation of Some Lignin and Carbohydrate Models and Pine Wood Shavings with Permanganate and Pyridinium Dichromate Before the Kraft Pulping Process. *Holzforschung* **1984**, *38* (2), 91–99. https://doi.org/10.1515/hfsg.1984.38.2.91.
(144) Rahimi, A.; Ulbrich, A.; Coon, J. J.; Stahl, S. S. Formic-Acid-Induced Depolymerization of Oxidized Lignin to Aromatics. *Nature* **2014**, *515* (7526), 249–252. https://doi.org/10.1038/nature13867.
(145) Yang, C.; Maldonado, S.; Stephenson, C. R. J. Electrocatalytic Lignin Oxidation. *ACS Catal.* **2021**, *11* (16), 10104–10114. https://doi.org/10.1021/acscatal.1c01767.
(146) Semmelhack, M. F.; Chou, C. S.; Cortes, D. A. Nitroxyl-Mediated Electrooxidation of Alcohols to Aldehydes and Ketones. *J. Am. Chem. Soc.* **1983**, *105* (13), 4492–4494. https://doi.org/10.1021/ja00351a070.
(147) Amorati, R.; Lucarini, M.; Mugnaini, V.; Pedulli, G. F.; Minisci, F.; Recupero, F.; Fontana, F.; Astolfi, P.; Greci, L. Hydroxylamines as Oxidation Catalysts: Thermochemical and Kinetic Studies. *J. Org. Chem.* **2003**, *68* (5), 1747–1754. https://doi.org/10.1021/jo026660z.
(148) Nutting, J. E.; Rafiee, M.; Stahl, S. S. Tetramethylpiperidine *N* -Oxyl (TEMPO), Phthalimide *N* -Oxyl (PINO), and Related *N* -Oxyl Species: Electrochemical Properties and Their Use in Electrocatalytic Reactions. *Chem. Rev.* **2018**, *118* (9), 4834–4885. https://doi.org/10.1021/acs.chemrev.7b00763.
(149) Sedai, B.; Díaz-Urrutia, C.; Baker, R. T.; Wu, R.; Silks, L. A. "Pete"; Hanson, S. K. Comparison of Copper and Vanadium Homogeneous Catalysts for Aerobic Oxidation of Lignin Models. *ACS Catal.* **2011**, *1* (7), 794–804. https://doi.org/10.1021/cs200149v.
(150) Osako, T.; Ohkubo, K.; Taki, M.; Tachi, Y.; Fukuzumi, S.; Itoh, S. Oxidation Mechanism of Phenols by Dicopper−Dioxygen (Cu_2/O_2) Complexes. *J. Am. Chem. Soc.* **2003**, *125* (36), 11027–11033. https://doi.org/10.1021/ja029380+.
(151) Guo, Q.-X.; Wu, Z.-J.; Luo, Z.-B.; Liu, Q.-Z.; Ye, J.-L.; Luo, S.-W.; Cun, L.-F.; Gong, L.-Z. Highly Enantioselective Oxidative Couplings of 2-Naphthols Catalyzed by Chiral Bimetallic Oxovanadium Complexes with Either Oxygen or Air as Oxidant. *J. Am. Chem. Soc.* **2007**, *129* (45), 13927–13938. https://doi.org/10.1021/ja074322f.
(152) Xin, X.; Li, Z.; Chi, M.; Zhang, M.; Dong, Y.; Lv, H.; Yang, G.-Y. A Recoverable Polyoxometalate-Ionic Liquid Catalyst for Selective Cleavage of Lignin β-O-4 Models under Mild Conditions. *Green Chem.* **2023**, *25* (7), 2815–2824. https://doi.org/10.1039/D3GC00087G.
(153) Yang, C.; Qin, J.; Sun, S.; Gao, D.; Fang, Y.; Chen, G.; Tian, C.; Bao, C.; Zhang, S. Progress in Developing Methods for Lignin Depolymerization and Elucidating the Associated Mechanisms. *Eur. Polym. J.* **2024**, *210*, 112995. https://doi.org/10.1016/j.eurpolymj.2024.112995.

(154) Pelckmans, M.; Renders, T.; Van De Vyver, S.; Sels, B. F. Bio-Based Amines through Sustainable Heterogeneous Catalysis. *Green Chem.* **2017**, *19* (22), 5303–5331. https://doi.org/10.1039/C7GC02299A.
(155) Dey, A.; Gunnoe, T. B.; Stamenkovic, V. R. Organic Electrosynthesis: When Is It Electrocatalysis? *ACS Catal.* **2020**, *10* (21), 13156–13158. https://doi.org/10.1021/acscatal.0c04559.
(156) Du, X.; Zhang, H.; Sullivan, K. P.; Gogoi, P.; Deng, Y. Electrochemical Lignin Conversion. *ChemSusChem* **2020**, *13* (17), 4318–4343. https://doi.org/10.1002/cssc.202001187.
(157) Jiang, H.; Xue, A.; Wang, Z.; Xia, R.; Wang, L.; Tang, Y.; Wan, P.; Chen, Y. Electrochemical Degradation of Lignin by ROS. *Sustainable Chem.* **2020**, *1* (3), 345–360. https://doi.org/10.3390/suschem1030023.
(158) Pardini, V. L.; Smith, C. Z.; Utley, J. H. P.; Vargas, R. R.; Viertler, H. Electroorganic Reactions. 38. Mechanism of Electrooxidative Cleavage of Lignin Model Dimers. *J. Org. Chem.* **1991**, *56* (26), 7305–7313. https://doi.org/10.1021/jo00026a022.
(159) Baciocchi, E.; Bietti, M.; Lanzalunga, O. Mechanistic Aspects of β-Bond-Cleavage Reactions of Aromatic Radical Cations. *Acc. Chem. Res.* **2000**, *33* (4), 243–251. https://doi.org/10.1021/ar980014y.
(160) Shiraishi, T.; Takano, T.; Kamitakahara, H.; Nakatsubo, F. Studies on Electrooxidation of Lignin and Lignin Model Compounds. Part 1: Direct Electrooxidation of Non-Phenolic Lignin Model Compounds. *Holzforschung* **2012**, *66* (3). https://doi.org/10.1515/hf.2011.069.
(161) Cabral Almada, C.; Kazachenko, A.; Fongarland, P.; Da Silva Perez, D.; Kuznetsov, B. N.; Djakovitch, L. Supported-Metal Catalysts in Upgrading Lignin to Aromatics by Oxidative Depolymerization. *Catalysts* **2021**, *11* (4), 467. https://doi.org/10.3390/catal11040467.
(162) Wang, Y.; Sun, S.; Li, F.; Cao, X.; Sun, R. Production of Vanillin from Lignin: The Relationship between β-O-4 Linkages and Vanillin Yield. *Ind. Crops Prod.* **2018**, *116*, 116–121. https://doi.org/10.1016/j.indcrop.2018.02.043.
(163) Sebhat, W.; El-Roz, A.; Crepet, A.; Ladavière, C.; Perez, D. D. S.; Mangematin, S.; Almada, C. C.; Vilcocq, L.; Djakovitch, L.; Fongarland, P. Comparative Study of Solvolysis of Technical Lignins in Flow Reactor. *Biomass Conv. Bioref.* **2020**, *10* (2), 351–366. https://doi.org/10.1007/s13399-019-00435-z.
(164) Schutyser, W.; Kruger, J. S.; Robinson, A. M.; Katahira, R.; Brandner, D. G.; Cleveland, N. S.; Mittal, A.; Peterson, D. J.; Meilan, R.; Román-Leshkov, Y.; Beckham, G. T. Revisiting Alkaline Aerobic Lignin Oxidation. *Green Chem.* **2018**, *20* (16), 3828–3844. https://doi.org/10.1039/C8GC00502H.
(165) Chen, J.; Yang, H.; Fu, H.; He, H.; Zeng, Q.; Li, X. Electrochemical Oxidation Mechanisms for Selective Products Due to C–O and C–C Cleavages of β-O-4 Linkages in Lignin Model Compounds. *Phys. Chem. Chem. Phys.* **2020**, *22* (20), 11508–11518. https://doi.org/10.1039/D0CP01091J.
(166) Hasan, M.; Akbari, A.; Greenlee, L. F. Combined Electrocatalytic Oxidation and Reduction to Selectively Cleave β-O-4 Linkage of Lignin over Platinum Electrode in Organic Solvent: Secondary Treatment Opportunity for CELF Process. *ACS Sustainable Chem. Eng.* **2023**, *11* (42), 15262–15272. https://doi.org/10.1021/acssuschemeng.3c03191.
(167) Bawareth, B.; Di Marino, D.; Nijhuis, T. A.; Jestel, T.; Wessling, M. Electrochemical Membrane Reactor Modeling for Lignin Depolymerization. *ACS Sustainable Chem. Eng.* **2019**, *7* (2), 2091–2099. https://doi.org/10.1021/acssuschemeng.8b04670.
(168) Jasiukaitytė-Grojzdek, E.; Huš, M.; Grilc, M.; Likozar, B. Acid-Catalysed α-O-4 Aryl-Ether Bond Cleavage in Methanol/(Aqueous) Ethanol: Understanding Depolymerisation

of a Lignin Model Compound during Organosolv Pretreatment. *Sci. Rep.* **2020**, *10* (1), 11037. https://doi.org/10.1038/s41598-020-67787-9.
(169) Lin, F.; Petrović, P. V.; Tse, H.-Y.; Erythropel, H. C.; Lam, J. C.-H.; Anastas, P. T. Mechanistic Investigation of a Ni-Catalyzed Electrochemical Reductive Cleavage of the α-O-4 Bond in the Lignin Model Compound Benzyl Phenyl Ether. *Green Chem.* **2023**, *25* (23), 9720–9732. https://doi.org/10.1039/D3GC01814H.
(170) Figueiredo, J. L.; Pereira, M. F. R. The Role of Surface Chemistry in Catalysis with Carbons. *Catalysis Today* **2010**, *150* (1–2), 2–7. https://doi.org/10.1016/j.cattod.2009.04.010.
(171) Hu, C.; Xiao, Y.; Zhao, Y.; Chen, N.; Zhang, Z.; Cao, M.; Qu, L. Highly Nitrogen-Doped Carbon Capsules: Scalable Preparation and High-Performance Applications in Fuel Cells and Lithium Ion Batteries. *Nanoscale* **2013**, *5* (7), 2726. https://doi.org/10.1039/c3nr34002c.
(172) Hu, C.; Dai, L. Doping of Carbon Materials for Metal-Free Electrocatalysis. *Adv. Mater.* **2019**, *31* (7), 1804672. https://doi.org/10.1002/adma.201804672.
(173) Ding, Y.; Greiner, M.; Schlögl, R.; Heumann, S. A Metal-Free Electrode: From Biomass-Derived Carbon to Hydrogen. *ChemSusChem* **2020**, *13* (16), 4064–4068. https://doi.org/10.1002/cssc.202000714.
(174) Park, J.; Kim, T. Biomass-Derived Sustainable Electrode Material for Low-Grade Heat Harvesting. *Nanomaterials* **2023**, *13* (9), 1488. https://doi.org/10.3390/nano13091488.
(175) Kroto, H. W.; Heath, J. R.; O'Brien, S. C.; Curl, R. F.; Smalley, R. E. C60: Buckminsterfullerene. *Nature* **1985**, *318* (6042), 162–163. https://doi.org/10.1038/318162a0.
(176) Xing, Y.; Dai, L. Nanodiamonds for Nanomedicine. *Nanomedicine* **2009**, *4* (2), 207–218. https://doi.org/10.2217/17435889.4.2.207.
(177) Jorge, A. B.; Jervis, R.; Periasamy, A. P.; Qiao, M.; Feng, J.; Tran, L. N.; Titirici, M. 3D Carbon Materials for Efficient Oxygen and Hydrogen Electrocatalysis. *Adv. Energy Mater.* **2020**, *10* (11), 1902494. https://doi.org/10.1002/aenm.201902494.
(178) Geim, A. K.; Novoselov, K. S. The Rise of Graphene. *Nat. Mater.* **2007**, *6* (3), 183–191. https://doi.org/10.1038/nmat1849.
(179) Novoselov, K. S. Graphene: The Magic of Flat Carbon. *ECS Trans.* **2009**, *19* (5), 3–7. https://doi.org/10.1149/1.3119522.
(180) Lorenz, H.; Fritzsche, J.; Das, A.; Stöckelhuber, K. W.; Jurk, R.; Heinrich, G.; Klüppel, M. Advanced Elastomer Nano-Composites Based on CNT-Hybrid Filler Systems. *Compos. Sci. Technol.* **2009**, *69* (13), 2135–2143. https://doi.org/10.1016/j.compscitech.2009.05.014.
(181) Dai, L.; Chang, D. W.; Baek, J.; Lu, W. Carbon Nanomaterials for Advanced Energy Conversion and Storage. *Small* **2012**, *8* (8), 1130–1166. https://doi.org/10.1002/smll.201101594.
(182) Iijima, S. Helical Microtubules of Graphitic Carbon. *Nature* **1991**, *354* (6348), 56–58. https://doi.org/10.1038/354056a0.
(183) Wen, Q.; Qian, W.; Nie, J.; Cao, A.; Ning, G.; Wang, Y.; Hu, L.; Zhang, Q.; Huang, J.; Wei, F. 100 Mm Long, Semiconducting Triple-Walled Carbon Nanotubes. *Adv. Mater.* **2010**, *22* (16), 1867–1871. https://doi.org/10.1002/adma.200902746.
(184) Dai, H. Carbon Nanotubes: Synthesis, Integration, and Properties. *Acc. Chem. Res.* **2002**, *35* (12), 1035–1044. https://doi.org/10.1021/ar0101640.
(185) Oh, H.; Choi, Y.; Shin, C.; Nguyen, T. V. T.; Han, Y.; Kim, H.; Kim, Y. H.; Lee, J.-W.; Jang, J.-W.; Ryu, J. Phosphomolybdic Acid as a Catalyst for Oxidative Valorization of Biomass and Its Application as an Alternative Electron Source. *ACS Catal.* **2020**, *10* (3), 2060–2068. https://doi.org/10.1021/acscatal.9b04099.

(186) Shao, Y.; Liu, J.; Wang, Y.; Lin, Y. Novel Catalyst Support Materials for PEMfuelcells: Current Status and Future Prospects. *J. Mater. Chem.* **2009**, *19* (1), 46–59. https://doi.org/10.1039/B808370C.
(187) Baglio, V.; Di Blasi, A.; D'Urso, C.; Antonucci, V.; Aricò, A. S.; Ornelas, R.; Morales-Acosta, D.; Ledesma-Garcia, J.; Godinez, L. A.; Arriaga, L. G.; Alvarez-Contreras, L. Development of Pt and Pt–Fe Catalysts Supported on Multiwalled Carbon Nanotubes for Oxygen Reduction in Direct Methanol Fuel Cells. *J. Electrochem. Soc.* **2008**, *155* (8), B829. https://doi.org/10.1149/1.2938368.
(188) Prabhuram, J.; Zhao, T. S.; Tang, Z. K.; Chen, R.; Liang, Z. X. Multiwalled Carbon Nanotube Supported PtRu for the Anode of Direct Methanol Fuel Cells. *J. Phys. Chem. B* **2006**, *110* (11), 5245–5252. https://doi.org/10.1021/jp0567063.
(189) Bateni, F.; Ghahremani, R.; Staser, J. A. Electrochemical Oxidative Valorization of Lignin by the Nanostructured PbO_2/MWNTs Electrocatalyst in a Low-Energy Depolymerization Process. *J. Appl. Electrochem.* **2021**, *51* (1), 65–78. https://doi.org/10.1007/s10800-020-01451-y.
(190) Tejral, G.; Panyala, N. R.; Havel, J. Carbon Nanotubes: Toxicological Impact on Human Health and Environment. *J. Appl. Biomed.* **2009**, *7* (1), 1–13. https://doi.org/10.32725/jab.2009.001.
(191) Pulskamp, K.; Diabate, S.; Krug, H. Carbon Nanotubes Show No Sign of Acute Toxicity but Induce Intracellular Reactive Oxygen Species in Dependence on Contaminants. *Toxicol. Lett.* **2007**, *168* (1), 58–74. https://doi.org/10.1016/j.toxlet.2006.11.001.
(192) Kagan, V. E.; Tyurina, Y. Y.; Tyurin, V. A.; Konduru, N. V.; Potapovich, A. I.; Osipov, A. N.; Kisin, E. R.; Schwegler-Berry, D.; Mercer, R.; Castranova, V.; Shvedova, A. A. Direct and Indirect Effects of Single Walled Carbon Nanotubes on RAW 264.7 Macrophages: Role of Iron. *Toxicol. Lett.* **2006**, *165* (1), 88–100. https://doi.org/10.1016/j.toxlet.2006.02.001.
(193) Tamura, K.; Takashi, N.; Akasaka, T.; Roska, I. D.; Uo, M.; Totsuka, Y.; Watari, F. Effects of Micro/Nano Particle Size on Cell Function and Morphology. *Key Eng. Mater.* **2003**, *254–256*, 919–922. https://doi.org/10.4028/www.scientific.net/KEM.254-256.919.
(194) Monteiro-Riviere, N. A.; Nemanich, R. J.; Inman, A. O.; Wang, Y. Y.; Riviere, J. E. Multi-Walled Carbon Nanotube Interactions with Human Epidermal Keratinocytes. *Toxicol. Lett.* **2005**, *155* (3), 377–384. https://doi.org/10.1016/j.toxlet.2004.11.004.
(195) Jia, G.; Wang, H.; Yan, L.; Wang, X.; Pei, R.; Yan, T.; Zhao, Y.; Guo, X. Cytotoxicity of Carbon Nanomaterials: Single-Wall Nanotube, Multi-Wall Nanotube, and Fullerene. *Environ. Sci. Technol.* **2005**, *39* (5), 1378–1383. https://doi.org/10.1021/es048729l.
(196) Pulskamp, K.; Wörle-Knirsch, J. M.; Hennrich, F.; Kern, K.; Krug, H. F. Human Lung Epithelial Cells Show Biphasic Oxidative Burst after Single-Walled Carbon Nanotube Contact. *Carbon* **2007**, *45* (11), 2241–2249. https://doi.org/10.1016/j.carbon.2007.06.054.
(197) Monteiro-Riviere, N. A.; Inman, A. O. Challenges for Assessing Carbon Nanomaterial Toxicity to the Skin. *Carbon* **2006**, *44* (6), 1070–1078. https://doi.org/10.1016/j.carbon.2005.11.004.
(198) Tian, L.; Li, Z.; Wang, P.; Zhai, X.; Wang, X.; Li, T. Carbon Quantum Dots for Advanced Electrocatalysis. *J. Energy Chem.* **2021**, *55*, 279–294. https://doi.org/10.1016/j.jechem.2020.06.057.
(199) Hoang, V. C.; Dave, K.; Gomes, V. G. Carbon Quantum Dot-Based Composites for Energy Storage and Electrocatalysis: Mechanism, Applications and Future Prospects. *Nano Energy* **2019**, *66*, 104093. https://doi.org/10.1016/j.nanoen.2019.104093.

(200) Liu, X.; Jiang, Z.; Cao, X.; Shen, Z.; Zhao, W.; Wang, F.; Cui, M.; Liang, C. Z-Scheme Heterojunction g-C 3 N 4 /CQD/CdZnS with High Redox Capability for Enhancing Visible Light-Driven Photocatalytic Depolymerization of Lignin into Aromatic Monomers. *Green Chem.* **2024**, *26* (4), 1935–1948. https://doi.org/10.1039/D3GC03929C.
(201) Friedrich, J. M.; Ponce-de-León, C.; Reade, G. W.; Walsh, F. C. Reticulated Vitreous Carbon as an Electrode Material. *J. Electroanal. Chem.* **2004**, *561*, 203–217. https://doi.org/10.1016/j.jelechem.2003.07.019.
(202) Fang, Z.; Jackson, J. E.; Hegg, E. L. Mild, Electroreductive Lignin Cleavage: Optimizing the Depolymerization of Authentic Lignins. *ACS Sustainable Chem. Eng.* **2022**, *10* (23), 7545–7552. https://doi.org/10.1021/acssuschemeng.2c00820.
(203) Lindenbeck, L. M.; Dahlhaus, S.; Wende, L. M.; Beele, B. B.; Frauscher, M.; Schebb, N. H.; Lehmann, C. W.; Bornhorst, J.; Slabon, A.; Rodrigues, B. V. M. Breaking down Lignin in Gamma-Valerolactone: Advances into a Bioelectrorefinery. *Green Chem. Lett. Rev.* **2024**, *17* (1), 2390867. https://doi.org/10.1080/17518253.2024.2390867.
(204) Song, J.; Cho, S. Catalytic Materials for Efficient Electrochemical Production of Hydrogen Peroxide. *APL Mater.* **2020**, *8* (5), 050701. https://doi.org/10.1063/5.0002845.
(205) Harris, D. C.; Werner, G. *Lehrbuch der quantitativen Analyse*, 8., vollst. überarb. erw. Aufl.; Springer-Lehrbuch; Springer Spektrum: Berlin, 2014.
(206) Schäfer, H. J. Contributions of Organic Electrosynthesis to Green Chemistry. *C. R. Chim.* **2011**, *14* (7–8), 745–765. https://doi.org/10.1016/j.crci.2011.01.002.
(207) Wang, J.; Yang, P.; Wei, X.; Zhou, Z. Preparation of NiO Two-Dimensional Grainy Films and Their High-Performance Gas Sensors for Ammonia Detection. *Nanoscale Res. Lett.* **2015**, *10* (1), 119. https://doi.org/10.1186/s11671-015-0807-5.
(208) Pai, S. H. S.; Pandey, S. K.; Samuel, E. J. J.; Jang, J. U.; Nayak, A. K.; Han, H. Recent Advances in NiO-Based Nanostructures for Energy Storage Device Applications. *J. Energy Storage* **2024**, *76*, 109731. https://doi.org/10.1016/j.est.2023.109731.
(209) Sergeev, A. G.; Webb, J. D.; Hartwig, J. F. A Heterogeneous Nickel Catalyst for the Hydrogenolysis of Aryl Ethers without Arene Hydrogenation. *J. Am. Chem. Soc.* **2012**, *134* (50), 20226–20229. https://doi.org/10.1021/ja3085912.
(210) Wang, M.; Zhao, Y.; Mei, D.; Bullock, R. M.; Gutiérrez, O. Y.; Camaioni, D. M.; Lercher, J. A. The Critical Role of Reductive Steps in the Nickel-Catalyzed Hydrogenolysis and Hydrolysis of Aryl Ether C−O Bonds. *Angew. Chem. Int. Ed.* **2020**, *59* (4), 1445–1449. https://doi.org/10.1002/anie.201909551.
(211) Molinari, V.; Giordano, C.; Antonietti, M.; Esposito, D. Titanium Nitride-Nickel Nanocomposite as Heterogeneous Catalyst for the Hydrogenolysis of Aryl Ethers. *J. Am. Chem. Soc.* **2014**, *136* (5), 1758–1761. https://doi.org/10.1021/ja4119412.
(212) Song, Q.; Wang, F.; Xu, J. Hydrogenolysis of Lignosulfonate into Phenols over Heterogeneous Nickel Catalysts. *Chem. Commun.* **2012**, *48* (56), 7019. https://doi.org/10.1039/c2cc31414b.
(213) Danlu, Z.; Xu, Z.; Sinong, W.; Yan, X.; Qiqi, D.; Fengxia, Y.; Peng, W.; Chuanfu, L.; Wu, L. Electrochemical Oxidation of Lignin Model Compounds over Metal Oxyhydroxides on Nickel Foam. *Green Chem.* **2024**, *26* (13), 7759–7768. https://doi.org/10.1039/D4GC02156H.
(214) Di Fidio, N.; Timmermans, J. W.; Antonetti, C.; Raspolli Galletti, A. M.; Gosselink, R. J. A.; Bisselink, R. J. M.; Slaghek, T. M. Electro-Oxidative Depolymerisation of Technical Lignin in Water Using Platinum, Nickel Oxide Hydroxide and Graphite Electrodes. *New J. Chem.* **2021**, *45* (21), 9647–9657. https://doi.org/10.1039/D1NJ01037A.

(215) Carkner, A.; Tageldin, I.; Han, J.; Seifitokaldani, A.; Kopyscinski, J. Impact of Temperature an Order of Magnitude Larger Than Electrical Potential in Lignin Electrolysis with Nickel. *ChemSusChem* **2023**, e202300795. https://doi.org/10.1002/cssc.202300795.
(216) Breiner, M.; Zirbes, M.; Waldvogel, S. R. Comprehensive Valorisation of Technically Relevant Organosolv Lignins via Anodic Oxidation. *Green Chem.* **2021**, *23* (17), 6449–6455. https://doi.org/10.1039/D1GC01995C.
(217) Klein, J.; Waldvogel, S. R. Selective Electrochemical Degradation of Lignosulfonate to Bio-Based Aldehydes. *ChemSusChem* **2023**, *16* (8), e202202300. https://doi.org/10.1002/cssc.202202300.
(218) Schmitt, D.; Regenbrecht, C.; Hartmer, M.; Stecker, F.; Waldvogel, S. R. Highly Selective Generation of Vanillin by Anodic Degradation of Lignin: A Combined Approach of Electrochemistry and Product Isolation by Adsorption. *Beilstein J. Org. Chem.* **2015**, *11*, 473–480. https://doi.org/10.3762/bjoc.11.53.
(219) Yan, K.; Zhang, Y.; Tu, M.; Sun, Y. Electrocatalytic Valorization of Organosolv Lignin Utilizing a Nickel-Based Electrocatalyst. *Energy Fuels* **2020**, *34* (10), 12703–12709. https://doi.org/10.1021/acs.energyfuels.0c02284.
(220) Aguillón-Rodríguez, P.; Pérez-Reyes, O.; Ortiz-Cervantes, C. Hydrogenolysis of Lignin and Lignin-Based Molecules Catalyzed by Nickel and $Sc(OTf)_3$. *Res. Chem.* **2023**, *5*, 100729. https://doi.org/10.1016/j.rechem.2022.100729.
(221) Ouyang, D.; Gao, D.; Qiang, Y.; Zhao, X. Highly-Efficient Conversion of Lignin to Electricity by Nickel Foam Anode Loaded with Solid Electrocatalysts. *Appl. Catal., B* **2023**, *328*, 122491. https://doi.org/10.1016/j.apcatb.2023.122491.
(222) Huang, J.; Jian, Y.; Zhou, M.; Wu, H. Oxidative C−C Bond Cleavage of Lignin via Electrocatalysis. *Front. Chem.* **2022**, *10*, 1007707. https://doi.org/10.3389/fchem.2022.1007707.
(223) Flora, G.; Gupta, D.; Tiwari, A. Toxicity of Lead: A Review with Recent Updates. *Interdiscip. Toxicol.* **2012**, *5* (2), 47–58. https://doi.org/10.2478/v10102-012-0009-2.
(224) Zhou, Q.; Zhou, X.; Zheng, R.; Liu, Z.; Wang, J. Application of Lead Oxide Electrodes in Wastewater Treatment: A Review. *Sci. Total Environ.* **2022**, *806*, 150088. https://doi.org/10.1016/j.scitotenv.2021.150088.
(225) Wang, X.; Wang, L.; Wu, D.; Yuan, D.; Ge, H.; Wu, X. PbO2 Materials for Electrochemical Environmental Engineering: A Review on Synthesis and Applications. *Sci. Total Environ.* **2023**, *855*, 158880. https://doi.org/10.1016/j.scitotenv.2022.158880.
(226) Bailey, A.; Brooks, H. M. Electrolytic Oxidation of Lignin. *J. Am. Chem. Soc.* **1946**, *68* (3), 445–446. https://doi.org/10.1021/ja01207a029.
(227) Pan, K.; Tian, M.; Jiang, Z.-H.; Kjartanson, B.; Chen, A. Electrochemical Oxidation of Lignin at Lead Dioxide Nanoparticles Photoelectrodeposited on TiO_2 Nanotube Arrays. *Electrochim. Acta* **2012**, *60*, 147–153. https://doi.org/10.1016/j.electacta.2011.11.025.
(228) Wang, Y.; Yang, F.; Liu, Z.; Yuan, L.; Li, G. Electrocatalytic Degradation of Aspen Lignin over Pb/PbO2 Electrode in Alkali Solution. *Catal. Commun.* **2015**, *67*, 49–53. https://doi.org/10.1016/j.catcom.2015.03.033.
(229) Lan, C.; Fan, H.; Shang, Y.; Shen, D.; Li, G. Electrochemically Catalyzed Conversion of Cornstalk Lignin to Aromatic Compounds: An Integrated Process of Anodic Oxidation of a Pb/PbO_2 Electrode and Hydrogenation of a Nickel Cathode in Sodium Hydroxide Solution. *Sustain. Energ. Fuels* **2020**, *4* (4), 1828–1836. https://doi.org/10.1039/C9SE00942F.
(230) Liu, M.; Wen, Y.; Qi, J.; Zhang, S.; Li, G. Fine Chemicals Prepared by Bamboo Lignin Degradation through Electrocatalytic Redox between Cu Cathode and Pb/PbO_2 Anode in Alkali Solution. *ChemistrySelect* **2017**, *2* (17), 4956–4962. https://doi.org/10.1002/slct.201700881.

(231) Wu, Z.; Zhang, X.; Fan, H.; Han, X.; Wen, Y.; Li, G.; Li, H. Allyl Halide Induced Electrochemical Degradation of Lignin into Double-Bonded Phenolic Monomers. *Int. J. Biol. Macromol.* **2023**, *242*, 124947. https://doi.org/10.1016/j.ijbiomac.2023.124947.
(232) Pourbaix, M. J. N.; Van Muylder, J.; de Zoubov, N. Electrochemical Properties of the Platinum Metals. *Platinum Metals Rev.* **1959**, *3*, 47–53.
(233) Martinsen, Ø. G.; Heiskanen, A. Electrodes. In *Bioimpedance and Bioelectricity Basics*; Elsevier, 2023; pp 175–248. https://doi.org/10.1016/B978-0-12-819107-1.00005-4.
(234) Jerkiewicz, G. Applicability of Platinum as a Counter-Electrode Material in Electrocatalysis Research. *ACS Catal.* **2022**, *12* (4), 2661–2670. https://doi.org/10.1021/acscatal.1c06040.
(235) Luo, Q.; Zhao, Y.; Sun, L.; Wang, C.; Xin, H.; Song, J.; Li, D.; Ma, F. Interface Oxygen Vacancy Enhanced Alkaline Hydrogen Evolution Activity of Cobalt-Iron Phosphide/CeO2 Hollow Nanorods. *Chem. Eng. J.* **2022**, *437*, 135376. https://doi.org/10.1016/j.cej.2022.135376.
(236) Xiao, X.; Sun, S.; Qi, Y.; Hao, S.; Zhang, W.; Qiu, X. Selective Electrocatalytic Oxidation of C(OH)–C Bond in Lignin with Pt@CeO_2 toward the Synthesis of Benzoic Acid. *Electrochim. Acta* **2023**, *470*, 143377. https://doi.org/10.1016/j.electacta.2023.143377.
(237) Ma, L.; Zhou, H.; Kong, X.; Li, Z.; Duan, H. An Electrocatalytic Strategy for C–C Bond Cleavage in Lignin Model Compounds and Lignin under Ambient Conditions. *ACS Sustainable Chem. Eng.* **2021**, *9* (4), 1932–1940. https://doi.org/10.1021/acssuschemeng.0c08612.
(238) Zhou, Y.; Zeng, Q.; He, H.; Wu, K.; Liu, F.; Li, X. Role of Methoxy and C -Based Substituents in Electrochemical Oxidation Mechanisms and Bond Cleavage Selectivity of β-O-4 Lignin Model Compounds. *Green Energy Environ.* **2024**, *9* (1), 114–125. https://doi.org/10.1016/j.gee.2022.05.006.
(239) Beliaeva, K.; Elsheref, M.; Walden, D.; Dappozze, F.; Nieto-Marquez, A.; Gil, S.; Guillard, C.; Vernoux, P.; Steinmann, S. N.; Caravaca, A. Towards Understanding Lignin Electrolysis: Electro-Oxidation of a β -O-4 Linkage Model on PtRu Electrodes. *J. Electrochem. Soc.* **2020**, *167* (13), 134511. https://doi.org/10.1149/1945-7111/abb8b5.
(240) Chen, R.; Yang, C.; Cai, W.; Wang, H.-Y.; Miao, J.; Zhang, L.; Chen, S.; Liu, B. Use of Platinum as the Counter Electrode to Study the Activity of Nonprecious Metal Catalysts for the Hydrogen Evolution Reaction. *ACS Energy Lett.* **2017**, *2* (5), 1070–1075. https://doi.org/10.1021/acsenergylett.7b00219.
(241) Nørskov, J. K.; Bligaard, T.; Logadottir, A.; Kitchin, J. R.; Chen, J. G.; Pandelov, S.; Stimming, U. Trends in the Exchange Current for Hydrogen Evolution. *J. Electrochem. Soc.* **2005**, *152* (3), J23. https://doi.org/10.1149/1.1856988.
(242) Da Cruz, M. G. A.; Rodrigues, B. V. M.; Ristic, A.; Budnyk, S.; Das, S.; Slabon, A. On the Product Selectivity in the Electrochemical Reductive Cleavage of 2-Phenoxyacetophenone, a Lignin Model Compound. *Green Chem. Lett. Rev.* **2022**, *15* (1), 153–161. https://doi.org/10.1080/17518253.2022.2025462.
(243) Dourado, A. H. B.; Santos, M.; Curvelo, A. A. S.; Varela, H. CuO as (Electro)Catalyst for Lignin Valorization. *Appl. Catal., A* **2024**, *671*, 119583. https://doi.org/10.1016/j.apcata.2024.119583.
(244) Han, J.; Lin, R.; Salehi, M.; Farzi, A.; Carkner, A.; Liu, K.; Abou El-Oon, O.; Ajao, O.; Seifitokaldani, A. Kraft Lignin Electro-Oxidation under Ambient Temperature and Pressure. *Energies* **2023**, *16* (24), 8007. https://doi.org/10.3390/en16248007.
(245) Rodriguez, P.; Koper, M. T. M. Electrocatalysis on Gold. *Phys. Chem. Chem. Phys.* **2014**, *16* (27), 13583–13594. https://doi.org/10.1039/C4CP00394B.

(246) Li, C.; Chai, O. J. H.; Yao, Q.; Liu, Z.; Wang, L.; Wang, H.; Xie, J. Electrocatalysis of Gold-Based Nanoparticles and Nanoclusters. *Mater. Horiz.* **2021**, *8* (6), 1657–1682. https://doi.org/10.1039/D0MH01947J.
(247) Naveen, M. H.; Khan, R.; Bang, J. H. Gold Nanoclusters as Electrocatalysts: Atomic Level Understanding from Fundamentals to Applications. *Chem. Mater.* **2021**, *33* (19), 7595–7612. https://doi.org/10.1021/acs.chemmater.1c02112.
(248) Song, Y.; Mobley, J. K.; Motagamwala, A. H.; Isaacs, M.; Dumesic, J. A.; Ralph, J.; Lee, A. F.; Wilson, K.; Crocker, M. Gold-Catalyzed Conversion of Lignin to Low Molecular Weight Aromatics. *Chem. Sci.* **2018**, *9* (42), 8127–8133. https://doi.org/10.1039/C8SC03208D.
(249) Qi, Y.; Liu, B.; Qiu, X.; Zeng, X.; Luo, Z.; Wu, W.; Liu, Y.; Chen, L.; Zu, X.; Dong, H.; Lin, X.; Qin, Y. Simultaneous Oxidative Cleavage of Lignin and Reduction of Furfural via Efficient Electrocatalysis by P-Doped $CoMoO_4$. *Adv. Mater.* **2023**, *35* (14), 2208284. https://doi.org/10.1002/adma.202208284.
(250) Du, X.; Liu, W.; Zhang, Z.; Mulyadi, A.; Brittain, A.; Gong, J.; Deng, Y. Low-Energy Catalytic Electrolysis for Simultaneous Hydrogen Evolution and Lignin Depolymerization. *ChemSusChem* **2017**, *10* (5), 847–854. https://doi.org/10.1002/cssc.201601685.
(251) Ko, M.; Pham, L. T. M.; Sa, Y. J.; Woo, J.; Nguyen, T. V. T.; Kim, J. H.; Oh, D.; Sharma, P.; Ryu, J.; Shin, T. J.; Joo, S. H.; Kim, Y. H.; Jang, J.-W. Unassisted Solar Lignin Valorisation Using a Compartmented Photo-Electro-Biochemical Cell. *Nat. Commun.* **2019**, *10* (1), 5123. https://doi.org/10.1038/s41467-019-13022-7.
(252) Rinaldi, R.; Jastrzebski, R.; Clough, M. T.; Ralph, J.; Kennema, M.; Bruijnincx, P. C. A.; Weckhuysen, B. M. Paving the Way for Lignin Valorisation: Recent Advances in Bioengineering, Biorefining and Catalysis. *Angew. Chem. Int. Ed.* **2016**, *55* (29), 8164–8215. https://doi.org/10.1002/anie.201510351.
(253) Radhika, N. L.; Sachdeva, S.; Kumar, M. Lignin Depolymerization and Biotransformation to Industrially Important Chemicals/Biofuels. *Fuel* **2022**, *312*, 122935. https://doi.org/10.1016/j.fuel.2021.122935.
(254) Sun, Z.; Fridrich, B.; De Santi, A.; Elangovan, S.; Barta, K. Bright Side of Lignin Depolymerization: Toward New Platform Chemicals. *Chem. Rev.* **2018**, *118* (2), 614–678. https://doi.org/10.1021/acs.chemrev.7b00588.
(255) Crook, J.; Mousavi, A. The Chlor-Alkali Process: A Review of History and Pollution. *Environ. Forensics* **2016**, *17* (3), 211–217. https://doi.org/10.1080/15275922.2016.1177755.
(256) Thannimalay, L. Life Cycle Assessment of Sodium Hydroxide. *Aust. J. Basic Appl. Sci.* **2013**, *7* (2), 421–431.
(257) Steinhauser, G. Cleaner Production in the Solvay Process: General Strategies and Recent Developments. *J. Cleaner Prod.* **2008**, *16* (7), 833–841. https://doi.org/10.1016/j.jclepro.2007.04.005.
(258) Sternberg, J.; Sequerth, O.; Pilla, S. Green Chemistry Design in Polymers Derived from Lignin: Review and Perspective. *Prog. Polym. Sci.* **2021**, *113*, 101344. https://doi.org/10.1016/j.progpolymsci.2020.101344.
(259) Chandna, S.; Olivares M., C. A.; Baranovskii, E.; Engelmann, G.; Böker, A.; Tzschucke, C. C.; Haag, R. Lignin Upconversion by Functionalization and Network Formation. *Angew. Chem. Int. Ed.* **2023**, e202313945. https://doi.org/10.1002/anie.202313945.
(260) Dier, T. K. F.; Rauber, D.; Durneata, D.; Hempelmann, R.; Volmer, D. A. Sustainable Electrochemical Depolymerization of Lignin in Reusable Ionic Liquids. *Sci. Rep.* **2017**, *7* (1), 5041. https://doi.org/10.1038/s41598-017-05316-x.

(261) Marino, D. D.; Stöckmann, D.; Kriescher, S.; Stiefel, S.; Wessling, M. Electrochemical Depolymerisation of Lignin in a Deep Eutectic Solvent. *Green Chem.* **2016**, *18* (22), 6021–6028. https://doi.org/10.1039/C6GC01353H.
(262) Wu, Z.; Jiang, Y.; Wang, X.; Xu, J.; Hu, L. A Review on the Separation of Lignin Depolymerized Products. *Biomass Conv. Bioref.* **2023**, *13* (18), 16667–16683. https://doi.org/10.1007/s13399-021-02266-3.
(263) Zirbes, M.; Graßl, T.; Neuber, R.; Waldvogel, S. R. Peroxodicarbonate as a Green Oxidizer for the Selective Degradation of Kraft Lignin into Vanillin. *Angew. Chem. Int. Ed.* **2023**, *62* (14), e202219217. https://doi.org/10.1002/anie.202219217.
(264) Kaya, K.; Atsay, A.; Gunduz, H.; Slabon, A.; Yagci, Y. Nature-Inspired Depolymerization of Soda Lignin: Light-Induced Free Radical Promoted Cleavage of β-O-4 Bonds. *Adv. Sustainable Syst.* **2023**, 2300366. https://doi.org/10.1002/adsu.202300366.
(265) Wiermans, L.; Schumacher, H.; Klaaßen, C.-M.; Domínguez De María, P. Unprecedented Catalyst-Free Lignin Dearomatization with Hydrogen Peroxide and Dimethyl Carbonate. *RSC Adv.* **2015**, *5* (6), 4009–4018. https://doi.org/10.1039/C4RA13113D.
(266) Thannimalay, L.; Yusoff, S.; Zawawi, N. Z. Life Cycle Assessment of Sodium Hydroxide. *Aust. J. Basic Appl. Sci.* **2013**, *7* (2), 421–431.
(267) Pichler, C. M.; Bhattacharjee, S.; Rahaman, M.; Uekert, T.; Reisner, E. Conversion of Polyethylene Waste into Gaseous Hydrocarbons via Integrated Tandem Chemical–Photo/Electrocatalytic Processes. *ACS Catal.* **2021**, *11* (15), 9159–9167. https://doi.org/10.1021/acscatal.1c02133.
(268) Wang, C.; Liu, K.; Jin, Y.; Huang, S.; Chun-Ho Lam, J. Amorphous RuO_2 Catalyst for Medium Size Carboxylic Acid to Alkane Dimer Selective Kolbe Electrolysis in an Aqueous Environment**. *ChemSusChem* **2023**, *16* (16), e202300222. https://doi.org/10.1002/cssc.202300222.
(269) Granatier, M.; Schlapp-Hackl, I.; Lê, H. Q.; Nieminen, K.; Pitkänen, L.; Sixta, H. Stability of Gamma-Valerolactone under Pulping Conditions as a Basis for Process Optimization and Chemical Recovery. *Cellulose* **2021**, *28* (18), 11567–11578. https://doi.org/10.1007/s10570-021-04243-5.
(270) Chen, Y.; Kanan, M. W. Tin Oxide Dependence of the CO2 Reduction Efficiency on Tin Electrodes and Enhanced Activity for Tin/Tin Oxide Thin-Film Catalysts. *J. Am. Chem. Soc.* **2012**, *134* (4), 1986–1989. https://doi.org/10.1021/ja2108799.
(271) Cheng, F.; Liu, S.; Karlen, S. D.; Kim, H.; Lu, F.; Ralph, J.; Ramos, L. M. V.; Huber, G. W.; Dumesic, J. A. Poplar Lignin Structural Changes during Extraction in γ-Valerolactone (GVL). *Green Chem.* **2023**, *25* (1), 336–347. https://doi.org/10.1039/D2GC03446H.
(272) Hadžija, O.; Špoljar, B. Quantitative Determination of Carboxylate by Infrared Spectroscopy: Application to Humic Acids. *Fresenius J. Anal. Chem.* **1995**, *351* (7), 692–693. https://doi.org/10.1007/BF00323352.
(273) Shi, Z.; Xu, G.; Deng, J.; Dong, M.; Murugadoss, V.; Liu, C.; Shao, Q.; Wu, S.; Guo, Z. Structural Characterization of Lignin from D. Sinicus by FTIR and NMR Techniques. *Green Chem. Lett. Rev.* **2019**, *12* (3), 235–243. https://doi.org/10.1080/17518253.2019.1627428.
(274) Sheldon, R. A. The E Factor at 30: A Passion for Pollution Prevention. *Green Chem.* **2023**, *25* (5), 1704–1728. https://doi.org/10.1039/D2GC04747K.
(275) Silverstein, R. M.; Webster, F. X.; Kiemle, D. J.; Bryce, D. L. *Spectrometric Identification of Organic Compounds*, Eighth edition.; Wiley: Hoboken, NJ, 2015.

(276) Haykir, N. I.; Viell, J. Challenges and Opportunities for Gamma-Valerolactone in Biomass Pretreatment. *Ind. Eng. Chem. Res.* **2024**, *63* (28), 12251–12264. https://doi.org/10.1021/acs.iecr.4c01277.
(277) Michels, J.; Wagemann, K. The German Lignocellulose Feedstock Biorefinery Project. *Biofuels, Bioprod. Biorefin.* **2010**, *4* (3), 263–267. https://doi.org/10.1002/bbb.216.
(278) Ragauskas, A. J. Lignin 'First' Pretreatments: Research Opportunities and Challenges. *Biofuels, Bioprod. Biorefin.* **2018**, *12* (4), 515–517. https://doi.org/10.1002/bbb.1900.
(279) Shuai, L.; Amiri, M. T.; Questell-Santiago, Y. M.; Héroguel, F.; Li, Y.; Kim, H.; Meilan, R.; Chapple, C.; Ralph, J.; Luterbacher, J. S. Formaldehyde Stabilization Facilitates Lignin Monomer Production during Biomass Depolymerization. *Science* **2016**, *354* (6310), 329–333. https://doi.org/10.1126/science.aaf7810.
(280) Luterbacher, J. S.; Alonso, D. M.; Rand, J. M.; Questell-Santiago, Y. M.; Yeap, J. H.; Pfleger, B. F.; Dumesic, J. A. Solvent-Enabled Nonenyzmatic Sugar Production from Biomass for Chemical and Biological Upgrading. *ChemSusChem* **2015**, *8* (8), 1317–1322. https://doi.org/10.1002/cssc.201403418.
(281) Pateromichelakis, A.; Psycha, M.; Pyrgakis, K.; Maréchal, F.; Kokossis, A. The Use of GVL for Holistic Valorization of Biomass. *Computers & Chemical Engineering* **2022**, *164*, 107849. https://doi.org/10.1016/j.compchemeng.2022.107849.
(282) Sun, W.; Trevorah, R.; Othman, M. Z. Fractionation of Spent Liquor from Organosolv-Pretreatment Using Lignin-Incompatible Extraction. *Bioresour. Technol.* **2018**, *269*, 255–261. https://doi.org/10.1016/j.biortech.2018.08.097.
(283) Wong, C. Y. Y.; Choi, A. W.-T.; Lui, M. Y.; Fridrich, B.; Horváth, A. K.; Mika, L. T.; Horváth, I. T. Stability of Gamma-Valerolactone under Neutral, Acidic, and Basic Conditions. *Struct. Chem.* **2017**, *28* (2), 423–429. https://doi.org/10.1007/s11224-016-0887-6.
(284) Collins, T. Toward Sustainable Chemistry. *Science* **2001**, *291* (5501), 48–49. https://doi.org/10.1126/science.291.5501.48.
(285) Sheldon, R. A. Engineering a More Sustainable World through Catalysis and Green Chemistry. *J. R. Soc. Interface* **2016**, *13* (116), 20160087. https://doi.org/10.1098/rsif.2016.0087.
(286) Arndt, J.-D.; Freyer, S.; Geier, R.; Machhammer, O.; Schwartze, J.; Volland, M.; Diercks, R. Rohstoffwandel in der chemischen Industrie. *Chem. Ing. Tech.* **2007**, *79* (5), 521–528. https://doi.org/10.1002/cite.200700025.
(287) Lei, L.; Wang, Y.; Zhang, Z.; An, J.; Wang, F. Transformations of Biomass, Its Derivatives, and Downstream Chemicals over Ceria Catalysts. *ACS Catal.* **2020**, *10* (15), 8788–8814. https://doi.org/10.1021/acscatal.0c01900.
(288) Li, C.; Zhao, X.; Wang, A.; Huber, G. W.; Zhang, T. Catalytic Transformation of Lignin for the Production of Chemicals and Fuels. *Chem. Rev.* **2015**, *115* (21), 11559–11624. https://doi.org/10.1021/acs.chemrev.5b00155.
(289) Stöcker, M. Biofuels and Biomass-To-Liquid Fuels in the Biorefinery: Catalytic Conversion of Lignocellulosic Biomass Using Porous Materials. *Angew. Chem. Int. Ed.* **2008**, *47* (48), 9200–9211. https://doi.org/10.1002/anie.200801476.
(290) Ansari, K. B.; Arora, J. S.; Chew, J. W.; Dauenhauer, P. J.; Mushrif, S. H. Fast Pyrolysis of Cellulose, Hemicellulose, and Lignin: Effect of Operating Temperature on Bio-Oil Yield and Composition and Insights into the Intrinsic Pyrolysis Chemistry. *Ind. Eng. Chem. Res.* **2019**, *58* (35), 15838–15852. https://doi.org/10.1021/acs.iecr.9b00920.
(291) Strassberger, Z.; Prinsen, P.; Klis, F. V. D.; Es, D. S. V.; Tanase, S.; Rothenberg, G. Lignin Solubilisation and Gentle Fractionation in Liquid Ammonia. *Green Chem.* **2015**, *17* (1), 325–334. https://doi.org/10.1039/C4GC01143K.
(292) Katahira, R.; Mittal, A.; McKinney, K.; Chen, X.; Tucker, M. P.; Johnson, D. K.; Beckham, G. T. Base-Catalyzed Depolymerization of Biorefinery Lignins. *ACS*

Sustainable Chem. Eng. **2016**, *4* (3), 1474–1486. https://doi.org/10.1021/acssuschemeng.5b01451.

(293) Chaudhary, R.; Dhepe, P. L. Solid Base Catalyzed Depolymerization of Lignin into Low Molecular Weight Products. *Green Chem.* **2017**, *19* (3), 778–788. https://doi.org/10.1039/C6GC02701F.

(294) Fang, Z.; Flynn, M. G.; Jackson, J. E.; Hegg, E. L. Thio-Assisted Reductive Electrolytic Cleavage of Lignin β-O-4 Models and Authentic Lignin. *Green Chem.* **2021**, *23* (1), 412–421. https://doi.org/10.1039/D0GC03597A.

(295) Yang, L.; Yuan, H.; Yang, Y.; Wang, R.; Wang, C.; Wei, X.; Chen, S.; Yu, J.; Ma, X. Enhanced Lignin Degradation in Tobacco Stalk Composting with Inoculation of White-Rot Fungi Trametes Hirsuta and Pleurotus Ostreatus. *Waste Biomass Valor.* **2020**, *11* (7), 3525–3535. https://doi.org/10.1007/s12649-019-00692-z.

(296) Hyde, K. D.; Xu, J.; Rapior, S.; Jeewon, R.; Lumyong, S.; Niego, A. G. T.; Abeywickrama, P. D.; Aluthmuhandiram, J. V. S.; Brahamanage, R. S.; Brooks, S.; Chaiyasen, A.; Chethana, K. W. T.; Chomnunti, P.; Chepkirui, C.; Chuankid, B.; De Silva, N. I.; Doilom, M.; Faulds, C.; Gentekaki, E.; Gopalan, V.; Kakumyan, P.; Harishchandra, D.; Hemachandran, H.; Hongsanan, S.; Karunarathna, A.; Karunarathna, S. C.; Khan, S.; Kumla, J.; Jayawardena, R. S.; Liu, J.-K.; Liu, N.; Luangharn, T.; Macabeo, A. P. G.; Marasinghe, D. S.; Meeks, D.; Mortimer, P. E.; Mueller, P.; Nadir, S.; Nataraja, K. N.; Nontachaiyapoom, S.; O'Brien, M.; Penkhrue, W.; Phukhamsakda, C.; Ramanan, U. S.; Rathnayaka, A. R.; Sadaba, R. B.; Sandargo, B.; Samarakoon, B. C.; Tennakoon, D. S.; Siva, R.; Sriprom, W.; Suryanarayanan, T. S.; Sujarit, K.; Suwannarach, N.; Suwunwong, T.; Thongbai, B.; Thongklang, N.; Wei, D.; Wijesinghe, S. N.; Winiski, J.; Yan, J.; Yasanthika, E.; Stadler, M. The Amazing Potential of Fungi: 50 Ways We Can Exploit Fungi Industrially. *Fungal Diversity* **2019**, *97* (1), 1–136. https://doi.org/10.1007/s13225-019-00430-9.

(297) Coconi Linares, N.; Fernández, F.; Loske, A. M.; Gómez-Lim, M. A. Enhanced Delignification of Lignocellulosic Biomass by Recombinant Fungus ***Phanerochaete Chrysosporium*** Overexpressing Laccases and Peroxidases. *Microb. Physiol.* **2018**, *28* (1), 1–13. https://doi.org/10.1159/000485976.

(298) Salem, M. Z. M.; Mansour, M. M. A.; Elansary, H. O. Evaluation of the Effect of Inner and Outer Bark Extracts of Sugar Maple (*Acer Saccharum* Var. *Saccharum*) in Combination with Citric Acid against the Growth of Three Common Molds. *J. Wood Chem. Technol.* **2019**, *39* (2), 136–147. https://doi.org/10.1080/02773813.2018.1547763.

(299) Spence, E. M.; Scott, H. T.; Dumond, L.; Calvo-Bado, L.; Di Monaco, S.; Williamson, J. J.; Persinoti, G. F.; Squina, F. M.; Bugg, T. D. H. The Hydroxyquinol Degradation Pathway in Rhodococcus Jostii RHA1 and *Agrobacterium* Species Is an Alternative Pathway for Degradation of Protocatechuic Acid and Lignin Fragments. *Appl. Environ. Microbiol.* **2020**, *86* (19), e01561-20. https://doi.org/10.1128/AEM.01561-20.

(300) Barton, N.; Horbal, L.; Starck, S.; Kohlstedt, M.; Luzhetskyy, A.; Wittmann, C. Enabling the Valorization of Guaiacol-Based Lignin: Integrated Chemical and Biochemical Production of Cis,Cis-Muconic Acid Using Metabolically Engineered Amycolatopsis Sp ATCC 39116. *Metab. Eng.* **2018**, *45*, 200–210. https://doi.org/10.1016/j.ymben.2017.12.001.

(301) Conde, J. J.; González-Rodríguez, S.; Chen, X.; Lu-Chau, T. A.; Eibes, G.; Pizzi, A.; Moreira, M. T. Electrochemical Oxidation of Lignin for the Simultaneous Production of Bioadhesive Precursors and Value-Added Chemicals. *Biomass and Bioenergy* **2023**, *169*, 106693. https://doi.org/10.1016/j.biombioe.2022.106693.

(302) Schotten, C.; Nicholls, T. P.; Bourne, R. A.; Kapur, N.; Nguyen, B. N.; Willans, C. E. Making Electrochemistry Easily Accessible to the Synthetic Chemist. *Green Chem.* **2020**, *22* (11), 3358–3375. https://doi.org/10.1039/D0GC01247E.
(303) Little, R. D.; Moeller, K. D. Introduction: Electrochemistry: Technology, Synthesis, Energy, and Materials. *Chem. Rev.* **2018**, *118* (9), 4483–4484. https://doi.org/10.1021/acs.chemrev.8b00197.
(304) Minteer, S. D.; Baran, P. Electrifying Synthesis: Recent Advances in the Methods, Materials, and Techniques for Organic Electrosynthesis. *Acc. Chem. Res.* **2020**, *53* (3), 545–546. https://doi.org/10.1021/acs.accounts.0c00049.
(305) Horn, E. J.; Rosen, B. R.; Baran, P. S. Synthetic Organic Electrochemistry: An Enabling and Innately Sustainable Method. *ACS Cent. Sci.* **2016**, *2* (5), 302–308. https://doi.org/10.1021/acscentsci.6b00091.
(306) Reichert, E.; Wintringer, R.; Volmer, D. A.; Hempelmann, R. Electro-Catalytic Oxidative Cleavage of Lignin in a Protic Ionic Liquid. *Phys. Chem. Chem. Phys.* **2012**, *14* (15), 5214. https://doi.org/10.1039/c2cp23596j.
(307) Pollet, P.; Davey, E. A.; Ureña-Benavides, E. E.; Eckert, C. A.; Liotta, C. L. Solvents for Sustainable Chemical Processes. *Green Chem.* **2014**, *16* (3), 1034–1055. https://doi.org/10.1039/C3GC42302F.
(308) Breeden, S. W.; Clark, J. H.; Macquarrie, D. J.; Sherwood, J. Green Solvents. In *Green Techniques for Organic Synthesis and Medicinal Chemistry*; Zhang, W., Cue, B. W., Eds.; Wiley, 2012; pp 241–261. https://doi.org/10.1002/9780470711828.ch9.
(309) Mellmer, M. A.; Sener, C.; Gallo, J. M. R.; Luterbacher, J. S.; Alonso, D. M.; Dumesic, J. A. Solvent Effects in Acid-Catalyzed Biomass Conversion Reactions. *Angew. Chem. Int. Ed.* **2014**, *53* (44), 11872–11875. https://doi.org/10.1002/anie.201408359.
(310) Zhao, X.; Zhou, Z.; Luo, H.; Zhang, Y.; Liu, W.; Miao, G.; Zhu, L.; Kong, L.; Li, S.; Sun, Y. γ-Valerolactone-Introduced Controlled-Isomerization of Glucose for Lactic Acid Production over an Sn-Beta Catalyst. *Green Chem.* **2021**, *23* (7), 2634–2639. https://doi.org/10.1039/D1GC00378J.
(311) Valentini, F.; Brufani, G.; Di Erasmo, B.; Vaccaro, L. γ-Valerolactone (GVL) as a Green and Efficient Dipolar Aprotic Reaction Medium. *Curr. Opin. Green Sustainable Chem.* **2022**, *36*, 100634. https://doi.org/10.1016/j.cogsc.2022.100634.
(312) Kerkel, F.; Markiewicz, M.; Stolte, S.; Müller, E.; Kunz, W. The Green Platform Molecule Gamma-Valerolactone – Ecotoxicity, Biodegradability, Solvent Properties, and Potential Applications. *Green Chem.* **2021**, *23* (8), 2962–2976. https://doi.org/10.1039/D0GC04353B.
(313) González, G.; Ehman, N.; Felissia, F. E.; Area, M. C. Strategies towards a Green Solvent Biorefinery: Efficient Delignification of Lignocellulosic Biomass Residues by Gamma-Valerolactone/Water Catalyzed System. *Ind. Crops Prod.* **2023**, *205*, 117535. https://doi.org/10.1016/j.indcrop.2023.117535.
(314) Raj, T.; Chandrasekhar, K.; Banu, R.; Yoon, J.-J.; Kumar, G.; Kim, S.-H. Synthesis of γ-Valerolactone (GVL) and Their Applications for Lignocellulosic Deconstruction for Sustainable Green Biorefineries. *Fuel* **2021**, *303*, 121333. https://doi.org/10.1016/j.fuel.2021.121333.
(315) Umland, J.; Witkowski, S. Notes - Reaction of Silver 4-Hydroxyvalerate with Bromine. *J. Org. Chem.* **1957**, *22* (3), 345–346. https://doi.org/10.1021/jo01354a618.
(316) Wang, T.; Tao, L.; Zhu, X.; Chen, C.; Chen, W.; Du, S.; Zhou, Y.; Zhou, B.; Wang, D.; Xie, C.; Long, P.; Li, W.; Wang, Y.; Chen, R.; Zou, Y.; Fu, X.-Z.; Li, Y.; Duan, X.; Wang, S. Combined Anodic and Cathodic Hydrogen Production from Aldehyde Oxidation and Hydrogen Evolution Reaction. *Nat. Catal.* **2021**, *5* (1), 66–73. https://doi.org/10.1038/s41929-021-00721-y.

(317) NaderiNasrabadi, M.; Rakshit, S. K.; Viswanathan, G.; Chen, Z.; Harrington, P. B.; Staser, J. A. A Techno-Economic Analysis for Integrating an Electrochemical Reactor into a Lignocellulosic Biorefinery for Production of Industrial Chemicals and Hydrogen. *Appl. Biochem. Biotechnol.* **2021**, *193* (3), 791–806. https://doi.org/10.1007/s12010-020-03452-1.

(318) Hinsch, J. J.; Liu, J.; White, J. J.; Wang, Y. The Role of Steps on Silver Nanoparticles in Electrocatalytic Oxygen Reduction. *Catalysts* **2022**, *12* (6). https://doi.org/10.3390/catal12060576.

(319) Sharma, R. K.; Yadav, S.; Dutta, S.; Kale, H. B.; Warkad, I. R.; Zbořil, R.; Varma, R. S.; Gawande, M. B. Silver Nanomaterials: Synthesis and (Electro/Photo) Catalytic Applications. *Chem. Soc. Rev.* **2021**, *50* (20), 11293–11380. https://doi.org/10.1039/D0CS00912A.

(320) Ibrahim, K. B.; Tsai, M.-C.; Chala, S. A.; Berihun, M. K.; Kahsay, A. W.; Berhe, T. A.; Su, W.-N.; Hwang, B.-J. A Review of Transition Metal-Based Bifunctional Oxygen Electrocatalysts. *Journal of the Chinese Chemical Society* **2019**, *66* (8), 829–865. https://doi.org/10.1002/jccs.201900001.

(321) Wolfsgruber, M.; Patil, P.; Pichler, C. M.; Bischof, R. H.; Budnyk, S.; Paulik, C.; Rodrigues, B. V. M.; Slabon, A. Potential Dependence of Gluconic Acid to Glucose Electroreduction on Silver. *Catal. Sci. Technol.* **2023**, *13* (20), 5998–6005. https://doi.org/10.1039/D3CY00897E.

(322) Wolfsgruber, M.; Bischof, R. H.; Paulik, C.; Slabon, A.; Rodrigues, B. V. M. Revisiting the Electrocatalytic Hydrogenation of Furfural to Furfuryl Alcohol Using Biomass-Derived Electrolytes. *RSC Sustain.* **2024**, *2* (4), 1142–1153. https://doi.org/10.1039/D4SU00040D.

(323) Ma, M.; Trześniewski, B. J.; Xie, J.; Smith, W. A. Selective and Efficient Reduction of Carbon Dioxide to Carbon Monoxide on Oxide-Derived Nanostructured Silver Electrocatalysts. *Angew. Chem. Int. Ed.* **2016**, *55* (33), 9748–9752. https://doi.org/10.1002/anie.201604654.

(324) Sapouna, I.; Van Erven, G.; Heidling, E.; Lawoko, M.; McKee, L. S. Impact of Extraction Method on the Structure of Lignin from Ball-Milled Hardwood. *ACS Sustainable Chem. Eng.* **2023**, *11* (43), 15533–15543. https://doi.org/10.1021/acssuschemeng.3c02977.

(325) Luo, J.; Liu, T. L. Electrochemical Valorization of Lignin: Status, Challenges, and Prospects. *J. Bioresour. Bioprod.* **2023**, *8* (1), 1–14. https://doi.org/10.1016/j.jobab.2022.11.003.

(326) Liu, X.; Wang, Y.; Duan, H. Recent Progress in Electrocatalytic Conversion of Lignin: From Monomers, Dimers, to Raw Lignin. *Precision Chemistry* **2024**. https://doi.org/10.1021/prechem.4c00024.

(327) Margellou, A. G.; Pappa, C. P.; Psochia, E. A.; Petala, M. D.; Triantafyllidis, K. S. Mild Isolation and Characterization of Surface Lignin from Hydrothermally Pretreated Lignocellulosic Forestry and Agro-Industrial Waste Biomass. *Sustainable Chem. Pharm.* **2023**, *33*, 101056. https://doi.org/10.1016/j.scp.2023.101056.

(328) Wang, D.; Yang, H.; Yang, J.; Wang, B.; Wasnik, P.; Xu, B. B.; Shi, Z. Efficient Visible Light-Induced Photodegradation of Industrial Lignin Using Silver-CuO Catalysts Derived from Cu-Metal Organic Framework. *Adv. Compos. Hybrid Mater.* **2023**, *6* (4), 138. https://doi.org/10.1007/s42114-023-00708-2.

(329) Yoo, H.; Lee, M.-W.; Lee, S.; Lee, J.; Cho, S.; Lee, H.; Cha, H. G.; Kim, H. S. Enhancing Photocatalytic β-O-4 Bond Cleavage in Lignin Model Compounds by Silver-Exchanged Cadmium Sulfide. *ACS Catal.* **2020**, *10* (15), 8465–8475. https://doi.org/10.1021/acscatal.0c01915.

(330) Linge, J. M.; Briega-Martos, V.; Hutzler, A.; Fritsch, B.; Erikson, H.; Tammeveski, K.; Cherevko, S. Stability of Carbon Supported Silver Electrocatalysts for Alkaline Oxygen Reduction and Evolution Reactions. *ACS Appl. Energy Mater.* **2023**, *6* (22), 11497–11509. https://doi.org/10.1021/acsaem.3c01717.
(331) Khaksar, Z.; Habibi, M. F.; Arvand, M.; Rezapour, R. Improving Oxygen Reduction Reaction of Microbial Fuel Cell by Silver Vanadate Blended Functionalized Multiwall Carbon Nanotubes as Cathode. *Fuel* **2024**, *373*, 132367. https://doi.org/10.1016/j.fuel.2024.132367.
(332) Linge, J. M.; Erikson, H.; Mooste, M.; Piirsoo, H.-M.; Kaljuvee, T.; Kikas, A.; Aruväli, J.; Kisand, V.; Tamm, A.; Kannan, A. M.; Tammeveski, K. Ag Nanoparticles on Mesoporous Carbon Support as Cathode Catalyst for Anion Exchange Membrane Fuel Cell. *Int. J. Hydrogen Energy* **2023**, *48* (29), 11058–11070. https://doi.org/10.1016/j.ijhydene.2022.12.138.
(333) Ding, J.; Wei, T.; Hou, T.; Liu, W.; Liu, Q.; Zhang, H.; Luo, J.; Liu, X. Easily Constructed Porous Silver Films for Efficient Catalytic CO_2 Reduction and Zn–CO_2 Batteries. *Nanoscale* **2024**, *16* (22), 10628–10636. https://doi.org/10.1039/D4NR00340C.
(334) Poolnapol, L.; Kao-ian, W.; Somwangthanaroj, A.; Mahlendorf, F.; Nguyen, M. T.; Yonezawa, T.; Kheawhom, S. Silver Decorated Reduced Graphene Oxide as Electrocatalyst for Zinc–Air Batteries. *Energies* **2020**, *13* (2), 462. https://doi.org/10.3390/en13020462.
(335) Lu, Q.; Rosen, J.; Zhou, Y.; Hutchings, G. S.; Kimmel, Y. C.; Chen, J. G.; Jiao, F. A Selective and Efficient Electrocatalyst for Carbon Dioxide Reduction. *Nat. Commun.* **2014**, *5* (1), 3242. https://doi.org/10.1038/ncomms4242.
(336) Ibrahim, K. B.; Tsai, M.; Chala, S. A.; Berihun, M. K.; Kahsay, A. W.; Berhe, T. A.; Su, W.; Hwang, B. A Review of Transition Metal-based Bifunctional Oxygen Electrocatalysts. *J. Chin. Chem. Soc.* **2019**, *66* (8), 829–865. https://doi.org/10.1002/jccs.201900001.
(337) Prat, D.; Wells, A.; Hayler, J.; Sneddon, H.; McElroy, C. R.; Abou-Shehada, S.; Dunn, P. J. CHEM21 Selection Guide of Classical- and Less Classical-Solvents. *Green Chem.* **2016**, *18* (1), 288–296. https://doi.org/10.1039/C5GC01008J.
(338) Kozmelj, T. R.; Bartolomei, E.; Dufour, A.; Leclerc, S.; Arnoux, P.; Likozar, B.; Jasiukaitytė-Grojzdek, E.; Grilc, M.; Le Brech, Y. Oligomeric Fragments Distribution, Structure and Functionalities upon Ruthenium-Catalyzed Technical Lignin Depolymerization. *Biomass and Bioenergy* **2024**, *181*, 107056. https://doi.org/10.1016/j.biombioe.2024.107056.
(339) Vuković, J. P.; Tišma, M. The Role of NMR Spectroscopy in Lignocellulosic Biomass Characterisation: A Mini Review. *Food Chem.: Mol. Sci.* **2024**, *9*, 100219. https://doi.org/10.1016/j.fochms.2024.100219.
(340) Jiang, B.; Zhang, Y.; Guo, T.; Zhao, H.; Jin, Y. Structural Characterization of Lignin and Lignin-Carbohydrate Complex (LCC) from Ginkgo Shells (Ginkgo Biloba L.) by Comprehensive NMR Spectroscopy. *Polymers* **2018**, *10* (7), 736. https://doi.org/10.3390/polym10070736.
(341) Lu, Y.; Lu, Y.-C.; Hu, H.-Q.; Xie, F.-J.; Wei, X.-Y.; Fan, X. Structural Characterization of Lignin and Its Degradation Products with Spectroscopic Methods. *J. Spectro.* **2017**, *2017*, 1–15. https://doi.org/10.1155/2017/8951658.
(342) Sher, M.; Khan, S. A.; Shahid, S.; Javed, M.; Qamar, M. A.; Chinnathambi, A.; Almoallim, H. S. Synthesis of Novel Ternary Hybrid G-C_3N_4@Ag-ZnO Nanocomposite with Z-Scheme Enhanced Solar Light-driven Methylene Blue Degradation and Antibacterial Activities. *J. Environ. Chem. Eng.* **2021**, *9* (4), 105366. https://doi.org/10.1016/j.jece.2021.105366.

(343) Boeriu, C. G.; Bravo, D.; Gosselink, R. J. A.; Van Dam, J. E. G. Characterisation of Structure-Dependent Functional Properties of Lignin with Infrared Spectroscopy. *Ind. Crops Prod.* **2004**, *20* (2), 205–218. https://doi.org/10.1016/j.indcrop.2004.04.022.
(344) Da Cruz, M. G. A.; Onwumere, J. N.; Chen, J.; Beele, B.; Yarema, M.; Budnyk, S.; Slabon, A.; Rodrigues, B. V. M. Solvent-Free Synthesis of Photoluminescent Carbon Nanoparticles from Lignin-Derived Monomers as Feedstock. *Green Chem. Lett. Rev.* **2023**, *16* (1), 2196031. https://doi.org/10.1080/17518253.2023.2196031.
(345) Riddell, L. A.; De Peinder, P.; Polizzi, V.; Vanbroekhoven, K.; Meirer, F.; Bruijnincx, P. C. A. Predicting Molecular Weight Characteristics of Reductively Depolymerized Lignins by ATR-FTIR and Chemometrics. *ACS Sustainable Chem. Eng.* **2024**, *12* (23), 8968–8977. https://doi.org/10.1021/acssuschemeng.4c03100.
(346) Riddell, L. A.; Lindner, J. B.; De Peinder, P.; Meirer, F.; Bruijnincx, P. C. A. Rapid Lignin Thermal Property Prediction through Attenuated Total Reflectance-Infrared Spectroscopy and Chemometrics. *ChemSusChem* **2024**, *17* (9), e202301464. https://doi.org/10.1002/cssc.202301464.
(347) Lucas, F. W. S.; Grim, R. G.; Tacey, S. A.; Downes, C. A.; Hasse, J.; Roman, A. M.; Farberow, C. A.; Schaidle, J. A.; Holewinski, A. Electrochemical Routes for the Valorization of Biomass-Derived Feedstocks: From Chemistry to Application. *ACS Energy Lett.* **2021**, *6* (4), 1205–1270. https://doi.org/10.1021/acsenergylett.0c02692.
(348) Liao, Y.; Koelewijn, S.-F.; Van Den Bossche, G.; Van Aelst, J.; Van Den Bosch, S.; Renders, T.; Navare, K.; Nicolaï, T.; Van Aelst, K.; Maesen, M.; Matsushima, H.; Thevelein, J. M.; Van Acker, K.; Lagrain, B.; Verboekend, D.; Sels, B. F. A Sustainable Wood Biorefinery for Low–Carbon Footprint Chemicals Production. *Science* **2020**, *367* (6484), 1385–1390. https://doi.org/10.1126/science.aau1567.
(349) Supriyanto; Usino, D. O.; Ylitervo, P.; Dou, J.; Sipponen, M. H.; Richards, T. Identifying the Primary Reactions and Products of Fast Pyrolysis of Alkali Lignin. *J. Anal. Appl. Pyrolysis* **2020**, *151*, 104917. https://doi.org/10.1016/j.jaap.2020.104917.
(350) Curet, L.; Lafargue dit-Hauret, W.; Benet-Buchholz, J.; Martínez-Belmonte, M.; Foix, D.; Palomares, E.; Billon, L.; Begué, D.; Viterisi, A. Self-Assembled Infinite Silver Cluster with Atomic Precision as a Scalable Catalyst for CO_2 -Electroreduction under Industry-Relevant Reaction Rates. *EES Catal.* **2025**, *3* (2), 286–296. https://doi.org/10.1039/D4EY00160E.
(351) Deng, X.; Alfonso, D.; Nguyen-Phan, T.-D.; Kauffman, D. R. Breaking the Limit of Size-Dependent CO_2RR Selectivity in Silver Nanoparticle Electrocatalysts through Electronic Metal–Carbon Interactions. *ACS Catal.* **2023**, *13* (23), 15301–15309. https://doi.org/10.1021/acscatal.3c03446.
(352) Spilarewicz-Stanek, K.; Kisielewska, A.; Ginter, J.; Bałuszyńska, K.; Piwoński, I. Elucidation of the Function of Oxygen Moieties on Graphene Oxide and Reduced Graphene Oxide in the Nucleation and Growth of Silver Nanoparticles. *RSC Adv.* **2016**, *6* (65), 60056–60067. https://doi.org/10.1039/C6RA10483E.
(353) Zhao, C.; Huang, J.; Yang, L.; Yue, F.; Lu, F. Revealing Structural Differences between Alkaline and Kraft Lignins by HSQC NMR. *Ind. Eng. Chem. Res.* **2019**, *58* (14), 5707–5714. https://doi.org/10.1021/acs.iecr.9b00499.
(354) Lindenbeck, L.; Brand, S.; Stallmann, F.; Barra, V.; Frauscher, M.; Beele, B. B.; Slabon, A.; Rodrigues, B. V. M. Silver-Catalyzed Aqueous Electrochemical Valorization of Soda Lignin into Aliphatics and Phenolics. *Polymers* **2024**, *16* (23), 3325–3338. https://doi.org/10.3390/polym16233325.
(355) Li, J.; Guan, D.; Xia, S.; Fan, Y.; Zhao, K.; Zhao, Z.; Zheng, A. Recent Advances, Challenges, and Opportunities in Lignin Valorization for Value-Added Chemicals, Biofuels, and Polymeric Materials. *Energy Convers. Manage.* **2024**, *322*, 119123. https://doi.org/10.1016/j.enconman.2024.119123.

(356) Liu, Z.-H.; Liu, H.; Xu, T.; Zhao, Z.-M.; Ragauskas, A. J.; Li, B.-Z.; Yuan, J. S.; Yuan, Y.-J. Lignin Valorization Reshapes Sustainable Biomass Refining. *Renewable Sustainable Energy Rev.* **2025**, *211*, 115296. https://doi.org/10.1016/j.rser.2024.115296.
(357) Wu, Y.; Restrepo-Flórez, J. M.; Vasco-Correa, J. A Superstructure-Based Lignin Valorization Process Optimization Model for Lignocellulosic Biorefineries through Biological Upgrading. *ACS Sustainable Chem. Eng.* **2024**, *12* (18), 6913–6926. https://doi.org/10.1021/acssuschemeng.3c08213.
(358) Chettri, D.; Ahmed, S.; Malik, A. A.; Verma, A. K. Lignin Depolymerization for Its Valorization. *Bioenerg. Res.* **2023**, *16* (3), 1264–1279. https://doi.org/10.1007/s12155-022-10561-8.
(359) Bawareth, B.; Di Marino, D.; Nijhuis, T. A.; Wessling, M. Unravelling Electrochemical Lignin Depolymerization. *ACS Sustainable Chem. Eng.* **2018**, *6* (6), 7565–7573. https://doi.org/10.1021/acssuschemeng.8b00335.
(360) Slabon, A.; Rodrigues, B. V. M. To Break, or Not to Break: Is Selective Depolymerization of Lignin a Riemann Hypothesis Rather than a Solution? *Green Chem.* **2024**, *27*, 2178–2183. https://doi.org/10.1039/D4GC05439C.
(361) Han, Y.; Simmons, B. A.; Singh, S. Perspective on Oligomeric Products from Lignin Depolymerization: Their Generation, Identification, and Further Valorization. *Ind. Chem. Mater.* **2023**, *1* (2), 207–223. https://doi.org/10.1039/D2IM00059H.
(362) Yan, B.; Lin, X.; Xiao, J.; Fu, Y.; Zhang, S. Comparative Study for the Separation and Depolymerization Behavior of Lignin from Different Separation Methods. *Fuel* **2024**, *358*, 130145. https://doi.org/10.1016/j.fuel.2023.130145.
(363) Di Marino, D.; Aniko, V.; Stocco, A.; Kriescher, S.; Wessling, M. Emulsion Electro-Oxidation of Kraft Lignin. *Green Chem.* **2017**, *19* (20), 4778–4784. https://doi.org/10.1039/C7GC02115A.
(364) Ibrahim, M. N. M.; Iqbal, A.; Shen, C. C.; Bhawani, S. A.; Adam, F. Synthesis of Lignin Based Composites of TiO_2 for Potential Application as Radical Scavengers in Sunscreen Formulation. *BMC Chem.* **2019**, *13* (1), 17. https://doi.org/10.1186/s13065-019-0537-3.
(365) Faix, O. Classification of Lignins from Different Botanical Origins by FT-IR Spectroscopy. *Holzforschung* **1991**, *45* (s1), 21–28. https://doi.org/10.1515/hfsg.1991.45.s1.21.
(366) Chen, Y.; Stark, N. M.; Cai, Z.; Frihart, C. R.; Lorenz, L. F.; Ibach, R. E. Chemical Modification of Kraft Lignin: Effect on Chemical and Thermal Properties. *BioRes.* **2014**, *9* (3), 5488–5500. https://doi.org/10.15376/biores.9.3.5488-5500.
(367) Hori, Y.; Takahashi, I.; Koga, O.; Hoshi, N. Selective Formation of C2 Compounds from Electrochemical Reduction of CO_2 at a Series of Copper Single Crystal Electrodes. *J. Phys. Chem. B* **2002**, *106* (1), 15–17. https://doi.org/10.1021/jp013478d.
(368) Jeon, H. S.; Kunze, S.; Scholten, F.; Roldan Cuenya, B. Prism-Shaped Cu Nanocatalysts for Electrochemical CO_2 Reduction to Ethylene. *ACS Catal.* **2018**, *8* (1), 531–535. https://doi.org/10.1021/acscatal.7b02959.
(369) Kim, D.; Kley, C. S.; Li, Y.; Yang, P. Copper Nanoparticle Ensembles for Selective Electroreduction of CO_2 to C_2 –C_3 Products. *Proc. Natl. Acad. Sci. U.S.A.* **2017**, *114* (40), 10560–10565. https://doi.org/10.1073/pnas.1711493114.
(370) Jiménez, C.; García, J.; Camarillo, R.; Martínez, F.; Rincón, J. Electrochemical CO_2 Reduction to Fuels Using Pt/CNT Catalysts Synthesized in Supercritical Medium. *Energy Fuels* **2017**, *31* (3), 3038–3046. https://doi.org/10.1021/acs.energyfuels.6b03017.
(371) Umeda, M.; Niitsuma, Y.; Horikawa, T.; Matsuda, S.; Osawa, M. Electrochemical Reduction of CO2 to Methane on Platinum Catalysts without Overpotentials: Strategies

for Improving Conversion Efficiency. *ACS Appl. Energy Mater.* **2020**, *3* (1), 1119–1127. https://doi.org/10.1021/acsaem.9b02178.

(372) Zhu, J.; Mulder, T.; Rokicińska, A.; Lindenbeck, L. M.; Van Den Hoek, J.; Havenith, R. W. A.; V. Cunha, A.; Kuśtrowski, P.; Slabon, A.; Das, S.; Cool, P. Synergistic Interaction between the Ni-Center and Glycine-Derived N-Doped Porous Carbon Material Boosts Electrochemical CO_2 Reduction. *ACS Catal.* **2024**, *14* (14), 10987–10997. https://doi.org/10.1021/acscatal.4c00881.

(373) Hao, Q.; Zhong, H.; Wang, J.; Liu, K.; Yan, J.; Ren, Z.; Zhou, N.; Zhao, X.; Zhang, H.; Liu, D.; Liu, X.; Chen, L.; Luo, J.; Zhang, X. Nickel Dual-Atom Sites for Electrochemical Carbon Dioxide Reduction. *Nat. Synth.* **2022**, *1* (9), 719–728. https://doi.org/10.1038/s44160-022-00138-w.

(374) Lu, P.; Yang, Y.; Yao, J.; Wang, M.; Dipazir, S.; Yuan, M.; Zhang, J.; Wang, X.; Xie, Z.; Zhang, G. Facile Synthesis of Single-Nickel-Atomic Dispersed N-Doped Carbon Framework for Efficient Electrochemical CO_2 Reduction. *Appl. Catal., B* **2019**, *241*, 113–119. https://doi.org/10.1016/j.apcatb.2018.09.025.

(375) García, J.; Jiménez, C.; Martínez, F.; Camarillo, R.; Rincón, J. Electrochemical Reduction of CO_2 Using Pb Catalysts Synthesized in Supercritical Medium. *J. Catal.* **2018**, *367*, 72–80. https://doi.org/10.1016/j.jcat.2018.08.017.

(376) Meng, D.; Li, G.; Liu, Z.; Yang, F. Study of Depolymerization of Cotton Cellulose by Pb/PbO_2 Anode Electrochemical Catalysis in Sulfuric Acid Solution. *Polym. Degrad. Stab.* **2011**, *96* (7), 1173–1178. https://doi.org/10.1016/j.polymdegradstab.2011.04.021.

(377) Heijnen, J. J.; Kleerebezem, R. Bioenergetics of Microbial Growth. *Encyclopedia of bioprocess technology: Fermentation, biocatalysis, and bioseparation* **1999**, *1*, 267–291.

(378) Wolfsgruber, M.; Rodrigues, B. V. M.; Da Cruz, M. G.; Bischof, R. H.; Budnyk, S.; Beele, B.; Monti, S.; Barcaro, G.; Paulik, C.; Slabon, A. Electrocatalytic Reduction of Aldonic Acids to Aldoses on Gold Electrodes. *ACS Sustainable Chem. Eng.* **2023**, *11* (1), 312–321. https://doi.org/10.1021/acssuschemeng.2c05576.

(379) Feijóo, J.; Yang, Y.; Fonseca Guzman, M. V.; Vargas, A.; Chen, C.; Pollock, C. J.; Yang, P. *Operando* High-Energy-Resolution X-Ray Spectroscopy of Evolving Cu Nanoparticle Electrocatalysts for CO_2 Reduction. *J. Am. Chem. Soc.* **2023**, *145* (37), 20208–20213. https://doi.org/10.1021/jacs.3c08182.

(380) Mir, S. H.; Yadav, V. K.; Singh, J. K. Efficient CO_2 Capture and Activation on Novel Two-Dimensional Transition Metal Borides. *ACS Appl. Mater. Interfaces* **2022**, *14* (26), 29703–29710. https://doi.org/10.1021/acsami.2c02469.

(381) Lin, Z.; Ammal, S. C.; Denny, S. R.; Rykov, S. A.; You, K.-E.; Heyden, A.; Chen, J. G. Unraveling Unique Surface Chemistry of Transition Metal Nitrides in Controlling Selective C–O Bond Scission Pathways of Glycerol. *JACS Au* **2022**, *2* (2), 367–379. https://doi.org/10.1021/jacsau.1c00403.

(382) Sahoo, S.; Reber, A. C.; Khanna, S. N. Conceptual Basis for Understanding C–C Bond Activation in Ethane by Second Row Transition Metal Carbides. *J. Phys. Chem. A* **2015**, *119* (51), 12855–12861. https://doi.org/10.1021/acs.jpca.5b09567.

(383) Zhao, M.; Zhao, L.; Cao, J.-P.; Jiang, W.; Xie, J.-X.; Zhu, C.; Wang, S.-Y.; Wei, Y.-L.; Zhao, X.-Y.; Bai, H.-C. Water-Involved Tandem Conversion of Aryl Ethers to Alcohols over Metal Phosphide Catalyst. *Chem. Eng. J.* **2022**, *435*, 134911. https://doi.org/10.1016/j.cej.2022.134911.

(384) Peng, P.; Gao, X.-H.; Yan, Z.-F.; Mintova, S. Diffusion and Catalyst Efficiency in Hierarchical Zeolite Catalysts. *Natl. Sci. Rev.* **2020**, *7* (11), 1726–1742. https://doi.org/10.1093/nsr/nwaa184.

(385) Tang, N.; Wang, W.; You, H.; Zhai, Z.; Hilario, J.; Zeng, L.; Zhang, L. Morphology Tuning of Porous CoO Nanowall towards Enhanced Electrochemical Performance as

Supercapacitors Electrodes. *Catal. Today* **2019**, *330*, 240–245. https://doi.org/10.1016/j.cattod.2018.03.024.
(386) Liu, X.; Zhang, J.; Liu, K.; Zhang, S.; Hou, R.; Hu, X.; Zhang, P.; Shao, G. Regulation of the Pore Structure of Carbon Nanosheets Based Electrocatalyst for Efficient Polysulfides Phase Conversions. *J. Mater. Sci. Technol.* **2024**, *171*, 37–46. https://doi.org/10.1016/j.jmst.2023.07.004.
(387) Du, H.-G.; Zhang, X.-F.; Ding, L.-W.; Liu, J.-L.; Yu, L.-H.; Zhang, X.-H.; Dou, Y.; Cao, L.-M.; Zhang, J.; He, C.-T. Engineering Pore-Size Distribution of Metal-Loaded Carbon Catalysts by in Situ Cavitation for Boosting Electrochemical Mass Transfer. *Appl. Catal. B: Environ.* **2024**, *342*, 123396. https://doi.org/10.1016/j.apcatb.2023.123396.
(388) Hong, J.; Mutalik, S.; Miola, M.; Gerlach, D.; Mehrabi K., R.; Ahmadi, M.; Kooi, B. J.; Portale, G.; Rudolf, P.; Pescarmona, P. P.; Protesescu, L. Nickel Boride ($Ni_x B$) Nanocrystals: From Solid-State Synthesis to Highly Colloidally Stable Inks. *Chem. Mater.* **2023**, *35* (4), 1710–1722. https://doi.org/10.1021/acs.chemmater.2c03478.
(389) Berzelius, J. J.; Berzelius, J. J.; Tischauser, A. S.; Mulder, G. J. *Leerboek Der Scheikunde*; Leerboek der scheikunde; P.H. van den Heuvell, 1835.
(390) Carnicom, E. M.; Strychalska-Nowak, J.; Wiśniewski, P.; Kaczorowski, D.; Xie, W.; Klimczuk, T.; Cava, R. J. Superconductivity in the Superhard Boride $WB_{4.2}$. *Supercond. Sci. Technol.* **2018**, *31* (11), 115005. https://doi.org/10.1088/1361-6668/aade5a.
(391) Nagamatsu, J.; Nakagawa, N.; Muranaka, T.; Zenitani, Y.; Akimitsu, J. Superconductivity at 39 K in Magnesium Diboride. *Nature* **2001**, *410* (6824), 63–64. https://doi.org/10.1038/35065039.
(392) Togano, K.; Badica, P.; Nakamori, Y.; Orimo, S.; Takeya, H.; Hirata, K. Superconductivity in the Metal Rich Li-Pd-B Ternary Boride. *Phys. Rev. Lett.* **2004**, *93* (24), 247004. https://doi.org/10.1103/PhysRevLett.93.247004.
(393) Degiorgi, L.; Felder, E.; Ott, H. R.; Sarrao, J. L.; Fisk, Z. Low-Temperature Anomalies and Ferromagnetism of EuB 6. *Phys. Rev. Lett.* **1997**, *79* (25), 5134–5137. https://doi.org/10.1103/PhysRevLett.79.5134.
(394) Hacker, H.; Shimada, Y.; Chung, K. S. Magnetic Properties of CeB6, PrB6, EuB6, and GdB6. *Phys. Stat. Sol. (a)* **1971**, *4* (2), 459–465. https://doi.org/10.1002/pssa.2210040221.
(395) Herbst, J. F.; Croat, J. J.; Pinkerton, F. E.; Yelon, W. B. Relationships between Crystal Structure and Magnetic Properties in Nd 2 Fe 14 B. *Phys. Rev. B* **1984**, *29* (7), 4176–4178. https://doi.org/10.1103/PhysRevB.29.4176.
(396) Mori, T.; Takimoto, T.; Leithe-Jasper, A.; Cardoso-Gil, R.; Schnelle, W.; Auffermann, G.; Rosner, H.; Grin, Yu. Ferromagnetism and Electronic Structure of TmB_2. *Phys. Rev. B* **2009**, *79* (10), 104418. https://doi.org/10.1103/PhysRevB.79.104418.
(397) Croat, J. J.; Herbst, J. F.; Lee, R. W.; Pinkerton, F. E. High-Energy Product Nd-Fe-B Permanent Magnets. *Appl. Phys. Lett.* **1984**, *44* (1), 148–149. https://doi.org/10.1063/1.94584.
(398) Bsenko, L.; Lundström, T. The High-Temperature Hardness of ZrB_2 and HfB_2. *J. less-common met.* **1974**, *34* (2), 273–278. https://doi.org/10.1016/0022-5088(74)90169-6.
(399) Akopov, G.; Yeung, M. T.; Sobell, Z. C.; Turner, C. L.; Lin, C.-W.; Kaner, R. B. Superhard Mixed Transition Metal Dodecaborides. *Chem. Mater.* **2016**, *28* (18), 6605–6612. https://doi.org/10.1021/acs.chemmater.6b02632.
(400) Akopov, G.; Yeung, M. T.; Turner, C. L.; Mohammadi, R.; Kaner, R. B. Extrinsic Hardening of Superhard Tungsten Tetraboride Alloys with Group 4 Transition Metals. *J. Am. Chem. Soc.* **2016**, *138* (17), 5714–5721. https://doi.org/10.1021/jacs.6b02676.

(401) Mohammadi, R.; Lech, A. T.; Xie, M.; Weaver, B. E.; Yeung, M. T.; Tolbert, S. H.; Kaner, R. B. Tungsten Tetraboride, an Inexpensive Superhard Material. *Proc. Natl. Acad. Sci. U.S.A.* **2011**, *108* (27), 10958–10962. https://doi.org/10.1073/pnas.1102636108.
(402) Mohammadi, R.; Xie, M.; Lech, A. T.; Turner, C. L.; Kavner, A.; Tolbert, S. H.; Kaner, R. B. Toward Inexpensive Superhard Materials: Tungsten Tetraboride-Based Solid Solutions. *J. Am. Chem. Soc.* **2012**, *134* (51), 20660–20668. https://doi.org/10.1021/ja308219r.
(403) Gürsoy, M.; Takeda, M.; Albert, B. High-Pressure Densified Solid Solutions of Alkaline Earth Hexaborides (Ca/Sr, Ca/Ba, Sr/Ba) and Their High-Temperature Thermoelectric Properties. *J. Solid State Chem.* **2015**, *221*, 191–195. https://doi.org/10.1016/j.jssc.2014.10.001.
(404) Sussardi, A.; Tanaka, T.; Khan, A. U.; Schlapbach, L.; Mori, T. Enhanced Thermoelectric Properties of Samarium Boride. *J. Materiomics* **2015**, *1* (3), 196–204. https://doi.org/10.1016/j.jmat.2015.07.007.
(405) Gupta, S.; Patel, M. K.; Miotello, A.; Patel, N. Metal Boride-Based Catalysts for Electrochemical Water-Splitting: A Review. *Adv. Funct. Mater.* **2020**, *30* (1), 1906481. https://doi.org/10.1002/adfm.201906481.
(406) Gupta, S.; Patel, N.; Fernandes, R.; Hanchate, S.; Miotello, A.; Kothari, D. C. Co-Mo-B Nanoparticles as a Non-Precious and Efficient Bifunctional Electrocatalyst for Hydrogen and Oxygen Evolution. *Electrochim. Acta* **2017**, *232*, 64–71. https://doi.org/10.1016/j.electacta.2017.02.100.
(407) Jiang, B.; Song, H.; Kang, Y.; Wang, S.; Wang, Q.; Zhou, X.; Kani, K.; Guo, Y.; Ye, J.; Li, H.; Sakka, Y.; Henzie, J.; Yusuke, Y. A Mesoporous Non-Precious Metal Boride System: Synthesis of Mesoporous Cobalt Boride by Strictly Controlled Chemical Reduction. *Chem. Sci.* **2020**, *11* (3), 791–796. https://doi.org/10.1039/C9SC04498A.
(408) Li, Y.; Xu, H.; Huang, H.; Gao, L.; Zhao, Y.; Ma, T. Synthesis of Co–B in Porous Carbon Using a Metal–Organic Framework (MOF) Precursor: A Highly Efficient Catalyst for the Oxygen Evolution Reaction. *Electrochem. Commun.* **2018**, *86*, 140–144. https://doi.org/10.1016/j.elecom.2017.12.011.
(409) Li, H.; Yang, H.; Li, H. Highly Active Mesoporous Co–B Amorphous Alloy Catalyst for Cinnamaldehyde Hydrogenation to Cinnamyl Alcohol. *J. Catal.* **2007**, *251* (1), 233–238. https://doi.org/10.1016/j.jcat.2007.07.022.
(410) Masa, J.; Weide, P.; Peeters, D.; Sinev, I.; Xia, W.; Sun, Z.; Somsen, C.; Muhler, M.; Schuhmann, W. Amorphous Cobalt Boride (Co_2B) as a Highly Efficient Nonprecious Catalyst for Electrochemical Water Splitting: Oxygen and Hydrogen Evolution. *Adv. Energy Mater.* **2016**, *6* (6), 1502313. https://doi.org/10.1002/aenm.201502313.
(411) Hong, J.; Mutalik, S.; Pescarmona, P. P.; Protesescu, L. Metal Borides: From Industrial Classics to Versatile Colloidal Nanocrystals for Energy, Catalysis, and Hard Coatings Applications. *Chem. Mater.* **2024**, *36* (5), 2147–2164. https://doi.org/10.1021/acs.chemmater.3c03029.
(412) Gupta, S.; Patel, N.; Fernandes, R.; Kadrekar, R.; Dashora, A.; Yadav, A. K.; Bhattacharyya, D.; Jha, S. N.; Miotello, A.; Kothari, D. C. Co–Ni–B Nanocatalyst for Efficient Hydrogen Evolution Reaction in Wide pH Range. *Appl. Catal., B* **2016**, *192*, 126–133. https://doi.org/10.1016/j.apcatb.2016.03.032.
(413) Yang, Y.; Zhuang, L.; Rufford, T. E.; Wang, S.; Zhu, Z. Efficient Water Oxidation with Amorphous Transition Metal Boride Catalysts Synthesized by Chemical Reduction of Metal Nitrate Salts at Room Temperature. *RSC Adv.* **2017**, *7* (52), 32923–32930. https://doi.org/10.1039/C7RA02558K.
(414) Nsanzimana, J. M. V.; Peng, Y.; Xu, Y. Y.; Thia, L.; Wang, C.; Xia, B. Y.; Wang, X. An Efficient and Earth-Abundant Oxygen-Evolving Electrocatalyst Based on

Amorphous Metal Borides. *Adv. Energy Mater.* **2018**, *8* (1), 1701475. https://doi.org/10.1002/aenm.201701475.

(415) Chen, H.; Ouyang, S.; Zhao, M.; Li, Y.; Ye, J. Synergistic Activity of Co and Fe in Amorphous Co *x* –Fe–B Catalyst for Efficient Oxygen Evolution Reaction. *ACS Appl. Mater. Interfaces* **2017**, *9* (46), 40333–40343. https://doi.org/10.1021/acsami.7b13939.

(416) Ma, X.; Wen, J.; Zhang, S.; Yuan, H.; Li, K.; Yan, F.; Zhang, X.; Chen, Y. Crystal Co_xB(x = 1–3) Synthesized by a Ball-Milling Method as High-Performance Electrocatalysts for the Oxygen Evolution Reaction. *ACS Sustainable Chem. Eng.* **2017**, *5* (11), 10266–10274. https://doi.org/10.1021/acssuschemeng.7b02281.

(417) Zieschang, A.-M.; Bocarsly, J. D.; Schuch, J.; Reichel, C. V.; Kaiser, B.; Jaegermann, W.; Seshadri, R.; Albert, B. Magnetic and Electrocatalytic Properties of Nanoscale Cobalt Boride, Co_3B. *Inorg. Chem.* **2019**, *58* (24), 16609–16617. https://doi.org/10.1021/acs.inorgchem.9b02617.

(418) Xu, X.; Deng, Y.; Gu, M.; Sun, B.; Liang, Z.; Xue, Y.; Guo, Y.; Tian, J.; Cui, H. Large-Scale Synthesis of Porous Nickel Boride for Robust Hydrogen Evolution Reaction Electrocatalyst. *Appl. Surf. Sci.* **2019**, *470*, 591–595. https://doi.org/10.1016/j.apsusc.2018.11.127.

(419) Arivu, M.; Masud, J.; Umapathi, S.; Nath, M. Facile Synthesis of Ni_3B/rGO Nanocomposite as an Efficient Electrocatalyst for the Oxygen Evolution Reaction in Alkaline Media. *Electrochem. Commun.* **2018**, *86*, 121–125. https://doi.org/10.1016/j.elecom.2017.12.002.

(420) Park, H.; Encinas, A.; Scheifers, J. P.; Zhang, Y.; Fokwa, B. P. T. Boron-Dependency of Molybdenum Boride Electrocatalysts for the Hydrogen Evolution Reaction. *Angew. Chem. Int. Ed.* **2017**, *56* (20), 5575–5578. https://doi.org/10.1002/anie.201611756.

(421) Okamoto, Y.; Nitta, Y.; Imanaka, T.; Teranishi, S. Surface Characterisation of Nickel Boride and Nickel Phosphide Catalysts by X-Ray Photoelectron Spectroscopy. *J. Chem. Soc., Faraday Trans. 1* **1979**, *75* (0), 2027. https://doi.org/10.1039/f19797502027.

(422) Carenco, S.; Portehault, D.; Boissière, C.; Mézailles, N.; Sanchez, C. Nanoscaled Metal Borides and Phosphides: Recent Developments and Perspectives. *Chem. Rev.* **2013**, *113* (10), 7981–8065. https://doi.org/10.1021/cr400020d.

(423) Ningthoujam, R. S.; Gajbhiye, N. S. Synthesis, Electron Transport Properties of Transition Metal Nitrides and Applications. *Prog. Mater Sci.* **2015**, *70*, 50–154. https://doi.org/10.1016/j.pmatsci.2014.11.004.

(424) Sher Shah, Md. S. A.; Jang, G. Y.; Zhang, K.; Park, J. H. Transition Metal Carbide-based Nanostructures for Electrochemical Hydrogen and Oxygen Evolution Reactions. *EcoEnergy* **2023**, *1* (2), 344–374. https://doi.org/10.1002/ece2.18.

(425) Weng, C.; Ren, J.; Yuan, Z. Transition Metal Phosphide-Based Materials for Efficient Electrochemical Hydrogen Evolution: A Critical Review. *ChemSusChem* **2020**, *13* (13), 3357–3375. https://doi.org/10.1002/cssc.202000416.

(426) Pu, Z.; Liu, T.; Zhang, G.; Liu, X.; Gauthier, Marc. A.; Chen, Z.; Sun, S. Nanostructured Metal Borides for Energy-Related Electrocatalysis: Recent Progress, Challenges, and Perspectives. *Small Methods* **2021**, *5* (10), 2100699. https://doi.org/10.1002/smtd.202100699.

(427) Zhou, Y.; Che, F.; Liu, M.; Zou, C.; Liang, Z.; De Luna, P.; Yuan, H.; Li, J.; Wang, Z.; Xie, H.; Li, H.; Chen, P.; Bladt, E.; Quintero-Bermudez, R.; Sham, T.-K.; Bals, S.; Hofkens, J.; Sinton, D.; Chen, G.; Sargent, E. H. Dopant-Induced Electron Localization Drives CO2 Reduction to C2 Hydrocarbons. *Nature Chem.* **2018**, *10* (9), 974–980. https://doi.org/10.1038/s41557-018-0092-x.

(428) Ashraf, I.; Rizwan, S.; Iqbal, M. A Comprehensive Review on the Synthesis and Energy Applications of Nano-Structured Metal Nitrides. *Front. Mater.* **2020**, *7*, 181. https://doi.org/10.3389/fmats.2020.00181.

(429) Porter, W. N.; Turaczy, K. K.; Yu, M.; Mou, H.; Chen, J. G. Transition Metal Nitride Catalysts for Selective Conversion of Oxygen-Containing Molecules. *Chem. Sci.* **2024**, *15* (18), 6622–6642. https://doi.org/10.1039/D4SC01314J.
(430) Sajkowski, D. J.; Oyama, S. T. Catalytic Hydrotreating by Molybdenum Carbide and Nitride: Unsupported Mo_2N and $Mo_2CAl_2O_3$. *Appl. Catal., A* **1996**, *134* (2), 339–349. https://doi.org/10.1016/0926-860X(95)00202-2.
(431) Denny, S. R.; Lin, Z.; Porter, W. N.; Artrith, N.; Chen, J. G. Machine Learning Prediction and Experimental Verification of Pt-Modified Nitride Catalysts for Ethanol Reforming with Reduced Precious Metal Loading. *Appl. Catal., B* **2022**, *312*, 121380. https://doi.org/10.1016/j.apcatb.2022.121380.
(432) Qin, T.; Wang, Z.; Wang, Y.; Besenbacher, F.; Otyepka, M.; Dong, M. Recent Progress in Emerging Two-Dimensional Transition Metal Carbides. *Nano-Micro Lett.* **2021**, *13* (1), 183. https://doi.org/10.1007/s40820-021-00710-7.
(433) Lin, Z.; Chen, R.; Qu, Z.; Chen, J. G. Hydrodeoxygenation of Biomass-Derived Oxygenates over Metal Carbides: From Model Surfaces to Powder Catalysts. *Green Chem.* **2018**, *20* (12), 2679–2696. https://doi.org/10.1039/C8GC00239H.
(434) Chan-Thaw, C.; Villa, A. Metal Carbides for Biomass Valorization. *Appl. Sci.* **2018**, *8* (2), 259. https://doi.org/10.3390/app8020259.
(435) Akmach, D.; Bathla, S.; Tran, C.-C.; Kaliaguine, S.; Mushrif, S. H. Transition Metal Carbide Catalysts for Upgrading Lignocellulosic Biomass-Derived Oxygenates: A Review of the Experimental and Computational Investigations into Structure-Property Relationships. *Catal. Today* **2023**, *423*, 114285. https://doi.org/10.1016/j.cattod.2023.114285.
(436) Mai, E. F.; Machado, M. A.; Davies, T. E.; Lopez-Sanchez, J. A.; Teixeira Da Silva, V. Molybdenum Carbide Nanoparticles within Carbon Nanotubes as Superior Catalysts for γ-Valerolactone Production via Levulinic Acid Hydrogenation. *Green Chem.* **2014**, *16* (9), 4092–4097. https://doi.org/10.1039/C4GC00920G.
(437) Ma, X.; Ma, R.; Hao, W.; Chen, M.; Yan, F.; Cui, K.; Tian, Y.; Li, Y. Common Pathways in Ethanolysis of Kraft Lignin to Platform Chemicals over Molybdenum-Based Catalysts. *ACS Catal.* **2015**, *5* (8), 4803–4813. https://doi.org/10.1021/acscatal.5b01159.
(438) Ma, R.; Hao, W.; Ma, X.; Tian, Y.; Li, Y. Catalytic Ethanolysis of Kraft Lignin into High-Value Small-Molecular Chemicals over a Nanostructured α-Molybdenum Carbide Catalyst. *Angew. Chem. Int. Ed.* **2014**, *126* (28), 7438–7443. https://doi.org/10.1002/ange.201402752.
(439) Broil, S.; Jeitschko, W. The Ternary Rare Earth Chromium Nitrides Ce_2CrN_3 and $Ln_3Cr_{10-x}N_1$ with Ln = La, Ce, Pr. *Z. Naturforsch.* **1995**, *50* (6), 905–912. https://doi.org/10.1515/znb-1995-0612.
(440) Woike, M.; Jeitschko, W. Preparation and Crystal Structure of the Nitridosilicates $Ln_3Si_6N_{11}$ (Ln = La, Ce, Pr, Nd, Sm) and $LnSi_3N_5$ (Ln = Ce, Pr, Nd). *Inorg. Chem.* **1995**, *34* (21), 5105–5108. https://doi.org/10.1021/ic00125a005.
(441) Vomhof, T.; Pöttgen, R.; Jeitschko, W. Magnetic Properties of the Carbides Ln_3C_4 (Ln ≡ Ho-Lu) and $Y_3B_{0.2}C_{3.8}$ with Sc_3C_4-Type Structure. *J. less-common met.* **1991**, *171* (1), 95–99. https://doi.org/10.1016/0022-5088(91)90266-7.
(442) Poettgen, R.; Jeitschko, W. Scandium Carbide, Sc_3C_4, a Carbide with C_3 Units Derived from Propadiene. *Inorg. Chem.* **1991**, *30* (3), 427–431. https://doi.org/10.1021/ic00003a013.
(443) Gesing, T.-M.; Pöttgen, R.; Jeitschko, W.; Wortmann, U. Crystal Structure and Physical Properties of the Carbides UAl_3C_3 and $YbAl_3C_3$. *J. Alloys Compd.* **1992**, *186* (2), 321–331. https://doi.org/10.1016/0925-8388(92)90019-6.

(444) Naguib, M.; Kurtoglu, M.; Presser, V.; Lu, J.; Niu, J.; Heon, M.; Hultman, L.; Gogotsi, Y.; Barsoum, M. W. Two-Dimensional Nanocrystals Produced by Exfoliation of Ti_3AlC_2. *Adv. Mater.* **2011**, *23* (37), 4248–4253. https://doi.org/10.1002/adma.201102306.
(445) Gogotsi, Y.; Anasori, B. The Rise of MXenes. *ACS Nano* **2019**, *13* (8), 8491–8494. https://doi.org/10.1021/acsnano.9b06394.
(446) Jin, D.; Johnson, L. R.; Raman, A. S.; Ming, X.; Gao, Y.; Du, F.; Wei, Y.; Chen, G.; Vojvodic, A.; Gogotsi, Y.; Meng, X. Computational Screening of 2D Ordered Double Transition-Metal Carbides (MXenes) as Electrocatalysts for Hydrogen Evolution Reaction. *J. Phys. Chem. C* **2020**, *124* (19), 10584–10592. https://doi.org/10.1021/acs.jpcc.0c01460.
(447) Oefner, N.; Shuck, C. E.; Schumacher, L.; Heck, F.; Hofmann, K.; Schmidpeter, J.; Li, W.; Bahri, M.; Mehdi, B. L.; Drochner, A.; Albert, B.; Hess, C.; Gogotsi, Y.; Etzold, B. J. M. MXene Aerogel Derived Ultra-Active Vanadia Catalyst for Selective Conversion of Sustainable Alcohols to Base Chemicals. *ACS Appl. Mater. Interfaces* **2023**, *15* (13), 16714–16722. https://doi.org/10.1021/acsami.2c22720.
(448) Von Schnering, H. G.; Hoenle, W. Chemistry and Structural Chemistry of Phosphides and Polyphosphides. 48. Bridging Chasms with Polyphosphides. *Chem. Rev.* **1988**, *88* (1), 243–273. https://doi.org/10.1021/cr00083a012.
(449) Li, S.-H.; Qi, M.-Y.; Tang, Z.-R.; Xu, Y.-J. Nanostructured Metal Phosphides: From Controllable Synthesis to Sustainable Catalysis. *Chem. Soc. Rev.* **2021**, *50* (13), 7539–7586. https://doi.org/10.1039/D1CS00323B.
(450) Lu, X.; Yan, K.; Yu, Z.; Wang, J.; Liu, R.; Zhang, R.; Qiao, Y.; Xiong, J. Transition Metal Phosphides: Synthesis Nanoarchitectonics, Catalytic Properties, and Biomass Conversion Applications. *ChemSusChem* **2024**, *17* (10), e202301687. https://doi.org/10.1002/cssc.202301687.
(451) Bhunia, K.; Chandra, M.; Kumar Sharma, S.; Pradhan, D.; Kim, S.-J. A Critical Review on Transition Metal Phosphide Based Catalyst for Electrochemical Hydrogen Evolution Reaction: Gibbs Free Energy, Composition, Stability, and True Identity of Active Site. *Coord. Chem. Rev.* **2023**, *478*, 214956. https://doi.org/10.1016/j.ccr.2022.214956.
(452) Lv, Y.; Wang, X. Nonprecious Metal Phosphides as Catalysts for Hydrogen Evolution, Oxygen Reduction and Evolution Reactions. *Catal. Sci. Technol.* **2017**, *7* (17), 3676–3691. https://doi.org/10.1039/C7CY00715A.
(453) Huang, C.-J.; Xu, H.-M.; Shuai, T.-Y.; Zhan, Q.-N.; Zhang, Z.-J.; Li, G.-R. A Review of Modulation Strategies for Improving Catalytic Performance of Transition Metal Phosphides for Oxygen Evolution Reaction. *Appl. Catal., B* **2023**, *325*, 122313. https://doi.org/10.1016/j.apcatb.2022.122313.
(454) Wu, W.; Luo, S.; Huang, Y.; He, H.; Shen, P. K.; Zhu, J. Recent Advances in Transition Metal Phosphide-Based Heterostructure Electrocatalysts for the Oxygen Evolution Reaction. *Mater. Chem. Front.* **2024**, *8* (4), 1064–1083. https://doi.org/10.1039/D3QM00793F.
(455) Yu, Y.; Ma, J.; Chen, C.; Fu, Y.; Wang, Y.; Li, K.; Liao, Y.; Zheng, L.; Zuo, X. General Method for Synthesis Transition-Metal Phosphide/Nitrogen and Phosphide Doped Carbon Materials with Yolk-Shell Structure for Oxygen Reduction Reaction. *ChemCatChem* **2019**, *11* (6), 1722–1731. https://doi.org/10.1002/cctc.201801935.
(456) Li, K.; Wang, R.; Chen, J. Hydrodeoxygenation of Anisole over Silica-Supported Ni_2P, MoP, and NiMoP Catalysts. *Energy Fuels* **2011**, *25* (3), 854–863. https://doi.org/10.1021/ef101258j.
(457) Duan, X.; Teng, Y.; Wang, A.; Kogan, V.; Li, X.; Wang, Y. Role of Sulfur in Hydrotreating Catalysis over Nickel Phosphide. *J. Catal.* **2009**, *261* (2), 232–240. https://doi.org/10.1016/j.jcat.2008.12.003.

(458) Bowker, R. H.; Smith, M. C.; Pease, M. L.; Slenkamp, K. M.; Kovarik, L.; Bussell, M. E. Synthesis and Hydrodeoxygenation Properties of Ruthenium Phosphide Catalysts. *ACS Catal.* **2011**, *1* (8), 917–922. https://doi.org/10.1021/cs200238v.
(459) Robinson, A. M.; Hensley, J. E.; Medlin, J. W. Bifunctional Catalysts for Upgrading of Biomass-Derived Oxygenates: A Review. *ACS Catal.* **2016**, *6* (8), 5026–5043. https://doi.org/10.1021/acscatal.6b00923.
(460) Fujita, S.; Nakajima, K.; Yamasaki, J.; Mizugaki, T.; Jitsukawa, K.; Mitsudome, T. Unique Catalysis of Nickel Phosphide Nanoparticles to Promote the Selective Transformation of Biofuranic Aldehydes into Diketones in Water. *ACS Catal.* **2020**, *10* (7), 4261–4267. https://doi.org/10.1021/acscatal.9b05120.
(461) Xu, M.; Xu, Y.; Liu, Y.; Zhao, D.; Ding, S.; Chen, C. NiyCo2-yP Alloy Catalysts with Assistance of Y for Boosting Low-Pressure Hydrogenation Transformation of Biomass-Derived Levulinic Acid or Furfural in Water. *Appl. Surf. Sci.* **2022**, *601*, 154142. https://doi.org/10.1016/j.apsusc.2022.154142.
(462) Chen, J.-Y.; Xiao, Y.; Guo, F.-S.; Li, K.-M.; Huang, Y.-B.; Lu, Q. Single-Atom Metal Catalysts for Catalytic Chemical Conversion of Biomass to Chemicals and Fuels. *ACS Catal.* **2024**, *14* (7), 5198–5226. https://doi.org/10.1021/acscatal.4c00208.
(463) Wang, W.; Li, S.; Qiang, Q.; Wu, K.; Pan, X.; Su, W.; Cai, J.; Shen, Z.; Yang, Y.; Li, C.; Zhang, T. Catalytic Refining Lignin-Derived Monomers: Seesaw Effect between Nanoparticle and Single-Atom Pt. *Angew. Chem. Int. Ed.* **2024**, *63* (34), e202404683. https://doi.org/10.1002/anie.202404683.
(464) Wu, Z.; Wang, T.; Zhao, Z.; Ji, Y.; Bai, H.; Jiang, Y.; Wang, X.; Nawaz, H.; He, A.; Xia, J.; Xu, J.; Chen, S.; Hu, L. Niobium-Based Single-Atom Catalyst Promoted Fractionation of Lignocellulose in Choline Chloride-Lactic Acid Deep Eutectic Solvent. *Int. J. Biol. Macromol.* **2024**, *269*, 132055. https://doi.org/10.1016/j.ijbiomac.2024.132055.
(465) Yang, H. B.; Hung, S.-F.; Liu, S.; Yuan, K.; Miao, S.; Zhang, L.; Huang, X.; Wang, H.-Y.; Cai, W.; Chen, R.; Gao, J.; Yang, X.; Chen, W.; Huang, Y.; Chen, H. M.; Li, C. M.; Zhang, T.; Liu, B. Atomically Dispersed Ni(i) as the Active Site for Electrochemical CO2 Reduction. *Nat. Energy* **2018**, *3* (2), 140–147. https://doi.org/10.1038/s41560-017-0078-8.
(466) Lin, F.; Xu, M.; Ramasamy, K. K.; Li, Z.; Klinger, J. L.; Schaidle, J. A.; Wang, H. Catalyst Deactivation and Its Mitigation during Catalytic Conversions of Biomass. *ACS Catal.* **2022**, *12* (21), 13555–13599. https://doi.org/10.1021/acscatal.2c02074.
(467) Argyle, M.; Bartholomew, C. Heterogeneous Catalyst Deactivation and Regeneration: A Review. *Catalysts* **2015**, *5* (1), 145–269. https://doi.org/10.3390/catal5010145.
(468) Bartholomew, C. H. Mechanisms of Catalyst Deactivation. *Appl. Catal. A: Gen.* **2001**, *212* (1–2), 17–60. https://doi.org/10.1016/S0926-860X(00)00843-7.
(469) Shah, M. A.; Farooq, W.; Shahnaz, T.; Akilarasan, M. Bioenergy and Value-Added Chemicals Derived Through Electrocatalytic Upgradation of Biomass: A Critical Review. *Bioenerg. Res.* **2024**. https://doi.org/10.1007/s12155-024-10797-6.
(470) Pan, H.; Xu, D.; He, C.; Shen, C. In Situ Regeneration and Deactivation of Co-Zn/H-Beta Catalysts in Catalytic Reduction of NOx with Propane. *Catalysts* **2018**, *9* (1), 23. https://doi.org/10.3390/catal9010023.
(471) Xie, C.; Chen, C.; Yu, Y.; Su, J.; Li, Y.; Somorjai, G. A.; Yang, P. Tandem Catalysis for CO_2 Hydrogenation to C_2–C_4 Hydrocarbons. *Nano Lett.* **2017**, *17* (6), 3798–3802. https://doi.org/10.1021/acs.nanolett.7b01139.
(472) Wu, J.; Wang, H.; Liu, N.; Jia, B.; Zheng, J. High-Entropy Materials in Electrocatalysis: Understanding, Design, and Development. *Small* **2024**, *20* (43), 2403162. https://doi.org/10.1002/smll.202403162.

(473) Folgueras, M. C.; Jiang, Y.; Jin, J.; Yang, P. High-Entropy Halide Perovskite Single Crystals Stabilized by Mild Chemistry. *Nature* **2023**, *621* (7978), 282–288. https://doi.org/10.1038/s41586-023-06396-8.
(474) Hao, J.; Zhuang, Z.; Cao, K.; Gao, G.; Wang, C.; Lai, F.; Lu, S.; Ma, P.; Dong, W.; Liu, T.; Du, M.; Zhu, H. Unraveling the Electronegativity-Dominated Intermediate Adsorption on High-Entropy Alloy Electrocatalysts. *Nat. Commun.* **2022**, *13* (1), 2662. https://doi.org/10.1038/s41467-022-30379-4.
(475) Ren, J.-T.; Chen, L.; Wang, H.-Y.; Yuan, Z.-Y. High-Entropy Alloys in Electrocatalysis: From Fundamentals to Applications. *Chem. Soc. Rev.* **2023**, *52* (23), 8319–8373. https://doi.org/10.1039/D3CS00557G.
(476) Yan, X.; Zhang, Y. Functional Properties and Promising Applications of High Entropy Alloys. *Scr. Mater.* **2020**, *187*, 188–193. https://doi.org/10.1016/j.scriptamat.2020.06.017.
(477) Ren, X.; Li, Y.; Qi, Y.; Wang, B. Review on Preparation Technology and Properties of Refractory High Entropy Alloys. *Materials* **2022**, *15* (8), 2931. https://doi.org/10.3390/ma15082931.
(478) Smith, S. M.; Fahrenholtz, W. G.; Hilmas, G. E. Pressureless Sintering of High-Entropy Boride Ceramics. *J. Eur. Ceram. Soc.* **2023**, *43* (12), 5168–5173. https://doi.org/10.1016/j.jeurceramsoc.2023.04.050.
(479) Zhao, L.; Sun, X.; Zeng, X.; Li, Y.; Fang, W.; Du, X.; He, X.; Wang, D.; Li, W.; Chen, H. Synthesis of a New Class of High-Entropy Nitride Ceramics and the Effects of Nitrogen Vacancies on Their Magnetic Properties. *Appl. Surf. Sci.* **2023**, *618*, 156543. https://doi.org/10.1016/j.apsusc.2023.156543.
(480) Wu, P.; Deng, C.; Liu, P.; Liu, F.; Chen, L.; Wang, B.; Zhu, W.; Xu, C. An Ultra-Stable High Entropy Metal Nitride for Aerobic Oxidative Desulfurization and Source Recovery of Aromatic Sulfides from Fuel Oils. *J. Chem. Eng.* **2023**, *474*, 145850. https://doi.org/10.1016/j.cej.2023.145850.
(481) Zhu, L.; Li, C.; Zheng, R.; Cheng, W.; He, Y.; Gong, C.; Liu, M.; Huang, Y.; Zhu, X.; Sun, Y. Design of High-Entropy Antiperovskite Metal Nitrides as Highly Efficient Electrocatalysts for Oxygen Evolution Reaction. *Int. J. Hydrog. Energy.* **2024**, *51*, 638–647. https://doi.org/10.1016/j.ijhydene.2023.07.011.
(482) Chen, P.; Zhong, W.; Gong, Z.; Cao, Q.; Tang, H.; Chu, Y.; Chen, Y. High Entropy Borides as Efficient Catalysts for Electrochemical Reduction of Nitrate to Ammonia. *Catal. Today* **2024**, *439*, 114809. https://doi.org/10.1016/j.cattod.2024.114809.
(483) Tong, X.; Zheng, J.; Xue, S.; Guo, S. High-Entropy Materials as the Catalysts for Valorization of Biomass and Biomass-Derived Platform Compounds. *ACS Sustain. Chem. Eng.* **2023**, *11* (28), 10203–10218. https://doi.org/10.1021/acssuschemeng.3c01602.
(484) Dai, J.; Patti, A. F.; Saito, K. Recent Developments in Chemical Degradation of Lignin: Catalytic Oxidation and Ionic Liquids. *Tetrahedron Lett.* **2016**, *57* (45), 4945–4951. https://doi.org/10.1016/j.tetlet.2016.09.084.
(485) Ardiyanti, A. R.; Khromova, S. A.; Venderbosch, R. H.; Yakovlev, V. A.; Heeres, H. J. Catalytic Hydrotreatment of Fast-Pyrolysis Oil Using Non-Sulfided Bimetallic Ni-Cu Catalysts on a δ-Al_2O_3 Support. *Appl. Catal., B* **2012**, *117–118*, 105–117. https://doi.org/10.1016/j.apcatb.2011.12.032.
(486) Brix, A. C.; Krysiak, O. A.; Cechanaviciutė, I. A.; Bjelovučić, G.; Banko, L.; Ludwig, A.; Schuhmann, W. Oxidative Depolymerisation of Kraft Lignin: From Fabrication of Multi-Metal-Modified Electrodes For Vanillin Electrogeneration via Pulse Electrolysis To High-Throughput Screening of Multi-Metal Composites. *ChemElectroChem* **2024**, *11* (3), e202300483. https://doi.org/10.1002/celc.202300483.

(487) Tamtaji, M.; Kim, M. G.; Wang, J.; Galligan, P. R.; Zhu, H.; Hung, F.; Xu, Z.; Zhu, Y.; Luo, Z.; Goddard, W. A.; Chen, G. A High-Entropy Single-Atom Catalyst Toward Oxygen Reduction Reaction in Acidic and Alkaline Conditions. *Adv. Sci.* **2024**, *11* (26), 2309883. https://doi.org/10.1002/advs.202309883.

(488) Liu, J.; Deng, C.; Liu, X.; Shao, S.; Zheng, P.; Chen, L.; Wu, P.; Li, H.; Ji, H.; Zhu, W. Single Mo Atoms Stabilized on High-Entropy Perovskite Oxide: A Frontier for Aerobic Oxidative Desulfurization. *Inorg. Chem.* **2023**, *62* (28), 11044–11055. https://doi.org/10.1021/acs.inorgchem.3c01085.

(489) Xu, H.; Zhang, Z.; Liu, J.; Do-Thanh, C.-L.; Chen, H.; Xu, S.; Lin, Q.; Jiao, Y.; Wang, J.; Wang, Y.; Chen, Y.; Dai, S. Entropy-Stabilized Single-Atom Pd Catalysts via High-Entropy Fluorite Oxide Supports. *Nat. Commun.* **2020**, *11* (1), 3908. https://doi.org/10.1038/s41467-020-17738-9.

(490) Yang, Y.; Xiong, Y.; Zeng, R.; Lu, X.; Krumov, M.; Huang, X.; Xu, W.; Wang, H.; DiSalvo, F. J.; Brock, Joel. D.; Muller, D. A.; Abruña, H. D. *Operando* Methods in Electrocatalysis. *ACS Catal.* **2021**, *11* (3), 1136–1178. https://doi.org/10.1021/acscatal.0c04789.

(491) Shan, Y.; Zhao, X.; Fonseca Guzman, M.; Jana, A.; Chen, S.; Yu, S.; Ng, K. C.; Roh, I.; Chen, H.; Altoe, V.; Gilbert Corder, S. N.; Bechtel, H. A.; Qian, J.; Salmeron, M. B.; Yang, P. Nanometre-Resolved Observation of Electrochemical Microenvironment Formation at the Nanoparticle–Ligand Interface. *Nat. Catal.* **2024**, *7* (4), 422–431. https://doi.org/10.1038/s41929-024-01119-2.

(492) Yang, Y.; Feijóo, J.; Briega-Martos, V.; Li, Q.; Krumov, M.; Merkens, S.; De Salvo, G.; Chuvilin, A.; Jin, J.; Huang, H.; Pollock, C. J.; Salmeron, M. B.; Wang, C.; Muller, D. A.; Abruña, H. D.; Yang, P. Operando Methods: A New Era of Electrochemistry. *Curr. Opin. Electrochem.* **2023**, *42*, 101403. https://doi.org/10.1016/j.coelec.2023.101403.

(493) Ito, Y.; Lee, C.; Miyahara, Y.; Miyazaki, K.; Abe, T. *Operando* Raman Spectroscopy Insights into the Electrochemical Formation of F-Graphite Intercalation Compounds. *ACS Energy Lett.* **2024**, *9* (4), 1473–1479. https://doi.org/10.1021/acsenergylett.4c00130.

(494) Liu, Y.; Wang, L.; Hübner, R.; Kresse, J.; Zhang, X.; Deconinick, M.; Vaynzof, Y.; Weidinger, I. M.; Eychmüller, A. Cobalt-based $Co_3Mo_3N/Co_4N/Co$ Metallic Heterostructure as a Highly Active Electrocatalyst for Alkaline Overall Water Splitting. *Angew. Chem. Int. Ed.* **2024**, *63* (14), e202319239. https://doi.org/10.1002/anie.202319239.

(495) Zhu, D. D.; Liu, J. L.; Qiao, S. Z. Recent Advances in Inorganic Heterogeneous Electrocatalysts for Reduction of Carbon Dioxide. *Adv. Mater.* **2016**, *28* (18), 3423–3452. https://doi.org/10.1002/adma.201504766.

(496) Montoya, J. H.; Seitz, L. C.; Chakthranont, P.; Vojvodic, A.; Jaramillo, T. F.; Nørskov, J. K. Materials for Solar Fuels and Chemicals. *Nature Mater.* **2017**, *16* (1), 70–81. https://doi.org/10.1038/nmat4778.

(497) Bushuyev, O. S.; De Luna, P.; Dinh, C. T.; Tao, L.; Saur, G.; Van De Lagemaat, J.; Kelley, S. O.; Sargent, E. H. What Should We Make with CO_2 and How Can We Make It? *Joule* **2018**, *2* (5), 825–832. https://doi.org/10.1016/j.joule.2017.09.003.

(498) De Luna, P.; Hahn, C.; Higgins, D.; Jaffer, S. A.; Jaramillo, T. F.; Sargent, E. H. What Would It Take for Renewably Powered Electrosynthesis to Displace Petrochemical Processes? *Science* **2019**, *364* (6438), eaav3506. https://doi.org/10.1126/science.aav3506.

(499) Lin, Z.; Chang, Y.; Chen, Y.; Hsu, Y.; Peng, K.; Hung, S. *Operando* Studies for CO_2/CO Reduction in Flow-Based Devices. *ChemNanoMat* **2024**, *10* (7), e202400070. https://doi.org/10.1002/cnma.202400070.

(500) *X-Ray Absorption: Principles, Applications, Techniques of EXAFS, SEXAFS and XANES*; Koningsberger, D. C., Ed.; Chemical analysis; Wiley: New York, 1988.
(501) Yuan, K.; Lu, C.; Sfaelou, S.; Liao, X.; Zhuang, X.; Chen, Y.; Scherf, U.; Feng, X. In Situ Nanoarchitecturing and Active-Site Engineering toward Highly Efficient Carbonaceous Electrocatalysts. *Nano Energy* **2019**, *59*, 207–215. https://doi.org/10.1016/j.nanoen.2019.02.043.
(502) Yuan, K.; Lützenkirchen-Hecht, D.; Li, L.; Shuai, L.; Li, Y.; Cao, R.; Qiu, M.; Zhuang, X.; Leung, M. K. H.; Chen, Y.; Scherf, U. Boosting Oxygen Reduction of Single Iron Active Sites via Geometric and Electronic Engineering: Nitrogen and Phosphorus Dual Coordination. *J. Am. Chem. Soc.* **2020**, *142* (5), 2404–2412. https://doi.org/10.1021/jacs.9b11852.
(503) Xue, J.; Dong, X.; Liu, C.; Li, J.; Dai, Y.; Xue, W.; Luo, L.; Ji, Y.; Zhang, X.; Li, X.; Jiang, Q.; Zheng, T.; Xiao, J.; Xia, C. Turning Copper into an Efficient and Stable CO Evolution Catalyst beyond Noble Metals. *Nat. Commun.* **2024**, *15* (1), 5998. https://doi.org/10.1038/s41467-024-50436-4.
(504) Meng, L.; Kao, C.-W.; Wang, Z.; Ma, J.; Huang, P.; Zhao, N.; Zheng, X.; Peng, M.; Lu, Y.-R.; Tan, Y. Alloying and Confinement Effects on Hierarchically Nanoporous CuAu for Efficient Electrocatalytic Semi-Hydrogenation of Terminal Alkynes. *Nat. Commun.* **2024**, *15* (1), 5999. https://doi.org/10.1038/s41467-024-50499-3.
(505) Timoshenko, J.; Roldan Cuenya, B. *In Situ* / *Operando* Electrocatalyst Characterization by X-Ray Absorption Spectroscopy. *Chem. Rev.* **2021**, *121* (2), 882–961. https://doi.org/10.1021/acs.chemrev.0c00396.
(506) Fabbri, E.; Abbott, D. F.; Nachtegaal, M.; Schmidt, T. J. Operando X-Ray Absorption Spectroscopy: A Powerful Tool toward Water Splitting Catalyst Development. *Curr. Opin. Electrochem.* **2017**, *5* (1), 20–26. https://doi.org/10.1016/j.coelec.2017.08.009.
(507) Fang, L.; Seifert, S.; Winans, R. E.; Li, T. Operando XAS/SAXS: Guiding Design of Single-Atom and Subnanocluster Catalysts. *Small Methods* **2021**, *5* (5), 2001194. https://doi.org/10.1002/smtd.202001194.
(508) Müller, O.; Nachtegaal, M.; Just, J.; Lützenkirchen-Hecht, D.; Frahm, R. Quick-EXAFS Setup at the SuperXAS Beamline for *in Situ* X-Ray Absorption Spectroscopy with 10 Ms Time Resolution. *J. Synchrotron Radiat.* **2016**, *23* (1), 260–266. https://doi.org/10.1107/S1600577515018007.
(509) Bornmann, B.; Kläs, J.; Müller, O.; Lützenkirchen-Hecht, D.; Frahm, R. The Quick EXAFS Setup at Beamline P64 at PETRA III for up to 200 Spectra per Second; Taipei, Taiwan, 2019; p 040008. https://doi.org/10.1063/1.5084609.
(510) Briois, V.; La Fontaine, C.; Belin, S.; Barthe, L.; Moreno, T.; Pinty, V.; Carcy, A.; Girardot, R.; Fonda, E. ROCK: The New Quick-EXAFS Beamline at SOLEIL. *J. Phys.: Conf. Ser.* **2016**, *712*, 012149. https://doi.org/10.1088/1742-6596/712/1/012149.
(511) Lin, S.-C.; Chang, C.-C.; Chiu, S.-Y.; Pai, H.-T.; Liao, T.-Y.; Hsu, C.-S.; Chiang, W.-H.; Tsai, M.-K.; Chen, H. M. Operando Time-Resolved X-Ray Absorption Spectroscopy Reveals the Chemical Nature Enabling Highly Selective CO_2 Reduction. *Nat. Commun.* **2020**, *11* (1), 3525. https://doi.org/10.1038/s41467-020-17231-3.
(512) Wurzler, N.; Schutter, J. D.; Wagner, R.; Dimper, M.; Lützenkirchen-Hecht, D.; Ozcan, O. Trained to Corrode: Cultivation in the Presence of Fe(III) Increases the Electrochemical Activity of Iron Reducing Bacteria – An in Situ Electrochemical XANES Study. *Electrochem. Commun.* **2020**, *112*, 106673. https://doi.org/10.1016/j.elecom.2020.106673.
(513) Genz, N. S.; Kallio, A.; Oord, R.; Krumeich, F.; Pokle, A.; Prytz, Ø.; Olsbye, U.; Meirer, F.; Huotari, S.; Weckhuysen, B. M. Operando Laboratory-Based Multi-Edge X-Ray Absorption Near-Edge Spectroscopy of Solid Catalysts. *Angew. Chem. Int. Ed.* **2022**, *61* (48), e202209334. https://doi.org/10.1002/anie.202209334.

(514) Ostervold, L.; Hoffman, A. S.; Thompson, D.; Bare, S. R.; Clark, E. L. A Versatile Electrochemical Cell for *Operando* XAS. *ChemCatChem* **2024**, *16* (15), e202400072. https://doi.org/10.1002/cctc.202400072.
(515) Lützenkirchen-Hecht, D.; Wagner, R.; Szillat, S.; Hüsecken, A. K.; Istomin, K.; Pietsch, U.; Frahm, R. The Multi-Purpose Hard X-Ray Beamline BL10 at the DELTA Storage Ring. *J. Synchrotron Radiat.* **2014**, *21* (4), 819–826. https://doi.org/10.1107/S1600577514006705.
(516) Li, R.; Wang, D. Superiority of Dual-Atom Catalysts in Electrocatalysis: One Step Further Than Single-Atom Catalysts. *Adv. Energy Mater.* **2022**, *12* (9), 2103564. https://doi.org/10.1002/aenm.202103564.
(517) Chen, F.; Jiang, X.; Zhang, L.; Lang, R.; Qiao, B. Single-Atom Catalysis: Bridging the Homo- and Heterogeneous Catalysis. *Chin. J. Catal.* **2018**, *39* (5), 893–898. https://doi.org/10.1016/S1872-2067(18)63047-5.
(518) Zhao, S.; Liu, M.; Qu, Z.; Yan, Y.; Zhang, Z.; Yang, J.; He, S.; Xu, Z.; Zhu, Y.; Luo, L.; Hui, K. N.; Liu, M.; Zeng, J. Cascade Synthesis of Fe-N_2-Fe Dual-Atom Catalysts for Superior Oxygen Catalysis. *Angew. Chem. Int. Ed.* **2024**, *63* (40), e202408914. https://doi.org/10.1002/anie.202408914.
(519) Li, Y.; Chen, C.; Cao, R.; Pan, Z.; He, H.; Zhou, K. Dual-Atom Ag_2/Graphene Catalyst for Efficient Electroreduction of CO_2 to CO. *Appl. Catal., B* **2020**, *268*, 118747. https://doi.org/10.1016/j.apcatb.2020.118747.
(520) Zhang, N.; Zhang, X.; Kang, Y.; Ye, C.; Jin, R.; Yan, H.; Lin, R.; Yang, J.; Xu, Q.; Wang, Y.; Zhang, Q.; Gu, L.; Liu, L.; Song, W.; Liu, J.; Wang, D.; Li, Y. A Supported Pd_2 Dual-Atom Site Catalyst for Efficient Electrochemical CO_2 Reduction. *Angew. Chem. Int. Ed.* **2021**, *60* (24), 13388–13393. https://doi.org/10.1002/anie.202101559.
(521) Wei, Y.; Sun, L.; Wang, M.; Hong, J.; Zou, L.; Liu, H.; Wang, Y.; Zhang, M.; Liu, Z.; Li, Y.; Horike, S.; Suenaga, K.; Xu, Q. Fabricating Dual-Atom Iron Catalysts for Efficient Oxygen Evolution Reaction: A Heteroatom Modulator Approach. *Angew. Chem. Int. Ed.* **2020**, *59* (37), 16013–16022. https://doi.org/10.1002/anie.202007221.
(522) Bai, L.; Hsu, C.-S.; Alexander, D. T. L.; Chen, H. M.; Hu, X. Double-Atom Catalysts as a Molecular Platform for Heterogeneous Oxygen Evolution Electrocatalysis. *Nat. Energy* **2021**, *6* (11), 1054–1066. https://doi.org/10.1038/s41560-021-00925-3.
(523) Bai, L.; Hsu, C.-S.; Alexander, D. T. L.; Chen, H. M.; Hu, X. A Cobalt–Iron Double-Atom Catalyst for the Oxygen Evolution Reaction. *J. Am. Chem. Soc.* **2019**, *141* (36), 14190–14199. https://doi.org/10.1021/jacs.9b05268.
(524) Chai, Y.; Chen, S.; Chen, Y.; Wei, F.; Cao, L.; Lin, J.; Li, L.; Liu, X.; Lin, S.; Wang, X.; Zhang, T. Dual-Atom Catalyst with N-Colligated Zn_1 Co_1 Species as Dominant Active Sites for Propane Dehydrogenation. *J. Am. Chem. Soc.* **2024**, *146* (1), 263–273. https://doi.org/10.1021/jacs.3c08616.
(525) Wang, Z.; Jin, X.; Xu, R.; Yang, Z.; Ma, S.; Yan, T.; Zhu, C.; Fang, J.; Liu, Y.; Hwang, S.-J.; Pan, Z.; Fan, H. J. Cooperation between Dual Metal Atoms and Nanoclusters Enhances Activity and Stability for Oxygen Reduction and Evolution. *ACS Nano* **2023**, *17* (9), 8622–8633. https://doi.org/10.1021/acsnano.3c01287.
(526) Zhang, H.; Guo, G.; Wang, Z.; He, X.; Ji, H. The Impact of Milling Energy on the Structure of Catalysts during the Mechanochemical Synthesis of Single-Atom Catalysts. *Ind. Eng. Chem. Res.* **2024**, *63* (45), 19530–19536. https://doi.org/10.1021/acs.iecr.4c03272.
(527) Wang, Y.; Wan, L.; Cui, P.; Tong, L.; Ke, Y.; Sheng, T.; Zhang, M.; Sun, S.; Liang, H.; Wang, Y.; Zaghib, K.; Wang, H.; Zhou, Z.; Yuan, J. Porous Carbon Membrane-Supported Atomically Dispersed Pyrrole-Type Fe-N_4 as Active Sites for Electrochemical Hydrazine Oxidation Reaction. *Small* **2020**, *16* (31), 2002203. https://doi.org/10.1002/smll.202002203.

(528) Dai, L.; Lv, J.; Xu, S.; Zong, J.; Liang, L.; Wang, B.; Li, P. Construction of Interlayered Single-Atom Active Sites on Bipyridine-Based 2D Conjugated Covalent-Organic Frameworks for Boosting the C_2 Products of Electrochemical CO_2 Reduction. *ACS Appl. Mater. Interfaces* **2024**, *16* (49), 67813–67820. https://doi.org/10.1021/acsami.4c16371.
(529) Huang, M.; Zhou, S.-H.; Yang, C.-J.; Dong, C.-L.; He, Y.; Wei, W.; Li, X.; Zhu, Q.-L.; Huang, Z. Selenic Acid Etching Assisted Atomic Engineering for Designing Metal-Semimetal Dual Single-Atom Catalysts for Enhanced CO_2 Electroreduction. *ACS Nano* **2024**, *18* (48), 33210–33219. https://doi.org/10.1021/acsnano.4c12576.
(530) Wagh, N. K.; Shinde, S. S.; Lee, J.-H. Atomically Modulated Cu Single-Atom Catalysts for Oxygen Reduction Reactions towards High-Power Density Zn– and Al–Air Batteries. *Chem. Commun.* **2024**, *60*, 15015–15018. https://doi.org/10.1039/D4CC05217J.
(531) Zhao, H.; Song, B.; Li, H.; Li, X.; Ge, C.; Wu, Q.; Chen, J.; Wang, Z.; Yan, G.; Fang, J. Controllable Microwave Heating for Energy-Efficient and Universal Synthesis of Atomically Dispersed Metals on Nitrogen-Doped Carbon Nanofibers. *Small* **2024**, *21* (4), 2407700. https://doi.org/10.1002/smll.202407700.
(532) Qian, K.; Kumar, A.; Zhang, H.; Bellmer, D.; Huhnke, R. Recent Advances in Utilization of Biochar. *Renewable Sustainable Energy Rev.* **2015**, *42*, 1055–1064. https://doi.org/10.1016/j.rser.2014.10.074.
(533) Vardon, D. R.; Moser, B. R.; Zheng, W.; Witkin, K.; Evangelista, R. L.; Strathmann, T. J.; Rajagopalan, K.; Sharma, B. K. Complete Utilization of Spent Coffee Grounds To Produce Biodiesel, Bio-Oil, and Biochar. *ACS Sustainable Chem. Eng.* **2013**, *1* (10), 1286–1294. https://doi.org/10.1021/sc400145w.
(534) Silva, M. A.; Nebra, S. A.; Machado Silva, M. J.; Sanchez, C. G. THE USE OF BIOMASS RESIDUES IN THE BRAZILIAN SOLUBLE COFFEE INDUSTRY. *Biomass Bioenergy* **1998**, *14* (5–6), 457–467. https://doi.org/10.1016/S0961-9534(97)10034-4.
(535) Pichler, J.; Maria Eder, R.; Widder, L.; Varga, M.; Marchetti-Deschmann, M.; Frauscher, M. Moving towards Green Lubrication: Tribological Behavior and Chemical Characterization of Spent Coffee Grounds Oil. *Green Chem. Lett. Rev.* **2023**, *16* (1), 2215243. https://doi.org/10.1080/17518253.2023.2215243.
(536) Yu, M.; Chan, C. K.; Tüysüz, H. Coffee-Waste Templating of Metal Ion-Substituted Cobalt Oxides for the Oxygen Evolution Reaction. *ChemSusChem* **2018**, *11* (3), 605–611. https://doi.org/10.1002/cssc.201701877.
(537) Tamtaji, M.; Li, Y.; Cai, Y.; Liu, H.; Goddard Iii, W. A.; Chen, G. Reaction Mechanism and Kinetics of Oxygen Reduction Reaction on the Iron–Nickel Dual Atom Catalyst. *J. Mater. Chem. A* **2023**, *11* (46), 25410–25421. https://doi.org/10.1039/D3TA05694E.
(538) Li, Q.; Luo, L.; Xu, C.; Song, S.; Wang, Y.; Zhang, L.; Tang, Y.; Texter, J. Palladium Enhanced Iron Active Site – An Efficient Dual-Atom Catalyst for Oxygen Electroreduction. *Small* **2023**, *19* (38), 2303321. https://doi.org/10.1002/smll.202303321.
(539) Chen, Y.; Zhao, J.; Pan, X.; Li, L.; Yu, Z.; Wang, X.; Ma, T.; Lin, S.; Lin, J. Tuning the Inter-Metal Interaction between Ni and Fe Atoms in Dual-Atom Catalysts to Boost CO_2 Electroreduction. *Angew. Chem. Int. Ed.* **2024**, *136* (44), e202411543. https://doi.org/10.1002/ange.202411543.
(540) Woo, D.; Kim, J.; Xu, L.; Park, J.; Park, C.; Yi, S. Y.; Kim, S.; Jun, H.; Kim, S.; Lee, J. Selective Self-Assembly of Atomically Dispersed Iron and Cobalt Dual Atom Catalyst on Anisotropic Mesoporous Carbon Particles for High Performance Seawater Batteries. *Adv. Funct. Materials* **2024**, 2414749. https://doi.org/10.1002/adfm.202414749.

(541) Jiang, M.; Wang, F.; Yang, F.; He, H.; Yang, J.; Zhang, W.; Luo, J.; Zhang, J.; Fu, C. Rationalization on High-Loading Iron and Cobalt Dual Metal Single Atoms and Mechanistic Insight into the Oxygen Reduction Reaction. *Nano Energy* **2022**, *93*, 106793. https://doi.org/10.1016/j.nanoen.2021.106793.
(542) Frahm, R. Quick Scanning Exafs: First Experiments. *Nucl. Instrum. Methods Phys. Res., Sect. A* **1988**, *270* (2–3), 578–581. https://doi.org/10.1016/0168-9002(88)90732-2.
(543) Yuan, J.; Giordano, C.; Antonietti, M. Ionic Liquid Monomers and Polymers as Precursors of Highly Conductive, Mesoporous, Graphitic Carbon Nanostructures. *Chem. Mater.* **2010**, *22* (17), 5003–5012. https://doi.org/10.1021/cm1012729.
(544) Baspinar, B.; Eskici, G.; Ozcelik, A. O. How Coffee Affects Metabolic Syndrome and Its Components. *Food Funct.* **2017**, *8* (6), 2089–2101. https://doi.org/10.1039/C7FO00388A.
(545) Alton Spiller, M. The Chemical Components of Coffee. In *Caffeine*; Spiller, G. A., Ed.; CRC Press, 2019; pp 97–161. https://doi.org/10.1201/9780429126789-6.
(546) Gómez-Ruiz, J. Á.; Leake, D. S.; Ames, J. M. In Vitro Antioxidant Activity of Coffee Compounds and Their Metabolites. *J. Agric. Food Chem.* **2007**, *55* (17), 6962–6969. https://doi.org/10.1021/jf0710985.
(547) Cano-Marquina, A.; Tarín, J. J.; Cano, A. The Impact of Coffee on Health. *Maturitas* **2013**, *75* (1), 7–21. https://doi.org/10.1016/j.maturitas.2013.02.002.
(548) Mussatto, S. I.; Machado, E. M. S.; Martins, S.; Teixeira, J. A. Production, Composition, and Application of Coffee and Its Industrial Residues. *Food Bioprocess Technol.* **2011**, *4* (5), 661–672. https://doi.org/10.1007/s11947-011-0565-z.
(549) Alcazar, A. Ion Chromatographic Determination of Some Organic Acids, Chloride and Phosphate in Coffee and Tea. *Talanta* **2003**, *61* (2), 95–101. https://doi.org/10.1016/S0039-9140(03)00244-3.
(550) Fraňková, A.; Drábek, O.; Havlík, J.; Száková, J.; Vaněk, A. The Effect of Beverage Preparation Method on Aluminium Content in Coffee Infusions. *J. Inorg. Biochem.* **2009**, *103* (11), 1480–1485. https://doi.org/10.1016/j.jinorgbio.2009.06.012.
(551) Jaramillo, D.; Alvarez, G.; Díaz, C.; Pérez, S.; Muñoz Saldaña, J.; Sierra, L.; López, B. L.; Moreno-Zuria, A.; Mohamedi, M.; Palacio, R. Porous Carbonaceous Materials Simultaneously Dispersing N, Fe and Co as Bifunctional Catalysts for the ORR and OER: Electrochemical Performance in a Prototype of a Zn–Air Battery. *Dalton Trans.* **2024**, *53* (7), 3143–3158. https://doi.org/10.1039/D3DT03330A.
(552) Szewczyk, I.; Rokicińska, A.; Michalik, M.; Chen, J.; Jaworski, A.; Aleksis, R.; Pell, A. J.; Hedin, N.; Slabon, A.; Kuśtrowski, P. Electrochemical Denitrification and Oxidative Dehydrogenation of Ethylbenzene over N-Doped Mesoporous Carbon: Atomic Level Understanding of Catalytic Activity by ^{15}N NMR Spectroscopy. *Chem. Mater.* **2020**, *32* (17), 7263–7273. https://doi.org/10.1021/acs.chemmater.0c01666.
(553) Lei, G.; Lin, X.; Yan, H.; Shen, L.; Wang, S.; Liang, S.; Zhao, Z.-J.; Liu, F.; Zhan, Y.; Jiang, L. Valence Electron and Coordination Structure Guided Metal Active Site Design for Hydrolytic Cleavage of Carbon–Sulfide Double Bonds. *ACS Catal.* **2024**, 17103–17112. https://doi.org/10.1021/acscatal.4c02921.
(554) Benedet, M.; Barreca, D.; Rizzi, G. A.; Maccato, C.; Wree, J.-L.; Devi, A.; Gasparotto, A. Fe_2O_3-Graphitic Carbon Nitride Nanocomposites Analyzed by XPS. *Surf. Sci. Spectra* **2023**, *30* (2), 024021. https://doi.org/10.1116/6.0002979.
(555) Lang, R.; Du, X.; Huang, Y.; Jiang, X.; Zhang, Q.; Guo, Y.; Liu, K.; Qiao, B.; Wang, A.; Zhang, T. Single-Atom Catalysts Based on the Metal–Oxide Interaction. *Chem. Rev.* **2020**, *120* (21), 11986–12043. https://doi.org/10.1021/acs.chemrev.0c00797.
(556) Sheng, B.; Chu, Y.; Cao, D.; Xia, Y.; Liu, C.; Chen, S.; Song, L. Application of X-Ray Absorption Spectroscopy in Carbon-Supported Electrocatalysts. *Nano Res.* **2023**, *16* (11), 12438–12452. https://doi.org/10.1007/s12274-023-6153-5.

(557) Lützenkirchen-Hecht, D.; Yuan, K.; Eckelt, F.; Braun, F.; Voss, L.; Li, L.; Tang, X.; Zhuang, X.; Chen, Y. Investigation of Single Atom Catalysts by X-Ray Absorption Spectroscopy. *Phys. Status Solidi A* **2024**, 2400606. https://doi.org/10.1002/pssa.202400606.
(558) Holmberg, K.; Erdemir, A. Influence of Tribology on Global Energy Consumption, Costs and Emissions. *Friction* **2017**, *5* (3), 263–284. https://doi.org/10.1007/s40544-017-0183-5.
(559) Lindenbeck, L.; Beele, B. B.; Morsali, M.; Budnyk, S.; Frauscher, M.; Chen, J.; Sipponen, M. H.; Slabon, A.; Rodrigues, B. V. M. MoS_2 Nanoflower-Decorated Lignin Nanoparticles for Superior Lubricant Properties. *Nanoscale* **2023**, *15* (20), 9014–9021. https://doi.org/10.1039/D3NR00458A.
(560) Plum, L. M.; Rink, L.; Haase, H. The Essential Toxin: Impact of Zinc on Human Health. *Int. J. Environ. Res. Public Health* **2010**, *7* (4), 1342–1365. https://doi.org/10.3390/ijerph7041342.
(561) Ruggiero, A.; D'Amato, R.; Merola, M.; Valašek, P.; Müller, M. Tribological Characterization of Vegetal Lubricants: Comparative Experimental Investigation on Jatropha Curcas L. Oil, Rapeseed Methyl Ester Oil, Hydrotreated Rapeseed Oil. *Tribol. Int.* **2017**, *109*, 529–540. https://doi.org/10.1016/j.triboint.2017.01.030.
(562) Emmanuel, O.; Rozina; Ezeji, T. C. Utilization of Biomass-Based Resources for Biofuel Production: A Mitigating Approach towards Zero Emission. *Sustainable Chemistry One World* **2024**, *2*, 100007. https://doi.org/10.1016/j.scowo.2024.100007.
(563) Movil, O.; Garlock, M.; Staser, J. A. Non-Precious Metal Nanoparticle Electrocatalysts for Electrochemical Modification of Lignin for Low-Energy and Cost-Effective Production of Hydrogen. *Int. J. Hydrogen Energy* **2015**, *40* (13), 4519–4530. https://doi.org/10.1016/j.ijhydene.2015.02.023.
(564) Hung, L.; Tsung, C.; Huang, W.; Yang, P. Room-Temperature Formation of Hollow Cu_2O Nanoparticles. *Adv. Mater.* **2010**, *22* (17), 1910–1914. https://doi.org/10.1002/adma.200903947.
(565) Mussatto, S. I.; Dragone, G.; Roberto, I. C. Brewers' Spent Grain: Generation, Characteristics and Potential Applications. *J. Cereal Sci.* **2006**, *43* (1), 1–14. https://doi.org/10.1016/j.jcs.2005.06.001.
(566) Lynch, K. M.; Steffen, E. J.; Arendt, E. K. Brewers' Spent Grain: A Review with an Emphasis on Food and Health. *J. Inst. Brew.* **2016**, *122* (4), 553–568. https://doi.org/10.1002/jib.363.
(567) Buffington, J. The Economic Potential of Brewer's Spent Grain (BSG) as a Biomass Feedstock. *ACES* **2014**, *04* (03), 308–318. https://doi.org/10.4236/aces.2014.43034.
(568) Mussatto, S. I. Brewer's Spent Grain: A Valuable Feedstock for Industrial Applications: Brewer's Spent Grain and Its Potential Applications. *J. Sci. Food Agric.* **2014**, *94* (7), 1264–1275. https://doi.org/10.1002/jsfa.6486.
(569) Steiner, J.; Procopio, S.; Becker, T. Brewer's Spent Grain: Source of Value-Added Polysaccharides for the Food Industry in Reference to the Health Claims. *Eur. Food Res. Technol.* **2015**, *241* (3), 303–315. https://doi.org/10.1007/s00217-015-2461-7.
(570) Bachmann, S. A. L.; Calvete, T.; Féris, L. A. Potential Applications of Brewery Spent Grain: Critical an Overview. *J. Environ. Chem. Eng.* **2022**, *10* (1), 106951. https://doi.org/10.1016/j.jece.2021.106951.
(571) Boubkr, L.; Bhakta, A. K.; Snoussi, Y.; Moreira Da Silva, C.; Michely, L.; Jouini, M.; Ammar, S.; Chehimi, M. M. Highly Active Ag-Cu Nanocrystal Catalyst-Coated Brewer's Spent Grain Biochar for the Mineralization of Methyl Orange and Methylene Blue Dye Mixture. *Catalysts* **2022**, *12* (11), 1475. https://doi.org/10.3390/catal12111475.

(572) Liu, C.; Qiao, B.; Zhang, T. Integration of Single Atoms for Tandem Catalysis. *JACS Au* **2024**, *4* (11), 4129–4140. https://doi.org/10.1021/jacsau.4c00784.
(573) Feng, Q.; Wang, B.; Chen, M.; Wu, P.; Lee, X.; Xing, Y. Invasive Plants as Potential Sustainable Feedstocks for Biochar Production and Multiple Applications: A Review. *Resour. Conserv. Recycl.* **2021**, *164*, 105204. https://doi.org/10.1016/j.resconrec.2020.105204.
(574) Dudek, K.; Wojtaszek, K.; Żabiński, P. Ni-Doped Activated Carbon from Invasive Plants as a Potential Catalyst. *Metals* **2024**, *14* (7), 790. https://doi.org/10.3390/met14070790.
(575) Lu, Y.-W.; Fan, Y.-H.; Chen, M. Synthesis of Invasive Plant Biochar Catalyst with Carbon Nitride Structure for Peroxymonosulfate Activation toward Efficient Ciprofloxacin Degradation. *Biochar* **2024**, *6* (1), 35. https://doi.org/10.1007/s42773-024-00325-2.
(576) Liang, J.; Chen, Y.; Cai, M.; Gan, M.; Zhu, J. One-Pot Pyrolysis of Metal-Embedded Biochar Derived from Invasive Plant for Efficient Cr(VI) Removal. *J. Environ. Chem. Eng.* **2021**, *9* (4), 105714. https://doi.org/10.1016/j.jece.2021.105714.
(577) Silva, M. P.; Moyano, E. L.; Scopel, A. L. Potential Applications of Biochar and Terpene-Enriched Bio-Oil Produced from a Semi-Arid Native Asteraceae. *J. Anal. Appl. Pyrolysis* **2017**, *126*, 39–49. https://doi.org/10.1016/j.jaap.2017.06.026.
(578) Rumlerová, Z.; Vilà, M.; Pergl, J.; Nentwig, W.; Pyšek, P. Scoring Environmental and Socioeconomic Impacts of Alien Plants Invasive in Europe. *Biol. Invasions* **2016**, *18* (12), 3697–3711. https://doi.org/10.1007/s10530-016-1259-2.
(579) Lavoie, C. The Impact of Invasive Knotweed Species (Reynoutria Spp.) on the Environment: Review and Research Perspectives. *Biol. Invasions* **2017**, *19* (8), 2319–2337. https://doi.org/10.1007/s10530-017-1444-y.
(580) Beerling, D. J.; Bailey, J. P.; Conolly, A. P. Fallopia Japonica (Houtt.) Ronse Decraene. *The Journal of Ecology* **1994**, *82* (4), 959. https://doi.org/10.2307/2261459.
(581) Tiébré, M.-S.; Saad, L.; Mahy, G. Landscape Dynamics and Habitat Selection by the Alien Invasive Fallopia (Polygonaceae) in Belgium. *Biodivers. Conserv.* **2008**, *17* (10), 2357–2370. https://doi.org/10.1007/s10531-008-9386-4.
(582) Duquette, M. -C.; Compérot, A.; Hayes, L. F.; Pagola, C.; Belzile, F.; Dubé, J.; Lavoie, C. From the Source to the Outlet: Understanding the Distribution of Invasive Knotweeds along a North American River. *River Res. Appl.* **2016**, *32* (5), 958–966. https://doi.org/10.1002/rra.2914.
(583) Watkins, D.; Nuruddin, Md.; Hosur, M.; Tcherbi-Narteh, A.; Jeelani, S. Extraction and Characterization of Lignin from Different Biomass Resources. *J. Mater. Res. Technol.* **2015**, *4* (1), 26–32. https://doi.org/10.1016/j.jmrt.2014.10.009.
(584) Alonso, D. M.; Gallo, J. M. R.; Mellmer, M. A.; Wettstein, S. G.; Dumesic, J. A. Direct Conversion of Cellulose to Levulinic Acid and Gamma-Valerolactone Using Solid Acid Catalysts. *Catal. Sci. Technol.* **2013**, *3* (4), 927–931. https://doi.org/10.1039/C2CY20689G.
(585) Han, Y.; Ye, L.; Gu, X.; Zhu, P.; Lu, X. Lignin-Based Solid Acid Catalyst for the Conversion of Cellulose to Levulinic Acid Using γ-Valerolactone as Solvent. *Ind. Crops Prod.* **2019**, *127*, 88–93. https://doi.org/10.1016/j.indcrop.2018.10.058.
(586) Ma, C.; Cai, B.; Zhang, L.; Feng, J.; Pan, H. Acid-Catalyzed Conversion of Cellulose Into Levulinic Acid With Biphasic Solvent System. *Front. Plant Sci.* **2021**, *12*, 630807. https://doi.org/10.3389/fpls.2021.630807.
(587) Lin, H.; Strull, J.; Liu, Y.; Karmiol, Z.; Plank, K.; Miller, G.; Guo, Z.; Yang, L. High Yield Production of Levulinic Acid by Catalytic Partial Oxidation of Cellulose in Aqueous Media. *Energy Environ. Sci.* **2012**, *5* (12), 9773. https://doi.org/10.1039/c2ee23225a.

(588) Yang, F.; Zhang, Q.; Fan, H.-X.; Li, Y.; Li, G. Electrochemical Control of the Conversion of Cellulose Oligosaccharides into Glucose. *J. Ind. Eng. Chem.* **2014**, *20* (5), 3487–3492. https://doi.org/10.1016/j.jiec.2013.12.039.
(589) Nagarajan, K. J.; Ramanujam, N. R.; Sanjay, M. R.; Siengchin, Suchart.; Surya Rajan, B.; Sathick Basha, K.; Madhu, P.; Raghav, G. R. A Comprehensive Review on Cellulose Nanocrystals and Cellulose Nanofibers: Pretreatment, Preparation, and Characterization. *Polym. Compos.* **2021**, *42* (4), 1588–1630. https://doi.org/10.1002/pc.25929.
(590) Li, X.; Wang, H.; Yang, H.; Cai, W.; Liu, S.; Liu, B. In Situ/Operando Characterization Techniques to Probe the Electrochemical Reactions for Energy Conversion. *Small Methods* **2018**, *2* (6), 1700395. https://doi.org/10.1002/smtd.201700395.
(591) Zhu, K.; Zhu, X.; Yang, W. Application of In Situ Techniques for the Characterization of NiFe-Based Oxygen Evolution Reaction (OER) Electrocatalysts. *Angew. Chem. Int. Ed.* **2019**, *58* (5), 1252–1265. https://doi.org/10.1002/anie.201802923.
(592) Yuan, Y.; Li, M.; Bai, Z.; Jiang, G.; Liu, B.; Wu, T.; Chen, Z.; Amine, K.; Lu, J. The Absence and Importance of Operando Techniques for Metal-Free Catalysts. *Adv. Mater.* **2019**, *31* (13), 1805609. https://doi.org/10.1002/adma.201805609.
(593) Lukashuk, L.; Foettinger, K. In Situ and Operando Spectroscopy: A Powerful Approach Towards Understanding Catalysts: Revealing Reaction Mechanisms to Find the Correlation between Structure and Surface Composition. *Johnson Matthey Technol. Rev.* **2018**, *62* (3), 316–331. https://doi.org/10.1595/205651318X15234323420569.
(594) Bañares, M. A. Operando Methodology: Combination of in Situ Spectroscopy and Simultaneous Activity Measurements under Catalytic Reaction Conditions. *Catal. Today* **2005**, *100* (1–2), 71–77. https://doi.org/10.1016/j.cattod.2004.12.017.
(595) Bañares, M. A. Operando Spectroscopy: The Knowledge Bridge to Assessing Structure–Performance Relationships in Catalyst Nanoparticles. *Adv. Mater.* **2011**, *23* (44), 5293–5301. https://doi.org/10.1002/adma.201101803.
(596) Fath, A. *Mikroplastik kompakt: Wissenswertes für alle*; essentials; Springer Fachmedien Wiesbaden: Wiesbaden, 2019. https://doi.org/10.1007/978-3-658-25734-7.
(597) Carlini, G.; Kleine, K. Advancing the International Regulation of Plastic Pollution beyond the United Nations Environment Assembly Resolution on Marine Litter and Microplastics. *Review of European, Comparative & International Environmental Law* **2018**, *27* (3), 234–244. https://doi.org/10.1111/reel.12258.
(598) Waldschläger, K. *Mikroplastik in der aquatischen Umwelt: Quellen, Senken und Transportpfade*; essentials; Springer Fachmedien Wiesbaden: Wiesbaden, 2019. https://doi.org/10.1007/978-3-658-27766-6.
(599) Zhao, B.; Rehati, P.; Yang, Z.; Cai, Z.; Guo, C.; Li, Y. The Potential Toxicity of Microplastics on Human Health. *Sci. Total Environ.* **2024**, *912*, 168946. https://doi.org/10.1016/j.scitotenv.2023.168946.
(600) Moog, D.; Schmitt, J.; Senger, J.; Zarzycki, J.; Rexer, K.-H.; Linne, U.; Erb, T.; Maier, U. G. Using a Marine Microalga as a Chassis for Polyethylene Terephthalate (PET) Degradation. *Microb Cell Fact* **2019**, *18* (1), 171. https://doi.org/10.1186/s12934-019-1220-z.
(601) Navarrete-Fernández, T.; Bermejo, R.; Hernández, I.; Deidun, A.; Andreu-Cazenave, M.; Cózar, A. The Role of Seagrass Meadows in the Coastal Trapping of Litter. *Marine Pollution Bulletin* **2022**, *174*, 113299. https://doi.org/10.1016/j.marpolbul.2021.113299.
(602) Kang, J.; Zhou, L.; Duan, X.; Sun, H.; Ao, Z.; Wang, S. Degradation of Cosmetic Microplastics via Functionalized Carbon Nanosprings. *Matter* **2019**, *1* (3), 745–758. https://doi.org/10.1016/j.matt.2019.06.004.

(603) Singh, N.; Walker, T. R. Plastic Recycling: A Panacea or Environmental Pollution Problem. *npj Mater. Sustain.* **2024**, *2* (1), 17. https://doi.org/10.1038/s44296-024-00024-w.
(604) Ragaert, K.; Delva, L.; Van Geem, K. Mechanical and Chemical Recycling of Solid Plastic Waste. *Waste Manage.* **2017**, *69*, 24–58. https://doi.org/10.1016/j.wasman.2017.07.044.
(605) Cestari, S. P.; Albitres, G. A. V.; Pires, H. M.; De França Da Silva Freitas, D.; Mendes, L. C. Study of the Interaction Between Oligomerised Recycled Poly(Ethylene Terephtalate) and Concrete Waste. *J. Polym. Environ.* **2019**, *27* (12), 2915–2924. https://doi.org/10.1007/s10924-019-01569-x.
(606) Syberg, K. Beware the False Hope of Recycling. *Nature* **2022**, *611* (7936), S6–S6. https://doi.org/10.1038/d41586-022-03645-0.
(607) Garcia, J. M.; Robertson, M. L. The Future of Plastics Recycling. *Science* **2017**, *358* (6365), 870–872. https://doi.org/10.1126/science.aaq0324.
(608) Castello, D.; Haider, M. S.; Rosendahl, L. A. Catalytic Upgrading of Hydrothermal Liquefaction Biocrudes: Different Challenges for Different Feedstocks. *Renewable Energy* **2019**, *141*, 420–430. https://doi.org/10.1016/j.renene.2019.04.003.
(609) Kim, S.; Kwon, E. E.; Kim, Y. T.; Jung, S.; Kim, H. J.; Huber, G. W.; Lee, J. Recent Advances in Hydrodeoxygenation of Biomass-Derived Oxygenates over Heterogeneous Catalysts. *Green Chem.* **2019**, *21* (14), 3715–3743. https://doi.org/10.1039/C9GC01210A.
(610) Webber, M. S.; Watson, J.; Zhu, J.; Jang, J. H.; Çağlayan, M.; Heyne, J. S.; Beckham, G. T.; Román-Leshkov, Y. Lignin Deoxygenation for the Production of Sustainable Aviation Fuel Blendstocks. *Nat. Mater.* **2024**, *23* (12), 1622–1638. https://doi.org/10.1038/s41563-024-02024-6.
(611) Laskar, D. D.; Yang, B.; Wang, H.; Lee, J. Pathways for Biomass-derived Lignin to Hydrocarbon Fuels. *Biofuels, Bioprod. Biorefin.* **2013**, *7* (5), 602–626. https://doi.org/10.1002/bbb.1422.
(612) Wijaya, Y. P.; Smith, K. J.; Kim, C. S.; Gyenge, E. L. Hydrodeoxygenation of Lignin Related Phenolic Monomers in Polar Organic Electrolyte *via* Electrocatalysis in a Stirred Slurry Catalytic Reactor. *Green Chem.* **2022**, *24* (19), 7469–7480. https://doi.org/10.1039/D2GC01997C.
(613) Garedew, M.; Young-Farhat, D.; Jackson, J. E.; Saffron, C. M. Electrocatalytic Upgrading of Phenolic Compounds Observed after Lignin Pyrolysis. *ACS Sustainable Chem. Eng.* **2019**, *7* (9), 8375–8386. https://doi.org/10.1021/acssuschemeng.9b00019.
(614) Weber, R. S.; Ramasamy, K. K. Electrochemical Oxidation of Lignin and Waste Plastic. *ACS Omega* **2020**, *5* (43), 27735–27740. https://doi.org/10.1021/acsomega.0c03989.
(615) Rani, S.; Aslam, S.; Lal, K.; Noreen, S.; Alsader, K. A. M.; Hussain, R.; Shirinfar, B.; Ahmed, N. Electrochemical C−H/C−C Bond Oxygenation: A Potential Technology for Plastic Depolymerization. *The Chemical Record* **2024**, *24* (3), e202300331. https://doi.org/10.1002/tcr.202300331.
(616) Cho, J.; Kim, B.; Kwon, T.; Lee, K.; Choi, S.-I. Electrocatalytic Upcycling of Plastic Waste. *Green Chem.* **2023**, *25* (21), 8444–8458. https://doi.org/10.1039/D3GC03337F.
(617) Karimi Estahbanati, M. R.; Kong, X. Y.; Eslami, A.; Soo, H. S. Current Developments in the Chemical Upcycling of Waste Plastics Using Alternative Energy Sources. *ChemSusChem* **2021**, *14* (19), 4152–4166. https://doi.org/10.1002/cssc.202100874.
(618) Nardella, S.; Conte, A.; Del Nobile, M. A. State-of-Art on the Recycling of By-Products from Fruits and Vegetables of Mediterranean Countries to Prolong Food Shelf Life. *Foods* **2022**, *11* (5), 665. https://doi.org/10.3390/foods11050665.

(619) Xue, L.; Liu, G.; Parfitt, J.; Liu, X.; Van Herpen, E.; Stenmarck, Å.; O'Connor, C.; Östergren, K.; Cheng, S. Missing Food, Missing Data? A Critical Review of Global Food Losses and Food Waste Data. *Environ. Sci. Technol.* **2017**, *51* (12), 6618–6633. https://doi.org/10.1021/acs.est.7b00401.
(620) Cederberg, C.; Sonesson, U. *Global Food Losses and Food Waste: Extent, Causes and Prevention; Study Conducted for the International Congress Save Food! At Interpack 2011, [16 - 17 May], Düsseldorf, Germany*; Gustavsson, J., Ed.; Food and Agriculture Organization of the United Nations: Rome, 2011.
(621) Kilcast, D. *Food and Beverage Stability and Shelf Life: Food and Beverage Stability and Shelf Life*; Woodhead Publishing Series in Food Science, Technology and Nutrition Ser; Elsevier Science & Technology: Cambridge, 2011.
(622) Amiri, H.; Aghbashlo, M.; Sharma, M.; Gaffey, J.; Manning, L.; Moosavi Basri, S. M.; Kennedy, J. F.; Gupta, V. K.; Tabatabaei, M. Chitin and Chitosan Derived from Crustacean Waste Valorization Streams Can Support Food Systems and the UN Sustainable Development Goals. *Nat. Food* **2022**, *3* (10), 822–828. https://doi.org/10.1038/s43016-022-00591-y.
(623) Gomes, L. P.; Souza, H. K. S.; Campiña, J. M.; Andrade, C. T.; Silva, A. F.; Gonçalves, M. P.; Paschoalin, V. M. F. Edible Chitosan Films and Their Nanosized Counterparts Exhibit Antimicrobial Activity and Enhanced Mechanical and Barrier Properties. *Molecules* **2018**, *24* (1), 127. https://doi.org/10.3390/molecules24010127.
(624) Khalifa, I.; Barakat, H.; El-Mansy, H. A.; Soliman, S. A. Improving the Shelf-Life Stability of Apple and Strawberry Fruits Applying Chitosan-Incorporated Olive Oil Processing Residues Coating. *Food Packaging and Shelf Life* **2016**, *9*, 10–19. https://doi.org/10.1016/j.fpsl.2016.05.006.
(625) Rai, S.; Dutta, P.; Mehrotra, G. Lignin Incorporated Antimicrobial Chitosan Film for Food Packaging Application. *J. Polym. Mater.* **2017**, *34*, 171–183.
(626) Pavoni, J. M. F.; dos Santos, N. Z.; May, I. C.; Pollo, L. D.; Tessaro, I. C. Impact of Acid Type and Glutaraldehyde Crosslinking in the Physicochemical and Mechanical Properties and Biodegradability of Chitosan Films. *Polym. Bull.* **2021**, *78* (2), 981–1000. https://doi.org/10.1007/s00289-020-03140-4.
(627) Al-Tayyar, N. A.; Youssef, A. M.; Al-hindi, R. Antimicrobial Food Packaging Based on Sustainable Bio-Based Materials for Reducing Foodborne Pathogens: A Review. *Food Chem.* **2020**, *310*, 125915. https://doi.org/10.1016/j.foodchem.2019.125915.
(628) Elsabee, M. Z.; Abdou, E. S. Chitosan Based Edible Films and Coatings: A Review. *Mater. Sci. Eng. C* **2013**, *33* (4), 1819–1841. https://doi.org/10.1016/j.msec.2013.01.010.
(629) Bojorges, H.; Fabra, M. J.; López-Rubio, A.; Martínez-Abad, A. Alginate Industrial Waste Streams as a Promising Source of Value-Added Compounds Valorization. *Sci. Total Environ.* **2022**, *838*, 156394. https://doi.org/10.1016/j.scitotenv.2022.156394.
(630) Araújo, R.; Vázquez Calderón, F.; Sánchez López, J.; Azevedo, I. C.; Bruhn, A.; Fluch, S.; Garcia Tasende, M.; Ghaderiardakani, F.; Ilmjärv, T.; Laurans, M.; Mac Monagail, M.; Mangini, S.; Peteiro, C.; Rebours, C.; Stefansson, T.; Ullmann, J. Current Status of the Algae Production Industry in Europe: An Emerging Sector of the Blue Bioeconomy. *Front. Mar. Sci.* **2021**, *7*, 626389. https://doi.org/10.3389/fmars.2020.626389.
(631) Gomaa, M.; Fawzy, M. A.; Hifney, A. F.; Abdel-Gawad, K. M. Use of the Brown Seaweed Sargassum Latifolium in the Design of Alginate-Fucoidan Based Films with Natural Antioxidant Properties and Kinetic Modeling of Moisture Sorption and Polyphenolic Release. *Food Hydrocolloids* **2018**, *82*, 64–72. https://doi.org/10.1016/j.foodhyd.2018.03.053.

(632) Díaz-Mula, H. M.; Serrano, M.; Valero, D. Alginate Coatings Preserve Fruit Quality and Bioactive Compounds during Storage of Sweet Cherry Fruit. *Food Bioprocess Technol.* **2012**, *5* (8), 2990–2997. https://doi.org/10.1007/s11947-011-0599-2.
(633) Stylianou, M.; Christou, A.; Dalias, P.; Polycarpou, P.; Michael, C.; Agapiou, A.; Papanastasiou, P.; Fatta-Kassinos, D. Physicochemical and Structural Characterization of Biochar Derived from the Pyrolysis of Biosolids, Cattle Manure and Spent Coffee Grounds. *J. Energy Inst.* **2020**, *93* (5), 2063–2073. https://doi.org/10.1016/j.joei.2020.05.002.
(634) Fornasini, P. Introduction to X-Ray Absorption Spectroscopy. In *Synchrotron Radiation*; Mobilio, S., Boscherini, F., Meneghini, C., Eds.; Springer Berlin Heidelberg: Berlin, Heidelberg, 2015; pp 181–211. https://doi.org/10.1007/978-3-642-55315-8_6.
(635) Ji, H.; Zhao, X.; Qiao, Z.; Jung, J.; Zhu, Y.; Lu, Y.; Zhang, L. L.; MacDonald, A. H.; Ruoff, R. S. Capacitance of Carbon-Based Electrical Double-Layer Capacitors. *Nat. Commun.* **2014**, *5* (1), 3317. https://doi.org/10.1038/ncomms4317.

Acknowledgements

Acknowledgements

First and foremost, I would like to express my deepest gratitude to Prof. Dr. Adam Slabon for welcoming me into his research group. Without his support and encouragement, I would not be where I am today. Thank you for giving me the freedom to pursue my own ideas, gain international experience, and participate in conferences.

I am also sincerely grateful to Prof. Dr. Christian W. Lehmann for his supervision and for the invaluable opportunity to learn electron microscopy at the Max Planck Institute for Coal Research. A special thanks goes to Nobbi and Silvia for their patience, explanations, and support with the instrumentation.

A very special thank you goes to Prof. Dr. Jiayin Yuan for allowing me to spend two months in his research group in Stockholm, where I had the opportunity to learn the fundamentals of catalyst development. These two months were incredibly enriching, both scientifically and personally, and I am grateful for this experience. I would also like to thank Anuja, whose support and kindness made my time there even more enjoyable and unforgettable.

My appreciation extends to my former colleagues Laura, Nicole, Julia, and Ferdi, as well as my current colleagues Fabi, Lara, Max, Sophie, Yanbing, Vanessa, Madlin, Andreas, and Nele, for making my time in the department both enjoyable and enriching. A special thanks goes to Bruno and Björn, not only for the scientific discussions and continuous support but also for their encouragement and help beyond research.

I would also like to thank everyone who contributed to making my research possible. My sincere gratitude goes to my dedicated students Houssein, Sira, Silas, Finn, Anton, and Franka – thank you for your excellent work and for helping me stay on track during busy times. I am also grateful to Dirk Lützenkirchen-Hecht for enabling us to conduct experiments at the synchrotron in Dortmund and for his continuous support with data interpretation. Furthermore, I would like to thank the analytical measurement team at BUW, as well as Ms. Litz for her administrative assistance and continuous support.

A heartfelt thank you goes to all my co-authors for their collaboration and contributions to my publications. This work was supported by the Austrian COMET-Program (K2, program InTribology, FFG-no. 906860, project coordinator AC2T research GmbH) and partially carried out at the “Excellence Center of Tribology” (AC2T research GmbH).

I would also like to thank my former teachers, Kai Dietrich, Karin Lender, and Simone Jentsch, for fostering my interest in the natural sciences, which continues to this day.

Finally, I am deeply grateful to my parents, my sister Hanna, my partner Patrick, and my friends for their patience, understanding, and support throughout my PhD journey. You gave me the support I needed in challenging moments.

Thank you!

Declaration

Declaration

The presented cumulative doctoral is composed of ten distinct chapters. Chapters 3, 4, 5, 6 and 8 have been published in international peer-reviewed scientific journals, while Chapter 7 and 9 have been submitted and are currently undergoing the peer-review process - Chapter 9 has been also published as a preprint. The published and submitted articles include suggestions from co-authors, editors and reviewers received during the peer-review process.

As the leading author of all chapters, the studies were conceptualized with my PhD supervisor Adam Slabon. I conducted the majority of the experiments, performed data analysis and data interpretation myself, with additional experiments carried out as part of thesis projects that I supervised. Further experimental work and data evaluation were conducted by the co-authors.

References to published data, methods, statements, and data interpretation of other researchers are properly cited in the relevant articles and across all other chapters of this thesis.

Lucie Marie Lindenbeck